Acylanthranilamidderivate als Partialagonisten des Farnesoid X Rezeptors

Dissertation

zur Erlangung des Doktorgrades

der Naturwissenschaften

vorgelegt beim Fachbereich

Biochemie, Chemie und Pharmazie

der Johann Wolfgang Goethe-Universität

in Frankfurt am Main

von

Daniel Merk

aus München

Frankfurt (2014)

(D30)

vom Fachbereich Biochemie, Chemie und Pharmazie der

Johann Wolfgang Goethe-Universität Frankfurt als Dissertation angenommen

Dekan:	Prof. Dr. Thomas Prisner
Gutachter:	Prof. Dr. Manfred Schubert-Zsilavecz
	Prof. Dr. Dieter Steinhilber
	Prof. Dr. Gisbert Schneider
Datum der Disputation:	16.2.2015

Inhaltsverzeichnis

1. Einleitung

Nukleäre Rezeptoren haben eine lange Tradition als pharmazeutische Targets. Ihre Geschichte als Zielstrukturen von Arzneistoffen nahm mit der Entwicklung oraler Kontrazeptiva als Estrogen- und Progesteronrezeptorliganden in den 1950er-Jahren ihren Anfang. Seitdem ist der Arzneischatz um Liganden zahlreicher nukleärer Rezeptoren bereichert und die Rolle der nukleären Rezeptoren in vielerlei physiologischen und pathophysiologischen Zusammenhängen intensiv beforscht worden. Modulatoren nukleärer Rezeptoren spielen eine große klinische Rolle in der Brustkrebstherapie (Tamoxifen, Fulvestrant), in der Osteoporosebehandlung (Raloxifen, Bazedoxifen), in der Therapie der Hyperlipidämie (Fibrate), des Diabetes mellitus Typ II (Glitazone) und zahlreicher weiterer pathophysiologischer Zustände.

Insbesondere der große klinische Erfolg der am Peroxisomen Proliferator-aktivierten Rezeptor γ (PPARγ) agonistischen Glitazone, den auch der Rückschlag seltener aber schwerwiegender kardiovaskulärer Nebenwirkungen nicht schmälern kann, zeigt, dass nukleäre Rezeptoren wertvolle Arzneistofftargets darstellen können. Die Geschichte von Rosiglitazon verdeutlicht aber auch die Gefahren, die aus einem Eingriff in das komplexe Netzwerk der nukleären Rezeptoren resultieren können. Die zukünftige Entwicklung von Liganden nukleärer Rezeptoren muss durch moderateren oder selektiveren Agonismus oder durch allosterische Modulation, wie sie für PPARγ zumindest in vitro schon gelungen scheint, das Nebenwirkungspotential gering halten. So stellt das kürzlich entwickelte Prinzip, die cdk5-abhängige Phosphorylierung von PPARγ durch PPARγ-Liganden zu hemmen, ohne den Rezeptor dabei zu aktivieren, einen äußerst vielversprechenden neuen Ansatz zur Therapie der Insulinresistenz und assoziierter Erkrankungen dar.

Um der weltweit stetig zunehmenden Inzidenz metabolischer Erkrankungen entgegen zu treten, werden neben vielen bekannten, erfolgreichen und hochwirksamen Arzneistoffen auch stetig neue Wirkstoffe an neuen Zielstrukturen dringend benötigt. Ein vielversprechendes Target für zukünftige Wirkstoffe zur Behandlung metabolischer Erkrankungen stellt der nukleäre Farnesoid X Rezeptor (FXR) dar. Als physiologischer Rezeptor für Gallensäuren kann FXR durch geeignete Fettsäuremimetika moduliert werden und bildet das Target der in dieser Arbeit entwickelten fettsäuremimetischen Acylanthranilamidderivate. Die vorliegende Arbeit widmet sich der Entwicklung neuer partialagonistischer FXR-Liganden.

1.1 Farnesoid X Rezeptor (FXR)

Der Farnesoid X Rezeptor (FXR) wurde 1995 als orphan nuclear receptor, also als nukleärer Rezeptor, für den der endogene Ligand unbekannt ist, entdeckt.[1,2] Seinen Namen hat FXR von der gleichzeitigen Beobachtung, dass Farnesolmetaboliten, die wichtige Zwischenprodukte im Cholesterol und Gallensäurestoffwechsel darstellen, den nukleären Rezeptor aktivieren können.[2] Vier Jahre später

wurden die Gallensäuren als endogene FXR-Liganden identifiziert und der Rezeptor somit deorphanisiert.[3,4] Seitdem sind die Struktur und Funktion von FXR intensiv beforscht sowie zahlreiche natürliche und synthetische Liganden des Rezeptors entdeckt worden.

Die Superfamile der nukleären Rezeptoren, zu denen FXR zählt, umfasst 48 sogenannte Liganden-aktivierte Transkriptionsfaktoren, die durch Steroidhormone, Lipide, Gallensäuren oder Xenobiotika aktiviert werden und zahlreiche Signalkaskaden der Zelldifferenzierung und des Metabolismus kontrollieren.[5]

1.1.1 Struktur und Funktion von FXR

Der Farnesoid X Rezeptor, auch NR1H4, gehört zur Superfamilie der Liganden-aktivierten Transkriptionsfaktoren und existiert beim Menschen nur als Isoform α, von der jedoch vier Splicevarianten identifiziert wurden (FXRα1-4).[6,7] Unterschiedliches Splicing hat jedoch kaum Einfluss auf die Funktion von FXR. Lediglich einzelne Targetgene werden durch FXRα1-4 unterschiedlich stark aktiviert.[7] FXR ist bei höher entwickelten Spezies konserviert, wobei in einigen Spezies, wie der Maus, mehrere Isoformen (FXRα und FXRβ) existieren.[7]

Der Rezeptor besteht aus 486 Aminosäuren, die zwei Hauptdomänen, eine DNA-Bindedomäne (DBD) und eine Ligandbindedomäne (LBD) bilden (Abbildung 1).[8] DBD und LBD sind durch eine hinge-Region miteinander verbunden. FXR liegt wie die meisten metabolischen nukleären Rezeptoren im ruhenden bzw. inaktiven Zustand gebunden an seine Response-Elemente (REs) auf der DNA als Heterodimer mit dem Retinoid X Rezeptor (RXR) vor, der auch mit anderen nukleären Rezeptoren Heterodimere bildet.[6,8]

Die N-terminale DNA-Bindedomäne ist innerhalb der Familie der nukleären Rezeptoren hochkonserviert, interagiert mit der DNA über zwei Zn^{2+}-Fingermotive und bindet selektiv an für FXR-spezifische DNA-Sequenzen, die sogenannten FXR-Response-Elemente (FXR-REs). Das erste identifizierte FXR-RE besteht aus Wiederholungen der Basensequenz AGGTCA, die jeweils durch eine Base getrennt sind und wird daher als *internal repeat 1* (IR-1) bezeichnet. Die Entdeckung von IR-1 hat zur Identifizierung zahlreicher direkter FXR-Targetgene geführt.[6,7]

Die für die Aktivierung von FXR entscheidende C-terminale Ligandbindedomäne wurde mit zahlreichen agonistischen Liganden co-kristallisiert, um ihre Struktur und Funktion aufzuklären. In der Übersichtsarbeit (Merk D, Steinhilber D, Schubert-Zsilavecz M. *Future Med. Chem.,* **2012**) sind die 24 bis 2012 verfügbaren FXR-Co-Kristallstrukturen und die unterschiedlichen Bindemodi der co-kristallisierten Liganden zusammengefasst und vergleichend untersucht. Die FXR-LBD besteht aus 12 α-Helices, die in drei Schichten übereinander liegen und ähnelt damit strukturell den Ligandbindedomänen anderer nukleärer Rezeptoren, von denen Co-Kristallstrukturen existieren (z.B.

PPARs).[6,8] Die Ligandbindetasche von FXR ist sehr hydrophob und wird durch die Helices 3, 5, 10 und 12 geformt. Sie ist mit 700 Å² relativ groß und kann sich durch die Variabilität der Helices 6 und 7 an eine Vielzahl verschiedener Liganden anpassen.[6,8,9] In Abwesenheit eines agonistischen Liganden ist die C-terminale Helix 12 destabilisiert und interagiert nicht mit der übrigen FXR-LBD.[6] Durch Bindung eines agonistischen Liganden wird die Liganden-abhängige Aktivierungsfunktion (AF-2) in Helix 12 dicht an die LBD gebunden und schließt dabei die Ligandbindetasche (vgl. Abbildung 1).[8] Zusammen mit den Helices 3, 4 und 5 bildet Helix 12 dadurch eine hydrophobe Rinne zur Bindung von Coaktivatoren.[8] Für die Bindung von Coaktivatorpeptiden ist daneben eine durch die Aminosäuren Lys_{300} in Helix 3 und Glu_{464} in Helix 12 gebildete dipolare „Zange“ von entscheidender Bedeutung.[6] Diese sogenannte „*charge clamp*“ wurde auch in anderen nuklerären Rezeptoren beobachtet.[6,10–12]

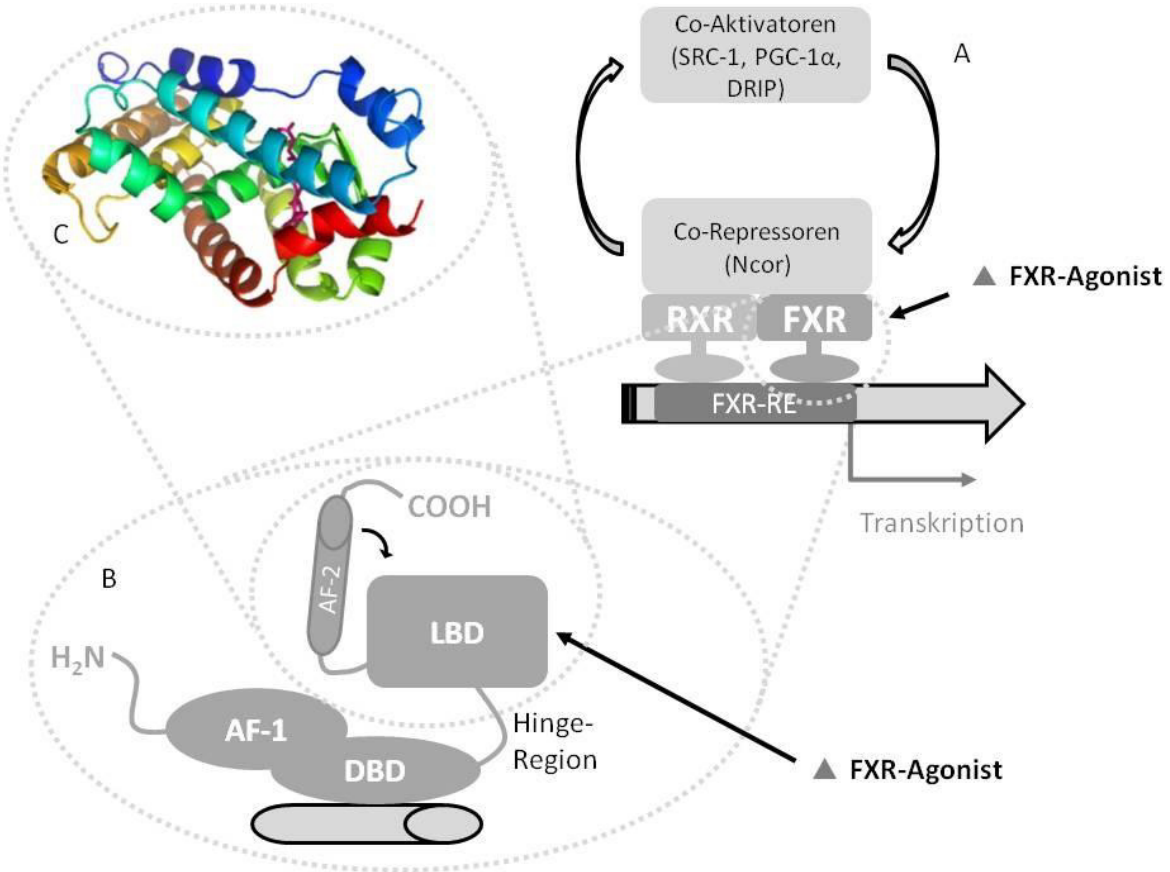

Abbildung 1: *Struktur und Funktion des nukleären Farnesoid-X-Rezeptors (FXR)*: (A) FXR bindet als Hetero-Dimer mit RXR an FXR-Response-Elemente (FXR-RE) auf der DNA. Im inaktiven Zustand sind Co-Repressoren wie NCor an das FXR-RXR-Heterodimer gebunden. Bindung eines FXR-Agonisten an die FXR-LBD bewirkt die Freisetzung von Co-Repressoren und die Rekrutierung von Co-Aktivatoren wie SRC-1 oder PGC-1α. (B) FXR besteht aus zwei Hauptdomänen, die über eine Hinge-Region verbunden sind. Die N-terminale DNA-Bindedomäne (DBD) bindet über zwei Zn^{2+}-Finger an die DNA und enthält die Liganden-unabhängige Aktivierungsfunktion 1 (AF-1). Die C-terminale Ligandbindedomäne (LBD) enthält die Liganden-abhängige Aktivierungsfunktion 2 (AF-2) in Helix 12. Durch Agonistenbindung wird die Helix 12/AF-2 an die LBD gebunden und ermöglich dadurch die Bindung von Co-Aktivatoren. (C) Die FXR-LBD besteht aus drei Schichten von insgesamt 12 α-Helices.

Im inaktiven Zustand binden Co-Repressorpeptide wie der *nuclear co-repressor* (NCor) an den FXR-RXR-Komplex und verhindern eine Transkription der Targetgene. Durch Bindung eines FXR-Liganden kommt es zu Konformationsänderungen in der Ligandbindedomäne, die wiederum zur Freisetzung

der Co-Repressorpeptide und zur Bindung von Co-Aktivatorpeptiden wie dem *steroid receptor coactivator 1* (SRC-1, nuclear receptor coactivator 1, NRC-1), dem *Vitamin D receptor interacting protein* (DRIP) oder dem *peroxisome proliferator-activated receptor gamma coactivator 1α* (PGC-1α) führen (Abbildung 1).[3,7,10] Solche Co-Aktivatorpeptide enthalten als entscheidendes Erkennungsmuster die Aminosäuresequenz LxxLL in einer α-Helix, wobei L für Leucin und x für eine beliebige Aminosäure steht.[3,4] Co-Aktivatorpeptide werden am C-Terminus von FXR nach Aktivierung der Liganden-abhängigen Aktivierungsfunktion 2 (AF-2) in Helix 12 der LBD mit Hilfe der *charge clamp* gebunden.[3,4] Die Rekrutierung von Co-Aktivatorpeptiden führt schließlich zur Aktivierung der Gentranskription. [8] Neben der Liganden-abhängigen Aktivierung über die AF-2 existiert auch eine Liganden-unabhängige Aktivierungsfunktion 1 (AF-1) in der Nähe des Aminoterminus des nukleären Rezeptors.[13]

FXR wird vor allem intensiv in Leber, Darm und Niere, also in Geweben, die mit Gallensäuren in Kontakt kommen, exprimiert.[4,8] Daneben wurde eine schwache FXR-Expression u.a. in Fettgewebe, glatten Gefäßmuskeln, Herzmuskelzellen, den Nebennieren, der Milz und dem Thymus beobachtet.[6,7] Diese Expression in für einen Gallensäurerezeptor eher untypischen Geweben verdeutlicht einerseits die noch nicht völlig aufgeklärte Rolle von Gallensäuren als Signalmolekülen und eröffnet andererseits zahlreiche potentielle therapeutische Verwendungsmöglichkeiten für FXR-Liganden.

1.2 Physiologische Rolle und klinischer Stellenwert von FXR

Als Sensor für Gallensäuren und metabolischer Regulator ist FXR in zahlreiche physiologische Vorgänge involviert und spielt daher diverse physiologische und pathophysiologische Rollen. Neben seiner Hauptfunktion in der Gallensäurehomöostase beeinflusst der nukleäre Rezeptor auch den Lipid- und Glucosestoffwechsel und ist essentiell für den Schutz und die Regeneration der Leber. Darüber hinaus rückt FXR auch im Zusammenhang mit Entzündungen und Krebs zunehmend in den Fokus.

1.2.1 Gallensäurestoffwechsel

Gallensäuren sind die natürlichen Liganden von FXR und erfüllen daneben zahlreiche weitere physiologische Funktionen. Sie sind zum einen essentiell für die Absorption von lipophilen Nährstoffen und Vitaminen, zum anderen stellen sie wichtige Abbau- und Eliminierungsprodukte des Cholesterolstoffwechsels dar. Außerdem fungieren sie als wichtige Signalmoleküle am nukleären Rezeptor FXR und dem membranständigen G-Protein-gekoppelten Rezeptor TGR5.[14,15]

In seiner physiologischen Funktion als Gallensäuresensor steuert FXR vor allem die Expression von Genen, die an der Gallensäurehomöostase beteiligt sind. Physiologisch wird FXR durch hohe Gallensäurespiegel aktiviert, um der Akkumulation (hepato-)toxischer Gallensäuren entgegen-

zuwirken. Eine FXR-Aktivierung führt zu verstärkter Expression von Gallensäuretransportproteinen in den Zellmembranen verschiedener Gewebe. FXR induziert die Expression der Transporter *multidrug resistance-associated protein 2* (MRP-2) und *bile salt export protein* (BSEP) in der kanalikularen Membran von Hepatozyten, sodass der Transport von Gallensäuren in die Galle zunimmt.[16] Gleichzeitig erhöht FXR die Expression der basolateralen Gallensäuretransporter *multidrug resistance-associated protein 3* (MRP-3) und *organic solute transporter* α und β (OSTα/β) in Hepatozyten.[16] In Niere und Gastrointestinaltrakt verstärkt FXR ebenfalls die Expression der Gallensäuren ausscheidenden Transportproteine MRP-2, MRP-3 und OSTα/β.[16] Gleichzeitig mit dem verstärkten Efflux von Gallensäuren aus den Zellen reduziert FXR außerdem durch Repression der basolateralen Gallensäuren aufnehmenden Transporter *Na^+-taurocholate cotransport peptide* (NTCP) und *organic anion transporting protein 1* und *4* (OATP 1/4) die Gallensäureaufnahme.[16] Eine erhöhte Expression des *ileal bile acid binding protein* (IBABP) komplettiert die FXR-induzierte Anpassung auf erhöhte Gallensäurespiegel und führt zu verstärkter Gallensäureausscheidung (vgl. Abbildung 2).[15,16]

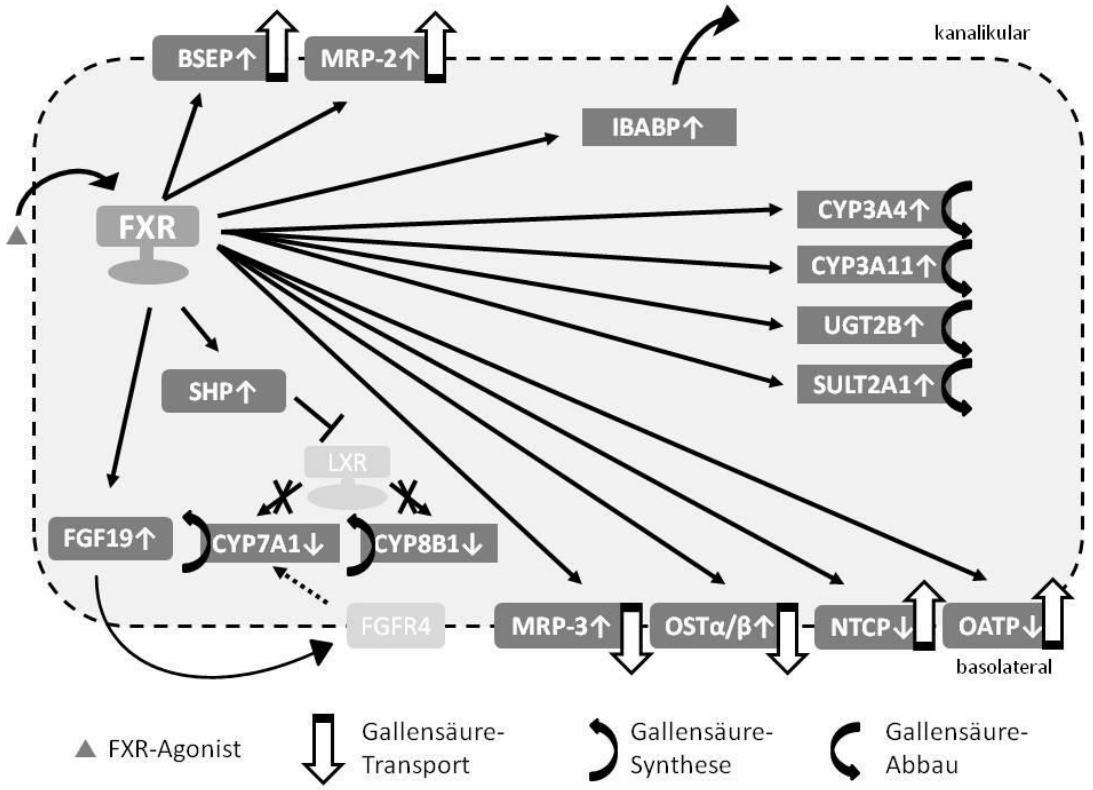

Abbildung 2: *Schematische Darstellung der genomischen Effekte einer FXR-Aktivierung auf den Gallensäurestoffwechsel*: FXR-Aktivierung erhöht die Expression von SHP und FGF19, was indirekt zur Repression der an der Gallensäuresynthese beteiligten Enzyme CYP7A1 und CYP8B1 führt. Daneben steigt die Expression der Gallensäuren metabolisierenden Enzyme CYP3A4, CYP3A11, UGT2B und SULT2A1. Der Gallensäuretransport wird durch Induktion der Gallensäureexporter BSEP, MRP-2, MRP-3 und OSTα/β und Repression der Gallensäuren aufnehmenden Transporter NTCP und OATP zur Gallensäureexkretion verschoben. Zusätzlich steigt die Expression des intestinalen Proteins IBABP.

Unterstützend zur verstärkten Gallensäureeliminierung kontrolliert FXR indirekt auch die Gene der Gallensäuresynthese. FXR-Aktivierung führt zu erhöhter Expression des nukleären Co-Rezeptors *small hetero-dimer partner* (SHP) und des *fibroblast growth factor 19* (FGF19). SHP inhibiert in der Folge

die Aktivität des Liver X Rezeptors (LXRα), zu dessen Targetgenen das Cytochrom P-450 Enzym *cholesterol 7α-hydroxylase* (CYP7A1) gehört, welches den geschwindigkeitsbestimmenden Schritt des klassischen (oder auch neutralen) Wegs der Synthese von Chenodeoxycholsäure (chenodeoxycholic acid, CDCA, **1**) aus Cholesterol katalysiert.[6,16–18] Durch gesteigerte SHP-Expression kommt es zur autokrinen Hemmung von LXRα und zur Repression von CYP7A1, wodurch die Gallensäuresynthese aus Cholesterol abnimmt. FGF19 (bzw. das murine Homolog FGF15) beeinflusst die CYP7A1-Expression als Signalmolekül parakrin durch Aktivierung des *fibroblast growth factor receptor 4* (FGFR4), der durch die intrazelluläre JNK-Kaskade die CYP7A1 Expression hemmt.[6,15,19,20]

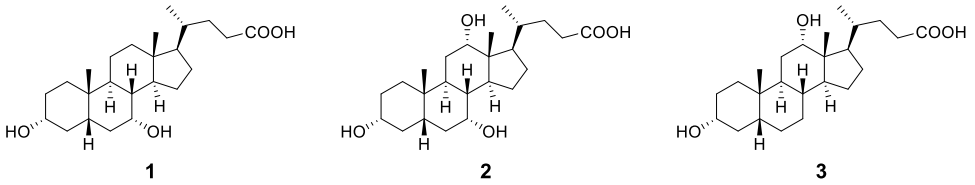

Abbildung 3: *Die Gallensäuren CDCA (**1**), CA (**2**) und DCA (**3**) sind wichtige physiologische FXR-Agonisten.*

Neben CYP7A1 spielt auch das Cytochrom P-450 Enzym *sterol 12α-hydroxylase* (CYP8B1) eine wichtige Rolle in der Gallensäuresynthese und beeinflusst die Zusammensetzung des Gallensäure-pools. CYP8B1 ist an der Biosynthese von Cholsäure (cholic acid, CA, **2**) und Deoxycholsäure (deoxycholic acid, DCA, **3**) beteiligt und damit für die Bildung bestimmter Gallensäuren essentiell. Die Aktivität von CYP8B1 bestimmt das Verhältnis der Gallensäuren CA und CDCA. CYP8B1 steht wie CYP7A1 über die nukleären Rezeptoren SHP und LRH-1 indirekt unter der Kontrolle von FXR.[6,7,15,19,20]

FXR beeinflusst außerdem den metabolischen Abbau von Gallensäuren, indem er die Expression der Cytochrom P-450 Enzyme CYP3A4 und CYP3A11 sowie der *UDP-glucuronosyltransferase-2B* (UGT2B) und der *sulfotransferase 2A1* (SULT2A1) induzieren kann, welche Gallensäuren metabolisieren.[7]

1.2.2 Lebererkrankungen

Der offensichtlichste therapeutische Nutzen einer FXR-Aktivierung besteht in der Behandlung von Lebererkrankungen, die im weitesten Sinn auf veränderten Spiegeln und erhöhter Toxizität von Gallensäuren beruhen. Dazu zählen die Cholestase, die primäre billiäre Zirrhose (PBC), die nicht-alkoholische Fettleber (NAFLD) und die nicht-alkoholische Steatohepatitis (NASH).

Cholestase ist durch einen gestörten Abfluss der Galle wegen einer mechanischen Blockade des Gallengangs oder durch die Insuffizienz von Hepatozyten charakterisiert. Die resultierende Akkumulation von Gallensäuren und anderen Metaboliten, wie Bilirubin, in der Leber führt zu Lebertoxizität und Leberschäden. In cholestatischen Zuständen verändert sich das Expressionsprofil von Gallensäuretransportern, sodass die Gallensäuren in Hepatozyten akkumulieren, von diesen aber nicht mehr kanalikular ausgeschieden werden. Daneben nimmt die renale Eliminierung als adaptiver Mechanismus zu. Therapeutisch kann eine FXR-Aktivierung in cholestatischen Zuständen den

normalen orthograden Gallensäuretransport und -abbau verbessern, indem die Expression von Gallensäuretransportern und Gallensäure metabolisierenden Enzymen induziert wird. Im Tiermodel zeigten die FXR-Agonisten GW4064 (**4**) und 6-α-Ethyl-CDCA (6-ECDCA, Obeticholsäure (OCA), **5**) entsprechend positive Effekte auf die Lebertoxizität bei Cholestase.[21,22] Allerdings wurde in anderen Tiermodellen beobachtet, dass durch FXR-Aktivierung bei Cholestase zwar die Lebertoxizität abnahm, gleichzeitig aber die Expression von Gallensäuretransportern (z.B. MRP-4), die für die basolaterale Ausscheidung von Gallensäuren aus Hepatozyten und die renale Eliminierung verantwortlich sind, zurückging. Somit scheint eine FXR-Aktivierung den physiologischen Anpassungsmechanismus auf einen cholestatischen Zustand zu stören.[23,24] Die Effekte von FXR-Liganden zur Behandlung der Cholestase sind also im Hinblick auf die Verbesserung des Gallensäuretransportes vielversprechend, bergen aber auch das Risiko schwerwiegender Nebenwirkungen und verstärkter Leberschädigung. Das Netzwerk der verschiedenen nukleären Rezeptoren wie dem Pregnan X Rezeptor (PXR) und dem konstitutiven Androstan Rezeptor (CAR), die als Sensoren für toxische Metaboliten und Xenobiotika fungieren, sowie LXR und PPARα muss noch besser verstanden werden, um die richtige Balance ihrer Aktivierung bzw. Hemmung zur Behandlung toxischer Erkrankungen wie der Cholestase zu finden.[7,14]

PBC ist eine chronische, autoimmun entzündliche Erkrankung der Leber, bei der es ausgehend von den Gallengängen zur entzündlichen Zerstörung des Lebergewebes kommt. Dabei wird das geschädigte Gewebe fibrotisiert und vernarbt. In der Folge kommt es zu portaler Hypertension und zur Zerstörung und Mangelfunktion der Leber als weiteren Sekundärmanifestationen. Die genauen Ursachen und Auslöser der PBC sind nicht vollständig aufgeklärt, es spielen jedoch Autoantikörper eine Rolle. Daneben gilt Alkohol als wichtiger Auslöser. Unbehandelt schreitet die Erkrankung fort und führt letztlich zum Tod. Die aktuelle Therapie beruht auf der Applikation der Gallensäure Ursodeoxycholsäure (UDCA, **6**), die an FXR nicht bzw. sehr schwach partialagonistisch aktiv ist. Die positiven Effekte von UDCA (**6**) bei PBC beruhen vermutlich auf Interaktionen mit anderen Rezeptoren, wie PXR und dem Glucocorticoidrezeptor (GR).[9,25,26] Aufgrund seiner antifibrotischen und choleretischen Effekte stellt FXR auch in der Behandlung der PBC ein attraktives Target dar.[14] Dafür spricht auch, dass die Regeneration der Leber nach partieller Resektion wahrscheinlich auf FXR-abhängigen Mechanismen beruht.[14]

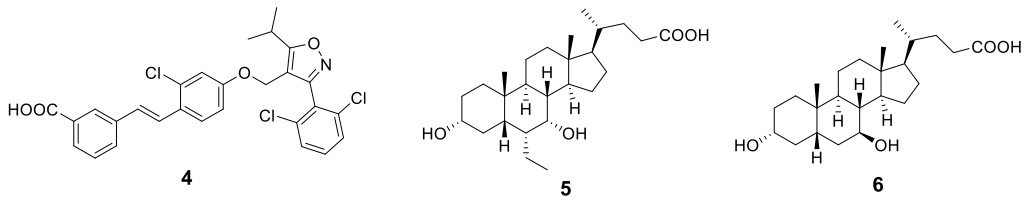

Abbildung 4: *Die synthetischen FXR-Agonisten GW4064 (**4**) und 6-ECDCA (**5**)* wurden als Modellsubstanzen in vielen in vitro und in vivo Untersuchungen verwendet. **5** befindet sich außerdem als erster FXR-Agonist in der fortgeschrittenen klinischen Entwicklung. Die natürliche Gallensäure UDCA (**6**) wird therapeutisch bei PBC eingesetzt, sie ist an FXR jedoch nur sehr schwach aktiv.

Die nicht-alkoholische Fettleber (NAFLD) und ihre fortgeschrittene Manifestation der nicht-alkoholischen Steatohepatitis (NASH) zählen zu den häufigsten Lebererkrankungen weltweit. Mit einer Inzidenz von 14-27% hat NAFLD eine deutlich höhere Prävalenz als Alkohol- oder Hepatitis C-assoziierte Leberpathophysiologien. NAFLD ist häufig verbunden mit metabolischen Erkrankungen wie Diabetes mellitus Typ II und Adipositas, kann aber auch ohne Begleiterkrankungen auftreten. Die erste Stufe der NAFLD ist durch einen erhöhten Fettgehalt der Leber charakterisiert. Schreitet die Erkrankung (in 5-20% der Fälle) zur NASH fort, kommen Lebertoxizität und erhöhte Apoptose von Hepatozyten hinzu. Ohne Behandlung oder Anpassung des Lebensstils kann NASH zu Leberzirrhose und im fortgeschrittenen Stadium zu Lebertumoren führen. Bislang existiert keine etablierte Therapie für NAFLD und ihre Folgeerkrankungen, doch aufgrund der hohen Prävalenz und der gravierenden Folgen ist die Entwicklung einer effektiven Behandlung dringend notwendig.[7,27,28]

Die Pathogenese der NAFLD ist nicht vollständig aufgeklärt, sie beruht jedoch offensichtlich auf einem Überangebot an Fett und erhöhten Triglyceridspiegeln aus zugeführten und im Körper gebildeten Lipiden.[28] Wie Tiermodelle mit FXR-Agonisten oder FXR-knockout demonstriert haben, spielt FXR eine entscheidende Rolle in der Regulation des Triglyceridstoffwechsels.[29–31] Reduktion von zirkulierenden Gallensäurespiegeln beim Menschen beispielsweise durch Colestyramin beeinflusste ebenfalls das Lipidprofil mit erhöhten HDL und VLDL und verringerten LDL-Spiegeln.[32,33]

FXR-Aktivierung induziert die Expression von SHP, was wiederum zu einer Repression des *sterol-regulatory-element-binding protein 1c* (SREBP-1c) führt. SREBP-1c kontrolliert die Expression zahlreicher für den Fettstoffwechsel entscheidender Gene, sodass eine Repression des Transkriptionsfaktors SREBP-1c die Lipidsynthese und -freisetzung reduziert.[28,34] FXR beeinflusst außerdem direkt oder indirekt die Expression der Apolipoproteine apoAI, apoCII, apoAIV, apoCIII sowie apoB und der Lipoproteinlipase (LPL).[28] Daneben antagonisiert der nukleäre Rezeptor den *nuclear factor kappa B* (NF-κB) Signalweg in Hepatozyten und wirkt dadurch der bei NAFLD/NASH auftretenden Lebertoxizität und -inflammation entgegen.[35] Durch die Repression von profibrotischen Faktoren wie des *transforming growth factor* β (TGFβ) reduziert FXR außerdem die Leberfibrose.[36] Somit bietet die Aktivierung von FXR in NAFLD/NASH einen breiten und vielversprechenden therapeutischen Ansatzpunkt. Allerdings besteht auch bei dieser wie bei allen FXR-abhängigen therapeutischen Strategien das Potential unerwünschter Wirkungen.[28]

Das synthetische Gallensäurederivat 6-ECDCA (**5**) befindet sich derzeit als erster FXR-Ligand in der späten klinischen Entwicklung zur Behandlung der NAFLD/NASH und der PBC. **5** ist ein Derivat des physiologischen FXR-Liganden CDCA (**1**) und hat etwa dessen 100-fache Potenz als FXR-Agonist. **5** stellt einen FXR-Vollagonisten mit EC_{50}-Werten von etwa 0,1 µM in Reportergen- und Co-Aktivatorrekrutierungsassay dar und ist selektiv für FXR über andere nukleäre Rezeptoren.[26,37,38] In

der präklinischen Entwicklung wurden für 6-ECDCA (**5**) anticholestatische und hepatoprotektive sowie positive metabolische Wirkungen beobachtet. 6-ECDCA (**5**) bewirkte in Tiermodellen des metabolischen Syndroms und des Diabetes mellitus Typ II eine verbesserte Glucosetoleranz und Lipidhomöostase, eine reduzierte Insulinresistenz und einen Rückgang des Leberfettgehaltes.[26,39,40,40,41] Daneben schützte **5** Mäuse vor chemisch induzierter Lebertoxizität und -fibrose.[26,42–44]

In der klinischen Entwicklung zur Behandlung der NAFLD/NASH verbesserte 6-ECDCA (**5**) in drei klinischen Phase II Studien verschiedene Biomarker der Leberfibrose und -schädigung. Auch in der experimentellen Behandlung der PBC zeigte **5** positive Effekte auf die Leberfibrose und -schädigung und senkte die Plasmaspiegel der alkalischen Phosphatase (AP) und der Gamma-Glutamyl-Transferase (GGT). Bei diabetischen Patienten mit NAFLD verbesserte **5** außerdem die hepatische und periphere Glucoseverwertung und führte zu einer Gewichtsreduktion. In den bisherigen klinischen Studien wurde der experimentelle Wirkstoff gut vertragen und verursachte keine schwerwiegenden Nebenwirkungen.[26] Weitere klinische Studien mit 6-ECDCA (**5**) zu den gleichen Indikationen werden aktuell durchgeführt und es spricht vieles dafür, dass Obethicholsäure (**5**) als erster FXR-Ligand eine Zulassung als Arzneistoff erhält. In diesem Fall könnte der Wirkstoff die derzeit nicht zufriedenstellende Behandlung der schwerwiegenden Lebererkrankungen PBC und NAFLD/NASH revolutionieren. Zudem besteht durch Studien zu anderen Indikationen die Möglichkeit, dass weitere mit FXR und Gallensäuren assoziierte pathophysiologische Zustände mit 6-ECDCA (**5**) therapiert werden können.[26]

1.2.3 Fettstoffwechsel und Arteriosklerose

Die Gallensäurehomöostase beeinflusst maßgeblich den Metabolismus von Cholesterol. Etwa die Hälfte des täglich aus dem Stoffwechsel entfernten Cholesterols wird durch Umwandlung in Gallensäuren eliminiert.[17] Somit kann durch eine Modulation von FXR der Cholesterolmetabolismus günstig beeinflusst werden. Die richtige Balance zwischen FXR-Aktivierung und -Hemmung für diesen Effekt ist jedoch bislang ungeklärt, da die FXR-Aktivierung zwar zu gesteigerter Gallensäureausscheidung führt, gleichzeitig aber durch reduzierte Gallensäuresynthese die Umwandlung von Cholesterol in Gallensäuren abnimmt. FXR knockout in Mäusen führte zu erhöhten Gallensäurespiegeln, da der negative Feedback-Mechanismus über FXR blockiert war. Daneben wurden ein gestörter Cholesterolmetabolismus, erhöhte Serumlipidspiegel und die Akkumulation von Lipiden in der Leber beobachtet. Insgesamt führte FXR knockout zu einem deutlich proatherogenen Lipidprofil, das sich auch im Phänotyp der Mäuse widerspiegelte.[7]

Der FXR-Agonist CDCA (**1**) wird seit Jahrzehnten zur Behandlung von Gallensteinen und der familiären Hypertriglyceridämie eingesetzt und bewirkt eine robuste Senkung der Plasmatriglyceridspiegel.[7]

Ähnliche Effekte wurden bei der Behandlung von Mäusen mit dem synthetischen FXR-Agonisten GW4064 (**4**) beobachtet.[7]

Die lipidsenkenden Effekte einer FXR-Aktivierung (Abbildung 5) beruhen dabei auf Einflüssen auf Gene der Fettsäure- und Triglyceridsynthese. FXR-Aktivierung unterdrückt über SHP die Expression von SREBP-1c, das wiederum die Expression lipogener Gene wie der *fatty acid synthase* (FAS) kontrolliert. FXR induziert außerdem den *low density lipoprotein receptor* (LDLR), den *very low density lipoprotein receptor* (VLDLR) und syndecan-1 in der Leber, was zu gesteigerter Lipidelimination führt.[45] Durch eine Induktion der Expression von PPARα führt FXR-Aktivierung daneben letztendlich zu einer gesteigerten β-Oxidation von Fettsäuren.[28,45]

Im Tiermodell bewirkte der synthetische FXR-Agonist GW4064 (**4**) ebenfalls eine Senkung des Cholesterolspiegels, doch dieser Effekt beruhte vor allem auf erniedrigten HDL-Cholesterol-Spiegeln. Im Einklang mit dieser Beobachtung zeigten $FXR^{-/-}$-Mäuse erhöhte HDL-Level. Somit hat FXR-Agonismus zwar einen positiven Effekt auf die Plasmatriglyceridspiegel und senkt damit das Arterioskleroserisiko, gleichzeitig wird aber durch Senkung der HDL-Spiegel die Lipidhomöostase gestört.[7]

Insgesamt hat eine FXR-Aktivierung pro- und anti-atherogene Wirkungen. FXR-Aktivierung bewirkt eine teilweise Verbesserung des Lipidprofils und scheint daneben die Expression des vasokonstriktiven Peptids Endothelin-1 zu reduzieren.[46] Demgegenüber steht eine FXR-abhängige Senkung der HDL-Spiegel und eine Induktion der proatherogenen Faktoren *intracellular adhesion molecule 1* (ICAM-1) und *vascular cell adhesion molecule 1* (VCAM-1), die zur Rekrutierung von Makrophagen in das vaskuläre Endothel führen.[47] Die Ergebnisse von Tiermodellen zur Arteriosklerose[48,49] sind bislang widersprüchlich, sodass die pro- und anti-atherogenen Wirkungen von FXR noch weiter zu untersuchen sind.

FXR-Aktivierung bewirkt also durch Hemmung verschiedener Stoffwechselenzyme eine Reduktion der hepatischen Lipogenese sowie durch zusätzliche Steigerung der Lipidelimination mittels Ausscheidung oder β-Oxidation eine Senkung der zirkulierenden Spiegel an Lipiden und Cholesterol.[45]

1.2.4 Glucosestoffwechsel

Die Rolle von FXR im Glucosestoffwechsel ist komplex und hängt mit zahlreichen anderen metabolischen Regulatoren zusammen. Die genomischen Effekte einer FXR-Aktivierung auf die Glucosehomöostase betreffen ähnlich wie bei der Lipidhomöostase sowohl die Glucosesynthese als auch die Glucoseelimination. Durch die Induktion von SHP hemmt FXR indirekt die Expression der beiden für die Glucosesynthese aus Pyruvat essenziellen Enzyme *phosphoenol-pyruvate carboxykinase* (PEPCK) und *glucose-6-phosphatase* (G6Pase), wodurch die Gluconeogenese in der Leber reduziert wird.[45,50,51] Daneben fördert FXR über nicht völlig aufgeklärte Mechanismen die

Glykogensynthese in der Leber und steigert die Glucoseaufnahme in Muskeln durch erhöhte Expression des Glucosetransporters GLUT-4 (Abbildung 5).[7,45,50,52]

In einigen Tiermodellen wurde außerdem eine Verbesserung der Insulinsensitivität durch FXR-Aktivierung bzw. eine Verschlechterung durch knockout beobachtet.[7,45,52] FXR knockout in Mäusen führte zu einem gestörten Glucosestoffwechsel, verschlechterter Glucosetoleranz und einer ausgeprägten Insulinresistenz, während Überexpression des nukleären Rezeptors in der Leber den Plasmaglucosespiegel senkte. Die Ergebnisse der Tiermodelle zur Untersuchung der Rolle von FXR in der Glucosehomöostase sind allerdings teilweise widersprüchlich, denn während $FXR^{-/-}$-Mäuse eine moderate Glucoseintoleranz und Insulinresistenz entwickeln, sind sie resistent gegen die metabolischen Konsequenzen einer fettreichen Ernährung (*high-fat diet*), die bei Wildtypmäusen zur Entwicklung eines diabetischen Phänotyps führen. Das lässt darauf schließen, dass andere Rezeptoren und Mechanismen die Folgen eines Mangels an FXR-Aktivität ausgleichen können.[7,50,53] Daher wäre auch ein synergistischer Effekt von FXR- und PPARγ-Aktivierung auf den Glucosestoffwechsel denkbar. Außerdem wurden auch für den nukleären Rezeptor PPARγ, dessen Aktivierung mit Glitazonen bekanntermaßen ein wertvolles therapeutisches Prinzip bei der Behandlung von Diabetes mellitus Typ II darstellt, widersprüchliche Ergebnisse in knockout Studien an Mäusen beobachtet.[54]

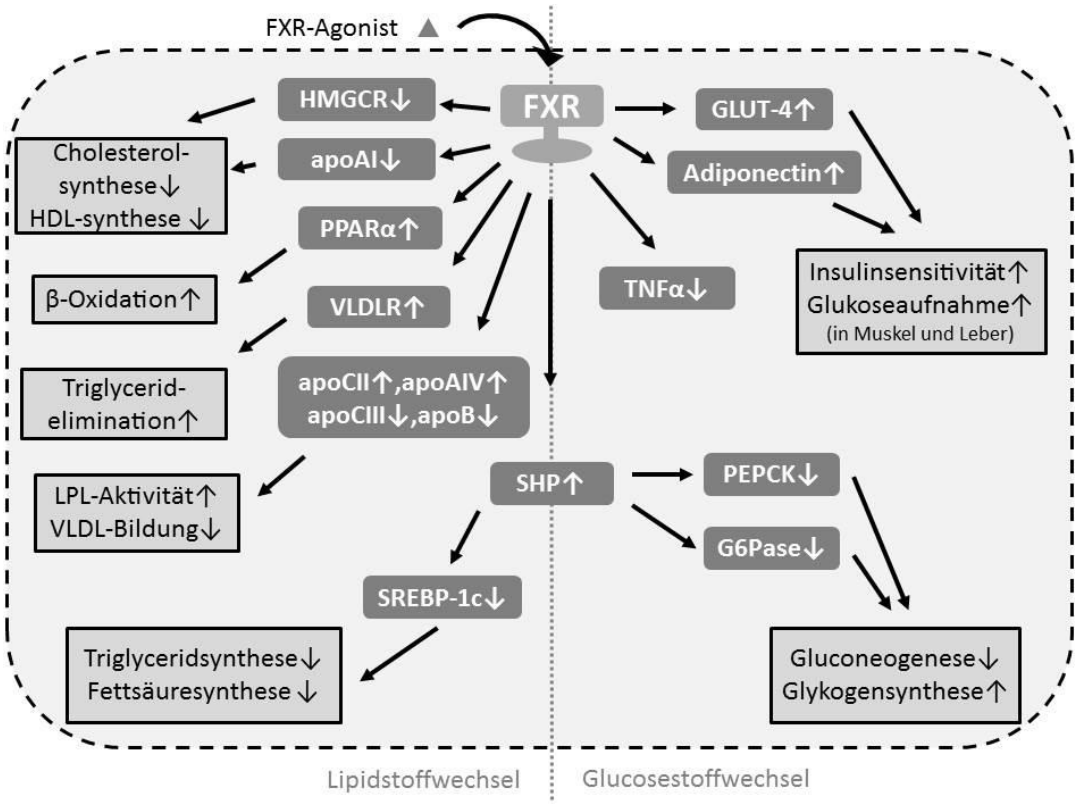

***Abbildung 5**: Schematische Darstellung der genomischen Effekte einer FXR-Aktivierung auf den Lipid- und Glucosestoffwechsel*: FXR-Aktivierung bewirkt durch Induktion oder Repression seiner Targetgene zahlreiche positive Wirkungen auf den Lipid- und Glucosemetabolismus. FXR-Aktivierung senkt unter anderem die Cholesterol-, Triglycerid- und Fettsäuresynthese sowie die Gluconeogenese. Daneben steigert sie die Triglyceridelimination u.a. durch vermehrte β-Oxidation und erhöht die Glucoseverwertung u.a. durch periphere und hepatische Glucoseaufnahme sowie durch gesteigerte Glykogensynthese.

In vitro wurden sehr positive Effekte von FXR-Agonisten auf die glucoseabhängige Insulinfreisetzung aus kultivierten β-Zellen von Mäusen beobachtet. Die FXR-Agonisten Tauro-CDCA und GW4064 (**4**) verstärkten die glucoseabhängige Insulinfreisetzung, während der FXR-Antagonist Guggulsteron (**7**) diesen Effekt hemmte.[55,56]

Kürzlich wurde FXR zumindest teilweise auch der drastische Gewichtsverlust nach operativer Magenverkleinerung als weiterer bedeutender metabolischer Effekt zugeschrieben. Diese ultima ratio in der Behandlung der Adipositas und assoziierter metabolischer Erkrankungen führt in sehr vielen Fällen zu großem Behandlungserfolg, denn etwa 40% der adipösen Diabetes mellitus Typ II Patienten, an denen eine operative Magenverkleinerung durchgeführt wird, erreichen eine vollständige Remission ihres Diabetes. Der Mechanismus, der der Effektivität dieser Behandlung zugrunde liegt, war lange Zeit unbekannt. Nun haben neue Ergebnisse belegt, dass FXR zumindest teilweise für die deutliche Verbesserung des metabolischen Zustands nach einer Magenverkleinerung verantwortlich ist.[57]

Dabei wurde zunächst beobachtet, dass eine Magenverkleinerung eine Zunahme des gesamten Gallensäurepools und der FXR-Aktivität bewirkt. Um die mechanistische Rolle von FXR zu bestätigen, wurden $FXR^{-/-}$- und Wildtypmäuse unter einer fettreichen Diät gehalten, bis sie einen deutlich adipösen Phänotyp entwickelt hatten und anschließend einer operativen Magenverkleinerung unterzogen. Sowohl $FXR^{-/-}$- als auch Wildtypmäuse verloren nach der Operation deutlich an Gewicht, doch während die Wildtypmäuse das nach der Magenverkleinerung reduzierte Gewicht hielten, erreichten die $FXR^{-/-}$-Mäuse nach 5 Wochen wieder das Gewicht von nicht operierten Mäusen. $FXR^{-/-}$-Mäuse nahmen dabei eine Woche nach der operativen Magenverkleinerung deutlich mehr Nahrung zu sich als Wildtypmäuse. Operierte Wildtypmäuse zeigten außerdem im Gegensatz zu $FXR^{-/-}$-Mäusen eine bessere Reaktion auf einen oralen Glucosetoleranztest. FXR scheint daher eine entscheidende Rolle bei der Aufrechterhaltung der äußerst positiven metabolischen Folgen einer operativen Magenverkleinerung zu spielen, womit sich weitere therapeutische Möglichkeiten zur Behandlung metabolischer Erkrankungen mit FXR-Agonisten eröffnen. Der konkrete Mechanismus für die metabolischen Verbesserungen nach einer Magenverkleinerung bleibt allerdings noch vollständig aufzuklären, wobei auch die Darmflora im Zusammenspiel mit FXR beteiligt zu sein scheint.[57]

1.2.5 FXR und Entzündung

Über genomische Effekte auf NF-κB scheint FXR zudem eine Rolle bei Entzündungen zu spielen. In einem Mausmodell entzündlicher Darmerkrankungen reduzierte die Applikation des synthetischen FXR-Agonisten 6-ECDCA (**5**) rektale Blutungen und die Entzündung im Gastrointestinaltrakt. Der FXR-Agonist schützte außerdem das intestinale Epithel und erhielt seine Barrierefunktion aufrecht.[43] Verglichen mit unbehandelten Mäusen wurden im Darm der mit 6-ECDCA (**5**) behandelten Mäuse

erniedrigte mRNA- und Protein-Level der inflammatorischen Gene Interleukin 1β (IL-1β), Interleukin 6 (IL-6) und *monocyte attractant protein-1* (MCP-1) beobachtet. Behandelte Mäuse hatten außerdem niedrigere Plasmaspiegel des Tumornekrosefaktors α (TNFα).[43]

In vitro Untersuchungen zeigten ähnliche Effekte und bestätigten die Rolle von FXR bei diesen antiinflammatorischen Effekten. Behandlung von kultivierten Enterozyten wie Caco-2 oder HT29 Zellen mit dem FXR-Agonisten GW4064 (**4**) antagonisierte die durch TNFα induzierte Expression von IL-1β. In kultivierten Immunzellen wie dendritischen Zellen oder mononukleären Zellen des peripheren Blutes (PBMCs) senkte der FXR-Agonist 6-ECDCA (**5**) außerdem die Expression und Freisetzung von TNFα.[43]

Im Darmgewebe von Morbus Crohn Patienten wurde eine verringerte Expression von FXR und seinen Targetgenen festgestellt, die möglicherweise auf verringerte zirkulierende Mengen von Gallensäuren bei den Patienten zurückzuführen ist.[58] In vitro Untersuchungen an Darmepithelzellen zeigten, dass sich NF-κB und FXR gegenseitig in ihrer Expression beeinflussen. FXR kann zwar die Inflammation im Darm reduzieren, wird aber bei Entzündung selbst durch NF-κB herunterreguliert, was wiederum das Fortschreiten der Entzündung begünstigt und den circulus vitiosus schließt.[59]

Aus den Erkenntnissen, dass die Expression und Aktivität von FXR bei entzündlichen Darmerkrankungen reduziert ist, FXR imstande ist, den TNFα-Spiegel zu senken und dass TNFα ein validiertes Target bei der Therapie chronisch entzündlicher Darmerkrankungen darstellt, ergibt sich eine mögliche therapeutische Verwendung von FXR-Agonisten bei der Behandlung von ulzerativer Colitis und Morbus Crohn.[43,59]

Ähnlich wie im Darmepithel beeinflusst FXR auch in der Leber die Entwicklung und Aufrechterhaltung von Entzündungen über NF-κB. In kultivierten Leberkarzinomzellen (HepG2) bewirkten FXR-Agonisten eine Repression von NF-κB. In primären Hepatozyten von $FXR^{-/-}$-Mäusen wurden zudem erhöhte mRNA-Level der inflammatorischen Gene induzierbare NO-Synthase (iNOS), Cyclooxygenase-2 (COX-2) und TNFα beobachtet.[35] Die Leber von $FXR^{-/-}$-Mäusen war außerdem anfälliger gegenüber einer Lipopolysaccharid(LPS)-induzierten Entzündung und Nekrose.[35] Diese Ergebnisse bestätigen die Funktion von FXR in der Protektion von Leberzellen.

1.2.6 FXR und Krebs

In den letzten Jahren wurde FXR auch im Kontext von Tumoren immer präsenter. Die FXR-assoziierten Effekte auf Tumorzellen sind in der Übersichtsarbeit (Lamers C, Schubert-Zsilavecz M, Merk D. *Current Trends in Medicinal Chemistry*, **2014**) zusammengefasst. FXR-Aktivierung führte in unterschiedlichen Tumorzelllinien in vitro und teilweise auch in vivo zu völlig unterschiedlichen

Effekten. Abhängig von der Tumorart bewirkte entweder ein FXR-Agonist oder ein FXR-Antagonist eine verringerte Proliferation, Migration und Invasion.

In Cholangiokarzinomgeweben wurde eine Repression der FXR-Expression beobachtet, die mit erhöhter Malignität der Tumoren einherging. In vitro und in Xenografts der Cholangiokarzinome bewirkten die FXR-Agonisten CDCA (**1**) und GW4064 (**4**) einen deutlichen antiproliferativen Effekt und reduzierten die Zellviabilität und Zellmigration. Diese Wirkungen ließen sich durch FXR-Antagonisten wie Guggulsteron (**7**) hemmen.[60,61] Außerdem zeigten FXR-Agonisten positive Effekte auf hepatozelluläre[62] und gastrointestinale[15,63] Karzinome.

Dagegen fand sich in Pankreas-[64] und Colonkarzinomen[65], in Zylinderepithelzellen eines Barrett-Ösophagus sowie in einigen Brustkrebszelllinien[66,67] eine FXR-Überexpression. Auf diese malignen bzw. prämalignen Zellen wurden entsprechend ungünstige Effekte von FXR-Agonisten beobachtet. FXR-Aktivierung bewirkte hier eine verstärkte Proliferation, während sich die Proliferation und Migration der Zellen durch FXR-Antagonisten deutlich reduzieren ließ.

Somit scheint FXR-Aktivierung in Tumoren von solchen Geweben, die üblicherweise mit Gallensäuren in Kontakt kommen, wie Cholangiokarzinomen, Lebertumoren oder gastrointestinalen Tumoren eine antiproliferative Wirkung zu entfalten, sodass hier FXR-Agonisten positive Effekte bewirken. In Tumoren von Geweben, die üblicherweise keinen hohen Konzentrationen an Gallensäuren ausgesetzt sind, wie die Speiseröhre oder die Bauchspeicheldrüse, bewirken Gallensäuren oder andere FXR-Agonisten dagegen eine verstärkte Proliferation und erhöhen die Progression des Tumors.

Diese Ergebnisse zeigen eine weitere Gefahr, die die therapeutische Verwendung von FXR-Liganden bergen kann, denn auf manche Tumorzelllinien wirken FXR-Agonisten bzw. -Antagonisten proliferations- und migrationsfördernd. Inwieweit dies auch für eine tumorigene Wirkung spricht, ist allerdings nicht bekannt. Auf der anderen Seite könnten FXR-Liganden, wenn sie zur Behandlung der richtigen Tumoren eingesetzt werden, aber auch als zukünftige Krebstherapeutika eine Rolle spielen, zumindest als adjuvante Co-Medikation. Dafür wäre allerdings eine genaue Typisierung der vorliegenden Tumorzellen essentiell.

Im Hinblick auf seine große Zahl an Targetgenen und seine komplexe Einbindung in diverse physiologische Zusammenhänge sind für FXR als Wirkstofftarget also zahlreiche therapeutische Anwendungsmöglichkeiten denkbar. Die Vielzahl der physiologischen Effekte weist aber gleichzeitig auf das Potential unerwünschter Effekte einer pharmakologischen FXR-Aktivierung hin. Um FXR als Wirkstofftarget vorteilhaft therapeutisch nutzen zu können, darf diese Gefahr nicht außer Acht gelassen werden.

1.3 FXR-Liganden

Seit seiner Entdeckung 1995[1,2] und spätestens nach Aufklärung seiner Rolle als Gallensäurerezeptor 1999[3,4] wurden für FXR zahlreiche natürliche Liganden identifiziert und synthetische Liganden entwickelt. Die Co-Kristallisation einiger dieser Liganden hat dabei wertvolle Informationen über die Beschaffenheit der FXR-LBD und ihre Funktion geliefert. Doch obwohl die Zahl der bekannten FXR-Liganden sehr groß ist, hat bislang nur 6-ECDCA (**5**) fortgeschrittene Phasen der klinischen Entwicklung erreicht. Nachdem lange Zeit vor allem FXR-Agonisten erforscht wurden, sind in den letzten Jahren auch zahlreiche antagonistische FXR-Liganden hinzugekommen.

Für den nukleären Rezeptor FXR sind Liganden mit unterschiedlicher Aktivität denkbar. FXR-Agonisten aktivieren den Rezeptor und führen zur Transkription der von FXR kontrollierten Targetgene. Die Amplitude der induzierten Targetgenexpression definiert dabei, ob ein Ligand vollagonistisch oder partialagonistisch wirkt. FXR-Antagonisten hemmen hingegen kompetitiv die Aktivierung des Rezeptors durch beispielsweise einen physiologischen Agonisten. In Abwesenheit eines Agonisten wäre ein Antagonist somit ohne Effekt. Zwischen Agonisten und Antagonisten liegen die sog. selektiven Gallensäurerezeptor-Modulatoren (SBARs), die eine unterschiedliche Wirkung auf verschiedene FXR-Targetgene ausüben, auf einen Teil der von FXR kontrollierten Gene also agonistisch wirken und die Expression anderer Gene antagonisieren. Ein inverser FXR-Agonist würde schließlich die Targetgenexpression in entgegengesetzter Richtung eines Agonisten beeinflussen und somit zu Expressionsraten unter dem Basallevel führen.[5,68]

Die Übersichtsarbeit (Merk D, Steinhilber D, Schubert-Zsilavecz M. *Future Med. Chem.*, **2012**) stellt die bekannten natürlichen und synthetischen FXR-Liganden sowie die vorhandenen Co-Kristallstrukturen zusammen und interpretiert die daraus gewonnenen Daten. Die verfügbaren FXR-Antagonisten und ihr möglicher pharmakologischer Stellenwert sind in (Lamers C, Schubert-Zsilavecz M, Merk D. *Current Trends in Medicinal Chemistry*, **2014**) näher betrachtet und bewertet.

1.3.1 Natürliche FXR-Liganden

Der erste mit der Entdeckung von FXR identifizierte Ligand Farnesol (**8**) ist ein schwacher Agonist und aktiviert FXR nur bei supraphysiologischen Konzentrationen.[2] Die physiologischen Agonisten von FXR stellen dagegen die Gallensäuren dar, unter denen die Chenodeoxychlosäure (CDCA, **1**) mit einem EC_{50}-Wert von etwa 8 µM die potenteste ist. Mit EC_{50}-Werten zwischen 10 und 50 µM sind Cholsäure (CA, **2**) und Deoxycholsäure (DCA, **3**) schwächere physiologische FXR-Agonisten.[9]

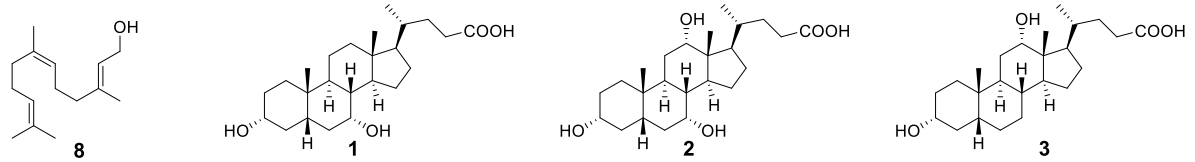

***Abbildung 6**: Natürliche FXR-Liganden*: Farnesol (**8**), CDCA (**1**), CA (**2**) und DCA (**3**)

Gallensäuren sind wasserlösliche Steroide mit amphiphatischer Struktur, welche für ihre Funktion als intestinale Tenside essentiell ist. Im Gegensatz zu den meisten anderen Steroiden steht das Proton an C-5 in Gallensäuren in β-Orientierung, sodass die Verbindung zwischen den Ringen A und B cis-konfiguriert ist. Dadurch liegt der Ring A nicht in einer Ebene mit den Ringen B, C und D, sodass Gallensäuren eine gebogene Form mit einer konvexen polaren und einer konkaven unpolaren Seite einnehmen. Diese Struktur unterscheidet sie von anderen Steroiden und trägt damit zur Selektivität für FXR bei, da der nukleäre Rezeptor die dipolare Form erkennt.[9,16]

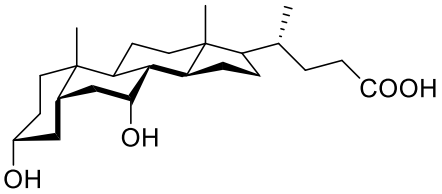

Abbildung 7: *Räumliche Struktur der Gallensäuren am Beispiel von CDCA (**1**)*

Neben den agonistischen Gallensäuren existieren auch Gallensäuremetaboliten, die antagonistisch an FXR wirken. Hierzu zählen die Lithocholsäure (LCA, **9**) sowie die murinen Gallensäuren α- und β-Muricholsäure (α-MCA, **10**; β-MCA, **11**). Die Ursodeoxycholsäure (UDCA, **6**) ist ein sehr schwacher Partialagonist an FXR und steht damit zwischen den agonistischen und antagonistischen Gallensäuren. Als antagonistische Gallensäuremetaboliten existieren außerdem Gallenalkohole mit einer α-Hydroxygruppe an C-5 wie 5α-Cyprinol (**12**) und 5α-Bufol (**13**).[9,19,20,69]

Außer den Gallensäuren und ihren Metaboliten ist eine Vielzahl natürlicher Steroide oder Steroidanaloga als FXR-Antagonisten charakterisiert. Sie sind zu einem Großteil marinen Ursprungs und spielen vor allem eine Rolle als Leitstrukturen zur Entwicklung neuer FXR-Liganden.[9,69]

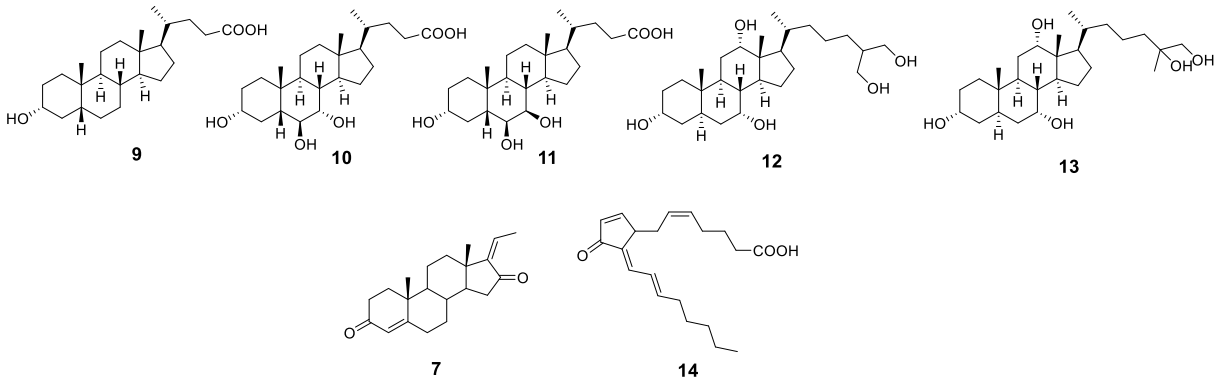

Abbildung 8: *Natürliche FXR-Antagonisten*: LCA (**9**), α-MCA (**10**), β-MCA (**11**), 5α-Cyprinol (**12**) und 5α-Bufol (**13**), sowie das Pflanzensteroid Guggulsteron (**7**) und der Arachidonsäuremetabolit 15d-PGJ_2 (**14**)

Eine Ausnahme bildet das Pflanzensteroid Guggulsteron (**7**), das in zahlreichen in vitro und in vivo Studien als FXR-Antagonist verwendet wurde und so zur Aufklärung vieler FXR-abhängiger Effekte beigetragen hat. Guggulsteron (**7**) ist kein FXR-Antagonist im klassischen Sinn, denn **7** verhält sich zwar antagonistisch in typischen in vitro Testsystemen und antagonisiert die Expression der meisten FXR-Targetgene, wirkt aber agonistisch auf die Expression von BSEP. Damit stellt **7** einen

genselektiven FXR-Modulator (SBARM) dar und zeigt, dass die Entwicklung selektiver FXR Modulatoren ähnlich den SERMs möglich ist.[9,69–72] Interessanterweise agierte auch der Arachidonsäuremetabolit 15d-Prostaglandin J_2 (15-PGJ_2, **14**) in vitro als FXR-Modulator. Ähnlich wie Guggulsteron (**7**) bewirkte **14** in vitro eine Repression der meisten FXR-Targetgene, seine Effekte auf BSEP und CYP7A1 waren aber agonistisch.[69,73]

1.3.2 Synthetische FXR-Liganden

Einer der wichtigsten synthetischen FXR-Liganden ist das steroidale CDCA-Derivat 6α-Ethyl-CDCA (**5**). Durch die Einführung der Ethylseitenkette gewinnt die Substanz fast um einen Faktor 100 an Potenz und hat einen EC_{50}-Wert an FXR von etwa 0,1 - 0,2 µM. Größere Substituenten wie eine Benzylgruppe in 6α-Position von CDCA (**1**) führten dagegen zu niedrigerer Potenz. Das Sulfatanalog **15** von 6-ECDCA ist mit einem EC_{50}-Wert von 30 nM noch etwas potenter an FXR, stellt aber auch einen potenten TGR5-Rezeptoragonisten dar. Durch Einführung eines Cinnamylcarbamats in der aziden Seitenkette von 6-ECDCA (**5**) in Derivat **16**, wurde eine weitere Potenzsteigerung zu einer Maximalaktivierung von 290% von CDCA (**1**) bei einem ähnlichen EC_{50}-Wert wie **5** von 0,15 µM erreicht. Der klinische Nutzen von **16** ist allerdings fraglich, da die Urethan-Funktion in vivo nicht stabil sein dürfte.[9,38,74–76]

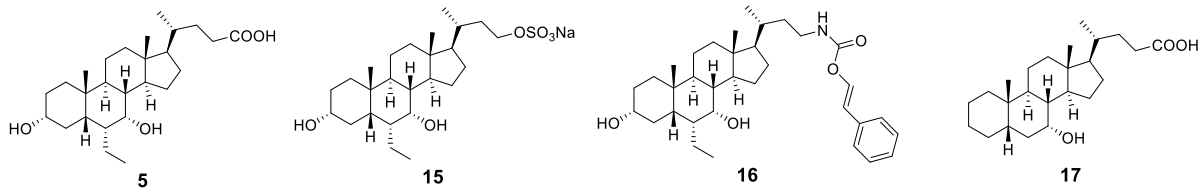

5 **15** **16** **17**

***Abbildung 9**: Synthetische steroidale FXR-Agonisten*: 6-ECDCA (**5**), seine Derivate **15** und **16** sowie 3-Deoxychenodeoxycholsäure (**17**), die wie **5** mit der FXR-LBD co-kristallisiert ist.

Kristallstrukturuntersuchungen (PDB-IDs: 1OSV, 1OT7) der steroidalen FXR-Liganden 6-ECDCA (**5**) und 3-Deoxychenodeoxycholsäure (**17**) zeigten eine potente Wechselwirkung der Carbonsäuren mit Arg331 in Helix 5, die keinen entscheidenden Einfluss auf die Aktivierung des Rezeptors zu haben scheint, sondern der Neutralisation der Carbonsäure in der sonst sehr lipophilen Ligandbindetasche dient. Daneben bildete die Hydroxyfunktion an C-7 der Steroide Wasserstoffbrückenbindungen mit den Hydroxygruppen von Ser_{332} und Tyr_{369} aus. Für die 3-OH-Gruppe in 6-ECDCA (**5**) wurden außerdem Wasserstoffbrückenbindungen zu Tyr_{361} und His_{447} beobachtet. Die 6α-Ethylgruppe füllte eine zusätzliche lipophile Untertasche in der FXR-LBD.[9,77]

Ebenfalls ein steroidähnlicher FXR-Agonist ist das von Merck entwickelte Derivat MFA-1 (**18**), in dem allerdings die Carbonsäurefunktion an Ring A sitzt und die Säureseitenkette der Steroide durch ein 4-Hydroxyphenylketon ersetzt ist. MFA-1 (**18**) ist ein hochpotenter FXR-Agonist mit einem EC_{50}-Wert von 17 nM, doch die Substanz erreichte nie die klinische Entwicklung. Zu den Struktur-Aktivitätsbeziehungen (SAR) von **18** ist wenig bekannt.[9,78]

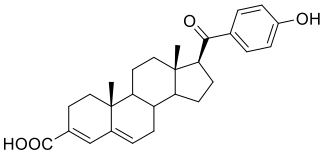

18

Abbildung 10: *Der synthetische steroidähnliche FXR-Agonist MFA-1 (**18**)*

Aufgrund der unterschiedlichen Position der Carbonsäurefunktion lag MFA-1 (**18**) in seiner Co-Kristallstruktur mit der FXR-LBD im Vergleich zu anderen steroidalen Liganden um etwa 180° gedreht in der Ligandbindetasche, sodass die Carbonsäuregruppe ebenfalls die neutralisierende Wechselwirkung mit Arg331 eingehen konnte. Der aromatische Ring des Phenylketons formte zudem potente π-Interaktionen mit den Seitenketten von Phe_{329} und Trp_{454} und die phenolische OH-Funktion bildete eine Wasserstoffbrücke mit Thr_{288} aus.[9,78]

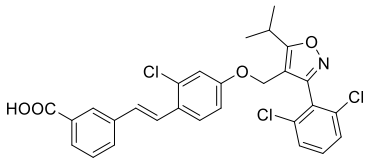

4

Abbildung 11: *Der synthetische FXR-Agonist GW4064 (**4**)*

Neben den synthetischen steroidalen FXR-Liganden wurden zahlreiche nicht-steroidale FXR-Agonisten entwickelt. Der als Referenzsubstanz am weitesten verbreitete FXR-Ligand ist das Isoxazolderivat GW4064 (**4**).[79] **4** aktiviert FXR mit einem niedrigen EC_{50}-Wert im Bereich von 0,1 µM und erreicht eine Maximalaktivierung des nukleären Rezeptors von etwa 140% von CDCA (**1**). Die in vitro Daten von GW4064 (**4**) schwanken allerdings abhängig vom verwendeten Testsystem.[9,80] Die SAR von GW4064 (**4**) wurden durch eine Vielzahl von Derivaten und mehrere Co-Kristallstrukturen (PDB-IDs: 3RUT, 3RUU, 3RVF, 3HC5, 3HC6, 3FXV, 3DCT, 3DCU, 3GD2, 3P89, 3P88) intensiv erforscht.[81–85] Dabei zeigte sich, dass die aromatische Carbonsäure in meta-Stellung für die FXR-Aktivierung am günstigsten ist und wichtige neutralisierende Wechselwirkungen mit Arg_{331}, His_{294} und Met_{265} eingeht. Eine Isopropyl- oder *tert*-Butylgruppe an Position 5 des zentralen Isoxazolringes zeigten bessere Aktivität als kleinere oder aromatische Substituenten und füllten eine lipophile Tasche innerhalb der FXR-Ligandbindetasche. Der zweifach in ortho-Position substituierte aromatische Ring an C-3 des Isoxazols war für die FXR-Aktivität essentiell und liegt aufgrund der beiden ortho-Substituenten um etwa 90° gedreht zum Isoxazol in der FXR-Ligandbindetasche, wo er eine potente π-Interaktion zur aromatischen Seitenkette der Aminosäure Phe_{329} ausbildet. Der zentrale Isoxazolring trägt ebenfalls entscheidend zur Aktivität von GW4064 (**4**) bei, indem er zum einen die an ihn gebundenen Substituenten in einem optimalen Winkel positioniert und andererseits über die beiden Heteroatome als Wasserstoffbrückenakzeptor potente Wechselwirkungen mit His_{447} eingeht. Der Bereich zwischen Säurefunktion und substituiertem Isoxazol kann durch unterschiedliche aromatische Gruppen gefüllt werden ohne die Potenz an FXR maßgeblich zu beeinflussen. Die ursprüngliche

Stilbenstruktur von GW4064 (**4**) wurde entsprechend durch zahlreiche Biphenyl-, Naphthyl- oder heteroaromatische Gruppen ersetzt, um zu ähnlich potenten Verbindungen zu gelangen.[9]

GW4064 (**4**) wurde intensiv zur Erforschung der physiologischen Funktionen von FXR verwendet und spielt eine wichtige Rolle als Referenzsubstanz in Testsystemen. Dabei stellte sich heraus, dass die Substanz ein anderes Profil bei der Aktivierung von FXR-Targetgenen zeigt als der physiologische Ligand CDCA (**1**). GW4064 wirkt agonistisch auf die Expression der meisten FXR-Targetgene, zeigt dabei jedoch eine superagonistische Tendenz insbesondere bei der Induktion von BSEP, dessen Expression **4** etwa doppelt so stark induziert wie CDCA (**1**).[8,86]

Die klinische Verwendbarkeit von GW4064 (**4**) als Wirkstoff ist jedoch begrenzt, da es eine Stilbenteilstruktur als potentiell toxisches Pharmakophor enthält und außerdem eine schlechte Bioverfügbarkeit bietet.[87,88] Daneben wurden zahlreiche off-target Effekte für **4** beobachtet, denn die Substanz ist zwar selektiv über andere nukleäre Rezeptoren[79], aktiviert aber G-Protein-gekoppelte Rezeptoren[89].

Eine weitere Klasse potenter FXR-Liganden stellen Fexaramine (**19**) und seine Derivate Fexarene (**20**) und Fexarine (**21**) dar. Fexaramine (**19**) ist ein FXR-Agonist mit einem EC_{50}-Wert von 25 nM und war der erste mit FXR co-kristallisierte Ligand. Die Kristallstruktur (PDB-ID: 1OSH) zeigte vor allem unpolare Wechselwirkungen und machte deutlich, dass für die Aktivierung von FXR nicht zwingend eine azide Funktion notwendig ist. Interessanterweise induzierte Fexaramine (**19**) ein anderes Expressionsprofil von FXR-Targetgenen als CDCA (**1**) und GW4064 (**4**).[8,9] Ähnlich wie GW4064 (**4**) eignet sich jedoch auch Fexaramine (**19**) wohl nicht für die weitere klinische Entwicklung, da zum einen in vivo der Methylester instabil sein und zum anderen die Zimtsäurepartialstruktur zur Isomerisierung und Dimerisierung neigen dürfte.

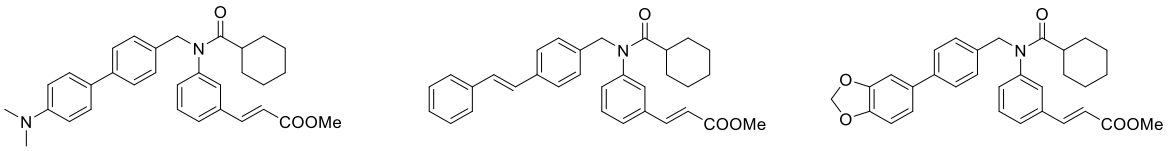

19 **20** **21**

Abbildung 12: *Die synthetischen FXR-Agonisten Fexaramine (**19**), Fexarene (**20**) und Fexarine (**21**)*

Die Klasse der 1,2,3,6-Tetrahydroazepino[4,5-*b*]indol-basierten FXR-Liganden um FXR-450 (XL335, WAY362450, **22**) enthält ebenfalls keine freie azide Funktion und stellt eine weitere Klasse potenter FXR-Agonisten dar. **22** aktiviert FXR mit einem EC_{50}-Wert von 4 nM und erreicht eine Maximalaktivierung von etwa 150% von CDCA (**1**). Die Kristallstruktur (PDB-ID: 3FLI) von **22** zeigte ebenfalls kaum polare Interaktion, aber eine Vielzahl lipophiler Wechselwirkungen und eine prominente π-Interaktion des Phenylrings im Azepinoindolsystem mit den aromatischen Seitenketten von Trp_{454} und Phe_{461}. FXR-450 (**22**) war in vitro selektiv über andere nukleäre Rezeptoren und zeigte trotz seiner schlechten Löslichkeit eine akzeptable orale Bioverfügbarkeit. **22** wurde deshalb in zwei kli-

nischen Phase I Studien untersucht, im Anschluss wurde die klinische Entwicklung jedoch aufgrund pharmakokinetischer Probleme eingestellt. Durch Einführung eines Morpholinopropylsubstituenten in **23** konnte die Löslichkeit deutlich gesteigert und die Potenz (EC_{50} = 0,09 µM, 200% max rel. Aktivierung) der Substanz weitgehend erhalten werden. Eine weitere klinische Entwicklung von **22** oder **23** ist jedoch nicht beschrieben.[9,90,91]

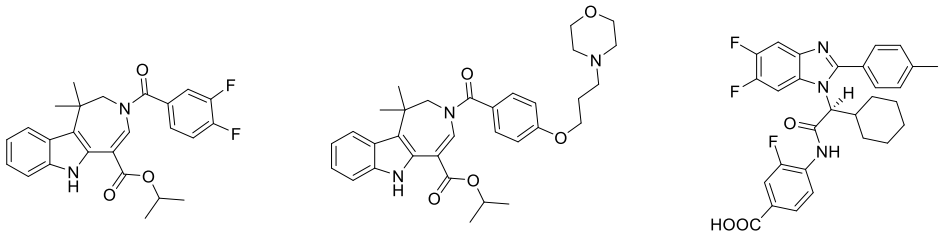

22 **23** **24**

Abbildung 13: *Die synthetischen, 1,2,3,6-Tetrahydroazepino[4,5-b]indol-basierten FXR-Agonisten FXR-450 (WAY362450, XL335, **22**) und sein besser lösliches Derivat **23**, sowie der Benzimidazol-basierte FXR-Agonist **24***

Die Entwicklungsgeschichte und die Co-Kristallstrukturanalysen der FXR-Liganden um GW4064 (**4**), Fexaramine (**19**) und FXR-450 (**22**) haben gezeigt, dass die FXR-Ligandbindetasche eine ausgeprägte Lipophilie aufweist, was dazu führt, dass potente FXR-Liganden ebenfalls sehr lipophil und schlecht wasserlöslich sind. Die Klasse der Benzimidazol-basierten FXR-Liganden um **24** wurde daher gezielt nicht nur auf ihre Potenz an FXR, sondern gleichzeitig auf eine akzeptable Polarität und Wasserlöslichkeit optimiert. In Kristallstrukturanalysen (PDB-ID: 3OLF, 3OKI, 3OKH, 3OMK, 3OMM, 3OOF, 3OOK) der Benzimidazole um **24** waren neben zahlreichen unpolaren Wechselwirkungen prominente Wasserstoffbrücken zwischen dem unsubstituierten Benzimidazolstickstoff und der Hydroxyfunktion von Tyr_{369} sowie zwischen dem Säureamidstickstoff und der Hydroxyfunktion mit Ser_{332} zu sehen. Daneben partizipierte die Carbonsäurefunktion in der typischen neutralisierenden Interaktion mit Arg_{331}. Diese Ergebnisse belegen, dass es mit geeigneten Liganden möglich ist, mehr polare Interaktionen mit der FXR-Ligandbindetasche auszubilden und auf diese Weise die Polarität und Löslichkeit der Liganden zu verbessern.[9,92,93]

Der FXR-Agonist **24** zeigte unter den Benzimidazolen das beste Gesamtprofil mit einem EC_{50}-Wert von 0,87 µM und gegenüber anderen FXR-Agonisten überlegenen physikochemischen Eigenschaften. In vivo Studien belegten bereits cholesterol- und lipidsenkende Wirkungen sowie einen anti-atherosklerotischen Effekt, sodass die Verbindungsklasse der Benzimidazole weitere präklinische und klinische Entwicklung erwarten lässt. [9,92–94]

Neben diesen wichtigsten und weitest entwickelten FXR-Aktivatoren wurden einige weitere an FXR agonistisch wirksame Substanzklassen entdeckt, darunter Pyrazolidin-3,5-dione um **25**[95], 1H-Pyrazolo[3,4-e][1,4]thiazepin-7-one um **26**[96] sowie die in silico entwickelten Verbindungen **27** und **28**[97,98]. Diese Substanzen stellen moderat potente FXR-Agonisten mit EC_{50}-Werten im niedrig micromolaren Bereich dar und könnten als Leitstrukturen zur Entwicklung weiterer potenter FXR-Liganden dienen.

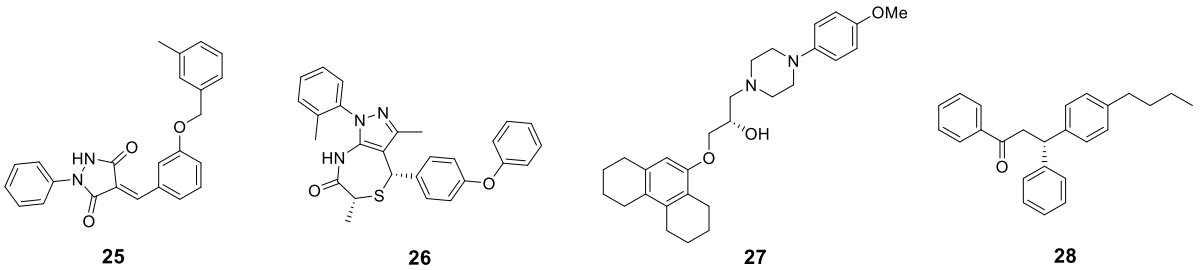

Abbildung 14: *Moderat potente synthetische FXR-Agonisten **25-28***

In den letzten Jahren hat außerdem das Interesse an FXR-Antagonisten zugenommen und zur Entwicklung einiger potenter synthetischer FXR-Antagonisten geführt. Ihre Strukturen sowie ihre potentielle pharmakologische Rolle sind in (Lamers C, Schubert-Zsilavecz M, Merk D. *Current Trends in Medicinal Chemistry*, **2014**) zusammengefasst und bewertet. Zu den wichtigsten synthetischen FXR-Antagonisten zählen unter anderen das Hydroxyacetophenonderivat **29**[99], das Pyrazolonderivat **30**[100] und insbesondere das Pyrazolderivat **31**[101], das mit einem IC_{50}-Wert von 0,47 µM in einem Reportergenassay den bisher potentesten FXR-Antagonisten darstellt.

Bislang ist keine Co-Kristallstruktur eines FXR-Antagonisten publiziert, sodass keine strukturellen Daten zum molekularen Mechanismus des FXR-Antagonismus zur Verfügung stehen. In silico Untersuchungen[102] haben jedoch angedeutet, dass Interaktionen eines Liganden mit der Helix 7 der FXR-LBD zu antagonistischer Aktivität führen könnten. Um antagonistisch zu wirken, kann ein FXR-Ligand entweder die Interaktion der FXR-LBD mit Co-Repressoren wie NCor stabilisieren oder die Rekrutierung von Co-Aktivatoren hemmen. Dazu dürfte die zur Aktivierung von FXR entscheidende Helix 12 durch einen Antagonisten nicht stabilisiert werden.[69]

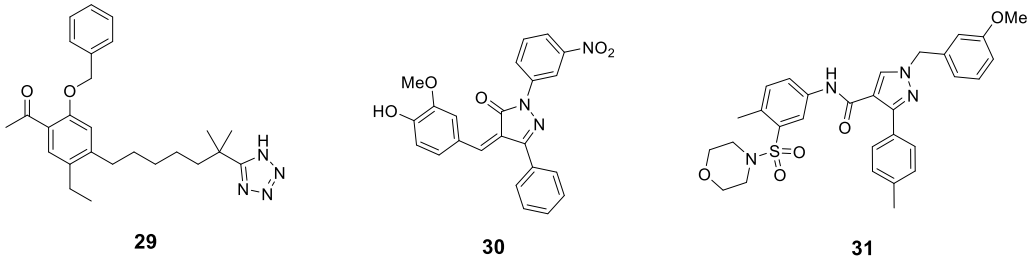

Abbildung 15: *Die potentesten synthetischen FXR-Antagonisten **29-31***

1.3.3 Charakterisierung von FXR-Liganden

Zur Charakterisierung von FXR-Liganden stehen zahlreiche in vitro Testsysteme zur Verfügung, die in der Übersichtsarbeit (Merk D, Steinhilber D, Schubert-Zsilavecz M. *Expert Opin Drug Discov*, **2014**) zusammengefasst und bewertet sind.

Bei der Entwicklung neuer biologisch aktiver Substanzen und der Durchführung von SAR-Studien ist ein Testsystem mit einem ausreichend hohen Durchsatz erforderlich, damit die Substanzentwicklung nicht durch eine allzu zeitaufwendige biologische Charakterisierung verzögert wird. Daneben ist bei SAR-Studien ein möglichst ökonomisches Testsystem wünschenswert, da während der Optimierung

eine große Zahl an Substanzen getestet werden muss. Für nukleäre Rezeptoren wie FXR sind hierfür drei Arten von Assays typisch: Reportergenassays, Bindungsassays, die auf Fluoreszenz oder Szintillation beruhen und Co-Aktivatorrekrutierungsassays. Alle drei Typen sind auch für FXR beschrieben und sollen im Folgenden kurz diskutiert werden.

Reportergenassays sind zelluläre Testsysteme, in denen die Aktivität eines Reportergens gemessen wird, welches durch die Wirkung eines am zu testenden Target aktiven Liganden exprimiert wird. Dazu werden Plasmide generiert, die die DNA-Sequenz des Targets, also des respektiven nukleären Rezeptors, enthalten, sowie die DNA-Sequenz eines Reportergens, die unter der Kontrolle eines Response-Elements des zu untersuchenden nukleären Rezeptors steht. Die Expression des nukleären Rezeptors muss dabei unter der Kontrolle eines konstitutiv aktivierten (in der Regel viralen) Promotors stehen, damit das Rezeptorprotein gebildet wird. Durch einen aktiven Liganden wird der nukleäre Rezeptor in der Folge aktiviert und induziert die Expression des Reportergens, das unter der Kontrolle seines RE steht.[80] Als Reportergen haben sich Luciferasen sowie die β-Galactosidase bewährt. Beide Enzyme bilden in Anwesenheit eines geeigneten Substrates ein messbares (Licht-)Signal. Eine elegante Alternative besteht in der Wahl eines fluoreszierenden Proteins als Reportergen.[103] Moderne Reportergenassays enthalten neben dem eigentlichen Reportergen ein zweites quantifizierbares Kontrollgen, das zur Überprüfung der Transfektionseffizienz und zur Messung von Toxizität dient. Dieses Kontrollgen ist ebenfalls eine Luciferase oder β-Galactosidase und steht unter der Kontrolle eines konstitutiv aktivierten Promotors.[80]

Der als Target dienende nukleäre Rezeptor wird entweder in seiner gesamten Sequenz (*full length* Assays), also inklusive der DBD, verwendet oder die LBD des Rezeptors wird mit der DBD des nukleären Rezeptors Gal4 aus der Hefe zu einem Hybridkonstrukt verbunden. Beide Varianten haben Vor- und Nachteile. Ein vollständiger nukleärer Rezeptor braucht für die Bindung an das Response-Element auf der DNA in der Regel einen Heterodimerpartner (RXR für FXR), sodass ein weiteres Plasmid, das für diesen Rezeptor codiert, benötigt wird. Dafür bietet die Verwendung des Volllängenrezeptors ein etwas weniger artifizielles Testsystem als ein Gal4-Hybridkonstrukt. Gal4-Hybridassays sind zwar noch artifizieller, besitzen jedoch meist ein besseres Signal-Rausch-Verhältnis, da natürliche Bestandteile der verwendeten Zellen weniger mit dem aus einer fremden Spezies stammenden Gal4-Promotor interagieren.[80]

Bei der Wahl der Zelllinie für den Reportergenassay ist darauf zu achten, dass ihr natürlicher Stoffwechsel möglichst wenig mit dem Testsystem interferiert, dass also beispielsweise eine Zelllinie für einen FXR-Reportergenassay möglichst keine Gallensäuren bildet und FXR nicht selbst exprimiert. Die Literatur beschreibt hierfür beispielsweise die Affennierenzelllinie Cos-7 und humane embryonale Nierenzellen (HEK293). Die Zellen werden mit den Plasmiden des Reportergenassays

transient transfiziert, anschließend mit den Testsubstanzen inkubiert und schließlich die Aktivität des Reportergens und des Kontrollgens vermessen. Nach Normalisierung auf das Kontrollgen und auf einen bekannten Agonisten des nukleären Rezeptors als Referenzsubstanz erhält man die relative Aktivität bei der eingesetzten Konzentration der Testsubstanz. Indem eine Testsubstanz bei mehreren Konzentrationen vermessen wird, ergibt sich eine sigmoidale Aktivitätskurve, die die Bestimmung des EC_{50}-Wertes ermöglicht. Auf die gleiche Weise kann auch ein Antagonist charakterisiert werden, wenn er in verschiedenen Konzentrationen zusammen mit einer festen Konzentration der Referenzsubstanz vermessen wird. Zusätzlich zu den Effekten einer Substanz an FXR kann ein Reportergenassay, der ein Kontrollgen enthält, außerdem erste Hinweise auf eine mögliche Toxizität der Substanz liefern.[80]

Eine Alternative zu Reportergenassays bieten zur Charakterisierung von FXR-Liganden vor allem Co-Aktivator-Rekrutierungsassays. Sie messen die Rekrutierung eines Co-Aktivatorpeptidfragments (meist SRC-1), das das Erkennungsmotiv LxxLL enthält, zum rekombinanten Rezeptorprotein in Gegenwart von Testsubstanzen. Die Rekrutierung, also die räumliche Nähe von Rezeptorprotein und Co-Aktivatorpeptid, wird dabei durch Fluoreszenz Resonanz Energie-Transfer (FRET) oder mit der alpha(amplified luminescent proximity homogenous assay)-Screen-Technologie durch die Übertragung chemischer Energie gemessen. Ähnlich wie bei Reportergenassays kann durch Co-Aktivatorrekrutierungsassays die Aktivität einer Substanz (alleine oder in Kompetition gegen eine Referenzsubstanz) bei verschiedenen Konzentrationen vermessen und so ihr EC_{50}/IC_{50} bestimmt werden.[80]

Zusätzlich zu diesen funktionellen FXR-Assays existieren verschiedene Systeme, um die Bindung einer Substanz an FXR zu quantifizieren. Diese beruhen auf bekannten Technologien wie scintillation proximity (SPA) oder Fluoreszenz-Polarisation und erfordern wie Co-Aktivatorrekrutierungsassays rekombinant hergestelltes FXR-LBD Protein. Sie liefern eine tatsächliche oder kompetitive Bindungsaffinität einer Testsubstanz an FXR, aber keine zusätzlichen Informationen zur funktionellen Aktivität einer Substanz.[80]

Die Funktion sowie die Vor- und Nachteile der verschiedenen in vitro Testsysteme für FXR-Liganden sind in der Übersichtsarbeit (Merk D, Steinhilber D, Schubert-Zsilavecz M. *Expert Opin Drug Discov*, **2014**) zusammengefasst und diskutiert.

Um neue, in einem Reportergen- oder Co-Aktivator-Rekrutierungsassay identifizierte FXR-Liganden genauer in vitro zu charakterisieren und mehr Informationen über einen möglichen in vivo Effekt zu erhalten, sind Daten zu ihren Effekten auf FXR-Targetgene wünschenswert. Die Rolle der einzelnen Targetgene für metabolische oder anti-inflammatorische in vivo Effekte wurde oben näher diskutiert.

Die Kenntnis der Modulation dieser Targetgene durch einen FXR-Liganden erlaubt eine begrenzte Vorhersage seiner in vivo Wirkungen.

Die Wirkung von FXR-Liganden auf FXR-Targetgene lässt sich mit Hilfe der quantitativen real time Polymerase-Kettenreaktion (qRT-PCR) vermessen. Dazu werden Zelllinien, die FXR exprimieren, also vorzugsweise Leber- oder Darmepithelzellen wie HepG2, Caco-2 oder HT29, verwendet. Die Zellen werden mit der Testsubstanz inkubiert und anschließend ihre RNA extrahiert. Nach Umschreiben der RNA in cDNA kann die ursprüngliche Menge an mRNA eines bestimmten Gens durch qRT-PCR quantifiziert werden. Diese Menge muss noch mit der mRNA-Menge eines konstitutiv hoch exprimierten, sogenannten *housekeeping* Gens wie der Glycerinaldehyd-3-phosphat-Dehydrogenase (GAPDH) oder β-Aktin normiert werden, um dann die mRNA-Menge des untersuchten Gens nach Behandlung mit einer Test- oder Referenzsubstanz bzw. ohne Behandlung vergleichen zu können und eine relative Induktion/Repression des Targetgens zu erhalten.[80]

1.4 Klinischer Stellenwert und Limitationen bekannter FXR-Liganden

Obwohl intensive Forschung eine Vielzahl physiologischer Funktionen von FXR charakterisiert hat und sich daraus einige vielversprechende therapeutische Einsatzgebiete für FXR-Liganden - insbesondere für FXR-Agonisten - ableiten lassen, hat bislang nur das synthetische Gallensäurederivat 6-ECDCA (**5**) eine fortgeschrittene Phase der klinischen Entwicklung erreicht. Daneben ist die Indikation NAFLD und PBC, für die 6-ECDCA (**5**) untersucht wird, im Vergleich zur Zahl der theoretisch über eine FXR-Aktivierung behandelbaren Erkrankungen eher schmal. Die geringe Zahl von FXR-Agonisten, die die klinische Entwicklung erreicht haben, mag zum Teil mit der hohen Lipophilie der FXR-Ligandbindetasche zusammenhängen, die dazu führt, dass die entwickelten potenten Liganden ebenfalls sehr lipophil sind und daher eine schlechte Löslichkeit und eine geringe Bioverfügbarkeit aufweisen. Daneben stellt sich aber auch die Frage, ob eine volle Aktivierung des nukleären Rezeptors FXR die richtige therapeutische Strategie bei der Behandlung metabolischer Erkrankungen darstellt. Die Therapie metabolischer Fehlregulationen wie Dyslipidämie oder Diabetes mellitus Typ II erfordert eine dauerhafte Einnahme eines Wirkstoffs über einen langen Zeitraum. Die Erfahrungen mit den antidiabetisch und an PPARγ vollagonistisch wirkenden Glitazonen und den z.B. postmenopausal therapeutisch eingesetzten, an Estrogenrezeptoren (ER) agonistischen Östrogenen zeigen, dass die Überaktivierung eines nukleären Rezeptors auch schwerwiegende unerwünschte Wirkungen wie kardiovaskuläre Komplikationen oder ein erhöhtes Tumorrisiko nach sich ziehen kann.[104–106]

Für die klinische Entwicklung des experimentellen FXR-Vollagonisten 6-ECDCA (**5**) mit den Indikationen PBC und NAFLD/NASH spielen diese Überlegungen dagegen eine untergeordnete Rolle, da die zu behandelnden Erkrankungen einerseits so gravierend sind, dass potentielle Nebenwir-

kungen vernachlässigbar scheinen und andererseits die Einnahme des Wirkstoffs auf einen kürzeren Zeitraum ausgelegt ist, als es bei metabolischen Erkrankungen notwendig wäre.

Im Falle von FXR wirkt der physiologische Ligand CDCA (**1**) zwar als Vollagonist, aufgrund seiner relativ geringen Affinität (EC_{50} ~ 8 µM) kommt es aber nur bei relativ hohen, annähernd toxischen Konzentrationen zu dieser vollen Aktivierung des Rezeptors, dessen physiologische Hauptfunktion darin besteht, als Sensor für eine Akkumulation potentiell toxischer Gallensäuren zu fungieren. Untersuchungen haben jedoch gezeigt, dass FXR und andere nukleäre Rezeptoren für einen in vivo Effekt nicht mit maximaler Amplitude aktiviert werden müssen. [92,107]

Um die Gefahr von Nebenwirkungen durch FXR-Überaktivierung zu minimieren, bestehen grundsätzlich zwei Möglichkeiten. Die Entwicklung gen- oder gewebespezifischer FXR-Modulatoren ähnlich den SERMs könnte eine gezielte und für eine bestimmte Wirkung optimierte Aktivierung von FXR ermöglichen und dabei FXR-Targetgene aussparen, die zu Nebenwirkungen führen könnten. Für diesen Ansatz fehlt jedoch noch weiteres Wissen um das Zusammenspiel des komplexen Netzwerks nukleärer Rezeptoren und Co-Aktivatoren, in das FXR eingebunden ist. Eine Alternative zu selektiven FXR-Rezeptormodulatoren bildet die Entwicklung partieller FXR Agonisten, die den Rezeptor selektiv und mit hoher Affinität aktivieren, aber nur eine moderate Amplitude in der Aktivierung hervorrufen. Auf diese Weise könnten die diversen positiven Effekte einer FXR-Aktivierung genutzt werden, ohne dass dabei durch eine Überaktivierung gravierende Nebenwirkungen ausgelöst werden.

1.5 Ursprung dieser Arbeit und Zielsetzung

Die vorliegende Arbeit widmet sich der Entwicklung solcher FXR-Partialagonisten ausgehend von den Ergebnissen eines Liganden- und Struktur-basierten virtuellen Screenings[108] der Asinex-Substanzdatenbank an FXR zur Identifikation neuer Leitstrukturen. Das Screening beruhte auf der Entwicklung zweier Liganden-basierter Konsensuspharmakophormodelle aus den verfügbaren FXR-Co-Kristallstrukturen und einem Screening der Substanzdatenbank an diesen Modellen. Die Zahl der in dieser ersten Runde identifizierten Treffer wurde anschließend durch Docking und mehrere Verfeinerungen eingeschränkt. Nach manueller Auswahl der besten Treffer wurden 27 Hits des Screenings in einem fl-FXR-Reportergenassay charakterisiert, wobei vier tatsächlich schwach aktive Verbindungen identifiziert wurden. Eine dieser Verbindungen, das Acylanthranilamid JA10 (**32**), das in vitro eine relative FXR-Aktivierung von 14,5 ± 1,3% bei 30 µM zeigte, wurde als Leitstruktur für die vorliegende Arbeit ausgewählt.

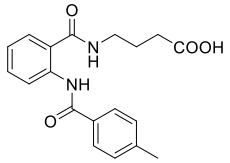

32

***Abbildung 16**: Leitstruktur JA10 (**32**)*

Basierend auf dem Acylanthranilamid **32** sollte durch Untersuchungen der Struktur-Aktivitätsbeziehungen (SAR) dieser Substanzklasse und daraus abgeleitete gezielte strukturelle Optimierungen ein potenter selektiver FXR-Partialagonist entwickelt und dessen in vitro Aktivität charakterisiert werden. Um der oben dargelegten Probleme von FXR-Vollagonisten zu begegnen, wurde eine moderate FXR-Aktivierung verbunden mit einem möglichst niedrigen EC_{50}-Wert angestrebt.

2. Ergebnisse und Diskussion

2.1 Synthese der Acylanthranilamidderivate

Zur Synthese der als Zielmoleküle gewünschten Acylanthranilamidderivate **33-106** und **127**-**138** wurden mehrere Synthesestrategien entwickelt und die zugehörigen Reaktionen optimiert. Für die Wahl einer der Syntheserouten für ein Zielmolekül war zum einen die Verfügbarkeit der benötigten Edukte, zum anderen aber vor allem die Reaktivität der Edukte entscheidend. Die Darstellung der Acylanthranilamidderivate erfolgte in zwei Synthesestufen. Im ersten Schritt wurde die Kopfgruppe durch eine nucleophile Substitution an den zentralen Anthranilsäuregrundkörper gebunden und anschließend der lipophile Acylsubstituent durch Reaktion des Anilins aus der ersten Stufe mit einem Acylchlorid eingeführt.

Zur Synthese der Zwischenstufen durch ortho-Aminobenzoylierung der Kopfgruppe wurden zwei unterschiedliche Synthesevarianten etabliert und in verschiedenen Modifikationen durchgeführt. Zur Einführung aliphatischer Kopfgruppen (**107**), deren Aminogruppe eine relativ hohe Nucleophilie aufwies, wurde als elektrophiler Reaktionspartner das Isatinsäureanhydrid (**108**) eingesetzt wie bereits von Venuti[109] veröffentlicht. Die Literatur beschreibt diese Reaktion mit aliphatischen Aminen in Gegenwart katalytischer Mengen 4-*N,N*-Dimethylaminopyridin (**109**, 4-DMAP), das das Elektrophil durch Bildung eines Aktivesters aktiviert. Die Literaturbedingungen sind allerdings auf wenig substituierte Amine ohne weitere funktionelle Gruppen beschränkt und lieferten mit den zur Darstellung der gewünschten Testverbindungen benötigten Edukten keine zufriedenstellenden Ergebnisse. Die Reaktion wurde daher in Anlehnung an die literaturbeschriebenen Synthesen auf die Verwendung von Aminen, die zusätzlich eine Carbonsäurefunktion tragen, optimiert. Dabei stellte sich heraus, dass insbesondere eine Temperatur von mindestens 80°C zur gewünschten Reaktion notwendig ist und der Einsatz eines Lösungsmittelgemisches von Pyridin und DMF mit Triethylamin als Hilfsbase den Bedingungen nach Venuti[109] überlegen ist. Diese optimierten Bedingungen ermöglichten eine ökonomische Darstellung der benötigten Zwischenstufen **110** durch die direkte Verwendung der freien Aminosäuren **107** ohne die Notwendigkeit einer Schutzgruppe wie beispielsweise eines Esters. Die Optimierung der Reaktion ist veröffentlicht (supporting information von Merk D et al. *Bioorg. Med. Chem.*, **2014**).

Zur ortho-Aminobenzoylierung von aromatischen Kopfgruppen mit durch Substituenteneinflüsse stark herabgesetzter N-Nucleophilie lieferte die obige Reaktion keine zufriedenstellenden Resultate, weshalb eine alternative Synthese etabliert wurde. Als Ausgangspunkt diente hierfür die in der Literatur[110] beschriebene Reaktion von Isatinsäureanhydrid (**108a**) mit substituierten Anilinen in absolutem Ethanol unter Rückfluss. Die Literaturbedingungen lieferten bereits annehmbare Ausbeuten des gewünschten Produkts und konnten durch den Einsatz eines doppelten Überschusses

des Nucleophils bei reduziertem Lösungsmittelvolumen und erhöhter Temperatur optimiert werden. Die Zugabe von 4-DMAP (**109**) als Katalysator oder der Hilfsbase NEt_3 brachten dagegen keine Verbesserung, sondern erhöhten die gebildete Menge des Nebenproduktes Anthranilsäureethylester (**111**). Um die Bildung des Nebenprodukts **111**, das durch Reaktion von Isatinsäureanhydrid (**108a**) mit dem Lösungsmittel Ethanol gebildet wird, zu reduzieren, wurden außerdem alternative Lösungsmittel untersucht. Bei der Verwendung von Essigsäure als ebenfalls protischem, aber weniger nucleophilem Lösungsmittel verschlechterte sich die Ausbeute. Mit dem sterisch etwas anspruchsvolleren Isopropylalkohol als Solvens wurde die Produktausbeute zwar leicht erhöht, die Aufarbeitung durch Fällung aber erschwert, weshalb die Reaktion zur Darstellung der Zwischenstufen **110** weiterhin in Ethanol durchgeführt wurde. Detaillierte experimentelle Bedingungen für diese Reaktion sind publiziert (Merk D et al. *J. Med. Chem.*, **2014**).

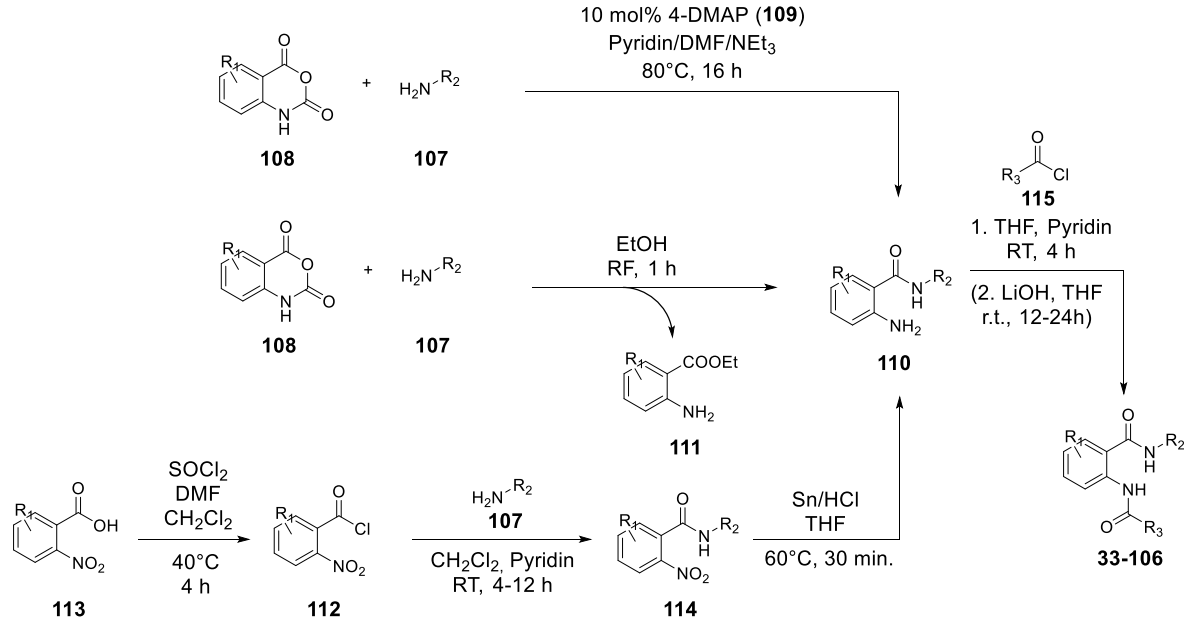

Abbildung 17: *Übersicht über die Synthesestrategie zur Darstellung der Acylanthranilamide **33-106***

Für einige wenige Kopfgruppen wie 3-Aminoacetophenon (**107a**) und 3-Aminobenzonitril (**107b**) mit stark erniedrigter N-Nucleophilie führte jedoch auch die Reaktion in Ethanol nicht zu akzeptablen Produktausbeuten. Daneben wurden für die SAR-Untersuchungen Anthranilamidderivate mit Substituenten am zentralen aromatischen Ring der Anthranilsäure benötigt, für die keine entsprechenden Isatinsäureanhydridderivate zur Verfügung standen. Somit war eine weitere Alternative zur Einführung der Kopfgruppen notwendig. Als dritte Syntheseroute zur ortho-Aminobenzoylierung wurde daher die Reaktion der Kopfgruppenaniline mit ortho-Nitrobenzoyl-chloridderivaten (**112**) mit anschließender Reduktion der Nitrogruppe gewählt. Hierfür wurden die Nitrobenzoesäurederivate (**113**) zunächst durch Chlorierung (**112**) aktiviert und anschließend mit den entsprechenden Anilinderivaten (**107**) zu **114** umgesetzt. Nach Reduktion der Nitrogruppe in **114** waren auch mit dieser Synthesestrategie die Zwischenstufen **110** zur Darstellung der

Acylanthranilamide zugänglich. Auch für diese Reaktion sind detaillierte experimentelle Bedingungen veröffentlicht (Merk D et al. *J. Med. Chem.*, **2014**).

Die Zwischenstufen (**110**) aus obigen Reaktionen wurden anschließend mit zahlreichen Acylchloriden (**115**) zur Reaktion gebracht und so die lipophilen Acylsubstituenten eingeführt. Die beste Produktzusammensetzung lieferte dabei unter zahlreichen untersuchten Bedingungen die Umsetzung der Zwischenstufen (**110**) mit den Acylchloriden (**115**) in THF in Gegenwart von Pyridin als Hilfsbase bei Raumtemperatur. Die experimentellen Bedingungen zur Durchführung der Reaktion sind publiziert (Merk D et al. *Bioorg. Med. Chem.*, **2014** und Merk D et al. *J. Med. Chem.*, **2014**).

Um gezielt den Einfluss bestimmter Molekülteile innerhalb der SAR zu untersuchen, waren außerdem Acylanthranilamidderivate notwendig, die nicht durch die beschriebene Grundsynthesestrategie zugänglich waren und daher durch andere Reaktionen dargestellt wurden. Die Synthese des sekundären Amins **51** erfolgte durch reduktive Aminierung aus dem bereits dargestellten ortho-Aminobenzoylderivat **110a** und 2-Napthylcarbaldehyd **116**. Dabei wurde auf die Verwendung einer Schutzgruppe für die freie Carbonsäure in **110a** verzichtet und zunächst in Eisessig aus **110a** und **116** innerhalb von zwei Stunden bei Raumtemperatur ein Imin gebildet. Nach Reduzieren der Menge an Eisessig im Vakuum und Verdünnen mit Dichlormethan wurde anschließend auf 0°C abgekühlt und als Reduktionsmittel Natriumborhydrid zugegeben. Durch die noch im Reaktionsansatz vorhandene Essigsäure bildete sich dabei in situ das weniger reaktive Natriumtriacetoxyborhydrid, welches selektiv das Imin zum sekundären Amin **51** reduzierte.

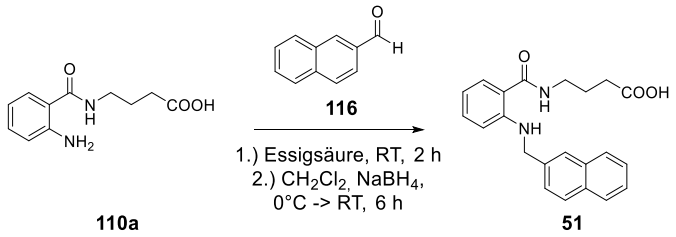

***Abbildung 18**: Darstellung des sekundären Amins **51** durch reduktive Aminierung*

Für die Darstellung des sekundären Amins **52** konnte nicht auf eine vorhandene Zwischenstufe zurückgegriffen werden. Als alternatives Edukt wurde ortho-Aminobenzylalkohol (**117**) mit Hilfe von Pyridiniumchlorochromat (PCC) in Dichlormethan selektiv zum ortho-Aminobenzaldehyd (**118**) oxidiert, der für die weitere Umsetzung nur noch die aromatische Aminofunktion als nucleophiles Zentrum enthielt und daneben über seine Aldehydgruppe in einer reduktiven Aminierung zum sekundären Amin umgesetzt werden konnte. Da jedoch durch die Einführung eines sekundären Amins in der reduktiven Aminierung ein weiteres nucleophiles Zentrum entsteht, das aufgrund seiner beiden aliphatischen Substituenten eine höhere Nucleophilie aufgewiesen hätte als die aromatische Aminofunktion, die mit dem Acylsubstituenten substituiert werden sollte, musste die reduktive

Aminierung im letzten Schritt durchgeführt werden. Also wurde zunächst durch Reaktion von **118** mit 2-Naphthoylchlorid (**115a**) zu **119** der lipophile Acylsubstituent addiert und anschließend die Kopfgruppe unter Bildung der gewünschten sekundären Aminofunktion in **52** durch reduktive Aminierung eingeführt, wobei zunächst wiederum das Imin aus **119** und **107c** gebildet und anschließend reduziert wurde.

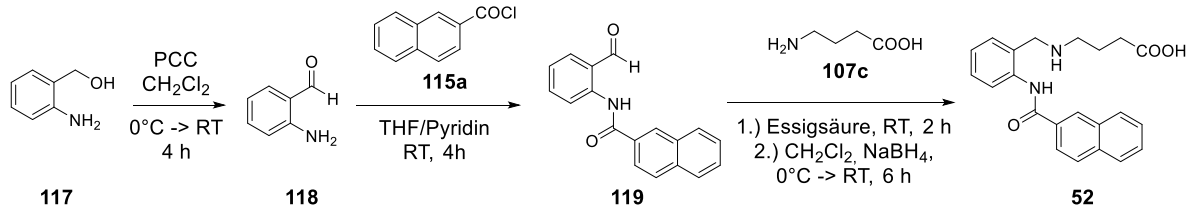

Abbildung 19: *Darstellung des sekundären Amins **52** durch Oxidation von **117** zu **118**, Acylierung von **118** mit **115a** und anschließende reduktive Aminierung mit **107c***

Die Darstellung von **66** mit invertierten Säureamidgruppen erfolgte analog zur Grundsynthesestrategie, wobei zunächst durch Reaktion von 4-*tert*-Butylanilin (**120**) mit Isatinsäureanhydrid (**108a**) in einem Gemisch aus Pyridin, DMF und NEt_3 zu **121** der lipophile Acylsubstituent mit umgekehrter Amidbindung eingeführt wurde. **121** reagierte anschließend mit dem Acylchlorid Methyl-3-chlorocarbonylbenzoat (**122**) zu Ester **123**, der nach alkalischer Hydrolyse mit LiOH in einem Gemisch aus THF und Wasser das gewünschte Produkt **66** lieferte, welches das Analog zu **64** mit invertierten Amidbindungen darstellte.

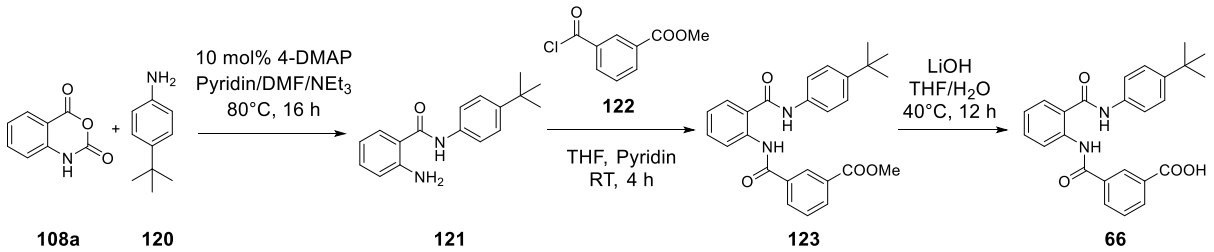

Abbildung 20: *Darstellung des invertierten Derivats **66** analog zur Grundsynthesestrategie durch Wahl der entsprechenden geeigneten Edukte **108a**, **120** und **122***

Bei der Synthese der bioisosteren Derivate **79** und **80** wurde auf bereits vorhandene Verbindungen zurückgegriffen und deren Kopfgruppen synthetisch modifiziert. Tetrazol **80** wurde durch eine dipolare [3+2]-Cycloaddition von Nitril **76** mit Natriumazid dargestellt. Die Durchführung der Reaktion erfolgte unter Cu(I)-Katalyse in einem Gemisch aus DMF und Methanol als Protonenquelle, wie in der Literatur[111] beschrieben. Im Katalysezyklus entsteht hierbei vermutlich zunächst Kupfer(I)azid, das durch eine koordinative Bindung zwischen Kupfer(I)kation und dem freien Elektronenpaar des Nitrilstickstoffatoms in räumliche Nähe zum Nitril gebracht wird. Die räumliche Nähe und die durch das Kupfer(I)kation bewirkte Polarisierung begünstigen dann die Cycloaddition von Nitril und Azid.

Zur Darstellung des Benzamids **79** konnte nicht die Grundsynthesestrategie beschritten werden, da das hierfür notwendige 3-Aminobenzamid zwei potentiell nucleophile Zentren enthält, die in jeder

Teilreaktion die Gefahr der Bildung von Produktgemischen bedingt hätten. Auch der Einsatz von Schutzgruppen, um dieses Problem zu umgehen, gestaltete sich schwierig. Als alternatives Edukt zur Synthese des Benzamids **79** bot sich die analoge Carbonsäure **64** an, die durch Aktivierung und anschließende Reaktion mit Ammoniak in **79** überführt werden konnte. Geeignete Bedingungen lieferten Khalafi-Nezhad et al.[112], die die Aktivierung von Carbonsäuren mit Tosylchlorid und Aminierung mit Ammoniumchlorid in einer einzigen Stufe und unter lösungsmittelfreien Bedingungen beschrieben haben.

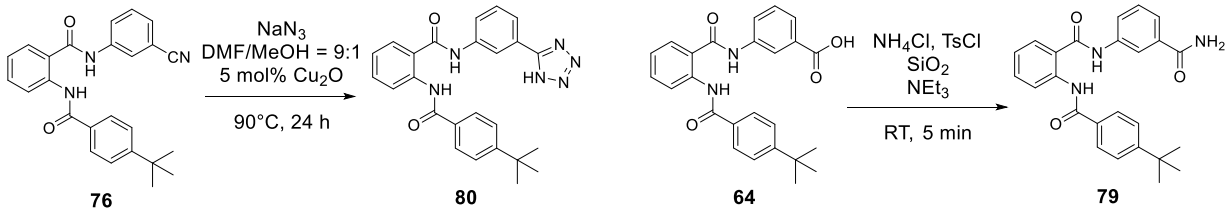

Abbildung 21**: Darstellung der bioisosteren Verbindungen **79** und **80: Tetrazol **80** wurde durch Cu(I)-katalysierte [3+2]-Cycloaddition von Nitril **76** und Natriumazid synthetisiert. Die Darstellung des primären Benzamids **79** erfolgte aus **64** mit Hilfe von Tosylchlorid, kieselgelgestütztem Ammoniumchlorid und Triethylamin.

Um die Relevanz der einzelnen Molekülteile der Acylanthranilamide für die FXR-Aktivierung zu untersuchen, sollten auch Fragmente der Substanzklasse bzw. der optimierten Substanz **58** an FXR charakterisiert werden (vgl. Abbildung 28). Das Fragment **110b** ohne lipophilen Acylsubstituenten war bereits in der Grundsynthesestrategie dargestellt worden, Anthranilsäure (**124a**) war kommerziell erhältlich. Das noch fehlende Fragment **67** wurde in zwei Stufen durch Reaktion von Anthranilsäure mit 4-*tert*-Butylbenzoylchlorid (**115b**) und anschließende Überführung der Carbonsäure in ein Säureamid, wie für **79** beschrieben, dargestellt. Eine direkte Umsetzung von Anthranilamid (**124b**) mit **115b** war aufgrund der zu hohen Nucleophilie der Säureamidgruppe ungünstig.

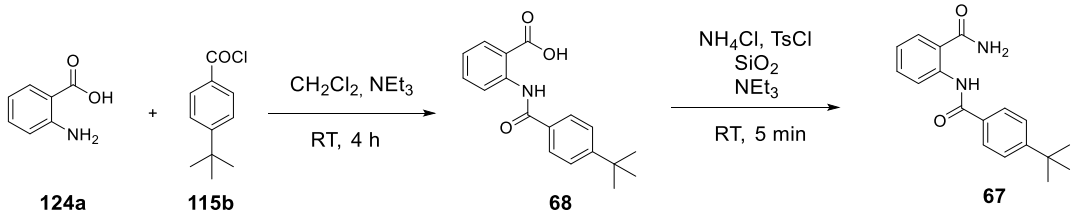

Abbildung 22: *Synthese der Fragmente **67** und **68***

Die experimentellen Bedingungen zur Darstellung aller beschriebenen Zwischen- und Endprodukte sowie deren analytische Daten sind in den Publikationen (Merk D et al. *Bioorg. Med. Chem.*, **2014** und Merk D et al. *J. Med. Chem.*, **2014**) sowie den zugehörigen supporting informations enthalten.

2.2 Biologische Aktivität der Acylanthranilamide und Struktur-Wirkungsbeziehungen

Den Ausgangspunkt der hier vorliegenden Entwicklung eines potenten FXR Partialagonisten stellte ein virtuelles Screening der Asinex-Substanzbibliothek an einem in silico Modell der FXR Ligandbindedomäne dar.[108] Ausgehend vom Screening-Hit JA10 (**32**, 14,5±1,3% FXR-Aktivierung bei 30 µM) wurden die Struktur-Aktivitätsbeziehungen der Verbindungsklasse der Acylanthranilamide als FXR-Liganden mit dem Ziel untersucht, einen potenten und selektiven FXR-Partialagonisten zu entwickeln.

2.2.1 In vitro-Charakterisierung der Testsubstanzen im FXR-Reportergenassay

Alle Testverbindungen der hier vorliegenden Arbeit wurden – wie auch die Ausgangsverbindung **32** – in einem *full-length* FXR-Reportergenassay biologisch charakterisiert. Dieser Reportergenassay basierte auf der transienten Transfektion von Hela-Zellen mit vier Plasmiden, die für die vollständigen (*full-length*) Rezeptoren FXR und RXR sowie für eine Firefly-Luciferase als Reportergen und eine Renilla-Luciferase als Kontrollgen codierten. Durch Verwendung eines konstitutiv aktiven CMV-Promotors wurden nach der Transfektion die Rezeptoren FXR und RXR von den Zellen exprimiert und konnten als Heterodimer an das FXR-spezifische Response-Element (BSEP-Promotor) binden, welches die Expression des Reportergens kontrollierte. Wurde das FXR-RXR-Heterodimer durch eine zugegebene Testsubstanz aktiviert, kam es zur Expression des Reportergens. Das Kontrollgen diente der Kontrolle von Transfektionseffizienz und potentieller Toxizität der getesteten Substanzen und stand daher wie die Rezeptoren FXR und RXR unter der Kontrolle eines konstitutiv aktiven Promotors (SV40). Die Aktivitäten von Reportergen und Kontrollgen wurden nach Lyse der Zellen mit Hilfe des DualGlo™ Kits als Lumineszenz gemessen und miteinander ins Verhältnis gesetzt. Die so ermittelten relative light units (RLU) für jeden Messpunkt (eine Konzentration einer Substanz) wurden anschließend auf den Wert unbehandelter Zellen normiert, was die fold-activation lieferte. Die fold-activation jedes Messpunkts wurde abschließend auf die fold-activation der Referenzsubstanz GW4064 (**4**) bei 3 µM als 100% bezogen. Auf diese Weise wurde die Aktivität aller Substanzen an FXR quantifiziert und durch Vermessung unterschiedlicher Konzentrationen der Testsubstanzen sigmoidale Aktivitätskurven erstellt, die die halbmaximale effektive Konzentration (EC_{50}) der Substanzen lieferten. Zur antagonistischen Charakterisierung erfolgte die Vermessung der Testsubstanzen in Gegenwart von 3 µM GW4064 (**4**). Jeder Messpunkt stellte den Mittelwert eines Triplikats dar und jedes Experiment wurde mindestens dreimal in unabhängigen Assays wiederholt. Testsubstanzen, die bis 30 µM keine signifikante FXR-Aktivierung zeigten, wurden als inaktiv angesehen. Der Reportergenassay wurde mit den FXR-Agonisten CDCA (**1**) und 6-ECDCA (**5**) validiert. Die Werte für beide Substanzen (CDCA (**1**): EC_{50} = 18±1 µM (88±3% max.); 6-ECDCA (**5**): EC_{50} = 0,161±0,025 µM (87±3% max.)) waren in gutem Einklang mit publizierten Daten[38,80].

2.2.2 Ergebnisse der ersten SAR-Studie (Merk et al. *Bioorg. Med. Chem*., **2014**)

Zur systematischen Untersuchung der Struktur-Aktivitäts-Beziehungen wurde die Ausgangssubstanz JA10 (**32**) in drei Molekülteile aufgetrennt und jeweils nur ein Teil variiert, um vergleichbare Ergebnisse zu erhalten. Abbildung 23 zeigt die Aufteilung von **32** und die Strategie der ersten SAR-Untersuchung. Die Ergebnisse dieser SAR-Studien sind mit allen zugehörigen in vitro Daten veröffentlicht (Merk D et al. *Bioorg. Med. Chem.*, **2014**).

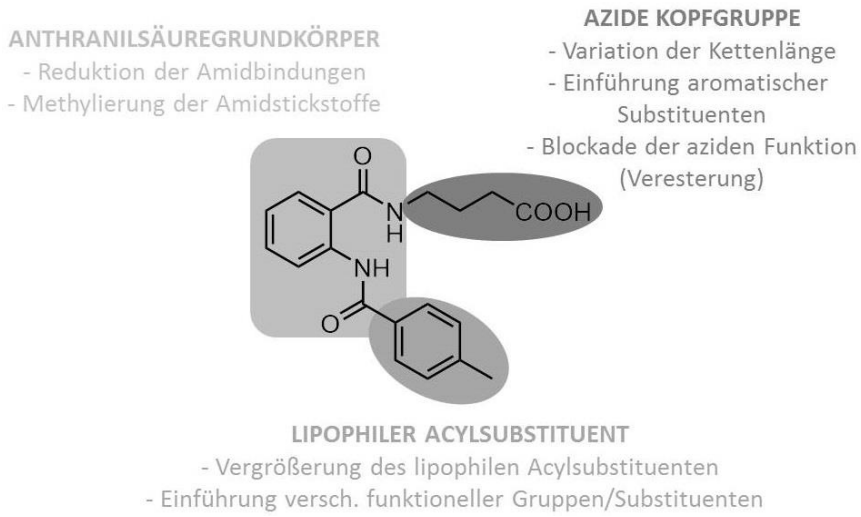

Abbildung 23: *Strategie der ersten Studie zu den Struktur-Aktivitätsbeziehungen* der Acylanthranilamide basierend auf der Ausgangssubstanz **32**

Um erste Hinweise auf einen möglichen Bindemodus von JA10 (**32**) und daraus resultierende Optimierungsmöglichkeiten zu erhalten, wurde **32** (und im Verlauf der SAR-Studien weitere Derivate) in silico an einem Modell von FXR untersucht. Als Grundlage für das hierzu notwendige virtuelle Modell der FXR-LBD fiel die Wahl auf die Co-Kristallstruktur des Benzimidazols **125** (PDB-ID: 3OLF)[92,93], da sie aufgrund ihres partialagonistischen Liganden am geeignetsten für die Entwicklung der Acylanthranilamide als FXR-Partialagonisten schien. (Abbildung 24)

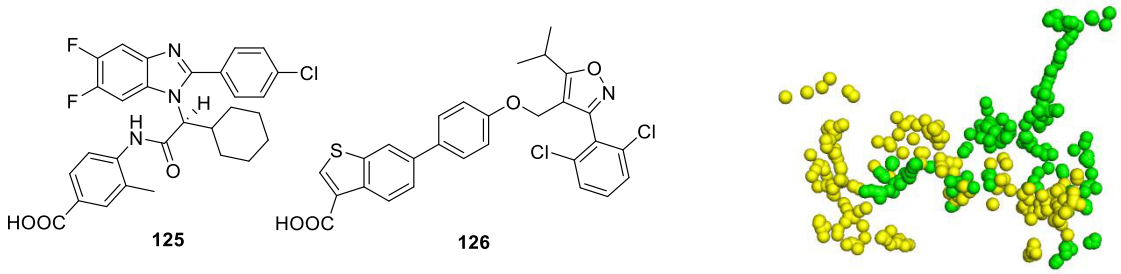

Abbildung 24: *Co-kristallisierte FXR-Liganden **125** (PDB-ID: 3OLF) und **126** (PDB-ID: 3RUT)*: In der partialagonistischen Konformation (**125**, grün) ist die FXR-Ligandbindetasche dreieckig, während sie in der vollagonistischen Konformation (**126**, gelb) eine längliche, schmale Form annimmt.

Kontrolluntersuchungen an mehreren Modellen der FXR-LBD zeigten, dass die Docking-Ergebnisse innerhalb aller partialagonistenbasierten Modelle (PDB-IDs: 3OLF, 3OKH, 3OKI, 3OMK, 3OMM, 3OOF, 3OOK)[92,93] um **125** identische Ergebnisse lieferten, während das docking der Acylanthranilamide in agonistenbasierte Modelle (z.B. PDB-ID: 3RUT; **126**)[113] zu keinen sinnvollen Ergebnissen kam. Beim

Vergleich der vollagonistischen und der partialagonistischen Strukturen fiel auf, dass sich die beiden Gruppen sowohl in der Proteinkonformation, als auch in der Form ihrer Ligandbindetasche unterscheiden. Zwischen den beiden Proteinkonformationen sind die Helices 3 und 7 stark verschoben, was dazu führt, dass die Ligandbindetasche der vollagonistischen Strukturen lang und schmal ist, während sie bei den partialagonistischen Strukturen eher eine dreieckige Form annimmt.

Die in silico Dockingstudien der Leitstruktur **32** (Abbildung 25A) deuteten an, dass im Bereich des Acylsubstituenten zusätzlicher Raum in der FXR-Bindetasche für größere Substituenten vorhanden sein könnte. Anstelle der relativ kleinen 4-Methylbenzoylgruppe in **32** wurden daher in **33-48** zunächst 16 alternative, vornehmlich lipophile Acylgruppen eingeführt, während der Anthranilsäure-grundkörper sowie die 4-Aminobuttersäure als Kopfgruppe nicht verändert wurden (Tabelle 1).

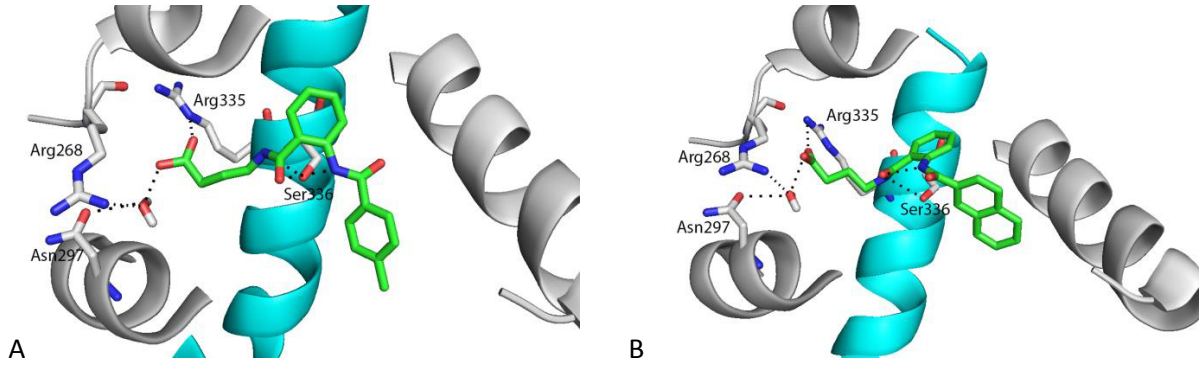

Abbildung 25: *Dockingposen der Leitstruktur **32** (A) und der ersten optimierten Verbindung **44** (B) in die FXR-LBD:* Die Carbonsäurekopfgruppe beider Verbindungen geht über einen Wassercluster eine neutralisierende Wechselwirkung mit Arg_{268} und Arg_{335} ein. Der vergrößerte Acylsubstituent von **44** wird besser in einer lipophilen Tasche gebunden. Die beiden Amidgruppen interagieren über eine intramolekulare Wasserstoffbrückenbindung. Modell basierend auf PDB-ID: 3OLF.

Der Großteil (**33**-**41**, Tabelle 1) der Acylanthranilamide mit vergrößertem Acylsubstituenten stellte sich als inaktiv an FXR heraus, lediglich das 4-Ethylbenzoylderivat **42**, das 4-*tert*-Butylbenzoylderivat **43**, das 2-Naphthoylderivat **44** und das Cinnamoylderivat **47** zeigten agonistische Aktivität an FXR. Die SAR des Acylsubstituenten zeigten sich als sehr schmal, denn gegenüber dem 2-Naphthoylderivat **44** waren sowohl das 1-Naphthoylderivat **45** als auch das um eine Methylengruppe verlängerte 2-Naphthylacetylderivat **46** inaktiv. Auch das Dihydrocinnamoylderivat **48** war gegenüber Cinnamoylderivat **47** nicht agonistisch an FXR.

Bezogen auf den EC_{50}-Wert sowie auf die maximale FXR-Aktivierung stellten sich also ein 2-Naphthoyl- (**44**) und ein 4-*tert*-Butylbenzoylsubstituent (**43**) als günstigste lipophile Acylsubstituenten heraus. Für die anschließenden Untersuchungen zur SAR der aziden Kopfgruppe und des zentralen Anthranilsäuresystems wurde die 2-Naphthoylgruppe aus **44** als Acylsubstituent gewählt, da sie bei nur geringfügig höherem EC_{50}-Wert die höhere Maximalaktivierung gezeigt hatte. Mit dieser höheren maximalen Aktivierung sollten falsch negative Ergebnisse aufgrund zu geringer und daher womöglich nicht signifikanter Aktivierung der Folgederivate ausgeschlossen werden.

Tabelle 1: *In vitro FXR-Aktivität der Derivate **33**-**48** mit variiertem Acylsubstituenten* (MW±SEM; n = 3-6; i.a. - inaktiv)

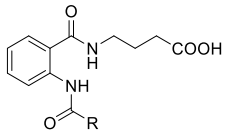

#	R	EC_{50} [µM] (max. rel. Aktivierung [%])	#	R	EC_{50} [µM] (max. rel. Aktivierung [%])
32	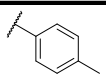	14,5±1,3% @ 30 µM	**41**	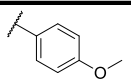	i.a.
33		i.a.	**42**	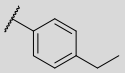	5,8±1,0 (28±2)
34		i.a.	**43**	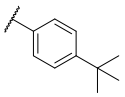	2,5±0,4 (19±1)
35	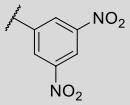	i.a.	**44**	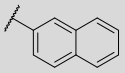	8,6±1,3 (37±2)
36	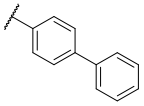	i.a.	**45**	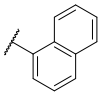	i.a.
37	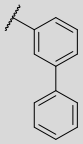	i.a.	**46**	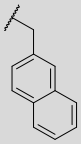	i.a.
38	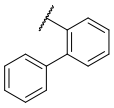	i.a.	**47**	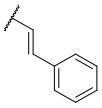	0,72±0,01 (12,4±0,1)
39	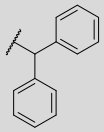	i.a.	**48**	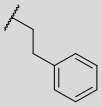	i.a.
40	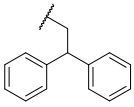	i.a.			

Um die SAR des zentralen Molekülteils, also des Anthranilsäuregrundkörpers, und insbesondere der beiden Säureamidgruppen zu untersuchen, wurden beide Amide selektiv reduziert bzw. am Stickstoff methyliert. Auf diese Weise wurde in der zugrunde liegenden Verbindung **44** jeweils eine Wasserstoffbrückenakzeptor- bzw. -donorfunktion blockiert, um festzustellen, welche Atome der beiden Amidbindungen womöglich entscheidende polare Wechselwirkungen mit der FXR-LBD eingehen. Neben Reduktion und Methylierung der Säureamidgruppen ersetzte außerdem in **53** eine Sulfonamidgruppe die Amidbindung des Acylsubstituenten. Interessanterweise waren sowohl die beiden sekundären Amine **51** und **52** als auch die beiden methylierten Derivate **49** und **50** sowie das Sulfonamid **53** inaktiv an FXR (vgl. Tabelle 2). Diese Ergebnisse deuteten darauf hin, dass die beiden Säureamidgruppen entweder von jedem der Heteroatome polare Wechselwirkungen mit der FXR-LBD eingehen oder dass die Geometrie der Säureamidbindungen für eine optimale Bindung in der

FXR-Ligandbindetasche essentiell ist. In Dockingstudien an Derivat **44** (vgl. Abbildung 25B) wurde beobachtet, dass womöglich zwischen dem Stickstoff der Amidfunktion der Kopfgruppe und dem Sauerstoff der zweiten Amidbindung eine intramolekulare Wasserstoffbrücke gebildet wird, die den FXR-Liganden in einer günstigen Geometrie für eine optimale Bindung hält. Durch Reduktion der Amidfunktion des Acylsubstituenten oder durch Methylierung der anderen Amidbindung am Stickstoff ist diese intramolekulare Wechselwirkung jedoch nicht mehr möglich.

Tabelle 2: *In vitro FXR-Aktivität der methylierten Derivate **49** und **50**, der sekundären Amine **51** und **52** sowie des Sulfonamids **53** im Vergleich zu **44*** (MW±SEM; n = 3-6; i.a. - inaktiv)

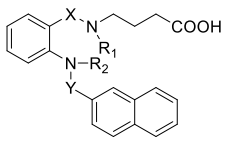

#	R_1	R_2	X	Y	EC_{50} [µM] (max. rel. Aktivierung [%])
44	H	H	C=O	C=O	8,6±1,3 (37±2)
49	Me	H	C=O	C=O	i.a.
50	H	Me	C=O	C=O	i.a.
51	H	H	C=O	CH_2	i.a.
52	H	H	CH_2	C=O	i.a.
53	H	H	C=O	SO_2	i.a.

Im Bereich der aziden Kopfgruppe hatten die Dockingstudien der Ausgangsverbindung JA10 (**32**, vgl. Abbildung 25A) angedeutet, dass eine Verlängerung der Alkylkette zu einer besseren Interaktion der Säurefunktion mit Arg_{335}/Arg_{268} führen und so die Aktivität der Substanzen steigern könnte. Tatsächlich änderte sich der EC_{50}-Wert bei Verlängerung der Kette um eine (**55**) oder zwei (**56**) Methylengruppen aber kaum, während die Maximalaktivierung der Derivate deutlich abnahm. Interessanterweise führte die Veresterung der Carbonsäure in **54** dagegen kaum zu einer Veränderung der Potenz, was dafür spricht, dass eine polare funktionelle Gruppe anstelle einer freien Carbonsäure für die FXR-Aktivierung ausreichend ist. Allerdings kann nicht ausgeschlossen werden, dass der Ester während der 24-stündigen Inkubation im Assay hydrolysiert wurde und die freie Säure **44** für die beobachtete FXR-Aktivierung verantwortlich war. (vgl. Tabelle 3)

Eine deutliche Verbesserung der Potenz wurde durch Einführung eines zusätzlichen aromatischen Ringes im Bereich der Kopfgruppe erzielt. Dies lässt zum einen Interaktionen des π-Elektronensystems mit der FXR-LBD vermuten, ist zum anderen aber auch durch günstige Effekte einer Rigidisierung zu erklären, da die Kopfgruppe durch den Ersatz der Alkylkette durch einen aromatischen Ring erheblich starrer wurde und Freiheitsgrade verlor. Sowohl eine meta- (**57**) als auch eine para-Aminobenzoesäure (**58**) als Kopfgruppe verbesserten den EC_{50}-Wert um etwa einen Faktor 8, wobei die Maximalaktivierung beim meta-Derivat **57** gleich hoch blieb, beim para-Derivat **58** hingegen abnahm. Das para-Aminobenzoesäurederivat **58** zeigte jedoch einen etwas niedrigeren EC_{50}-Wert, weshalb ausgehend von **58** 4-Aminophenylessigsäure (**59**) und 4-Aminomethylbenzoesäure (**60**) als wietere aromatische Kopfgruppen eingeführt wurden. Beide Derivate konnten die Potenz jedoch weder bezogen auf den EC_{50}-Wert, noch auf die relative Maximalaktivierung steigern. Auch der Versuch, die

beiden Sauerstoffe der Carbonsäure mit einem 1,3-Dioxolring (**61**, **62**) zu imitieren und die Kopfgruppe auf diese Weise weiter zu rigidisieren, führte nicht zu gesteigerter Potenz, sondern zu Inaktivität an FXR. (vgl. Tabelle 3)

Tabelle 3: *In vitro FXR-Aktivität der Derivate **54**-**62** mit variierter azider Kopfgruppe* (MW±SEM; n = 3-6; i.a. - inaktiv)

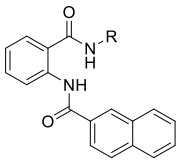

#	R	EC_{50} [µM] (max. rel. Aktivierung [%])
44	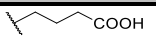	8,6±1,3 (37±2)
54	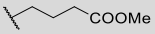	7,1±0,6 (19,0±0,6)
55	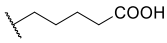	8,3±1,0 (11,4±0,4)
56		4,4±0,6 (10,4±0,4)
57	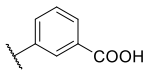	1,5±0,2 (37±1)
58	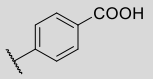	1,0±0,2 (23±1)
59	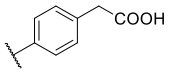	3,1±0,3 (9,8±0,4)
60	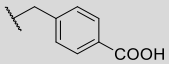	1,3±0,1 (10,0±0,1)
61	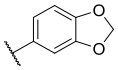	i.a.
62	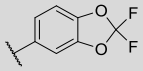	i.a.

Als bestes Acylanthranilamidderivat der ersten SAR-Studie stellte sich somit das 3-Aminobenzoesäurederivat **57** heraus und wurde daher hinsichtlich seiner physikochemischen und in vitro pharmakologischen Eigenschaften genauer untersucht. Mit guter metabolischer Stabilität und geringer Toxizität (vgl. Abbildung 26) stellte **57** eine potente Leitstruktur für weitere SAR-Untersuchungen dar.

A

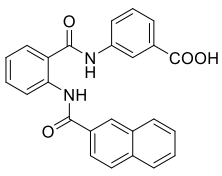

57

EC_{50}(hFXR) = 1.54±0.19 µM (37±1% max.)
Molekulargewicht= 410
H-Brückendonoren: 3 ; H-Brückenakzeptoren: 6
clogP = 4.96, Löslichkeit in H_2O: 0.3 mg/L
LE = 0.26; SILE = 2.08
nicht toxisch bis 60 µM

B

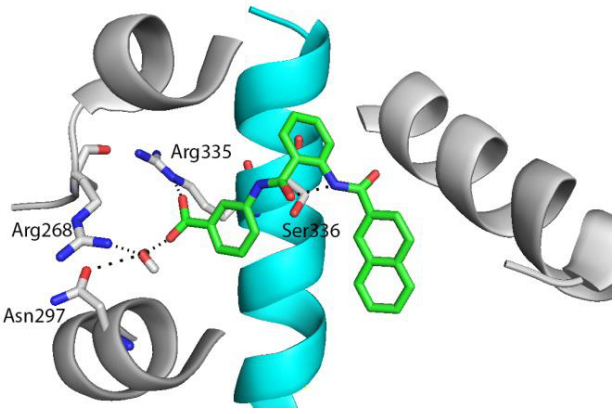

Abbildung 26: *Charakteristika (A) und Dockingpose (B) der optimierten Verbindung **44***

Die erste SAR-Studie (Merk D et al. *Bioorg. Med. Chem.*, **2014**) der Acylanthranilamide als FXR-Liganden führte von einem moderat aktiven Screeninghit (**32**) mit einer Restaktivität von 14,5±1,3% bei 30 µM zu potenten und vielversprechenden Leitstrukturen (**43**, **57**, **58**) mit EC_{50}-Werten zwischen 1,0 und 2,5 µM. Die Untersuchungen zeigten, dass die zentrale Anthranilamid-Teilstruktur für

potente FXR-Aktivität essentiell ist und dass sich die Potenz sowohl durch Einführung größerer lipophiler Acylsubstituenten als auch durch Erweiterung der aziden Kopfgruppe um einen zusätzlichen aromatischen Ring steigern ließ. Im Bereich des Acylsubstituenten stellten sich die SAR allerdings als relativ schmal heraus.

2.2.3 Ergebnisse der zweiten SAR-Studie (Merk et al. *J. Med. Chem.*, **2014**)

Die Erkenntnisse aus den ersten SAR-Untersuchungen wurden anschließend durch Rekombination der besten Teilstrukturen vereint (vgl. Abbildung 27). Dabei boten sich die Kopfgruppen der Benzoesäurederivate **57** und **58** sowie die Acylsubstituenten von 4-*tert*-Butylbenzoylderivat **43** und Cinnamoylderivat **47** an.

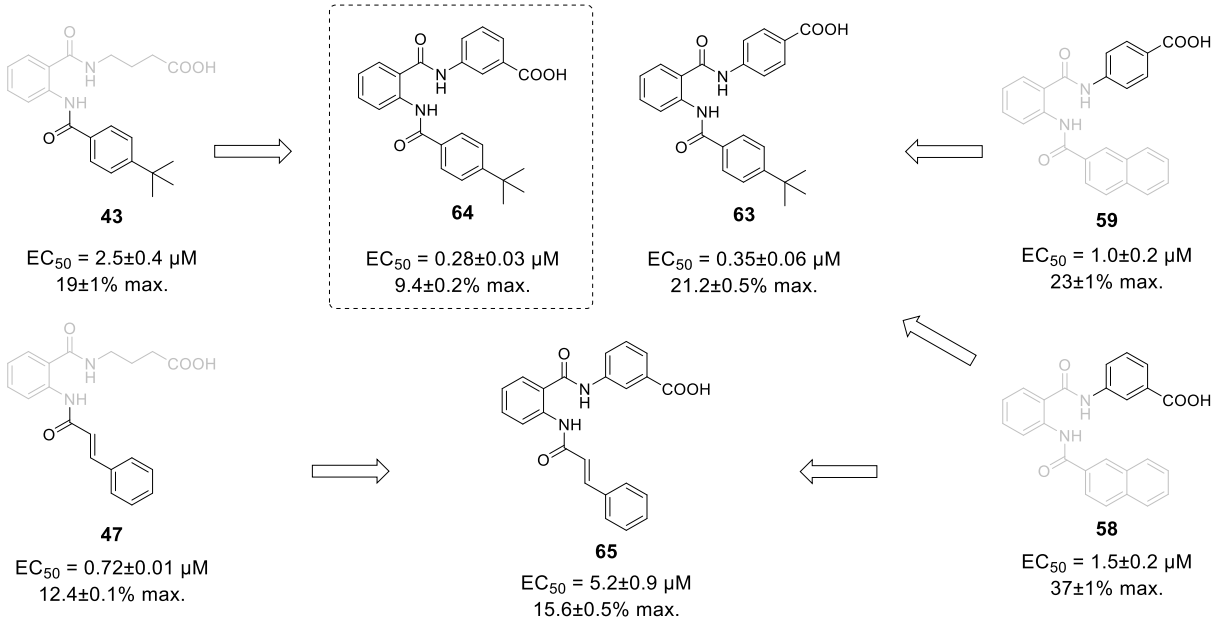

Abbildung 27: *Rekombination der besten Substituenten der ersten SAR-Studie zu den potenten FXR-Partialagonisten **63** und **64***: Die rekombinierte Verbindung **65** erreichte dagegen keine verbesserte Potenz. (MW±SEM)

Die Kombination der Benzoesäurekopfgruppen mit einem 4-*tert*-Butylbenzoylsubstituenten lieferte erwartungsgemäß die beiden deutlich potenteren Derivate **63** und **64**, während sich die hohe Aktivität des Cinnamoylderivates **47** aus der ersten SAR-Untersuchung nicht durch Kombination mit einer besseren Kopfgruppe in **65** optimieren ließ. Hinsichtlich des EC_{50}-Wertes erwies sich **64** als potenteste Rekombination der Ergebnisse aus der ersten SAR-Studie und wurde deshalb als Leitstruktur für die folgenden SAR-Untersuchungen gewählt.

Um Anhaltspunkte über die Rolle der einzelnen Molekülteile der Acylanthranilamide bei der FXR-Aktivierung zu erhalten, wurde die Ausgangsverbindung **64** anschließend in Fragmente (vgl. Abbildung 28) zerlegt. Dabei zeigte die Anthranilsäure (**124a**) keine FXR-Aktivierung und auch das Fragment **110b** ohne Acylsubstituenten erwies sich als inaktiv. Interessanterweise stellte sich jedoch das Fragment **67** aus zentralem Anthranilsäuregrundkörper und 4-*tert*-Butylbenzoylsubstituenten als potenter FXR-Partialagonist heraus. Diese Ergebnisse legten nahe, dass die 4-*tert*-Butylbenzoyl-

gruppe als Acylsubstituent einen entscheidenden Teil der Aktivität der Verbindungen ausmachte und dass daher vor allem der zentrale Anthranilsäuregrundkörper sowie die Kopfgruppe für höhere Potenz weiter optimiert werden mussten.

[redacted]

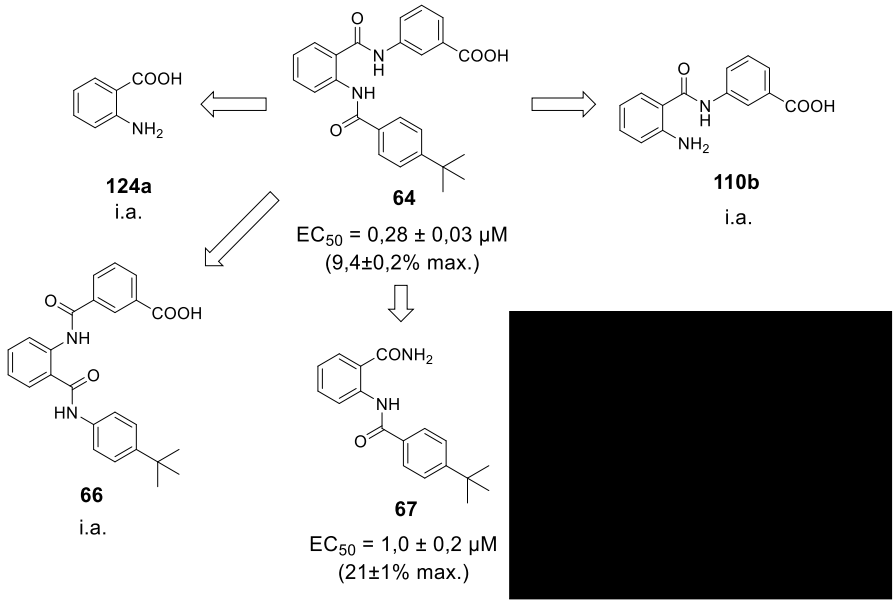

Abbildung 28: *Fragmentierung und Inversion der optimierten Leitstruktur **64*** mit in vitro Aktivität der resultierenden Derivate **66**, **67**, **68**, **69** und **110b** sowie der Anthranilsäure (**124a**) an FXR (MW±SEM; i.a. - inaktiv)

In der ersten SAR-Studie wurde bereits in den Derivaten **49**-**52** die entscheidende Rolle der Säureamidbindungen für die Aktivität an FXR gezeigt. Ausgehend von **64** wurde nun die noch ausstehende Inversion der Amidbindungen durchgeführt. Wie bereits die reduzierten und methylierten Derivate **49**-**52** war auch das invertierte Derivat **66** inaktiv.

Damit bestätigte sich die Wahl der durch Rekombination erhaltenen Verbindung **64** als Leitstruktur für die folgenden Untersuchungen der SAR und die Optimierung der Potenz der Verbindungsklasse. Auch in dieser SAR-Studie wurde ausgehend von **64** systematisch immer nur ein Molekülteil variiert, um vergleichbare Ergebnisse zu erhalten und am Ende wiederum die besten Derivate rekombinieren zu können. Die Strategie für die zweite SAR-Studie zeigt Abbildung 29.

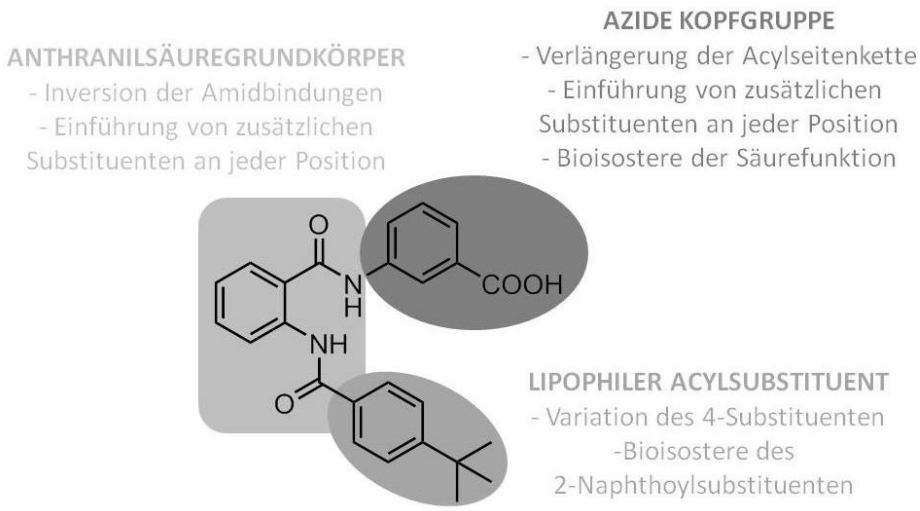

Abbildung 29: *Strategie der zweiten Studie zu den Struktur-Aktivitätsbeziehungen* der Acylanthranilamide basierend auf der in der ersten Studie optimierten Substanz **64**

Die zweite SAR-Studie wurde wiederum mit dem Versuch begonnen, den lipophilen Acylsubstituenten zu optimieren, wobei in diesem Fall gezielt Analoga der bereits als potent charakterisierten Substituenten, nämlich der 2-Naphthoylgruppe (**58**) und der 4-*tert*-Butylbenzoyl-gruppe (**64**), eingeführt wurden. Dabei wurde auch versucht, durch das Einbringen polarerer Substituenten die Löslichkeit der Verbindungen zu verbessern.

Tabelle 4: *In vitro FXR-Aktivität der Derivate **69**-**74** mit variiertem Acylsubstituenten* (MW±SEM; n = 3-6; i.a. - inaktiv)

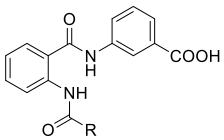

#	R	EC_{50} [µM] (max. rel. Aktivierung [%])
64	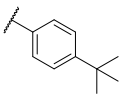	0,28±0,03 (9,4±0,2)
69	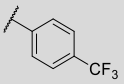	6,9±0,2 (26,2±0,4)
70	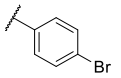	3,7±0,9 (14,3±0,9)
71	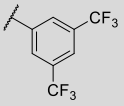	i.a.
58	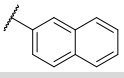	1,5±0,2 (37±1)
72	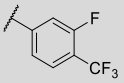	5.0±0,2 (32,4±0,5)
73	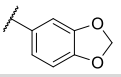	10,0±1,2 (12,2±0,5)
74	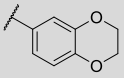	4,9±0,4 (23,3±0,4)

Die Potenz des 4-*tert*-Butylbenzoylderivates **64** konnte jedoch durch keine andere 4-substituierte Benzoylgruppe (**69**, **70**, **72**) oder Analoga des 2-Naphthoylsystems (**72**, **73**, **74**) gesteigert werden. Lediglich die Maximalaktivierung der Acylanthranilamidderivate nahm durch Verwendung eines 2-

Naphthoylsystems (**58**) oder der 3,4-disubstituierten Benzoylgruppe in **72** als Acylsubstituenten zu (vgl. Tabelle 4). Die 4-*tert*-Butylbenzoylgruppe (**64**) stellte also mit einem gutem EC_{50}-Wert sowie ausreichender Maximalaktivierung den günstigsten Acylsubstituenten dar und wurde für die weiteren SAR-Untersuchungen beibehalten. Im nächsten Schritt wurden ausgehend von **64** die SAR der 3-Aminobenzoesäure als azider Kopfgruppe untersucht und dabei bioisostere Derivate der Carbonsäure hergestellt, die Kettenlänge zwischen aromatischem Ring und Carbonsäurefunktion variiert sowie zusätzliche Substituenten an verschiedenen Positionen des aromatischen Rings der Kopfgruppe eingeführt.

Bioisosterer Ersatz der Carbonsäurefunktion (vgl. Tabelle 5) war interessanterweise weitgehend ohne große Veränderungen in der Potenz durch diverse bioisostere Gruppen möglich. Ein Methylketon (**75**), ein Nitril (**76**), eine Methoxygruppe (**77**) sowie ein Methylmercaptosubstituent (**78**) als Carbonsäureersatz führten zu vergleichbar potenten Verbindungen. Zur FXR-Aktivierung ist also offenbar nicht zwingend eine azide Funktion erforderlich.

Tabelle 5: *In vitro FXR-Aktivität der bioisosteren Derivate **75**-**82*** (MW±SEM; n = 3-6; i.a. - inaktiv)

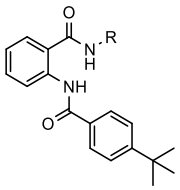

#	R	EC_{50} [µM] (max. rel. Aktivierung [%])
64	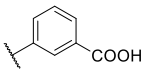	0,28±0,03 (9,4±0,2)
75	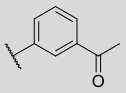	0,48±0,07 (18,8±0,5)
76	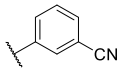	0,23±0,05 (17,5±0,8)
77	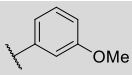	0,38±0,06 (13,3±0,7)
78	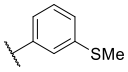	0,20±0,03 (8,6±0,3)
79	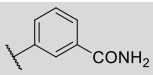	0,074±0,011 (14,8±0,3)
80	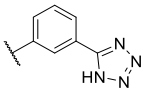	2,85±0,78 (39,3±4,5)
81	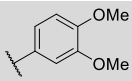	0,071±0,022 (12,7±0,2)
82	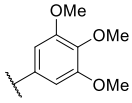	i.a.

Einen erheblich größeren Einfluss auf die Aktivität zeigte dagegen der bioisostere Ersatz (vgl. Tabelle 5) der Carbonsäure durch ein primäres Carbonsäureamid (**79**) bzw. ein 1*H*-Tetrazol (**80**). Carbonsäureamid **79** war bezogen auf seinen EC_{50}-Wert um etwa einen Faktor 5 potenter als die Carbonsäure **64** bei vergleichbarer Maximalaktivierung, zeigte jedoch auch starke Toxizität im zellulären Testsystem, weshalb **79** nicht zur weiteren Optimierung der Substanzklasse dienen konnte.

Die Einführung eines 1*H*-Tetrazols als Kopfgruppe in **80** bewirkte jedoch den gegensätzlichen Effekt. **80** hatte einerseits einen etwa 10-fach schlechteren EC_{50}-Wert, erreichte auf der anderen Seite aber mit knapp 40% die höchste Maximalaktivierung aller beschriebenen Acylanthranilamidderivate.

Auch die Einführung zusätzlicher Methoxygruppen in **77** beeinflusste die Aktivität der Verbindungen deutlich. Eine weitere Methoxygruppe in **81** verbesserte den EC_{50}-Wert um etwa einen Faktor 5, die Maximalaktivierung blieb allerdings auf dem niedrigen Niveau von **77**. Eine dritte Methoxygruppe in **82** führte dagegen zu Inaktivität. (vgl. Tabelle 5)

Bemerkenswerte Unterschiede in der FXR-Aktivierung wurden auch bei der Variation der Kettenlänge zwischen aromatischem Ring der Kopfgruppe und Carbonsäurefunktion beobachtet. Durch Einführen einer Methylengruppe als Spacer im 3-Aminophenylessigsäurederivat **83** wurde im Vergleich zum 3-Aminobenzoesäurederivat **64** der EC_{50}-Wert etwas schlechter, die Maximalaktivierung nahm aber zu. Verlängerung um eine weitere Methylengruppe im 3-Aminopropansäurederivat **84** führte dagegen zu einer deutlichen Verbesserung des EC_{50}-Wertes bei ähnlich hoher Maximalaktivierung. (vgl. Tabelle 6)

Tabelle 6: *In vitro FXR-Aktivität der Substanzen **83** und **84** mit verlängerter Kopfgruppe* (MW±SEM; n = 3-6)

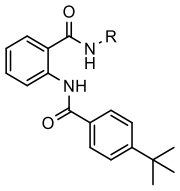

#	R	EC_{50} [µM] (max. rel. Aktivierung [%])
64	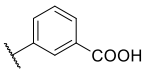	0,28±0,03 (9,4±0,2)
83	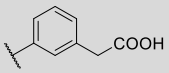	0,42±0,13 (26,4±1,4)
84	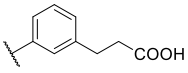	0,064±0,013 (21,8±0,6)

Als mögliche Erklärung für diese Potenzunterschiede deuteten virtuelle Studien (vgl. Abbildung 30) an, dass die Säurefunktion des 3-Aminobenzoesäurederivates **64** potente Wechselwirkungen mit Arg_{268} und Arg_{335} der FXR-LBD eingeht, die durch einen Wassercluster vermittelt werden, sodass ein Wassermolekül zwischen dem Liganden **64** und den Aminosäuren des Rezeptors als ‚Überträger' von Wasserstoffbrücken fungiert. Eine Verlängerung um eine Methyleneinheit in 3-Aminophenylessigsäurederivat **83** führt dazu, dass die Abstände und Winkel zwischen der Säurefunktion, dem Wassercluster sowie Arg_{268}/Arg_{335} nicht mehr optimal für günstige Wechselwirkungen sind. Durch weitere Verlängerung um eine Methyleneinheit in **84** kann die Carbonsäuregruppe jedoch ein Wassermolekül verdrängen und dessen räumliche Position in der Bindetasche einnehmen, sodass die Säurefunktion direkt mit Arg_{268}/Arg_{335} interagiert. Der Entropiegewinn durch das Verdrängen eines Wassermoleküls kann den deutlich besseren EC_{50}-Wert für das 3-Aminopropansäurederivat **84** erklären.

Im nächsten Schritt der SAR-Studie wurde die Möglichkeit untersucht, weitere Substituenten an den freien Positionen des aromatischen Ringes der Kopfgruppe einzuführen. Mit solchen Substituenten könnte die Potenz der Verbindungen einerseits durch zusätzliche Interaktionen mit dem Rezeptor

verbessert werden. Andererseits besteht bei benachbarten Substituenten an einem aromatischen Ring die Möglichkeit, durch intramolekulare Wechselwirkungen die freie Drehbarkeit von Bindungen einzuschränken und durch diese Art der Rigidisierung potenzsteigernde Entropiegewinne zu erzielen.

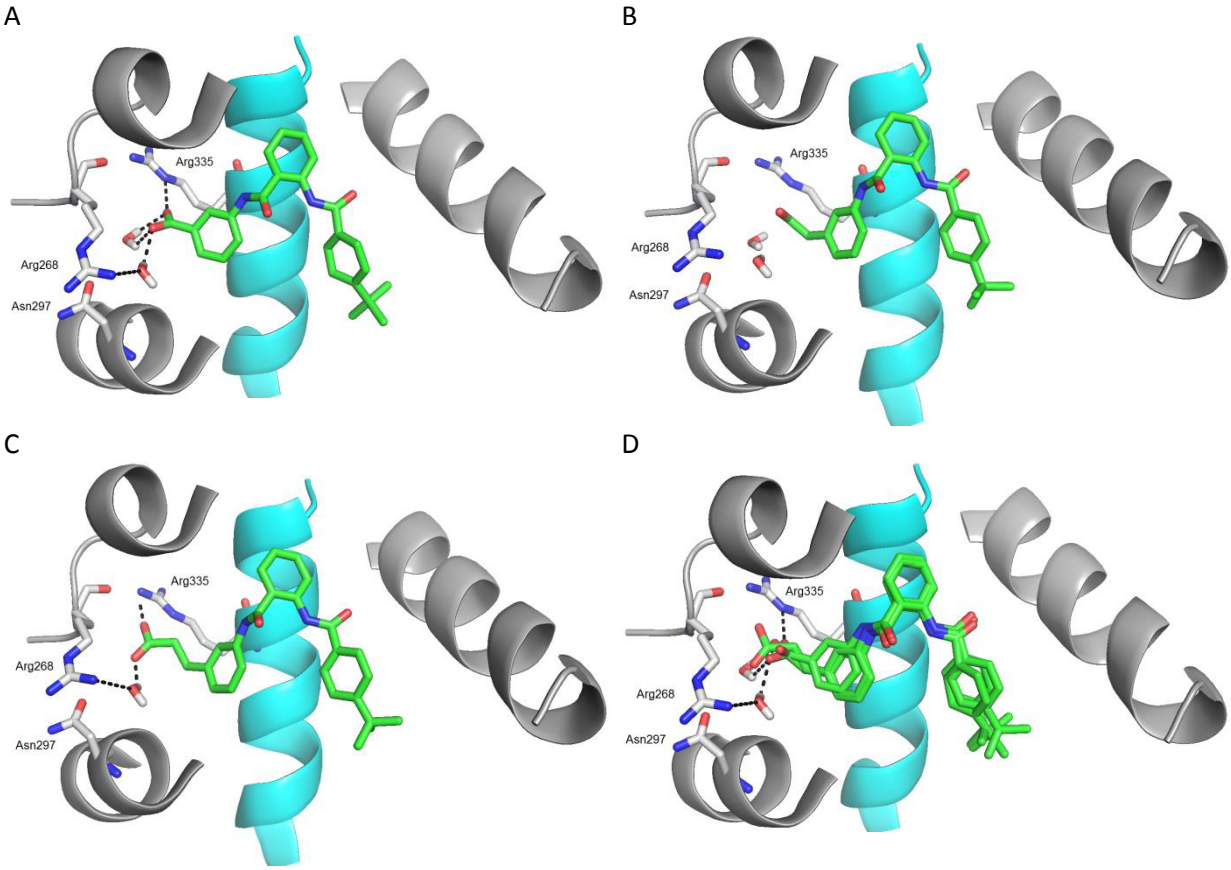

Abbildung 30: *Dockingposen der Derivate **64** (A), **83** (B) und **84** (C) sowie **64**, **83** und **84** im Vergleich (D):* Kettenverlängerung um eine Methyleneinheit von **64** zu **83** bewirkt ungünstige Winkel und Abstände für potente Wechselwirkungen des Derivates **83**. Eine weitere Methyleneinheit in **84** führt dagegen zu optimaler Platzierung der Carbonsäure für Wechselwirkungen mit Arg268/Arg335 und zur Verdrängung eines Wassermoleküls aus dem mit Arg268/Arg335 assoziierten Wassercluster.

Die Dockingpose von **64** (vgl. Abbildung 30A) ließ vermuten, dass Substituenten in 4-Position des aromatischen Ringes der Kopfgruppe eine zusätzliche, noch unbelegte kleine Tasche der Ligandbindedomäne ausfüllen könnten. Daher wurden zunächst an dieser Position verschiedene Substituenten eingeführt (**85**-**88**, vgl. Tabelle 7). Entgegen der Ergebnisse der in silico Studien führten jedoch alle 4-Substituenten zu einem Aktivitätsverlust. Das 4-Methylderivat **85** war gänzlich inaktiv, während das 4-Chlor- (**86**) und 4-Methoxyderivat (**87**) noch moderat aktiv, aber gegenüber der unsubstituierten Ausgangsverbindung **64** hinsichtlich des EC_{50}-Wertes um etwa einen Faktor 4-8 weniger potent waren. Lediglich das 4-Fluorderivat **88** mit dem kleinsten Substituenten in 4-Position behielt annähernd die gleiche Potenz wie die Ausgangsverbindung **64**. Die Beobachtung, dass durch den kleinsten 4-Substituenten der geringste Aktivitätsverlust verursacht wurde, aber bereits eine Methylgruppe an 4-Position zu Inaktivität führte, legt die Vermutung nahe, dass womöglich sterische Wechselwirkungen zwischen dem 4-Substituenten und der benachbarten Säureamidgruppe zu einer

für die Bindung an FXR ungünstigen Geometrie führten und so die verringerte Potenz erklären. Diese These wurde ebenfalls durch Dockingstudien unterstützt, in denen das in 4-Position methylierte Derivat **85** in einen deutlich unterschiedlichen Bindungsmodus gezwungen wurde.

Tabelle 7: *In vitro FXR-Aktivität der in 4-Position der Kopfgruppe substituierten Derivate **85**-**88*** (MW±SEM; n = 3-6; i.a. - inaktiv)

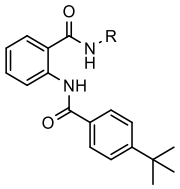

#	R	EC_{50} [µM] (max. rel. Aktivierung [%])
64	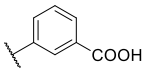	0,28±0,03 (9,4±0,2)
85	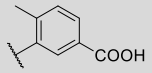	i.a.
86	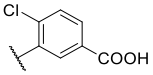	1,12±0,27 (15,6±0,7)
87	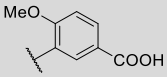	4,7±0,3 (14,9±0,2)
88	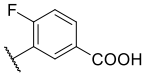	0,48±0,14 (12,0±0,4)

Im Gegensatz zu den ungünstigen Effekten von Substituenten in 4-Position des aromatischen Rings der Kopfgruppe führte eine Methylierung an den Positionen 2 (**89**) und 6 (**90**) zu einer erheblichen Verbesserung des EC_{50}-Wertes (vgl. Tabelle 8). Beide Derivate **89** und **90** waren hinsichtlich des EC_{50}-Wertes um etwa einen Faktor 6 potenter als die unsubstituierte Ausgangsverbindung **64** und zeigten beide eine günstige Maximalaktivierung von etwa 20%. Da im Falle einer Substitution in 2-Position (**89**) ähnlich wie bei den 4-substituierten Derivaten **85**-**88** die Möglichkeit sterischer Wechselwirkungen mit der benachbarten Säureamidgruppe bestand und sich diese in **85**-**88** als potentiell ungünstig erwiesen hatten, wurde von der 2-Substitution abgesehen.

Stattdessen wurden die SAR der aktivitätssteigernden Substitution in 6-Position genauer untersucht (vgl. Tabelle 8) und die Methylgruppe in **90** durch andere Substituenten ersetzt, um die Möglichkeit einer weiteren Potenzsteigerung durch alternative Substituenten in dieser Position zu studieren. Die SAR waren in diesem Fall jedoch relativ schmal und nur eine Methoxygruppe (**91**) in 6-Position erzielte vergleichbare Potenz wie **90**, während ein Chlor- (**92**) oder Bromatom (**93**) sowie eine Nitrogruppe (**94**) zu Aktivitätsverlust führten. Die 3-Amino-6-Methylbenzoesäure (**90**) stellte sich somit als günstigste Kopfgruppe heraus. Ihre Dockingpose (vgl. Abbildung 31A) deutete darauf hin, dass durch die zusätzliche Methylgruppe ähnlich wie beim 3-Aminophenylpropansäurederivat ein Wassermolekül aus dem mit Arg_{268} und Arg_{335} assoziierten Wassercluster verdrängt wird, was den Aktivitätsgewinn erklären würde. Für größere Substituenten wie ein Bromatom (**93**) oder eine Nitrogruppe (**94**) bot die FXR-Ligandbindetasche an dieser Position gemäß der in silico Ergebnisse jedoch nicht genügend Platz, was wiederum die geringere Aktivität von **93** und **94** bekräftigte.

Tabelle 8: *In vitro FXR-Aktivität der in 2- und 6-Position der Kopfgruppe substituierten Derivate* ***89-94*** (MW±SEM; n = 3-6; i.a. - inaktiv)

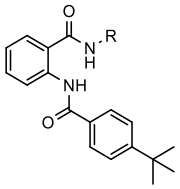

#	R	EC_{50} [µM] (max. rel. Aktivierung [%])
64	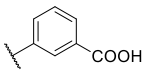	0,28±0,03 (9,4±0,2)
89	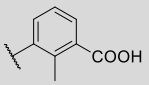	0,042±0,001 (19,0±0,2)
90	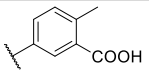	0,045±0,009 (22,4±0,5)
91	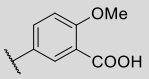	0,047±0,001 (19,1±0,5)
92	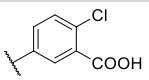	0,28±0,04 (18,7±0,4)
93	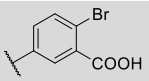	0,15±0,01 (16,4±0,2)
94	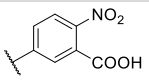	i.a.

Nach den Studien zu den SAR des Acylsubstituenten und der Kopfgruppe blieb noch der zentrale Anthranilamidgrundkörper zu untersuchen. Ähnlich wie bei der Optimierung der Kopfgruppe wurde hier durch Erweiterung des zentralen Aromaten (vgl. Tabelle 9) in der Leitstruktur **64** durch zusätzliche Substituenten überprüft, ob etwaige noch unbelegte Taschen innerhalb der FXR-Ligandbindedomäne ausgefüllt werden könnten, um die Potenz der Verbindungen durch zusätzliche Interaktionen mit dem Rezeptor zu erhöhen. Aufgrund der für erste Untersuchungen leichten synthetischen Zugänglichkeit wurde dabei zunächst an jeder freien Position des aromatischen Ringes ein Chloratom eingeführt. Ein zusätzliches Chloratom in 3- (**95**) oder 6-Position (**98**) des zentralen Aromaten führte zu Inaktivität, was entweder durch sterische Wechselwirkungen mit den benachbarten Amidfunktionen oder mit dem Rezeptor zu erklären war. Chlorierung in 4-Position (**96**) führte dagegen zu einer Potenzsteigerung um einen Faktor 2,5, sodass eine Vergrößerung der Leitstruktur **64** durch Substituenten in 4-Position des zentralen aromatischen Ringes zu einer Optimierung der Aktivität zu führen schien.

Interessanterweise machte ein Chloratom in 5-Position (**97**) dagegen aus der partialagonistischen Ausgangsverbindung **64** einen moderat potenten FXR-Antagonisten. Dockingstudien (vgl. Abbildung 31B) wiesen darauf hin, dass **97** durch den zusätzlichen Substituenten einen leicht verschobenen Bindemodus einnimmt und eine zusätzliche Wechselwirkung mit Tyr_{373} in Helix 7 eingeht. Ähnliche Interaktionen mit Helix 7 sind auch für den FXR-Antagonisten Suvanin beschrieben[102], was die antagonistische Aktivität von **97** erklären kann. Um die überraschende antagonistische Aktivität von **97** aber auch in vitro zu bekräftigen, wurde zusätzlich das an 5-Position mit einer Methoxygruppe substituierte Derivat **99** synthetisiert und ebenfalls als FXR-Antagonist mit vergleichbarer Potenz identi-

fiziert. Dadurch eröffnet sich die Möglichkeit, mit **97** und **99** als vielversprechenden Leitstrukturen die Substanzklasse der Acylanthranilamide auch zu potenten FXR-Antagonisten zu optimieren.

Tabelle 9: *In vitro FXR-Aktivität der am zentralen Anthranilamidgrundkörper substituierten Derivate* ***95-103*** (MW±SEM; n = 3-6; i.a. - inaktiv)

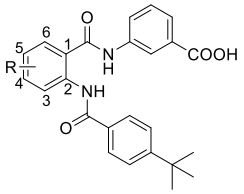

#	R	EC_{50} [µM] (max. rel. Aktivierung [%])
64	-	0,28±0,03 (9,4±0,2)
95	3-Cl	i.a.
96	4-Cl	0,123±0,007 (22,0±0,3)
97	5-Cl	IC_{50} = 12,3±0,6 (15±4 min.)
98	6-Cl	i.a.
99	5-OMe	IC_{50} = 15,1±0,1 (10±1 min.)
100	4-Me	0,061±0,014 (21±1)
101	**4-OMe**	**0,008±0,003 (18±1)**
102	4-Br	0,048±0,016 (15±1)
103	4-NO_2	i.a.

Mit dem Ziel, die partialagonistische Aktivität der Acylanthranilamide weiter zu optimieren, wurde jedoch von den Antagonisten **97** und **99** abgesehen und die SAR einer Derivatisierung in 4-Position des zentralen aromatischen Ringes mit verschiedenen Substituenten weiter untersucht (vgl. Tabelle 9). Austausch des Chloratoms (**96**) gegen eine Methylgruppe (**100**) oder ein Bromatom (**102**) verbesserte den EC_{50}-Wert um einen weiteren Faktor 2, während eine Nitrogruppe in 4-Position (**103**) zu Inaktivität führte. Eine weitere deutliche Potenzsteigerung gelang durch Einführung einer Methoxygruppe (**101**) in 4-Position des zentralen Aromaten, was den gewünschten hochpotenten FXR-Partialagonisten **101** mit einem EC_{50}-Wert von 8±3 nM und 18±1% relativer Aktivierung lieferte.

Die hohe Potenz des optimierten Derivates **101** schien gemäß virtueller Studien (vgl. Abbildung 31C) wiederum von der Verdrängung eines Wassermoleküls aus dem Wassercluster um Arg_{268}/Arg_{335} herzurühren, die schon für **83** und **90** beobachtet worden war. Zusätzlich war **101** in der FXR-Bindetasche verglichen mit den Vorgängersubstanzen leicht verschoben, wodurch der 4-*tert*-Butylbenzoylsubstituent noch tiefer in einer lipophilen Tasche platziert wurde (vgl. Abbildung 31D).

Ähnlich wie nach der ersten SAR-Studie wurde nach Abschluss der SAR-Untersuchungen an allen Molekülteilen versucht, die Erkenntnisse über die besten Teilstrukturen in einer Verbindung zu vereinen und die Potenz auf diese Weise noch weiter zu steigern. Als Kopfgruppe bot sich dabei insbesondere die 3-Amino-6-Methylbenzoesäure aus **90** an, während im Bereich der zentralen Anthranilsäuregrundstruktur vor allem die Substitution mit einer Methoxygruppe in 4-Position (**101**) herausstach. Eine Rekombination dieser beiden Teilstrukturen mit dem 4-*tert*-Butylbenzoylsubstituenten in **104** führte jedoch nicht zu einer Steigerung der Potenz, sondern senkte sie auf einen EC_{50}-Wert von 87±20 nM. Auch die Kombination der besten Kopfgruppe mit einem 4-Chlorsubstituenten am zentralen aromatischen Ring in **105** lieferte mit einem EC_{50}-Wert von 110±16 nM zwar einen sehr potenten, der Verbindung **101** aber nicht überlegenen FXR-Partialagonisten.

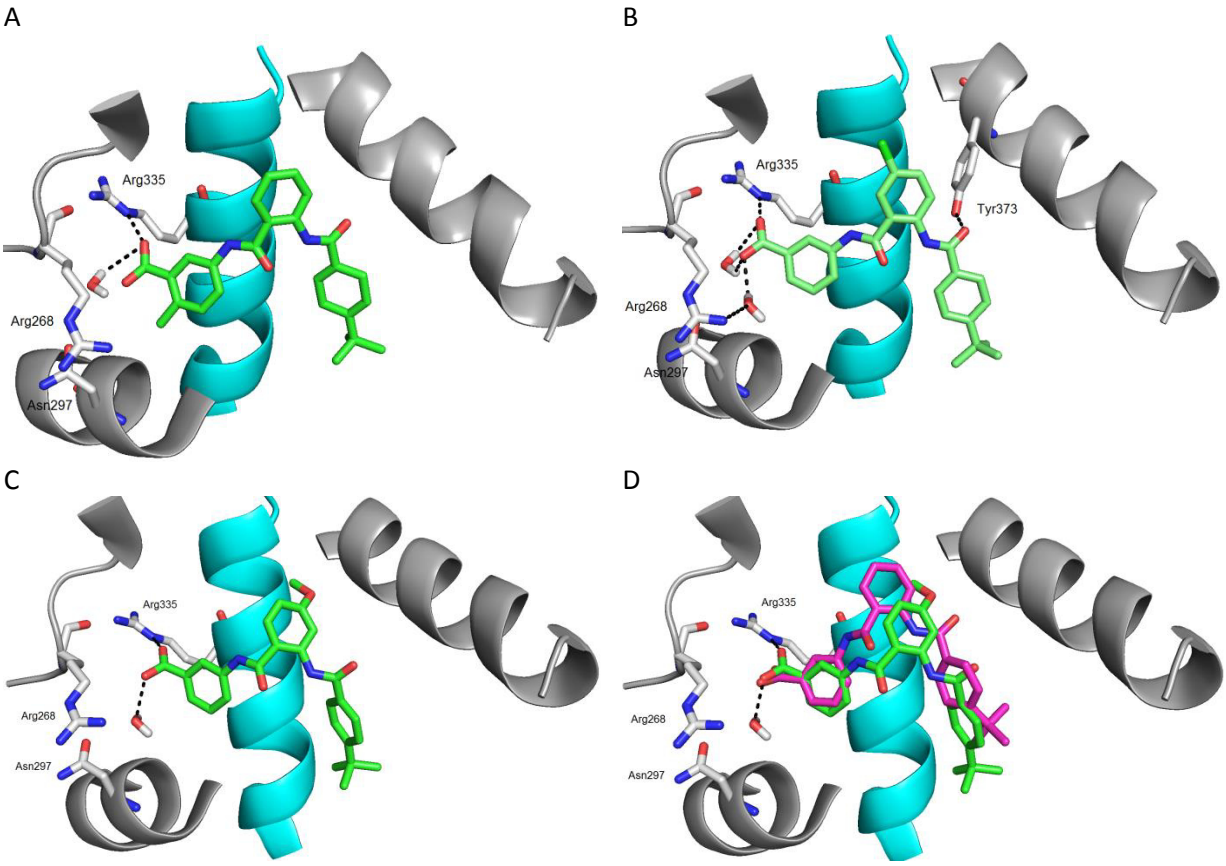

***Abbildung 31**: Dockingposen von **90** (A), **97** (B) und **101** (C) sowie **101** (grün, D) im Vergleich mit **84** (violett, D):* Methylierung in 6-Position der Kopfgruppe (**90**, A) führt zur Verdrängung eines Wassermoleküls, der Platz für Substituenten an dieser Stelle der FXR-Ligandbindetasche ist jedoch begrenzt. Durch Substituenten in 5-Position des zentralen Aromaten (**97**, B) wird ein anderer Bindemodus erzwungen und eine Interaktion mit Tyr_{373} in Helix 7 ermöglicht, was den Antagonismus von **97** erklären könnte. Substitution in 4-Position des zentralen Aromaten (**101**, C) führt ebenfalls zu einem leicht verschobenen Bindemodus (D), wodurch ein Wassermolekül verdrängt und die Lage der Carbonsäure von **101** zu Arg_{335} verbessert wird. Zusätzlich wird der 4-*tert*-Butylbenzoylsubstituent tiefer in einer lipophilen Tasche platziert.

Diese Ergebnisse legten nahe, dass die Rekombination der besten Substituenten womöglich ein insgesamt zu großes Molekül für additive Effekte der Teilstrukturen lieferte. Dafür sprachen auch die in silico Ergebnisse des Dockings (vgl. Abbildung 31A/C) von **90** und **101** in die FXR-LBD, da für beide Derivate das Verdrängen eines Wassermoleküls aus dem Wassercluster um Arg_{268} und Arg_{335} als möglicher aktivitätssteigernder Effekt beobachtet wurde, der jedoch durch Kombination nicht doppelt ausgenutzt werden kann.

Tabelle 10**: In vitro FXR-Aktivität der durch Rekombination der besten Teilstrukturen generierten Derivate **104**-**106 (MW±SEM; n = 3-6)

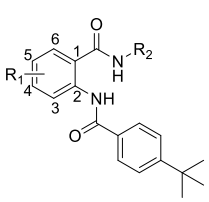

#	R_1	R_2	EC_{50} [µM] (max. rel. Aktivierung [%])
104	4-OMe	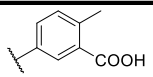	0,087±0,020 (22,3±0,7)
105	4-Cl	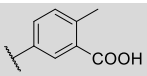	0,110±0,016 (20,1±0,5)
106	4-Me	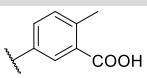	0,030±0,008 (18,2±0,5)

Der Aktivitätsverlust der rekombinierten Verbindungen kann außerdem von sterischer Überlappung mit der Ligandbindetasche des Rezeptors herrühren. Deshalb wurde das kleinstmögliche Derivat mit doppelter Substitution, nämlich die in 6-Position des Aromaten der Kopfgruppe und in 4-Position des zentralen Aromaten methylierte Verbindung **106** synthetisiert und charakterisiert (vgl. Tabelle 10). Das doppelt methylierte Derivat **106** war mit einem EC_{50}-Wert von 30±8 nM zwar die potenteste der rekombinierten Verbindungen, übertraf aber **101** weder hinsichtlich des EC_{50}-Wertes noch hinsichtlich der Maximalaktivierung. Somit blieb DM336 (**101**) der potenteste FXR-Partialagonist unter den Acylanthranilamidderivaten.

2.2.4. Ergebnisse und Zusammenfassung der SAR-Studien

Die aus dieser Arbeit resultierende Verbindung DM336 (**101**) stellt mit einem EC_{50}-Wert von 8±3 nM und einer Maximalaktivierung von 18±1% einen hochpotenten FXR-Partialagonisten dar. Ausgehend von der Leitstruktur JA10 (**32**) wurde die Potenz der Verbindungsklasse der Acylanthranilamide als FXR-Partialagonisten damit um mehr als einen Faktor 1000 gesteigert. DM336 (**101**) bietet die in vitro pharmakologischen Voraussetzungen, um bei der weiteren Untersuchung der potentiellen therapeutischen Strategie des FXR-Partialagonismus in vitro und in vivo eine Rolle zu spielen.

Im Zuge der in SAR-Studien (Merk D et al. *Bioorg. Med. Chem.*, **2014** und Merk D et al. *J. Med. Chem.*, **2014**) wurde die Leitstruktur JA10 (**32**) durch Vergrößerung des Substituenten in 4-Position des aromatischen Ringes im Acylsubstituenten, durch Einführung eines zusätzlichen Aromaten in der aziden Kopfgruppe sowie durch Addition einer Methoxygruppe in 4-Postion der zentralen Anthranilamidgrundstruktur zu DM336 (**101**) optimiert und dabei die essentielle Notwendigkeit der Amidbindungen demonstriert. Außerdem wurden die Möglichkeiten aufgezeigt, durch Vergrößerung des Acylsubstituenten die Maximalaktivierung der Verbindungsklasse zu erhöhen und durch Einführen eines Substituenten in 5-Position des zentralen aromatischen Ringes acylanthranilamidbasierte FXR-Antagonisten zu entwickeln. (vgl. Abbildung 32)

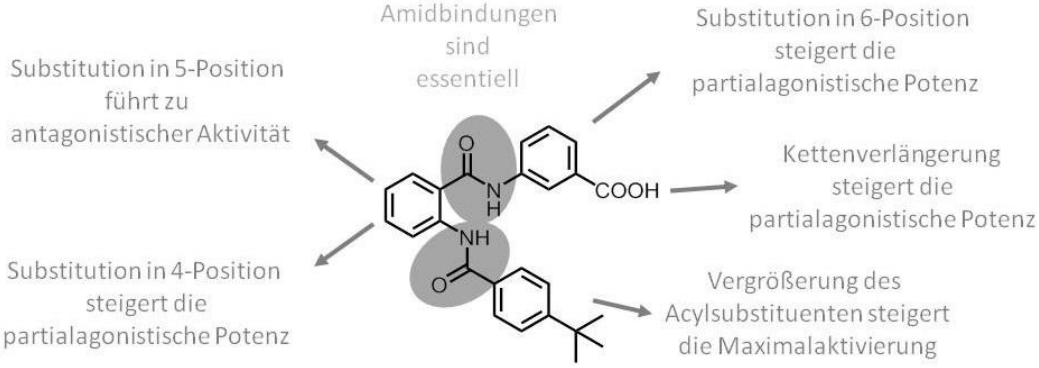

Abbildung 32: *Übersicht über die in dieser Arbeit ermittelten Struktur-Aktivitäts-Beziehungen der Acylanthranilamide als FXR-Partialagonisten*

2.3 Offtargetaktivität der Acylanthranilsäurederivate und Entwicklung von PPAR-Liganden

Da das Ziel der vorliegenden Arbeit die Entwicklung eines selektiven und potenten FXR-Partialagonisten darstellte, wurden während der SAR-Studien ausgewählte potente Derivate auch hinsichtlich ihrer Aktivität an anderen, sog. *off-targets* charakterisiert. Ein wichtiges off-target stellte dabei der membranständige G-Proteingekoppelte Gallensäurerezeptor TGR5 dar, da er die gleichen physiologischen Liganden wie FXR aufweist und daher mit einer Kreuzreaktivität von FXR-Liganden an TGR5 zu rechnen war. Die Acylanthranilamide **58**, **64** und **101** stellten sich jedoch als inaktiv an TGR5 heraus.

Aufgrund struktureller Ähnlichkeit der Acylanthranilamide mit den nicht-steroidalen Antiphlogistika (NSAR) und Cyclooxigenasehemmern Mefenaminsäure (**125**) und Flufenaminsäure (**126**) wurde außerdem die Aktivität der Acylanthranilamidderivate **44** und **64** an Enzymen der Arachidonsäurekaskade, nämlich der 5-Lipoxigenase (5-LO) und den Cyclooxigenasen COX-1 und COX-2 untersucht. Auch hier stellten sich **44** und **64** als inaktiv und somit selektiv heraus.

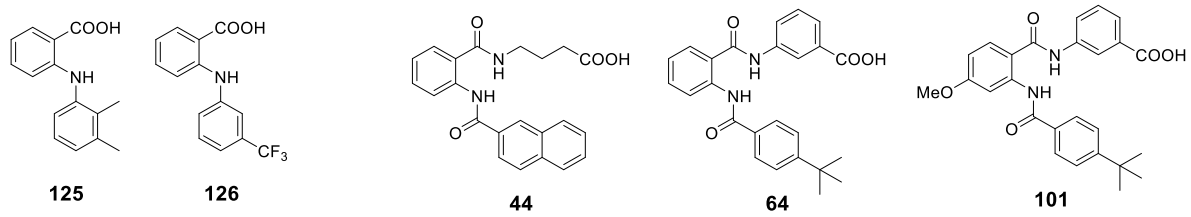

125 **126** **44** **64** **101**

Abbildung 33: *NSAR Mefenaminsäure (**125**) und Flufenaminsäure (**126**) im Vergleich zu den Acylanthranilamiden **44**, **64** und **101***

Schließlich stellten noch die Peroxisomen Proliferator-aktivierten Rezeptoren PPARα, PPARγ und PPARδ wichtige off-targets dar, da sie zusammen mit FXR und dem Corezeptor RXR ein komplexes Netzwerk metabolischer Regulatoren bilden, sodass auch Selektivität über PPARs für einen potenten FXR-Partialagonisten essentiell ist.

Die nukleären PPARs umfassen die drei Subtypen PPARα, PPARγ und PPARδ, die alle durch Fettsäuren und Eicosanoide aktiviert werden und die Expression metabolischer und inflammatorischer Targetgene kontrollieren, sich jedoch in ihrem Expressionsmuster unterscheiden.[114–117] PPARα findet sich vor allem in der Leber und im Fettgewebe, wo der Rezeptor unter anderem die β-Oxidation von Fettsäuren fördert, und wird als Hauptregulator des hepatischen Nährstoffmetabolismus im nüchternen Zustand angesehen. Die PPARα-agonistischen Fibrate spielen seit Jahrzehnten eine große Rolle in der Therapie von Dyslipidämien.[118,119]

PPARγ kontrolliert vor allem die Differenzierung von Adipozyten und die Adipogenese. Außerdem spielt der Rezeptor eine große Rolle im Glucose- und Lipidstoffwechsel sowie in der Insulinsensitivität. Entsprechend wird PPARγ insbesondere im Fettgewebe, in Makrophagen und in Skelettmuskeln exprimiert. Mit den Thiazolidindionen existieren auch für PPARγ klinisch verwendete

Agonisten, die trotz ernstzunehmender Nebenwirkungen[120] weiterhin die Behandlung des Diabetes mellitus Typ 2 mitbestimmen.[118]

Im Gegensatz zu den Subtypen α und γ, die validierte und klinisch relevante Arzneistofftargets darstellen, existiert bislang kein zugelassener Wirkstoff, der seine Aktivität über PPARδ entfaltet. PPARδ wird im Körper ubiquitär exprimiert und erfüllt zahlreiche physiologische Funktionen. Zum einen spielt PPARδ in zahlreichen Geweben wie in Skelettmuskeln eine wichtige Rolle in der Fettsäureoxidation, zum anderen ist der Rezeptor in das komplexe Geschehen bei der Entstehung und Auflösung von Entzündungen eingebunden.[121] Klinische Studien mit einem PPARδ-Agonisten[122,123] deuteten auf wertvolle metabolische Effekte, wie gesenkte Triglyceridspiegel und verbesserte Insulinsensitivität hin, doch die Untersuchungen wurden aufgrund des Verdachts auf Kanzerogenität des experimentellen Wirkstoffs eingestellt.[124]

Alle drei PPAR Subtypen stellen also attraktive Wirkstofftargets dar. Wie in (Lamers C, Schubert-Zsilavecz M, Merk D. *Expert Opin. Ther. Patents*, **2012**) dargelegt ist, wird intensive akademische und industrielle Forschung an diesen Rezeptoren betrieben, sowohl bei der Entwicklung neuer Liganden der nukleären Rezeptoren, als auch bei der Suche nach neuen therapeutischen Anwendungsmöglichkeiten. Dabei steht insbesondere der Rezeptor PPARδ im Fokus, da er aktuellen Erkenntnissen zufolge einen neuen Ansatzpunkt zur Therapie metabolischer Erkrankungen bieten könnte.

Das erste im Zuge dieser Arbeit an PPARs getestete Acylanthranilamid **44** zeigte mit einem EC_{50}-Wert von 18,1±0,9 µM und einer Maximalaktivierung von 432±13% deutliche Aktivität an PPARγ, die vor allem aufgrund der extremen Maximalaktivierung für die Entwicklung selektiver FXR-Partialagonisten nicht wünschenswert war. Auch die optimierte Verbindung **57** der ersten SAR-Studie stellte sich als PPAR-Agonist heraus und war interessanterweise an allen drei Subtypen aktiv. Um das verfolgte Ziel eines selektiven FXR-Partialagonisten zu realisieren, musste also neben der Optimierung der Aktivität an FXR die off-target-Aktivität an PPARs reduziert werden. Aufgrund der therapeutischen Relevanz der PPARs schien es außerdem interessant, die Acylanthranilamide an PPARs, insbesondere am aufstrebenden Wirkstoff-Target PPARδ, einer eigenen SAR-Studie zu unterziehen. Auf diese Weise wurden zum einen Strukturelemente identifiziert, die zur Selektivität der Acylanthranilamide für FXR führten und zum anderen potente PPAR-Liganden entwickelt. Die Ergebnisse dieser SAR-Studie sind zur Publikation eingereicht (Merk D et al. *Bioorg. Med. Chem.*, submitted).

Die Charakterisierung der PPAR-Aktivität erfolgte für jeden Subtypen in Gal4-Hybrid-Reportergenassays, in denen jeweils die LBD des PPARs mit der DBD des Transkriptionsfaktors Gal4 aus der Hefe *Saccharomyces cerevisiae* zu einem Hybridrezeptor fusioniert ist. Als Reportergen fungierte entsprechend eine Firefly-Luziferase mit einem Gal4-Response-Element.[125] Die Auswertung des

Testsystems erfolgte analog zum FXR-Reportergenassay. Eine genaue Methodenbeschreibung der PPAR-Reportergenassays findet sich im Manuskript (Merk D et al. *Bioorg. Med. Chem.*, submitted).

Tabelle 11**: In vitro PPAR-/FXR-Aktivität der Derivate **36**-**39**, **42**-**45**, **49**, **50** und **55**-**60 (MW±SEM; n = 3-6; i.a. - inaktiv)

	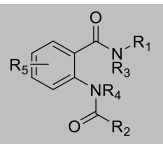					**EC_{50} [µM] (max. rel. Aktivierung [%])**			
#	**R_1**	**R_2**	**R_3**	**R_4**	**R_5**	**PPARα**	**PPARγ**	**PPARδ**	**FXR**
36	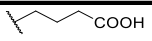	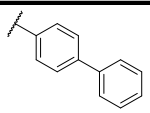	H	H	-	i.a.	13±1 (135±6)	i.a.	i.a.
37	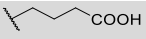	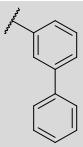	H	H	-	10±1 (260±5)	37±11 (229±44)	i.a.	i.a.
38	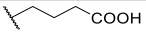	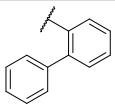	H	H	-	i.a.	23±6 (45±6)	i.a.	i.a.
39	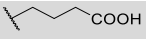	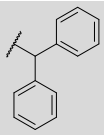	H	H	-	i.a.	i.a.	i.a.	i.a.
42	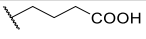	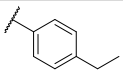	H	H	-	15,7±2,7 (100±11)	39±10% @10 µM	i.a.	5,8±1,0 (28±2)
43	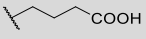	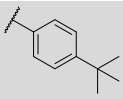	H	H	-	i.a.	i.a.	i.a.	2,5±0,4 (19±1)
44	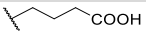	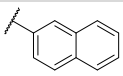	H	H	-	i.a.	18,1±0,9 (432±13)	i.a.	8,6±1,3 (37±2)
45	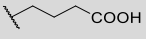	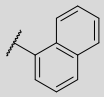	H	H	-	12±3% @10µM	41±5 (397±39)	i.a.	i.a.
49	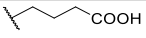	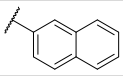	Me	H	-	i.a.	i.a.	i.a.	i.a.
50	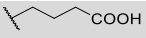	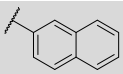	H	Me	-	i.a.	i.a.	i.a.	i.a.
55	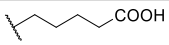	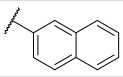	H	H	-	i.a.	26±4 (269±29)	i.a.	8,3±1,0 (11,4±0,4)
56	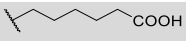	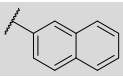	H	H	-	38±9% @10 µM	40±10% @10 µM	i.a.	4,4±0,6 (10,4±0,4)
57	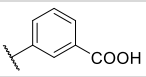	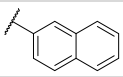	H	H	-	1,96±0,13 (73±2)	5,5±0,6 (126±19)	4,7±0,6 (51±5)	1,5±0,2 (37±1)
58	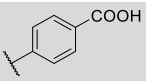	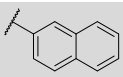	H	H	-	i.a.	21±1 (639±22)	i.a.	1,0±0,2 (23±1)
59	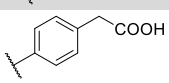	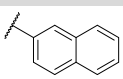	H	H	-	i.a.	25±7% @10 µM	i.a.	3,1±0,3 (9,8±0,4)
60	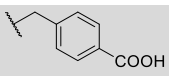	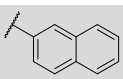	H	H	-	17±9% @10 µM	56±5% @10 µM	i.a.	1,3±0,1 (10,0±0,1)

Innerhalb der ersten SAR-Studie (vgl. Tabelle 11) der Acylanthranilamide an PPARs stellten sich die Verbindungen vor allem als aktiv an PPARγ heraus. PPARγ wurde durch die beiden Naphthylderivate **44** und **45** sowie durch die Biphenyle **36** und **37** aktiviert, wobei die Substanzen mit micromolaren EC_{50}-Werten nur moderate Affinität zeigten, den Rezeptor aber mit Maximalaktivierungen bis über 400% von Pioglitazon sehr effektiv aktivierten. Wie schon an FXR führte die Methylierung der Amidfunktionen von **44** in **49** und **50** auch an PPARγ zu Inaktivität. An PPARα waren nur das 4-Etylbenzoylderivat **42** sowie das 3-Biphenylderivat **37** aktiv, wobei **37** ebenfalls superagonistische Aktivität entfaltete. Interessanterweise zeigte das an FXR aktive 4-*tert*-Butylbenzoylderivat **43** keine PPAR-Aktivierung. Bereits die SAR des Acylsubstituenten zeigten also deutliche Unterschiede zwischen FXR und PPARs sowie innerhalb der PPAR Subtypen. Die meisten der getesteten Verbindungen waren aktiv an PPARγ, was darauf hindeutete, dass dieser Rezeptor viele unterschiedliche Liganden binden kann und durch die Größe der PPARγ-Ligandbindetasche zu erklären ist. Hinsichtlich der FXR-Aktivierung stach vor allem das 4-*tert*-Butylbenzoylderivat **43** heraus, da es die gewünschte partialagonistische Wirkung an FXR bot und gleichzeitig an allen PPARs inaktiv war.

Ausgehend von der an PPARγ superagonistisch aktiven Verbindung **44** wurde anschließend der Einfluss der aziden Kopfgruppe auf die Aktivität an PPARs untersucht (vgl. Tabelle 11). Eine Verlängerung der aliphatischen Kopfgruppe um eine (**55**) oder zwei (**56**) Methylengruppen führte zur Verschlechterung der Potenz, während die Einführung einer 3-Aminobenzoesäure (**57**) als Kopfgruppe, die die Potenz an FXR erheblich gesteigert hatte, auch die PPAR-Aktivität erhöhte, sodass **57** an allen drei PPAR-Subtypen aktiv war. Das 4-Aminobenzoesäurederivat **58** zeigte hingegen nur PPARγ-Agonismus, bewirkte aber wie schon **44** und **45** eine extreme Maximalaktivierung. Andere aromatische Kopfgruppen wie 4-Aminophenylessigsäure (**59**) oder 4-Aminomethylbenzoesäure (**60**) waren deutlich weniger aktiv an PPARs.

Hinsichtlich der aziden Kopfgruppe war im Gegensatz zum Acylsubstituenten also keine deutliche Unterscheidung zwischen FXR und den PPARs sowie zwischen den PPAR Subtypen möglich. An allen vier Rezeptoren erwies sich das 3-Aminobenzoesäurederivat **57** als potenteste Verbindung und stellte einen moderat potenten pan-PPAR- und FXR-Agonisten dar. Lediglich das para-Isomer **58** war an FXR etwa gleichwertig aktiv und dabei selektiv über PPARα und PPARδ. An PPARγ zeigte **58** aber extreme superagonistische Aktivität.

Aufgrund ihrer überlegenen Aktivität an FXR wurde die 3-Aminobenzoesäurekopfgruppe (**57**) für die weiteren SAR-Studien ausgewählt und zunächst zur Steigerung der Aktivität an und der Selektivität für FXR mit dem 4-*tert*-Butylbenzoylsubstituenten (**43**) kombiniert. Aufgrund ihrer gesteigerten Potenz an FXR war die resultierende Verbindung **64** deutlich selektiver über alle PPAR Subtypen als **57**. Basierend auf **64** bzw. **57** wurden anschließend Analoga der 4-*tert*-Butylbenzoyl- und der 2-

Naphthoylgruppe als Acylsubstituenten eingeführt, wodurch jedoch keine Verbesserung der FXR-Aktivität und -Selektivität gelang (vgl. Tabelle 12).

Tabelle 12**: In vitro PPAR-/FXR-Aktivität der Derivate **64, 69, 70-73, 95-98** und **101 (MW±SEM; n = 3-6; i.a. - inaktiv)

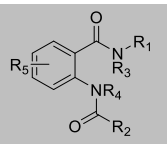

#	R_1	R_2	R_3	R_4	R_5	EC_{50} [µM] (max. rel. Aktivierung [%]) PPARα	PPARγ	PPARδ	FXR
57	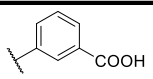	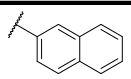	H	H	-	1,96±0,13 (73±2)	5,5±0,6 (126±19)	4,7±0,6 (51±5)	1,5±0,2 (37±1)
64	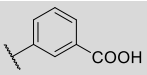	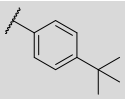	H	H	-	1,3±0,3 (37±3)	3,9±0,5 (348±26)	i.a.	0,28±0,03 (9,4±0,2)
69	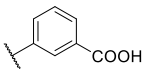	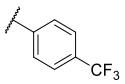	H	H	-	5,8±2,8 (79±15)	8,5±0,5 (384±13)	3,2±0,7 (46±5)	6,9±0,2 (26±1)
70	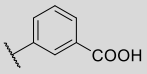	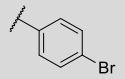	H	H	-	3,6±0,1 (38±1)	4,5±1,9 (58±12)	12±1 (44±2)	3,7±0,9 (14,3±0,9)
71	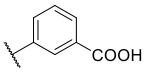	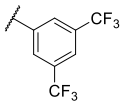	H	H	-	15±6% @10 µM	11±2 (114±17)	i.a.	i.a.
72	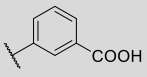	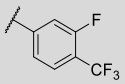	H	H	-	2,2±0,3 (34±2)	6,9±0,4 (240±14)	3,0±0,3 (37±2)	5,0±0,2 (32±1)
73	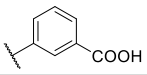	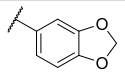	H	H	-	19±2 (54±2)	25±5 (221±59)	i.a.	10±1 (12±1)
95	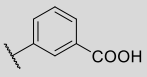	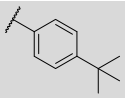	H	H	3-Cl	i.a.	i.a.	i.a.	i.a.
96	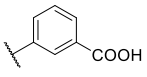	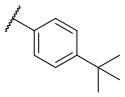	H	H	4-Cl	44±1% @10 µM	9±1 (256±16)	i.a.	0,12±0,01 (22±1)
97	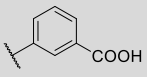	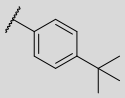	H	H	5-Cl	18±1% @10 µM	5,4±0,3 (132±5)	i.a.	*antago-nistisch*
98	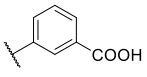	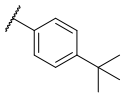	H	H	6-Cl	i.a.	i.a.	i.a.	i.a.
101	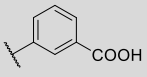	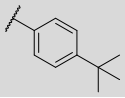	H	H	4-OMe	44±5% @10 µM	3,0±0,1 (81±2)	i.a.	0,008±0,003 (18±1)

Durch die Einführung einer 4-*tert*-Butylbenzoylgruppe als Acylsubstituenten (**64**) war es zwar gelungen, die Selektivität für FXR zu steigern, doch lag zwischen den EC_{50}-Werten von Verbindung **64** an FXR und PPARα bzw. PPARγ nur etwa ein Faktor 4 bzw. 13, was für die Entwicklung eines selektiven FXR-Partialagonisten noch nicht ausreichend war. Eine weitere Selektivitätssteigerung wurde durch die Einführung eines zusätzlichen Substituenten in 4-Position des zentralen aromatischen Ringes (**96**) erzielt (vgl. Tabelle 12). Das zusätzliche Chloratom in 4-Position (**96**) steigerte die Aktivität an FXR um einen Faktor 2,5 während die Aktivität an PPARγ leicht und an

PPARα erheblich abnahm, sodass **96** mit einem Faktor von mindestens 75 selektiv über alle PPAR-Subtypen war. Dieses Selektivitätsprofil konnte durch Ersetzen des Chloratoms in **96** durch eine Methoxygruppe in **101** weiter gesteigert werden (vgl. Tabelle 12). **101** ist mit einem Faktor von mindestens 375 hochselektiv für FXR über alle PPAR Subtypen.

Tabelle 13**: In vitro PPAR-/FXR-Aktivität der Derivate **76, 77, 79** und **83-93 (MW±SEM; n = 3-6; i.a. - inaktiv)

#	R_1	R_2	R_3	R_4	R_5	EC_{50} [µM] (max. rel. Aktivierung [%]) PPARα	PPARγ	PPARδ	FXR
76	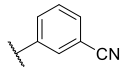	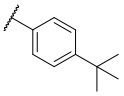	H	H	-	i.a.	i.a.	i.a.	0,23±0,05 (18±1)
77	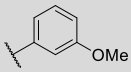	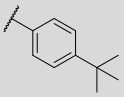	H	H	-	i.a.	i.a.	i.a.	0,38±0,06 (13±1)
79	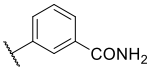	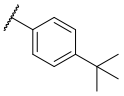	H	H	-	i.a.	i.a.	i.a.	0,07±0,01 (15±1)
83	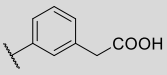	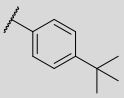	H	H	-	4,4±0,5 (155±11)	6,2±0,8 (121±1)	5,4±0,3 (46±1)	0,42±0,13 (26±1)
84	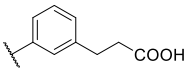	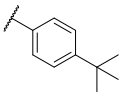	H	H	-	5,4±0,7 (115±12)	5,0±0,8 (175±23)	i.a.	0,06±0,01 (22±1)
85	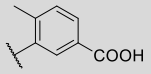	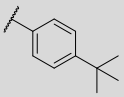	H	H	-	i.a.	6,3±1,3 (163±26)	i.a.	i.a.
86	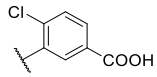	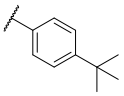	H	H	-	16±4% @10 µM	1,9±0,5 (154±23)	i.a.	1,1±0,3 (16±1)
87	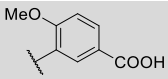	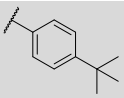	H	H	-	2,9±0,3 (16±1)	4,5±1,6 (154±36)	i.a.	4,7±0,3 (15±1)
88	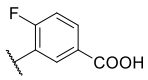	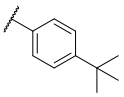	H	H	-	17±2% @10 µM	5,8±1,6 (735±112)	i.a.	0,48±0,14 (12±1)
90	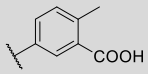	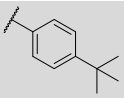	H	H	-	0,21±0,02 (34±1)	5,0±0,2 (98±3)	i.a.	0,045±0,009 (22±1)
91	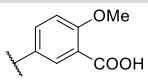	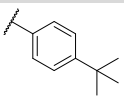	H	H	-	0,74±0,09 (13,7±0,4)	4,4±1,0 (96±12)	i.a.	0,047±0,001 (19±1)
92	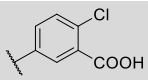	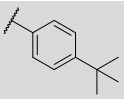	H	H	-	9,1±1,0 (91±6)	5,4±0,3 (98±6)	i.a.	0,28±0,04 (19±1)
93	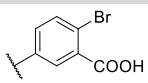	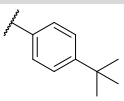	H	H	-	4,1±0,5 (42±4)	6,3±1,1 (82±15)	i.a.	0,15±0,01 (16±1)

Obwohl das Ziel der Selektivität für FXR über die PPARs in Verbindung **101** verwirklicht war, wurden die Struktur-Wirkungsbeziehungen der Acylanthranilamide an den PPARs weiter untersucht, um

neben dem selektiven FXR-Partialagonisten potentere PPAR-Agonisten als Leitstrukturen für weitere Optimierungen und SAR-Studien zu generieren.

Im Vergleich zu 3-Aminobenzoesäurederivat **64** war das um eine Methylengruppe verlängerte 3-Aminophenylessigsäurederivat **83** an PPARα und PPARγ ähnlich und an FXR etwas schwächer potent, an PPARδ zeigte **83** aber agonistische Aktivität, während **64** inaktiv war. Dieser Trend setzte sich bei weiterer Kettenverlängerung (**84**) jedoch nicht fort, denn 3-Aminophenylpropansäurederivat **84** war an FXR deutlich potenter, an PPARα und PPARγ gleich potent und an PPARδ inaktiv (vgl. Tabelle 13). Der bioisostere Ersatz der Carbonsäure (**76**, **77**, **79**, vgl. Tabelle 13), der die Potenz der Verbindungen an FXR kaum beeinflusst hatte, führte interessanterweise zu einem völligen Aktivitätsverlust an allen PPARs, was darauf schließen ließ, dass zur Aktivierung der PPARs eine ionisierbare Kopfgruppe notwendig ist, während an FXR eine polare Funktion ausreicht. Die Einführung bioisosterer Kopfgruppen böte somit eine weitere Möglichkeit zur Steigerung der FXR-Selektivität.

Zusätzliche Substituenten am aromatischen Ring der Kopfgruppe (vgl. Tabelle 13) hatten im Gegensatz zu den Carbonsäurebioisosteren große Auswirkungen auf die Aktivität der Substanzen an FXR und beeinflussten auch die Aktivität an PPARs. Es stellte sich heraus, dass Substituenten in 6-Position des aromatischen Ringes der Kopfgruppe (**85**-**88**) die Aktivität an PPARγ erhöhten und an FXR und PPARα verringerten, wodurch die Substanzen Selektivität für PPARγ gewannen. Innerhalb der 6-substituierten Derivate wies **85** hinsichtlich PPARγ das beste Aktivitäts- und Selektivitätsprofil auf und stellt eine potente superagonistische Leitstruktur zur Entwicklung von Acylanthranilamid-basierten PPARγ-Liganden dar.

Durch Methylierung in 4-Position des aromatischen Ringes der Kopfgruppe (**90**) wurde die Aktivität an PPARγ hingegen kaum beeinflusst, die Potenz an FXR und PPARα aber beträchtlich gesteigert. Die SAR an PPARα waren hierbei jedoch sehr schmal und neben der 6-Methylgruppe in Verbindung **90**, die sich als an PPARα potentestes Derivat herausstellte, wurde lediglich noch eine Methoxygruppe (**91**) vergleichbar gut toleriert.

Docking der Verbindung **90** in die PPARα-LBD (vgl. Abbildung 34) deutete darauf hin, dass die 6-Methylgruppe eine kleine lipophile Untertasche füllt und dabei hydrophobe Kontakte mit Val_{444} ausbildet. In PPARγ(Leu_{453}) und in PPARδ(Met_{417}) ist die Aminosäure Val_{444} von PPARα jeweils durch eine größere Aminosäure ersetzt, sodass die Größe der Subtasche an der Spitze von Arm I in diesen beiden Rezeptoren reduziert ist und eine zusätzliche Substitution der 6-Position schlechter toleriert wird, was die PPARα Selektivität erhöht. Möglicherweise trägt zur hohen Potenz von **90** an PPARα außerdem die sterische Wechselwirkung der Methylgruppe mit der benachbarten Carbonsäure bei, die dazu führt, dass die Carbonsäure keine co-planare Lage zum aromatischen Ring behalten kann.

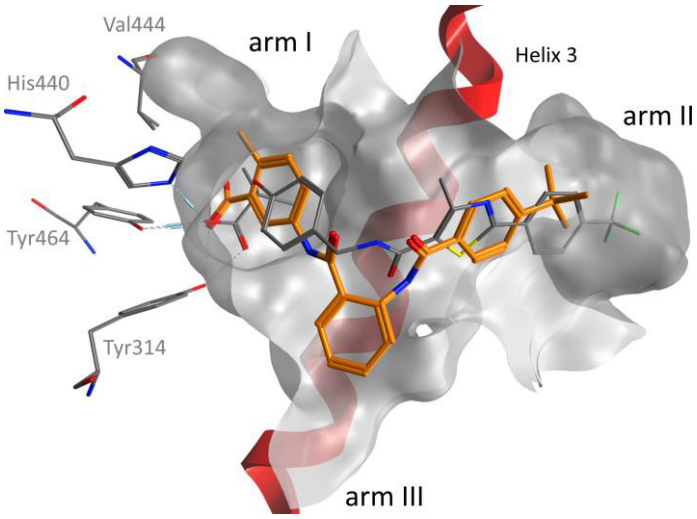

Abbildung 34: *Dockingpose von **90** in der PPARα-LBD (basierend auf der Co-Kristallstruktur des PPARα-Agonisten GW735 (grau, PDB-ID: 2P54):* Die Carbonsäure von **90** (orange) interagiert mit dem Wasserstoffbrückennetzwerk von His440, Tyr464, Ser280 und Tyr314. Die Methylgruppe in 6-Position der Kopfgruppe füllt eine kleine Tasche nahe Val444, wodurch womöglich die Selektivität von **90** für PPARα gegenüber den anderen PPAR Subtypen zustande kommt. In PPARγ(Leu453) und PPARδ(Met417) ist das relativ kleine Val444 von PPARα durch größere Aminosäuren ersetzt, die den Raum an der Spitze von Arm I limitieren. (Helix 3 (rot); Oberfläche der Ligandbindetasche (grau))

Mit seiner hohen Aktivität an PPARα und FXR ist **90** ein potenter dualer PPARα/FXR Partialagonist. Da beide Rezeptoren im Zusammenspiel wichtige Rollen im Metabolismus und Transport von Lipiden[45,126,127] erfüllen, bietet die duale Aktivität von **90** ein neues Prinzip, parallel über zwei Angriffspunkte in die Lipidhomöostase einzugreifen, das ausgehend von **90** weiter in vitro und in vivo untersucht werden kann. Die Verbindung **90** könnte dabei die antiarteriosklerotischen und lipidsenkenden Wirkungen der PPARα-Aktivierung mit den triglyceridsenkenden und hepatoprotektiven Effekten von FXR vereinen und dadurch mögliche Synergien erzeugen. **90** ist außerdem selektiv über PPARγ und PPARδ und zeigte erst ab 50 µM schwache toxische Effekte in vitro.

Durch geeignete Substituenten konnte also die Selektivität der Acylanthranilamide zu FXR, PPARα und PPARγ verschoben und so neben dem selektiven FXR-Partialgonisten **101** auch die PPARγ-superagonistische Leitstruktur **85** sowie der duale PPARα/FXR Partialagonist **90** identifiziert werden. Durch Rekombination der Ergebnisse obiger SAR-Studien wurde außerdem versucht, die Potenz und Selektivität der Acylanthranilamide an PPARδ zu verbessern. Da der für die meisten Untersuchungen eingesetzte 4-*tert*-Butylbenzoylsubstituent sich jedoch an PPARδ als weitgehend inaktiv herausgestellt hatte, besaßen die Ergebnisse für PPARδ nur eine begrenzte Aussagekraft, sodass die SAR an PPARδ durch Synthese geeigneterer Derivate ergänzt wurden (vgl. Tabelle 14). Insbesondere die Derivate für die Untersuchungen der SAR einer Substitution des zentralen aromatischen Ringes (**95**-**98**) waren für PPARδ ungeeignet, da die unsubstituierte Vergleichssubstanz **64** an PPARδ inaktiv war und somit womöglich eine Aktivitätssteigerung sowie vor allem ein Aktivitätsverlust durch einen zusätzlichen Substituenten verborgen blieben. Daher wurden basierend auf der an PPARδ

agonistischen Verbindung **69** neue am zentralen aromatischen Ring substituierte Derivate (**127**-**129**) synthetisiert und charakterisiert. Dabei zeigte sich, dass ein zusätzliches Chloratom in 4-Position (**127**) die Maximalaktivierung deutlich senkte, während ein zusätzliches Chloratom in 5-Position (**128**) den EC_{50}-Wert verschlechterte und Chlorierung in 6-Position (**129**) des zentralen aromatischen Ringes gänzlich zur Inaktivität führte. Eine zusätzliche Substitution am zentralen Aromaten schien also keine Verbesserung der PPARδ-Aktivität zu ermöglichen.

In den obigen SAR-Studien hatten sich im Gegensatz zum 4-*tert*-Butylbenzoylsubstituenten kleinere 4-substituierte Benzoylgruppen (**62**, **69**, **70**) an PPARδ als aktiv erwiesen, wobei der 4-Trifluoromethylbenzoylsubstituent (**69**) die höchste Aktivität lieferte. Daneben war das 4-*tert*-butylbenzoylsubstituierte 3-Aminophenylessigsäurederivat **83** an PPARδ aktiv, während die jeweils um eine Methylengruppe verkürzte (**64**) bzw. verlängerte (**84**) Verbindung inaktiv war. Diese Erkenntnisse wurden in Verbindung **130** kombiniert und dadurch eine leichte Aktivitätssteigerung an PPARδ erzielt. Wie bereits für **84** beobachtet, führte die Verlängerung der aziden Seitenkette von **130** in **131** zur Verschlechterung des EC_{50}-Wertes, **131** zeigte jedoch als erstes Acylanthranilamidderivat voll- bis superagonistische Aktivität an PPARδ. Interessanterweise bewirkte auch eine Verlängerung des Acylsubstituenten von **69** durch Einführung einer 4-Biphenylgruppe in **132** superagonistische Aktivität. **132** war an allen drei PPAR-Subtypen mit niedrig micromolaren EC_{50}-Werten superagonistisch aktiv und kann daher als Leitstruktur zur Entwicklung von pan-PPAR-Superagonisten dienen.

Innerhalb der Verbindungen **69**, **130** und **131** erwies sich die 3-Aminophenylessigsäure (**130**) als geeignetste azide Kopfgruppe zur Entwicklung potenter PPARδ-Agonisten. Abschließend wurde daher versucht, mit dieser Kopfgruppe durch Variation des Acylsubstituenten (**133**-**138**) die Potenz und Selektivität an PPARδ zu steigern. Da besonders kleine 4-substituierte Benzoylgruppen (**62**, **69**, **70**) sowie die 2-Naphthoylgruppe (**57**) gute Ergebnisse an PPARδ gezeigt hatten, wurden dabei Analoga dieser Acylsubstituenten eingeführt.

Ersetzen der 4-Trifluoromethylgruppe (**69**) mit einer 4-Methylmercaptogruppe (**133**) steigerte deutlich die Maximalaktivierung bei etwas schlechterem EC_{50}-Wert, während eine 4-Trifluoromethylmercaptogruppe (**134**) wiederum partialagonistische Aktivität bei niedrigerem EC_{50}-Wert aufwies. Beide Verbindungen waren jedoch nicht selektiv für PPARδ, sondern ähnlich aktiv an PPARα, PPARγ und FXR. Das 4-Cyanoderivat **135** war hingegen an allen PPARs und an FXR inaktiv. Erst die Einführung einer 4-Methoxygruppe (**136**) führte zu gewisser Selektivität für PPARδ. **136** zeigte partialagonistische Aktivität mit einem niedrig micromolaren EC_{50}-Wert an PPARδ, war inaktiv an FXR und nur schwach aktiv an PPARα und PPARγ. Das potenteste Acylanthranilamidderivat an PPARδ war jedoch **137** mit einem 2-Naphthoylsubstituenten. **137** zeigte PPARδ-superagonistische Aktivität mit einem EC_{50}-Wert von 1,3±0,1 µM und Präferenz für PPARδ über PPARα und PPARγ. Der abschließende

Versuch, die potente PPARδ-agonistische Aktivität sowie die Tendenz zur Selektivität des 4-Methoxybenzoyl- (**136**) und des 2-Naphthoylsubstituenten (**137**) in einer 3,4-Dimethoxygruppe (**138**) zu vereinen, führte zu Inaktivität an allen PPARs und FXR.

Tabelle 14**: In vitro PPAR-/FXR-Aktivität der Derivate **127-138 (MW±SEM; n = 3-6; i.a. - inaktiv)

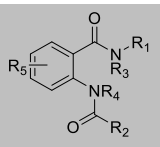

#	R_1	R_2	R_3	R_4	R_5	EC_{50} [µM] (max. rel. Aktivierung [%]) PPARα	PPARγ	PPARδ	FXR
69	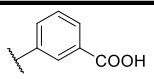	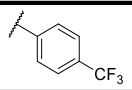	H	H	-	5,8±2,8 (79±15)	8,5±0,5 (384±13)	3,2±0,7 (46±5)	6,9±0,2 (26±1)
127	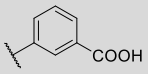	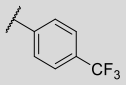	H	H	4-Cl	18,6±0,5 (255±11)	8,7±1,3 (420±49)	3,4±0,3 (16,5±0,5)	2,1±0,3 (17,8±1,0)
128	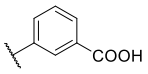	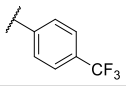	H	H	5-Cl	25±2% @10 µM	4,7±1,4 (415±49)	6,3±0,4 (24±1)	3,4±0,5 (16,9±0,5)
129	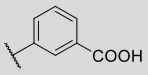	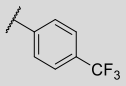	H	H	6-Cl	i.a.	i.a.	i.a.	i.a.
130	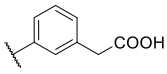	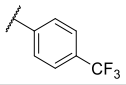	H	H	-	5,4±1,4 (69±9)	9,4±3,4 (161±37)	2,2±0,1 (58±1)	2,60±0,02 (14,8±0,1)
131	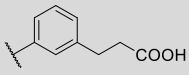	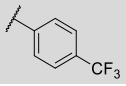	H	H	-	5,9±0,4 (101±1)	6,9±0,3 (70±3)	6,8±2,2 (120±23)	2,3±0,1 (13,0±0,1)
132	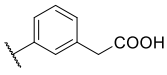	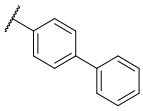	H	H	-	3,0±0,2 (109±5)	2,6±0,2 (125±7)	6,4±1,0 (175±23)	0,7±0,1 (18,8±0,3)
133	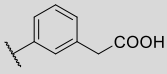	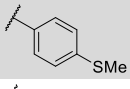	H	H	-	14,4±3,6 (250±47)	17,4±1,7 (200±15)	7,4±0,6 (133±6)	8,5±2,2,0 (16,9±1,3)
134	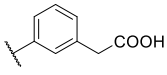	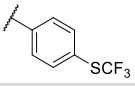	H	H	-	1,3±0,2 (73±3)	4,4±0,1 (158±2)	2,3±0,5 (64±6)	7,0±2,5 (23±2)
135	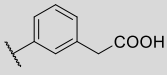	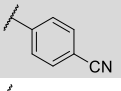	H	H	-	i.a.	i.a.	i.a.	i.a.
136	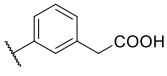	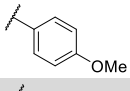	H	H	-	17,3±0,2% @10 µM	13,2±0,6% @ 10 µM	5,9±0,5 (54±2)	i.a.
137	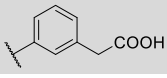	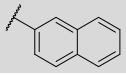	H	H	-	14,4±2,5 (248±22)	18,0±4,7 (335±58)	1,3±0,1 (147±3)	2,5±0,2 (20,9±0,3)
138	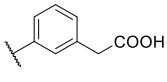	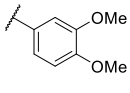	H	H	-	i.a.	i.a.	i.a.	i.a.

Das 2-Naphthoylderivat **137** zeigte somit das beste Aktivitätsprofil mit Präferenz für PPARδ über PPARα (Faktor 11) und PPARγ (Faktor 13) sowie relativer Selektivität über FXR (Superagonismus gegenüber Partialagonismus). **137** war daneben in vitro metabolisch sehr stabil (80,5±0,3% nach 60 min.), hatte akzeptable physikochemische Eigenschaften (Wasserlöslichkeit: 2,5 mg/L; clogP = 4,2) und zeigte erst ab 50 µM leichte toxische Effekte auf Leberzellen (HepG) in vitro. Die Verbindung stellt somit eine potente Leitstruktur zur Entwicklung von selektiven PPARδ Agonisten dar, wobei

Dockingstudien von **137** an PPARδ (vgl. Abbildung 35) nahe legen, dass die Potenz der Verbindung mittels einer weiteren Vergrößerung des Acylsubstituenten durch kleine lipophile Gruppen noch gesteigert werden könnte.

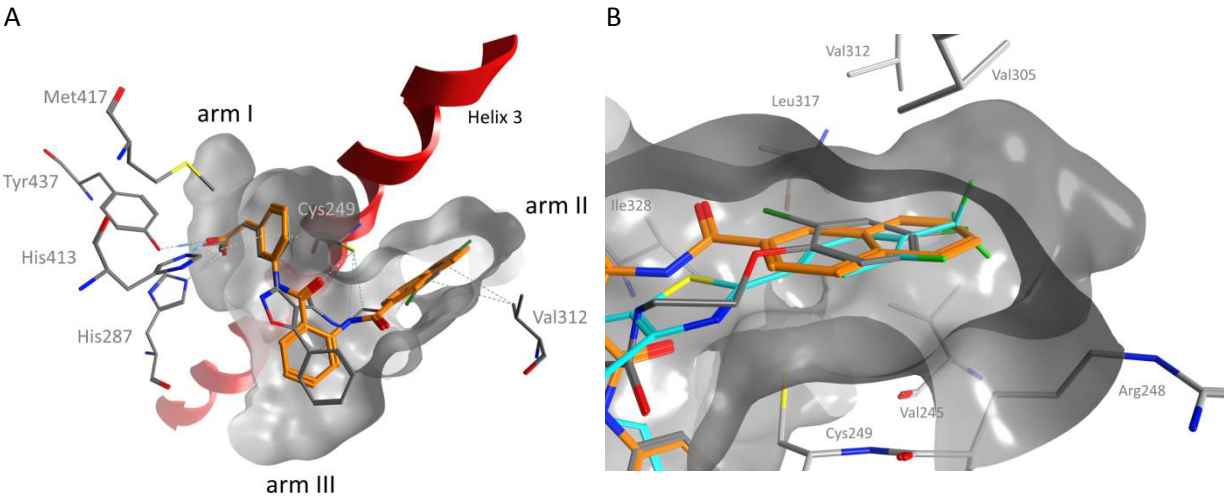

***Abbildung 35**: Dockingpose von **137** in der PPARδ-LBD:* (A) Aufgrund der verlängerten Säureseitenkette kann **137** besser mit dem H-Brückennetzwerk der Aminosäuren Tyr437, His413, Thr253 und His287 interagieren. (B) Das 2-Naphthylsystem (orange) von **137** belegt wie die lipophilen Substituenten der PPARδ-Agonisten LCI765 (grau) und GW0742 (blau) die lipophile Tasche von Arm II. Möglicherweise könnte die Potenz von **137** an PPARδ durch Erweiterung der 2-Naphthoylgruppe mit lipophilen Substituenten noch gesteigert werden.

Mit dem selektiven PPARγ-Superagonisten **85**, dem PPARδ-Superagonisten **137**, dem pan-PPAR-Superagonisten **132** sowie dem dualen PPARα/FXR-Partialagonisten **90** wurden somit zusätzlich zum selektiven FXR-Partialagonisten **101** Acylanthranilamidderivate mit variablen Aktivitätsprofilen an unterschiedlichen nukleären Rezeptoren identifiziert, die als potente Leitstrukturen für weitere Studien dienen können. Die dual aktive Verbindung **90** besitzt dabei bereits ausreichend hohe Potenz, um eventuelle synergistische Effekte von PPARα- und FXR-Aktivierung in vitro oder in vivo studieren zu können. Im Zuge der SAR-Studien wurden konkrete strukturelle Elemente zur selektiven Aktivitätssteigerung an den einzelnen PPARs sowie FXR identifiziert (vgl. Abbildung 36) und dadurch das große Potential der Acylanthranilamide als Modulatoren verschiedener nukleärer Rezeptoren aufgezeigt.

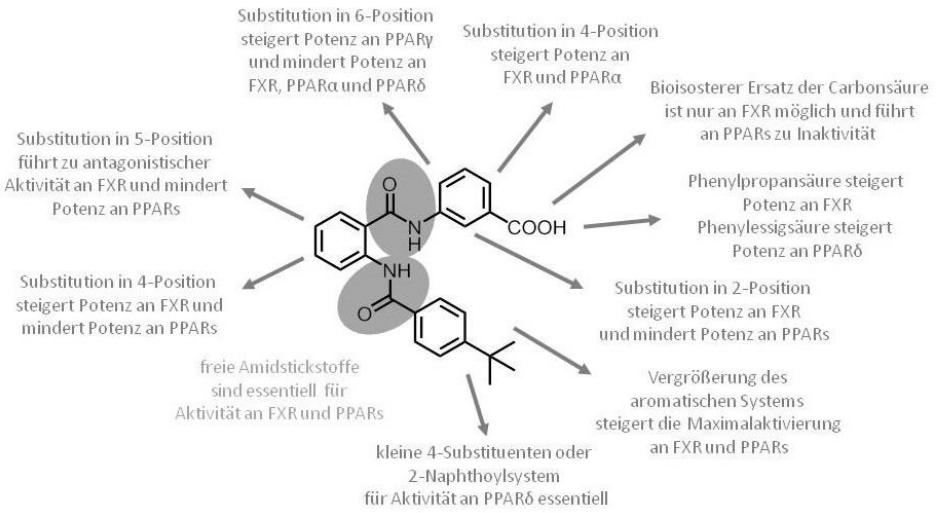

***Abbildung 36**: Struktur-Aktivitätsbeziehungen der Acylanthranilamide an FXR und PPARs und Möglichkeiten der Selektivitätssteigerung durch geeignete Substituenten*

2.4 In vitro pharmakologische Charakterisierung von DM336 (101)

2.4.1 Effekt von DM336 (101) auf FXR-Targetgene

Um die FXR-agonistische Aktivität der optimierten Verbindung DM336 (**101**) in einem weniger artifiziellen Testsystem als dem Reportergenassay näher zu untersuchen und die partialagonistische Aktivität zu belegen, wurde der Effekt der Substanz auf die Expression von FXR-Targetgenen auf mRNA-Ebene mit Hilfe der quantitativen real time PCR (qRT-PCR) bestimmt. Als positive Kontrolle diente hierbei der natürliche FXR-Agonist CDCA (**1**), um möglichst physiologische Bedingungen zu schaffen. Um einen reproduzierbaren Effekt der Testsubstanzen auf die Genexpression zu erzielen, wurden zunächst die Bedingungen bei der Kultivierung der Zellen optimiert. Da FXR vor allem in der Leber und im Darm eine wichtige Rolle spielt und in Hepatozyten und Darmepithelzellen konstitutiv exprimiert wird, wurden die Leberkarzinomzelllinie HepG2 sowie die Adenomzelllinie HT29 für die Untersuchungen mittels qRT-PCR gewählt. In Anlehnung an publizierte Methoden erfolgte vor der Behandlung mit den Testsubstanzen eine Kultivierung der Zellen in einem Minimalkulturmedium über 24-48 Stunden, um Einflüsse von im Medium enthaltenen Wachstumsfaktoren und einem Überangebot an Nährstoffen auf die FXR-Aktivität auszuschließen. Die Zellen wurden außerdem nach unterschiedlichen Inkubationszeiten mit den Testsubstanzen untersucht, um festzustellen, nach welcher Zeitspanne die Effekte am ausgeprägtesten waren. Es zeigte sich, dass in HepG2-Zellen zur Quantifizierung von BSEP 6 Stunden Inkubation am günstigsten sind, für SHP ein Zeitraum von 18 Stunden und für CYP7A1, das ein indirektes FXR-Targetgen darstellt, 24 Stunden. Die Quantifizierung von OSTα lieferte sowohl nach 6 Stunden Inkubation als auch nach 18 Stunden reproduzierbare Ergebnisse. IBABP wurde in HT29-Zellen nach 24 Stunden quantifiziert.

Bei der Wahl der Primer wurde zunächst auf in der Literatur beschriebene Primer zurückgegriffen und bezüglich der Targetgene SHP und CYP7A1 lieferten die publizierten Primer reproduzierbare Ergebnisse. Für die Targetgene BSEP, OSTα und IBABP zeigte sich jedoch, dass die in der Literatur beschriebenen Primer fehlerhaft waren, sodass für diese Gene neue Primer entwickelt wurden. Eine detaillierte Methodenbeschreibung zur Targetgenquantifizierung mit allen Primersequenzen ist publiziert (Merk D et al. *J. Med. Chem.*, **2014**).

Um die partialagonistische Aktivität von DM336 (**101**) durch Quantifizierung der FXR-Targetgen-mRNA zu belegen, wurde der Effekt von **101** bei mehreren Konzentrationen (0,1 µM, 0,3 µM, 1,0 µM, 3,0 µM, 10 µM) oberhalb des EC_{50}-Wertes (0,008±0,003 µM) bestimmt und jeweils mit dem Effekt von CDCA (**1**) verglichen. Es stellte sich heraus, dass DM336 (**101**) bei allen untersuchten Konzentrationen auf alle fünf untersuchten Targetgene jeweils einen konstanten, also konzentrationsunabhängigen Effekt hervorrief. Der beobachtete Effekt erreichte zudem für alle untersuchten Targetgene etwa 40-50% des Effektes von CDCA (**1**), sodass FXR durch **101** nur partial aktiviert wurde. Für

das Targetgen BSEP wurde außerdem die Aktivität von GW4064 (**4**) untersucht und mit DM336 (**101**) verglichen, da GW4064 (**4**) BSEP besonders[8,86] effektiv aktiviert und zudem im auf einem BSEP-Promotor-basierten Reportergenassay als Referenzsubstanz zum Einsatz kam. Wie bereits im Reportergenassay erreichte der Maximaleffekt von DM336 (**101**) auch bei der Quantifizierung der BSEP-mRNA etwa 20% des Effekts von GW4064 (**4**). Damit stellt DM336 (**101**) einen echten FXR-Partialagonisten dar, der den nukleären Rezeptor nur mit einer moderaten Amplitude aktiviert.

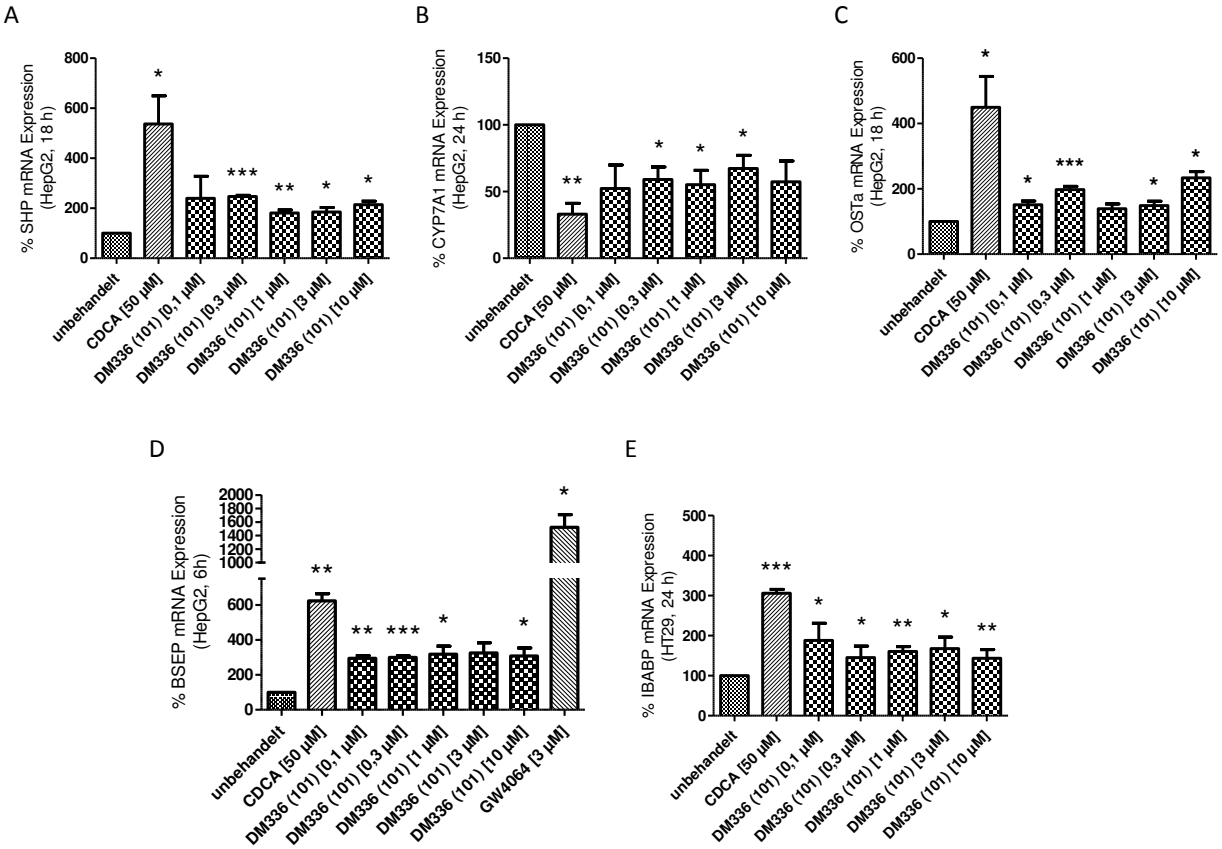

Abbildung 37: *Effekt von DM336 (**101**) auf die FXR-Targetgene SHP (A), CYP7A1 (B), OSTα (C), BSEP (D) und IBABP (E) in vitro*: **101** stellt einen echten FXR-Partialagonisten dar, da sein Effekt auf die Targetgene bei unterschiedlichen Konzentrationen (0,1; 0,3; 1; 3 und 10 µM) oberhalb des EC_{50}-Wertes (8±3 nM) konstant ist und etwa 40% des Effektes des physiologischen FXR-Agonisten CDCA (**1**) ausmacht.

2.4.2 In vitro Toxizität von DM336 (101)

Die pharmakologische Wirkung von FXR-Liganden entfaltet sich insbesondere in Leberzellen, wo FXR konstitutiv exprimiert wird und eine wichtige Rolle in der Kontrolle von Metabolismus und Homöostase, aber auch in der Leberprotektion spielt. Daher ist für die Charakterisierung von an FXR aktiven Substanzen vor allem die Toxizität auf Hepatocyten interessant. DM336 (**101**) wurde deshalb hinsichtlich seiner Toxizität auf HepG2-Zellen mit zwei typischen Testsystemen untersucht. Zur Bestimmung einer möglichen antiproliferativen Wirkung eignete sich dabei ein WST-1-Assay, in dem DM336 (**101**) ab einer Konzentration von 30 µM einen nennenswerten antiproliferativen Effekt zeigte, der bei 100 µM sehr stark ausgeprägt war. Die Charakterisierung der akuten Toxizität erfolgte

durch Messung der LDH-Aktivität, wobei etwa das gleiche Ergebnis eines moderat toxischen Effekts bei 30 µM mit einer erheblichen Steigerung bei 100 µM beobachtet wurde (vgl. Abbildung 38).

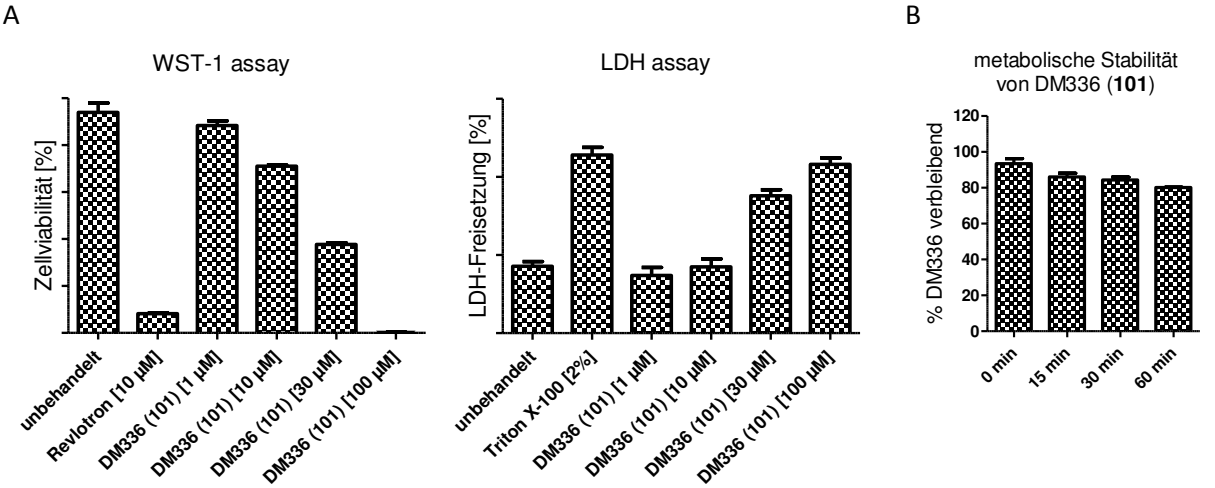

Abbildung 38: *In vitro Toxizität (A) von DM336 (**101**) auf HepG2-Zellen und metabolische Stabilität (B)*: **101** zeigte bis zu Konzentrationen von 10 µM, was mehr als die 1000-fache Konzentration seines EC_{50}-Wertes darstellt, keine nennenswerte Toxizität. **101** war in vitro außerdem sehr stabil gegen eine Metabolisierung durch Lebermikrosomen.

Insgesamt stellte sich die Toxizität von DM336 (**101**) gemessen an seiner hohen Potenz an FXR jedoch als vernachlässigbar heraus, denn bis zu einer Konzentration von 10 µM wurden keine nennenswerte Akuttoxizität oder antiproliferative Wirkung beobachtet. Die in vitro pharmakologischen Effekte von **101** im Reportergenassay und bei der FXR-Targetgen-Quantifizierung erreichten ihr Maximum jedoch spätestens bei einer Konzentration von 0,3 µM, also weit unterhalb toxischer Konzentrationen.

2.4.3 Metabolische Stabilität von DM336 (101)

Als potentiell für in vivo Untersuchungen geeignete Substanz bedurfte DM336 (**101**) außerdem guter metabolischer Stabilität. In in vitro Metabolisierungsstudien wurde in Lebermikrosomen von Sprague−Dawley Ratten innerhalb einer Stunde nur etwa ein Fünftel von DM336 (**101**) verstoffwechselt, was für eine sehr gute metabolische Stabilität spricht (vgl. Abbildung 38). Allerdings ist zu beachten, dass die in vitro Metabolisierung mit Lebermikrosomen nur Phase-1-Metabolismusreaktionen abbildet. Da sich die freie Carbonsäure von DM336 (**101**) aber für Phase-2-Reaktionen wie eine Glucoronidierung anbietet, besteht hier dennoch die Möglichkeit intensiver Verstoffwechselung von **101**. Die SAR-Studien haben aber gezeigt, dass ein bioisosterer Ersatz der freien Carbonsäure in **101** beispielsweise durch ein Nitril (**76**) oder ein Methylketon (**75**) ohne nennenswerten Verlust an Aktivität toleriert wird, sollte eine zu hohe Phase-2-Metabolisierung auftreten.

2.4.4 Selektivität von DM336 (101)

Zur Bestimmung der Selektivität von DM336 (**101**) für FXR wurde seine Aktivität an wichtigen off-targets untersucht. Für einen FXR-Partialagonisten spielt dabei vor allem die Aktivität am zweiten Rezeptor für Gallensäuren, nämlich dem membranständigen G-Proteingekoppelten Rezeptor TGR5,

eine große Rolle. Hier zeigte sich DM336 (**101**) als inaktiv bis zu Konzentrationen von 100 µM. Da für so hohe Konzentrationen aber auch Toxizität beobachtet wurde, kann nur von einer Inaktivität an TGR5 bis zu 30 µM ausgegangen werden. Damit ist DM336 (**101**) selektiv für FXR über TGR5 mit einem Faktor >1000.

Neben TGR5 war außerdem, wie bereits dargelegt, die Aktivität von **101** an den PPARs von großem Interesse, da sie zusammen mit FXR und weiteren nukleären Rezeptoren ein komplexes Netzwerk metabolischer Regulatoren bilden. Während sich DM336 (**101**) als inaktiv an PPARδ herausstellte, zeigte die Substanz schwache agonistische Aktivität an den PPAR-Subtypen α und γ (vgl. Abildung 39). Für PPARα lag der EC_{50}-Wert dabei über 10 µM und wurde nicht bestimmt. Für PPARγ ergab sich ein EC_{50}-Wert von 3,0±0,1 µM (81±2% max.). Somit war DM336 (**101**) auch selektiv über PPARα (Faktor >1000), PPARγ (Faktor ~ 375) und PPARδ (Faktor >1000). Da sich außerdem die Leitstruktur **64** inaktiv an 5-Lipoxigenase (5-LO) und den Cyclooxygenasen COX-1 und COX-2 gezeigt hatte, kann erwartet werden, dass auch DM336 (**101**) selektiv über diese beiden off-targets ist. Somit stellt **101** einen hochselektiven FXR-Partialagonisten dar.

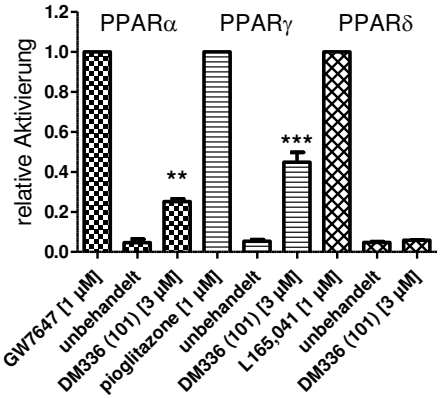

***Abbildung 39**: Aktivität von DM336 (**101**) an PPARs*: **101** ist mit einem Faktor >1000 selektiv über PPARα und PPARδ und mit einem Faktor von etwa 375 selektiv über PPARγ.

3. Ausblick

In den SAR-Studien dieser Arbeit wurde die Aktivität der Substanzklasse der Acylanthranilamide als FXR-Liganden ausgehend von der schwach aktiven Leitstruktur JA10 (**32**) in mehreren Schritten um mehr als einen Faktor 1000 optimiert und mit DM336 (**101**) ein hochpotenter FXR-Partialagonist identifiziert (vgl. Abbildung 40). Mit seinem guten Aktivitäts- und Selektivitätsprofil, seiner geringen Toxizität und seiner großen metabolischen Stabilität kann sich DM336 (**101**) für in vivo Studien des FXR-Partialagonismus empfehlen.

Neben **101** wurde der potente duale PPARα/FXR-Partialagonist **90** entwickelt, der ebenfalls gute Eigenschaften für weitere in vitro und in vivo Studien bietet. Aus den in dieser Arbeit beschrie-benen Verbindungen ergeben sich außerdem potente neue Leitstrukturen als Ausgangspunkte von SAR- und Optimierungsstudien zu FXR-Antagonisten (**97**), pan-PPAR-Superagonisten (**132**), PPARγ-Superagonisten (**85**) und PPARδ-Superagonisten (**137**).

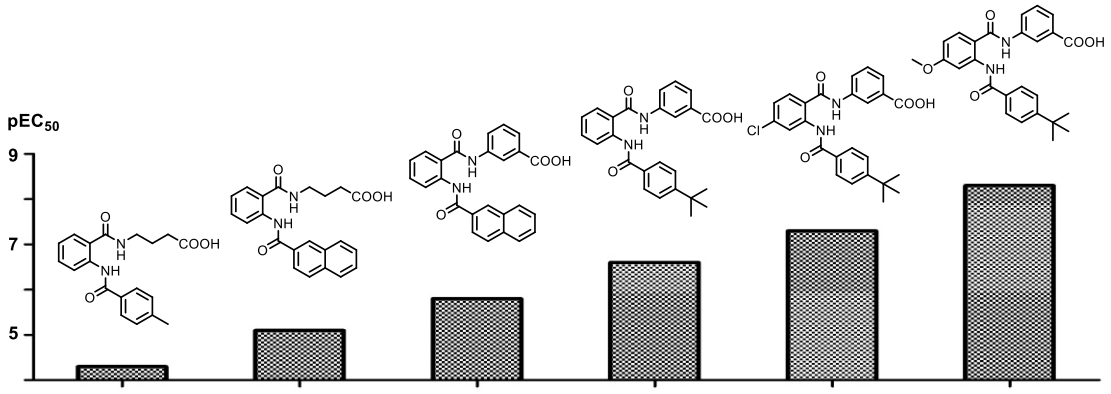

	JA10 (**32**)	DM21 (**44**)	DM113 (**57**)	DM179 (**64**)	DM224 (**96**)	DM336 (**101**)
EC_{50}	n.b.	8,6±1,3 µM	1,5±0,2 µM	0,28±0,03 µM	123±7 nM	8±3 nM
pEC_{50}	(4-5)	5,1	5,8	6,6	6,9	8,1
max. Akt.	11% @30 µM	37±2%	37±1%	9,4±0,2%	22,0±0,3%	17,5±0,7%
MG	340	376	410	416	451	447
Löslichkeit (H_2O)	n.b.	45 mg/L 120 µM	0,3 mg/L 0,7 µM	n.b.	n.b.	2,6 mg/L 5,8 µM
clogP	2,68	3,35	4,96	5,62	6,44	5,65
metabolische Stabilität	n.b.	92±2% (60 min.)	61±2% (60 min.)	n.b.	n.b.	80,2±0,2% (60 min.)
Toxizität	n.b.	≥100 µM	≥30 µM	n.b.	n.b.	≥30 µM
off-targets			*EC_{50} (Maximalaktivierung)*			
PPARα	n.b.	i.a.	2,0 µM (73%)	1,3 µM (37%)	>10 µM	>10 µM
PPARγ	n.b.	18 µM (432%)	5,5 µM (126%)	3,9 µM (348%)	9 µM (256%)	3,0 µM (81%)
PPARδ	n.b.	i.a.	4,7 µM (51%)	i.a.	i.a.	i.a.
TGR5	n.b.	n.b.	inaktiv	inaktiv	n.b.	inaktiv

Abbildung 40: *Evolution der Acylanthranilamide als FXR-Partialagonisten*: Im Zuge der in dieser Arbeit durchgeführten SAR- und Optimierungsstudien wurde die Aktivität der Acylanthranilamide an FXR ausgehend von der Leitstruktur JA10 (**32**) in mehreren Schritten um mehr als einen Faktor 1000 gesteigert und der hochpotente und selektive FXR-Partialagonist DM336 (**101**) entwickelt. **101** weist neben seiner großen Potenz an FXR hohe Selektivität, geringe Toxizität und gute physikochemische Eigenschaften auf. (n.b. - nicht bestimmt; i.a. - inaktiv, MG - Molekulargewicht)

Daneben wird derzeit mit dem ebenfalls in dieser Arbeit identifizierten FXR-Partialagonisten DM175 (**63**) der molekulare Mechanismus des FXR-Partialagonismus auf Basis von Co-Kristallstrukturen der FXR-LBD mit dem physiologischen Liganden CDCA (pdb-ID: 4QE8, **1**) und mit DM175 (**63**, pdb-ID: 4QE6) sowie einer Apostruktur der FXR-LBD analysiert. Die zur Kristallisation verwendete Verbindung **63** wurde wie **101** eingehend in vitro pharmakologisch charakterisiert und ihr partialagonistisches Profil an zahlreichen FXR-Targetgenen bestätigt (vgl. Abbildung 41).

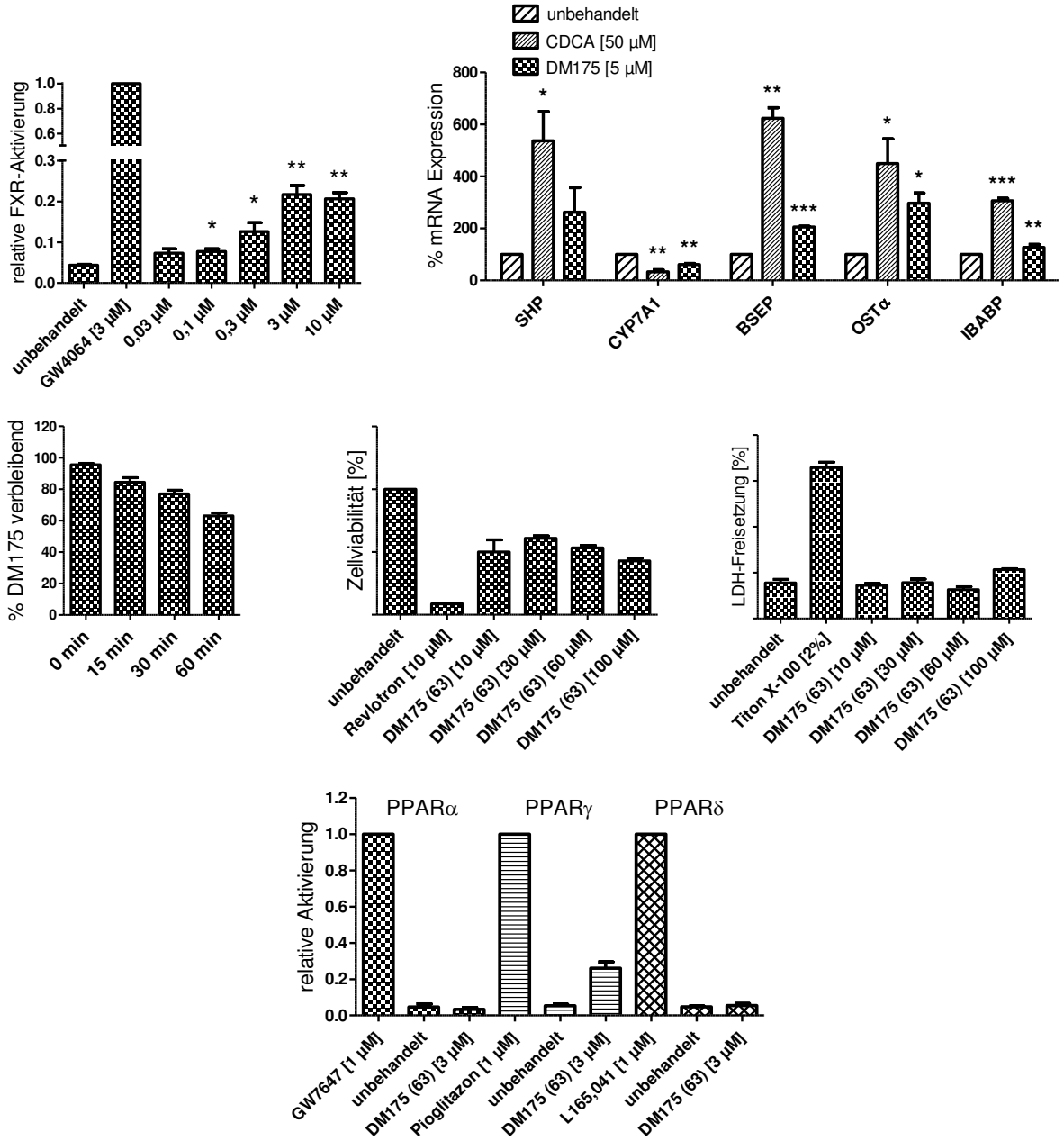

Abbildung 41: *In vitro pharmakologische Charakterisierung von DM175 (**63**)*: (A) **63** zeigte einen EC_{50}-Wert von 0,35±0,06 µM im Reportergenassay und erreichte bereits bei 3 µM sein Aktivitätsmaximum von etwa 20% der Aktivität von GW4064 (**4**). (B) Effekt von **63** auf die FXR-Targetgene SHP, CYP7A1, BSEP, OSTα, und IBABP in vitro: **63** stellt einen echten FXR-Partialagonisten dar, da sein Effekt auf die Targetgene bei 5 µM – einer Konzentration auf dem Plateau des Aktivitätsmaximums – nur etwa 40% des Effektes von CDCA (**1**) ausmachte. (C) **63** zeigte gute metabolische Stabilität in Lebermikrosomen. (D) **63** wirkte im Konzentrationsbereich 10-100 µM schwach antiproliferativ auf HepG2-Zellen, aber nicht akut toxisch. (E) **63** zeigte Selektivitäz über PPARα und PPARδ und Präferenz für FXR über PPARγ (Faktor ~ 15). **63** war außerdem inaktiv an TGR5.

4. Zusammenfassung

Als zellulärer Regulator, der eine Vielzahl metabolischer und inflammatorischer Gene kontrolliert, stellt der nukleäre Farnesoid X Rezeptor (FXR) ein vielversprechendes neues Wirkstofftarget dar. Physiologisch wird FXR durch Gallensäuren wie die Chenodeoxycholsäure (CDCA, **1**) aktiviert und spielt dadurch eine wichtige Rolle in Gallensäuremetabolismus und -homöostase. Die Aktivierung von FXR mit natürlichen oder synthetischen Liganden führte in vitro und in vivo zu zahlreichen wünschenswerten Effekten wie gesteigerter Insulinfreisetzung, verringerter Insulinresistenz oder verbessertem Lipidprofil. Daneben stellt die Aktivierung von FXR ein Prinzip zur Behandlung der Lebererkrankungen nicht-alkoholische Fettleber und primäre billiäre Zirrhose dar. Mit 6-ECDCA (**5**) befindet sich derzeit der erste FXR-Ligand in Phase 3 der klinischen Entwicklung zur Therapie dieser gravierenden Leberpathophysiologien.

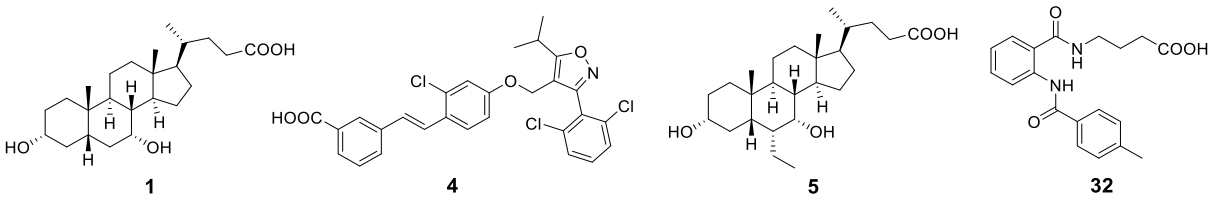

***Abbildung 43**: Physiologischer FXR-Agonist CDCA (**1**), synthetische FXR-Agonisten GW4064 (**4**) und 6-ECDCA (**5**) und Leitstruktur JA10 (**32**)*

Existierende synthetische FXR-Liganden stellen strukturell Fettsäure- bzw. Gallensäuremimetika dar und imitieren auf diese Weise den physiologischen FXR-Agonisten CDCA (**1**). In den Übersichtsarbeiten (Merk D, Steinhilber D, Schubert-Zsilavecz M. *Future Med Chem,* **2012** und Lamers C, Schubert-Zsilavecz M, Merk D. *Current Trends in Medicinal Chemistry,* **2014**) sind die verfügbaren agonistischen und antagonistischen FXR-Liganden sowie deren Co-Kristallstrukturen und deren pharmakologische Wirkungen zusammengefasst und diskutiert. Die meisten dieser synthetischen FXR-Liganden sind jedoch aufgrund von Toxizität, geringer Selektivität oder schlechter Bioverfügbarkeit nicht zur weiteren klinischen Entwicklung geeignet. Sie stellen außerdem vornehmlich vollagonistische FXR-Liganden dar. Wie jedoch die klinischen Erfahrungen mit Liganden anderer nukleärer Rezeptoren wie den Peroxisomen Proliferator-aktivierten Rezeptoren (PPAR) oder den Estrogenrezeptoren (ER) gezeigt haben, birgt eine zu starke Aktivierung eines Liganden-aktivierten Transkriptionsfaktors Risiken erheblicher Nebenwirkungen. Im Tiermodell wurden für FXR bereits vergleichbare unerwünschte Wirkungen einer Überaktivierung beschrieben. Eine Möglichkeit, dieser Gefahr vorzubeugen, stellt die Entwicklung partialagonistischer FXR-Liganden dar, die den Rezeptor nur mit moderater Amplitude aktivieren.

In dieser Arbeit wurde ausgehend von der Leitstruktur JA10 (**32**), die in einem virtuellen Struktur- und Liganden-basierten Screening als moderat potenter FXR-Ligand identifiziert wurde, durch medizinisch chemische Optimierung und Untersuchungen zu den Struktur-Aktivitäts-Beziehungen

(SAR) ein potenter und selektiver FXR-Partialagonist entwickelt. JA10 (**32**) zeigte im *full-length* FXR Reportergenassay eine Aktivität von 14,5±1,3% bei 30 µM verglichen mit der Aktivität der Referenzsubstanz GW4064 (**4**) bei 3 µM.

Die Leitstruktur JA10 (**32**) wurde in drei Molekülteile – die azide Kopfgruppe, den zentralen Anthranilamidkörper und den Acylsubstituenten – aufgespalten und jeder dieser Molekülbausteine hinsichtlich der Potenz an FXR optimiert. Ausgehend von JA10 (**32**) wurden zunächst mit geeigneten Derivaten die SAR des Acylsubstituenten untersucht, wobei sich ein 2-Naphthoyl- (**44**) und ein 4-*tert*-Butylbenzoylsubstituent (**43**) als der in JA10 (**32**) enthaltenen 4-Methylbenzoylgruppe überlegen zeigten. Mit EC_{50}-Werten von 8,6±1,3 µM (37±2% Maximalaktivierung) für **44** bzw. 2,5±0,4 µM (19±1% max.) für **43** stellten beide Verbindungen eine deutliche Verbesserung gegenüber der Leitstruktur **32** dar.

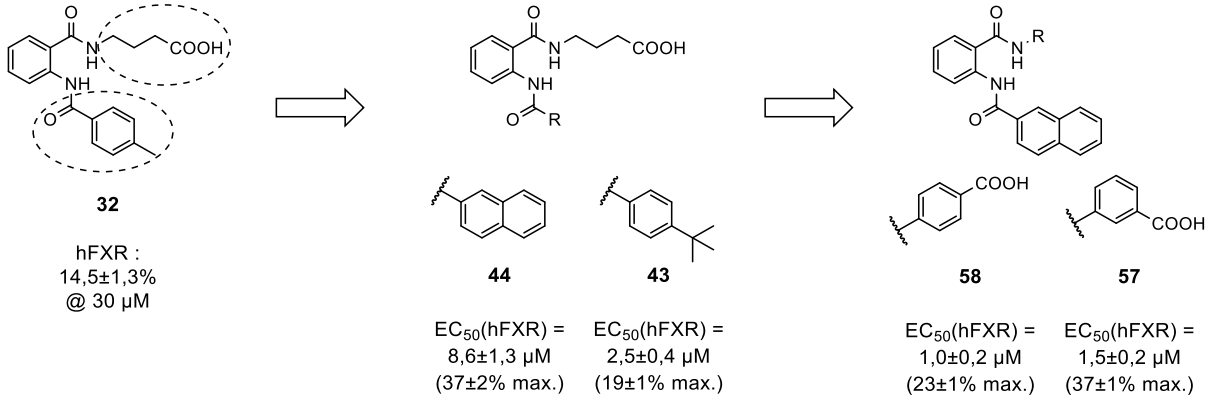

(Merk D et al. *Bioorg. Med. Chem.*, **2014**)

***Abbildung 44**: Ergebnisse der ersten SAR-Studie mit **57** als potentestem Derivat* (MW±SEM; n = 3-6)

In den folgenden SAR-Studien wurde die 2-Naphthoylgruppe als Acylsubstituent beibehalten. Eine selektive Reduktion bzw. Methylierung zeigte, dass beide Amidbindungen der Acylanthranilamide für die Aktivität an FXR essentiell sind. Dockinguntersuchungen deuteten darauf hin, dass dies einerseits mit der Geometrie der Säureamidgruppen und zum anderen durch spezifische Wechselwirkungen mit dem Rezeptor zu erklären ist. Bei der anschließenden Variation der aziden Kopfgruppe gelang ein weiterer Aktivitätsgewinn durch die Einführung eines zusätzlichen aromatischen Ringes mit einer 3-Aminobenzoesäure (**57**, EC_{50} = 1,5±0,2 µM, 37±1% max.) oder einer 4-Aminobenzoesäure (**58**, EC_{50} = 1,0±0,2 µM, 23±1% max.) statt der 4-Aminobuttersäure in JA10 (**32**). Das beste Derivat **57** dieser ersten SAR-Studie (Merk D et al. *Bioorg. Med. Chem.*, **2014**) zeigte gute metabolische Stabilität, geringe Toxizität sowie akzeptable Löslichkeit und stellte damit eine gute Leitstruktur für weitere Optimierungen dar. **57** aktivierte neben FXR allerdings auch alle PPAR Subtypen, sodass parallel zur Steigerung der Potenz an FXR auch die SAR der Acylanthranilamide an PPARs untersucht wurden, welche zur Publikation eingereicht sind (Merk D et al. *Bioorg. Med. Chem.*, submitted).

Die hinsichtlich des EC_{50}-Wertes besten Substituenten der obigen Untersuchungen, nämlich der 4-*tert*-Butylbenzoylsubstituent und die 3-Aminobenzoesäure als Kopfgruppe, wurden in **64** rekombiniert und auf diese Weise eine weitere deutliche Potenzsteigerung an FXR erreicht (EC_{50} = 0,28±0,03 µM, 9,4±0,2% max.). Mit **64** als optimierter Leitstruktur wurden anschließend in einer weiteren SAR-Studie (Merk D et al. *J. Med. Chem.*, **2014**) alle Molekülteile des Acylanthranilamidgerüstes weiter untersucht und optimiert. Während dabei im Bereich des Acylsubstituenten keine weitere Potenzsteigerung durch strukturelle Variation gelang, wurden sowohl im Bereich des zentralen Anthranilsäurekörpers als auch bei der aziden Kopfgruppe zusätzliche Substituenten und Molekülerweiterungen identifiziert, welche die Aktivität der Verbindungen an FXR erheblich verbesserten.

In der aziden Kopfgruppe konnte die freie Carbonsäurefunktion bei etwa gleicher Potenz der resultierenden Derivate durch verschiedene Bioisostere wie ein Nitril (**76**), ein Methylketon oder eine Methoxygruppe ersetzt werden. Diese bioisostere Substitution der potentiell gegen Metabolismus anfälligen Carbonsäure erlaubt eine mögliche Steigerung der metabolischen Stabilität. Daneben gewannen die bioisosteren Derivate Selektivität über alle PPAR Subtypen.

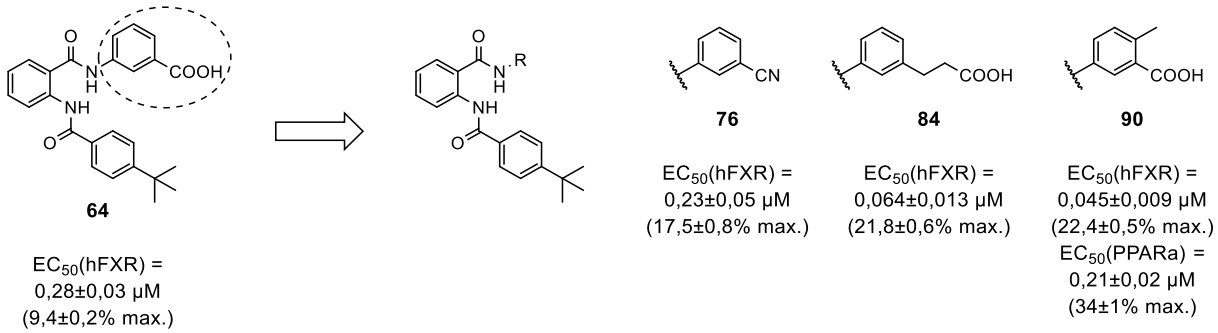

(Merk D et al. *J. Med. Chem.*, **2014**)

***Abbildung 45**: Ergebnisse der Untersuchungen zu den SAR der Kopfgruppe*; **90** stellt einen potenten dualen FXR/PPARα-Partialagonisten dar. (MW±SEM; n = 3-6)

Eine Verlängerung der Säureseitenkette um zwei Methyleneinheiten in Phenylpropansäurederivat **84** (EC_{50} = 0,064±0,013 µM, 21,8±0,6% max.) steigerte die Potenz an FXR deutlich, wobei interessanterweise das Phenylessigsäurederivat (**83**, EC_{50} = 0,42±0,13 µM, 26,4±1,4% max.) eine geringere Aktivität zeigte als das ursprüngliche Benzoesäurederivat **64**. Durch die Einführung eines zusätzlichen Substituenten in 6-Position der aziden Kopfgruppe in **90** (EC_{50} = 0,045±0,009 µM, 22,4±0,5% max.) konnte die FXR-Aktivität ebenfalls erhöht werden. Die SAR war hier jedoch sehr schmal, da neben der 6-Methylgruppe (**90**) nur eine 6-Methoxygruppe (**91**, EC_{50} = 0,047±0,001 µM, 19,1±0,5% max.) vergleichbare Potenz aufwies. Substitution in 6-Position der Kopfgruppe erhöhte allerdings auch die Aktivität an PPARα (**90**, EC_{50}(PPARα) = 0,21±0,02 µM, 34±1% max.), sodass für **90** keine ausreichende FXR-Selektivität gegeben war. **90** stellt jedoch einen potenten dualen FXR/PPARα-Partialagonisten

dar, der als Modellsubstanz zur Untersuchung eventueller Synergien aus dualer FXR/PPARα-Aktivierung dienen kann.

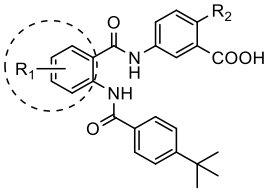

#	R_1	R_2	EC_{50} [µM] (max. rel. Aktivierung [%]) FXR	PPARα	PPARγ	PPARδ
64	-	H	0,28±0,03 (9,4±0,2)	1,3±0,3 (37±3)	3,9±0,5 (348±26)	i.a.
96	4-Cl	H	0,12±0,01 (22±1)	> 10	9±1 (256±16)	i.a.
97	5-Cl	H	IC_{50} = 12,3±0,6 (15±4% min.)	> 10	5,4±0,3 (132±5)	i.a.
101	4-OMe	H	**0,008±0,003 (18±1)**	> 10	3,0±0,1 (81±2)	i.a.
104	4-OMe	Me	0,087±0,020 (22±1)	n.b.	n.b.	n.b.

(Merk D et al. *J. Med. Chem.*, **2014**)

***Abbildung 46**: Ergebnisse der Untersuchungen zu den SAR des zentralen aromatischen Ringes mit **101** als potentestem FXR-Partialagonisten in dieser Arbeit* (MW±SEM; n = 3-6; n.b. - nicht bestimmt; i.a. - inaktiv)

Die entscheidende selektive Steigerung der Potenz an FXR gelang durch Einführung zusätzlicher Substituenten in 4-Position des zentralen aromatischen Ringes. Bereits ein zusätzlicher Chlorsubstituent in dieser Position (**96**, EC_{50} = 0,12±0,01 µM, 22±1% max.) steigerte die Aktivität an FXR um einen Faktor 2,5, während die Aktivität an PPARs gleichzeitig ab- und die FXR-Selektivität somit zunahm. Interessanterweise bewirkte ein Chloratom in 5-Position (**97**, IC_{50} = 12,3±0,6 15±4% min.) eine Umkehrung der Aktivität und führte zu Antagonismus an FXR. **97** bildet somit eine Leitstruktur zur Entwicklung neuer FXR-Antagonisten in weiteren SAR-Studien.

Durch den Austausch des Chloratoms gegen eine Methoxygruppe (**101**, EC_{50} = 0,008±0,003 µM, 18±1% max.) in 4-Position konnte die in **96** beobachtete Potenz- und Selektivitätssteigerung an FXR zu einem niedrig nanomolaren EC_{50}-Wert weiter optimiert werden. Die abschließende Kombination der unterschiedlichen Substituenten, die die FXR-Aktivität unabhängig voneinander verbessert hatten, in einer Substanz (**104**, EC_{50} = 0,087±0,020 µM, 22±1% max.) führte dagegen zu keiner weiteren Potenzsteigerung.

Die resultierende Verbindung DM336 (**101**) der in dieser Arbeit durchgeführten SAR-Studien und Optimierungen stellt einen hochpotenten und selektiven FXR-Partialagonisten dar. **101** wurde daher ausführlich in vitro charakterisiert, um seine partialagonistische Aktivität an FXR genauer zu untersuchen und dadurch seine Eignung für künftige in vivo Studien zu untermauern.

Als Fettsäure- bzw. Gallensäuremimetikum spielten für **101** nicht nur die PPARs eine wichtige Rolle als potentielle off-targets, sondern auch der membranständige G-Proteingekoppelte Gallensäure-rezeptor TGR5. **101** war jedoch wie schon über die PPARs selektiv über TGR5. DM336 (**101**) stellte sich in vitro außerdem als metabolisch sehr stabil (80,2±0,2% nach 60 min.) und gemessen an seiner Potenz ausreichend löslich (2,6 mg/L; 5,8 µM) in Wasser heraus. Die ab einer Konzentration von

30 µM beobachtete moderate Toxizität von **101** auf die Leberzelllinie HepG ist aufgrund der nanomolaren Potenz der Substanz vernachlässigbar.

Zur ausführlichen Charakterisierung von DM336 (**101**) als FXR-Partialagonist wurden die Effekte der Substanz auf die Expression von FXR-Targetgenen in mehreren FXR-exprimierenden Zelllinien studiert und mit dem physiologischen Liganden CDCA (**1**) verglichen. In Leber- (HepG) und Darmzellen (HT29) bewirkte **101** über den Konzentrationsbereich 0,1 µM bis 10 µM eine konstante, konzentrationsunabhängige, partielle Induktion der direkten FXR-Targetgene *small hetero-dimer partner* (SHP), *bile salt export protein* (BSEP), *organic solute transporter α* (OSTα) und *ileal bile acid binding protein* (I-BABP) sowie eine partielle Repression des indirekten Targetgens *cholesterol 7α-hydroxylase* (CYP7A1). DM336 (**101**) wirkte dabei auf alle Targetgene mit einer Amplitude von etwa 40% des Effektes von CDCA (**1**) und verhielt sich somit nicht nur im relativ artifiziellen Reportergenassay, sondern auch unter in vitro größtmöglichen physiologischen Bedingungen als hochpotenter FXR-Partialagonist.

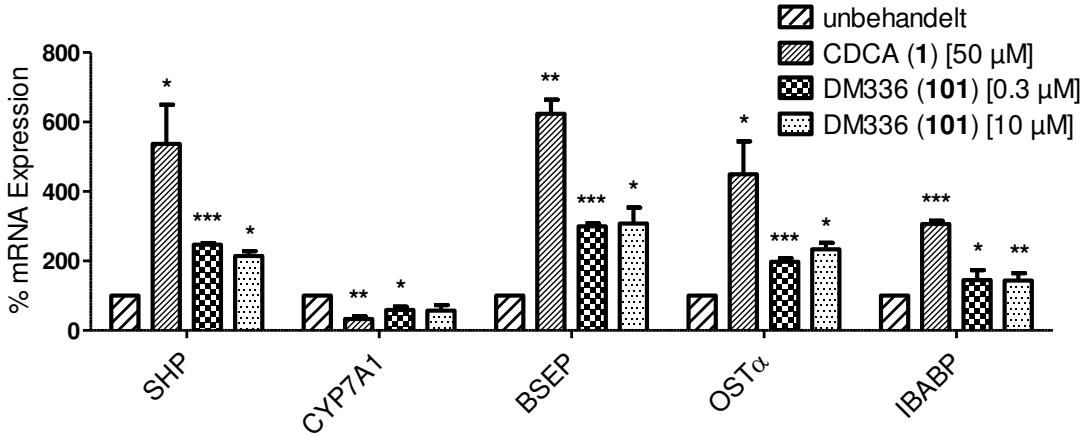

(Merk D et al. *J. Med. Chem.*, **2014**)

***Abbildung 47**: Effekt von DM336 (**101**) auf die FXR-Targetgene SHP, CYP7A1, BSEP, OSTα und IBABP in vitro*

Im Zuge dieser Arbeit wurde somit aus der schwach an FXR aktiven Leitstruktur JA10 (**32**) in mehreren SAR-Studien und Optimierungsschritten die Potenz der Acylanthranilamidderivate als FXR-Partialagonisten um mehr als einen Faktor 1000 gesteigert. Die Identifikation mehrerer Acylanthranilamidderivate mit variabler Aktivität an unterschiedlichen nukleären Rezeptoren als Leitstrukturen für weitere SAR-Studien zeigte außerdem das große Potential dieser Substanzklasse. Mit der Verbindung DM336 (**101**) wurde ein hochpotenter und selektiver FXR-Partialagonist mit akzeptabler Löslichkeit und Toxizität sowie guter metabolischer Stabilität entwickelt, der sich für künftige in vitro und in vivo Studien zu partieller FXR-Aktivierung empfehlen kann.

5. Dieser Arbeit zugrunde liegende Publikationen

Merk, D.; Schubert-Zsilavecz, M. Nuclear receptors as pharmaceutical targets: rise of FXR and rebirth of PPAR? *Future Med Chem*, **2012**, *4(*5), 587–588.
eigener Beitrag: Konzeption und Verfassen des Editorials

Merk, D.; Steinhilber, D.; Schubert-Zsilavecz, M. Medicinal chemistry of farnesoid X receptor ligands: from agonists and antagonists to modulators. *Future Med Chem*, **2012**, *4(*8), 1015–1036.
eigener Beitrag: Konzeption und Verfassen des gesamten Reviews, Entwurf der Abbildungen.

Lamers, C.; Schubert-Zsilavecz, M.; Merk, D. Therapeutic modulators of peroxisome proliferator-activated receptors (PPAR): a patent review (2008–present). *Expert Opin. Ther. Patents*, **2012**, *22(*7), 803–841.
eigener Beitrag: Konzeption des Reviews, teilweises Verfassen der Einleitung, Verfassen der Kapitel ‚selektive PPARα Liganden', ‚selektive PPARγ Liganden' und ‚pan-PPAR Liganden', sowie der ‚expert opinion'.

Merk, D.; Steinhilber, D.; Schubert-Zsilavecz, M. Characterizing ligands for farnesoid X receptor--available in vitro test systems for farnesoid X receptor modulator development. *Expert Opin Drug Discov*, **2014**, *9(*1), 27–37.
eigener Beitrag: Konzeption und Verfassen des gesamten Reviews.

Merk, D.; Gabler, M.; Gomez, R.C.; Flesch, D.; Hanke, T.; Kaiser, A.; Lamers, C.; Werz, O.; Schneider, G.; Schubert-Zsilavecz, M. Anthranilic acid derivatives as novel ligands for farnesoid X receptor (FXR). *Bioorg. Med. Chem.*, **2014**, *22(*8), 2447–2460.
eigener Beitrag: Synthese aller beschriebenen Verbindungen, Mitarbeit an der in vitro pharmakologischen Charakterisierung der Verbindungen im Reportergenassay, Bestimmung der in vitro Toxizität der Verbindungen, Konzeption und Verfassen des gesamten Papers.

Merk, D.; Lamers, C.; Ahmad, K.; Carrasco Gomez, R.; Schneider, G.; Steinhilber, D.; Schubert-Zsilavecz, M. Extending the structure-activity relationship of anthranilic acid derivatives as farnesoid X receptor modulators - Development of a highly potent partial farnesoid X receptor agonist. *J Med Chem*, **2014**, doi: 10.1021/jm500937v, in press.
eigener Beitrag: Synthese aller beschriebenen Verbindungen, in vitro pharmakologische Charakterisierung der Verbindungen im Reportergenassay und mittels qRT-PCR, Bestimmung der in vitro Toxizität der Verbindungen, Konzeption und Verfassen des gesamten Papers.

Lamers, C.; Schubert-Zsilavecz, M.; Merk, D. Medicinal Chemistry and Pharmacological Potential of FXR antagonists. *Current Trends in Medicinal Chemistry*, **2014**, in press.
eigener Beitrag: Konzeption des Reviews, Verfassen der Einleitung, der Kapitel ‚Medizinische Chemie von FXR-Antagonisten' und ‚In vitro Pharmakologie von FXR-Antagonisten' sowie der Diskussion.

Merk, D.; Lamers, C.; Weber, J.; Flesch, D.; Gabler M.; Proschak, E.; Schubert-Zsilavecz, M. Anthranilic acid derivatives as nuclear receptor modulators – development of novel PPAR selective and dual PPAR/FXR ligands. *Bioorg. Med. Chem.*, 2014, *submitted*.
eigener Beitrag: Synthese aller beschriebenen Verbindungen, Teilweise in vitro pharmakologische Charakterisierung der Verbindungen in den Reportergenassays, Bestimmung der in vitro Toxizität der Verbindungen, Konzeption und Verfassen des gesamten Papers.

6. Literaturverzeichnis

1. Seol W, Choi HS, Moore DD. Isolation of proteins that interact specifically with the retinoid X receptor: two novel orphan receptors. *Mol. Endocrinol.* **1995,** *9*(1), 72–85.
2. Forman BM, Goode E, Chen J, Oro AE, Bradley DJ, Perlmann T, Noonan DJ, Burka LT, McMorris T, Lamph WW, Evans RM, Weinberger C. Identification of a nuclear receptor that is activated by farnesol metabolites. *Cell* **1995,** *81*(5), 687–693.
3. Parks DJ, Blanchard SG, Bledsoe RK, Chandra G, Consler TG, Kliewer SA, Stimmel JB, Willson TM, Zavacki AM, Moore DD, Lehmann JM. Bile acids: natural ligands for an orphan nuclear receptor. *Science* **1999,** *284*(5418), 1365–1368.
4. Makishima M, Okamoto AY, Repa JJ, Tu H, Learned RM, Luk A, Hull MV, Lustig KD, Mangelsdorf DJ, Shan B. Identification of a nuclear receptor for bile acids. *Science* **1999,** *284*(5418), 1362–1365.
5. Gronemeyer H, Gustafsson J, Laudet V. Principles for modulation of the nuclear receptor superfamily. *Nat Rev Drug Discov* **2004,** *3*(11), 950–964.
6. Pellicciari R, Costantino G, Fiorucci S. Farnesoid X receptor: from structure to potential clinical applications. *J. Med. Chem.* **2005,** *48*(17), 5383–5403.
7. Fiorucci S, Mencarelli A, Distrutti E, Palladino G, Cipriani S. Targetting farnesoid-X-receptor: from medicinal chemistry to disease treatment. *Curr. Med. Chem.* **2010,** *17*(2), 139–159.
8. Downes M, Verdecia MA, Roecker AJ, Hughes R, Hogenesch JB, Kast-Woelbern HR, Bowman ME, Ferrer J, Anisfeld AM, Edwards PA, Rosenfeld JM, Alvarez, Jacqueline G A, Noel JP, Nicolaou KC, Evans RM. A chemical, genetic, and structural analysis of the nuclear bile acid receptor FXR. *Mol. Cell* **2003,** *11*(4), 1079–1092.
9. Merk D, Steinhilber D, Schubert-Zsilavecz M. Medicinal chemistry of farnesoid X receptor ligands: from agonists and antagonists to modulators. *Future Med Chem* **2012,** *4*(8), 1015–1036.
10. Savkur RS, Thomas JS, Bramlett KS, Gao Y, Michael LF, Burris TP. Ligand-dependent coactivation of the human bile acid receptor FXR by the peroxisome proliferator-activated receptor gamma coactivator-1alpha. *J. Pharmacol. Exp. Ther.* **2005,** *312*(1), 170–178.
11. Molnár F, Matilainen M, Carlberg C. Structural determinants of the agonist-independent association of human peroxisome proliferator-activated receptors with coactivators. *J. Biol. Chem.* **2005,** *280*(28), 26543–26556.
12. Wu Y, Chin WW, Wang Y, Burris TP. Ligand and coactivator identity determines the requirement of the charge clamp for coactivation of the peroxisome proliferator-activated receptor gamma. *J. Biol. Chem.* **2003,** *278*(10), 8637–8644.
13. Zhang Y, Kast-Woelbern HR, Edwards PA. Natural structural variants of the nuclear receptor farnesoid X receptor affect transcriptional activation. *J. Biol. Chem.* **2003,** *278*(1), 104–110.
14. Lindor KD. Farnesoid X receptor agonists for primary biliary cirrhosis. *Curr. Opin. Gastroenterol.* **2011,** *27*(3), 285–288.
15. Maran, Rengasamy R M, Thomas A, Roth M, Sheng Z, Esterly N, Pinson D, Gao X, Zhang Y, Ganapathy V, Gonzalez FJ, Guo GL. Farnesoid X receptor deficiency in mice leads to increased intestinal epithelial cell proliferation and tumor development. *J. Pharmacol. Exp. Ther.* **2009,** *328*(2), 469–477.
16. Fiorucci S, Mencarelli A, Distrutti E, Zampella A. Farnesoid X receptor: from medicinal chemistry to clinical applications. *Future Med Chem* **2012,** *4*(7), 877–891.

17. Goodwin B, Jones SA, Price RR, Watson MA, McKee DD, Moore LB, Galardi C, Wilson JG, Lewis MC, Roth ME, Maloney PR, Willson TM, Kliewer SA. A regulatory cascade of the nuclear receptors FXR, SHP-1, and LRH-1 represses bile acid biosynthesis. *Mol. Cell* **2000,** *6*(3), 517–526.

18. Lu TT, Makishima M, Repa JJ, Schoonjans K, Kerr TA, Auwerx J, Mangelsdorf DJ. Molecular basis for feedback regulation of bile acid synthesis by nuclear receptors. *Mol. Cell* **2000,** *6*(3), 507–515.

19. Hu X, Bonde Y, Eggertsen G, Rudling M. Muricholic bile acids are potent regulators of bile acid synthesis via a positive feedback mechanism. *J. Intern. Med.* **2014,** *275*(1), 27–38.

20. Sayin SI, Wahlström A, Felin J, Jäntti S, Marschall H, Bamberg K, Angelin B, Hyötyläinen T, Orešič M, Bäckhed F. Gut microbiota regulates bile acid metabolism by reducing the levels of tauro-beta-muricholic acid, a naturally occurring FXR antagonist. *Cell Metab.* **2013,** *17*(2), 225–235.

21. Liu Y, Binz J, Numerick MJ, Dennis S, Luo G, Desai B, MacKenzie KI, Mansfield TA, Kliewer SA, Goodwin B, Jones SA. Hepatoprotection by the farnesoid X receptor agonist GW4064 in rat models of intra- and extrahepatic cholestasis. *J. Clin. Invest.* **2003,** *112*(11), 1678–1687.

22. Fiorucci S, Clerici C, Antonelli E, Orlandi S, Goodwin B, Sadeghpour BM, Sabatino G, Russo G, Castellani D, Willson TM, Pruzanski M, Pellicciari R, Morelli A. Protective effects of 6-ethyl chenodeoxycholic acid, a farnesoid X receptor ligand, in estrogen-induced cholestasis. *J. Pharmacol. Exp. Ther.* **2005,** *313*(2), 604–612.

23. Denk GU, Soroka CJ, Takeyama Y, Chen W, Schuetz JD, Boyer JL. Multidrug resistance-associated protein 4 is up-regulated in liver but down-regulated in kidney in obstructive cholestasis in the rat. *J. Hepatol.* **2004,** *40*(4), 585–591.

24. Mennone A, Soroka CJ, Cai S, Harry K, Adachi M, Hagey L, Schuetz JD, Boyer JL. Mrp4-/- mice have an impaired cytoprotective response in obstructive cholestasis. *Hepatology* **2006,** *43*(5), 1013–1021.

25. Vetter C. Cholestatische Lebererkrankungen: Neue Therapeutika in der Pipeline. *Dtsch Arztebl* **2012** *109*(51-52), A-2599.

26. Adorini L, Pruzanski M, Shapiro D. Farnesoid X receptor targeting to treat nonalcoholic steatohepatitis. *Drug Discov. Today* **2012,** *17*(17-18), 988–997.

27. Weiß J, Rau M, Geier A. Non-alcoholic fatty liver disease— epidemiology, clincal course, investigation and treatment. *Dtsch Arztebl Int* **2014.**(111), 447–452.

28. Fuchs M. Non-alcoholic Fatty liver disease: the bile Acid-activated farnesoid x receptor as an emerging treatment target. *J Lipids* **2012,** *2012*, 934396.

29. Watanabe M, Houten SM, Wang L, Moschetta A, Mangelsdorf DJ, Heyman RA, Moore DD, Auwerx J. Bile acids lower triglyceride levels via a pathway involving FXR, SHP, and SREBP-1c. *J. Clin. Invest.* **2004,** *113*(10), 1408–1418.

30. Trauner M, Halilbasic E. Nuclear receptors as new perspective for the management of liver diseases. *Gastroenterology* **2011,** *140*(4), 1120-1125.e1-12.

31. Hylemon PB, Zhou H, Pandak WM, Ren S, Gil G, Dent P. Bile acids as regulatory molecules. *J. Lipid Res.* **2009,** *50*(8), 1509–1520.

32. Nestel PJ, Grundy SM. Changes in plasma triglyceride metabolism during withdrawal of bile. *Metab. Clin. Exp.* **1976,** *25*(11), 1259–1268.

33. Angelin B, Einarsson K, Hellström K, Leijd B. Effects of cholestyramine and chenodeoxycholic acid on the metabolism of endogenous triglyceride in hyperlipoproteinemia. *J. Lipid Res.* **1978,** *19*(8), 1017–1024.

34. Horton JD, Goldstein JL, Brown MS. SREBPs: activators of the complete program of cholesterol and fatty acid synthesis in the liver. *J. Clin. Invest.* **2002,** *109*(9), 1125–1131.

35. Wang Y, Chen W, Wang M, Yu D, Forman BM, Huang W. Farnesoid X receptor antagonizes nuclear factor kappaB in hepatic inflammatory response. *Hepatology* **2008,** *48*(5), 1632–1643.

36. Fiorucci S, Antonelli E, Rizzo G, Renga B, Mencarelli A, Riccardi L, Orlandi S, Pellicciari R, Morelli A. The nuclear receptor SHP mediates inhibition of hepatic stellate cells by FXR and protects against liver fibrosis. *Gastroenterology* **2004,** *127*(5), 1497–1512.

37. Fiorucci S, Cipriani S, Mencarelli A, Baldelli F, Bifulco G, Zampella A. Farnesoid X receptor agonist for the treatment of liver and metabolic disorders: focus on 6-ethyl-CDCA. *Mini Rev Med Chem* **2011,** *11*(9), 753–762.

38. Pellicciari R, Fiorucci S, Camaioni E, Clerici C, Costantino G, Maloney PR, Morelli A, Parks DJ, Willson TM. 6alpha-ethyl-chenodeoxycholic acid (6-ECDCA), a potent and selective FXR agonist endowed with anticholestatic activity. *J. Med. Chem.* **2002,** *45*(17), 3569–3572.

39. Wang XX, Jiang T, Shen Y, Caldas Y, Miyazaki-Anzai S, Santamaria H, Urbanek C, Solis N, Scherzer P, Lewis L, Gonzalez FJ, Adorini L, Pruzanski M, Kopp JB, Verlander JW, Levi M. Diabetic nephropathy is accelerated by farnesoid X receptor deficiency and inhibited by farnesoid X receptor activation in a type 1 diabetes model. *Diabetes* **2010,** *59*(11), 2916–2927.

40. Cipriani S, Mencarelli A, Palladino G, Fiorucci S. FXR activation reverses insulin resistance and lipid abnormalities and protects against liver steatosis in Zucker (fa/fa) obese rats. *J. Lipid Res.* **2010,** *51*(4), 771–784.

41. Miyazaki-Anzai S, Levi M, Kratzer A, Ting TC, Lewis LB, Miyazaki M. Farnesoid X receptor activation prevents the development of vascular calcification in ApoE-/- mice with chronic kidney disease. *Circ. Res.* **2010,** *106*(12), 1807–1817.

42. Vavassori P, Mencarelli A, Renga B, Distrutti E, Fiorucci S. The bile acid receptor FXR is a modulator of intestinal innate immunity. *J. Immunol.* **2009,** *183*(10), 6251–6261.

43. Gadaleta RM, van Erpecum, Karel J, Oldenburg B, Willemsen, Ellen C L, Renooij W, Murzilli S, Klomp, Leo W J, Siersema PD, Schipper, Marguerite E I, Danese S, Penna G, Laverny G, Adorini L, Moschetta A, van Mil SW. Farnesoid X receptor activation inhibits inflammation and preserves the intestinal barrier in inflammatory bowel disease. *Gut* **2011,** *60*(4), 463–472.

44. Fickert P, Fuchsbichler A, Moustafa T, Wagner M, Zollner G, Halilbasic E, Stöger U, Arrese M, Pizarro M, Solís N, Carrasco G, Caligiuri A, Sombetzki M, Reisinger E, Tsybrovskyy O, Zatloukal K, Denk H, Jaeschke H, Pinzani M, Trauner M. Farnesoid X Receptor Critically Determines the Fibrotic Response in Mice but Is Expressed to a Low Extent in Human Hepatic Stellate Cells and Periductal Myofibroblasts. *The American Journal of Pathology* **2009,** *175*(6), 2392–2405.

45. Zhang Y, Edwards PA. FXR signaling in metabolic disease. *FEBS Lett.* **2008,** *582*(1), 10–18.

46. He F, Li J, Mu Y, Kuruba R, Ma Z, Wilson A, Alber S, Jiang Y, Stevens T, Watkins S, Pitt B, Xie W, Li S. Downregulation of endothelin-1 by farnesoid X receptor in vascular endothelial cells. *Circ. Res.* **2006,** *98*(2), 192–199.

47. Qin P, Tang X, Elloso MM, Harnish DC. Bile acids induce adhesion molecule expression in endothelial cells through activation of reactive oxygen species, NF-kappaB, and p38. *Am. J. Physiol. Heart Circ. Physiol.* **2006,** *291*(2), H741-7.

48. Zhang Y, Wang X, Vales C, Lee FY, Lee H, Lusis AJ, Edwards PA. FXR deficiency causes reduced atherosclerosis in Ldlr-/- mice. *Arterioscler. Thromb. Vasc. Biol.* **2006,** *26*(10), 2316–2321.

49. Hanniman EA, Lambert G, McCarthy TC, Sinal CJ. Loss of functional farnesoid X receptor increases atherosclerotic lesions in apolipoprotein E-deficient mice. *J. Lipid Res.* **2005,** *46*(12), 2595–2604.

50. Zhang Y, Lee FY, Barrera G, Lee H, Vales C, Gonzalez FJ, Willson TM, Edwards PA. Activation of the nuclear receptor FXR improves hyperglycemia and hyperlipidemia in diabetic mice. *Proc. Natl. Acad. Sci. U.S.A.* **2006,** *103*(4), 1006–1011.

51. Ma K, Saha PK, Chan L, Moore DD. Farnesoid X receptor is essential for normal glucose homeostasis. *J. Clin. Invest.* **2006,** *116*(4), 1102–1109.

52. Cariou B, Staels B. FXR: a promising target for the metabolic syndrome? *Trends Pharmacol. Sci.* **2007,** *28*(5), 236–243.

53. Prieur X, Coste H, Rodriguez JC. The human apolipoprotein AV gene is regulated by peroxisome proliferator-activated receptor-alpha and contains a novel farnesoid X-activated receptor response element. *J. Biol. Chem.* **2003,** *278*(28), 25468–25480.

54. Miles PD, Barak Y, He W, Evans RM, Olefsky JM. Improved insulin-sensitivity in mice heterozygous for PPAR-gamma deficiency. *J. Clin. Invest.* **2000,** *105*(3), 287–292.

55. Düfer M, Hörth K, Wagner R, Schittenhelm B, Prowald S, Wagner, Thomas F J, Oberwinkler J, Lukowski R, Gonzalez FJ, Krippeit-Drews P, Drews G. Bile acids acutely stimulate insulin secretion of mouse β-cells via farnesoid X receptor activation and K(ATP) channel inhibition. *Diabetes* **2012,** *61*(6), 1479–1489.

56. Düfer M, Hörth K, Krippeit-Drews PDrews G. The significance of the nuclear farnesoid X receptor (FXR) in β cell function. *Islets* **2012,** *4*(5), 333–338.

57. Ryan KK, Tremaroli V, Clemmensen C, Kovatcheva-Datchary P, Myronovych A, Karns R, Wilson-Pérez HE, Sandoval DA, Kohli R, Bäckhed F, Seeley RJ. FXR is a molecular target for the effects of vertical sleeve gastrectomy. *Nature* **2014,** *509*(7499), 183–188.

58. Nijmeijer RM, Gadaleta RM, van Mil, Saskia WC, van Bodegraven, Adriaan A, Crusius, Bart A, Dijkstra G, Hommes DW, de Jong DJ, Stokkers, Pieter CF, Verspaget HW, Weersma RK, van der Woude, C Janneke, Stapelbroek JM, Schipper, Marguerite EI, Wijmenga C, van Erpecum KJ, Oldenburg B. Farnesoid X receptor (FXR) activation and FXR genetic variation in inflammatory bowel disease. *PLoS ONE* **2011,** *6*(8), e23745.

59. Gadaleta RM, Oldenburg B, Willemsen, Ellen CL, Spit M, Murzilli S, Salvatore L, Klomp LW, Siersema PD, van Erpecum KJ, van Mil SW. Activation of bile salt nuclear receptor FXR is repressed by pro-inflammatory cytokines activating NF-κB signaling in the intestine. *Biochim. Biophys. Acta* **2011,** *1812*(8), 851–858.

60. Dai J, Wang H, Shi Y, Dong Y, Zhang Y, Wang J. Impact of bile acids on the growth of human cholangiocarcinoma via FXR. *J Hematol Oncol* **2011,** *4*, 41.

61. Meng Z, Wang Y, Wang L, Jin W, Liu N, Pan H, Liu L, Wagman L, Forman BM, Huang W. FXR regulates liver repair after CCl4-induced toxic injury. *Mol. Endocrinol.* **2010,** *24*(5), 886–897.

62. Ohno T, Shirakami Y, Shimizu M, Kubota M, Sakai H, Yasuda Y, Kochi T, Tsurumi H, Moriwaki H. Synergistic growth inhibition of human hepatocellular carcinoma cells by acyclic retinoid and GW4064, a farnesoid X receptor ligand. *Cancer Lett.* **2012,** *323*(2), 215–222.

63. Modica S, Murzilli S, Salvatore L, Schmidt DR, Moschetta A. Nuclear bile acid receptor FXR protects against intestinal tumorigenesis. *Cancer Res.* **2008,** *68*(23), 9589–9594.

64. Lee JY, Lee KT, Lee JK, Lee KH, Jang K, Heo JS, Choi SH, Kim Y, Rhee JC. Farnesoid X receptor, overexpressed in pancreatic cancer with lymph node metastasis promotes cell migration and invasion. *Br. J. Cancer* **2011,** *104*(6), 1027–1037.

65. Gottardi A de, Touri F, Maurer CA, Perez A, Maurhofer O, Ventre G, Bentzen CL, Niesor EJ, Dufour J. The bile acid nuclear receptor FXR and the bile acid binding protein IBABP are differently expressed in colon cancer. *Dig. Dis. Sci.* **2004,** *49*(6), 982–989.

66. Journe F, Durbecq V, Chaboteaux C, Rouas G, Laurent G, Nonclercq D, Sotiriou C, Body J, Larsimont D. Association between farnesoid X receptor expression and cell proliferation in estrogen receptor-positive luminal-like breast cancer from postmenopausal patients. *Breast Cancer Res. Treat.* **2009,** *115*(3), 523–535.

67. Swales KE, Korbonits M, Carpenter R, Walsh DT, Warner TD, Bishop-Bailey D. The farnesoid X receptor is expressed in breast cancer and regulates apoptosis and aromatase expression. *Cancer Res.* **2006,** *66*(20), 10120–10126.

68. Germain P, Staels B, Dacquet C, Spedding M, Laudet V. Overview of nomenclature of nuclear receptors. *Pharmacol. Rev.*, **2006**, *58*(4), 685–704.

69. Lamers C, Schubert-Zsilavecz M, Merk D. Medicinal Chemistry and Pharmacological Potential of FXR antagonists. *Current Trends in Medicinal Chemistry* **2014,** *accepted*.

70. Ulbricht C, Basch E, Szapary P, Hammerness P, Axentsev S, Boon H, Kroll D, Garraway L, Vora M, Woods J. Guggul for hyperlipidemia: a review by the Natural Standard Research Collaboration. *Complement Ther Med* **2005,** *13*(4), 279–290.

71. Cui J, Huang L, Zhao A, Lew J, Yu J, Sahoo S, Meinke PT, Royo I, Pelaez FWright SD. Guggulsterone is a farnesoid X receptor antagonist in coactivator association assays but acts to enhance transcription of bile salt export pump. *J. Biol. Chem.* **2003,** *278*(12), 10214–10220.

72. Urizar NL, Liverman AB, Dodds DT, Silva FV, Ordentlich P, Yan Y, Gonzalez FJ, Heyman RA, Mangelsdorf DJ, Moore DD. A natural product that lowers cholesterol as an antagonist ligand for FXR. *Science* **2002,** *296*(5573), 1703–1706.

73. Xu X, Lu Y, Chen L, Chen J, Luo X, Shen X. Identification of 15d-PGJ2 as an antagonist of farnesoid X receptor: molecular modeling with biological evaluation. *Steroids* **2013,** *78*(9), 813–822.

74. Rizzo G, Passeri D, Franco F de, Ciaccioli G, Donadio L, Rizzo G, Orlandi S, Sadeghpour B, Wang XX, Jiang T, Levi M, Pruzanski M, Adorini L. Functional characterization of the semisynthetic bile acid derivative INT-767, a dual farnesoid X receptor and TGR5 agonist. *Mol. Pharmacol.* **2010,** *78*(4), 617–630.

75. Costantino G, Macchiarulo A, Entrena-Guadix A, Camaioni E, Pellicciari R. Binding mode of 6ECDCA, a potent bile acid agonist of the farnesoid X receptor (FXR). *Bioorg. Med. Chem. Lett.* **2003,** *13*(11), 1865–1868.

76. Gioiello A, Macchiarulo A, Carotti A, Filipponi P, Costantino G, Rizzo G, Adorini L, Pellicciari R. Extending SAR of bile acids as FXR ligands: discovery of 23-N-(carbocinnamyloxy)-3α,7α-dihydroxy-6α-ethyl-24-nor-5β-cholan-23-amine. *Bioorg. Med. Chem.* **2011,** *19*(8), 2650–2658.

77. Mi L, Devarakonda S, Harp JM, Han Q, Pellicciari R, Willson TM, Khorasanizadeh S, Rastinejad F. Structural basis for bile acid binding and activation of the nuclear receptor FXR. *Mol. Cell* **2003,** *11*(4), 1093–1100.

78. Soisson SM, Parthasarathy G, Adams AD, Sahoo S, Sitlani A, Sparrow C, Cui J, Becker JW. Identification of a potent synthetic FXR agonist with an unexpected mode of binding and activation. *Proc. Natl. Acad. Sci. U.S.A.* **2008,** *105*(14), 5337–5342.

79. Maloney PR, Parks DJ, Haffner CD, Fivush AM, Chandra G, Plunket KD, Creech KL, Moore LB, Wilson JG, Lewis MC, Jones SA, Willson TM. Identification of a chemical tool for the orphan nuclear receptor FXR. *J. Med. Chem.* **2000,** *43*(16), 2971–2974.

80. Merk D, Steinhilber D, Schubert-Zsilavecz M. Characterizing ligands for farnesoid X receptor--available in vitro test systems for farnesoid X receptor modulator development. *Expert Opin Drug Discov* **2014,** *9*(1), 27–37.

81. Feng S, Yang M, Zhang Z, Wang Z, Di Hong, Richter H, Benson GM, Bleicher K, Grether U, Martin RE, Plancher J, Kuhn B, Rudolph MG, Chen L. Identification of an N-oxide pyridine GW4064 analog as a potent FXR agonist. *Bioorg. Med. Chem. Lett.* **2009,** *19*(9), 2595–2598.

82. Abel U, Schlüter T, Schulz A, Hambruch E, Steeneck C, Hornberger M, Hoffmann T, Perović-Ottstadt S, Kinzel O, Burnet M, Deuschle U, Kremoser C. Synthesis and pharmacological validation of a novel series of non-steroidal FXR agonists. *Bioorg. Med. Chem. Lett.* **2010,** *20*(16), 4911–4917.

83. Kainuma M, Kasuga J, Hosoda S, Wakabayashi K, Tanatani A, Nagasawa K, Miyachi H, Makishima M, Hashimoto Y. Diphenylmethane skeleton as a multi-template for nuclear receptor ligands: preparation of FXR and PPAR ligands. *Bioorg. Med. Chem. Lett.* **2006,** *16*(12), 3213–3218.

84. Akwabi-Ameyaw A, Bass JY, Caldwell RD, Caravella JA, Chen L, Creech KL, Deaton DN, Madauss KP, Marr HB, McFadyen RB, Miller AB, Navas F, Parks DJ, Spearing PK, Todd D, Williams SP, Bruce Wisely G. FXR agonist activity of conformationally constrained analogs of GW 4064. *Bioorg. Med. Chem. Lett.* **2009,** *19*(16), 4733–4739.

85. Akwabi-Ameyaw A, Bass JY, Caldwell RD, Caravella JA, Chen L, Creech KL, Deaton DN, Jones SA, Kaldor I, Liu Y, Madauss KP, Marr HB, McFadyen RB, Miller AB, Iii FN, Parks DJ, Spearing PK, Todd D, Williams SP, Wisely GB. Conformationally constrained farnesoid X receptor (FXR) agonists: Naphthoic acid-based analogs of GW 4064. *Bioorg. Med. Chem. Lett.* **2008,** *18*(15), 4339–4343.

86. Vaquero J, Monte MJ, Dominguez M, Muntané J, Marin J. Differential activation of the human farnesoid X receptor depends on the pattern of expressed isoforms and the bile acid pool composition. *Biochem. Pharmacol.* **2013,** *86*(7), 926–939.

87. Howarth DL, Law, Sheran H W, Law JM, Mondon JA, Kullman SW, Hinton DE. Exposure to the synthetic FXR agonist GW4064 causes alterations in gene expression and sublethal hepatotoxicity in eleutheroembryo medaka (Oryzias latipes). *Toxicol. Appl. Pharmacol.* **2010,** *243*(1), 111–121.

88. Chiang P, Thompson DC, Ghosh S, Heitmeier MR. A formulation-enabled preclinical efficacy assessment of a farnesoid X receptor agonist, GW4064, in hamsters and cynomolgus monkeys. *J Pharm Sci* **2011,** *100*(11), 4722–4733.

89. Singh N, Yadav M, Singh AK, Kumar H, Dwivedi, Shailendra Kumar Dhar, Mishra JS, Gurjar A, Manhas A, Chandra S, Yadav PN, Jagavelu K, Siddiqi MI, Trivedi AK, Chattopadhyay N, Sanyal S. Synthetic FXR agonist GW4064 is a modulator of multiple G protein-coupled receptors. *Mol. Endocrinol.* **2014,** *28*(5), 659–673.

90. Flatt B, Martin R, Wang T, Mahaney P, Murphy B, Gu X, Foster P, Li J, Pircher P, Petrowski M, Schulman I, Westin S, Wrobel J, Yan G, Bischoff E, Daige C, Mohan R. Discovery of XL335 (WAY-362450), a highly potent, selective, and orally active agonist of the farnesoid X receptor (FXR). *J. Med. Chem.* **2009,** *52*(4), 904–907.

91. Mehlmann JF, Crawley ML, Lundquist JT, Unwalla RJ, Harnish DC, Evans MJ, Kim CY, Wrobel JE, Mahaney PE. Pyrrole[2,3-d]azepino compounds as agonists of the farnesoid X receptor (FXR). *Bioorg. Med. Chem. Lett.* **2009,** *19*(18), 5289–5292.

92. Richter, Hans G F, Benson GM, Blum D, Chaput E, Feng S, Gardes C, Grether U, Hartman P, Kuhn B, Martin RE, Plancher J, Rudolph MG, Schuler F, Taylor S, Bleicher KH. Discovery of novel and orally active FXR agonists for the potential treatment of dyslipidemia & diabetes. *Bioorg. Med. Chem. Lett.* **2011,** *21*(1), 191–194.

93. Richter, Hans G F, Benson GM, Bleicher KH, Blum D, Chaput E, Clemann N, Feng S, Gardes C, Grether U, Hartman P, Kuhn B, Martin RE, Plancher J, Rudolph MG, Schuler F, Taylor S. Optimization of a novel class of benzimidazole-based farnesoid X receptor (FXR) agonists to

improve physicochemical and ADME properties. *Bioorg. Med. Chem. Lett.* **2011,** *21*(4), 1134–1140.

94. Hambruch E, Miyazaki-Anzai S, Hahn U, Matysik S, Boettcher A, Perović-Ottstadt S, Schlüter T, Kinzel O, Krol HD, Deuschle U, Burnet M, Levi M, Schmitz G, Miyazaki M, Kremoser C. Synthetic farnesoid X receptor agonists induce high-density lipoprotein-mediated transhepatic cholesterol efflux in mice and monkeys and prevent atherosclerosis in cholesteryl ester transfer protein transgenic low-density lipoprotein receptor (-/-) mice. *J. Pharmacol. Exp. Ther.* **2012,** *343*(3), 556–567.
95. Marinozzi M, Carotti A, Sansone E, Macchiarulo A, Rosatelli E, Sardella R, Natalini B, Rizzo G, Adorini L, Passeri D, de Franco F, Pruzanski M, Pellicciari R. Pyrazole[3,4-e][1,4]thiazepin-7-one derivatives as a novel class of Farnesoid X Receptor (FXR) agonists. *Bioorg. Med. Chem.* **2012,** *20*(11), 3429–3445.
96. Marinozzi M, Carotti A, Sardella R, Buonerba F, Ianni F, Natalini B, Passeri D, Rizzo G, Pellicciari R. Asymmetric synthesis of the four diastereoisomers of a novel non-steroidal farnesoid X receptor (FXR) agonist: role of the chirality on the biological activity. *Bioorg. Med. Chem.* **2013,** *21*(13), 3780–3789.
97. Schuster D, Markt P, Grienke U, Mihaly-Bison J, Binder M, Noha SM, Rollinger JM, Stuppner H, Bochkov VN, Wolber G. Pharmacophore-based discovery of FXR agonists. Part I: Model development and experimental validation. *Bioorg. Med. Chem.* **2011,** *19*(23), 7168–7180.
98. Grienke U, Mihály-Bison J, Schuster D, Afonyushkin T, Binder M, Guan S, Cheng C, Wolber G, Stuppner H, Guo D, Bochkov VN, Rollinger JM. Pharmacophore-based discovery of FXR-agonists. Part II: identification of bioactive triterpenes from Ganoderma lucidum. *Bioorg. Med. Chem.* **2011,** *19*(22), 6779–6791.
99. Liu P, Xu X, Chen L, Ma L, Shen X, Hu L. Discovery and SAR study of hydroxyacetophenone derivatives as potent, non-steroidal farnesoid X receptor (FXR) antagonists. *Bioorg. Med. Chem.* **2014,** *22*(5), 1596–1607.
100. Huang H, Yu Y, Gao Z, Zhang Y, Li C, Xu X, Jin H, Yan W, Ma R, Zhu J, Shen X, Jiang H, Chen L, Li J. Discovery and optimization of 1,3,4-trisubstituted-pyrazolone derivatives as novel, potent, and nonsteroidal farnesoid X receptor (FXR) selective antagonists. *J. Med. Chem.* **2012,** *55*(16), 7037–7053.
101. Yu DD, Lin W, Forman BM, Chen T. Identification of trisubstituted-pyrazol carboxamide analogs as novel and potent antagonists of farnesoid X receptor. *Bioorg. Med. Chem.* **2014,** *22*(11), 2919–2938.
102. Di Leva, Francesco Saverio, Festa C, D'Amore C, Marino S de, Renga B, D'Auria MV, Novellino E, Limongelli V, Zampella A, Fiorucci S. Binding mechanism of the farnesoid X receptor marine antagonist suvanine reveals a strategy to forestall drug modulation on nuclear receptors. Design, synthesis, and biological evaluation of novel ligands. *J. Med. Chem.* **2013,** *56*(11), 4701–4717.
103. Suzuki T, Nishimaki-Mogami T, Kawai H, Kobayashi T, Shinozaki Y, Sato Y, Hashimoto T, Asakawa Y, Inoue K, Ohno Y, Hayakawa T, Kawanishi T. Screening of novel nuclear receptor agonists by a convenient reporter gene assay system using green fluorescent protein derivatives. *Phytomedicine* **2006,** *13*(6), 401–411.
104. Cheatham WW. Peroxisome proliferator-activated receptor translational research and clinical experience. *Am. J. Clin. Nutr.* **2010,** *91*(1), 262S-266S.
105. Kung J, Henry RR. Thiazolidinedione safety. *Expert Opin Drug Saf* **2012,** *11*(4), 565–579.
106. Beral V. Ovarian cancer and hormone replacement therapy in the Million Women Study. *The Lancet* **2007,** *369*(9574), 1703–1710.

107. Pirat C, Farce A, Lebègue N, Renault N, Furman C, Millet R, Yous S, Speca S, Berthelot P, Desreumaux P, Chavatte P. Targeting peroxisome proliferator-activated receptors (PPARs): development of modulators. *J. Med. Chem.* **2012,** *55*(9), 4027–4061.

108. Achenbach J, Gabler M, Steri R, Schubert-Zsilavecz M, Proschak E. Identification of novel farnesoid X receptor modulators using a combined ligand- and structure-based virtual screening. *Med. Chem. Commun.* **2013,** *4*(6), 920.

109. Venuti MC. Isatoic Anhydride/4-Dimethylaminopyridine as a Reagent for ortho -Aminobenzoylation. *Synthesis* **1982,** *1982*(04), 266–268.

110. Astra Zeneca UK Limited. Benzimidazole Derivatives and Their Use As Antiviral Agents. WO 2010/103306 A1 **2010.**.

111. Jin T, Kitahara F, Kamijo S, Yamamoto Y. Copper-catalyzed synthesis of 5-substituted 1H-tetrazoles via the [3+2] cycloaddition of nitriles and trimethylsilyl azide. *Tetrahedron Letters* **2008,** *49*(17), 2824–2827.

112. Khalafi-Nezhad A, Parhami A, Soltani R, Mohammad N, Zarea A. Efficient method for the direct preparation of amides from carboxylic acids using tosyl chloride under solvent-free conditions. *Tetrahedron Letters* **2005,** *46*(40), 6879–6882.

113. Akwabi-Ameyaw A, Caravella JA, Chen L, Creech KL, Deaton DN, Madauss KP, Marr HB, Miller AB, Navas F, Parks DJ, Spearing PK, Todd D, Williams SP, Wisely GB. Conformationally constrained farnesoid X receptor (FXR) agonists: Alternative replacements of the stilbene. *Bioorganic & Medicinal Chemistry Letters* **2011,** *21*(20), 6154–6160.

114. Keller H, Dreyer C, Medin J, Mahfoudi A, Ozato K, Wahli W. Fatty acids and retinoids control lipid metabolism through activation of peroxisome proliferator-activated receptor-retinoid X receptor heterodimers. *Proc. Natl. Acad. Sci. U.S.A.* **1993,** *90*(6), 2160–2164.

115. Kliewer SA, Sundseth SS, Jones SA, Brown PJ, Wisely GB, Koble CS, Devchand P, Wahli W, Willson TM, Lenhard JM, Lehmann JM. Fatty acids and eicosanoids regulate gene expression through direct interactions with peroxisome proliferator-activated receptors alpha and gamma. *Proc. Natl. Acad. Sci. U.S.A.* **1997,** *94*(9), 4318–4323.

116. Xu HE, Lambert MH, Montana VG, Parks DJ, Blanchard SG, Brown PJ, Sternbach DD, Lehmann JM, Wisely GB, Willson TM, Kliewer SA, Milburn MV. Molecular recognition of fatty acids by peroxisome proliferator-activated receptors. *Mol. Cell* **1999,** *3*(3), 397–403.

117. Forman BM, Chen J, Evans RM. Hypolipidemic drugs, polyunsaturated fatty acids, and eicosanoids are ligands for peroxisome proliferator-activated receptors alpha and delta. *Proc. Natl. Acad. Sci. U.S.A.* **1997,** *94*(9), 4312–4317.

118. Staels B, Fruchart J. Therapeutic roles of peroxisome proliferator-activated receptor agonists. *Diabetes* **2005,** *54*(8), 2460–2470.

119. Staels B, Dallongeville J, Auwerx J, Schoonjans K, Leitersdorf E, Fruchart JC. Mechanism of action of fibrates on lipid and lipoprotein metabolism. *Circulation* **1998,** *98*(19), 2088–2093.

120. Mahaffey KW, Hafley G, Dickerson S, Burns S, Tourt-Uhlig S, White J, Newby LK, Komajda M, McMurray J, Bigelow R, Home PD, Lopes RD. Results of a reevaluation of cardiovascular outcomes in the RECORD trial. *American Heart Journal* **2013,** *166*(2), 240–249.e1.

121. Neels JG, Grimaldi PA. Physiological functions of peroxisome proliferator-activated receptor β. *Physiol. Rev.* **2014,** *94*(3), 795–858.

122. Sprecher DL, Massien C, Pearce G, Billin AN, Perlstein I, Willson TM, Hassall DG, Ancellin N, Patterson SD, Lobe DC, Johnson TG. Triglyceride:High-Density Lipoprotein Cholesterol Effects in Healthy Subjects Administered a Peroxisome Proliferator Activated Receptor Agonist. *Arteriosclerosis, Thrombosis, and Vascular Biology* **2006,** *27*(2), 359–365.

123. Riserus U, Sprecher D, Johnson T, Olson E, Hirschberg S, Liu A, Fang Z, Hegde P, Richards D, Sarov-Blat L, Strum JC, Basu S, Cheeseman J, Fielding BA, Humphreys SM, Danoff T, Moore NR, Murgatroyd P, O'Rahilly S, Sutton P, Willson T, Hassall D, Frayn KN, Karpe F. Activation of Peroxisome Proliferator-Activated Receptor (PPAR) Promotes Reversal of Multiple Metabolic Abnormalities, Reduces Oxidative Stress, and Increases Fatty Acid Oxidation in Moderately Obese Men. *Diabetes* **2007,** *57*(2), 332–339.

124. Gupta RA, Wang D, Katkuri S, Wang H, Dey SK, DuBois RN. Activation of nuclear hormone receptor peroxisome proliferator-activated receptor-delta accelerates intestinal adenoma growth. *Nat. Med.* **2004,** *10*(3), 245–247.

125. Rau O, Wurglics M, Paulke A, Zitzkowski J, Meindl N, Bock A, Dingermann T, Abdel-Tawab M, Schubert-Zsilavecz M. Carnosic acid and carnosol, phenolic diterpene compounds of the labiate herbs rosemary and sage, are activators of the human peroxisome proliferator-activated receptor gamma. *Planta Med.* **2006,** *72*(10), 881–887.

126. Kersten S. Integrated physiology and systems biology of PPARα. *Mol Metab* **2014,** *3*(4), 354–371.

127. Feige JN, Gelman L, Michalik L, Desvergne B, Wahli W. From molecular action to physiological outputs: peroxisome proliferator-activated receptors are nuclear receptors at the crossroads of key cellular functions. *Prog. Lipid Res.* **2006,** *45*(2), 120–159.

7. Verzeichnis der Abkürzungen

4-DMAP	4-*N,N*-Dimethylaminopyridin
5-LO	5-Lipoxigenase
AF-1	Aktivierungsfunktion 1
AF-2	Aktivierungsfunktion 2
alpha-Screen	*amplified luminescent proximity homogenous assay* Screen
AP	alkalische Phosphatase
apoAI	Apolipoprotein A1
apoAIV	Apolipoprotein A4
apoB	Apolipoprotein B
apoCII	Apolipoprotein C2
apoCIII	Apolipoprotein C3
BSEP	*bile salt export protein*
bzw.	beziehungsweise
CA	*cholic acid* (Cholsäure)
CAR	*constitutive androstane receptor*
CDCA	*chenodeoxycholic acid* (Chenodeoxycholsäure)
cdk5	*cyclin-dependent kinase 5*
clogP	*calculated partition-coefficient* (Verteilungskoeffizient)
CMV	Zytomegalievirus
COX-1	Cyclooxygenase-1
COX-2	Cyclooxygenase-2
CYP3A4	*cytochrome P450, family 3, subfamily a, polypeptide 4*
CYP3A4	*cytochrome P450, family 3, subfamily a, polypeptide 11*
CYP7A1	*cytochrome P450, family 7, subfamily a, polypeptide 1* (Cholesterol 7α-hydroxylase)
CYP8B1	*cytochrome P450, family 8, subfamily b, polypeptide 1* (Sterol 12α-hydroxylase)
DNA	Desoxyribonukleinsäure
DBD	DNA-Bindedomäne
DCA	*deoxycholic acid* (Deoxycholsäure)
DMF	*N,N*-Dimethylformamid
DRIP	Vitamin D receptor interacting protein
EC_{50}	halbmaximale effektive Konzentration
ER	Estrogenrezeptor
EtOH	Ethanol
FAS	*fatty acid synthase* (Fettsäuresynthase)
FGF15	*fibroblast growth factor 15* (Fibroblastenwachstumsfaktor 15)
FGF19	*fibroblast growth factor 19* (Fibroblastenwachstumsfaktor 19)
FGFR4	*fibroblast growth factor receptor 4* (Fibroblastenwachstumsfaktorrezeptor 4)
fl	*full length*
FRET	*fluorescence resonance energy transfer* (Fluoreszenz-Resonanz-Energie-Transfer)
FXR	Farnesoid X Rezeptor
G6Pase	Glucose-6-Phosphatase
GAPDH	Glycerinaldehyd-3-phosphat-Dehydrogenase
GGT	Gamma-Glutamyl-Transferase
GLUT-4	Glucosetransporter Typ4
GR	Glucocorticoidrezeptor
HDL	*high-density lipoprotein*
HMGCR	3-Hydroxy-3methylglutaryl-CoA-Reduktase
i.a.	inaktiv
IBABP	*ileal bile acid binding protein*
IC_{50}	halbmaximale inhibitorische Konzentration
ICAM-1	*intracellular adhesion molecule 1*
IL-1β	Interleukin-1β
IL-6	Interleukin-6
iNOS	induzierbare NO-Synthase
IR-1	*internal repeat 1*
JNK	c-Jun N-terminale Kinasen
LBD	Ligandbindedomäne
LCA	*lithocholic acid* (Lithocholsäure)
LDH	Lactatdehydrogenase
LDL	*low-density lipoprotein*
LDLR	*low-density lipoprotein receptor*
LE	*ligand efficiency*
LPL	Lipoproteinlipase

LPS	Lipopolysaccharid
LXR	liver X receptor
max.	maximal
MCA	*muricholic acid* (Muricholsäure, murine Gallensäure)
MCP-1	*monocyte chemoattractant protein-1*
MRP-2	*multidrug resistance-associated protein 2*
MRP-3	*multidrug resistance-associated protein 3*
MRP-4	*multidrug resistance-associated protein 4*
MW	Mittelwert
NCor	*nuclear co-repressor*
n.b.	nicht bestimmt
NAFLD	*non-alcoholic fatty liver disease* (nichtalkoholische Fettlebererkrankung)
NASH	*non-alcoholic steatohepatitis* (nichtalkoholische Steatohepatitis)
NEt3	Triethylamin
NF-κB	*nuclear factor kappa B*
NR1H4	*nuclear receptor subfamily 1, group H, member 4*
NRC-1	*nuclear receptor coactivator 1*
NSAR	nichtsteroidale Antirheumatika
NTCP	*Na^+-taurocholate cotransport peptide* (Natriumtaurocholatcotransporter)
OATP	*organic anion transporting protein*
OCA	*obeticholic acid* (Obeticholsäure)
OSTα/β	*organic solute transporter α/β*
PBC	*primary biliary cirrhosis* (Primäre Biliärzirrhose)
PBMCs	*peripheral blood mononuclear cells* (mononukleäre Zellen des peripheren Blutes)
PCC	Pyridiniumchlorochromat
PDB	Protein Data Bank
PEPCK	*phosphoenol-pyruvate carboxykinase*
PGC-1α	*peroxisome proliferator-activated receptor gamma coactivator 1α*
PPAR	*peroxisome proliferator-activated receptor* (Peroxisomen Proliferator-aktivierte Rezeptoren)
PXR	Pregnan X Rezeptor
qRT-PCR	*quantitative real-time polymerase chain reaction* (quantitative Echtzeit-Polymerase-Ketten-Reaktion)
RE	*resonse element*
rel.	relativ
RF	Rückfluss
RLU	*relative light units* (relative Lichteinheiten)
RT	Raumtemperatur
RXR	Retinoid X Rezeptor
SAR	*structure-activity relationship* (Struktur-Wirkungsbeziehungen)
SEM	*standard error of the mean* (Standard error)
SHP	*small hetero-dimer partner*
SILE	*size-independent ligand efficiency*
SPA	*scintillation proximity assay*
SRC-1	*steroid receptor coactivator 1*
SREBP-1c	*sterol-regulatory-element-binding protein 1c*
SULT2A1	*sulfotransferase 2A1*
SV40	Simian-Virus 40
sog.	sogenannt(e)
TGFβ	*transforming growth factor β* (Transformierender Wachstumsfaktor β)
TGR5	*G protein-coupled bile acid receptor 1*
THF	Tetrahydrofuran
TNFα	Tumornekrosefaktor α
UDCA	*ursodeoxycholic acid* (Ursodeoxycholsäure)
UGT2B	*UDP-glucoronosyltransferase-2B*
VCAM-1	*vascular cell adhesion molecule 1*
vgl.	vergleiche
VLDL	*very low-density lipoprotein*
VLDLR	*very low-density lipoprotein receptor*
WST-1	*water soluble tetrazolium 1* (*4-[3-(4-Iodophenyl)-2-(4-nitrophenyl)-2H-5-tetrazolio]-1,3-benzene sulfonate*)

8. Curriculum Vitae

Name	**Daniel Merk**
Adresse	[redacted]
Staatsangehörigkeit	**Deutsch**
Geburtsdatum	**13. November 1985**
Geburtsort	**München**

Werdegang

09/1992 - 08/1996	**Grundschule an der Nadistraße, München**
09/1996 - 06/2005	**Maximiliansgymnasium München**
24.6.2005	**Abitur (allg. Hochschulreife)**
10/2006 - 03/2009	**Studium ‚Bachelor of Pharmaceutical Sciences' an der Ludwig-Maximilians-Universität München** Bachelorarbeit: „Untersuchungen des protektiven Effektes auf Signaltransduktionsebene von Crataegusextrakt WS1442 auf die endotheliale Permeabilität" im Arbeitskreis von Prof. Dr. A. Vollmar
27.3.2009	**‚Bachelor of Pharmaceutical Sciences'**
04/2009 - 02/2011	**Studium ‚Master of Pharmaceutical Sciences' und Pharmazie (Staatsexamen) an der Ludwig-Maximilians-Universität München** Masterarbeit: „4-substituierte Nipecotinsäurederivate als GABA-uptake-Inhibitoren" im Arbeitskreis von Prof. Dr. K.T. Wanner
9.2.2011	**‚Master of Pharmaceutical Sciences' mit Gewinn des 'Daiichi Sankyo Master Preises'**
20.4.2011	**Zweites Pharmazeutisches Staatsexamen**
seit 1.7.2011	**Wissenschaftlicher Mitarbeiter im Arbeitskreis von Prof. Dr. M. Schubert-Zsilavecz an der Goethe Universität Frankfurt**

Tagungsbesuche

2.-4.10.2011	**27th Ernst Klenk Symposium in Molecular Medicine: Lipid metabolic diseases: novel developments in molecular pathology and therapy (Köln)**
5.-10.2.2012	**Pharmacon (Davos, Schweiz)**
2.-6.9.2012	**International Symposium Medicinal Chemistry (Berlin)** *Beitrag:* Poster: „Structure and ligand based identification of novel synthetic ligands for farnesoid X receptor"
28.9.-3.10.2012	**2nd International PhD Summer-School (Chieti, Italien)** *Beitrag:* Vortrag: „Anthranilic acid derivatives as novel ligands for farnesoid X receptor"
3.-8.2.2013	**Pharmacon (Davos, Schweiz)**
3.-8.4.2013	**Keystone Symposium ‚Nuclear Receptors and Friends' (Alpbach, Österreich)** *Beitrag:* Poster: „Novel ligands for farnesoid X receptor"
5.-7.12.2013	**18th Lipid Meeting Leipzig (Leipzig)**
2.-7.2.2014	**Pharmacon (Davos, Schweiz)**
16.-19.3.2014	**Frontiers in Medicinal Chemistry (Tübingen)** *Beitrag:* Poster: „Novel ligands for farnesoid X receptor"

Lehrerfahrung

10/2007 - 03/2010	**Betreuung des Tutoriums ‚Stöchiometrie' an der Ludwig-Maximilians-Universität München**
10/2008 - 08/2010	**Betreuung des Tutoriums ‚Organische Chemie' an der Ludwig-Maximilians-Universität München**
seit 10/2011	**Betreuung des Praktikums , Allgemeine und analytische Chemie der anorganischen Arznei-, Hilfs- und Schadstoffe (unter Einbeziehung von Arzneibuchmethoden)' an der Goethe Universität Frankfurt**
seit 10/2011	**Betreuung der Seminare ‚Stöchiometrie' (erstes Semester Pharmazie) und ‚Medizinische Chemie' (drittes Semester Pharmazie) an der Goethe Universität Frankfurt**
seit 10/2011	**Betreuung jeweils einer Gruppe pro Semester im ‚Fertigarzneimittelseminar' des achten Semesters Pharmazie an der Goethe Universität Frankfurt**
seit 10/2011	**Regelmäßige Vertretung der Vorlesung ‚Chemie für Pharmazeuten' (zweites und drittes Semester Pharmazie) an der Goethe Universität Frankfurt**
22.1.2014	**Erwerb des ‚Zertifikates Hochschullehre' des Interdisziplinären Kollegs Hochschullehre der Goethe Universität Frankfurt**

Sprachkenntnisse

Englisch	**fließend**
Spanisch	**Grundkenntnisse**
	Graecum, Latinum

Akademische Lehrer

Prof. Dr. Martin Biel

Prof. Dr. Franz Bracher

Prof. Dr. Wolfgang Frieß

Prof. Dr. Angelika Vollmar

Prof. Dr. Ernst Wagner

Prof. Dr. Christian Wahl-Schott

Prof. Dr. Gerhard Winter

Prof. Dr. Stefan Zahler

Prof. Dr. Klaus Wanner

Prof. Dr. Manfred Schubert-Zsilavecz

9. Publikationsliste

Publikationen in peer-review journals

Schubert-Zsilavecz, M.; Merk, D. Innovations in the treatment of cystic fibrosis: outriders for the treatment of diseases with other genetic defects? *Future Med Chem*, **2011**, *3*(16), 1969–1970.

Merk, D.; Schubert-Zsilavecz, M. New hope or drawbacks: will chronic kidney disease be treatable with small molecules in the near future? *Future Med Chem*, **2012**, *4*(3), 269–271.

Merk, D.; Schubert-Zsilavecz, M. Nuclear receptors as pharmaceutical targets: rise of FXR and rebirth of PPAR? *Future Med Chem*, **2012**, *4*(5), 587–588.

Merk, D.; Steinhilber, D.; Schubert-Zsilavecz, M. Medicinal chemistry of farnesoid X receptor ligands: from agonists and antagonists to modulators. *Future Med Chem*, **2012**, *4*(8), 1015–1036.

Lamers, C.; Schubert-Zsilavecz, M.; Merk, D. Therapeutic modulators of peroxisome proliferator-activated receptors (PPAR): a patent review (2008–present). *Expert Opin. Ther. Patents*, **2012**, *22*(7), 803–841.

Merk, D.; Schubert-Zsilavecz, M. Novel strategies to control lipid metabolism: can the antisense drug mipomersen fulfill the unmet need? *Future Med Chem*, **2012**, *4*(14), 1773–1775.

Lamers, C.; Flesch, D.; Schubert-Zsilavecz, M.; Merk, D. Novel prostaglandin receptor modulators: a patent review (2002 - 2012) - part I: non-EP receptor modulators. *Expert Opin Ther Pat*, **2013**, *23*(1), 47–77.

Flesch, D.; Merk, D.; Lamers, C.; Schubert-Zsilavecz, M. Novel prostaglandin receptor modulators: a patent review (2002 - 2012) - part II: EP receptor modulators. *Expert Opin Ther Pat*, **2013**, *23*(2), 233–267.

Pellowska, M.; Merk, D.; Schubert-Zsilavecz M. Advances in personalized medicine - medicinal chemistry and pharmacology of vemurafenib and ivacaftor. *Pharmazie*, **2013**, *68*(7), 484–491.

Merk, D.; Schubert-Zsilavecz, M. Repairing mutated proteins - development of small molecules targeting defects in the cystic fibrosis transmembrane conductance regulator. *Expert Opin Drug Discov*, **2013**, *8*(6), 691–708.

Merk, D.; Steinhilber, D.; Schubert-Zsilavecz, M. Characterizing ligands for farnesoid X receptor--available in vitro test systems for farnesoid X receptor modulator development. *Expert Opin Drug Discov*, **2014**, *9*(1), 27–37.

Merk, D.; Gabler, M.; Gomez, R.C.; Flesch, D.; Hanke, T.; Kaiser, A.; Lamers, C.; Werz, O.; Schneider, G.; Schubert-Zsilavecz, M. Anthranilic acid derivatives as novel ligands for farnesoid X receptor (FXR). *Bioorg. Med. Chem.*, **2014**, *22*(8), 2447–2460.

Merk, D.; Lamers, C.; Ahmad, K.; Carrasco Gomez, R.; Schneider, G.; Steinhilber, D.; Schubert-Zsilavecz, M. Extending the structure-activity relationship of anthranilic acid derivatives as farnesoid X receptor modulators - Development of a highly potent partial farnesoid X receptor agonist. *J Med Chem*, **2014**, *57*(19), 8035-8055.

Lamers, C.; Schubert-Zsilavecz, M.; Merk, D. Medicinal Chemistry and Pharmacological Potential of FXR antagonists. *Current Trends in Medicinal Chemistry*, **2014**, *14*(19), 2188-2205.

Pellowska, M.; Stein, C.; Pohland, M.; Merk, D.; Klein, J., Eckert, G.P.; Schubert-Zsilavecz, M.; Wurglics, M. Pharmakokinetic properties of MH84, a γ-secretase modulator with PPARγ agonistic activity. *J. Pharm. Biomed. Analysis*, **2014**, *102c*, 417-424.

Merk, D.; Lamers, C.; Weber, J.; Flesch, D.; Gabler M.; Proschak, E.; Schubert-Zsilavecz, M. Anthranilic acid derivatives as nuclear receptor modulators – development of novel PPAR selective and dual PPAR/FXR ligands. *Bioorg. Med. Chem.*, **2015**, *23*(3), 499-514.

andere Publikationen

Merk, D.; Schubert-Zsilavecz, M. Neue Ansätze bei Mukoviszidose. *Pharmazeutische Zeitung*, **2011**, *156*(37).

Merk, D.; Schubert-Zsilavecz, M. Chronische Niereninsuffizienz: Triterpenoid als Hoffnungsträger. *Pharmazeutische Zeitung*, **2012**, *157*(1).

Merk, D.; Schubert-Zsilavecz, M. Mukoviszidose: Erster Wirkstoff für kausale Therapie. *Pharmazeutische Zeitung*, **2012**, *157*(9).

Merk, D.; Schubert-Zsilavecz, M. Nicht-agonistische Inhibitoren der Cdk5-abhängigen Phosphorylierung von PPARγ als Insulin-Sensitizer der Zukunft? *Pharm Unserer Zeit*, **2012**, *41(*3).

Merk, D.; Schubert-Zsilavecz, M. Diabetes: Neue Wirkstoffe in Aussicht. *Pharmazeutische Zeitung*, **2012**, *157*(28).

Merk, D.; Schubert-Zsilavecz, M. Schilddrüsentherapeutika. *Pharmazie in unserer Zeit*, **2012**, *41(*5).

Merk, D.; Schubert-Zsilavecz, M. Nicht-agonistische Inhibitoren der Cdk5-abhängigen Phosphorylierung von PPARγ als Insulin-Sensitizer der Zukunft? *Pharm Unserer Zeit*, **2012**, *41(*3), 182–183.

Merk, D.; Schubert-Zsilavecz, M. Influence of genetic variability on drug actions. *Pharmakon*, **2013**, *1(*1).

Lamers, C.; Merk, D.; Schubert-Zsilavecz, M. Onychomycosis: drugs in the pipeline. *Pharmakon*, **2014**, *2(*3).

Lamers, C.; Schubert-Zsilavecz, M.; Merk, D. Drugs for the treament of hyper- and hypotrichosis. *Pharmakon*, **2014**, *2(*3).

Buchbeiträge

Mitarbeit an:

Ammon, Hermann P. T. (Hrsg.): **Hunnius Pharmazeutisches Wörterbuch.** 11. neu bearb. u. erw. Aufl., Walter de Gruyter: 2014.

10. Eidesstattliche Versicherung

ERKLÄRUNG

Ich erkläre hiermit, dass ich mich bisher keiner Doktorprüfung im Mathematisch-Naturwissenschaftlichen Bereich unterzogen habe.

Frankfurt am Main, den ……
Unterschrift

EIDESSTATTLICHE VERSICHERUNG

Ich erkläre hiermit an Eides Statt, dass ich die vorgelegte Dissertation über

……

Acylanthranilamidderivate als

……

Partialagonisten des Farnesoid X Rezeptors

……

selbstständig angefertigt und mich anderer Hilfsmittel als der in ihr angegebenen nicht bedient habe, insbesondere, dass alle Entlehnungen aus anderen Schriften mit angabe der betreffenden Schrift gekennzeichnet sind.

Ich versichere, die Grundsätze der guten wissenschaftlichen Praxis beachtet und nicht die Hilfe einer kommerziellen Promotionsvermittlung in Anspruch genommen zu haben.

Frankfurt am Main, den ……
Unterschrift

11. Danksagung

Allen voran danke ich Corina für ihre Unterstützung und ihr Verständnis während der gesamten Zeit meiner Promotion. Danke, dass du da bist!

Ganz besonders danke ich meinem Doktorvater Prof. Dr. Manfred Schubert-Zsilavecz als Betreuer, Lehrer und Förderer für seine Ideen, seine Unterstützung, seine Kritik und alle Freiheiten während der Promoition. Außerdem danke ich ihm für die Möglichkeiten, Tagungen und Kongresse zu besuchen, Publikationen zu verfassen und Kooperationen zu knüpfen, für die Arbeitsgruppen-seminare in Aigen und die Reisen zu Pharmacon in Davos.

Meinem Co-Betreuer Prof. Dr. Dieter Steinhilber danke ich für seine fachliche Unterstützung, seine Hilfe beim Verfassen von Publikationen und die Möglichkeit zur Nutzung von Geräten und Ressourcen.

Ich danke Jun.-Prof. Dr. Eugen Proschak und seinen Mitarbeitern für die Identifikation meiner sehr wertvollen Leitstruktur und alle Zusammenarbeit.

Danke, Christina für all unsere Zusammenarbeit in der Uni, viele gemeinsame Publikationen, unzählige nicht immer wissenschaftliche Diskussionen und für die guten, frohen Zeiten außerhalb der Uni! :p

Vielen Dank an meine Familie für ihre Unterstützung und meiner Mutter für den ersten Anstoß diese Promotion anzutreten!

Maren danke ich für die herzliche Aufnahme in Frankfurt und die gemeinsame Zeit im AK MSZ

Prof. Dr. K. Wanner danke ich für die erste Anleitung zum strikt korrekten wissenschaftlichen Arbeiten während meiner Masterarbeit, die später vieles erleichtert hat.

Dr. Eva Schaffert danke ich für die erste Ausbildung in der organischen Synthese und viel gute Zeit im Labor.

Mein besonderer Dank gilt außerdem…

… Matthias W. für jeden Ausgleich zum Promotionsalltag

… Mario für Unterstützung, Verständnis und die entspannte Leitung des Praktikums

… Matthias als Labornachbar für die gute Zusammenarbeit in Labor und Zellkultur und viel Spaß auch nach Feierabend

... meinen Labornachbarn Dalibor und Stefano für die entspannte und lustige Zeit im Labor

… Simon für seine Mitarbeit und sehr viel Spaß im Labor

… Astrid für ihre immer gute Laune und ihre Unterstützung bei der Carakterisierung meiner Substanzen und bei der Organisation von Davos

… Khalil für die gute Zusammenarbeit und die Hilfe bei jedem Zellkulturproblem

… Daniel für die gute Zusammenarbeit beim Assay

… Thomas

… Roberto für viele gute Dockingergebnisse

… Stefan für unzählige NMRs

… allen Kooperationspartnern, die zu dieser Arbeit beigetragen haben

… meinen Freunden in München dafür, dass sich trotz der wenigen Zeit, die ich zuhause bin, nichts geändert hat

… und allen meinen Kollegen im Arbeitskreis MSZ und Franca für die gute Zeit bei der Arbeit, im Praktikum, beim Grillen, beim Korrigieren, bei den Arbeitsgruppenseminaren in Aigen und bei Tagungen.

12. Anhang: Nachdrucke der Publikationen

Anhang I: Merk, D.; Schubert-Zsilavecz, M. Nuclear receptors as pharmaceutical targets: rise of FXR and rebirth of PPAR? *Future Med Chem*, **2012**, *4(*5), 587–588.

Anhang II: Merk, D.; Steinhilber, D.; Schubert-Zsilavecz, M. Medicinal chemistry of farnesoid X receptor ligands: from agonists and antagonists to modulators. *Future Med Chem*, **2012**, *4(*8), 1015–1036.

Anhang III: Lamers, C.; Schubert-Zsilavecz, M.; Merk, D. Therapeutic modulators of peroxisome proliferator-activated receptors (PPAR): a patent review (2008–present). *Expert Opin. Ther. Patents*, **2012**, *22(*7), 803–841.

Anhang IV: Merk, D.; Steinhilber, D.; Schubert-Zsilavecz, M. Characterizing ligands for farnesoid X receptor--available in vitro test systems for farnesoid X receptor modulator development. *Expert Opin Drug Discov*, **2014**, *9(*1), 27–37.

Anhang V: Merk, D.; Gabler, M.; Gomez, R.C.; Flesch, D.; Hanke, T.; Kaiser, A.; Lamers, C.; Werz, O.; Schneider, G.; Schubert-Zsilavecz, M. Anthranilic acid derivatives as novel ligands for farnesoid X receptor (FXR). *Bioorg. Med. Chem.*, **2014**, *22(*8), 2447–2460.

Anhang VI: Merk, D.; Lamers, C.; Ahmad, K.; Carrasco Gomez, R.; Schneider, G.; Steinhilber, D.; Schubert-Zsilavecz, M. Extending the structure-activity relationship of anthranilic acid derivatives as farnesoid X receptor modulators - Development of a highly potent partial farnesoid X receptor agonist. *J Med Chem*, **2014**, *57*(19), 8035-8055.

Anhang VII: Lamers, C.; Schubert-Zsilavecz, M.; Merk, D. Medicinal Chemistry and Pharmacological Potential of FXR antagonists. *Current Trends in Medicinal Chemistry*, **2014**, *14*(19), 2188-2205.

Anhang VIII: Merk, D.; Lamers, C.; Weber, J.; Flesch, D.; Gabler M.; Proschak, E.; Schubert-Zsilavecz, M. Anthranilic acid derivatives as nuclear receptor modulators – development of novel PPAR selective and dual PPAR/FXR ligands. *Bioorg. Med. Chem.*, **2015**, *23*(3), 499-514.

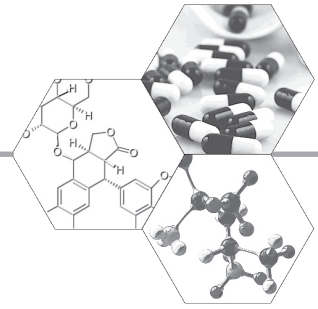

Nuclear receptors as pharmaceutical targets: rise of FXR and rebirth of PPAR?

"*The future research into modulators of nuclear receptors will have to respect the high physiologic impact of its targets and avoid compounds that exhibit full agonism.*"

Keywords: cdk5 ■ fibrates ■ FXR ■ glitazars ■ metabolic disorders ■ PPAR ■ thiazolidindiones

Nuclear receptors have gained a lot of pharmaceutical and medicinal interest in recent decades as they emerged as potential targets for the treatment of several endocrinologic diseases. In particular, targeting the receptor family of the peroxisome proliferator-activated receptors (PPAR) proved to be an effective strategy in medicating metabolic disorders. The joy of this success, however, was short-lived. As with the insulin-sensitizing thiazolidinediones (TZDs), rosiglitazone and troglitazone, the most clinically relevant PPARγ agonists were taken off the market due to adverse effects. Rosiglitazon showed an increased risk for cardiovascular events while troglitazone exhibited hepatotoxicity. Most recently the last available TZD, pioglitazone, was suspended by some authorities as it is suspected to promote bladder cancer. In addition, all TZDs showed fluid retention, weight gain and loss of bone mineral density as common side effects [1]. These adverse effects are partly explicable with the fact that PPARγ is not only expressed in adipose tissue where the desired effects are effectuated but, for example, also in the cardiovascular system and cardiomyocytes [2]. Additionally PPARγ-dependent activation of the epithelial sodium channel in the kidney has been shown for the TZD rosiglitazone [3]. The suitability of PPARγ as a target is therefore reasonably doubted, at least for the use of full agonists.

Fibrates, as another clinically important class of PPAR agonists, are indeed still available for treatment of dyslipidemia, especially hypertriglyceridemia, but they also have numerous undesirable effects – the most important of which are muscle toxicity and rhabdomyolysis [4]. The fibrates, which can be considered as fatty acid mimetics, in contrast to the TZDs activate PPARα, which is predominantly expressed in the liver where it controls the expression of several genes involved in fatty acid metabolism but can also be found in skeletal muscle and in the heart [2,5].

Before the market withdrawal of the TZDs and clofibrate, a lot of research has been carried out on the development of dual-PPARα/γ agonists that were thought to combine the beneficial effects of dual-PPAR agonism on metabolic disorders such as diabetes and dyslipidemia. This combination of agonism at two PPAR subtypes was chosen because of the fact that diabetes mellitus is in many cases associated with hypertriglyceridemia. Dual-PPARα/γ agonists were therefore thought to be effective agents against two metabolic disorders that often appear together. Tesaglitazar, as the most developed candidate of dual-PPARα/γ agonists, had advanced to clinical Phase III studies when it failed due to disadvantageous risk–benefit profiles as treatment with tesaglitazar, for example, increased serum creatinine levels [5]. Besides the metabolic side effects of PPAR agonists, most recently the suspicion of cancerogenicity was demonstrated for some compounds in several animal studies [6].

The development of PPAR agonists has until now been characterized by numerous drawbacks and the fact that most of the observed side effects of the compounds are dependent on the PPAR agonism itself, hinder further development of this class of pharmaceutical agents. On the other hand PPARs and other nuclear receptors are still very attractive targets for the development of new therapeutic strategies and have gained particular interest as they are highly involved in metabolism and metabolic disorders.

Most recently a second biochemical effect of the TZDs besides their PPARγ agonism was discovered. Rosiglitazone and some other PPARγ ligands have been shown to effectively inhibit the phosphorylation of Ser-273 in PPARγ by the cycline-dependent kinase (cdk) 5 *in vitro* and *in vivo*. This effect, however, was independent

Daniel Merk

Institute for Pharmaceutical Chemistry, Goethe University Frankfurt, Max-von-Laue-Str. 9, 60438 Frankfurt, Germany

Manfred Schubert-Zsilavecz

Institute for Pharmaceutical Chemistry, Goethe University Frankfurt, Max-von-Laue-Str. 9, 60438 Frankfurt, Germany
Tel.: +49 69 798 29339
E-mail: schubert-zsilavecz@pharmchem.uni-frankfurt.de

FUTURE SCIENCE part of fsg

of the agonistic activity of the compounds. As phosphorylation of Ser-273 is obesity-linked and as blocking of this phosphorylation exhibited PPARγ agonism-independent antidiabetic effects in animal studies, this might be a new promising approach for the development of antidiabetic PPAR ligands in case the side effects of the TZDs are only dependent on PPARγ agonism. A first set of nonagonistic PPARγ ligands that block Cdk5-mediated phosphorylation of Ser-273 has been described yet. In docking studies the compounds showed a different way of binding to PPARγ than the TZDs as they do not stabilize helix 12, which is crucial for activation and co-activator recruitment. SR1664, as the most promising compound, has already been shown to exhibit antidiabetic effects *in vivo* without being a PPARγ agonist. Should these results be clinically proven, the first nonagonistic PPARγ modulating drugs for treatment of diabetes might be on their way [1].

But not PPARy alone does hold promises as a pharmaceutical target for the treatment of metabolic disorders. With the farnesoid-X receptor (FXR), another nuclear receptor is in the focus of research. FXR was first reported in 1995 and later described as a receptor for bile acids [7]. Since then, research efforts have resulted in the development of several synthetic FXR agonists and with their help many physiologic effects of FXR activation have been discovered. Some of these effects are also desirable for the treatment of several diseases. FXR activation, for example, reduced plasma triglyceride levels *in vivo* by altering triglyceride synthesis and plasma glucose levels, by influencing insulin signaling [7,8]. FXR-overexpressing mice showed comparable results; while FXR-knockout mice developed hyperglycemia and insulin resistance [7]. Unfortunately, the available FXR ligands are not applicable as therapeutic drugs as they exhibit high toxicity or are not bioavailable. The intense academic and industrial interest, however, has already yielded 24 co-crystal structures of the FXR ligand-binding domain with several ligands and generated a strong SAR for FXR ligands. The SAR reveals that the FXR ligand-binding domain favors quite hydrophobic compounds as ligands, but the extensive research into FXR modulating agents justifies the hope that potent compounds with drug like properties might be developed in the future.

It is not only the required high lipophilicity of putative FXR ligands but also the fact that full FXR agonists might effect too many undesired side effects, which hinder the development of FXR modulating agents. The story of drugs that modulate nuclear receptors, especially the TZDs, has taught that full agonists at these receptors show quite a lot of physiologic effects because their target is nearly omnipresent in the body and has different functions dependent on the target tissue. The future research into modulators of nuclear receptors will have to respect the high physiologic impact of its targets and avoid compounds that exhibit full agonism. In addition, new insights into the pharmacology of PPAR, including the possibility to selectively block its phosphorylation without causing agonism, show that there may be many molecular ways to modulate nuclear receptors that we have not yet discovered.

Financial & competing interests disclosure

The authors have no relevant affiliations or financial involvement with any organization or entity with a financial interest in or financial conflict with the subject matter or materials discussed in the manuscript. This includes employment, consultancies, honoraria, stock ownership or options, expert testimony, grants or patents received or pending, or royalties.

No writing assistance was utilized in the production of this manuscript.

References

1 Choi JH, Banks AS, Kamenecka AM *et al.* Antidiabetic actions of a non-agonist PPARγ ligand blocking Cdk5-mediated phosphorylation. *Nature* 477, 477–483 (2011).

2 Wang N, Yin R, Liu Y, Mao G, Xi F. Role of peroxisome proliferator-activated receptor-γ in atherosclerosis. *Circ. J.* 75, 528–535 (2011).

3 Renauld S, Tremblay K, Ait-Benichou S *et al.* Stimulation of ENaC activity by rosiglitazone is PPARc-dependent and correlates with SGK1 expression increase. *J. Membrane Biol.* 236, 259–270 (2010).

4 Florentin M, Liberopoulos EN, Mikhailidis DP, Elisaf MS. Fibrate-associated adverse effects beyond muscle and liver toxicity. *Curr. Pharm. Des.* 14, 574–587 (2008).

5 Lindblom P, Berg AL, Zhang H *et al.* Tesaglitazar, a dual PPAR-a/g agonist. Hamster carcinogenicity, investigative animal and clinical studies. *Toxicol. Pathol.* 40, 18–32 (2011).

6 Ratner RE, Parikh S, Tou C. Efficacy, safety and tolerability of tesaglitazar when added to the therapeutic regimen of poorly controlled insulin-treated patients with type 2 diabetes. *Diab. Vas. Dis. Res.* 4, 214–221 (2007).

7 Fiorucci S, Mencarelli A, Distrutti E, Palladino G, Cipriani S. Targeting farnesoid-X-receptor: from medicinal chemistry to disease treatment. *Curr. Med. Chem.* 17, 139–159 (2010).

8 Lundquist JT, Harnish DC, Kim CY *et al.* Improvement of physiochemical properties of the tetrahydroazepinoindole series of farnesoid X receptor (FXR) agonists: beneficial modulation of lipids in primates. *J. Med. Chem.* 53, 1774–1787 (2010).

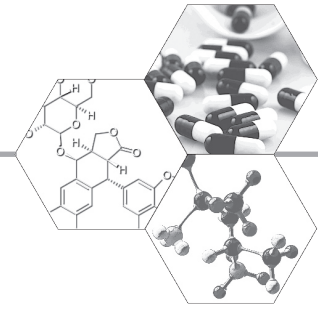

Medicinal chemistry of farnesoid X receptor ligands: from agonists and antagonists to modulators

The nuclear receptor farnesoid X receptor (FXR) has emerged as a highly promising target in preclinical development in recent years. A significant amount of research has been conducted and, although none has reached clinical use, many synthetic ligands of FXR have been described. This review outlines the available knowledge regarding the medicinal chemistry and SAR of these FXR ligands, and discusses the molecular interactions of the compounds with the FXR ligand-binding domain by interpreting the existing co-crystal structures.

Daniel Merk*, Dieter Steinhilber & Manfred Schubert-Zsilavecz

Institute of Pharmaceutical Chemistry, Goethe University, Frankfurt, Max-von-Laue-Straße 9, D-60438 Frankfurt am Main, Germany
*Author for correspondence:
E-mail: merk@pharmchem.uni-frankfurt.de

In its function as a ligand-activated transcription factor, the farnesoid X receptor (FXR) is, besides its primary role in bile acid homeostasis, involved in the regulation of genes related to metabolic processes. It is primarily expressed in the liver, kidneys, intestine and adrenal glands, where it is activated by its physiological ligands, the bile acids **(1–5)**. Chenodeoxycholic acid (CDCA) **(1)** is the most potent physiological FXR ligand, while the other bile acids are less active and ursodeoxycholic acid (UDCA) **(5)** is not an FXR agonist. The role of FXR as a bile acid sensor was first reported in 1999 when three groups found that certain bile acids activate FXR and modulate expression of its target genes [1–4]. Since then, FXR has gained a lot of academic and industrial interest. New physiological roles of FXR were discovered leading to reasonable hope that the **nuclear receptor** could serve as a pharmacological target in several pathophysiological conditions.

In humans, the four isoforms (hFXRα_{1-4}) are encoded by a single gene by alternative splicing of the RNA and by transcription using different promoters. Most target genes of FXR can be activated by all four isoforms although some are more responsive to certain isoforms [5,6]. As with all members of the nuclear receptor superfamily, all four isoforms consist of a ligand-binding domain (LBD) in the C-terminal region and a N-terminal DNA-binding domain with two cysteine-rich Zn^{2+} finger motifs for DNA binding. *FXR*β is a pseudogene in humans [7].

After activation by bile acids, FXR binds to its response elements on the DNA as a heterodimer with the retinoid X receptor (RXR) **(Figure 1)**. The physiological effects of FXR activation are, in several cases, mediated by upregulation of the inhibitory nuclear receptor small hetereodimer partner (SHP), which reduces the expression of genes such as SREBP1c [8] and eventually regulates PEPCK1, although the regulation of PEPCK1 is not clear [3,9–11]. Additionally, FXR directly upregulates the expression of the bile salt export pump (BSEP) [12,13]. The function as a sensor and regulator in cholesterol and bile acid metabolism is thought to be the major physiological role of FXR; however, in recent years, many more functions of FXR have been discovered. FXR activation has been found to reduce plasma triglyceride levels by altering triglyceride synthesis and metabolism [14,15], and to be involved in insulin sensitivity and glucose homeostasis [16,17]. Recent animal studies indicate that FXR-mediated effects on glucose levels are mainly due to modulation of insulin signaling. FXR activation with GW4064 **(9a)** or FXR overexpression in mice resulted in reduced plasma glucose levels, while FXR-deficient mice developed insulin resistance and hyperglycemia over time [1,18,19]. Although the results regarding the influence of FXR activation on glucose homeostasis in animal models are conflicting, the effects are certainly dependent on a complex interaction of FXR with other nuclear receptors [1,16,17,20]. At least one beneficial effect of FXR activation could be shown in a mouse model of renal injury in diabetic nephropathy. In this model, FXR knockout accelerated renal damage, while FXR activation by the agonist INT-747 **(6)** attenuated renal injury [21]. Other animal models of diabetes showed a protective effect of FXR agonists on kidney function and

FUTURE SCIENCE part of fsg

Key Term

Nuclear receptors: Ligand-activated transcription factors.

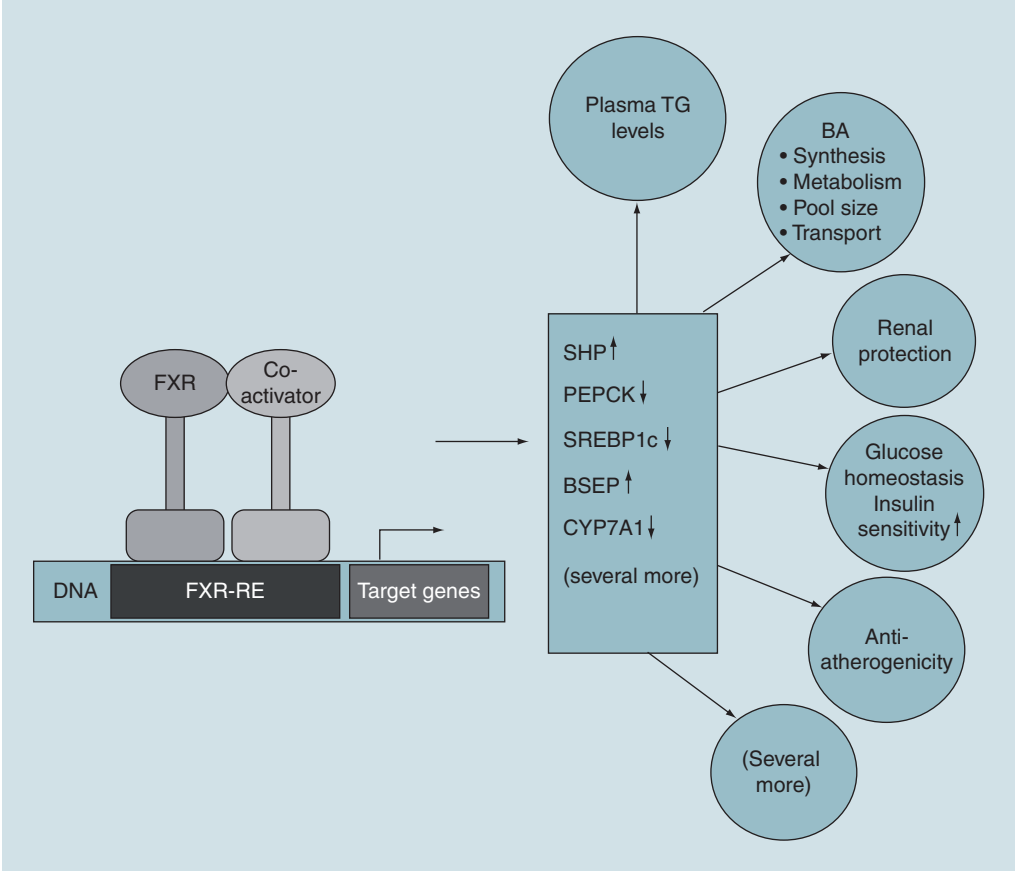

Figure 1. Target scheme of the farnesoid X receptor. Activated FXR binds to the DNA as a heterodimer with a co-activator (retinoid X receptor). Consequently, FXR target genes are transcribed, which leads to the physiologic effects. Here, only the most prominent target genes and physiological effects are depicted.
BA: Bile acid; FXR: Farnesoid X receptor; RE: Response element; TG: Triglyceride.

improvements of proteinuria, glomerulosclerosis and macrophage infiltration [22]. Furthermore a possible beneficial effect of FXR activation in atherosclerosis was discussed as animal models indicated that FXR activation with synthetic agonists protects against development of aortic plaques [23,24]. Additionally, *in vitro* studies showed antiproliferative effects of FXR agonists in MCF-7 TR1 and cholangiocarcinoma cells, which denotes an eventual role of FXR in breast cancer and cholangiocarcinoma cell growth [25,26]. Furthermore, FXR mediates pronounced effects on the liver including liver regeneration [27], while FXR-deficient mice spontaneously developed liver tumors [28,29]. Therefore, FXR activation might also be a promising strategy to treat liver diseases such as non-alcoholic fatty liver disease and liver fibrosis. Hence, the development of small molecules targeting FXR is a very promising approach for the treatment of certain forms of cancer as well as various metabolic diseases, such as dyslipidemia, hypertriglyceridemia and diabetes, including their secondary outcomes, such as chronic renal disease [15,22].

Co-crystal structures

At the time of writing, there are 24 co-crystal structures of the LBD of FXR (FXR–LBD) with several ligands including steroidal and nonsteroidal structures but no physiological ligand has been co-crystallized yet. For some structural classes the co-crystal structures give many insights into the SARs of FXR ligands. Unfortunately, neither the full length receptor is crystallized nor any native FXR protein without a ligand. An overview of the various crystal structures is given in **Table 1**. The numbering of amino acids in the various co-crystal structures of the human FXR–LBD differs in the literature. For better understanding, the numbering has been adjusted in this review; **Table 2 and Figure 2** give an overview over the relevant amino acids and their numbering.

Physiological FXR ligands

As stated above, bile acids are the most important physiological ligands of FXR. Among these, CDCA (3α,7α-dihydroxy-5β-cholane-24-oic acid, **1**; **FIGURE 3**) is the most effective activator (EC_{50} ~8 μM), while cholic acid (3α,7α,12α-trihydroxy-5β-cholane-24-oic acid, **2**), deoxycholic acid (3α,12α-dihydroxy-5β-cholane-24-oic acid, **3**) and lithocholic acid (3α-hydroxy-5β-cholane-24-oic acid, **4**) are weaker agonists (EC_{50} values of 10–50 μM) [4]. UDCA (3α,7β-dihydroxy-5β-cholane-24-oic acid, **5**), the 7-β-epimer of CDCA, is a poor partial agonist of FXR. Even at supraphysiological concentrations it does not activate FXR to the full extent, indicating that the configuration of the hydroxyl group in position 7 is highly important for the ability to activate FXR.

Some other metabolites, such as polyunsaturated fatty acids, are known to be weak FXR agonists [30]. Since the pharmacological use of bile acids is restricted by high toxicity, in recent years many synthetic FXR ligands have been reported. However, none of them has yet reached the status for clinical use.

Steroidal FXR ligands

Comprehensive work has been conducted with regards to the synthesis and biological evaluation of steroidal FXR ligands. Emanating from the structure of the bile acids as physiological ligands, many derivatives have been synthesized. A series of 6-α-alkyl-substituted CDCA derivatives showed high potency in FXR activation with small linear alkyl side chains, while bulkier substituents, such as benzyl, were inactive. 6-ethyl-chenodeoxycholic acid (6-ECDCA; obeticholic acid, INT-747, **6**) emerged as the most potent candidate among the 6-alkyl derivatives with an EC_{50} value of 99 nM and indicated the presence of an additional hydrophobic cage inside the LBD of FXR [31,32]. Most recently, INT-767 **(6a)** has been described as dual FXR/TGR5 agonist. **6a** is a sulfate homologue of **6** and has with an EC_{50} value of 0.03 μM; a slightly higher potency at FXR activation than **6** [33]. **6a** was selective for FXR over other nuclear receptors and for TGR5 over other G-protein-coupled receptors *in vitro*. It was also more effective in FXR activation than 6-ECDCA **(6)** and CDCA **(1)**. No toxicity was observed in human HepG2 liver

Table 1. Available co-crystal structures of farnesoid X receptor and ligands†.

Species	Protein	Ligand	PDB ID	Ref.
Homo sapiens	hFXR-LBD	**9j**	3RUT	[47]
Homo sapiens	hFXR-LBD	**9i**	3RUU	[47]
Homo sapiens	hFXR-LBD	**9h**	3RVF	[47]
Homo sapiens	hFXR-LBD	**9g**	3HC5	[45]
Homo sapiens	hFXR-LBD	**9f**	3HC6	[45]
Rattus norvegicus	rFXR-LBD	**Ia**	1OT7	[38]
Homo sapiens	hFXR-LBD	**9e**	3P88	[47]
Homo sapiens	hFXR-LBD	**9d**	3P89	[47]
Homo sapiens	hFXR-LBD	**9c**	3FXV	[42]
Homo sapiens	hFXR-LBD	**9a**	3DCT	[64]
Homo sapiens	hFXR-LBD	**9b**	3DCU	[47]
Homo sapiens	hFXR-LBD	**16e**	3OKH	[15]
Homo sapiens	hFXR-LBD	**16f**	3OKI	[15]
Homo sapiens	hFXR-LBD	**9m**	3GD2	[65]
Homo sapiens	hFXR-LBD	**8**	3BEJ	[37]
Rattus norvegicus	rFXR-LBD	**6**	1OSV	[38]
Homo sapiens	hFXR-LBD	**10**	1OSH	[34]
Homo sapiens	hFXR-LBD	**16d**	3OLF	[53]
Homo sapiens	hFXR-LBD	**16c**	3OMK	[53]
Homo sapiens	hFXR-LBD	**16**	3OMM	[53]
Homo sapiens	hFXR-LBD	**16a**	3OOK	[53]
Homo sapiens	hFXR-LBD	**16b**	3OOF	[53]
Homo sapiens	hFXR-LBD	**15b**	3L1B	[14]
Homo sapiens	hFXR-LBD	**15**	3FLI	[51]

†*Ligands refer to the structures discussed later in this review.*
hFXR: Human farnesoid X receptor; LBD: Ligand-binding domain; rFXR: Rat farnesoid X receptor.

Table 2. Relevant amino acids of the human farnesoid X receptor for interaction with known ligands†.

Number in review	Number in PDB sequence	Number in review	Number in PDB sequence
M_{265}	M_{279}	I_{335}	I_{349}
L_{287}	L_{301}	L_{340}	L_{354}
T_{288}	T_{302}	L_{348}	L_{362}
M_{290}	M_{304}	I_{352}	I_{366}
A_{291}	A_{305}	I_{357}	I_{371}
H_{294}	H_{308}	Y_{369}	Y_{383}
M_{328}	M_{342}	H_{447}	H_{461}
F_{329}	F_{343}	W_{454}	W_{468}
R_{331}	R_{345}	F_{461}	F_{475}
S_{332}	S_{346}	T_{474}	T_{488}

†*Numbering differs in several publications and the PDB and was adjusted for better understanding in this review.*

cells and in several mouse models of diabetes the compound ameliorated serum cholesterol and triglyceride levels. INT-767 **(6a)** might, therefore, be a possible candidate for further clinical development [33].

In contrast to the activity-increasing alkylation of the 6α-position of CDCA **(1)**, alkyl substituents in 3-α-position of CDCA or 7α-position of UDCA **(5)** had little influence on the FXR activation activity, while side chains in 3β- and 7β-position decreased the ability to activate FXR with increasing length of the side chain, suggesting that steric hindrance was responsible for the decreased activity [34].

Human FXR: (full-length receptor)

MVMQFQGLENPIQISPHCSCTPSGFFMEMMSMKPAKGVLTEQVAGPLGQN 50
LEVEPYSQYSNVQFPQVQPQISSSSYYSNLGFYPQQPEEWYSPGIYELRR 100
MPAETLYQGETEVAEMPVTKKPRMGASAGRIKGDELCVVCGDRASGYHYN 150
ALTCEGCKGFFRRSITKNAVYKCKNGGNCVMDMYMRRKCQECRLRKCKEM 200
GMLAECMYTGLLTEIQCKSKRLRKNVKQHADQTVNEDSEGRDLRQVTSTT 250
KSCREKTELTPDQQTLLHFIMDSYNKQRMPQEITNKILKEEFSAEENFLI 300
LTEMATNHVQVLVEFTKKLPGFQTLDHEDQIALLKGSAVEAMFLRSAEIF 350
NKKLPSGHSDLLEERIRNSGISDEYITPMFSFYKSIGELKMTQEEYALLT 400
AIVILSPDRQYIKDREAVEKLQEPLLDVLQKLCKIHQPENPQHFACLLGR 450
LTELRTFNHHHAEMLMSWRVNDHKFTPLLCEIWDVQ

Rat FXR: (LBD)

TELTVDQQTLL 250
DYIMDSYSKQRMPQEITNKILKEEFSAEENFLILTEMATSHVQILVEFTK 300
RLPGFQTLDHEDQIALLKGSAVEAMFLRSAEIFNKKLPAGHADLLEERIR 350
KSGISDEYITPMFSFYKSVGELKMTQEEYALLTAIVILSPDRQYIKDREA 400
VEKLQEPLLDVLQKLCKIYQPENPQHFACLLGRLTELRTFNHHHAEMLMS 450
WRVNDHKFTPLLCEIWDV

Figure 2. Amino acid sequences of human farnesoid X receptor and rat farnesoid X receptor. Important amino acids for ligand interaction are highlighted.
FXR: Farnesoid X receptor; LBD: Ligand-binding domain.
Data derived from PDB.

Further evaluation of steroidal FXR ligands yielded 23-*N*-(carbocinnamyloxy)-3α-7α-dihydroxy-6α-ethyl-24-nor-5β-cholane-23-amine **(7)**, a cinnamylcarbamate derivative of CDCA, as a potent FXR ligand with an EC_{50} of 150 nM, which is similarly potent as 6-ECDCA **(6)**, although the carboxylic acid moiety is substituted. These results suggested that no negative charge in the side chain is necessary to activate FXR and that additional hydrophobic space could be present in the receptor's binding pocket [35,36].

Furthermore, several bile alcohols have been investigated as FXR ligands. Conversion of the carboxylic group in CDCA to an alcohol hardly affected the ability to activate FXR, while the same conversion in cholic acid **(2)** even increased the activity [34]. However, epimerization of the hydroxyl groups in the 3- and 12-position of deoxycholic acid **(3)** decreased the activity on FXR, again indicating that the original 3α,12α-stereochemistry of the natural bile acids has to be maintained for FXR activation.

Another series of CDCA derivatives focused on substitution in the side chain. Hydrophilic as well as hydrophobic substituents have been introduced at positions 22–26. Little influence on the FXR activation activity was observed for 26- and 25-hydroxy derivatives of CDCA **(1)** as well as for all stereoisomers of 24- and 23-hydroxy-CDCA. However, 22-hydroxy-CDCA showed different results. While (22*R*)-hydroxy and (22*R*)-methyl-CDCA showed FXR agonistic activity comparable to that of CDCA **(1)**, the (22*S*)-isomers were inactive [36].

Bile acid derivatives with a shorter side chain were less potent in FXR activation than the native C_{24}-bile acids. C_{22}-steroids are no FXR

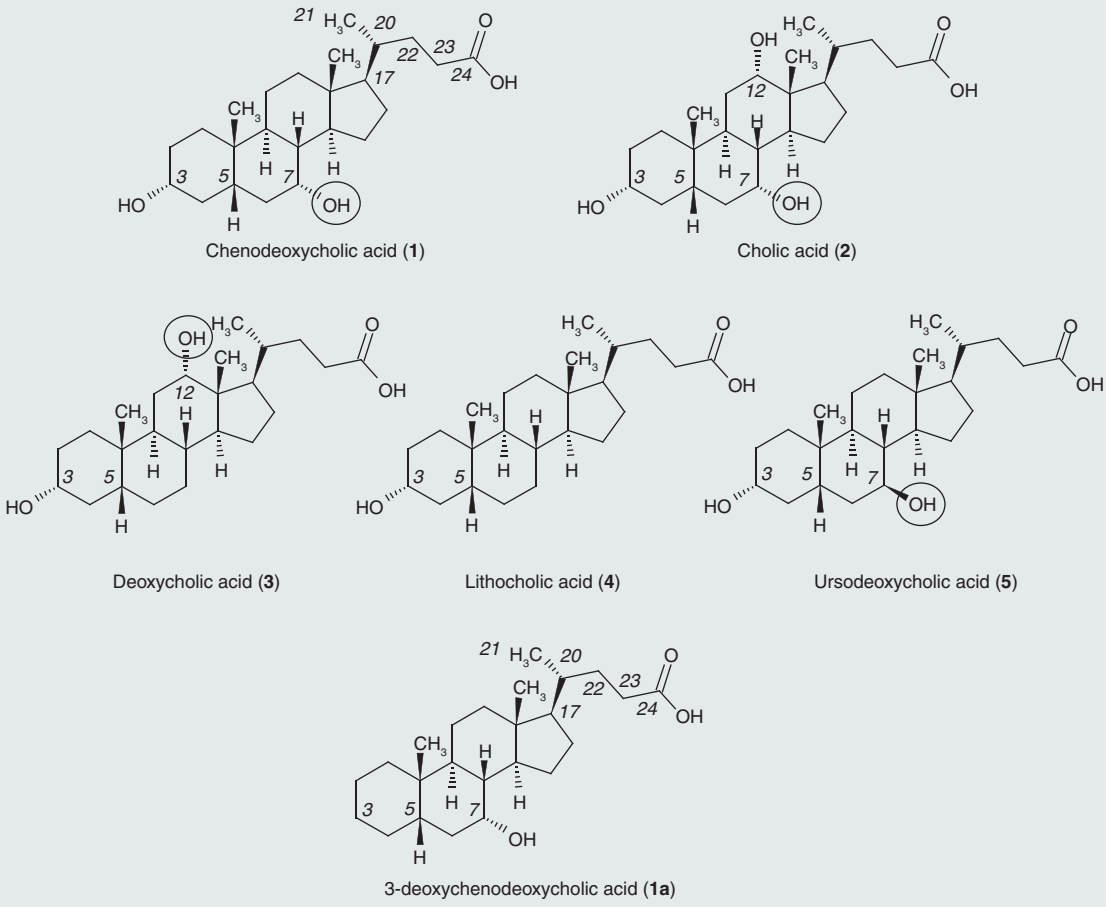

Figure 3. Physiological bile acids.

agonists, consistent with the fact that steroid hormones with a C_{21}-body do not activate FXR [36].

Finally, some work addressed the importance of the annealing conformation between rings A and B in bile acids for their ability to activate FXR. Natural bile acids always occur in A/B-*cis* conformation with the substituent at position 5 in β-orientation. This conformation distinguishes the bile acids from other steroids, as the A/B-*cis* conformation makes ring A stick out of the plane of the ring system. Some 5α-isomers of bile acids with a *trans* ring juncture conformation were examined on their ability to activate FXR, but the results were inconsistent. 5α-CDCA and some other 5α-bile acids matched the FXR activity of their natural 5β-isomers, while other 5α-derivatives were inactive on FXR.

6-ECDCA (INT-747, **6**) is the first steroidal FXR agonist that has advanced into clinical Phase II trials in patients with primary biliary cirrhosis (PBC) or non-alcoholic fatty liver disease. Most recently, the developer has announced positive results for INT-747 **(6)** as monotherapy for PBC. Until now, UDCA **(5)** is the only approved medication for PBC. A dosage of 10–50 mg of **6** per day significantly improved liver enzyme levels compared with placebo **(FIGURE 4)** [101].

Another more potent steroidal FXR ligand is MFA-1 **(8)** with an EC_{50} value of 17 nM. It was discovered in a high-throughput screening based on coactivator recruitment to FXR. MFA-1 contains the same methylation pattern as CDCA but no hydroxyl groups at positions 3 and 7 **(FIGURE 5)**. Instead, the steroid core is substituted with a carboxylic acid moiety at position 3 and the rings A and B are unsaturated, while the side chain of CDCA is replaced by benzyl ketone. Co-crystallization of MFA-1 with the LBD of FXR (residues 235–472) showed a different binding mode compared with the natural ligands **(FIGURE 6)**. The steroid ring was rotated approximately 180°, positioning the carboxylic

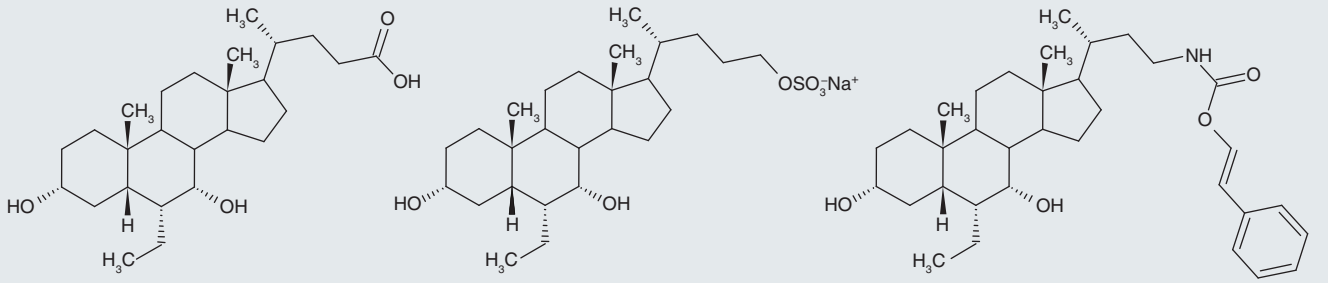

Figure 4. 6-ethyl-chenodeoxycholic acid (6) and derivative 7.

acid at ring A at the same site as the carboxylic acid in the side chain of bile acids is bound. However, MFA-1 **(8)** has not been applied in clinical trials [37].

For the synthetic steroid **8**, a co-crystal structure with the LBD of human FXR exists. As described above, this did not reveal the expected binding mode in accordance with **6**, but **8** was bound in a 180°-rotated position. In this orientation it formed hydrogen bonds between the carboxylate and Arg-331, and between the phenolic hydroxyl group and Thr-288. In addition, a π–π interaction among the phenyl ring and Phe-329 or Trp-454 might be present **(Figure 6)** [37].

Two more x-ray co-crystal structures of the FXR–LBD with a steroidal ligand exist so far. The bile acid derivative **6** was crystallized with the LBD of rat FXR **(Figure 7)**. It showed a strong electrostatic interaction between the carboxylate moiety and Arg-328, which is the same as Arg-331 in human FXR. In addition, the two hydroxyl groups at positions 3 and 7 both form two hydrogen bonds. The 3-hydroxy group interacts with Tyr-358 and His-444 while the 7-hydroxy group forms hydrogen bonds with Ser-329 and Tyr-366. The 6-ethyl moiety, which distinguishes **6** from the natural ligand **1**, lies in a hydrophobic cavity near Ile-349. To investigate the importance of the 3-hydroxy group for binding 3-deoxyCDCA **(1a)** was also co-crystallized with the rat FXR–LBD. **1a** lacks 3-OH and the 6-ethyl side chain of **6** while the 7-OH and 8-H stand in α-orientation. However, it showed the same binding position as **6** with the carboxylate forming an electrostatic interaction with Arg-328, and the 7-OH forming hydrogen bonds to Ser-329 and Tyr-366 **(Figure 7)** [38].

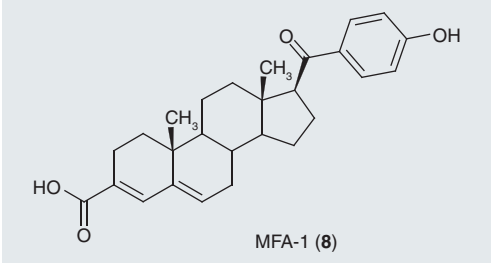

Figure 5. MFA-1 (8).

Nonsteroidal FXR-ligands

Due to the high potential for side effects of steroidal compounds, the search for nonsteroidal FXR ligands started soon after the discovery of FXR. Bile acids activate the pregnane X receptor, vitamin D receptor (VDR) and other nuclear receptor besides FXR, and interact with bile salt transport and binding proteins. Thus, there is a need for more selective ligands, which has led to the synthesis and biological evaluation of several compound classes.

GW4064

The first identified nonsteroidal high-affinity ligand of FXR, GW4064 **(9a)**, is still one of the most important chemical tools to study the molecular and physiological characteristics of FXR *in vitro* and *in vivo*. However, due to poor bioavailability [39] and toxicological issues [40], especially concerning the stilbene moiety, it is not suited for clinical use. The isoxazole derivative was optimized from a hit of a combinatorial library screening in a cell-free ligand-sensing assay [41]. Compound **9a** has an EC_{50} value of approximately 90 nM on FXR with a relative efficacy of 140% compared with CDCA **(1)**. During the development process of GW4064, **(9a)** other isoxazole derivatives were also identified. Thereby, it was found that the carboxylic acid at the stilbene moiety is most effective in *meta*-position and that larger lipophilic

substituents at position 5 of the isoxazole are favored. The fact that 5-methylisoxazoles failed to activate FXR, but 5-isopropyl and 5-tert-butyl derivatives were highly active, suggested that a lipophilic subpocket has to be filled for FXR activation. However, the crucial step in optimization was the introduction of a bi-*ortho*-substituted aryl moiety at position 3 of the isoxazole as the *ortho* substitution forces the aryl ring out of the plane of the isoxazole [41].

GW4064 **(9a)** is a full FXR agonist and shows no activity on other nuclear receptors such as RXR at concentrations up to 1 µM. Several series of structural analogues of GW4064 **(9a)** have been synthesized, but none of the derivatives could clearly outmatch the potency of the original isoxazole derivative. Replacement of the dichlorophenyl substituent at position 3 of the isoxazole by a dichloropyridine *N*-oxide **(9l)** only slightly improved the potency of the substance but enhanced aqueous solubility and membrane permeability [42]. In addition, the potentially toxic chlorosubstituted stilbene moiety could be replaced in **9k** and **9l** by methyl(2-(trifluormethyl)pyridin-3-yl)aminomethylbenzoic acids to yield structures with slightly higher potency than **9a** [43]. However, the new derivatives showed that the 3-(2,6-dichlorophenyl)-5-isopropyl-isoxazole moiety is essential for the FXR activity of the compounds. In contrast with the agonistic activity of GW4064 with an isopropyl-group in the 5-position of isoxazole, introduction of bulky residues, such as phenyl **(9o)**, 2-naphthyl **(9p)** or 4-biphenyl-substituents **(9q)**, at that position yielded FXR antagonists **(FIGURE 8)** [44]. In addition to expanding the SAR of isoxazoles as FXR ligands, some pharmacokinetic and physicochemical properties, such as cell permeability, have been improved using new derivatives [41–46].

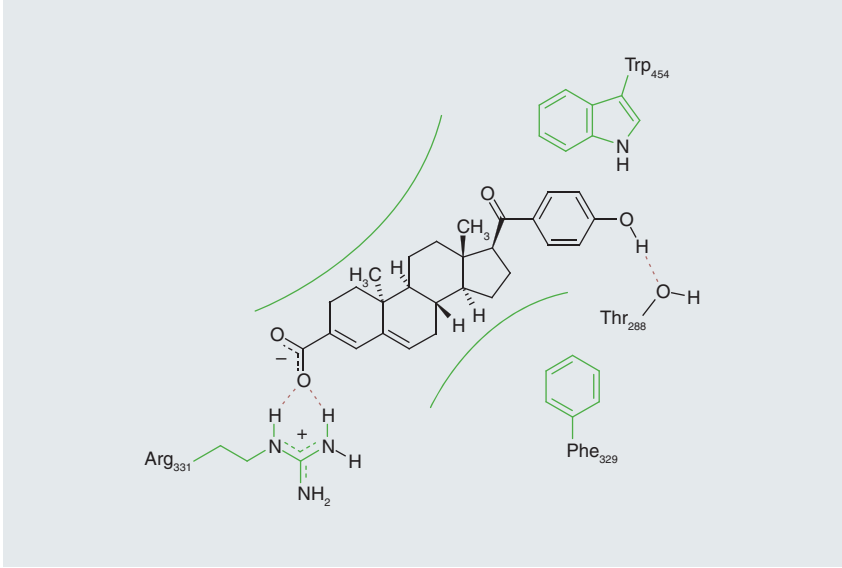

Figure 6. Binding mode of MFA-1 (8) to human farnesoid X receptor.

The most potent of the 3-(2,6-dichlorophenyl)-5-isopropyl-isoxazole derivatives have been co-crystallized with the FXR–LBD and x-ray analysis of the crystal structures revealed the most important interactions of the agonists with the receptor **(FIGURE 9)**. A strong electrostatic interaction is formed between the carboxylic acid moiety

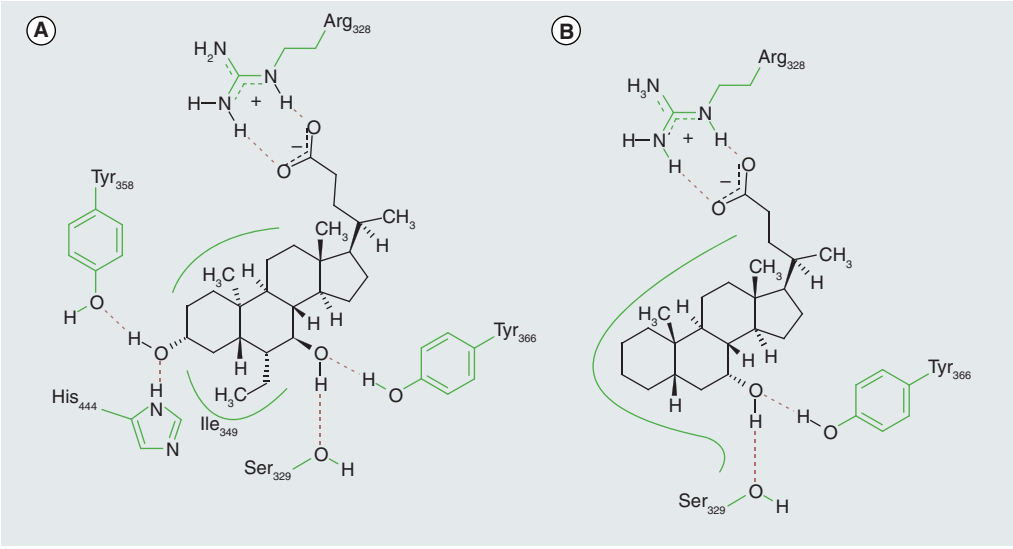

Figure 7. Binding mode of bile acids to rat farnesoid X receptor.
(A) 6-ethyl-chenodeoxycholic acid **(6)** and **(B)** 3-deoxychenodeoxycholic acid **(1a)**.

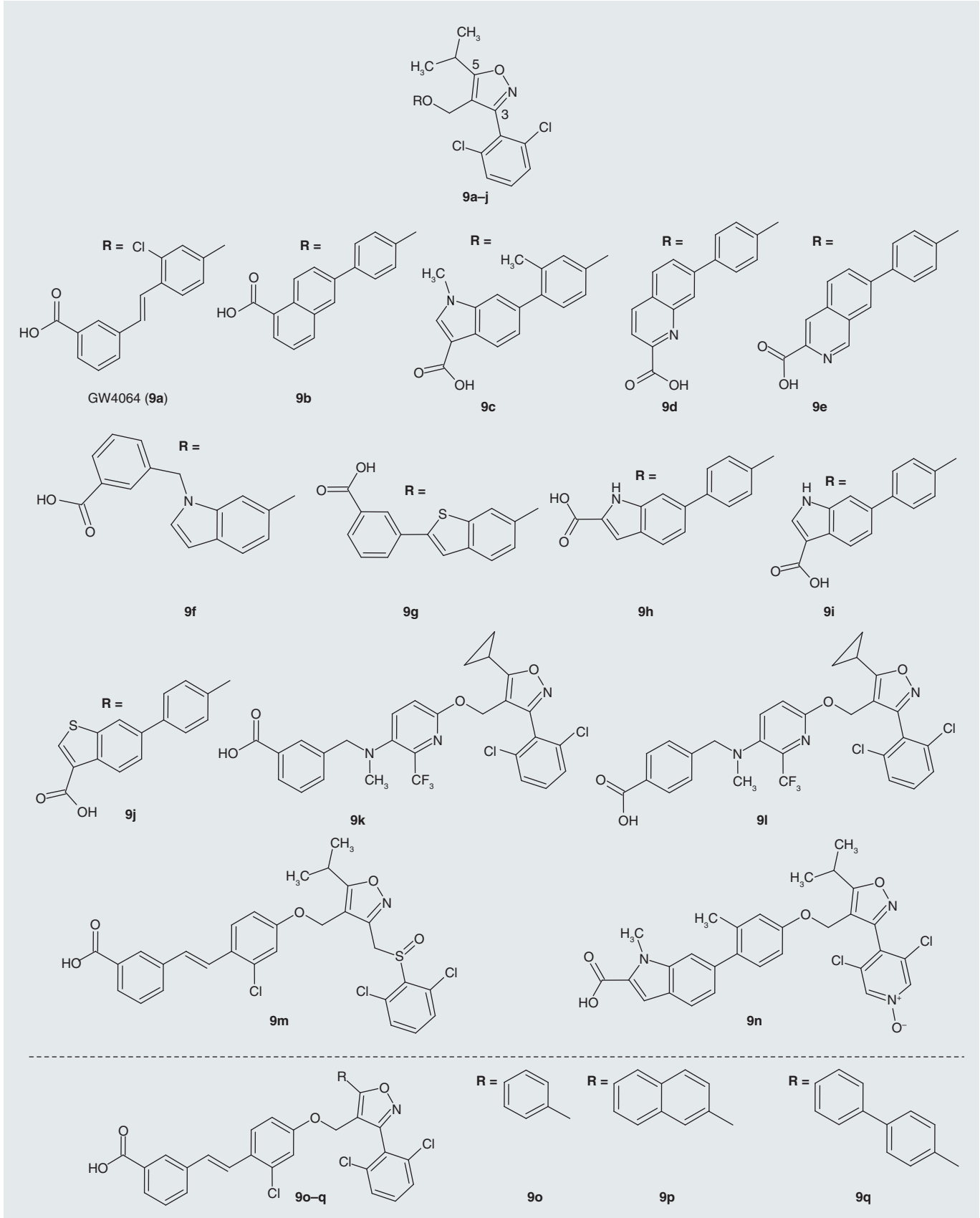

Figure 8. GW4064 (9a) and derivatives 9b-q.

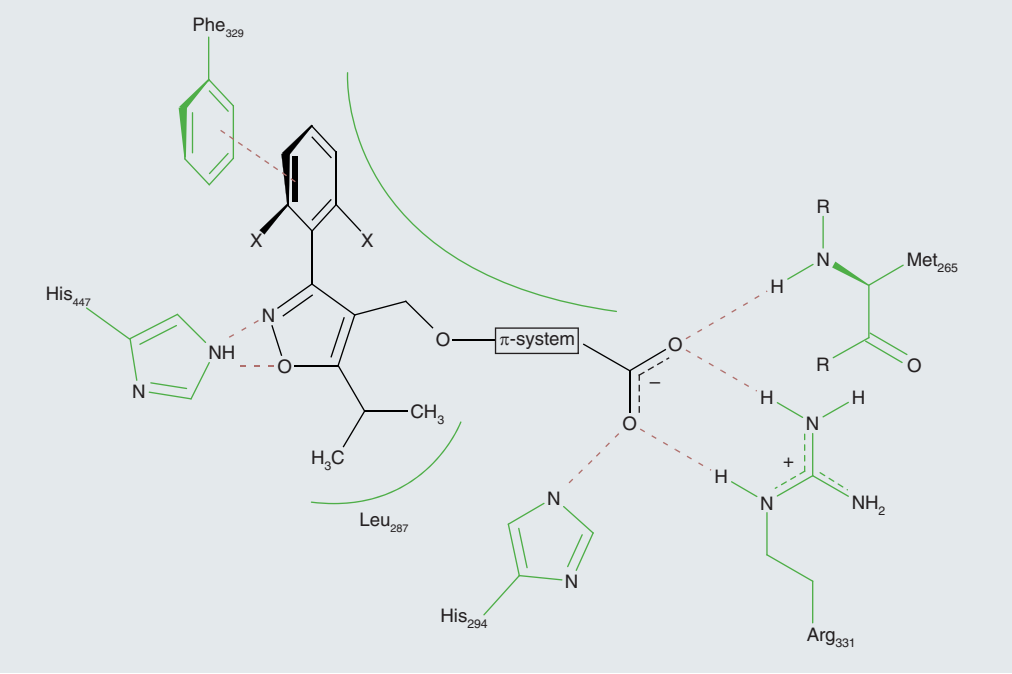

Figure 9. Binding mode of GW4064 (9a) and derivatives 9b–k to human farnesoid X receptor.

of **9a** and the guanidine side chain of Arg-331. This interaction is weakened when the carboxylic acid functionality is moved from the *meta* position of the terminal ring to the *para* position, while it is well tolerated in *ortho* position indicating that the orientation of the carboxylic acid is highly important for binding to FXR [47]. The electrostatic interaction with Arg-331 was present in derivatives **9a, 9c 9g, 9i, 9j** and **9m** but not in the other co-crystallized compounds **(FIGURE 9)**. Besides the ionic bonding to Arg-331, the carboxylic acid in some derivatives was able to accept an hydrogen bond from Met-265 and His-294 but none of these interactions alone could compensate the loss of the ionic interaction with Arg-331 [42,45,47]. The second important polar interaction is formed from the isoxazole nitrogen to His-447, but this hydrogen bond was not present in the crystal structures of all 3-(2,6-dichlorophenyl)-5-isopropyl-isoxazole derivatives (e.g., it was not observable in the co-crystal structure of **9a**) [42,44,47]. However, no further polar interactions with the FXR–LBD could yet be found for 3-(2,6-dichlorophenyl)-5-isopropyl-isoxazole derivatives.

Important hydrophobic interactions are formed between the isopropyl moiety and Leu-287 that provides a hydrophobic cavity as well as between the dichlorophenyl ring and Phe-329 [42,45,47]. The π–π interaction with Phe-329 is only possible with two substituents in the ortho position that make the aromatic ring flip out of plane [45]. **FIGURE 9** summarizes the interactions of the isoxazole derivatives **9a–k** with the FXR–LBD.

In addition, the analysis of the interactions of the isoxazole derivatives with the nuclear receptor obtained from the co-crystal structures revealed that the geometry at the isoxazole core is a very important factor. The angles between the substituents at positions 3, 4 and 5 of the isoxazole place the interacting groups in perfect orientation and explain the fact that GW4064 is still one of the most potent FXR agonists.

Fexaramine

After the isoxazole GW4064 **(9a)**, fexaramine **(10)** was the next high-affinity nonsteroidal FXR agonist that was discovered **(FIGURE 10)**. It was obtained by lead optimization from a benzopyrane-based combinatorial library that was screened with a luciferase reporter gene assay [48]. The first hit was optimized systematically in three regions whereupon the original benzopyrane moiety was replaced with biaryl and styrenyl units. The entire optimization process yielded three highly potent FXR ligands – fexaramine **(10)**, fexarine **(10a)** and fexarene **(10b)** – all containing a 3-methylcinnamate and a cyclohexanecarboxamide moiety **(FIGURE 10)**. The most potent compound, fexaramine, has an

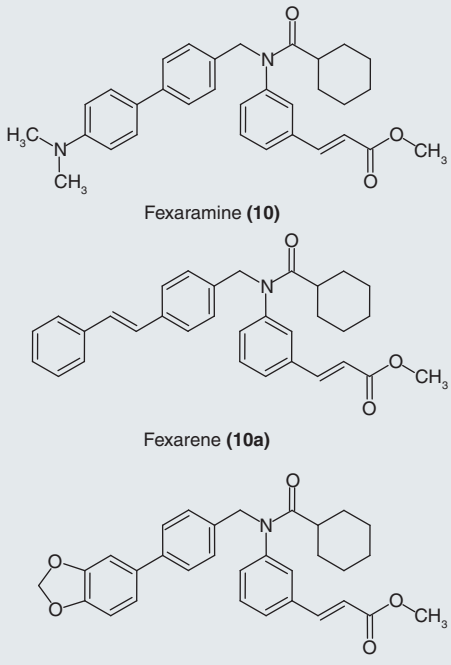

Figure 10. Fexaramine (10) and derivatives 10a and 10b.

EC_{50} value of 25 nM on FXR and was the first substance co-crystallized inside the FXR–LBD [4,34]. This co-crystal structure revealed only two polar interactions of **10** with the receptor (i.e., two hydrogen bonds from the amide carbonyl oxygen to His-294 and Ser-332; **Figure 11**). Van der Waals' interactions are present between the cyclohexyl moiety and Ile-335 and Leu-340 as well as between the methyl ester and Met-291, Leu-348 and Ile-352. Furthemore, the biphenyl moiety has van der Waals' contacts with two aliphatic and aromatic residues, but there is no defined π–π interaction **(Figure 11)** [34].

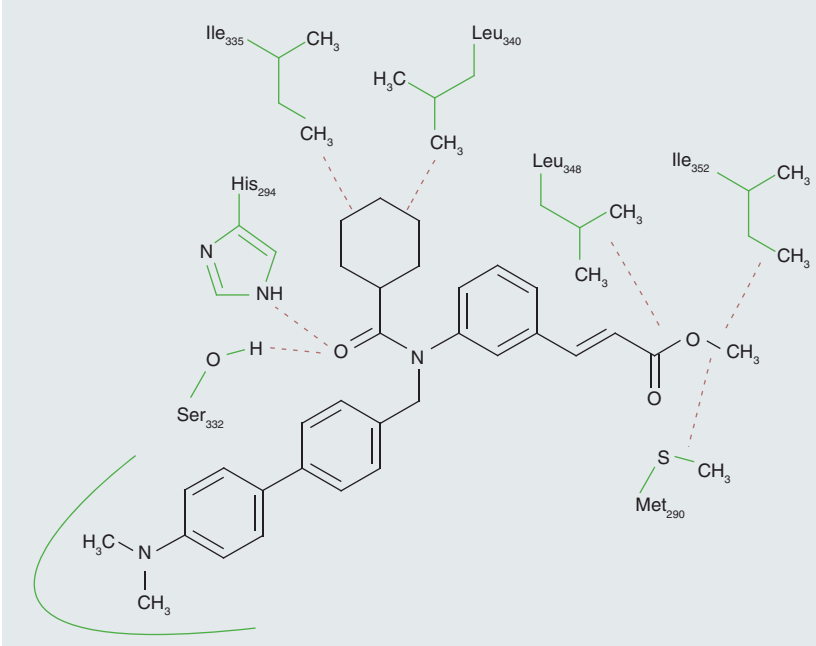

Figure 11. Binding mode of fexaramine (10) to human farnesoid X receptor.
Data from [34].

Biological characterization of fexaramine **(10)** revealed some very interesting facts. In mRNA-expression experiments with high-density oligonucleotide arrays, CDCA **(1)**, GW4064 **(9a)** and fexaramine **(10)** showed different profiles of gene regulation and expression. This observation led to the assumption that small molecules could act as specific FXR modulators activating only certain target genes. The development of FXR modulators with a specific profile could be of great therapeutic benefit and such modulators could outmatch full FXR agonists as FXR is involved in many physiological processes and animal studies have shown that full activation of the nuclear receptor can lead to serious physiological imbalances and pathophysiological conditions [1,34].

AGN31 & AGN29

The synthetic retinoid TTNPB (4-[(E)-2-(5,6,7,8-tetrahydro-5,5,8,8-tetramethyl-2-naphthalenyl)-1-propenyl]benzoic acid, Arotinoid acid, **11**) was also found to have a low affinity for FXR, although it is actually a ligand of the retinoic acid receptor **(Figure 12)**. It was optimized for better FXR affinity by introducing bulky substituents at the central isoprene moiety. Introduction of trimethylsilyl and *n*-butyl units at this position yielded AGN29 **(12)** and AGN31 **(13)**, respectively, which are two medium potent activators of the FXR–RXR heterodimer with EC_{50} values of approximately 2 µM. Since both compounds also have a significant affinity to RXR, it is not proven that their action is mediated by direct binding to FXR [49].

Pyrazolidine-3,5-diones

A virtual screening program including more than 120,000 compounds revealed pyrazolidine-3,5-diones as potential lead structures for the development of FXR agonists. The first 200 hits of the screening were filtered for drug-like properties and docked into the FXR binding pocket. This led to the discovery of the pyrazolidine-3,5-dione derivative **14** with an EC_{50} value of 5 µM as potential lead structure for

further optimization **(FIGURE 13)**. By variation of the substituents at the pyrazolidine-3,5-dione core structure, a couple of compounds including **14a** and **b** were generated, which exhibited full or partial agonistic activity at FXR comparable with the activity of CDCA **(1)** with EC_{50} values ranging from 2 to 6 µM [50].

FXR-450 & derivatives

Most recently, a luciferase reporter gene assay-based high-throughput screening of the Exelixis compound library identified a class of azepino[4,5-b]indoles as potent FXR agonists **(FIGURE 14)**. The first hit of this screening was optimized to yield the compound FXR-450 (WAY-362450, XL335, **15**), which exceeds the activity of both GW4064 **(9a)** and fexaramine with an EC_{50} value of 4 nM and 149% efficacy compared with CDCA. In addition, the derivative was selective for FXR compared with other nuclear receptors up to concentrations of 1 µM and showed acceptable oral bioavailability despite its poor aqueous solubility. The compound reached two clinical Phase I trials of which one was completed and one was terminated due to pharmacokinetic issues but not due to safety or tolerability [51,102].

Since FXR-450 **(15)** showed poor aqueous solubility due to its high lipophilicity and its planar structure, a series of analogues with improved hydrophilicity was synthesized. In this series, the indole core was replaced by a 2-cyano-pyrrole moiety and the azepine olefin was reduced, twisting the azepine ring out of its planar conformation **(FIGURE 14)**. The resulting compounds showed highly improved aqueous solubility but also a significant loss in potency with the most potent derivative **15a** having an EC_{50} value of 280 nM. This might be due to the nonplanar structure of the compounds with the substituents not in optimal position for binding to the cavities of the nuclear receptor [52].

In another approach, to improve the physicochemical and pharmacokinetic properties

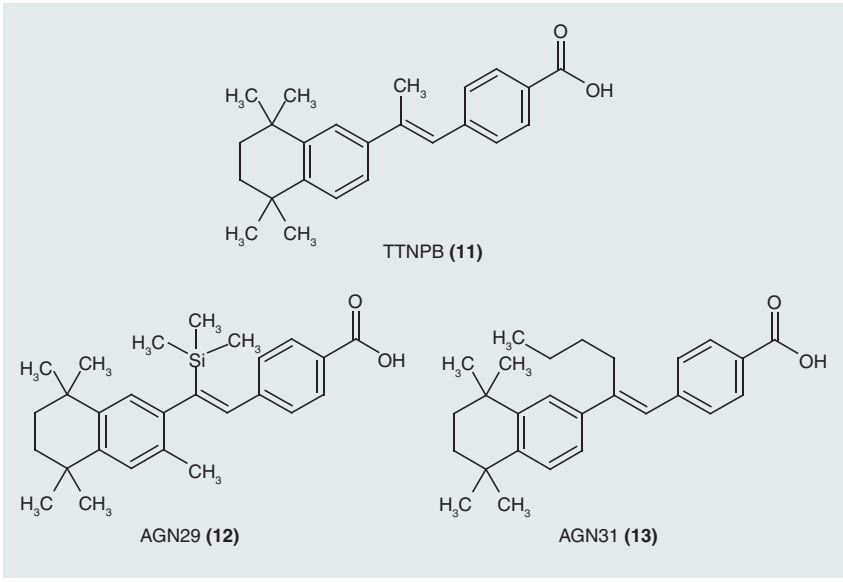

Figure 12. Retinoid TTNPB (11) and derivatives AGN29 (12) and AGN31 (13).

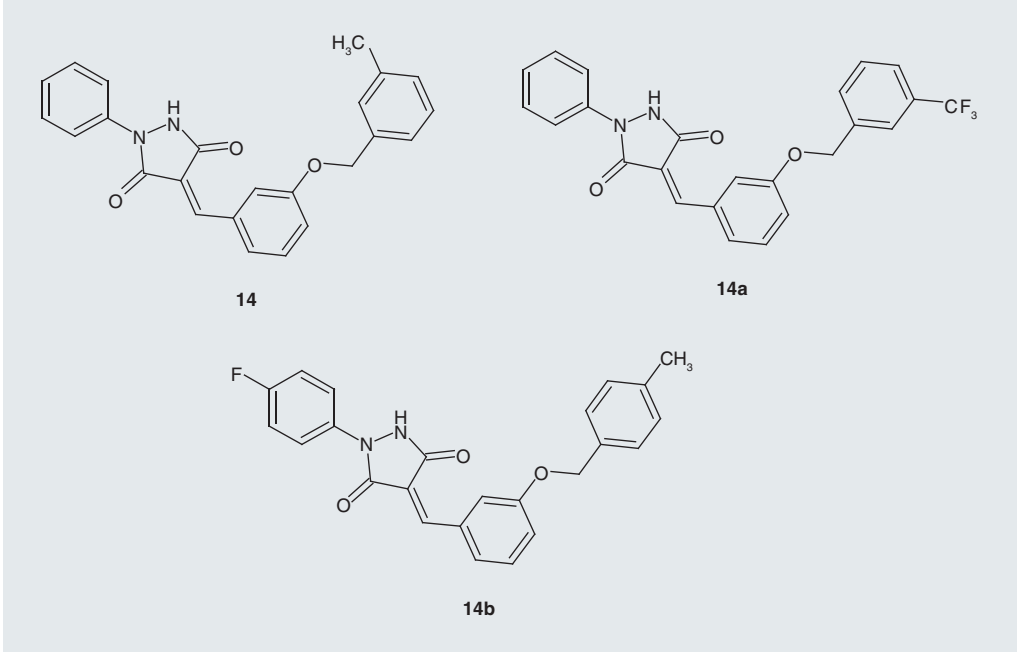

Figure 13. Pyrazolidine-3,5-dione 14 and derivatives 14a and 14b.

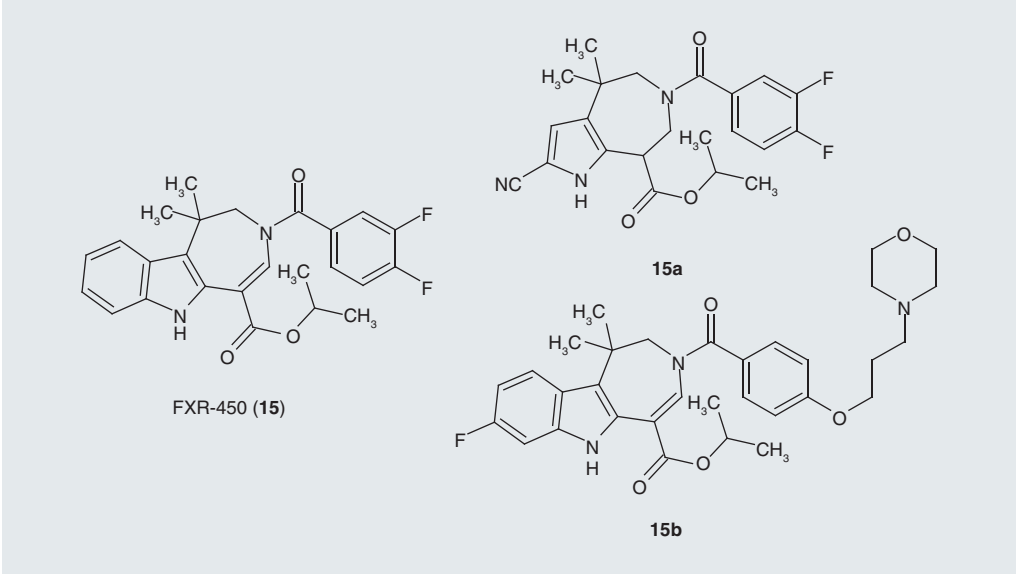

Figure 14. Farnesoid X receptor-450 (15) and derivatives 15a and 15b.

of FXR-450 **(15)**, the azepino[4,5-b]indole core structure was unchanged but polar amino substituents were introduced in *meta-* or *para-*position of the benzoyl moiety. This led to a strong improvement in the aqueous solubility of the compounds while the loss of agonistic potency was still acceptable. Introduction of a morpholinopropyloxy or morpholinoethyloxy moiety in *para* position proved to be the most suitable derivatisation. In addition, a fluorine atom was introduced at position 8 of the indole core to improve metabolic stability. The resulting compound **15b** showed good solubility in aqueous vehicles, an EC_{50} of 88 nM for hFXR with approximately 200% efficacy compared with GW4064 **(9a)** and high microsomal stability. In animal studies with rhesus monkeys, it significantly lowered TG, VLDL and LDL [14,52].

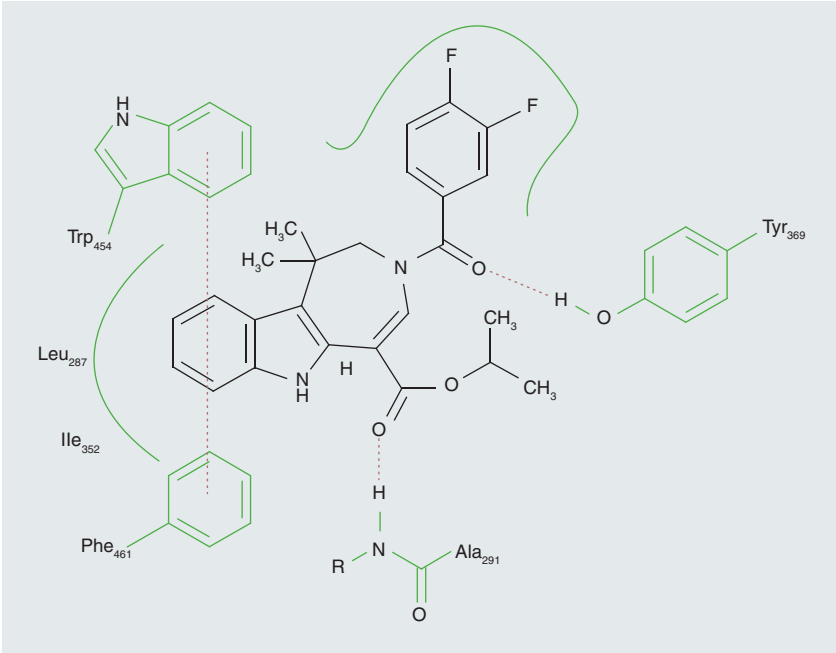

Figure 15. Binding mode of farnesoid X receptor-450 (15) to human farnesoid X receptor.

Two co-crystal structures have been generated with **15** and **15b**. x-ray analysis of **15** bound to the FXR–LBD revealed four important interactions **(Figure 15)**. There are two strong hydrogen bonds formed between the ester carbonyl oxygen and the amide hydrogen of Ala-291, and between the amide carbonyl oxygen and Tyr-369. In addition, the indole core structure is kept between the aromatic systems of residues Phe-461 and Trp-474 inside helix 12 **(Figure 15)** [51].

The co-crystal structure of **15b** with the FXR–LBD shows a binding orientation comparable to **15** with the same molecular interactions **(Figure 16)**. In addition, one internal hydrogen bond is formed between the indole-NH and the ester carbonyl oxygen, which rigidifies the molecule. The propylmorpholine moiety is oriented towards a hydrophobic space of helix 2 (residues Ile-335, Leu-340 and Leu-348), which is also occupied in the co-crystal structure of **10** and changes its position in comparison with the crystal structure of **15 (Figure 15)** [14]. An additional hydrogen bond might be formed between the phenolic ether oxygen and the amide NH of Ser-332 **(Figure 16)**.

Benzimidazole-based FXR ligands

One crucial problem of all potent FXR ligands developed so far is their poor aqueous solubility, which is attributed to the high lipophilicity of the FXR target site. Since the lipophilic bile acids are the natural ligands of FXR, the LBD essentially contains hydrophobic areas and few polar groups. This makes the development of hydrophilic FXR ligands a challenging problem.

The design of the benzimidazole-based FXR ligands starting from hits of a scintillation proximity assay-based screening with the LBD of hFXR considered this fact from an early point in development. The SAR of the benzimidazole derivatives **16a–f (FIGURE 17)** displayed a broad range of possible lipophilic substituents at the imidazole moiety (R^1) and the side chain (R^2) but with the introduction of polar residues the potency was significantly lowered. The variability of the substituent at the amide nitrogen (R^3) was even lower with phenyl and cyclohexyl as the

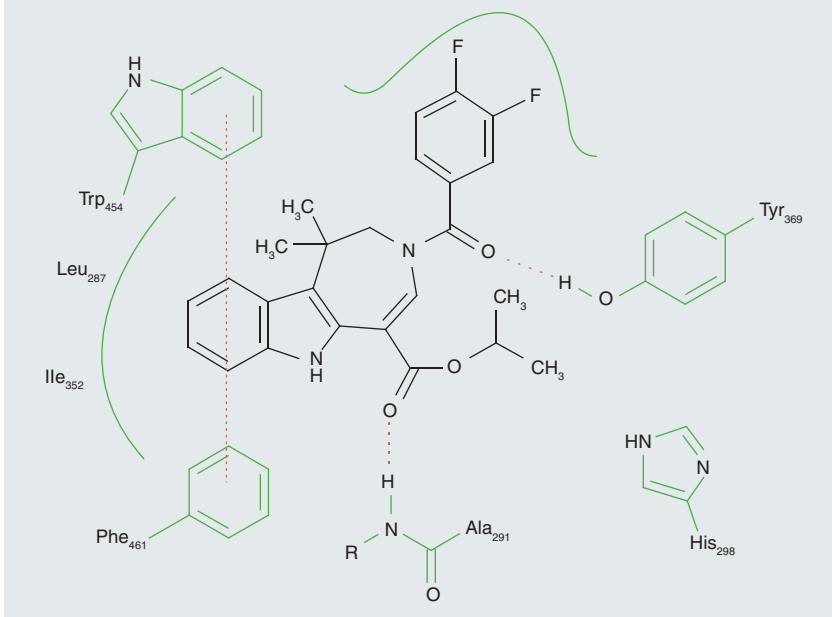

Figure 16. Binding mode of 15b to human farnesoid X receptor.

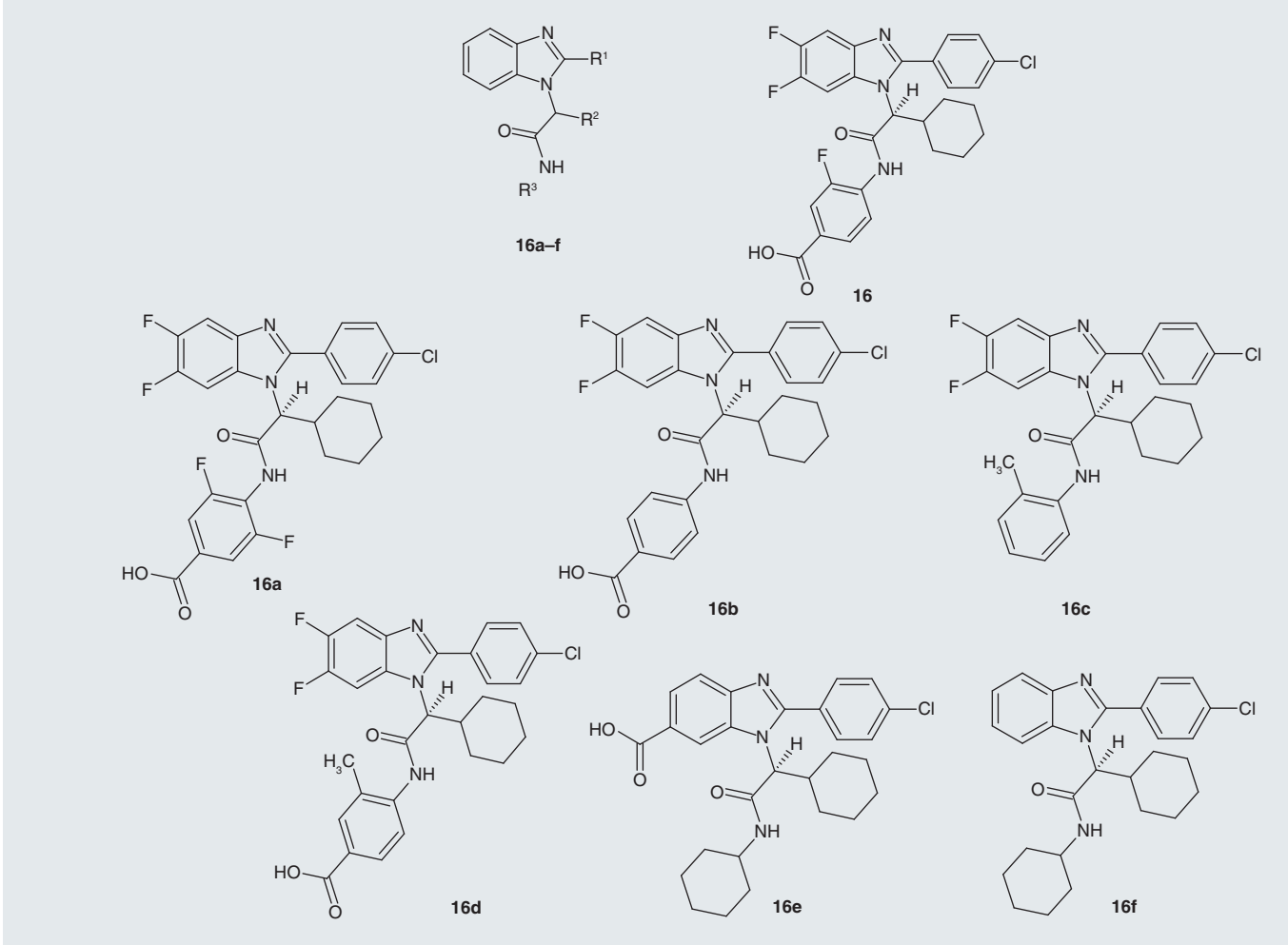

Figure 17. Benzimidazoles 16 and 16a–f.

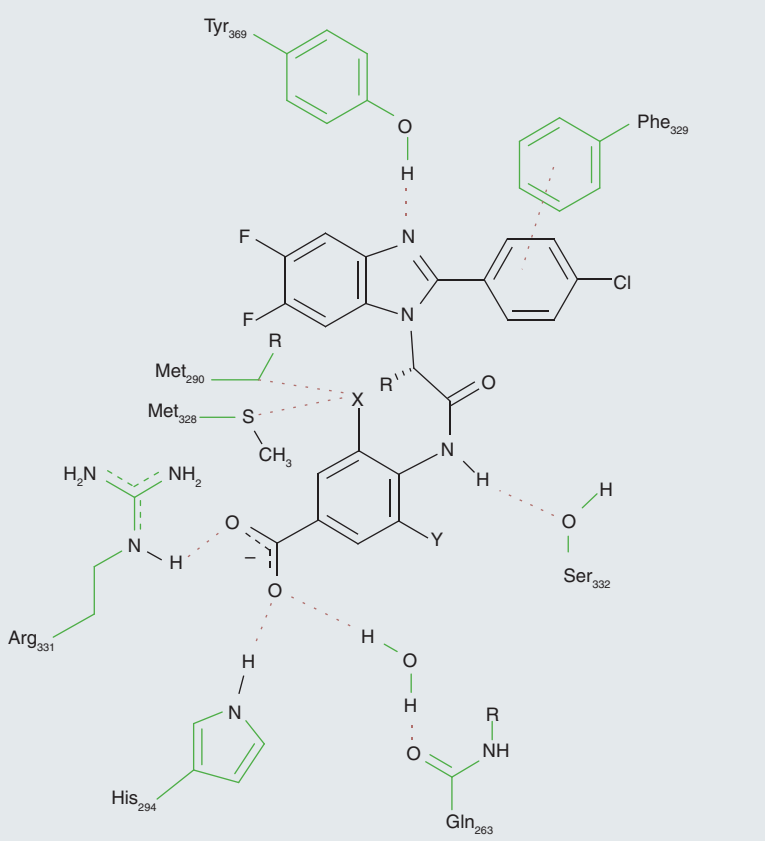

Figure 18. Binding mode of benzimidazoles 16a–f to human farnesoid X receptor.

only tolerated moieties. The only polar interactions of the first set of benzimidazole derivatives and FXR were observed for the imidazole nitrogen and the amide nitrogen as hydrogen bond acceptors [15].

Analysis of the binding mode of the first benzimidazole derivatives revealed an unexplored and more polar region in the FXR–LBD in proximity to the amide nitrogen **(Figure 18)**. Further optimization of the lead structures by variation of the substituent at the amide nitrogen (R^3) and introduction of several carboxylic acids and tetrazoles yielded 4-{(*S*)-2-[2-(4-chlorophenyl)-5,6-difluorobenzimidazol-1-yl]-2-cyclohexylacetylamino}-3-fluorobenzoic acid **(16)** as a potent FXR agonist with an EC_{50} value of 0.87 μM, no activation of other nuclear receptors and with superior physicochemical properties compared with established FXR ligands. The compound also showed plasma triglyceride and cholesterol lowering activities *in vivo*. Hence, the benzimidazole core provides a promising lead for FXR ligands and further exploration and research of this substance class will doubtless be conducted [53].

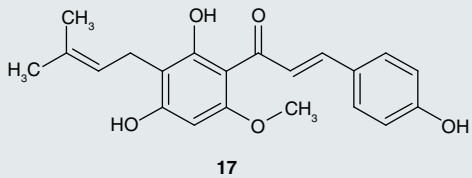

17

Figure 19. Xanthohumol (17).

Benzimidazole derivatives represent another class of nonsteroidal FXR agonists that are well investigated with co-crystal structures in the LBD of the nuclear receptor. The crystal structures revealed a hydrogen bond between the N3 of the benzimidazole core and Tyr-369 as important polar interaction by this substance class with FXR **(Figure 18)**. The fact that the corresponding indole derivatives (CH for N3) fail to bind and activate FXR is in accordance with this finding [15,53]. Another (although, much weaker) hydrogen bond is formed by the amide nitrogen with Ser-332, but this interaction was not present in every derivative co-crystallized [15,53]. Comparable with the results of the crystal structure analysis of compound **9a** and derivatives, there were no further polar interactions found in the first set of benzimidazoles. However, the crystal structures revealed a more polar region in the receptor next to the amide-bound cyclohexyl moiety of **16f**, which was not yet occupied by the ligand. This polar region consisted of the amino acids His-294 and Arg-331 that have already been shown to form polar interactions with the carboxylates of **6** and **9a**. Introduction of a benzoic acid moiety at the amide yielded the benzimidazole derivatives **16, 16a, b** and **d** that formed an additional polar interaction with the carboxylate acting as a hydrogen bond acceptor for Arg-331 **(Figure 18)** [15,53]. The carboxylate also forms a hydrogen bond with a water molecule that is coordinated with Gln-263 [53]. The fluorine atom at the amide bound phenyl ring (X in **Figure 18**) interacts with the sulfur atom of Met-328 and the β-carbon atom of Met-290 [53]. In addition, there are some hydrophobic interactions with the hydrophobic FXR–LBD (e.g., a π–π interaction between the *p*Cl-phenyl ring and Phe-329) **(Figure 18)** [15,53].

Besides the described key interaction with Tyr-369, the benzimidazole core, similarly to the isoxazole in **9a**, provides a very advantageous geometry that places its substituents in perfect orientation for binding to FXR.

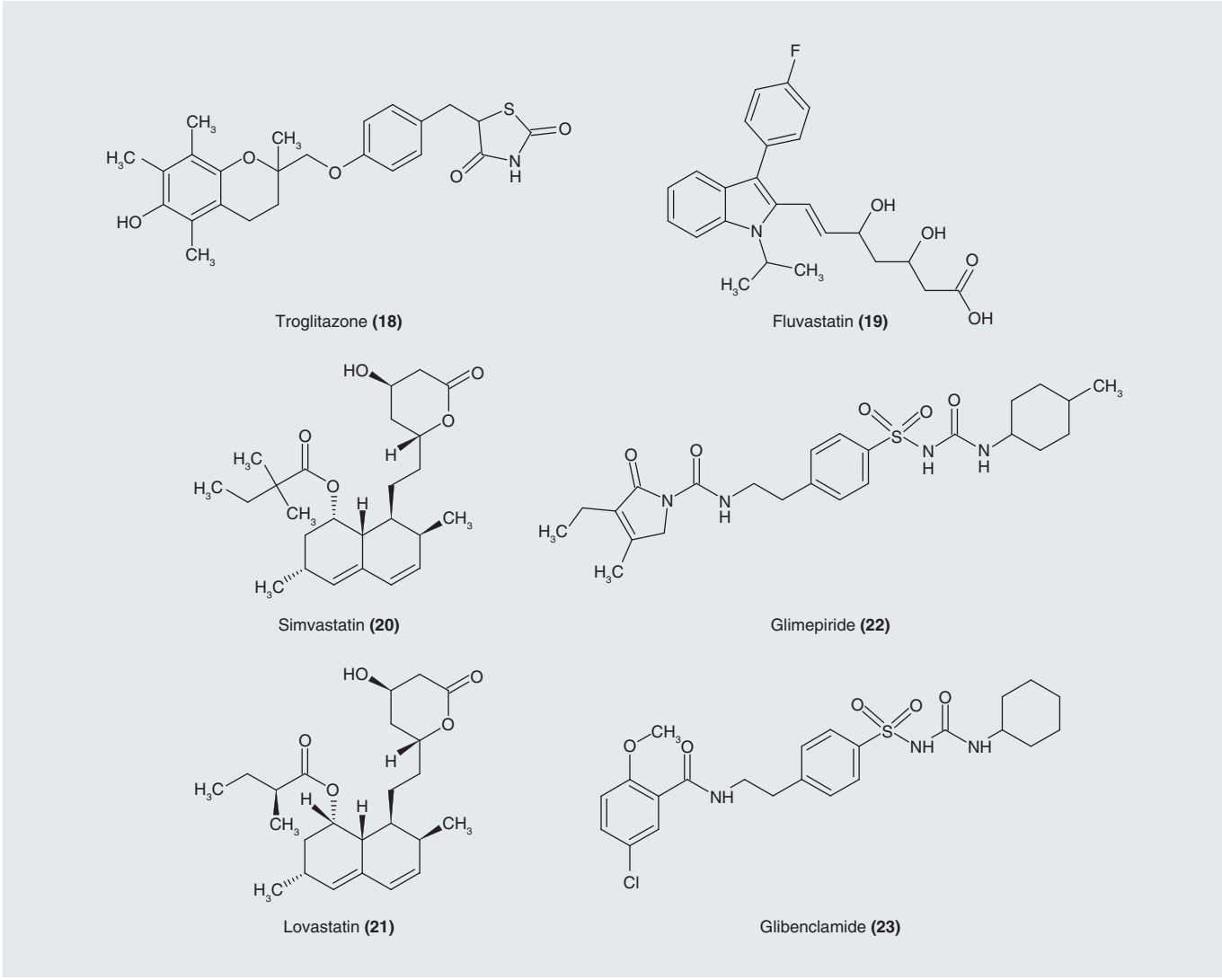

Figure 20. Approved drugs with farnesoid X receptor agonistic activity.

Xanthohumol

Xanthohumol **(17)**, a natural prenylated flavonoid from beer hops (*Humulus lupulus L.*) has been discovered as FXR agonist as well **(FIGURE 19)**. It activates FXR in a transient transfection assay and shows positive effects on glucose and lipid metabolism in a mouse model of Type 2 diabetes mellitus and obesity [54].

Approved drugs as FXR ligands

The high diversity of available FXR ligands indicates that the LBD of the nuclear receptor is capable of binding a large number of structurally distinct compounds. This suggests that approved drugs, especially those targeting other nuclear receptors, might also be active on FXR.

Therefore, several approved (or formerly approved) drugs have been investigated on their ability to bind and activate or modulate FXR. The ability of some of these drugs to act as weak FXR ligands, however, does not implicate that this action is pharmacologically relevant. But for completeness and because they might contribute to the SAR of FXR ligands, these drugs shall be mentioned.

It was found that troglitazone **(18)** but not the other glitazones exerted partial agonistic activity on FXR being a weak agonist for BSEP and SHP expression, but an antagonist in the presence of bile acids [55].

In addition, some members of the class of statins have been found to be FXR agonists *in vitro*. Although they activated FXR to a lower extent than CDCA, fluvastatin **(19)**, simvastatin **(20)** and lovastatin **(21)** exhibited significant FXR agonistic activity whereupon the

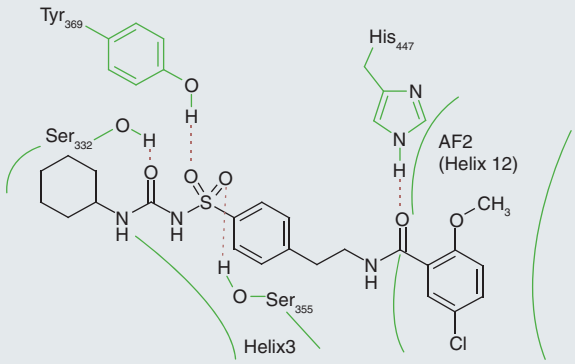

Figure 21. Interactions of Glibenclamide (23) docked into the farnesoid X receptor binding pocket.

lactone forms were more potent than the acids **(Figure 20)** [56].

Recently, an *in vitro* and *in silico* study revealed that the antidiabetic sulfonylureas modulate FXR activation. In a luciferase-based transactivation assay, both glimepiride **(22)** and Glibenclamide **(23)** decreased the luciferase activity induced by GW4064 **(9a)** or CDCA **(1)**. A real-time qPCR study showed that both sulfonylureas increased mRNA levels of FXR target genes in HepG2 cells comparable to fexaramine **(10)**. Glibenclamide **(23)** formed several interactions with the FXR–LBD in the *in silico* experiments and stabilized helix 12, which is known to be crucial for nuclear receptor activation **(Figure 21)** [57].

The study revealed several possible polar interactions of Glibenclamide **(23)** with the FXR–LBD including hydrogen bonds between Ser-332 and the urea carbonyl oxygen, between Tyr-369, Ser-355 and the sulfonyl oxygens, as well as between His-447 and the benzyl amide carbonyl oxygen. In this docked orientation, **23** stabilized the activated conformation of helix 12 (AF-2) **(Figure 21)** [57].

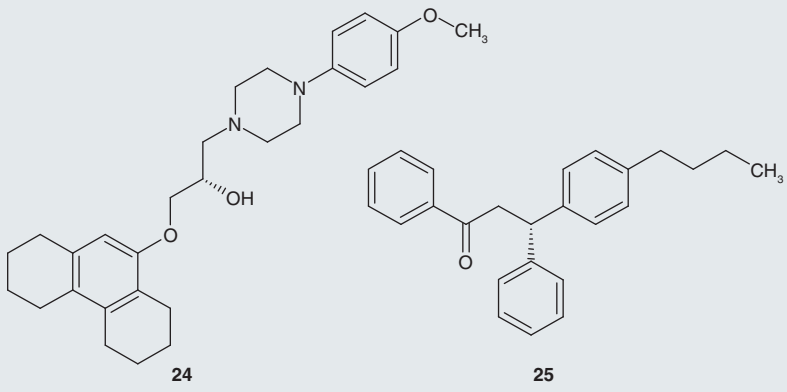

Figure 22. Weak farnesoid X receptor ligands from a recently published *in silico* study [58].

Virtual evaluation of FXR ligands

Most recently, the first *in silico* pharmacophore model of FXR has been published, which incorporates data derived from nine co-crystal structures of four chemically distinct classes of FXR ligands. It primarily shows that the high flexibility of the FXR–LBD and the chemical diversity of known FXR ligands complicates the generation of *in silico* models. Only few precise interactions with the nuclear receptor are present in chemically different classes of ligands and models that combine data from different co-crystal structures are, therefore, quite difficult to generate. Hence, virtual models derived from single co-crystal structures of FXR predominantly yield structurally very similar hits, especially when the models contain a shape restriction. However, some of the generated pharmacophore models recognized known FXR ligands belonging to chemically different compound classes than the underlying co-crystallized ligand. In this manner validated models were used to screen virtual drug databases, which yielded a few new steroidal and nonsteroidal hits. Biological evaluation of the *in silico* hits proved FXR agonistic activity for compounds **24** and **25** with EC_{50} values of 3.2 µM and 6.2 µM, respectively **(Figure 22)**. Whilst **25** presents itself as highly lipophilic and hardly drug-like, **24** might serve as a lead structure for a new class of FXR agonists. Docking experiments suggested that **24** binds to FXR in a manner comparable to fexaramine **(10)** [58].

FXR antagonists

An antagonist of FXR is a molecule that binds with high affinity to the LBD of the nuclear receptor but does not activate it and, therefore, does not evoke the physiologic effects of FXR activation. Moreover, an FXR antagonist is supposed to inhibit the activation of the receptor by agonistic ligands. This could, for example, be possible by stabilizing complexes of FXR with corepressors such as the nuclear corepressor NCoR or by binding the LBD with high affinity but without stabilizing AF-2, also referred to as transactivation function 2. Binding the nuclear receptor with high affinity without stabilizing helix 12 in an active conformation would hinder co-activator recruitment and, therefore, not evoke FXR activation [59].

The first FXR antagonist described in the literature [60] was guggulsterone **(26)** the active

compound in guggulipid, an extract from *Commiphora mukul* **(Figure 22)**. Guggulsterone **(26)** appears in two isomers (*E*/*Z*) and is active at many nuclear receptors including the estrogene receptor, the glucocorticoid receptor, the mineralocorticoid receptor, the pregnane X receptor and FXR. First experiments with guggulsterone indicated that it is a FXR antagonist as it inhibits the activation of FXR by CDCA **(1)** *in vitro*. Later, it was shown that guggulsterone acts as an antagonist for most FXR target genes, but has agonistic effects concerning the expression of *BSEP*, a well-known target gene of FXR [60,61]. However, whether guggulsterone can be classified as an FXR modulator is questionable since it acts on many nuclear receptors and the effects on gene expression cannot be attributed to FXR alone. Therefore, results obtained with guggulsterone used as FXR antagonist in *in vitro* assays to investigate the mechanism of action of new FXR ligands have to be interpreted with care.

Besides a couple of other weak steroidal FXR antagonists, a sulfated sterol **27** from the marine organism *Ophialepis superba* has recently been reported to be the first potent FXR antagonist. The tested sterols share the A/B *cis* ring conformation, the negative charge in the side chain and polar groups in α-position of ring A as key elements with the bile acids **(Figure 23)**. All described compounds contain sulfate groups at C-3 and C-21. The most potent agonistic compound **27**, however, contains a longer and bulkier side chain than bile acids with a hydroxyl group at C-26, which appears to be critical for antagonistic activity. The sterol almost completely inhibited the effects of FXR activation by CDCA **(1)** at a concentration of 100 μM probably by stabilizing the complex with the nuclear corepressor NCoR [62].

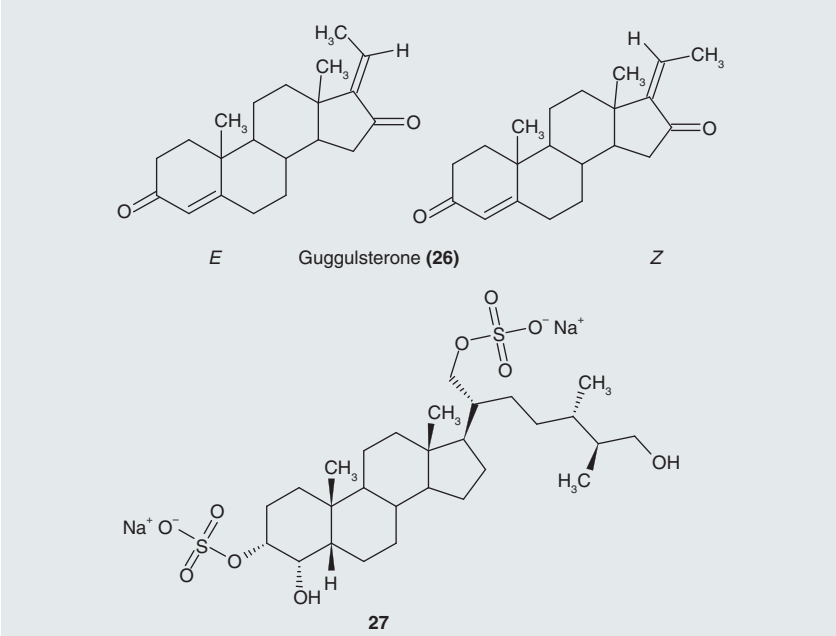

Figure 23. Farnesoid X receptor antagonists guggulsterone (26) and the sulfated sterol 27.

FXR modulators

As described above, great efforts have been made to develop FXR agonists yielding potent steroidal and nonsteroidal compounds. In addition, some FXR antagonists have been developed as research tools although their potential therapeutic use is uncertain. With FXR emerging as a potential pharmacological target, the development of selective FXR modulators is coming into focus as both the activation of FXR with agonists or the inhibition of FXR with antagonists produce beneficial and also undesirable effects. Full FXR agonism (in other words transactivation of all FXR target genes by full extent) would, besides the desired effects, particularly inhibit physiological synthesis and transport of bile acids, which might impair cholesterol homeostasis.

It is, therefore, a future challenge to design potent FXR ligands that induce or inhibit certain patterns of FXR target genes, while other target genes are not affected. A possible approach to obtain such FXR modulators might be to target certain interactions with specific areas of the LBD causing different recruitment of coactivators or corepressors. The only compound that so far exhibits such characteristics is the synthetic retinoid derivative, AGN34 **(28)**, which increases CYP7A1 expression and lowers IBABP expression, while other FXR target genes, such as *SHP*, are not

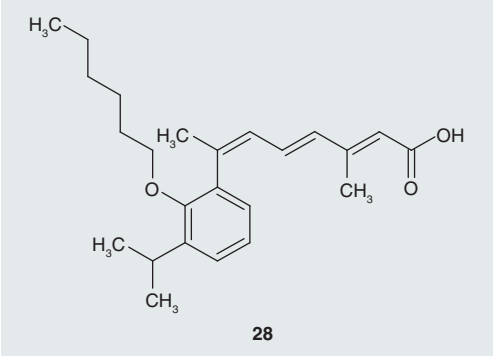

Figure 24. AGN34 (28).

affected (FIGURE 24). These effects of AGN34 are visible even at concentrations as low as 10 nM but the retinoid also has a high affinity to RXR and the action requires a FXR–RXR heterodimer; AGN34 does not bind to the regular FXR–LBD. The compound must, therefore, be considered as an allosteric FXR modulator and cannot contribute to the SAR of FXR ligands [49].

Conclusion

The available knowledge about the SAR of FXR ligands – especially agonists – and their co-crystal structures indicate that the development of new FXR ligands has to consider that there are few polar interactions possible and that the FXR–LBD requires quite hydrophobic ligands. This makes the design of ligands with drug-like properties a challenging topic.

Few prominent interactions have been found in the crystal structures of more than one chemical class of FXR ligands (TABLE 3). Those are a hydrogen bond from Tyr-369 to a carbonyl oxygen (FIGURES 15 & 16) or to N3 of the benzimidazole core of **16** (FIGURE 17), an ionic interaction between a carboxylic acid function and Arg-331 (FIGURES 6 & 8) or Arg-328 (FIGURE 7) and a π–π interaction with Phe-329 (FIGURES 7 & 8). Some additional polar interactions are possible with residues near the Arg-331-bound carboxylic acid moiety (e.g., His-294). The interactions of the co-crystallized ligands with the FXR binding site are depicted in TABLE 3.

Table 3. Interactions of farnesoid X receptor ligands with the nuclear receptor.

Amino acid	Compound							
	6	**5a**	**8**	**9a–k**	**10**	**15**	**15b**	**16a–f**
H-447				H				
F-329			P	P				P
L-287				L		L	L	
H-294				H	H			H
R-331			H	I				H
M-265				H				
Y-369						H	H	H
S-332					H		H	H
W-454			P			P	P	
T-288			H					
I-335					L		L	
L-340					L		L	
L-348					L		L	
I-352					L	L		
M-290					L			S/X
M-328								S/X
F-461						P	P	
A-291						H	H	
I-357							L	
T-358 (rFXR-LBD)	H							
H-444 (rFXR-LBD)	H							
R-328 (rFXR-LBD)	I	I						
I-349 (rFXR-LBD)	L							
S-329 (rFXR-LBD)	H	H						
T-366 (rFXR-LBD)	H	H						
EC_{50} (nM)	99		17	90 **(9a)**	25	4	88	870 **(16)**

Numbering of amino acids was adjusted for better understanding (numbering differs in published co-crystal structures of **9c, 10, 15, 15b** *and* **16a–f** *by +4, compared with the data in* [58]*; compounds* **5a** *and* **6** *are co-crystallized with rFXR-LBD).*
H: Hydrogen bond; I: Ionic interaction; L: Hydrophobic interaction; P: π–π interaction; rFXR-LBD: Rat farnesoid X receptor ligand-binding domain; S/X: Sulfur-hal interaction.

Besides these most prominent FXR–ligand interactions, the co-crystal structures have revealed that FXR ligands require a very special geometry, which is predominantly provided by a central five-membered heterocycle, such as isoxazole, benzimidazole or indole. These central moieties position their substituents in optimal directions for FXR binding. In the case of fexaramine **(10)**, a tertiary amine allocates the required geometry.

In addition to a fitting geometry and optimal utilization of the possible polar interactions, a good balance between hydrophobic surface for van der Waals' interactions with the receptor and hydrophilicity for drug likeness is necessary for the development of highly potent FXR ligands. How these ligands can be chemically divided into agonists and true modulators is a challenging and as yet unanswered question, but, to our current knowledge, the interaction with helix 12 plays a crucial role. To activate FXR an agonist has to stabilize AF-2 in a position that is tightly packed to the LBD and near the ligand [37,59]. In such an active conformation co-activator recruitment is enabled and the nuclear receptor can exhibit its functions. An active position of helix 12 can be achieved by interaction of the ligand with residues such as Trp-469 (H12), His-447 (H11) and Tyr-361 (H10) and no direct contact of the ligand with helix 12 is necessary in order to make recruitment of coactivators possible [63]. Moreover, an agonistic ligand of FXR has to increase the overall stability of the LBD including not only helix 12 but also the other helices, especially helices 3 and 11 [37]. By formation of hydrogen bonds between the helices inside the ligand-stabilized FXR–LBD protein, the AF-2 can be sufficiently stabilized, which is, for example, the case for the activation of FXR by bile acids [37]. The synthetic FXR ligands MFA-1 **(8)** and fexaramine **(10)** on the other hand directly interact with helices 3, 11 and 12. Both methods of activation, however, lead to the formation of a cation–π interaction between His-447 in helix 11 and Trp-469 in helix 12 [37].

For the reasons that several ways of molecular interaction are able to activate FXR and that FXR has a quite flexible LBD, which is capable of binding many different chemical structures, it is very difficult to define interactions that an FXR ligand has to form with the LBD in order to act as agonist, antagonist or modulator as any molecule that binds with high affinity to the LBD will increase its stability. More research is therefore necessary to predict the physiologic actions of FXR ligands by their mode of binding. Until then, FXR ligands will have to be characterized by functional *in vitro* assays.

Table 4. Most important farnesoid X receptor ligands with EC_{50} values.

Ligand	EC_{50}	Ref.
CDCA **(1)**	8.3 μM	[1]
6-ethyl-chenodeoxycholic acid/INT-747 **(6)**	99 nM	[31]
INT-767 **(6a)**	30 nM	[33]
7	150 nM	[35]
MFA-1 **(8)**	17 nM	[37]
GW4064 **(9a)**	90 nM	[41]
Fexaramine **(10)**	25 nM	[48]
Fexarene **(10a)**	36 nM	[48]
Fexarine **(10b)**	38 nM	[48]
AGN29 **(12)**	~2 μM	[49]
AGN31 **(13)**	~2 μM	[49]
FXR-450/WAY-362450 **(15)**	4 nM	[51]
15a	280 nM	[52]
15b	88 nM	[14]
16	870 nM	[53]
24	3.2 μM	[58]
25	6.2 μM	[58]

CDCA: Chenodeoxycholic acid; ECDCA: Obeticholic acid; FXR: Farnesoid X receptor.

A considerable number of FXR ligands (the most important are depicted in **Table 4**) are known, although several FXR agonists are in preclinical and clinical development, a satisfying FXR modulator has not yet been discovered.

Future perspective

The story of the rise and fall of PPARγ ligands, as a warning, and the unfavorable highly lipophilic nature of the FXR–LBD, as a separation hurdle, will ensure the development of FXR ligands that have the physicochemical and pharmacological properties to achieve drug status an acanthous and stony way. But with the intense academic and industrial interest in FXR as a pharmacological target, a hope for FXR-targeting drugs is justified.

Financial & competing interests disclosure

The authors gratefully acknowledge financial support by LOEWE Schwerpunkt Onkogene Signaltransduktion Frankfurt (OSF). The authors have no other relevant affiliations or financial involvement with any organization or entity with a financial interest in or financial conflict with the subject matter or materials discussed in the manuscript apart from those disclosed.

No writing assistance was utilized in the production of this manuscript.

Executive summary

- The nuclear receptor for bile acids, the farnesoid X receptor (FXR), has emerged as a highly interesting drug target and several synthetic ligands have been described. However, the existing ligands for the nuclear receptor have, for various reasons, not reached a status for clinical use.
- As FXR modulation might be a successful strategy in the treatment of several diseases, there is a need for new FXR ligands with drug-like properties.
- The examination and interpretation of co-crystal structures of the FXR ligand-binding domain with potent agonists shows a couple of polar interactions that ligands of the nuclear receptor can form. However, the co-crystal structures predominantly reveal that the ligand-binding site of FXR is lipophilic and very flexible.
- Therefore, it remains a challenging topic to design potent ligands for FXR with drug-like properties.
- This review summarizes the opportunities and challenges of FXR as a pharmaceutical target; gathers and interprets the available knowledge about medicinal chemistry and SAR of FXR ligands; draws an overview over the known agonists and antagonists; and attempts to give a future perspective on where the research on FXR might proceed.

References

Papers of special note have been highlighted as:
▪ of interest
▪▪ of considerable interest

1 Fiorucci S, Mencarelli A, Distrutti E, Palladino G, Cipriani S. Targeting farnesoid-X-receptor: from medicinal chemistry to disease treatment. *Curr. Med. Chem.* 17(2), 139–159 (2010).

▪▪ **Reviews, among others, the physiological effects of the farnesoid X receptor (FXR).**

2 Parks DJ. Bile acids: natural ligands for an orphan nuclear receptor. *Science* 284(5418), 1365–1368 (1999).

3 Wang H, Chen J, Hollister K, Sowers LC, Forman BM. Endogenous bile acids are ligands for the nuclear receptor FXR/BAR. *Mol. Cell* 3(5), 543–553 (1999).

4 Makishima M. Identification of a nuclear receptor for bile acids. *Science* 284(5418), 1362–1365 (1999).

5 Huber RM, Murphy K, Miao B *et al.* Generation of multiple farnesoid-X-receptor isoforms through the use of alternative promoters. *Gene* 290(1-2), 35–43 (2002).

6 Zhang Y. Natural structural variants of the nuclear receptor farnesoid X receptor affect transcriptional activation. *J. Biol. Chem.* 278(1), 104–110 (2002).

7 Otte K, Kranz H, Kober I *et al*. Identification of farnesoid X receptor beta as a novel mammalian nuclear receptor sensing lanosterol. *Mol. Cell. Biol* 23(3), 864–872 (2003).

8 Watanabe M, Houten SM, Wang L *et al*. Bile acids lower triglyceride levels via a pathway involving FXR, SHP, and SREBP-1c. *J. Clin. Invest.* 113(10), 1408–1418 (2004).

9 Kalaany NY, Mangelsdorf DJ. LXRS AND FXR: the yin and yang of cholesterol and fat metabolism. *Annu. Rev. Physiol.* 68(1), 159–191 (2006).

10 Cariou B, Van Harmelen K, Duransandoval D *et al*. Transient impairment of the adaptive response to fasting in FXR-deficient mice. *FEBS Lett.* 579(19), 4076–4080 (2005).

11 Stayrook KR. Regulation of carbohydrate metabolism by the farnesoid x receptor. *Endocrinology* 146(3), 984–991 (2004).

12 Zollner G, Marschall HU, Wagner M, Trauner M. Role of nuclear receptors in the adaptive response to bile acids and cholestasis: pathogenetic and therapeutic considerations. *Mol. Pharm.* 3(3), 231–251 (2006).

13 Ananthanarayanan M. Human bile salt export pump promoter is transactivated by the farnesoid X receptor/bile acid receptor. *J. Biol. Chem.* 276(31), 28857–28865 (2001).

14 Lundquist JT, Harnish DC, Kim CY *et al*. Improvement of physiochemical properties of the tetrahydroazepinoindole series of farnesoid X receptor (FXR) agonists: beneficial modulation of lipids in primates. *J. Med. Chem.* 53(4), 1774–1787 (2010).

15 Richter HG, Benson GM, Blum D *et al*. Discovery of novel and orally active FXR agonists for the potential treatment of dyslipidemia and diabetes. *Bioorg. Med. Chem. Lett.* 21(1), 191–194 (2011).

▪ **Contributes to SAR of FXR ligands.**

16 Watanabe M, Horai Y, Houten SM *et al*. Lowering bile acid pool size with a synthetic farnesoid X receptor (FXR) agonist induces obesity and diabetes through reduced energy expenditure. *J. Biol. Chem.* 286 (30), 26913–26920 (2011).

17 Ge X, Yin L, Ma H, Li T, Chiang JYL, Zhang Y. Aldo-keto reductase 1B7 is a target gene of FXR and regulates lipid and glucose homeostasis. *J. Lipid Res.* 52(8), 1561–1568 (2011).

18 Prieur X. The human apolipoprotein AV gene is regulated by peroxisome proliferator-activated receptor-alpha and contains a novel farnesoid X-activated receptor response element. *J. Biol. Chem.* 278(28), 25468–25480 (2003).

19 Zhang Y, Lee FY, Barrera G *et al*. Activation of the nuclear receptor FXR improves hyperglycemia and hyperlipidemia in diabetic mice. *Proc. Natl Acad. Sci. USA* 103(4), 1006–1011 (2006).

20 Prawitt J, Abdelkarim M, Stroeve JHM *et al*. Farnesoid X receptor deficiency improves glucose homeostasis in mouse models of obesity. *Diabetes* 60(7), 1861–1871 (2011).

21 Wang XX, Jiang T, Shen Y *et al*. Diabetic nephropathy is accelerated by farnesoid X receptor deficiency and inhibited by farnesoid X receptor activation in a Type 1 diabetes model. *Diabetes* 59(11), 2916–2927 (2010).

22 Levi M. Nuclear receptors in renal disease. *Biochim. Biophys. Acta* 1812(8), 1061–1067 (2011).

23 Mencarelli A, Fiorucci S. FXR an emerging therapeutic target for the treatment of atherosclerosis. *J. Cell. Mol. Med.* 14(1–2), 79–92 (2010).

24 Hartman HB, Gardell SJ, Petucci CJ, Wang S, Krueger JA, Evans MJ. Activation of farnesoid X receptor prevents atherosclerotic lesion formation in LDLR$^{-/-}$ and apoE$^{-/-}$ mice. *J. Lipid Res.* 50(6), 1090–1100 (2009).

25 Giordano C, Catalano S, Panza S *et al*. Farnesoid X receptor inhibits tamoxifen-resistant MCF-7 breast cancer cell growth through downregulation of HER2 expression. *Oncogene* 30(39), 4129–4140 (2011).

26 Dai J, Wang H, Shi Y, Dong Y, Zhang Y, Wang J. Impact of bile acids on the growth of human cholangiocarcinoma via FXR. *J. Hematol. Oncol.* 4(1), 41 (2011).

27 Huang W. Nuclear receptor-dependent bile acid signaling is required for normal liver regeneration. *Science* 312(5771), 233–236 (2006).

28 Lindor KD. Farnesoid X receptor agonists for primary biliary cirrhosis. *Curr. Opin. Gastroenterol.* 27(3), 285–288 (2011).

29 Yang F, Huang X, Yi T, Yen Y, Moore DD, Huang W. Spontaneous development of liver tumors in the absence of the bile acid receptor farnesoid X receptor. *Cancer Res.* 67 (3), 863–867 (2007).

30 Zhao A, Yu J, Lew J, Huang L, Wright S, Cui J. Polyunsaturated fatty acids are FXR ligands and differentially regulate expression of FXR targets. *DNA Cell Biol.* 23(8) 519–526 (2004).

31 Pellicciari R, Fiorucci S, Camaioni E *et al*. 6α-ethyl-chenodeoxycholic acid (6-ECDCA), a potent and selective FXR agonist endowed with anticholestatic activity. *J. Med. Chem.* 45(17), 3569–3572 (2002).

32 Costantino G, Macchiarulo A, Entrena-Guadix A, Camaioni E, Pellicciari R. Binding mode of 6ECDCA, a potent bile acid agonist of the farnesoid X receptor (FXR). *Bioorg. Med. Chem. Lett.* 13(11), 1865–1868 (2003).

▪ **Contributes to SAR of FXR ligands**

33 Rizzo G, Passeri D, Franco F *et al*. Functional characterization of the semisynthetic bile acid derivative INT-767, a dual farnesoid X receptor and TGR5 agonist. *Mol. Pharmacol* 78(4), 617–630 (2010).

34 Downes M, Verdecia MA, Roecker AJ *et al*. A chemical, genetic, and structural analysis of the nuclear bile acid receptor FXR. *Mol. Cell* 11(4), 1079–1092 (2003).

▪▪ **Describes development and optimization of FXR ligands of the fexaramine series**

35 Gioiello A, Macchiarulo A, Carotti A *et al*. Extending SAR of bile acids as FXR ligands: discovery of 23-N-(carbocinnamyloxy)-3α,7α-dihydroxy-6α-ethyl-24-nor-5β-cholan-23-amine. *Bioorg. Med. Chem.* 19 (8), 2650–2658 (2011).

▪ **Contributes to SAR of FXR ligands**

36 Fujino T. Structure-activity relationship of bile acids and bile acid analogs in regard to FXR activation. *J. Lipid Res.* 45(1), 132–138 (2003).

37 Soisson SM, Parthasarathy G, Adams AD *et al.* Identification of a potent synthetic FXR agonist with an unexpected mode of binding and activation. *Proc. Natl Acad. Sci. USA* 105(14), 5337–5342 (2008).

▪ **Contributes to SAR of FXR ligands.**

38 Mi LZ, Devarakonda S, Harp JM *et al*. Structural basis for bile acid binding and activation of the nuclear receptor FXR. *Mol. Cell* 11(4), 1093–1100 (2003).

39 Chiang PC, Thompson DC, Ghosh S, Heitmeier MR. A formulation-enabled preclinical efficacy assessment of a farnesoid X receptor agonist, GW4064, in hamsters and cynomolgus monkeys. *J. Pharm. Sci.* 100(11), 4722–4733 (2011).

40 Howarth DL, Law SH, Law JM, Mondon J, Kullman SW, Hinton DE. Exposure to the synthetic FXR agonist GW4064 causes alterations in gene expression and sublethal hepatotoxicity in eleutheroembryo medaka (*Oryzias latipes*). *Toxicol. Appl. Pharm.* 243(1), 111–121 (2010).

41 Maloney PR, Parks DJ, Haffner CD *et al*. Identification of a chemical tool for the orphan nuclear receptor FXR. *J. Med. Chem.* 43(16), 2971–2974 (2000).

▪ **Contributes to SAR of FXR ligands.**

42 Feng S, Yang M, Zhang Z *et al*. Identification of an N-oxide pyridine GW4064 analog as a potent FXR agonist. *Bioorg. Med. Chem. Lett.* 19(9), 2595–2598 (2009).

▪ **Contributes to SAR of FXR ligands.**

43 Abel U, Schlüter T, Schulz A *et al*. Synthesis and pharmacological validation of a novel series of non-steroidal FXR agonists. *Bioorg. Med. Chem. Lett.* 20(16), 4911–4917 (2010).

▪ **Contributes to SAR of FXR ligands.**

44 Kainuma M, Kasuga JI, Hosoda S *et al*. Diphenylmethane skeleton as a multi-template for nuclear receptor ligands: preparation of FXR and PPAR ligands. *Bioorg. Med. Chem. Lett.* 16(12), 3213–3218 (2006).

45 Akwabi-Ameyaw A, Bass JY, Caldwell RD *et al*. FXR agonist activity of conformationally constrained analogs of GW 4064. *Bioorg. Med. Chem. Lett.* 19(16), 4733–4739 (2009).

46 Kainuma M, Makishima M, Hashimoto Y, Miyachi H. Design, synthesis, and evaluation of non-steroidal farnesoid X receptor (FXR) antagonist. *Bioorg. Med. Chem.* 15(7), 2587–2600 (2007).

47 Akwabi-Ameyaw A, Caravella J, Chen L *et al*. Conformationally constrained farnesoid X receptor (FXR) agonists: alternative replacements of the stilbene. *Bioorg. Med. Chem. Lett.* 21, 6154–6160 (2011).

48 Nicolaou KC, Evans RM, Roecker AJ, Hughes R, Downes M, Pfefferkorn JA. Discovery and optimization of non-steroidal FXR agonists from natural product-like libraries. *Org. Biomol. Chem* 1(6), 908–920 (2003).

▪ **Contributes to SAR of FXR ligands.**

49 Dussault I. Identification of gene-selective modulators of the bile acid receptor FXR. *J. Biol. Chem.* 278(9), 7027–7033 (2002).

50 Deng G, Li W, Shen J, Jiang H, Chen K, Liu H. Pyrazolidine-3,5-dione derivatives as potent non-steroidal agonists of farnesoid X receptor: virtual screening, synthesis, and biological evaluation. *Bioorg. Med. Chem. Lett.* 18(20), 5497–5502 (2008).

▪ **Contributes to SAR of FXR ligands.**

51 Flatt B, Martin R, Wang TL *et al*. Discovery of XL335 (WAY-362450), a highly potent, selective, and orally active agonist of the farnesoid X receptor (FXR). *J. Med. Chem.* 52(4), 904–907 (2009).

▪ **Contributes to SAR of FXR li**gands.

52 Mehlmann JF, Crawley ML, Lundquist TL *et al*. Pyrrole[2,3-d]azepino compounds as agonists of the farnesoid X receptor (FXR). *Bioorg. Med. Chem. Lett.* 19(18), 5289–5292 (2009).

53 Richter HG, Benson G, Bleicher K *et al*. Optimization of a novel class of benzimidazole-based farnesoid X receptor (FXR) agonists to improve physicochemical and ADME properties. *Bioorg. Med. Chem. Lett.* 21(4), 1134–1140 (2011).

54 Nozawa H. Xanthohumol, the chalcone from beer hops (*Humulus lupulus* L.), is the ligand for farnesoid X receptor and ameliorates lipid and glucose metabolism in KK-Ay mice. *Biochem. Biophys. Res. Commun.* 336(3), 754–761 (2005).

55 Kaimal R, Song X, Yan B, King R, Deng R. Differential modulation of farnesoid X receptor signaling pathway by the thiazolidinediones. *J. Pharmacol. Exp. Ther.* 330(1), 125–134 (2009).

56 Howe K, Sanat F, Thumser AE, Coleman T, Plant N. The statin class of HMG-CoA reductase inhibitors demonstrate differential activation of the nuclear receptors PXR, CAR and FXR, as well as their downstream target genes. *Xenobiotica* 41(7), 519–529 (2011).

57 Steri R, Kara M, Proschak E, Steinhilber D, Schneider G, Schubert-Zsilavecz M. Antidiabetic sulfonylureas modulate farnesoid X receptor activation and target gene transcription. *Future Med. Chem.* 2(4), 575–586 (2010).

58 Schuster D, Markt P, Grienke U *et al*. Pharmacophore-based discovery of FXR agonists. Part I: model development and experimental validation. *Bioorg. Med. Chem.* 19(23), 7168–7180 (2011).

59 Gronemeyer H, Gustafsson JA, Laudet V. Principles for modulation of the nuclear receptor superfamily. *Nat. Rev. Drug Discov.* 3, 950–964 (2004).

▪▪ **Reviews successful approaches of selective modulation of nuclear receptors**

60 Urizar NL, Liverman AB, Dodds DT *et al*. A natural product that lowers cholesterol as

an antagonist ligand for FXR. *Science* 296(5573), 1703–1706 (2002).

61 Burris TP, Montrose C, Houck KA *et al*. The hypolipidemic natural product guggulsterone is a promiscuous steroid receptor ligand. *Mol. Pharmacol.* 67(3), 948–954 (2005).

62 Sepe V, Bifulco G, Renga B, D'Amore C, Fiorucci S, Zampella A. Discovery of sulfated sterols from marine invertebrates as a new class of marine natural antagonists of farnesoid-X-receptor. *J. Med. Chem.* 54(5), 1314–1320 (2011).

63 Pellicciari R, Gioiello A, Costantino G *et al*. Back door modulation of the farnesoid X receptor: design, synthesis, and biological evaluation of a series of side chain modified chenodeoxycholic acid derivatives. *J. Med. Chem.* 49(14), 4208–4215 (2006).

64 Akwabi-Ameyaw A, Bass JY, Caldwell RD *et al*. Conformationally constrained farnesoid X receptor (FXR) agonists: Naphthoic acid-based analogs of GW 4064. *Bioorg. Med. Chem. Lett.* 18(15), 4339–4343 (2008).

▪ **Contributes to SAR of FXR ligands.**

65 Bass JY, Caldwell RD, Caravella JA *et al*. Substituted isoxazole analogs of farnesoid X receptor (FXR) agonist GW4064. *Bioorg. Med. Chem. Lett.* 19(11), 2969–2973 (2009).

■ Websites

101 Intercept Pharmaceuticals, Inc, press release. Intercept pharmaceuticals' FXR agonist INT-747 meets primary end point in a Phase II clinical trial in Type 2 diabetic patients with nonalcoholic fatty liver disease. 2 October 2009. www.genextra.it/docs/intercept_02_10_09.pdf

102 ClinicalTrials. Study Evaluating FXR-450 in Healthy Japanese Men. http://clinicaltrials.gov/ct2/show/NCT00509756

EXPERT OPINION

Therapeutic modulators of peroxisome proliferator-activated receptors (PPAR): a patent review (2008–present)

Christina Lamers, Manfred Schubert-Zsilavecz & Daniel Merk†
†*Goethe University Frankfurt, Institute of Pharmaceutical Chemistry, Frankfurt, Germany*

Introduction: Peroxisome proliferator-activated receptors (PPAR) are ligand-activated transcription factors belonging to the nuclear receptor superfamily. The three known subtypes PPARα, PPARγ and PPARδ have different tissue distribution and play a key role as regulators of glucose and lipid homeostasis as well as in cell proliferation, differentiation and inflammatory responses. They have gained a lot of interest as pharmaceutical targets over the last years and with the antidiabetic thiazolidindiones (TZDs) and the hypolipidemic fibrates, two classes of drugs had entered the market. Early observations of severe adverse events changed the situation in the recent past.

Areas covered: Herein the authors summarize recent (2008–present) patent applications concerning PPAR ligands claimed for the use in metabolic disorders as well as patents indicating new applications for modulators of the PPAR subtypes.

Expert opinion: Looking at the recent patent activity regarding novel compounds, there have not been real innovations. As major applications for therapeutic PPAR ligands cancer therapy, skin-related disorders and systemic anti-inflammatory therapies might arise in the mid-term future. The known PPAR targeting drugs might see a repurposing for novel indications.

Keywords: cancer, CS-7017, dyslipidemia, fibrates, GW-501516, GW-590735, hyperglycemia, inflammatory diseases, nuclear receptor modulators, nuclear receptors, PAM-1616, PAR-1622, PAR-5359, skin disorders, thiazolidindiones

Expert Opin. Ther. Patents [Early Online]

1. Introduction

Nuclear receptors have gained a lot of interest as pharmaceutical targets over the last years. Besides nuclear hormone receptors, especially the family of the peroxisome proliferator-activated receptors (PPAR) has been in the focus of academic and industrial research and with the antidiabetic thiazolidindiones (TZDs) and the hypolipidemic fibrates two classes of quite successful drugs had entered the market. But as early observations of severe adverse events had indicated, the situation has intensely changed in the recent past.

While the PPARα agonistic fibrates are still in clinical use the PPARγ agonistic TZDs have seen a serious fall as troglitazone, rosiglitazone and most recently pioglitazone were suspended at least by some authorities because of severe adverse events [1].

However, against these disillusioning progressions also a very promising finding on the field of PPAR as pharmaceutical target has been made. A group of US-researchers has shown that the antidiabetic effects of the TZDs are not alone mediated by PPARγ agonism but at least in part by the inhibition of the cyclin-dependent kinase 5 (Cdk5)-mediated PPARγ phosphorylation at Ser_{273} [2,3].

informa healthcare

Article highlights.

- Many novel PPAR ligands have been patented, but there are no real innovations concerning affinity, selectivity or pharmacological profile of the compounds.
- Most novel compounds are in preclinical development and only a few have entered clinical trials.
- Instead, there is a strong trend towards new indications for PPAR-modulating compounds such as cancer, inflammatory diseases and skin disorders with repurposing of known PPAR targeting drugs such as the thiazolidindiones and the fibrates for novel indications.
- Antidiabetic inhibition of the Cdk5-mediated phosphorylation of PPARγ arises as a very promising new development.
- Evolution of PPARδ as a promising drug target of the future.

This box summarizes key points contained in the article.

This review is supposed to list the recent (2008–present) movements in therapeutical patents on the field of PPAR, to evaluate their potential and to deal with the question whether PPARs have a chance to play a major role as a drug target in the mid-term future.

1.1 PPARs as drug target

Peroxisome proliferator-activated receptors belong to the nuclear receptor superfamily. They are built up of a C-terminal ligand-binding domain (LBD) and a N-terminal DNA-binding domain (DBD), which are linked by a hinge region. The three known subtypes PPARα, PPARγ and PPARδ (sometimes referred to as PPARβ) have distinct physiological roles that are predominantly linked to regulation of lipid and glucose homeostasis. As physiological ligands for PPARs serve unsaturated fatty acid derivatives such as prostaglandins [4].

In accordance with the physiological role as regulator of lipid and glucose homeostasis, the most prominent indications for PPAR ligands are metabolic disorders. PPARγ agonists (the TZDs) have been among the most-used antidiabetics until their market withdrawal and PPARγ is still in the focus of diabetes research. Furthermore, the fibrates as PPARα agonists still play a great role as hypolipidemics. But over time the nuclear receptors also have emerged as targets for several other diseases.

One possible future indication for PPAR modulators are skin disorders. Peroxisome proliferator-activated receptors are involved in skin development and differentiation of several cell types that are found in the skin. Additionally they play a role in the homeostasis of the skins barrier function and in animal models PPAR activation showed anti-inflammatory effects in the skin. Peroxisome proliferator-activated receptor agonists are therefore intensely investigated as novel agents for the treatment of skin disorders such as psoriasis, atopic dermatitis and skin cancer [5,6].

A growing amount of research also focuses on involvement and therapeutic potential of PPARs in systemic auto-immune and inflammatory diseases [7]. In this field some clinical trials are conducted yet.

Finally, PPAR modulating agents might be useful in adjuvant treatment of cancer as the nuclear receptors also are involved in cell differentiation [8].

1.2 Medicinal chemistry and SAR of PPAR ligands

As PPARs are ligand-activated transcription factors, an agonist at PPAR induces transcription of the target genes of the activated receptor isoform. For this action endogenous co-activators have to bind to PPAR besides the agonistic compound. The resulting complex then binds to certain response elements on the DNA and induces transcription of target genes [9].

An antagonist, on the other hand, indeed binds to the nuclear receptor but does not activate the transcription of target genes, whereas a partial agonist binds to PPAR with high affinity but only activates the transcription to a partial extent [9].

To determine the particular action of a nuclear receptor ligand *in vitro*, especially cell-based reporter gene assays are standard. They usually comprise hybrid constructs of the nuclear receptor-binding domain and a DBD such as GAL-4. Agonistic compounds activate the hybrid construct, which then binds to DNA response elements (i.e. a GAL-4 promotor) and induces the transcription of a reporter-gene such as a luciferase. After addition of a luciferase substrate the resulting luminescence is measured as read-out (for details see e.g. [10]).

Extensive research over the last years has drawn a vast SAR of PPAR ligands, especially in case of PPARγ. Although there are several exceptions, the molecular structure of most ligands for PPARs can be summarized in quite simple chemical determinants. A typical PPARγ agonist comprises a polar head with a carboxylic acid or a suitable bioisosteric group that is over an aromatic linker bound to a lipophilic and typically hetero-aromatic tail (**Figure 1**). The acidic head can form several polar interactions with one subpocket of the PPARγ ligand-binding site, while the aromatic tail binds to the second and highly hydrophobic subpocket. As the ligand-binding site of PPARγ has the shape of a Y, a ligand has to feature a certain angle. This overall molecular structure can be found in the TZDs, phenylpropionic or phenylacetic acid derivatives as well as in indole derivatives and mimics the structure of the endogenous ligands [11-14].

Among all isoforms of the nuclear receptor, PPARγ has the largest ligand-binding pocket with about 1600 $A^{\circ 3}$. The binding pockets of PPARα and PPARδ are slightly smaller with 1400 and 1300 $A^{\circ 3}$, respectively, and with about 70% the identity between the amino acid sequences of the LBDs of all subtypes is quite high. Hence, it is difficult to define certain molecular determinants that guide the selectivity of ligands for a single PPAR isoform and development of

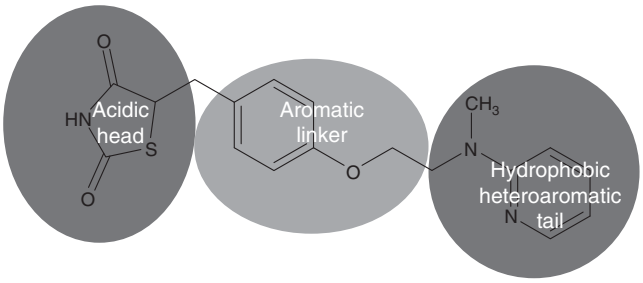

Figure 1. General SAR of PPAR ligands with example rosiglitazone.

selective PPAR modulators is a challenging topic. But many chemical classes of subtype selective PPAR ligands have been generated. Actually a strong focus of basic research lies on the development of selective modulators that are either tissue or gene selective. However, such activity is difficult to distinguish from partial agonism as often not enough data are available. Selective PPAR modulation can eventually be obtained by compounds that induce a certain conformational shift in the LBD or specifically interact with the activation function 2 (AF-2) in helix 12 of PPAR. This leads to selective recruitment of certain co-activators, which in consequence transactivates only a subset of target genes [11-14].

2. Selective PPARα ligands

Although the fibrates are still the only approved PPARα active drugs, there are several approaches for novel compounds that modulate PPARα or novel indications for known ligands of this nuclear receptor.

2.1 PPARα ligands for hypolipidemic indications

With 4-Phenoxy-nicotinic acid as molecular scaffold *Bayer Schering* has filed two patents [15,16] claiming compounds of the general formula **1** for their use as PPARα modulators. The patents address the disadvantage of the fibrates that they have only medium affinity to their target wit EC_{50} values in a µM range that leads to a merely modest pharmacological effect. The novel compounds of formula **1** have significantly higher affinity to PPARα and might therefore be beneficial in the treatment of dyslipidemias and cardiovascular disorders. The most potent derivatives **1a and b** exhibited PPARα agonism in a reportergene assay with EC_{50} values of 59 and 87 nM (**Figure 2**).

Also quite potent PPARα agonistic compounds of the formula **2** have been claimed by *Aryx Therapeutics* [17] to be used in the therapy of several hyperlipidemic conditions. The derivatives have been characterized in *in vitro* studies but no detailed values for affinity or activity nor any *in vivo* data are available (**Figure 3**).

Indole-based selective PPARα modulators of the general formula **3** have been patented by *Smithkline Beecham* [18]. The carboxyl substituted compounds comprise a mono- or bicyclic aromatic moiety for Z and various substituents at the indole nitrogen. The affinities of the derivatives to the PPAR subtypes have been examined in scintillation proximity-based binding assays and most of the compounds were highly selective for the α isoform with EC_{50} values ranging from 1 nM to 0.5 µM for PPARα binding. However, the patents do not give insight whether the compounds exhibit full or partial agonism nor is any *in vivo* data incorporated. Hence, the claimed use for the indole derivatives as agents to treat PPAR-related disorders is only vaguely defined (**Figure 4**).

Two sets of fatty acid amide derivatives have been claimed by *Fundación IMABIS (Instituto Mediterraneo para el avance de la biotechnologia y la investigación sanitaria)* to be used in the control of eating disorders. In the first patent [19], pyrazole derivatives of the general formula **4** wherein R represents a fatty acid described as selective ligands of PPARα.

The second invention from 2011 [20] claims fatty acids coupled with amphetamines. The resulting compounds of the general formula **5** are dual PPARα/cannabinoid receptor 1 (CB1) ligands and therefore especially supposed to induce satiety and to control food intake (**Figure 5**).

Although PPARα is a crucial regulator of lipid metabolism in cells, the acyl CoA:diacylglycerolacyltransferase (DGAT), in particular, DGAT1, is a key enzyme of lipid synthesis. Hence activation of PPARα and inhibition of DGAT1 might be a synergistic strategy to significantly reduce triglyceride levels, which in turn is beneficial for the treatment of obesity and related diseases such as type II diabetes and cardiovascular disorders. Additionally it has recently been observed that co-administration of a PPARα agonist and a DGAT1 inhibitor can increase levels of glucagon like peptide 1 (GLP-1), a saturation hormone reducing food intake. A patent [21] by *Janssen Pharmaceutica* claims the described use of a PPARα agonist combined with a DGAT1 inhibitor. As DGAT1 inhibitors the patent describes several new compounds while fenofibrate is used as PPARα agonistic component. When fed to mice the combination significantly increased GLP-1 levels and reduced food intake. Hence this combination might have future use for treating obesity and related disorders but no clinical development has been announced yet.

2.2 Natural PPARα modulators

Excelside A (**6**), a substituted diglucopyranoside, which is one of the major active compounds found in an extract from *fraxinus excelsior* seeds and several other ingredients from the same extract have been found to activate PPARα. Hence preparation and pharmaceutical use of the extract have been patented [22] in 2009. The extract is supposed to be effective for blocking fat synthesis as well as reducing body weight and eventually to control plasma insulin levels. In a PPARα reportergene assay the extract slightly activated the nuclear receptor at concentrations between 100 and 1000 µg/mL and in animal models beneficial effects on

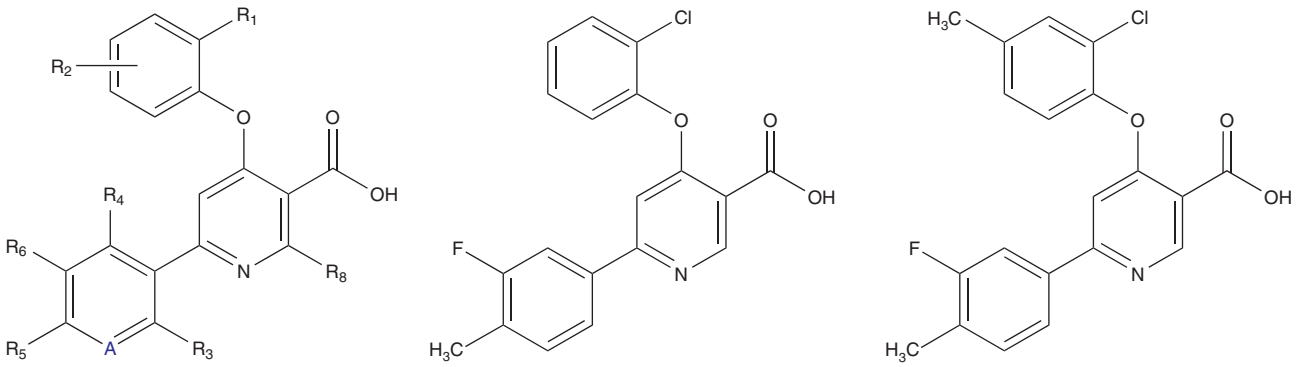

1 1a 1b

Figure 2. PPARα ligands by Bayer Schering.

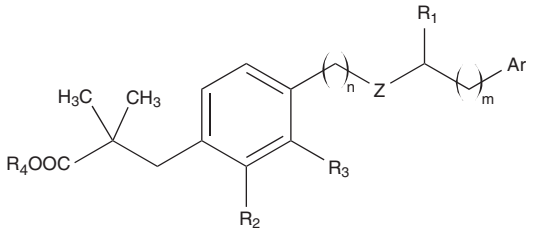

2

Figure 3. General formula of PPARα ligands by Aryx Therapeutics.

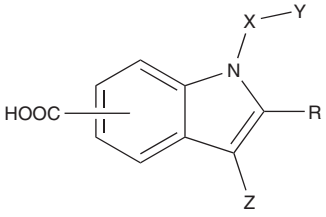

3

Figure 4. General formula of PPARα ligands by Smithkline Beecham.

body weight, body fat, serum glucose and serum insulin levels were observable (**Figure 6**).

With the isoflavone-C-glycoside puerarin (7) from *Puerira Lobata* another natural compound is patented [23] as PPARα modulator. However, the compound does not bind to the nuclear receptor but upregulates its expression [23].

2.3 Novel indications of PPARα ligands

Especially in recent years several new indications for PPARα targeting agents have been developed and patented including the use of known PPARα ligands for novel indications as well as new compounds. The novel approaches can be divided in topical and systemic application.

2.3.1 Topical application

A structurally quite simple class of PPARα agonists has been patented [24] by *Neopharm* in 2010. The compounds of the general formula **8** wherein R1 and R2 are alkyl groups or monocyclic aromatic moieties intensely remind of fatty acids and fatty acid amides, respectively. By dermal application the compounds exhibit anti-inflammatory effects in the skin and are therefore useful for the treatment of skin disorders such as acne, dermatitis and urticaria. The anti-inflammatory effects of the claimed substances have been proven in several *in vivo* models (**Figure 7**).

2.3.2 Systemic application

2.3.2.1 Cartilage protection against inflammation in arthritis

A very interesting novel indication for PPARα agonists has been discovered and patented [25] by *Johns Hopkins University*. In an *in vitro* model of cartilage inflammation, human chondrocytes are exposed to shear stress that leads to upregulation of stress-induced genes such as the COX-2. In this model it was observed that selective PPARα agonists can antagonize the stress-induced upregulation of COX-2 and might therefore be an effective alternative to COX-inhibitors in prevention and treatment of cartilage inflammation as it, for example, occurs in arthritis.

2.3.2.2 Muscle wasting disorders

PPARα is among other tissues highly expressed in skeletal muscles where it is involved in the muscles' metabolism control. Congruently, side effects affecting muscles occurred in the clinical use of the PPARα agonistic fibrates. Hence PPARα ligands have been examined for their effects on muscle cells and it has been observed that activation of the nuclear receptor can protect muscles from ischemic damage [26,27]. In several animal

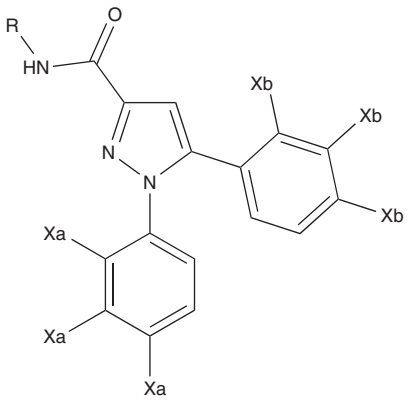

4

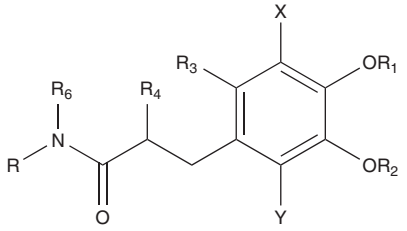

5

Figure 5. General formulas of PPARα ligands by IMABIS.

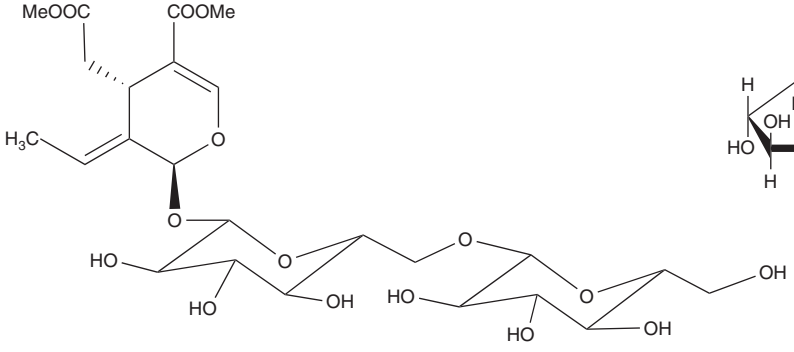

6

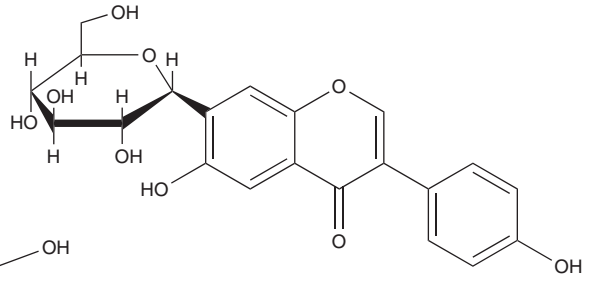

7

Figure 6. Natural PPARα modulators 6 and 7.

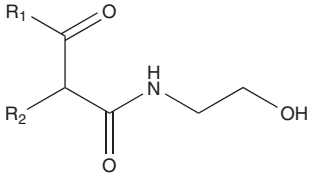

8

Figure 7. General formula of PPARα ligands by Neopharm.

models of ischemic muscle necrosis and muscle dystrophy, the application of fibrates was effective to reduce necrotic area after ischemic events or reduce lesions related to dystrophy. Fibrates or other PPARα agonists have therefore been patented [26,27] for the use in treatment of several myopathies but there are no clinical trials for this indication yet.

2.3.2.3 Reduction of side effects of glucocorticoid therapy

With the intention to lower the side effects induced by a systemic therapy with glucocorticoids (GCs) the combination of GCs with PPAR agonists, especially fibrates has been studied *in vitro* and *in vivo*. It was thereby observed that by adding a PPARα agonist to a GC therapy the effective dose of GC can be significantly reduced, which in turn lowers the GC side effects. Hence the use of a combination of a GC and a PPARα agonist has been patented [28] for the treatment of glucocorticoid-responsive conditions.

3. Selective PPARγ ligands

Despite the fall of the TZDs [1], also quite a lot of new patents regarding PPARγ have been filed over the last few years including new ligands and novel methods or uses for known compounds.

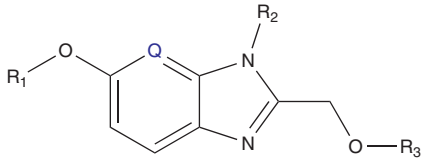

9

Figure 8. General formula of PPARγ ligands by Daiichi Sankyo.

3.1 PPARγ ligands for antidiabetic and metabolic indications

In 2008, *Daiichi Sankyo* has patented [29] a broad range of PPARγ modulating aryl derivatives. The claim includes monocyclic aryl derivatives, naphtyl derivatives and 5-membered heteroaromatic compounds that are all highly substituted. The huge variability of this patent does not yet admit any significant conclusion about the concrete structure of potent PPARγ ligands inside this series of compounds and there has not been a succeeding claim that specifies either the structural properties or the use of these compounds.

However, in 2009, Daiichi Sankyo filed a patent [30] on fused bicyclic heteroaryl derivatives, which was renewed with more specified compounds in 2012 [31]. The first of these patents claims compounds of the general formula **9** with various alkyl or aryl substituents. In 2012, R^3 has been specified as a 3-benzoic acid substituent, R^2 as a methyl group and Q as CH, which makes the core structure of the compounds a benzimidazole. For R^1 the patent claims substituted pyridyl groups. All these compounds are described as PPARγ agonistic antidiabetics but also several other indications including cancer, inflammatory and neurodegenerative diseases are mentioned in the patents. In several *in vitro* assays the compounds exhibited PPARγ agonistic or partial agonistic activity and the proposed antidiabetic effects have been proven in mouse models of diabetes (**Figure 8**).

Merck has focused on benzisoxazoles and other fused bicyclic heteroaromates as PPARγ ligands over the last years. In 2008, benzisoxazole **10** has been claimed [32] as anhydrous crystalline tosylate salt, which is stable and suitable for pharmaceutical use. Compound **10** is described as selective PPARγ partial agonist and as effective agent to treat disorders related to diabetes and hyperglycemia by reducing serum glucose.

Later in 2008 [33] the structural space of Merck's PPARγ ligands was expanded to fused aromatic and heteroaromatic core structures with several substituents of the general formula **11**. All compounds are claimed as PPARγ agonists or partial agonists that are useful to treat and control type II diabetes and related disorders by weekly application.

One year later, Merck filed a patent [34] claiming azaindoles and diazaindoles as therapeutic compounds for the treatment of type II diabetes. The compounds of the general formula **12** share a similar core structure compared to **10** and **11**. All derivatives are described as PPARγ ligands with predominantly agonistic or partial agonistic activity but it is not excluded that also some antagonistic ligands are contained. In contrast to the prior patents by Merck that claim selective ligands for PPARγ, some of the compounds of general formula **12** may also have an activity at PPARα.

Since 2009 there has not been any activity in patents concerning PPAR ligands by Merck, which might be due to the recent events concerning the TZDs (**Figure 9**).

Dong-A Pharmaceuticals has filed two patents [35,36] claiming phenylpropionic acid derivatives of formula **13** as PPARγ modulators that exhibit partial agonism and are thereby effective to treat type II diabetes with reduced side effects compared to the TZDs. Disclosed are free α-ethoxy-dihydrocinnamic acids, their alkali salts or ethyl esters that are substituted with several biaryl moieties in para position. In reportergene assays the compounds exhibited partial PPARγ agonism with EC_{50} values ranging from 7 to 1000 nM and transactivation efficacy of 15–80% compared to full agonistic reference muraglitazar (**14**; the IUPAC name in the patent does not make sense but probably refers to **14**). The most potent derivative **13a** showed 27% PPARγ transactivation with an EC_{50} of 7 nM and good selectivity (> 400) over PPARα. In diabetic (db/db) mice compound **13a** and four others exhibited a significant blood glucose lowering effect within 5 days.

Furthermore, several of the compounds showed a reduced binding capacity to PPARγ in the presence of Trap220. As Trap220 is an essential cofactor for adipocyte differentiation, PPARγ ligands that have reduced affinity to PPARγ in the presence of Trap220 are thought to exhibit less weight gain as side effects compared to the TZDs [37]. Hence the compounds are true PPAR modulators and with PAM-1616 [37] (**13b**), PAR-1622 [38] (**13c**) and PAR-5359 [39] (**13d**) there are currently three compounds with different balances in PPARα/γ activities in preclinical development. Although **13b** and **13c** are selective, PPARγ partial agonists **13d** also exhibits PPARα partial agonism. All compounds showed antidiabetic effects *in vivo* and might enter clinical development in near future (**Figure 10**).

Another series of partial PPARγ agonists for the use as antidiabetics has been claimed in two patents [40,41] filed by *Evolva SA*. The compounds of the general formula **15** contain a central 1,3-dioxane structure with an olefinic carboxylic acid side chain and various aromatic substituents. Derivative **15a** exhibited concentration-dependent partial agonism in PPARγ transactivation assays and was inactive at PPARδ and RXRα, but a slight activity at PPARα was observable. In a competitive binding assay, a K_d of 15 μM was determined for its affinity to PPARγ and several beneficial effects such as enhanced insulin-stimulated glucose uptake without promotion of adipocyte differentiation were observed for **15a** *in vitro*. However, **15a** has probably too weak affinity to its target for clinical development and further structural optimization has to be conducted (**Figure 11**).

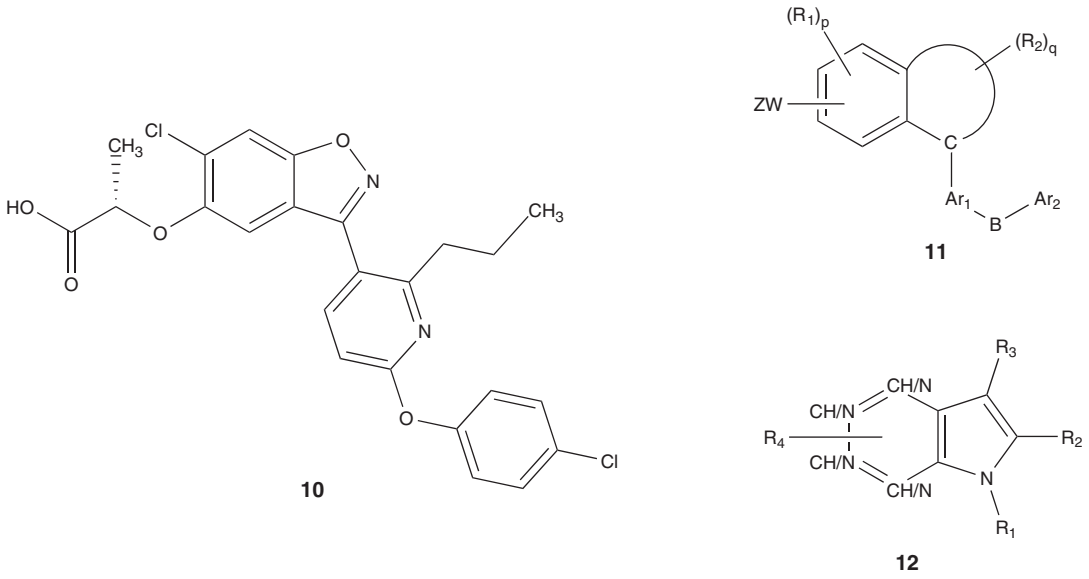

Figure 9. General formulas of PPARγ ligands by Merck.

Smithkline Beecham has claimed [42] PPARγ-modulating indole derivatives of formula **16** for the use as antidiabetics. With respect to the good efficacy but unfavorable side effects of full agoniostic TZDs, these indole derivatives are partial agonists at PPARγ. The patent claims their use for the treatment of diabetes and related disorders, but on the other hand also describes the recent findings about involvement of PPARγ in several other pathologic conditions such as Alzheimer's disease, rheumatoid arthritis and cancer (**Figure 12**).

3.1.1 *Dual PPARγ-agonists/AT1-inhibitors*

With respect to the growing incidence of type II diabetes, dyslipidemia and obesity and the fact that these disorders are potential risk factors for arteriosclerotic diseases, *Kowa* is developing compounds with a dual activity as angiotensin II receptor antagonists (AT_1-blockers) and PPARγ agonists. In 2011, two similar structural classes with the general formulas **17** and **18** have been patented [43,44] for this activity. Both share a 4-biphenyl moiety that is substituted with a bioisosteric group for a carboxylic acid, for example, with a tetrazole or an 1,2,4-oxadiazol-5(4*H*)-one. Comparable bioisosteric use of a tetrazole has already been successful in the AT_1-blocker losartan and the structures **17** and **18** generally have a close relation to the sartans except that the patented compounds are significantly greater to be able to activate PPARγ. The biphenyl moiety further carries a substituted imidazole or 2-pyridone.

Later the pyrimidinone derivative **19** and closely related structures along with their synthesis were also claimed [45] as dual angiotensin II receptor antagonists/PPARγ agonists. The angiotensin II receptor antagonistic/PPARγ agonistic activities were evaluated in *in vitro* assays with transfected CHO-K1-cells that expressed either human AT_1 or human PPARγ and in animal models the compounds significantly reduced blood pressure (**Figure 13**).

Similar to the inventions by Kowa also *Kyowa Hako Kirin Co.* has filed patents on dual angiotensin II receptor antagonists/PPARγ agonists. But compared to the predominantly mono- and bicyclic compounds active at PPARγ, Kyowa developed a structurally quite different scaffold. Tricyclic compounds represented by the general formula **20** are claimed [46] as dual angiotensin II receptor antagonists/PPARγ agonists. In addition to their tricyclic core structure all derivatives possess carboxylic acid moieties or suitable bioisosteric groups such as tetrazoles, oxadiazoles, oxadiazolones or sulfonic amides. The compounds are disclosed as potential agents for the treatment of various disorders in which PPARγ is involved such as metabolic, vascular, inflammatory and neurodegenerative diseases.

The most potent derivatives **20a** and **20b** exhibited PPARγ agonism with EC_{50} values of 48 and 73 nM, but also several other highly potent structures are included. Dibenzo[b,f] azepine **20a** and dihydrodibenzo[a,d]annulene **20b** are substituted with a benzimidazole and an 1,2,4-oxadiazol-5(4H)-one as bioisosteric group for the required carboxylic acid. Additionally to their PPARγ activity the affinity of the compounds to the angiotensin II receptor was examined in a radio ligand-binding assay where several of the substances including **20b** had affinities below 10 nM. Administration of some of the patented compounds to diabetic and obese mice showed a significant amelioration of plasma glucose and triglyceride levels and an improved reaction to oral glucose tolerance tests [46].

The succeeding patent [47] from 2011 claims compounds of the general formula **21** that are selective agonists for PPARγ. They again share a substituted tricyclic core structure that holds a carboxylic acid moiety or a suitable bioisosteric

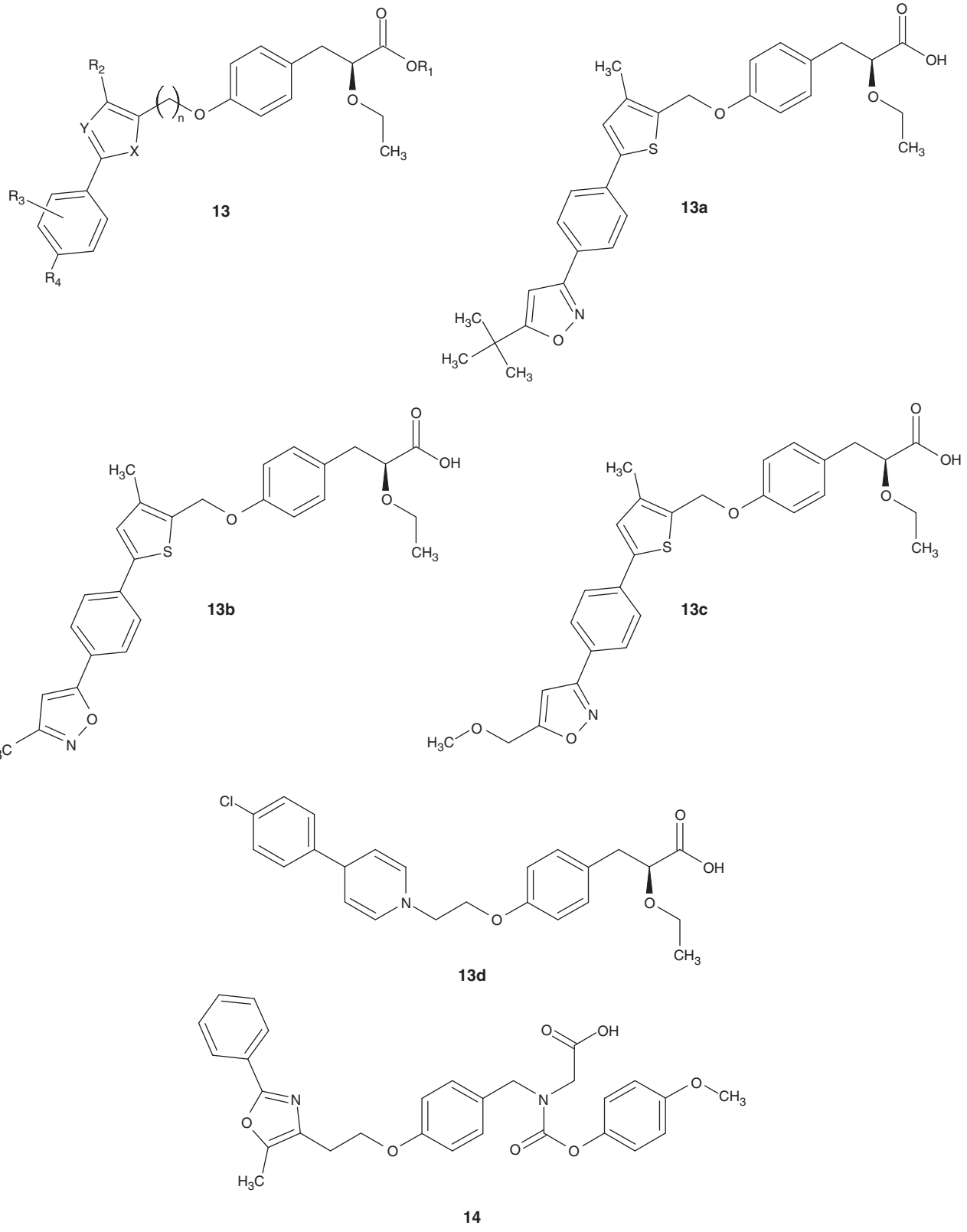

Figure 10. PPARγ ligands by Dong-A Pharmaceuticals.

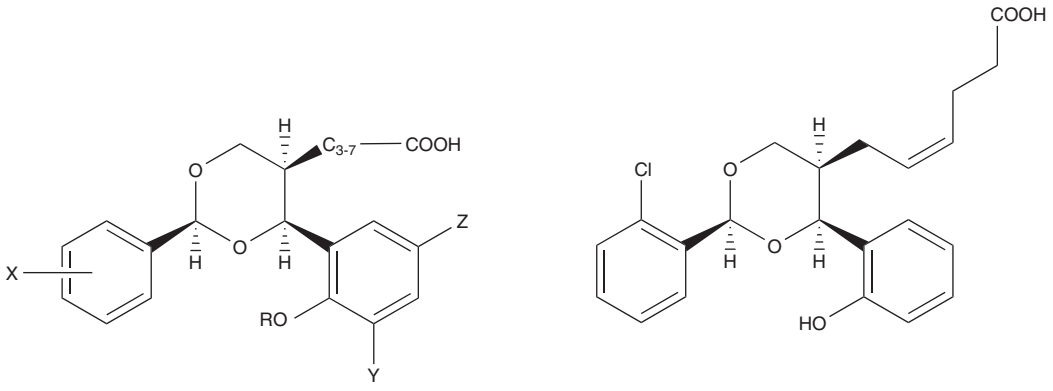

Figure 11. PPARγ ligands by Evolva SA.

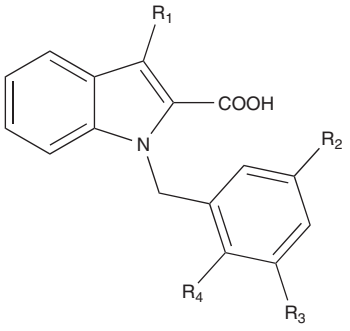

Figure 12. General formula of PPARγ ligands by Smithkline Beecham.

group. **21a** and **21b** exhibited PPARγ agonism with EC_{50} values of 2.6 and 2.4 nM and are thus even more potent than the former compounds. Accordingly they were effective in reducing plasma glucose and triglycerides in mice. However, the patent does not comment on their activity at the angiotensin II receptor but due to the close relationship to the former compounds, which are antagonistic at AT_1 a comparable activity is likely (**Figure 14**).

3.1.2 PPARγ ligands by other patent assignees

Some other, though, less potent structural classes of PPARγ ligands have been patented including coumaperine derivatives related to **22** by *Kaneka Corp.* [48] as well as cannabinoid chinone derivatives of general formula **23** by *Vivacell Biotechnology Espana* [49].

Additionally *Shenzhen Neptunus Pharmaceutical Co.* has claimed [50] diphenylethene derivatives of formula **24** as PPARγ agonists with EC_{50} values of around 30 nM for the most potent candidates. But as the compounds comprise a potentially toxic stilbene moiety as central structure, their pharmaceutical applicability is questionable (**Figure 15**).

3.1.3 Combinations to reduce side effects of antidiabetic PPARγ agonists

A possible way to reduce side effects is by lowering the administered dose of the responsible agent. Such an approach has been patented [51,52] for the TZDs by *Epax* in 2010. In animal models of diabetes a combination of a TZD with a phospholipid composition showed synergistic beneficial effects on weight gain and plasma glucose levels. Hence the combination might be useful to reduce the dose of TZDs necessary to control type II diabetes, which in turn could minimize side effects.

With *Boehringer Ingelheim* [53] and *Theracos, Inc.* [54], two companies have patented the combined use of a PPARγ agonist and a sodium-dependent glucose cotransporter 2 (SGLT2) inhibitor for the treatment of type II diabetes. SGLT2 is exclusively expressed in the kidney and responsible for reuptake of filtered glucose. Background of this strategy is that by inhibiting SGLT2 the renal excretion of glucose is enhanced and thereby a hyperglycemic condition is supposed to be ameliorated. As PPARγ agonistic component of the patented pharmaceutical combinations TZDs, in particular, rosiglitazone or pioglitazone, are described. In animal studies with diabetic rodents the combination of a SGLT2 inhibitor and a TZD was effective in controlling plasma glucose levels but led to significantly less weight gain than the application of a TZD alone. In another *in vivo* study a SGLT2 inhibitor significantly reduced the plasma volume of rats that were chronically treated with pioglitazone. SGLT2 inhibitors might therefore be useful to suppress weight gain and fluid retention which are major side effects of the TZDs.

Also for the indication to reduce side effects of PPARγ agonists acetyl L-carnitine in combination with a TZD or other PPARγ agonists has been disclosed [55]. In patients that were affected by osteoporosis due to treatment with rosiglitazone previously, the combination of rosiglitazone and acetyl L-carnitine was effective to reduce osteoporotic side effects.

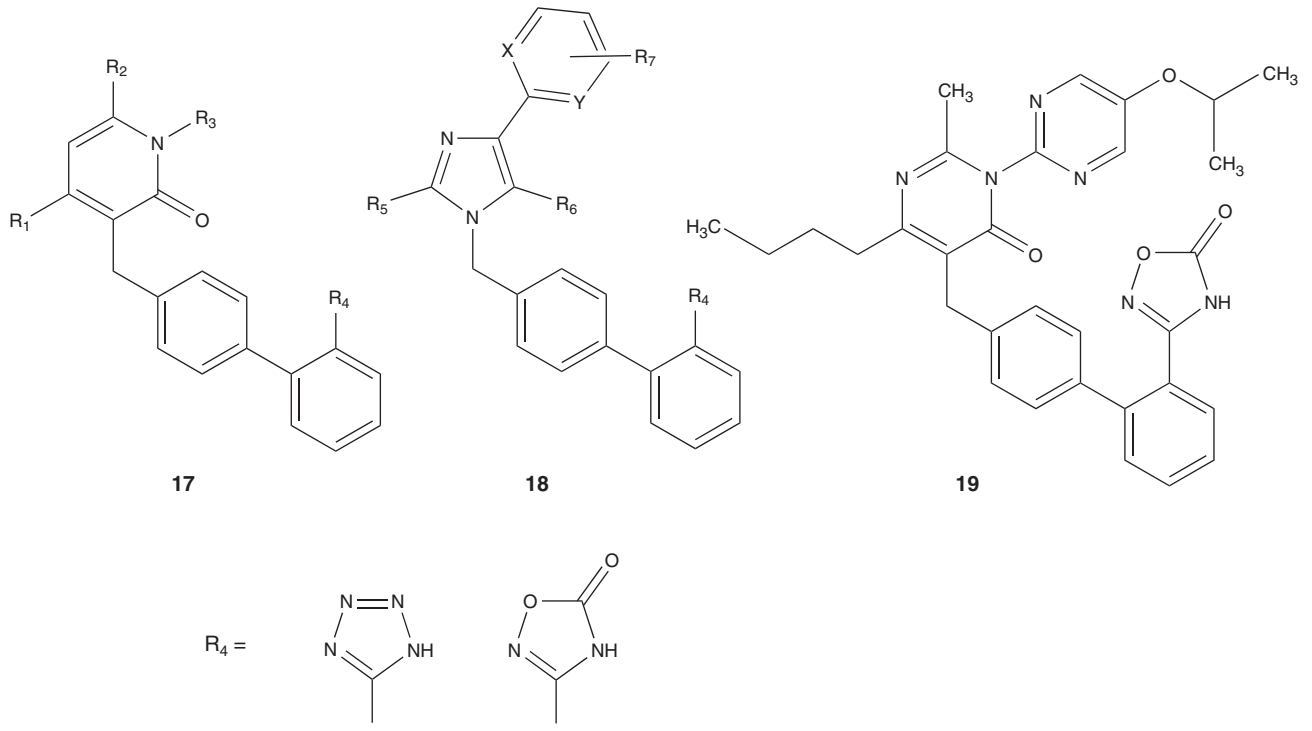

Figure 13. Dual PPARγ-agonists/AT_1-inhibitors by Kowa.

Furthermore, the same combination led to a slight but significant reduction in body weight. Hence, acetyl L-carnitine might arise as suitable co-medication for antidiabetic therapies with TZDs or other PPARγ agonists.

3.1.4 *Cdk5-dependent phosphorylation of PPARγ*

As mentioned, a very recent new finding might revolutionize PPAR-targeted antidiabetic therapy in the mid-term future. Researchers at Harvard Medical School have discovered that not the PPARγ agonism of rosiglitazone and other agonists alone is effective to ameliorate type II diabetes, but that the ability of the compounds to inhibit the obesity-linked phosphorylation of PPARγ at Ser_{273} by the Cdk5 also has antidiabetic effects [3]. Furthermore, novel ligands SR1824 (**25a**) and SR1664 (**25b**) of the nuclear receptor have been described that block the Cdk5-dependent PPARγ phosphorylation without being agonists at PPARγ. Such modulators might be effective PPAR-targeted antidiabetics that lack the adverse effects of classic PPARγ agonists such as the TZDs. However, further optimization of the indole-based compounds **25a and b**, which structurally remind of the sartanes, will probably have to be conducted before suitable drug-like derivatives for clinical development are available. According to this the inventors of **25a and b** have recently patented [56] methods for identifying compounds that inhibit said Cdk5-dependent PPARγ phosphorylation (**Figure 16**).

3.2 Novel indications for PPARγ ligands

Despite the recent decline of PPARγ ligands in clinical use for the treatment of metabolic diseases and especially type II diabetes, several other possible indications for activation or modulation of this nuclear receptor have emerged.

3.2.1 *Topical application*

Recently, growing interest has focused on the possible use of PPARγ agonists in skin-related disorders associated with diabetes or aging. As PPARγ agonists such as rosiglitazone have been observed to cause weight gain by promoting the differentiation of adipocytes, these full agonistic agents might have a future role in, for example, restoring subcutaneous fat or treating lipodystrophy. Furthermore, for the fact that topical or subcutaneous application of these might circumvent the severe adverse events associated with systemic application of TZDs, the cutaneous use could help a rebirth of PPARγ agonists [57].

Galderma Research & Development developed PPARγ modulators for the use in skin disorders associated with an anomaly of epidermal cell differentiation. Three similar structural classes with the general formulas **26**, **27** and **28** have been patented so far. The compounds of the general formulas **26** [58] and **27** [59] share a cinnamoyl moiety that was eventually because of unfavorable stability replaced by a dihydrocinnamoyl structure in **28** [60,61]. In a HeLN-cell-based reportergene assay the compounds were examined for their affinity to PPARγ and the most potent derivatives had K_d values

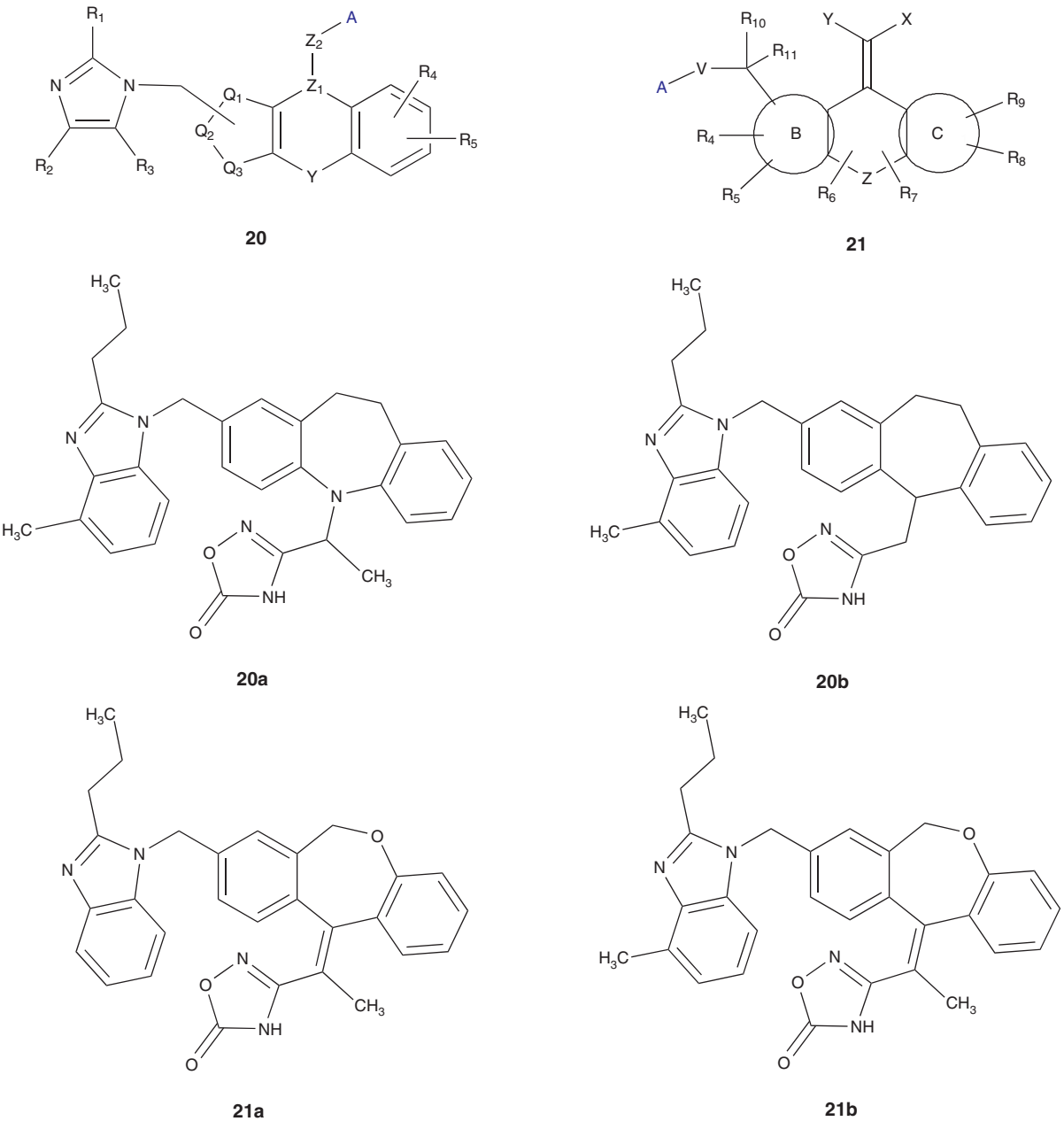

Figure 14. Dual PPARγ-agonists/AT_1-inhibitors by Kyowa Hako Kirin Co.

between 1 and 10 nM for affinity to PPARγ with excellent selectivity over other PPAR subtypes (**Figure 17**).

Topical compositions that comprise weaker PPARγ agonists such as lipoic acid in combination with corticosteroids and antibiotics for the treatment of inflammatory skin disorders including dermatitis, acne, psoriasis, alopecia and others are claimed in several patents [62-64]. In these drug combinations for topic application the PPARγ agonistic compound is said to act as an antioxidant.

A predominantly cosmetic invention [65] of *Johnson & Johnson* relates to the use of TZDs or other PPARγ agonists for the treatment of facial skin defects, which includes scars, skin atrophy, sagging skin and many others. The PPARγ active agent is supposed to be subcutaneously delivered together with various carriers and held in place by a filling material that is not immediately degraded or absorbed.

Also the use of PPARγ antagonists for topical application has been claimed. In contrast to PPARγ agonists that promote fat synthesis and storage in adipocytes, antagonists at the nuclear receptor reduce lipid synthesis and accumulation. This action might be useful for the cosmetic treatment of cellulite and related skin-associated defects as they depend

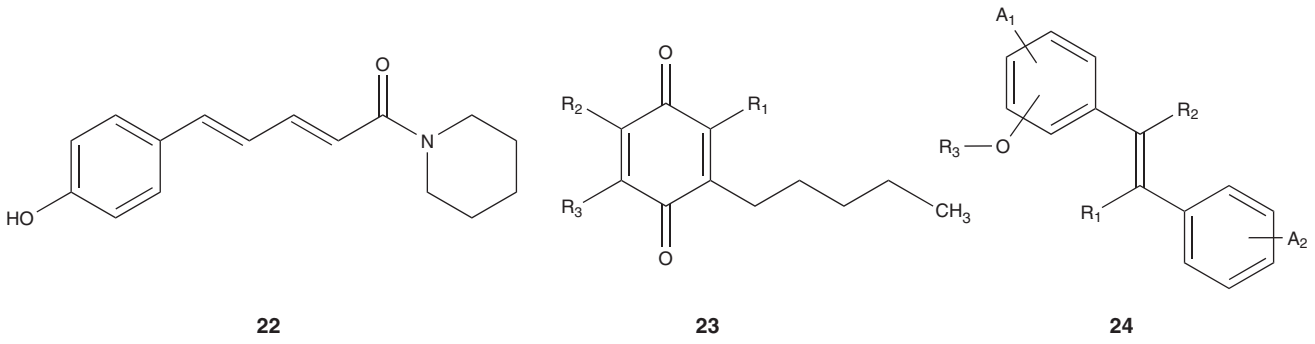

22 23 24

Figure 15. PPARγ ligands by Kaneka Corp., Vivacell Biotechnology and Shenzhen Neptunus Pharmaceutical Co.

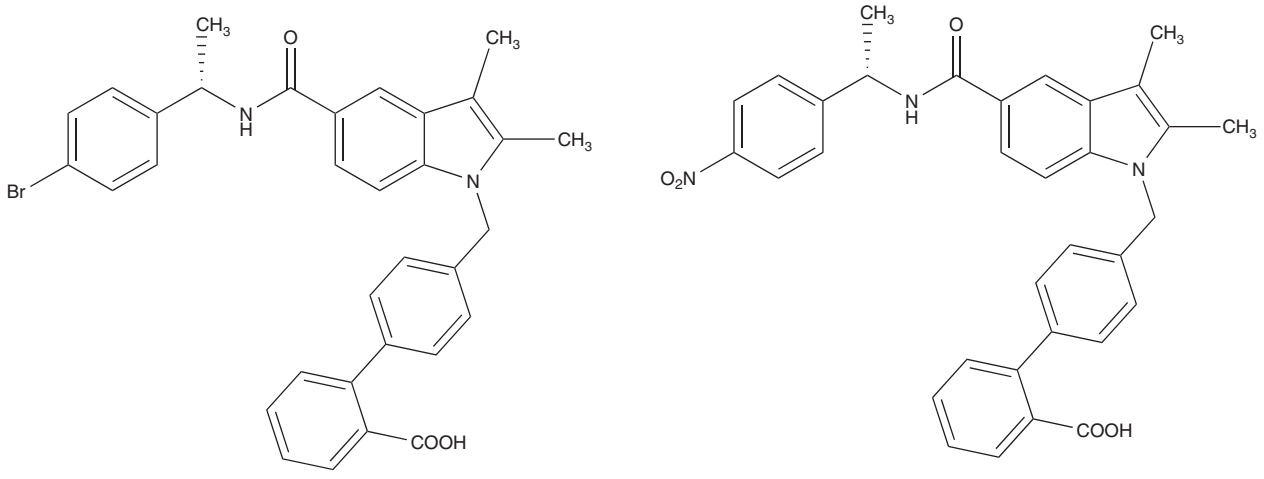

25a 25b

Figure 16. Non-agonistic PPARγ ligands SR1824 (25a) and SR1664 (25b) that inhibit the obesity-linked phosphorylation of PPARγ by the Cdk5.

on lipid accumulation in subcutaneous adipose tissue. A patent [66] by *Avon Products* claims the use of an extract from *Eclipta prostrata* or other PPARγ antagonists in cosmetic compositions for this purpose.

3.2.2 Systemic application

3.2.2.1 Autoimmune diseases

Recently a very interesting observation has led to a patent [67] claiming the use of PPARγ agonists in autoimmune diseases that are associated with T_{H17} lymphocytes. This specialized population of immune cells predominantly produces the cytokine IL-17A and has been shown to be intensely involved in the pathogenesis of multiple sclerosis and other inflammatory diseases. In *in vitro* studies, activation of PPARγ with rosiglitazone or pioglitazone significantly reduced the production of IL-17A. This was accompanied by anti-inflammatory effects in animal models of multiple sclerosis, colitis and arthritis. However, the certain physiologic and pharmacologic correlations of these effects are not yet understood and more research will have to be conducted before PPAR agonists can reach clinical relevance for the treatment of inflammatory diseases.

A possible role of PPARγ activation was also discovered [68] in inflammatory bowel diseases (IBD) including Crohn's disease (CD) and ulcerative colitis (UC). Recent experiments indicated that the nuclear receptor might be involved in anti-inflammatory actions by inducing defensins. In *in vitro* studies a strong induction of mRNA of defensins HD-5, HD-6 and others was observed by qPCR in Caco-2 cells after stimulation with rosiglitazone. Hence the use of PPARγ agonists such as the TZDs and several others is patented [69] for the treatment of inflammatory diseases of the intestine such as CD, UC, inflammatory bowel syndrome and diverticulitis.

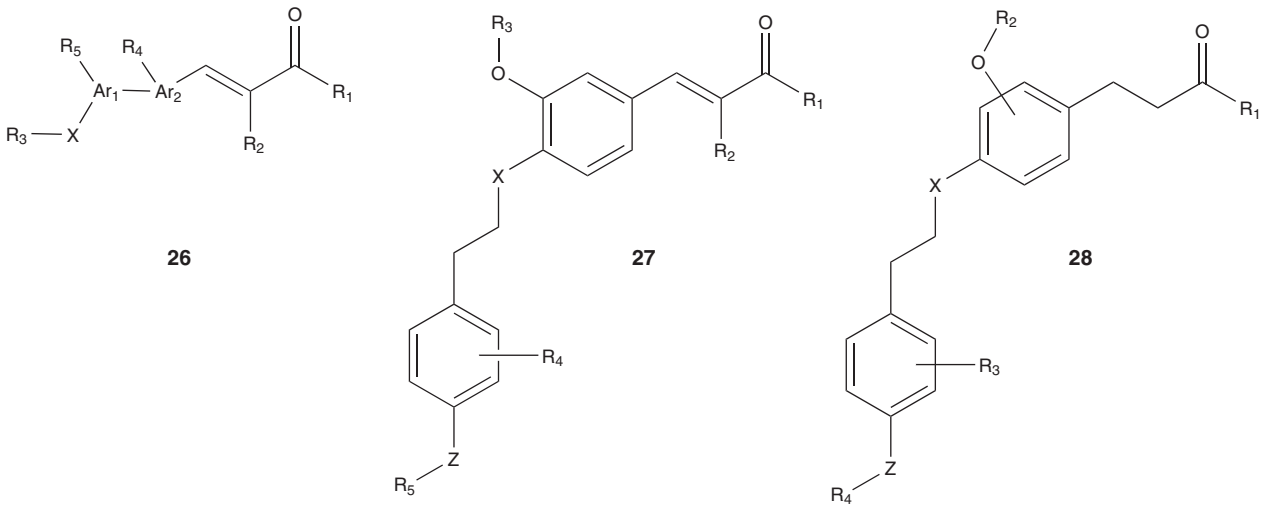

Figure 17. General formulas of PPARγ ligands by Galderma R&D.

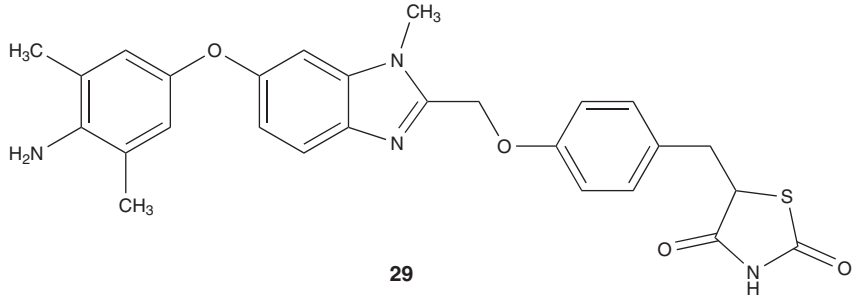

Figure 18. Daiichi Sankyo's PPARγ ligand CS-7017.

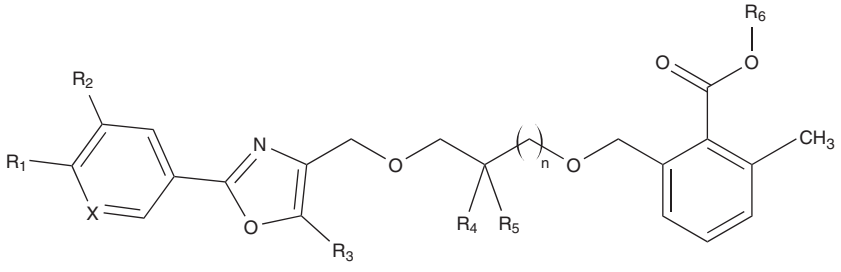

Figure 19. General formula of dual PPARα/γ ligands by Sanofi-Aventis.

Furthermore, a potential therapeutic use for other inflammatory disorders including allergic rhinitis and dermatitis is claimed.

3.2.2.2 Cancer

As PPARs are ligand-activated transcription factors and hence involved in regulation of genes, a potential involvement in cancer development as well as a possible role for cancer therapy is obvious and the fact that pioglitazone was recently found to promote bladder cancer proves this assumption [70]. Many *in vitro* and *in vivo* studies have therefore been conducted with known PPARγ ligands to determine the risk of therapeutic PPARγ activation on one hand, and a possible use thereof for cancer treatment on the other hand. As PPARγ

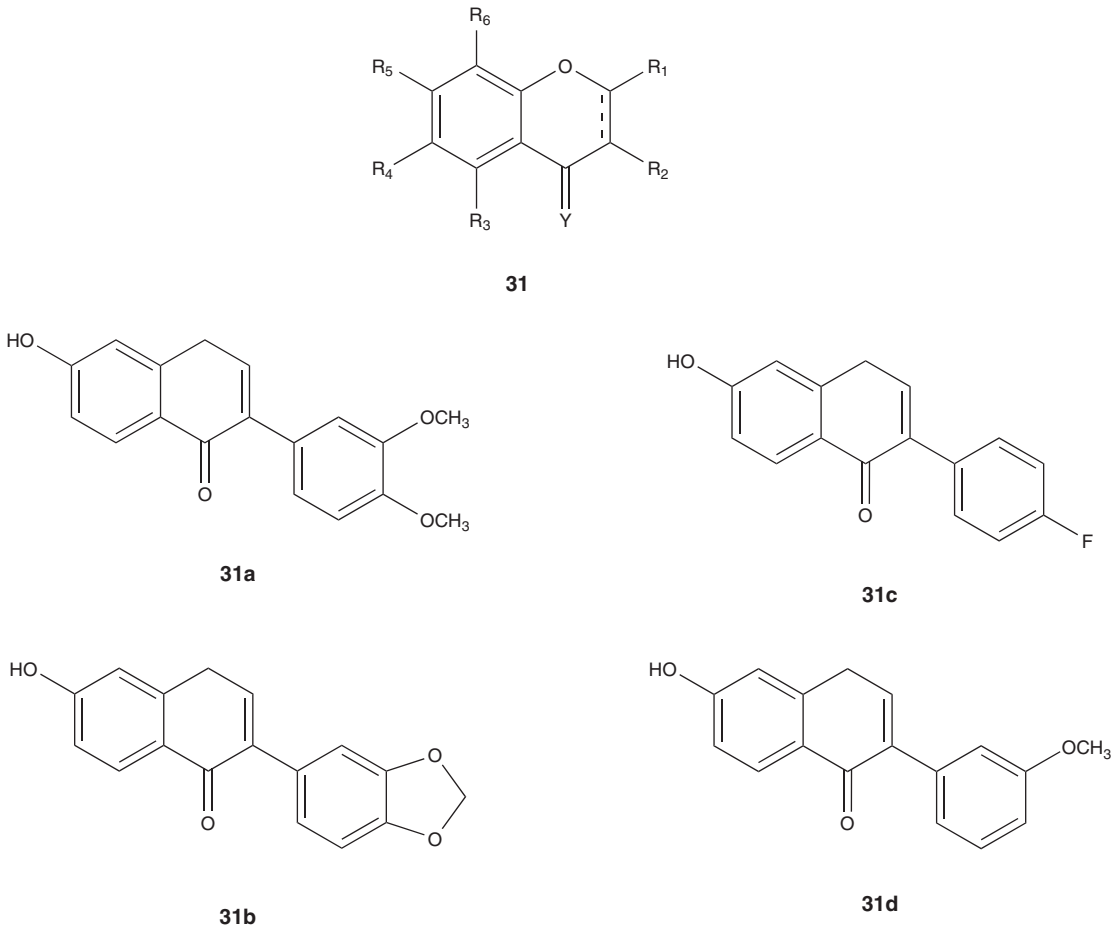

Figure 20. Dual PPARα/γ ligands by the University of Sidney.

activation is a promising strategy to inhibit tumor growth of several cancer forms and proved to be effective *in vitro* and *in vivo* the TZDs and other PPARγ agonists entered clinical trials for the treatment of cancer in recent past [8].

Consequently, some patent activity has taken place on this sector including novel PPARγ agonistic compounds for cancer treatment as mentioned above but also concerning established agents for this new indication. The use of TZDs in combination with a caspase-dependent chemotherapeutic agent is patented [71] for treatment of several very common cancer forms. The patent relies on *in vitro* observations that PPARγ agonists enhance the pro-apoptotic effects of said chemotherapeutics by upregulation of pro-apoptotic factors such as Bax and Bcl-2. It will have to be awaited if these effects will be confirmed and beneficial in clinical development.

The PPARγ agonistic thiazolidinedione derivative CS-7017 (**29**) [72] by *Daiichi Sankyo* that belongs to the same chemical class as **9** is patented [73-77] as anticancer pharmaceutical along with its manufacturing method and compositions containing **29**. compound **29** was investigated in *in vitro* assays and animal models where it had significant antiproliferative effects on several human tumor cell lines (non-small-cell lung cancer cell lines A549 and SN12-PM6) and tumor xenografts (colorectal tumor HT-29). Parallel experiments with the same cell lines also showed synergistic effects of **29** with the epidermal growth factor receptor (EGFR) inhibitor gefitinib and the dual vascular endothelial growth factor receptor (VEGFR) inhibitor and Raf kinase inhibitor sorafenib. CS-7017 (**29**) recently completed clinical Phase I/II trials for several cancer forms but no results are available yet (**Figure 18**).

3.2.2.3 Age-related macular degeneration

The age-related macular degeneration (AMD) is thought to be at least in part dependent on oxidative processes that damage the polyunsaturated fatty acids, which are present in the membranes of photoreceptive cells. As PPARγ is intensely involved in lipid metabolism and degradation as well as in the regulation of antioxidative genes, there are experimental approaches to use PPARγ agonists for the treatment of AMD. In particular, the use of docosahexaenoic acid, an endogenous omega-3 fatty acid that is a weak activator of PPARγ, has been patented [78] recently.

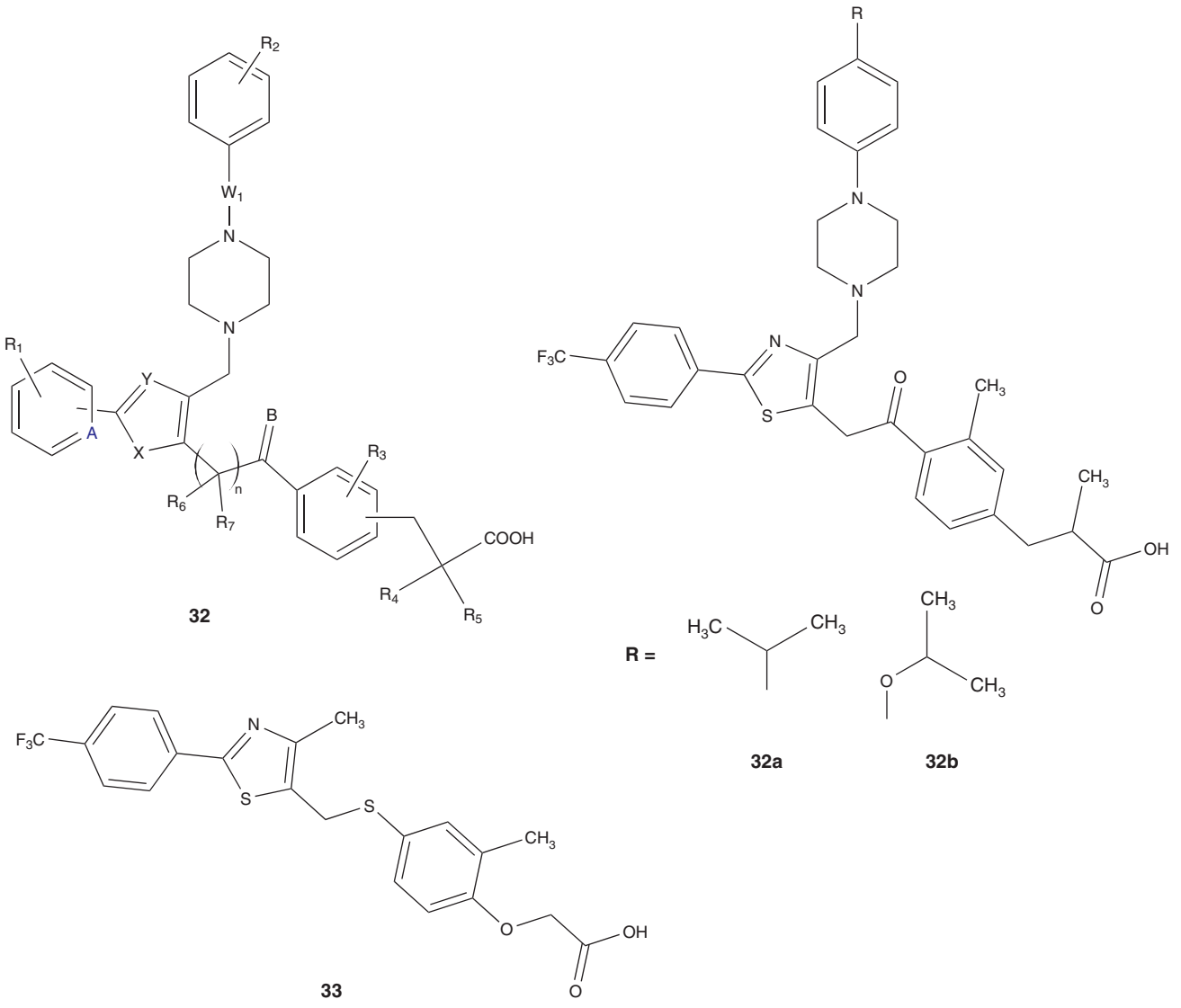

Figure 21. Dual PPARα/γ ligands by Nippon Chemiphar.

3.2.2.4 *Addiction*

Various animal studies have recently indicated that the use of a potent PPARγ agonist such as the TZDs can be effective to prevent or to treat addictions. This includes addictions to a certain substance such as alcohol, nicotine, opioids or cocaine but also addictive behavior as, for example, kleptomania and others. In congruence with these findings it was observed that diabetic patients with alcoholism that received a TZD as antidiabetic medication reduced their alcohol intake.

This novel use of PPARγ agonists has been claimed in two patents [79,80] by the *Omeros Corporation*. As PPARγ active agent the patents describe the use of glitazones eventually combined with an opioid receptor antagonist, an antidepressant or an anticonvulsive drug. However, besides the observations in diabetic patients with alcoholism there is no data from clinical studies that confirms any antiaddictive action of PPARγ activation up to now.

3.2.2.5 *Brain damage*

A patent published in 2010 by the *Rhode Island Hospital* reports a relationship between alcohol-induced brain damage and insulin resistance [81]. This could be demonstrated by findings of impaired insulin response and alterations in the insulin/IGF pathways in the brains of animals with chronic alcohol intake. Animal models of alcohol-induced brain damage revealed that administration of PPAR agonists can prevent oxidative stress and DNA damage in the brain. The patent claims treating, preventing or reversing alcohol-induced brain damage by administering selective agonists of PPARα, PPARγ or PPARδ.

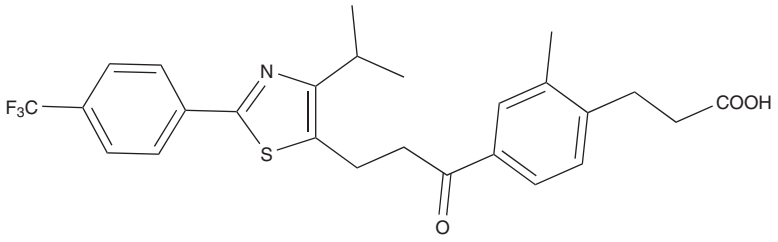

34

Figure 22. PPARδ ligand by Nippon Chemiphar.

Another patent application of Rhode Island Hospital published in 2010 claims methods for treating, preventing or reversing liver disease or damage produced by chronic alcohol intake by administering PPAR agonists as similarly impaired insulin response and signaling was observed in the liver of animals with chronic alcohol intake. Congruently, administration of PPAR agonists inhibited oxidative stress and DNA damage and enhanced liver regeneration [82].

4. Dual PPARα/γ ligands

In many cases metabolic disorders including hyperglycemia and dyslipidemia occur together and have to be treated simultaneously. It has therefore been a logical approach to combine PPARα and PPARγ agonistic activity in one compound that led to the development of the glitazars. However, although these dual PPARα/γ agonists advanced to clinical development and tesaglitazar even reached Phase III trials none of the compounds is approved as a drug because in several cases adverse events and infavorable risk–benefit profiles finished the development. Yet there are still approaches for novel dual PPARα/γ agonists.

Sanofi-Aventis has claimed [83] a series of benzoic acid derivatives with dual agonistic activity at PPARα and PPARγ in 2008. The compounds of the general formula **30** show EC_{50} values of 1.4–88 nM/17–710 nM for PPARα/PPARγ and structurally belong to the class of the mentioned glitazars. But as the glitazars failed due to adverse risk–benefit profiles this project was probably discontinued (**Figure 19**).

Flavonoid-derived compounds of the general formula **31** patented [84] by the *University of Sidney* also have a dual activity at PPARα and PPARγ. From a large library of substituted chromen-4-ones, four derivatives **31a–d** comprising the crucial 7-OH group have emerged as the most potent compounds with strong agonistic activity at both PPAR subtypes at concentrations of 5 μM determined in usual reportergene assays. Psi-baptigenin (**31b**) showed the best overall profile and is in preclinical development (**Figure 20**).

Further dual PPARα/γ agonists have been developed and patented [85,86] by *Nippon Chemiphar*. The compounds with the general formula **32** are structurally derived from the known selective PPARδ agonist GW-501516 (**33**). By introduction of a bulky phenylpiperazine moiety in **33** and some other minor modifications, the activity at PPARδ was lowered while the compounds gained agonism at PPARα and PPARγ. Among these derivatives **32a and b** are most potent with EC_{50} values between 0.1 and 0.3 μM for PPARα and PPARγ (**Figure 21**).

5. PPARδ

In contrast to PPARα and PPARγ that have already gained status as clinically addressed drug targets, PPARδ still has not seen a clinically relevant ligand. However, at present several clinical Phase II trials concerning PPARδ targeting agents are conducted or have recently been completed (NCT00388180, NCT00158899, NCT00701883, NCT01271777, NCT01275469, NCT01271751). The trials focus on the use of previously patented PPARδ ligands such as **33** for the treatment of dyslipidemic or diabetes-related conditions. These clinical studies and the intense patent activity concerning PPARδ indicate that this subtype of the nuclear receptor might more and more come into focus.

In the field of PPARδ agonistic compounds several patent applications have been published in recent years. Most of the claimed PPARδ-activating compounds are structurally similar to **33**, which was first published in 2001 [87]. *Nippon Chemiphar* claimed most of the recently published patent applications and has filed several patents disclosing compounds that have a PPARδ transcription-activating activity and are structurally based on **33**.

Nippon Chemiphar claimed that the disclosed compounds can be used to treat metabolic diseases such as diabetes, syndrome X, obesity, hypercholesterolemia, hyperlipoproteinemia, hyperlipidemia and atherosclerosis as well as for cardiovascular, inflammatory and neurodegenerative diseases including Alzheimer's disease.

In 2009, Nippon Chemiphar disclosed a series of phenylpropionic/phenoxyacetic acid derivatives related to structure **34** with thiazole, oxazole, pyrazole or thiophene rings instead of the thiazole ring in GW501516 (**33**) [88]. Mostly

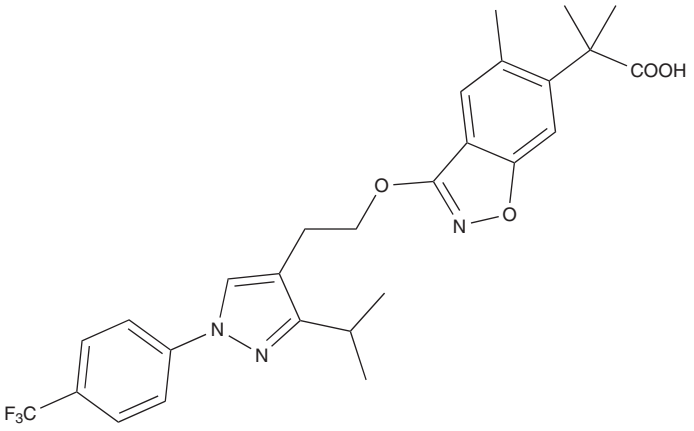

35

Figure 23. PPARδ ligand by Nippon Chemiphar.

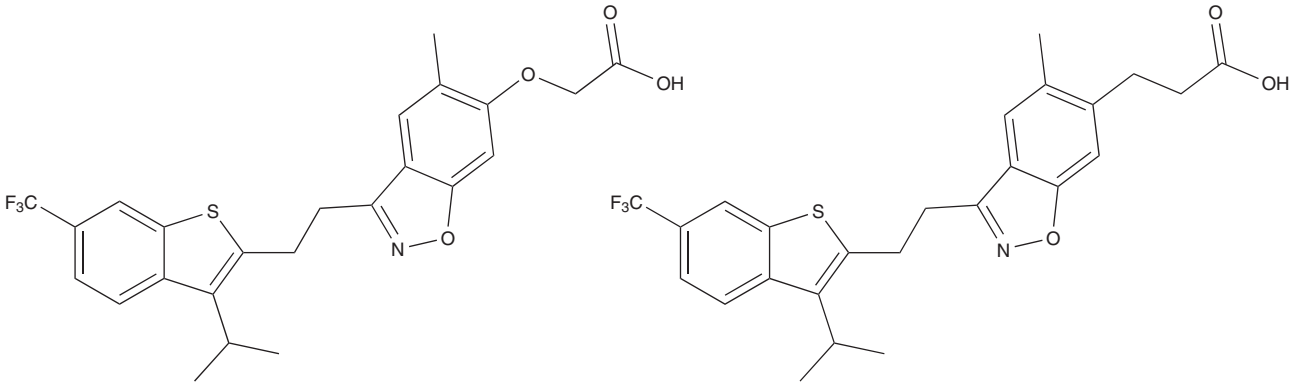

36a 36b

Figure 24. PPARδ ligands by Nippon Chemiphar.

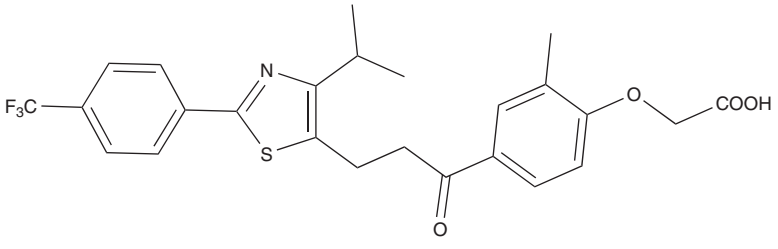

37

Figure 25. PPARδ ligand by Nippon Chemiphar.

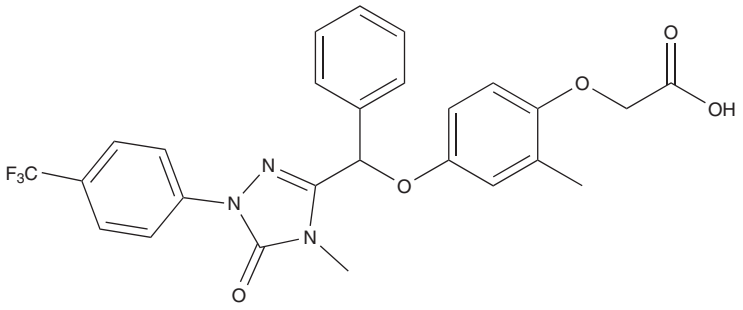

38a

Figure 26. PPARδ ligand by Zhejiang Hisun Pharm.

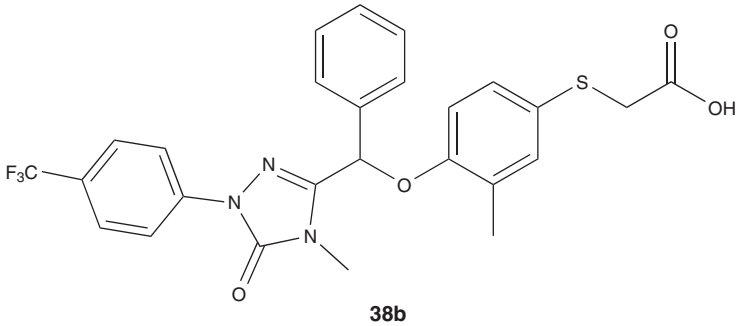

38b

Figure 27. PPARδ ligand by Zhejiang Hisun Pharm.

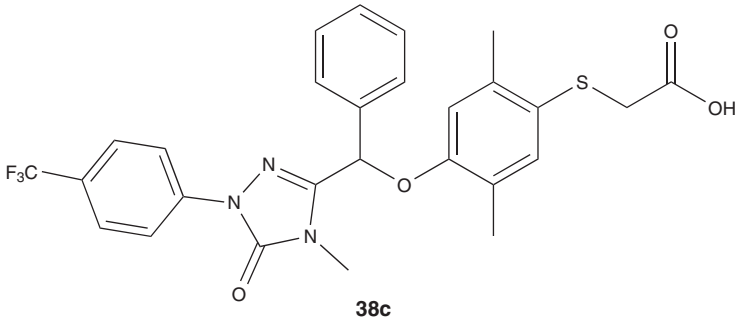

38c

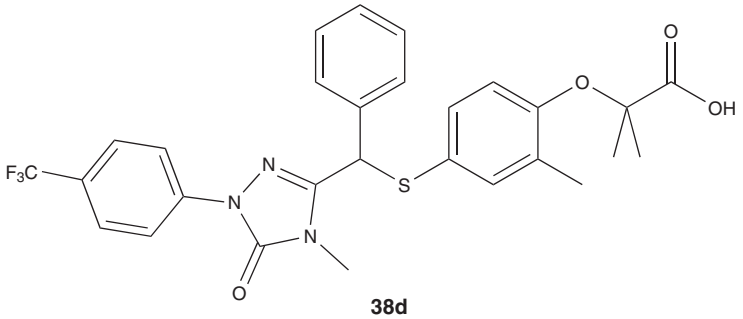

38d

Figure 28. PPARδ ligands by Zhejiang Hisun Pharm.

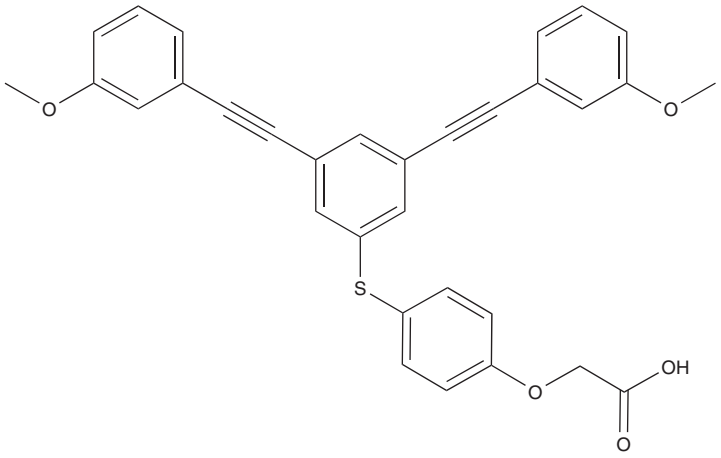

39

Figure 29. PPARδ ligand by Novo Nordisk.

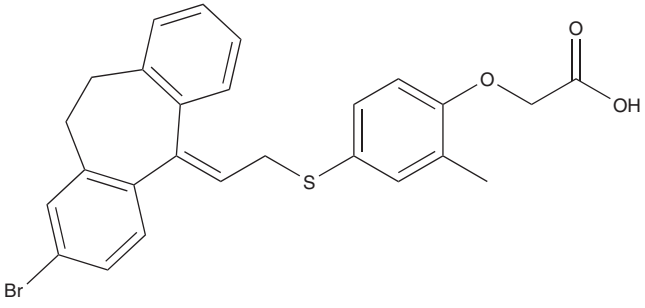

40

Figure 30. PPARδ ligand by Novo Nordisk.

the substitution pattern is analog to GW501516 (**33**) with a 4-trifluoromethylphenyl moiety. The claimed compounds show selective PPARδ activation with the best derivative **34** as active as GW501516 (**33**, EC_{50} PPARα 1,1 μM, PPARγ 0,85 μM, PPARδ 0,001 μM) with 114% activation compared to same (**Figure 22**).

The following patent applications are based on another previously published patent [89] containing different bicyclic ring systems such as indoles, benzofurans and benzisoxazoles. Nippon Chemiphar continued to build their work on the benzisoxazole derivatives with a patent published in 2010 [90]. The claimed compounds exhibit PPAR-activating effects at all three subtypes compared to known potent activators (PPARα: GW590735, PPARγ: Rosiglitazone, PPARδ: GW 501516). Potency is declared as relative value of test compound to control compounds. This patent comprises a huge amount of benzisoxazole derivatives wherein the monocyclic heteroaromatic ring of GW501516 (**33**) is varied to furan, thiophene, pyrazole, isoxazole and thiazole rings. Within this patent Nippon Chemiphar could increase the selectivity towards PPARδ for compound **35** wherein the linker between the pyrazole and the benzyl was increased to two carbon atoms (**Figure 23**).

The compounds differ from previously claimed [91] benzothiophene or benzofuran derivatives of **33** in the linker and the condensed ring (benzisoxazole).

A further patent application from 2011 [92] claims several derivatives of previously disclosed compounds with benzisoxazole scaffold. The 4-trifluoromethylphenylthiazole moiety of **33** is substituted in this series with benzothiophene and similar condensed aromatic rings. However, not only benzothiophene derivatives are claimed but also benzofuran and indole derivatives. Inside this series of derivatives the ketone moiety can be replaced by oxim or CH_2 moieties and the carboxylic acid by a tetrazole or cinnamic acid as bioisosters. The most potent examples **36a** and **36b** show EC_{50} values of 4.8 nM (**36a**) and 1.3 nM (**36b**) (**Figure 24**).

The most recent patent [93] by Nippon sums up all previously published structures. In this application, compound **37** is highlighted that selectively activates PPARδ with an EC_{50} value of 18 nM determined in a Gal4-transactivation assay. Additionally several pharmacological data are mentioned. Treatment of rats on high-fat diet with **37** resulted in decreased body weight. Furthermore, an oral glucose tolerance was assessed after 21 days of treatment with **37** (10 mg/kg), which was significantly improved. The patent also describes a small SAR for compound **37** by replacing the ether by a thioether or varying the linker by substitution of the ketone by an allyl or alcohol moiety. Interestingly, the thioether derivative exhibited activity at all three subtypes of PPAR, whereas all other derivatives were selective for PPARδ. The alcohol derivative showed a significant loss in activation (**Figure 25**).

Zhejiang Hisun Pharmaceutical disclosed compounds that incorporate the core structure of GW501516 (**33**) with

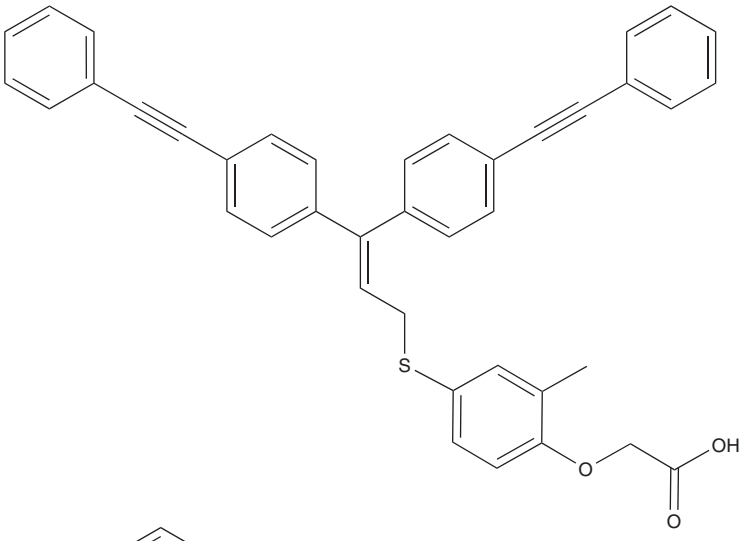

41a

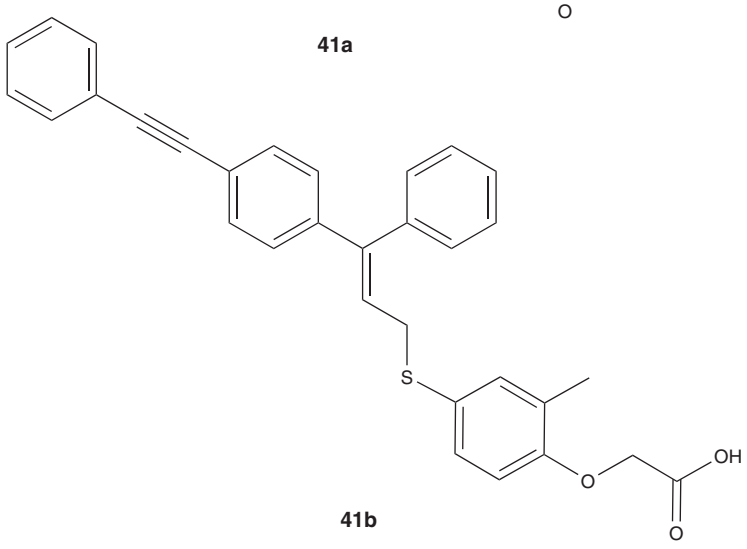

41b

Figure 31. PPARδ ligands by High Point Pharmaceuticals.

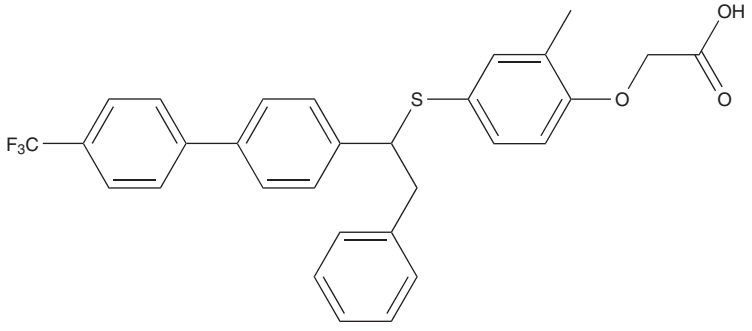

42

Figure 32. PPARδ ligand by the Seoul National University.

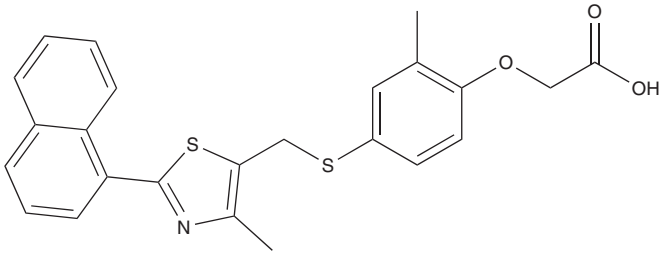

43

Figure 33. PPARδ ligand by SRI International.

differences in the substitution pattern in alpha carboxyl position or replacement of the thiazole by a tetrazole moiety leading to compounds **38a–d** [94]. Activity was measured in a transactivation assay where the compounds exhibited high activity at PPARδ. However, no data on whether they can activate PPARγ or PPARα is available (**Figure 26**).

The activity at PPARδ could be increased by replacing one ether moiety by a thioether from EC_{50} of 468 nM (**38a**) to 10 nM (**38b**) and 1 nM (**38c**, **38d**). The exemplified four substances were tested *in vivo* in ApoE mouse, SD rat and Mesocricetus aureus models with high-fat diet-induced hyperlipidemia. Compounds **38a–d** showed activity in decreasing blood lipid levels such as cholesterol, triglyceride and LDL levels in an amount of 30–60% while HDL was increased. Especially (**38b**) showed good *in vivo* activity, so further conferment of the efficacy was tested in a Macaca rhesus model of hyperlipidemia. Insulin concentration, serum total cholesterol and LDL were decreased after three months of administration. The therapeutic effect was better than that of GW501516 (**33**) (**Figure 27**).

Further pharmacological activities of **38a and b** were investigated such as weight loss as well as serum lipid and glucose levels. The compounds significantly decreased serum levels of triglycerides and glucose with higher efficacy than orlistat. Also pharmacokinetic data were collected in SD rats, showing a tissue distribution to liver (65% for **38a**) and liver and heart (**38b** liver 36%, heart 26%), respectively (**Figure 28**).

In 2009, a disclosure from *Novo Nordisk* [95] highlighted a series of phenoxyacetic acids with a central aromatic core and a triangle structure with two alkine substituents exemplified in compound **39**. The aromatic core can be a phenyl or a pyridinyl with variously substituted aromatic substituents (**Figure 29**).

In addition, Novo Nordisk filed a patent [96], which claimed phenoxyacetic acid derivatives where a dihydrodibenzocycloheptane moiety replaces the aromatic core of the previous structures (exemplified in **40**). However, both patents do not supply any pharmacological data (**Figure 30**).

High Point Pharmaceuticals continued the work of Novo Nordisk in the phenoxyaceticacid series with triangle structure, when they filed two patents in 2011 [97,98] where the central aromatic core was replaced by a diphenylmethyl moiety (**41a, b**). While in the first disclosure the diphenylmethylene structure was symmetrically substituted as in **41a**, in the recently published patents only one of the arylalkine moieties is maintained leading to compounds such as **41b** (**Figure 31**).

A patent application by *Seoul National University Industry Foundation* [99], published in 2008, claimed compounds highly selective to PPARδ represented by **42**. The disclosed compounds showed EC_{50} values for PPARδ in the range of 2–200 nM. The substances differ in substitution pattern in alpha carboxylic position or in different substituents at the biphenyl moiety which is, for example, substituted with fluorine. In addition, the biphenyl moiety can be replaced by a trifluoromethylphenyloxazole moiety and there are also untypical selenethers claimed with EC_{50} values comparable to the thioether derivatives (**Figure 32**).

In 2009, *SRI International* has disclosed a series of PPARδ antagonistic phenoxyacetic acid derivatives such as **43** that are also derived from GW501516 (**33**) [100]. The compounds bind to the LBD of PPARδ and inhibit binding of GW501516 (**33**) at concentrations in the low micromolar range (1–10 μM). SAR studies showed that modifications of the aryl thiazole scaffold of GW501516 (**33**) such as replacement of the 4-trifluoromethylphenylgroup with a 1-naphthyl group resulted in antagonistic activity. SRI International claimed that this antagonistic activity could be used in treatment of several cancer types. They showed that cancer cell lines express significant levels or PPARδ and that treatment with PPARδ antagonists has inhibitory effects on the cell cycle (**Figure 33**).

The inventors of a patent application published in 2009 [101] have carried out a virtual screening using a three-dimensional database of commercially available compounds and the structure of the PPAR LBD. Based on this, *Shionogi Co.* claimed a huge amount of benzthiazoles linked to nitrogen containing aliphatic rings. Most of the derivatives comprise a piperazine ring, which can also be replaced by piperidine or homopiperazine, whereas the benzothiazole moiety can be replaced by the trifluoromethylphenylthiazol moiety known from GW501516 (**33**). The claimed compounds exemplified by **44** are selective PPARδ agonists with EC_{50} values lower than 100 nM for most derivatives. This PPARδ agonistic activity can be used for the treatment of hyperlipidemia, diabetes, obesity, atherosclerosis, hyperglycemia and syndrome X (**Figure 34**).

While all compounds described to this point are structurally derived from GW501516 (**33**), there have also been patents claiming completely different structures as follows.

In 2008, *Kalypsys, Inc.* patented sulfonyl-substituted bicyclic aryl derivatives illustrated by **45** [102] as selective PPARδ modulators. Several derivatives are disclosed wherein the exemplified oxim moiety is replaced by an ether or tertiary amine. The activity is only vaguely described with EC_{50} values < 5 μM, 5–100 μM or > 100 μM so that no

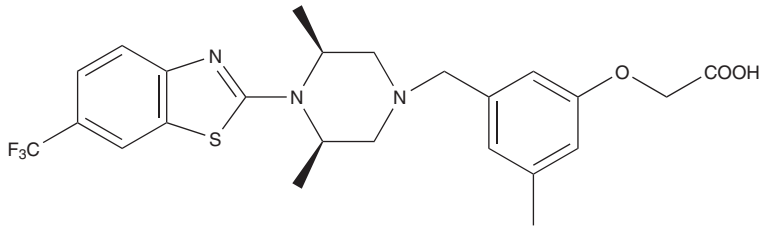

44

Figure 34. PPARδ ligand by Shionogi Co.

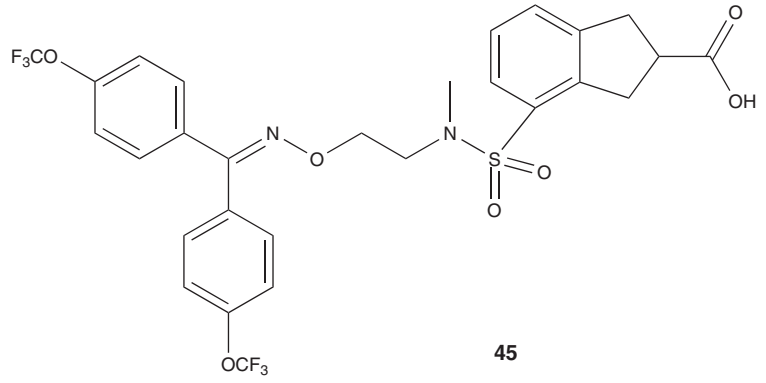

45

Figure 35. PPARδ ligand by Kalypsys, Inc.

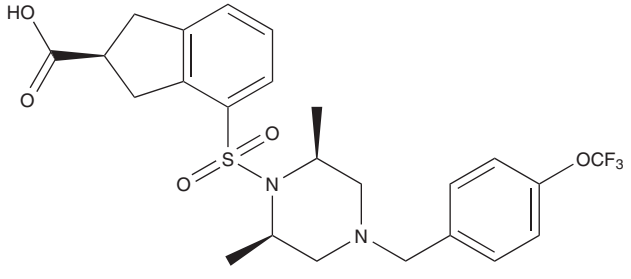

46

Figure 36. PPARδ ligand by Kalypsys, Inc.

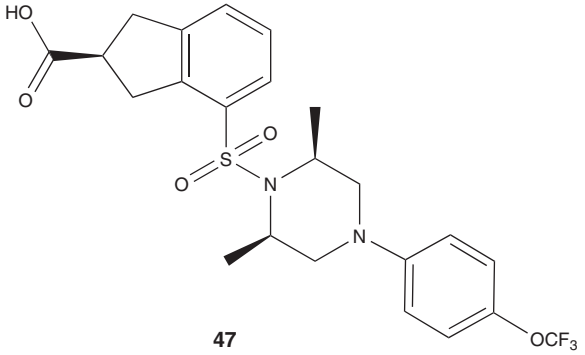

47

Figure 37. PPARδ ligand by Kalypsys, Inc.

SAR can be highlighted. The invention provides methods of raising HDL, lowering LDLc, shifting LDL particle size from low density to normal LDL and inhibiting cholesterol absorption thereby leading to compounds which can be used for the treatment of metabolic disorders and related conditions (**Figure 35**).

In addition to the described novel ligands of PPARδ, various patents indicate new fields of application of PPARδ ligands or disclose novel insights in the role of PPARδ activation.

A patent assigned by Kalypsys claims selective activation of PPARδ as therapeutic approach for the treatment of nonalcoholic steato hepatitis (NASH) [103]. The incorporated compound **46** was first disclosed in 2006 as part of a patent [104] showing several sulfonyl-substituted bicyclic compounds with PPAR modulatory activity. The recent patent focuses on treatment with compound **46** which was pharmacologically characterized in a mouse model of

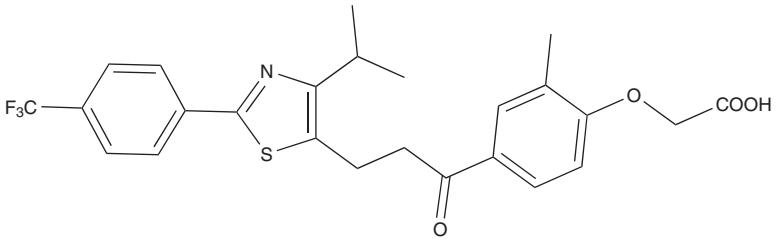

48a

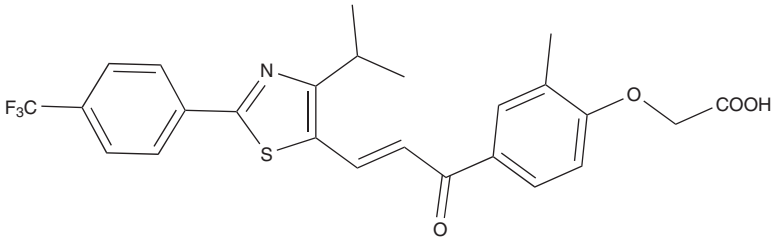

48b

Figure 38. PPARδ ligands by Cerenis Therapeutics.

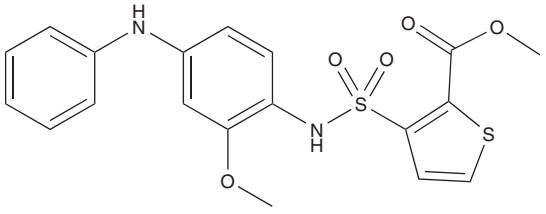

49

Figure 39. PPARδ ligand by the University of Dundee.

steatosis. Treatment with **46** for 42 days significantly reduced levels of serum transaminases AST and ALT. Additionally, the lipid accumulation in the liver was reduced, the progression to fibrosis attenuated and inflammatory markers such as TGFβ-1 were normalized (**Figure 36**).

Another patent application of Kalypsys published in 2008 [105] claimed an oral pharmaceutical formulation compromising a PPARδ agonistic compound **47**, which was first disclosed in 2006 [106]. This compound shows selectivity towards PPARδ with an EC_{50} value < 5μM for PPARδ. Specific diseases modulated by PPARδ for which the composition is useful include but are not limited to dyslipidemia, syndrome X, atherosclerosis, obesity, heart failure, hypercholesteremia, cardiovascular disease and inflammation. Other indications include reduction of scarring and wound healing (**Figure 37**).

Teijin Limited in 2008 claimed a method for screening a substance having a thermogenesis enhancing effect by measuring a PPARδ activating effect [107]. Application of these compounds is claimed to enhance uncoupling respiration in mitochondria, enhancing proton leak in inner membranes of mitochondria and increasing expression of UCP1 in mitochondria-containing cells.

A patent application by *Toudai TLO* could show that GW501516 (**33**) acts as an insulin secretagogoues agent through activation of PPARδ, which directly addresses pancreatic β-cells potently stimulating glucose-dependent insulin secretion in response to hyperglycemia. The patent application clearly describes that the insulin secretion-stimulating action is pharmacologically different from the insulin-sensitizing action [108].

Cerenis Therapeutics S.A. disclosed a patent application in 2008, which is based on any compound possessing PPARδ agonistic activity exemplified by compounds **48a and b** [109]. The patent claims methods for treatment of diseases related to atherosclerotic plaque formation by increasing pre-β HDL, ApoA-I levels and HDL levels. In hAPOA-I transgenic mice activation of PPARδ by a selective agonist could increase ApoA-I levels up to 25%. Studies in male cynomolgus monkeys treated with a selective PPARδ agonist for two weeks confirmed these *in vivo* results (**Figure 38**).

In 2009, the *University of Dundee* filed a patent indicating that PPARδ fulfills a critical role in the activation of macrophages and that selective inhibition of PPARδ activity can prevent foam cell formation. They claimed that compounds that interfere with the formation of foam cell development inhibit PPARδ activity. As possible therapeutic agent siRNA selective for PPARδ is described [110].

A recently published patent application [111] claimed a mouse model which overexpress PPARδ and can be used as model for inflammatory skin conditions. This model can be

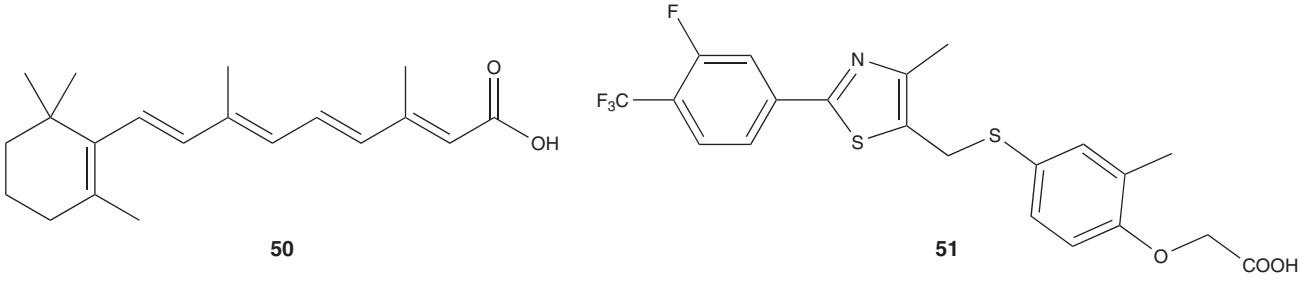

50 **51**

Figure 40. PPARδ ligands 50 and 51.

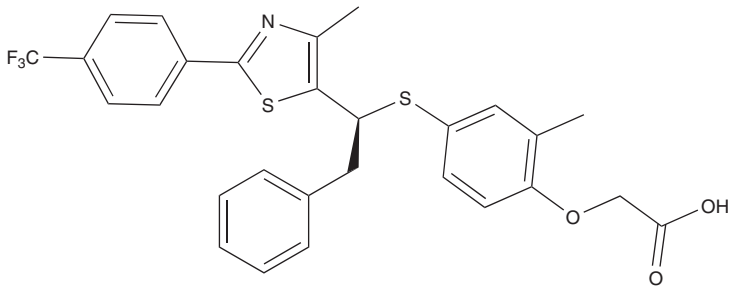

52-*R*

Figure 41. PPARδ ligand by the Seoul National University.

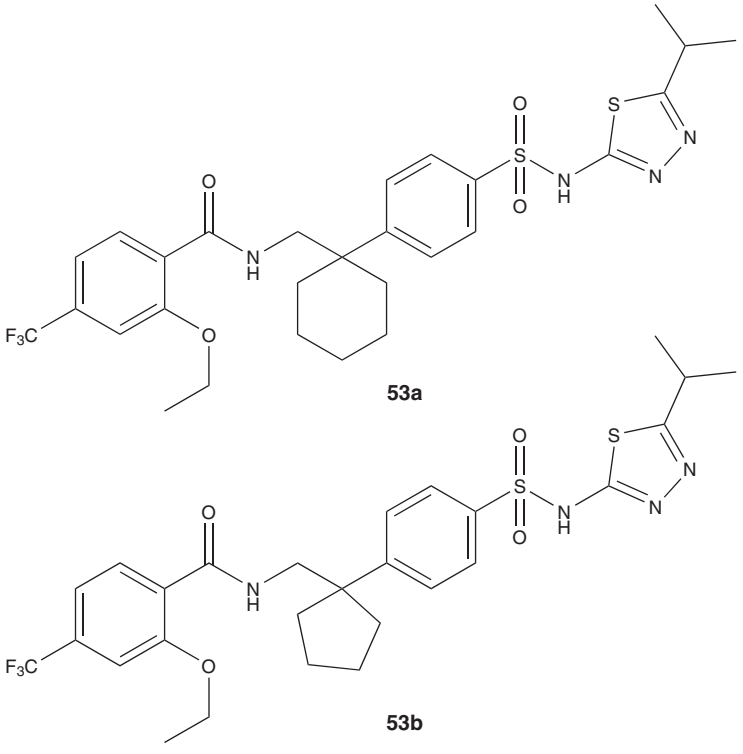

53a

53b

Figure 42. Dual PPARγ/δ ligands by Sanofi-Aventis.

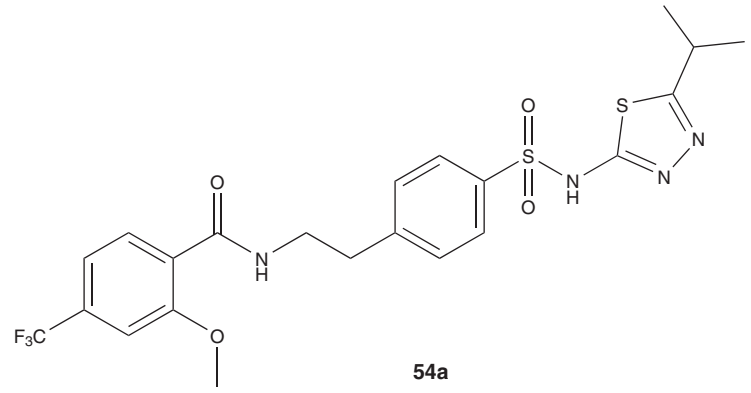

54a

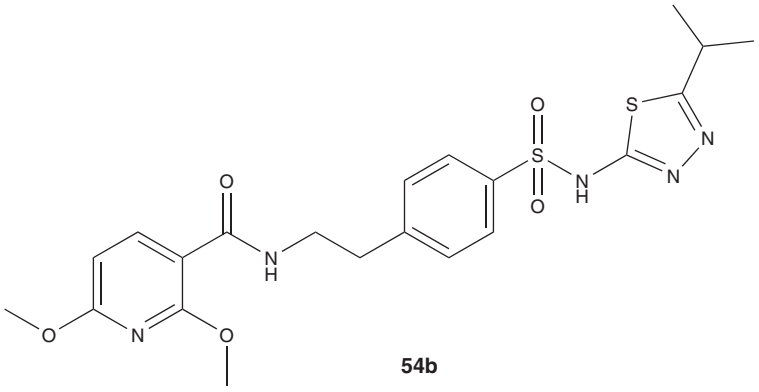

54b

Figure 43. Dual PPARγ/δ ligands by Sanofi-Aventis.

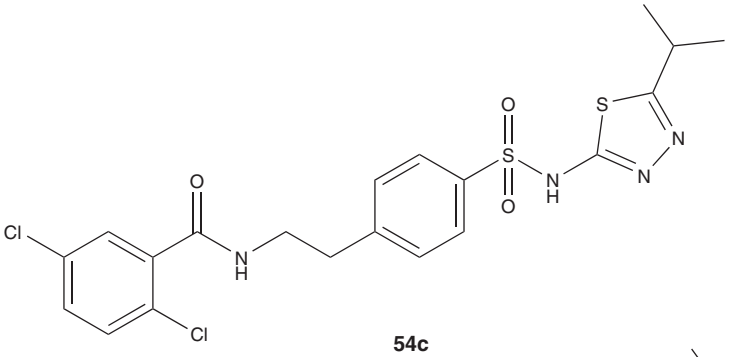

54c

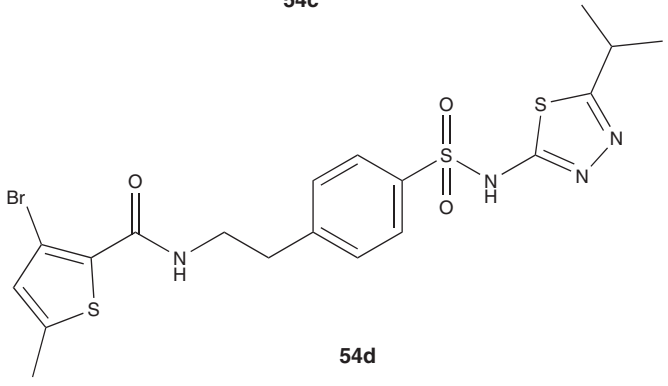

54d

Figure 44. Dual PPARγ/δ ligands by Sanofi-Aventis.

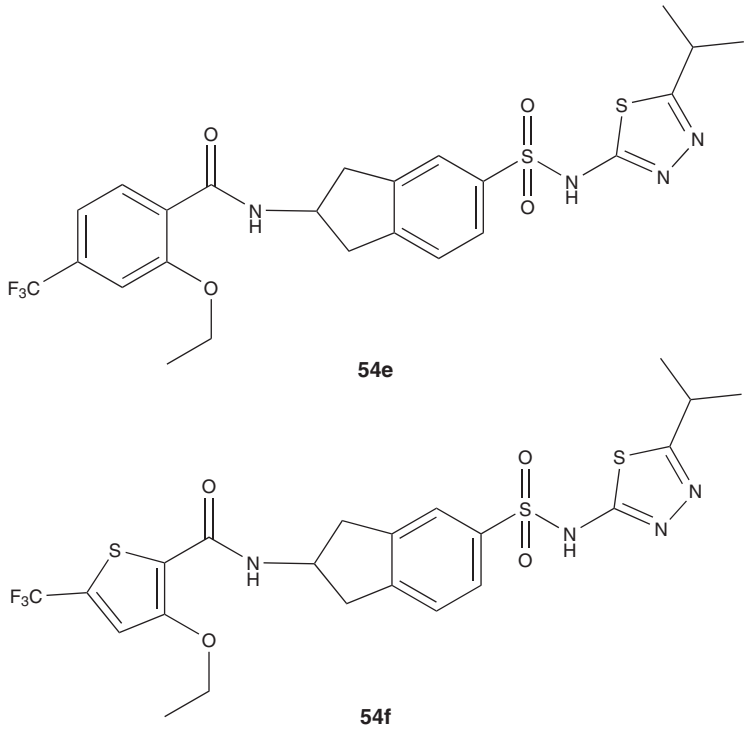

Figure 45. Dual PPARγ/δ ligands by Sanofi-Aventis.

used to assess the efficiency of test compounds for treating this skin conditions. The patent application also disclosed compounds with PPARδ antagonistic effect, which can be administered topically for the prevention or treatment of psoriasis. Exemplified (**49**) is GSK 0660, which was first described in 2007 (**Figure 39**) [112].

A patent application [113] supported by the United States government and published in 2009 claims a method of increasing insulin sensitivity of insulin-resistant cells by administering all-trans-retinoic acid (**50**) to the cells. The invention is based on the discovery that **50** is effective to activate PPARδ in cells expressing fatty acid binding protein 5 (FABP5). The patent contains *in vitro* data showing that **50** as well as PPARδ agonistic compound GW 0742 (**51**) upregulates the expression of PPARδ target genes. Furthermore, *in vivo* experiments with a high fat/high sucrose diet-induced mouse model of obesity showed a loss of 15% of body weight with more than twofold decrease of fat tissue after administration of **50**. A glucose tolerance test in the same mouse model treated with **50** was highly improved as the results were comparable to lean mice. Additionally the liver of said mice was all but devoid of lipid stores. Hence, this patent claims the use of **50** for the treatment of type II diabetes, syndrome X, obesity and hepatic steatosis (**Figure 40**).

A patent by *Seoul National University Industry Foundation* is based on the racemate of structure **52** which was previously disclosed by Eli Lilly [114]. Seoul National University declares the optical active R-Enantiomer **52-R** having high PPARδ selectivity with an EC_{50} value of 0.6 nM versus 5.1 nM for the S-Enantiomer. **52-R** can be used for the treatment of obesity, hyperlipidemia, arteriosclerosis, diabetes, dementia, Alzheimer's and Parkinson's disease and for strengthening muscles or improving memory. Said effects were tested in animal models described in the patent (**Figure 41**) [115].

Sanofi-Aventis filed several patents disclosing dual PPARγ/δ agonists that contain thiadiazolebenzensulfonamides as general scaffold. The compounds exemplified in **53a** are claimed for treatment of fatty acid metabolism and glucose utilization disorders, disorders related to insulin resistance as well as demyelinization and neurodegenerative disorders of the central and peripheral nervous system. Compounds in the first application showed a slight selectivity towards PPARδ with **53a** comprising EC_{50} values of 0.12 μM for PPARδ versus > 10 μM for PPARγ activation. PPARγ activity could be increased in **53b** by replacing the spirocyclohexyl moiety by a spirocylcopentan (EC_{50} PPARδ: 0.021 μM, PPARγ: 0.007 μM) (**Figure 42**) [116].

A succeeding patent application [117] is based on previous compounds. The novel derivatives differ in substituents at the alkyl spacer between thiadiazolebenzensulfonamide moiety and benzamide. However, the most compounds lack substituents and are illustrated by **54a**. Claimed compounds exhibited a balanced activity at PPARδ and PPARγ with EC_{50} values in low μM to low nM range (**54a**: EC_{50} PPARδ 0.11 μM, PPARγ 0.38 μM) (**Figure 43**).

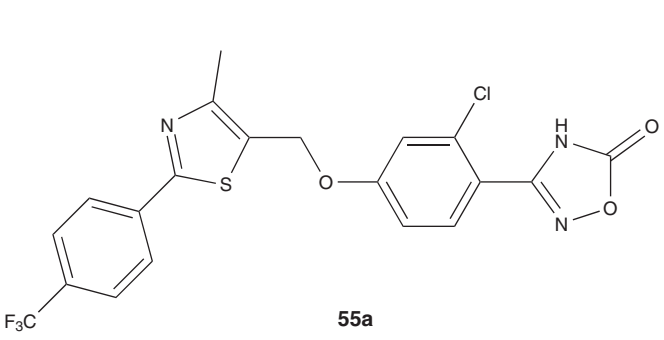

55a

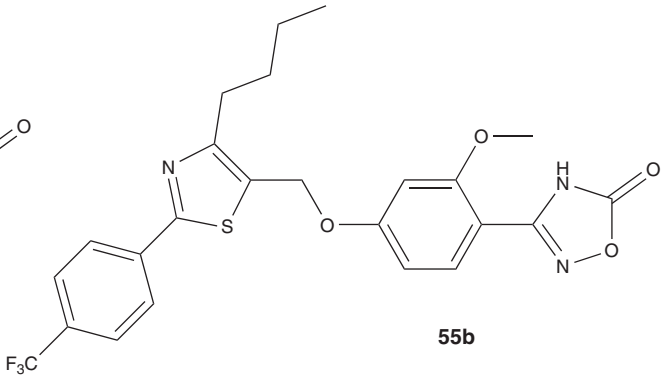

55b

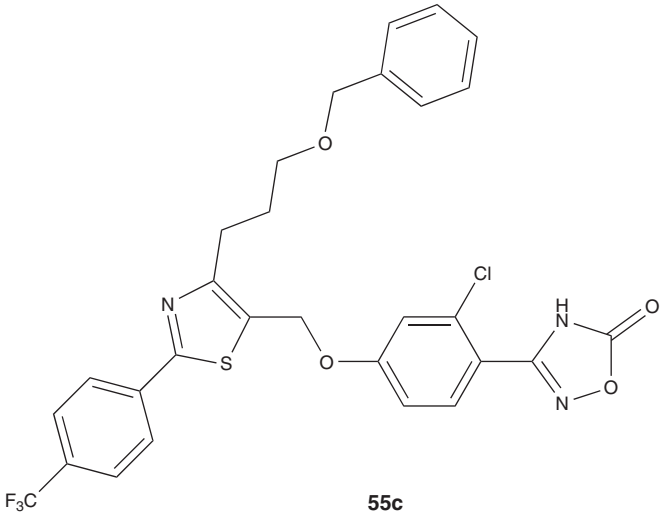

55c

Figure 46. Dual PPARα/δ ligands by Sanofi-Aventis.

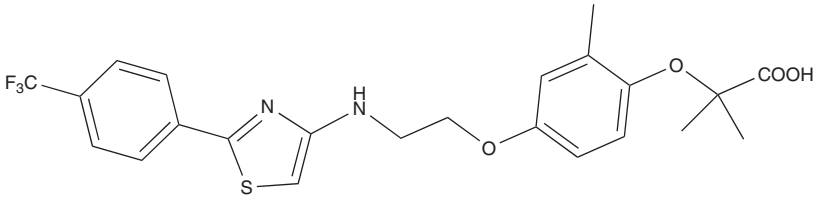

56a

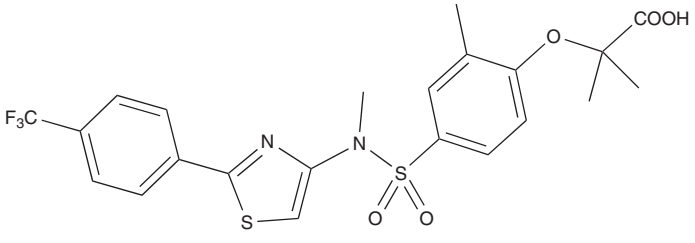

56b

Figure 47. Dual PPARα/δ ligands by Novartis.

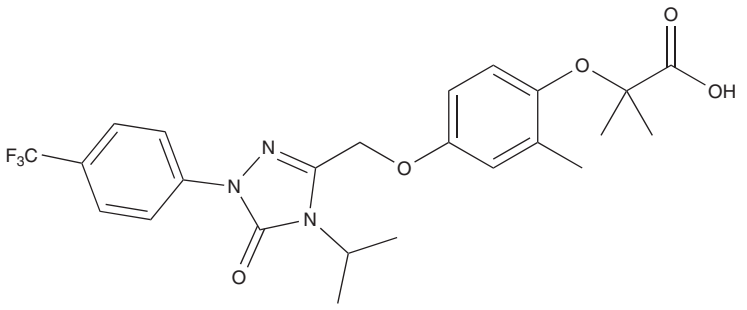

57a

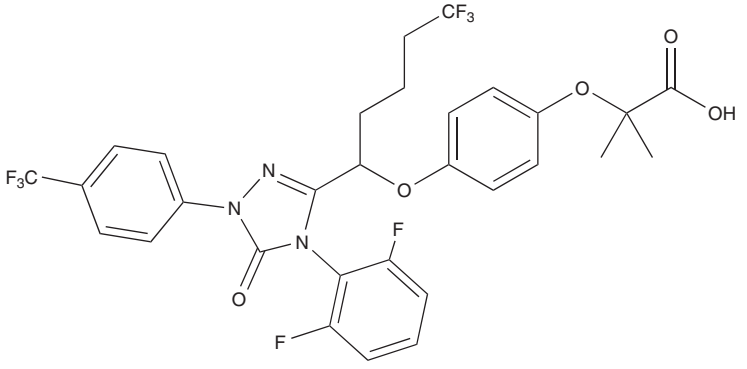

57b

Figure 48. Dual PPARα/δ ligands by Eli Lilly.

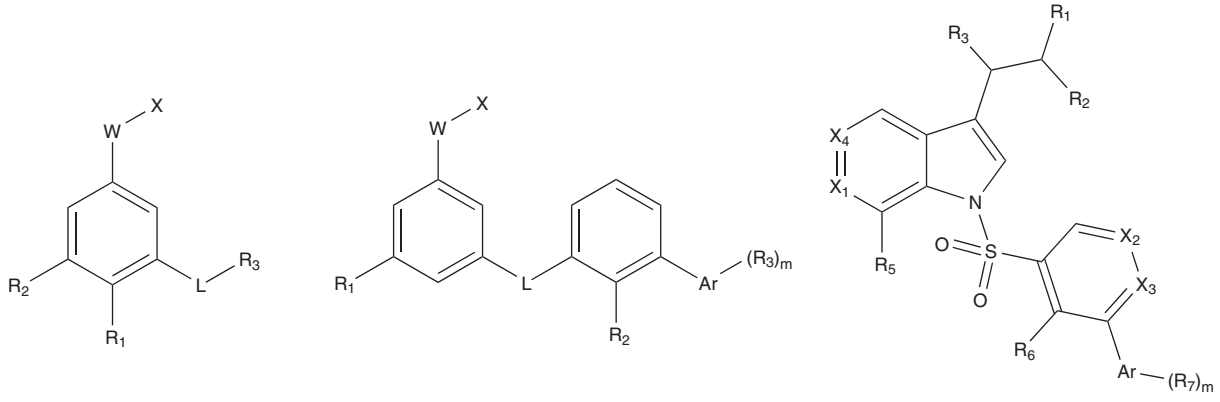

58 **59** **60**

Figure 49. Pan-PPAR ligands by Plexxikon.

Variation of the substitution pattern at the benzamide to 2,6-methoxy substitution resulted in loss of activity at both PPAR subtypes (**54b**: EC_{50} PPARδ 1.1 μM; PPARγ 1.11 μM). Selectivity towards PPARγ could be realized with 2,5-chloro derivative **54c** (EC_{50} PPARδ 2.80 μM; PPARγ 0.27 μM) whereas **54d** (EC_{50} PPARδ 0.06 μM; PPARγ 1.87 μM) comprising a 3-bromo-5-methyl-thiophenyl moiety was selective towards PPARδ (**Figure 44**).

In another patent [118] based on the previously claimed compounds the spacer between the aromatic moieties is fixed

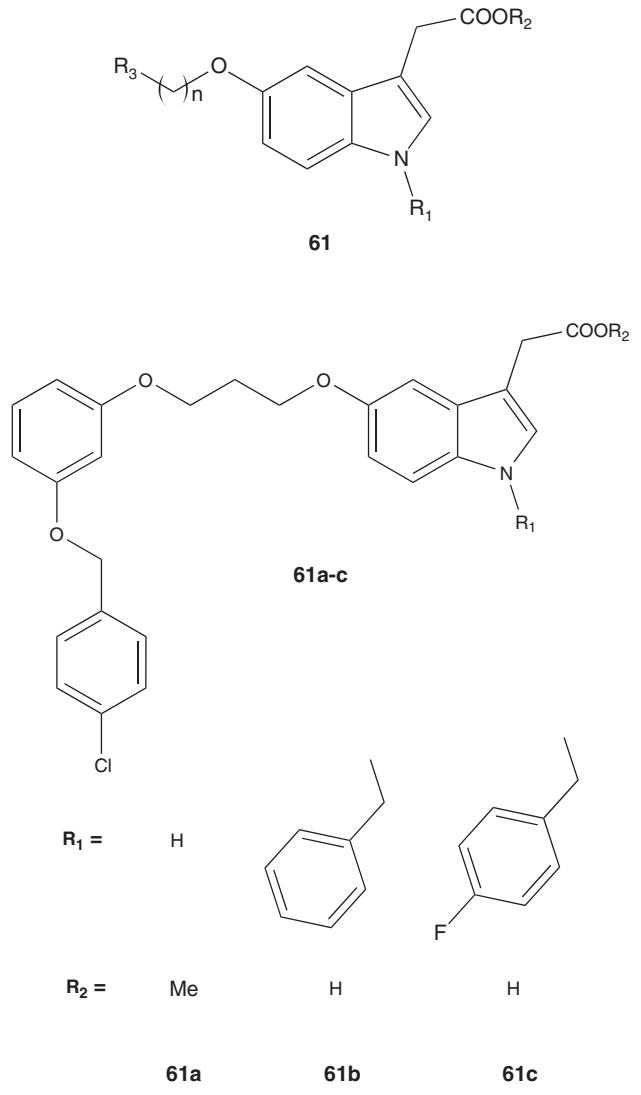

Figure 50. Pan-PPAR ligands.

with condensed rings like indan or tetrahydronaphthalene exemplified by **54e**. **54e** exhibited the highest activity with EC_{50} values of 0.001 μM at both, PPARγ and PPARδ. According to the previous applications selectivity towards PPARδ could be achieved by replacing the 4-trifluoromethyl-2-methoxyphenyl by thiophene (**54f**: EC_{50} PPARδ 0.001 μM; PPARγ >10 μM) (**Figure 45**).

In addition to dual PPARγ/δ ligands Sanofi Aventis has also disclosed dual PPARα/δ agonists [119] that can be used for the treatment of lipid and glucose metabolism related disorders as well as neurodegenerative diseases. The compounds exemplified by **55a** show PPARα and PPARδ activating properties with selectivity towards PPARδ with EC_{50} values for PPARα from 100 nM to >10 μM and for PPARδ predominantly in the low nanomolar range.

Structurally the compounds can be described as oxadiazolones illustrated by **55a** (EC_{50} PPARα 1.66 μM; PPARδ 0.056 μM) wherein the trifluoromethylphenylthiazole moiety is comparable to the derivatives claimed by GSK and Nippon. In **55b** the 5-substituent of the thiazole is changed to larger groups (**55b**: EC_{50} PPARα >10 μM; PPARδ 0.015 μM). Interestingly, compound **55c** with a quite large substituent is highly active at PPARδ (**55c**: EC_{50} PPARα 0.42 μM; PPARδ 0.0007 μM) (**Figure 46**).

Another company active in the field of dual PPARα/δ agonists is *Novartis*. In 2009 they claimed compounds with structures exemplified by **56a** [120] that are varied in N-alkyl substituents, substitution pattern of methyl substituents at the phenoxyacetic acid or in 4-position of the phenylthiazol moiety. Furthermore, the thiazole ring can be replaced by oxazole and the ether linking the phenoxyacetic acid to the alkylspacer can be replaced by a thioether or a sulfone resulting in a sulfonamide moiety in **56b** (**Figure 47**).

Furthermore, the patent provides a method of treating several diseases in animals. As the compounds of the invention modulate the activity of PPARs they can be used for the treatment of disorders such as dyslipidemia, atherosclerosis, obesity, inflammation, arthritis, cancer, Alzheimer's disease, skin disorders, respiratory diseases, ophthalmic disorders and IBDs.

However, no pharmacological data are supplied in the patent. Novartis only claimed preferable EC_{50} values below 5 μM with a subtype activity preferable towards PPARδ. In particular the EC_{50} values at PPARδ should preferably be lower or equal to PPARα and at least tenfold lower than at PPARγ.

In 2008, *ELI LILLY* claimed a series of compounds with a triazolone moiety instead of the thiazole used in GW501516 (**33**) [121]. The derivatives illustrated by **57a and b** (**57a**: EC_{50} PPARδ 63.4 nM, PPARα 308.9 nM, **57b**: EC_{50} PPARδ 46.4 nM, PPARα 872.1 nM) are potent dual agonists of PPARδ/α with EC_{50} values lower than 600 nM for PPARδ and lower than 3 μM for PPARα. The disclosed compounds differ in substitution at position 4 of the triazolone or in alpha position to the triazolone moiety (**Figure 48**).

The PPARα and PPARδ-modulating compounds are believed to be especially useful for cardiovascular diseases such as hyperlipidemia, hypertriglyceridemia and atherosclerosis. In addition, Eli Lilly claimed that the compounds can minimize the incidence of undesired drug interactions by exhibiting low PXR modulation.

6. pan-PPAR ligands

A novel trend in development of PPAR-targeting compounds is leading towards pan-PPAR ligands that interact with all subtypes of the nuclear receptor and three chemical classes of such compounds have been patented.

Researchers of *Plexxikon, Inc.* filed three patents [122-124] on PPAR modulators with similar structural properties. Claimed are compounds of the general formulas **58** [122], **59** [123] and **60**

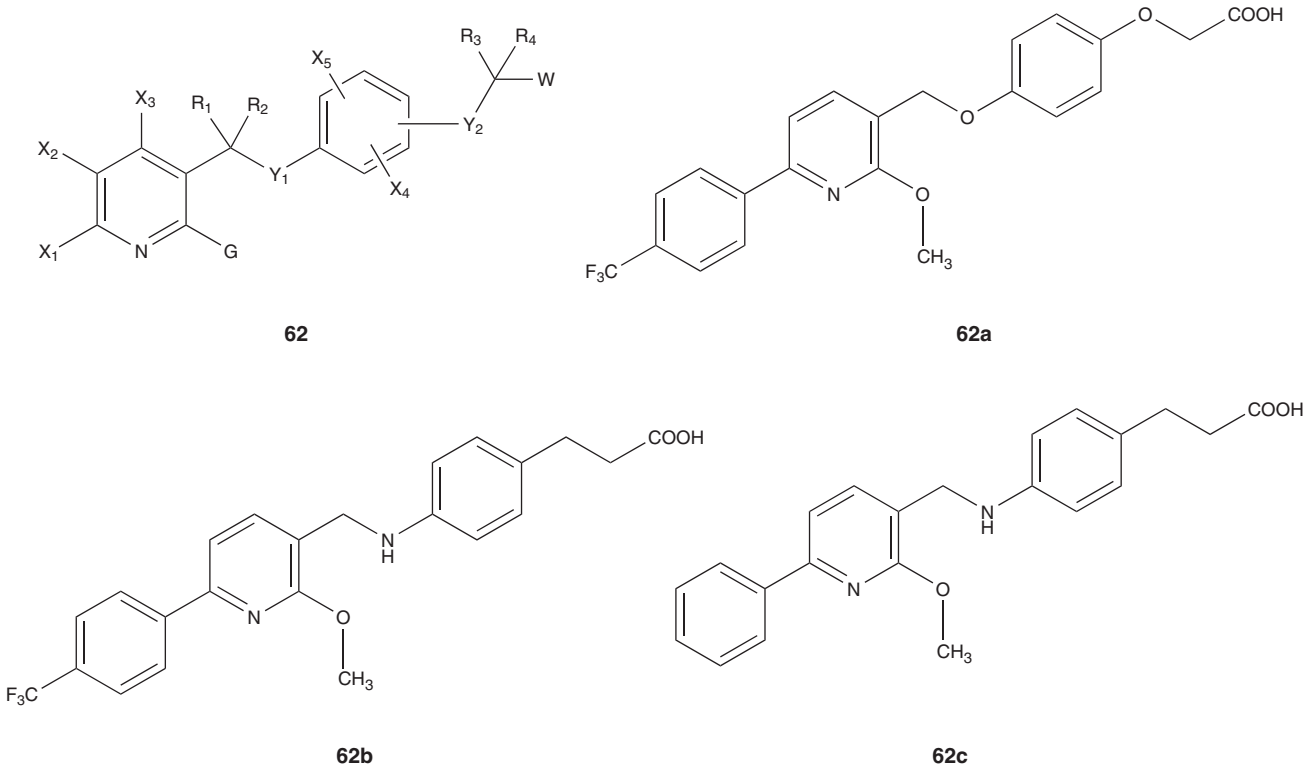

Figure 51. Pan-PPAR ligands.

[124] wherein each patent draws a structural improvement. The derivatives are described as active at least at one PPAR subtype but no detailed data for affinity or activity nor a concrete therapeutic use of the compounds is published. However, it is stated that the compounds include pan-PPAR ligands but also ligands with up to 100-fold selectivity for one subtype. As the structural properties of the claimed compounds are quite variably patented and there are no detailed *in vitro* or *in vivo* data available, there is probably more research necessary before the compounds achieve a status for preclinical or clinical development (**Figure 49**).

Furthermore, alkoxyindole-3-acetic acid derivatives of general formula **61** have been patented [125] by Korean researchers as pan-PPAR agonists. The compounds are described to be useful for treating or preventing metabolic and cardiovascular as well as inflammatory diseases. *In vitro* experiments revealed **61a–c** as the most potent derivatives with agonistic activity at all PPAR subtypes and EC_{50} values between 0.8 and 13 µM. The highest affinity and best-balanced activity at the three receptor isoforms showed **61c**. However, as the compounds have only modest affinity with EC_{50} values in a micromolar range, further optimization has to be conducted to achieve potent pan-PPAR agonists with minimal off-target effects at therapeutic concentrations (**Figure 50**).

Slightly higher affinity to all PPAR subtypes is exhibited by several compounds of the general formula **62** that have been patented [126] recently along with their proposed use for the therapy of metabolic, cardiovascular and inflammatory disorders. The derivatives all comprise a carboxylic acid function or a bioisosteric group thereof (W in formula **62**) according to the SAR of PPAR ligands. *In vitro* characterization showed EC_{50} values between 0.3 and 4.5 µM for the most potent substances **62a and b** at the three PPAR subtypes. Compound **62a** was selected for *in vivo* experiments and exhibited beneficial effects on glycemic profiles and insulin resistance in diabetic mice. Furthermore, compound **62c**, which is slightly selective for PPARα with an EC_{50} of 0.143 µM, was investigated for its influence on lipid profiles *in vivo*. As expected, **62c** increased plasma levels of HDL-cholesterol and lowered free fatty acids. Hence compounds **62a–c** might be suitable for further preclinical and clinical development. Additionally the series of derivatives revealed that only modest variation of chemical properties such as interchanging hetero atoms can lead to selectivity for single PPAR subtypes (**Figure 51**).

7. Expert opinion

Although the TZDs as most widely used PPAR-targeting drugs have recently been suspended, several new findings have led to quite a lot of patents concerning novel PPAR ligands and their use. Although still some approaches tend to develop PPAR ligands for the use as antidiabetics, more

PPAR subtype	Potential future indication
PPARα	Hypolipidemic, anorectic, body-weight control Inflammatory skin disorders Cartilage protection (e.g., in arthritis) Muscle wasting disorders
PPARγ	Metabolic diseases, especially hyperglycemia Cardiovascular disorders Inflammatory and auto-immune diseases: multiple sclerosis, inflammatory bowel diseases, rheumatoid arthritis Cancer Alzheimer's disease Age-related macular degeneration Skin related disorders Addiction control
PPARδ	Metabolic diseases: e.g., anti-diabetic (by stimulation of insulin secretion) Cardiovascular diseases Inflammatory diseases: e.g., psoriasis, inflammatory bowel diseases Neurodegenerative diseases: e.g., demyelinization, Alzheimer's disease, dementia, Parkinson's disease Cancer Non-alcoholic fatty liver disease

Scheme 1. Possible future indications for ligands of the three PPAR subtypes.

and more new indications for modulators of PPARs are coming up. This repurposing of known PPAR-targeting drugs might help them to gain more relevance again. An overview over possible future indications of PPAR ligands is given in Scheme 1.

The most recent patent activity along with the few clinical trials that are presently being conducted indicate that especially three major applications for therapeutic PPAR ligands might arise in the mid-term future. On one hand, the adjuvant use of PPAR modulators in cancer therapy is promising and corresponding clinical studies are ongoing, for example, with the experimental agent CS-7017 (**10**). On the other hand, topic use of PPAR ligands could be an upcoming strategy for several skin-related disorders as the side effects in non-systemic application are minimal. The third highly interesting development is the possible use of PPAR ligands in anti-inflammatory therapies. Especially, chronic inflammatory diseases such as multiple sclerosis, rheumatoid arthritis and IBDs affect large patient collectives and the available therapies on this sector are insufficient. Hence, any new approach on this field is desirable and PPAR modulators are a promising strategy for systemic anti-inflammatory therapies.

Yet the antidiabetic use of PPARγ modulators can still play a role because of the huge patient collective for this indication. However, PPARγ agonists may not fulfill this role but the recent findings and developments concerning the obesity-linked Cdk5-dependent phosphorylation of PPARγ and its inhibition are very promising though not yet ready for clinical use.

Another possible progression could be the several approaches to reduce the adverse effects of systemic administration of PPARγ agonists in antidiabetic therapy by drug combinations. But it is questionable whether these strategies can outmatch other available therapeutic options for type II diabetes as every additional agent bares additional risks for side effects and drug interactions.

Compound number	Inventor/ company	Activity (EC_{50} [μM], E_{max} [%])			Further activity	Indication	Development status
		PPARα	PPARγ	PPARδ			
1a	Bayer Schering	agonistic (0.059)	n.d.	n.d.	-	hyperlipidemia	preclinical
1b	Bayer Schering	agonistic (0.087)	n.d.	n.d.	-	hyperlipidemia	preclinical
29 (CS-7017)	Daiichi Sankyo	n.d.	n.d.	n.d.	-	cancer	Phase I/II completed
13a	Dong-A Pharm.	> 2	partial agonistic (0.007, 27 %)	n.d.	-	anti-diabetic	preclinical
13b (PAM-1616)	Dong-A Pharm.	> 2	partial agonistic (0.08, 25 %)	> 30	-	anti-diabetic	preclinical
13c (PAR-1622)	Dong-A Pharm.	> 2	partial agonistic (0.04, 37 %)	n.d.	-	anti-diabetic	preclinical
13d (PAR-5359)	Dong-A Pharm.	agonistic (1.7)	agonistic (0.6)	n.d.	-	anti-diabetic	preclinical
15a	Evolva	n.a. at 10 μM	partial agonistic (15)	n.a. at 10 μM	-	-	-
20a	Kyowa	n.d.	agonistic (0.048)	n.d.	AT_1-antagonist	metabolic disorders and others	preclinical
20b	Kyowa	n.d.	agonistic (0.073)	n.d.	AT_1-antagonist	metabolic disorders	preclinical
21a	Kyowa	n.d.	agonistic (0.0026)	n.d.	?AT_1-antagonist ?	metabolic disorders and others	preclinical
21b	Kyowa	n.d.	agonistic (0.0024)	n.d.	?AT_1-antagonist ?	metabolic disorders and others	preclinical
31b	University of Sidney	active at 5 μM	agonistic (2.9)	n.d.	-	-	preclinical

Scheme 2. Selected novel compounds patented since 2008, their pharmacological properties, indications and development status. Novel compounds (Most potent and promising compounds of selected companies.

n.d.: No data available; n.a.: Not active.

Compound number	Inventor/ company	Activity (EC_{50} [μM], E_{max} [%])			Further activity	Indication	Development status
		PPARα	PPARγ	PPARδ			
32a	Nippon Chemiphar Co	agonistic (0.092)	agonistic (0.30)	agonistic (3.0)	-	metabolic disorders	-
32b	Nippon Chemiphar Co	agonistic (0.18)	agonistic (0.29)	agonistic (2.3)	-	metabolic disorders	-
33 GW-501516	GSK	agonistic (1.1)	agonistic (0.85)	agonistic (0.001)	-	dyslipidemia	Phase II
35	Nippon Chemiphar Co	0.2% (at 1 μM)	0.3% (at 1 μM)	87.8% (at 1 μM)	-	metabolic/ cardiovascular disorders, cancer, inflammatory disease	-
36a	Nippon Chemiphar Co	> 10 μM	> 10 μM	agonistic (0.0048)	-	metabolic disorders, cancer, Alzheimer's disease inflammatory disease	-
36b	Nippon Chemiphar Co	> 10 μM	> 10 μM	agonistic (0.0013)	-	metabolic disorders, cancer, Alzheimer's disease inflammatory disease	-
37	Nippon Chemiphar Co	> 10 μM	> 8 μM	agonistic (0.018)	-	Metabolic disorders, inflammation, diseases of the lung, disorders of the kidney	preclinical
38a	Zhejang Hisun Ph.	n.d.	n.d.	agonistic (0.468)	-	-	-

Scheme 2. Selected novel compounds patented since 2008, their pharmacological properties, indications and development status. (Most potent and promising compounds of selected companies) (Continued).

n.d.: No data available; n.a.: Not active.

Compound number	Inventor/ company	Activity (EC_{50} [μM], E_{max} [%])			Further activity	Indication	Development status
		PPARα	PPARγ	PPARδ			
38b	Zhejang Hisun Ph.	n.d.	n.d.	agonistic (0.010)	-	hypolipidemic	preclinical
38c	Zhejang Hisun Ph.	n.d.	n.d.	agonistic (0.001)	-	hypolipidemic	preclinical
38d	Zhejang Hisun Ph.	n.d.	n.d.	agonistic (0.001)	-	hypolipidemic	preclinical
39	Novo Nordisk	n.d.	n.d.	n.d.	-	metabolic/cardio-vascular disorders, cancer, renal disease, cognitive function, osteoporosis	-
42	Seoul National University	n.a.	n.a.	agonistic (0.0026)	-	-	-
43	SRI International	n.d.	n.d.	n.d.	-	cancer	-
44	Kalypsys	> 100 μM	< 5 μM	< 5 μM	-	metabolic disorders	-
45	Shionogi Co.	> 10 μM	> 10 μM	agonistic (0.026)	-	metabolic disorders	-
46	Kalypsys	n.d.	n.d.	n.d.	-	NASH	-
47	Kalypsys	> 100 μM	> 100 μM	< 5 μM	-	metabolic disorders	-
52-R	Seoul National University	n.a.	n.a.	0.0006	-	various	preclinical
52-*S*	Seoul National University	n.a.	n.a.	0051	-	various	-

Scheme 2. Selected novel compounds patented since 2008, their pharmacological properties, indications and development status. (Most potent and promising compounds of selected companies) (Continued).

n.d.: No data available; n.a.: Not active.

Compound number	Inventor/ company	Activity (EC_{50} [μM], E_{max} [%])			Further activity	Indication	Development status
		PPARα	PPARγ	PPARδ			
53	Sanofi-Aventis	n.d.	0.007	0.021	-	various	-
54a	Sanofi-Aventis	n.d.	0.38	0.11	-	various	-
54b	Sanofi-Aventis	n.d.	1.11	1.1	-	various	-
54c	Sanofi-Aventis	n.d.	0.27	2.8	-	various	-
54d	Sanofi-Aventis	n.d.	1.87	0.06	-	various	-
54e	Sanofi-Aventis	n.d.	0.001	0.001	-	various	-
54f	Sanofi-Aventis	n.d.	> 10 μM	0.001	-	various	-
55a	Sanofi-Aventis	1.66	n.d.	0.056	-	various	-
55b	Sanofi-Aventis	> 10 μM	n.d.	0.015	-	various	-
55c	Sanofi-Aventis	0.42	n.d.	0.0007	-	various	-
57a	Eli Lilly	0.3089	n.d.	0.0634	-	cardiovascular diseases	-
57b	Eli Lilly	0.8721	n.d.	0.0464	-	cardiovascular diseases	-
62a	Masson C. *et al.*	partial agonistic (0.371, 77%)	partial agonistic (4.49, 66%)	agonistic (0.784)	-	metabolic/ cardiovascular diseases	preclinical
62b	Masson C. *et al.*	partial agonistic (0.304, 78%)	agonistic (1.52)	agonistic (0.595)	-	metabolic/ cardiovascular diseases	preclinical
62c	Masson C. *et al.*	partial agonistic (0.143, 48%)	> 10	2.0	-	hypolipidemic	preclinical

Scheme 2. Selected novel compounds patented since 2008, their pharmacological properties, indications and development status. (Most potent and promising compounds of selected companies) (Continued).

n.d.: No data available; n.a.: Not active.

Also PPARδ has a good chance to emerge as clinically relevant drug target as the first PPARδ-targeting agents are in clinical trials for hyperlipidemic and diabetes-related disorders. However, whether these metabolic diseases or other conditions will be the major indication for future PPARδ-targeting drugs is hardly foreseeable. Additionally, it has to be awaited how the side effects of these PPARδ-targeted agents and their incidence look like.

Looking at the recently patented novel compounds (the most interesting are depicted in Scheme 2), there have not been real innovations. Several new agonistic or partial agonistic ligands have been claimed but up to now they are neither notably more potent or selective than former compounds nor do they exhibit extraordinary pharmacological effects. Eventually, due to the severity of adverse effects that have been observed in the clinical use of the TZDs nearly none of the novel compounds has reached clinical development but the companies stopped many development programs at preclinical stage. Furthermore, a surprising trend is tending towards pan-PPAR ligands and leads away from selectivity for one isoform.

Summing up, there will most probably be an important future role for PPARs in pharmacotherapy. However, the major indication for PPAR-modulating agents will change as the antidiabetic use has come out of focus and will not play the star role, at least not alone.

Declaration of interest

The authors gratefully acknowledge financial support by LOEWE Schwerpunkt onkogene Signaltransduktion Frankfurt (OSF). The authors declare no other conflicts of interest.

Bibliography

Papers of special note have been highlighted as either of interest (•) or of considerable interest (••) to readers.

1. Merk D, Schubert-Zsilavecz M. Nuclear receptors as pharmaceutical targets: rise of FXR and rebirth of PPAR? Future Med Chem 2012;4(5):587-8
2. Crunkhorn S. Diabetes: Safer PPARgamma-targeted drugs on the horizon? Nat Rev Drug Discov 2011;10(11):814
3. Choi JH, Banks AS, Kamenecka TM, et al. Antidiabetic actions of a non-agonist PPARgamma ligand blocking Cdk5-mediated phosphorylation. Nature 2011;477(7365):477-81

•• **Highly interesting novel findings concerning the Cdk5-dependent phosphorylation of PPARγ.**

4. Berger J, Moller DE. The mechanisms of action of PPARs. Annu Rev Med 2002;53:409-35
5. Michalik L, Wahli W. Peroxisome proliferator-activated receptors (PPARs) in skin health, repair and disease. Biochim Biophys Acta BBAMol Cell Biol Lipids 2007;1771(8):991-8

• **Summarizes and reviews the role of PPARs in the skin.**

6. Schmuth M, Jiang YJ, Dubrac S, et al. Thematic review series: skin Lipids. Peroxisome proliferator-activated receptors and liver X receptors in epidermal biology. J Lipid Res 2008;49(3):499-509

• **Summarizes and reviews the role of PPARs in the skin.**

7. Neher MD, Weckbach S, Huber-Lang MS, Stahel PF. New insights into the role of peroxisome proliferator-activated receptors in regulating the inflammatory response after tissue injury. PPAR Res 2012;2012:728461
8. Peters JM, Shah YM, Gonzalez FJ. The role of peroxisome proliferator-activated receptors in carcinogenesis and chemoprevention. Nat Rev Cancer 2012;12(3):181-95

•• **Reviews the role of PPARs in cancer development and therapy.**

9. Gronemeyer H, Gustafsson J, Laudet V. Principles for modulation of the nuclear receptor superfamily. Nat Rev Drug Discov 2004;3(11):950-64
10. Zettl H, Steri R, Lammerhofer M, Schubert-Zsilavecz M. Discovery of a novel class of 2-mercaptohexanoic acid derivatives as highly active PPARalpha agonists. Bioorg Med Chem Lett 2009;19(15):4421-6
11. Giaginis C, Theocharis S, Tsantili-Kakoulidou A. Structural basis for the design of PPAR-gamma ligands: a survey on quantitative structure-activity relationships. Mini Rev Med Chem 2009;9(9):1075-83
12. Gelman L, Feige J, Desvergne B. Molecular basis of selective PPARgamma modulation for the treatment of Type 2 diabetes. Biochim Biophys Acta BBAMol Cell Biol Lipids 2007;1771(8):1094-107
13. Miyachi H. Design, synthesis, and structure-activity relationship study of peroxisome proliferator-activated receptor (PPAR) delta-selective ligands. Curr Med Chem 2007;14(22):2335-43
14. Feldman PL, Lambert MH, Henke BR. PPAR modulators and PPAR pan agonists for metabolic diseases: the next generation of drugs targeting peroxisome proliferator-activated receptors? Curr Top Med Chem 2008;8(9):728-49
15. Bayer Healthcare AG. 4-Phenoxy-nicotine acid derivatives and use thereof as PPAR-modulators: WO2008031500A1; 2008
16. Bayer Schering Pharma Aktiengesellschaft. 4-Phenoxy-nicotine acid derivatives and use thereof as PPAR-modulators: US20100160386A1; 2010
17. Aryx Therapeutics, Inc. Agonist of peroxisome proliferator activated receptor alpha: WO2010071813A1; 2010
18. Smithkline Beecham Corp. Carboxyl substituted indoles for use as PPAR alpha modulators: WO2009147121A1; 2009
19. Fundacion Instituto Mediterraneo para el Avance de la Biotecnologia y la Investigacion Sanitaria (IMABIS). Pyrazole derivatives of fatty acid amides as PPAR-alpha specific activators, preparation method thereof and use of same: WO2009050318A1; 2009
20. Fundacion Instituto Mediterraneo para el Avance de la Biotecnologia y la Investigacion Sanitaria (IMABIS). Fatty acid amide derivatives with amphetamines for the treatment of eating disorders: WO2011076966A1; 2011

21. Janssen Pharmaceutica NV. Drug combinations comprising a DGAT inhibitor and a PPAR-agonist: WO2009147170A2; 2009
22. He K. Extract of fraxinus excelsior seeds and therapeutic applications therefor: US20090117214A1; 2009
23. Wang H. Isoflavone glycosides as peroxisome proliferator-activated receptor-alpha modulator: US20090099099A1; 2009
24. Neopharm Co., Ltd. Use of PPAR alpha activator as inflammatory skin disease-treating agent and method for treating skin diseases using the same: US20100173995A1; 2010
25. Johns Hopkins University. Phase 2 inducers and related signaling pathways protect cartilage against inflammation/ infection, apoptosis and stress: US20100015085A1; 2010
26. Carmeliet P. Use of PPAR alpha agonists to treat skeletal muscle wasting disorders: WO2008006819A2; 2008
27. Carmeliet P. Use of PPAR alpha agonists to treat skeletal muscle wasting disorders: US20090234150A1; 2009
28. Ghent University. Compositions and methods relating to glucocorticoid receptor alpha and peroxisome proliferator-activated receptors: US20090111782A1; 2009
29. Daiichi Sankyo Co., Ltd. Aryl derivatives: WO2008126731A1; 2008
30. Daiichi Sankyo Co., Ltd. Fused bicyclic heteroaryl derivatives: EP2138484A1; 2009
31. Daiichi Sankyo Co., Ltd. Pyridine derivative: EP2404918A1; 2012
32. Merck & Co., Inc. Novel crystalline salt form of an antidiabetic compound: WO2008109334A1; 2008
33. Merck & Co., Inc. Method of treatment using fused aromatic compounds having anti-diabetic activity: WO2008137105A1; 2008
34. Merck & Co., Inc. Antidiabetic azaindoles and diazaindoles: WO2009005672A1; 2009
35. Dong-A Pharm. Co., Ltd. Novel phenylpropionic acid derivatives as peroxisome proliferator-activated gamma receptor modulators, method of the same and pharmaceutical composition comprising the same: WO2008108602A1; 2008

- **Promising novel compounds PAM-1616, PAR1622, PAR-5359.**

36. Moon H-S. Novel phenylpropionic acid derivatives as peroxisome proliferator-activated gamma receptor modulators, method of the same and pharmaceutical composition comprising the same: US20100063041A1; 2010
37. Kim M, Chae YN, Choi S, et al. PAM-1616, a selective peroxisome proliferator-activated receptor gamma modulator with preserved anti-diabetic efficacy and reduced adverse effects. Eur J Pharmacol 2011;650(2-3):673-81
38. Kim M, Chae YN, Kim HS, et al. PAR-1622 is a selective peroxisome proliferator-activated receptor gamma partial activator with preserved antidiabetic efficacy and broader safety profile for fluid retention. Arch Pharm Res 2009;32(5):721-7
39. Kim M, Chae YN, Son MH, et al. PAR-5359, a well-balanced PPARalpha/ gamma dual agonist, exhibits equivalent antidiabetic and hypolipidemic activities in vitro and in vivo. Eur J Pharmacol 2008;595(1-3):119-25
40. Evolva SA. Substituted 1,3-dioxanes useful as PPAR modulators: WO2008089461A1; 2008
41. Evolva SA. PPAR modulators: US20110178112A1; 2011
42. Smithkline Beecham Corp. 1H-Indole-2-carboxylic acid derivatives useful as PPAR modulators: WO2008028118A1; 2008
43. Kowa Co., Ltd. Novel compounds comprising a 3-(5-alkoxypyrimidin-2-yl)-pyrimidin-4(3H)-one structure and drugs that comprise same: US20110306623A1; 2011
44. Kowa Co., Ltd. Novel 1-(biphenyl-4-yl-methyl)-1H-imidazole derivative and pharmaceutical product containing same: WO2011077712A1; 2011
45. Kowa Co., Ltd. Novel 2-pyridone derivative and pharmaceutical product containing same: WO2011077711A1; 2011
46. Kyowa Hakko Kogyo Co., Ltd. Tricyclic compounds: EP1988091A1; 2008
47. Kyowa Hakko Kirin Co., Ltd. Tricyclic compounds: EP2327690A1; 2011
48. Kaneka Corp. Peroxisome proliferator-activated receptor ligand: US20080132544A1; 2008
49. Vivacell Biotechnology Espana, S.L. Cannabinoid quinone derivatives: WO2011117429A1; 2011
50. Shenzhen Neptunus Pharmaceutical Co., Ltd. Diphenylethene derivatives and uses thereof: WO2011075935A1; 2011
51. Epax AS. Composition comprising a PPAR agonist and a phospholipid component: WO2010039040A1; 2010
52. Epax AS. Composition comprising at least one PPAR agonist and a lipid component: US20100081694A1; 2010
53. Boehringer Ingelheim International GmbH. Pharmaceutical composition comprising an SGLT2 inhibitor and a PPAR-gamma agonist and uses thereof: WO2011120923A1; 2011
54. Theracos, Inc. Therapeutic uses of SGLT2 inhibitors: US20110077212A1; 2011
55. Sigma-Tau Industrie Farmaceutiche Riunite S.p.A. Composition useful for the prevention of adverse effects due to the use of PPAR-gamma agonists: WO2008141897A1; 2008
56. Dana-Farber Cancer Institute, Inc. Compositions, kits and methods for identification, assessment, prevention and therapy of metabolic disorders: WO2011091134A2; 2011

- **Methods to identify inhibitors of the Cdk5-dependent phosphorylation of PPARγ.**

57. Rivier M, Castiel I, Safonova I, et al. Peroxisome proliferator-activated receptor-alpha enhances lipid metabolism in a skin equivalent model. J Invest Dermatol 2000;114(4):681-7
58. Galderma Research & Development. Novel biaromatic compounds that modulate PPAR-receptors: US20090012129A1; 2009
59. Galderma Research & Development. Novel 3-phenyl acrylic acid compound activators of type PPAR receptors and pharmaceutical/cosmetic compositions comprised thereof: US20100144884A1; 2010
60. Galderma Research & Development. Novel derivatives of 3-phenyl propanoic acid activating PPAR-type receptors, method for preparing same and use thereof in cosmetic or pharmaceutical compositions: WO2008152333A2; 2008

61. Galderma Research & Development. Novel 3-phenylpropanpoic compound activators receptors of PPAR type and pharmaceutical/cosmetic compositions comprised thereof: US20100158843A1; 2010

62. Umbert Millet, Ignacio. Dermatological pharmaceutical composition for the treatment of skin inflammation diseases, such as dermatitis, atopic dermatitis, vitiligo, alopecia areata, acne, psoriasis, pruritus or combinations of same: EP2311454A2; 2011

63. Umbert Millet, Ignacio. Dermatological pharmaceutical composition for the treatment of skin inflammation diseases, such as dermatitis, atopic dermatitis, vitiligo, alopecia areata, acne, psoriasis, pruritus or combinations of same: WO2009153373A2; 2009

64. Umbert Millet, Ignacio. Dermatological pharmaceutical composition for the treatment of skin inflammation diseases, such as dermatitis, atopic dermatitis, vitiligo, alopecia areata, acne, psoriasis, pruritus or combinations of same: US20110129546A1; 2011

65. Johnson and Johnson Consumer Companies, Inc. A composition comprising a PPAR-gamma agonist and method of treating facial skin defect: EP2123248A1; 2009

66. Avon Products, Inc. Use of eclipta prostrata and other PPAR-gamma inhibitors in cosmetics and compositions thereof: US20110305781A1; 2011

67. Rheinische Friedrich-Wilhelms Universitat. PPAR-gamma agonisten zur Behandlung von Erkrankungen mit pathophysiologischer Beteiligung von TH17-Lymphozyten: EP2301539A1; 2011

- **PPARs in inflammatory diseases.**

68. Peyrin-Biroulet L, Beisner J, Wang G, et al. Peroxisome proliferator-activated receptor gamma activation is required for maintenance of innate antimicrobial immunity in the colon. Proc Natl Acad Sci USA 2010;107(19):8772-7

69. Giuliani International, Ltd. PPAR-gamma agonists for the induction of cationic antimicrobial peptide expression as immunoprotective stimulants: WO2008104557A1; 2008

- **PPARs in inflammatory diseases.**

70. Neumann A, Weill A, Ricordeau P, et al. Pioglitazone and risk of bladder cancer among diabetic patients in France: a population-based cohort study. Diabetologia 2012;55(7):1953-62

71. Cedars-Sinai Medical Center. Methods of using PPAR-gamma agonists and caspase-dependent chemotherapeutic agents for the treatment of cancer: US20090264483A1; 2009

72. Shimazaki N, Togashi N, Hanai M, et al. Anti-tumour activity of CS-7017, a selective peroxisome proliferator-activated receptor gamma agonist of thiazolidinedione class, in human tumour xenografts and a syngeneic tumour implant model. Eur J Cancer 2008;44(12):1734-43

- **Preclinical development of CS-7017 as anti-cancer agent.**

73. Daiichi Sankyo Co., Ltd. Crystal of thiazolidinedione compound and process for production thereof: EP2311834A1; 2011

74. Daiichi Sankyo Co., Ltd. Crystal of thiazolidinedione compound and process for production thereof: EP2305673A1; 2011

75. Daiichi Sankyo Co., Ltd. Crystal of thiazolidinedione compound and process for production thereof: WO2010013769A1; 2010

76. Daiichi Sankyo Co., Ltd. Crystalline forms of thiazolidinedione derivative and its manufacturing method: WO2008099944A1; 2008

77. Daiichi Sankyo Co., Ltd. Crystal of thiazolidinedione compound and process for production thereof: WO2010013768A1; 2010

78. Soluciones Extractivas Alimentarias, S.L. Solutex. Docosahexaenoic acid ethyl esters and/or its derivatives for prevention and/or treatment of age-related macular degeneration: WO2011095837A1; 2011

79. Omeros Corp. Compositions and methods for prophylaxis and treatment of addictions: WO2010105103A1; 2010

80. Ciccocioppo R. Compositions and methods for prophylaxis and treatment of addictions: WO2008128126A1; 2008

81. Rhode Island Hospital. Treatment, prevention and reversal of alcohol-induced brain disease: US20100055037A1; 2010

82. Rhode Island Hospital. Treatment, prevention and reversal of alcohol-induced brain disease: US20100021386A1; 2010

83. Sanofi-Aventis. 6-Oxazol-4-ylmetholmethoxy-alko-alkoxymethyl substituted benzoic acid derivatives forming peroxisome proliferator activated receptor (PPAR) ligands, process for their preparation and methods of use thereof: US20080171776A1; 2008

84. The University of Sidney. Flavonoid PPAR agonists: WO2009026657A1; 2009

85. Nippon Chemiphar Co., Ltd. Activator for peroxisome proliferator activated receptor: WO2008016175A1; 2008

86. Nippon Chemiphar Co., Ltd. Activator for peroxisome proliferator activated receptor: WO2009128558A1; 2009

87. Glaxo Group Ltd. Thiazole and oxazole derivatives and their pharmaceutical use: WO002001000603; 2001

88. Nippon Chemiphar Co., Ltd. Activating agent for peroxisome proliferator activated receptor delta: US20090298896A1; 2009

89. Nippon Chemiphar Co., Ltd. Activating agent of peroxisome proliferator activated receptor delta: US000007119104B2; 2000

90. Nippon Chemiphar Co., Ltd. Activator for peroxisome proliferator activated receptor: US20100029949A1; 2010

91. Smithkline Beecham Corp. Chemical compounds: WO2005077926A2; 2005

92. Nippon Chemiphar Co., Ltd. Activator agent for peroxisome proliferator activated receptor: US20110090098480A1; 2011

93. Nippon Chemiphar Co., Ltd., Cerenis Therapeutics S.A. Use of PPAR delta ligands for the treatment of prevention of inflammation or energy metanolism/ production related diseases: US20110092517A1; 2011

- **Summarizes the most promising compounds of Nippon Chemiphar.**

94. Zhejiang Hisun Pharmaceutical Co., Ltd. Compound with agitation effect on peroxisome proliferator-activated receptor delta, and preparation method and use thereof: US20110319458A1; 2011

95. Novo Nordisk A/S. Novel compounds, their preparation and use: US20090209588A1; 2009

96. Novo Nordisk A/S. Novel compounds, their preparation and use: US20090012171A1; 2009

97. Novo Nordisk A/S; High Point Pharmaceuticals, LLC. Novel compounds, their preparation and use: US20110039841A1; 2011

98. High Point Pharmaceuticals, LLC. Phenoxy acetic acids as PPAR delta activators: US20110245244A1; 2011

99. Seoul National University Industry Foundation. Aryl compounds as PPAR ligands and their use: WO2008066356A1; 2008

100. SRI International. PPAR-delta ligands and methods of their use: US20090163481A1; 2009

101 Shionogi Co., Ltd.; Institute of medicinal molecular design. Derivative having PPAR agonistic activity: US20090286974A1; 2009

102. Kalypsys, Inc. Novel compounds as modulators of PPAR: US20080287477A1; 2008

103. Kalypsys, Inc. Sulfonyl-substituted bicyclic compounds as PPAR modulators for the treatment of non-alcoholic steatohepatitis: US20080176861A1; 2008

104. Kalypsys, Inc. Sulfonyl-substituted bicyclic compounds as modulators of PPAR: US20060205736A1; 2006

105. Kalypsys, Inc. Oral Pharmaceutical formulation compromising a sulfonyl bicyclic modulator of PPAR for the treatment of disease: WO2008043024A2; 2008

106. Kalypsys, Inc. Sulfonyl-substituted bicyclic compounds as modulators of PPAR: US20060167012A1; 2006

107. Teijin Ltd. Method for screening substance by measuring PPAR delta activating effect and agent: US20080287544A1; 2008

108. Toudai TLO, Ltd. Insuline secretagogue drugs: US20080207710A1; 2008

109. Cerenis Therapeutics S.A. Novel uses of PPAR delta agonists: WO2008154023A1; 2008

110. The University of Dundee. PPAR delta Inhibitors for treatment of cardiovascular diseases: EP1200114B1; 2009

111. University Court of the University of Dundee. Methods concerning PPAR delta and antagonists thereof: US20110263691A1; 2011

112. Shearer BG, Steger DJ, Way JM, et al. Identification and characterization of a selective peroxisome proliferator-activated receptor/(NR1C2) antagonist. Mol Endocrinol 2007;22(2):523-9

113. Noa Noy. Methods of treating metabolic disorders: US20090137671A1; 2009

114. Eli Lilly and Co. Peroxisome proliferator activated receptor modulators: WO2003072100; 2003

115. Seoul National University Foundation. Thiazole compound (as PPAR delta) ligand and pharmaceutical, cosmetic and health food comprised thereof: US20100041723A1; 2010

116. Sanofi-Aventis U.S. LLC. Cyclic N-[1,3,4].thiadiazol-2-yl-benzene sulfonamides, pharmaceutical compositions and methods for the therapeutic use thereof: US20080280959A1; 2008

117. Sanofi-Aventis U.S. LLC. N-[1,3,4]-thiadiazol-2-yl-benzene sulfonamides, pharmaceutical compositions thereof and methods for their therapeutic use: US20090054494A1; 2009

118. Sanofi-Aventis U.S. LLC. Bicyclic aryl-sulfonic acid [1,3,4]-thiadiazol-2-yl-amides, processes for their preparation, pharmaceutical compositions and methods for their use: US20100022603A1; 2010

119. Sanofi-Aventis Deutschland GmbH. Oxadizolones and derivatives thereof as peroxisome proliferator-activated receptor delta agonists: US7709509B2; 2010

120. Genomics Institute of the Novartis Research Foundation. Compounds and compositions as PPAR modulators: US20090192203A1; 2009

121. Eli Lilly and Co. Peroxisome proliferator activated receptor modulator: WO2008103574A3; 2008

122. Plexxikon, Inc. PPAR active compounds: US20080249137A1; 2008

123. Plexxikon, Inc. PPAR active compounds: US20080221127A1; 2008

124. Plexxikon, Inc. PPAR active compounds: WO2008109700A1; 2008

125. Ryu J-H. Alkoxy indole-3-acetic acid derivative acting as PPAR alpha/gamma/delta agonists, preparation method thereof, and pharmaceutical composition containing same as active ingredient: WO2011031111A2; 2011

126. Masson C. PPAR agonist compounds, preparation and uses: US20110195993A1; 2011

- **pan-PPAR ligands.**

Affiliation

Christina Lamers, Manfred Schubert-Zsilavecz & Daniel Merk†
†Author for correspondence
Goethe University Frankfurt,
Institute of Pharmaceutical Chemistry,
Max-von-Laue-Str. 9, Frankfurt, Germany
E-mail: merk@pharmchem.uni-frankfurt.de

EXPERT OPINION

informa healthcare

Characterizing ligands for farnesoid X receptor – available *in vitro* test systems for farnesoid X receptor modulator development

Daniel Merk†, Dieter Steinhilber & Manfred Schubert-Zsilavecz
Goethe-University Frankfurt, Institute of Pharmaceutical Chemistry, Frankfurt am Main, Germany

Introduction: Farnesoid X receptor (FXR) is an ascending target for metabolic and inflammatory diseases. As a nuclear receptor, FXR exhibits many physiological effects in transcription control of several genes. Therefore, the development of synthetic FXR ligands requires elaborate *in vitro* test systems to characterize novel ligands and to estimate their *in vivo* activities.
Areas covered: This work gathers and describes published *in vitro* test systems for FXR ligands including cell-based functional assays as well as binding assays. It also evaluates the information which can be provided by these assays.
Expert opinion: *In vitro* screening of FXR ligands widely relies on reporter gene assays. Additionally, some co-activator re-cruitment assays are described and for the characterization of potent compounds the pattern of affected target genes is evaluated by qPCR. Compared to other nuclear receptors such as PPARs the variety of test systems is quite low for FXR and might eventually not be enough to sufficiently characterize FXR targeting drug candidates.

Keywords: assay, chenodeoxycholic acid (CDCA), coactivator recruitment assay, farnesoid X receptor, GW4064, nuclear receptors, reporter gene assay

Expert Opin. Drug Discov. [Early Online]

1. Introduction

The ligand-activated transcription factor farnesoid X receptor (FXR) is a member of the nuclear receptor superfamily. It is highly expressed in liver, intestine and kidney and binds to specific DNA response elements (REs) as heterodimer with the retinoid X receptor (RXR). Physiologically activated by bile acids such as chenodeoxycholic acid (CDCA, **1a**), FXR regulates a large number of target genes involved in the metabolism and homeostasis of bile acids, lipids and glucose [1-3].

Several pathophysiological conditions have been discovered in which FXR plays a role. *In vitro* and *in vivo* models indicate a possible use of FXR ligands in the treatment of metabolic [4-10] and inflammatory [11-13] diseases as well as a role of FXR in development and growth of certain cancer cells [14,15]. Hence, FXR ligands might be beneficial in the treatment of, for example, diabetes, dyslipidemia, cancer and other disorders.

Intense research on FXR ligands has yielded several potent steroidal and non-steroidal compounds (reviewed in Ref. [16]). Among the bile acids as physiological ligands of FXR, CDCA (**1a**) is the most potent. Medicinal chemistry efforts have optimized compound **1a** leading to 6-ethyl-CDCA [17] (INT-747, **1b**). Among the number of non-steroidal FXR ligands, GW4064 [18] (**2**) and its derivatives are most potent so far (**Figure 1**).

10.1517/17460441.2014.860129 © 2013 Informa UK, Ltd. ISSN 1746-0441, e-ISSN 1746-045X

Article highlights.

- Various *in vitro* assay systems for FXR ligands are available including cell-based and cell-free, functional and binding assays.
- Each of these assays can provide certain information on the characterized ligands, such as functional activity, affinity or *in vitro* genomic activity. For a good *in vitro* characterization, novel FXR ligands should be applied to more than one test system.
- The most widely used reporter gene assays provide much information but are time-consuming. Stably transfected cell lines for reporter gene assays might help but the described systems rely on hybrid constructs that might falsify the results.
- Assays that provide more functional insights into the activity of novel compounds and that could better predict *in vivo* effects are not available but conceivable.
- Compared to other nuclear receptors, such as PPARs, the knowledge on FXR is still narrow and, therefore, the present test systems might not be comprehensive yet.

This box summarizes key points contained in the article.

Since FXR controls various target genes and interacts with several coactivators and corepressors, the *in vitro* pharmacological characterization of FXR ligands is difficult. Distinct FXR agonists have been shown to activate different patterns of genes [19] which make a number of test systems necessary for their complete characterization. Additionally, the definition and distinction of agonists, modulators and antagonists is difficult. Since the first discovery of FXR as bile acid receptor [1,2], there has been growing interest in this nuclear receptor. Besides the number of synthetic ligands, many test systems have been developed including cell-based and cell-free, functional and affinity-based assays and test systems to investigate the activated gene pattern or the involved coactivators/corepressors. This article describes the available assays for FXR ligands and evaluates which information can be provided by each assay.

2. Cell-based assays

Cell-based test systems are standard in nuclear receptor ligand characterization and development. They provide a cellular background and can give information on functional activities of test compounds. With cell-based assays, no recombinant protein expression and purification is required. On the other hand, cell-based test systems are characterized by many possible influences of cellular factors that can sophisticate the results. Cell-based assays provide information on functional activities of compounds but binding affinity and kinetics cannot be determined directly.

2.1 Reporter gene-/transactivation assays

Reporter gene assays are most common and widespread among test systems to discover and characterize nuclear receptor ligands. The first FXR reporter gene assays were described right with the discovery of the receptor [1,2]. With the growing interest in FXR as target, many more optimized systems were developed. For these assays, an expression plasmid for the respective receptor under the control of a constitutive promoter (e.g., simian virus 40 promoter (SV40) or cytomegalovirus promoter (CMV)) is transfected into an eukaryotic cell line such as HeLa cells, Cos7 cells or HepG2 cells. The constructs either contain the sequence for the nuclear receptor ligand binding domain (LBD) as hybrid with the DNA-binding domain (DBD) of another non-human nuclear receptor, for example, GAL4 from yeast or the full-length nuclear receptor (flFXR). A second plasmid containing the reporter gene under the control of a RE for the respective used DNA-binding domain is cotransfected. The most common REs for flFXR reporter gene assays are the promoter of the FXR target gene bile salt export protein (BSEP) and the internal repeat 1 (IR-1) which is found in the promoter region of heat shock protein 27 (hsp27).

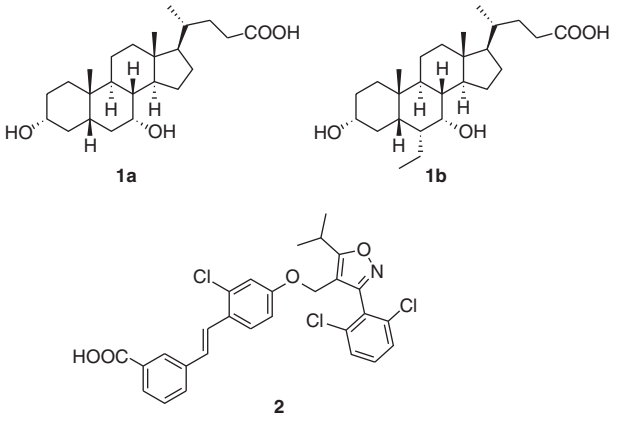

Figure 1. Schematic representation of FXR ligands CDCA (**1a**), 6-ECDCA (**1b**) and GW4064 (**2**).

When the flFXR is used in a reporter gene assay, a plasmid for RXR expression under a constitutive promoter is also usually cotransfected, since FXR only functions as heterodimer with RXR. Only few systems rely on endogenously expressed RXR [20].

Both systems, the one-hybrid system of chimeric fusion proteins and flFXR reporter gene assays, have certain advantages. Chimeric fusion proteins when activated bind to REs which are not found in human cells, such as the GAL4-RE, and are not affected by cellular proteins which lowers the background and can enhance the signal: noise ratio. A flFXR-based reporter gene assay, on the other hand, provides more physiological conditions, since the target receptor itself is not modified and can detect modulations of FXR activity by interactions outside of the ligand-binding domain.

Most of the FXR reporter gene assays are based on a transient transfection of the used cells. For the transfection, many protocols are described which are optimized for a

certain cell line and the best suited transfection method for the respective cells. Only a few stable cell lines for FXR reporter gene assays are described in literature and shall be discussed later.

While the first assays were only based on the reporter gene as single readout, newer systems include a control gene as internal standard that has several advantages and enhances the power of the assay. This second gene is another luciferase, a β-galactosidase or a fluorescent protein that can be detected simultaneously without affecting the reporter gene or vice versa. The internal control gene is under the control of a constitutive promoter and is located on an additional plasmid that is cotransfected.

Predominantly, the constitutively expressed reporter gene is used as a transfection control on which the reporter gene signal is normalized. The normalized results are independent from the transfection efficiency which makes the assay more robust and reduces the standard error. In addition, the constitutively expressed control gene can serve as a marker for toxicity when its signal is strongly reduced.

In contrast to these advantages of a second readout, it cannot sometimes be excluded that tested compounds interact with a reporter gene or affect its expression in any way. This can falsify the assay result for the respective compound and in the worst case make the assay unreliable. Further, controls with empty plasmid and/or with mutated REs should be performed in order to be sure that the observed effects are mediated by FXR-binding to the reporter gene promoter.

For a good performance, a reporter gene assay has to be optimized concerning cell number/density, DNA amount and plasmid ratios, transfection protocol, incubation time and many more.

In general, reporter gene assays can serve for agonist and antagonist characterization. For agonist testing, the transfected cells are incubated with varying concentrations of the test compound. In case of an agonistically active substance, this yields a sigmoidal curve which provides an EC_{50} value and the maximum FXR activation activity compared to a known full agonist as control which is set as 100%. The most widely used full agonist as control for FXR assays is GW4064 (**2**).

The characterization of antagonists can be achieved by incubating the transfected cells with varying concentrations of the test compound and a constant concentration of a known agonist (e.g., GW4064 (**2**)) which leads to an inverse sigmoidal curve providing an IC_{50} value. For a more physiological setting, CDCA (**3**) can be used as agonist instead of compound **2** since compound **3** is the most potent physiological FXR agonist. When a reporter gene assay is used for antagonist testing, it should contain a control gene because without such second reporter gene toxic effects of a test compound could be misinterpreted as antagonistic activity. When a luciferase is used as reporter gene also a possible light absorption of the test compounds has to be considered and must not be misinterpreted as antagonism.

A problem of cell-based reporter gene assays is that some test compounds may not only interact with the target protein FXR but also influence reporter proteins such as a luciferase or even the protein synthesis machinery of the cells. Such effects falsify and disturb the results of reporter gene assays and make the respective compounds difficult to characterize. In case the compounds interact with the protein product of reporter or control gene, such as a luciferase, an alternative reporter gene construct such as a β-galactosidase can be used to overcome the problem. In case the compounds influence the protein synthesis machinery or other basic cellular processes, the problem is not easily solvable but such compounds will probably be toxic either.

A reporter gene assay in stably transfected cells is superior to transiently transfected cells since, on one hand, the transfection is omitted which is time-consuming. The other advantage is the constant expression level that is not dependent on transfection efficacy. One reporter gene assay system for FXR in stably transfected cells is described in literature [21,22]. It uses HEK293 cells that stably express a GAL4–FXR–LBD chimera and a suitable (but not specified) luciferase reporter construct. This cell line can directly be incubated with test compounds and evaluated for luciferase activity after the incubation period (24 h). A control gene is not required.

The discussed reporter gene assays are all suited for miniaturization and can be performed in a format between 24- and 384-well plates. They provide a lot of information including EC_{50} and IC_{50} values, maximum FXR activation activity and toxicity. **Table 1** gives an overview over published FXR reporter gene assays.

2.2 Quantitative (real-time) polymerase chain reaction

Since the ligand-activated transcription factor FXR exhibits effects on various genes via interactions with different coactivators, corepressors and REs on the DNA, constants for binding and transactivation alone cannot characterize a ligand sufficiently. Thus, the pattern of genes that are changed in their expression rate by an FXR ligand is another important option to characterize FXR ligands. The influence of a compound on the expression of FXR-dependent genes can be evaluated by quantitative (real-time) polymerase chain reaction (qPCR). For this purpose, cells are incubated (6 – 24 h) with the respective test compound and then harvested. Subsequently, the total RNA is extracted and translated into cDNA. For both steps, many kits are commercially available. With the cDNA, qPCR experiments can be performed for any FXR-dependent gene with suitable primers (**Table 2**). Methods for the performance of qPCR experiments are summarized in Refs. [23,24]. The obtained data for the mRNA level of an FXR target gene have to be normalized to the mRNA level of a ubiquitously expressed gene such as the glyceraldehyde 3-phosphate dehydrogenase, actin or β2-microglobulin that is not affected by FXR. Finally, the expression profile of FXR-dependent genes

Table 1. FXR reporter gene assay systems (examples).

Cell line	Transfection method/reagent	Receptor (promoter)	Reporter gene (RE)	Control gene (promoter)	Ref.
CV-1	n.d.	rat flFXR	β-galactosidase (IR-1)	-	[2]
HepG2	FuGENE HD	flFXR (CMV), RXR (SG5)	Firefly luciferase (IR-1 in hsp27 promoter)	β-galactosidase (CMV)	[25]
HepG2	FuGENE HD	flFXR (CMV), RXR (SG5)	Firefly luciferase (IR-1 in hsp27 promoter)	Renilla luciferase (GL4.70)	[58]
HepG2	FuGENE HD	flFXR (SG5), RXR (SG5)	Firefly luciferase (IR-1 in hsp27 promoter)	β-galactosidase (CMV)	[26]
HepG2	SuperFect transfection Kit	GAL4–DBD–FXR–LBD (CMV)	Firefly luciferase (GAL4-RE × 5)	β-galactosidase (CMV)	[59]
HEK293	$Ca_3(PO_4)_2$	Murine flFXR, Murine RXR	Firefly luciferase $((ECRE)_5TK)$	Renilla luciferase (SV40)	[27]
HepG2	SuperFect transfection Kit	flFXR (CMV)	Firefly luciferase (SHP promoter or CYP7A1 promoter)	β-galactosidase (CMV)	[20]
COS-7	Effectene transfection reagent	flFXR (CMV), RXR (CMV)	Enhanced yellow fluorescent protein (IR-1)	Enhanced cyan fluorescent protein (thymidine kinase promoter)	[60]
HEK293	[Stable]	GAL4–FXR–LBD	Luciferase	-	[22]
CV-1	DOTAP	flFXR (CMX), RXR (CMX)	Luc12-luciferase (ECREx7)	β-galactosidase (CMX)	[61]
CV-1	FuGENE HD	GAL4–DBD–FXR–LBD (CMV)	Firefly luciferase (GAL4-RE)	-	[39]

Table 2. Primers for qPCR experiments for FXR target genes.

FXR target gene (human)	Primer(s)	Ref.
BSEP	gggccattgtacgagatcctaa/tgcaccgtcttttcactttctg	[25,32]
SHP	gctgtctggagtccttctgg/ccaatgatagggcgaaagaagag	[32,33]
OSTα	tgttgggccctttccaatac/ggctcccatgttctgctcac	[25,32,33]
CYP7A1*	caccttgaggacggttccta/cgatccaaagggcatgtagt	[32,33]

*CYP7A1 is not a direct FXR target gene but affected via SHP.

obtained with a test compound can be compared to the expression profile of a positive and negative control and insights into the effects of a test compound on gene expression via FXR can be given.

For significant results, a suitable cell line has to be selected for qPCR experiments. Since the experiment should reflect physiological conditions, the receptor is not transfected into the cells as in common transactivation assays so that cells which express FXR should be used. The literature describes qPCR experiments with the human hepatoma cell lines HepG2 [25-35] and Huh-7 [36] as well as with primary hepatocytes [25].

With qPCR experiments, the impact of any FXR modulator on FXR-dependent gene expression can be evaluated. In contrast to reporter gene assays, FXR agonism or antagonism for each single FXR-dependent gene can be investigated. It has turned out that regulation of target gene expression by FXR is complex so that FXR ligands might affect expression of certain genes, whereas others remain unaffected in a compound-specific manner. Under pharmacological aspects, FXR agonism may be beneficial for some genes, whereas other genes should not be eventually affected by a synthetic ligand. Therefore, the impact of a compound on the expression profile of FXR-dependent genes is a valuable information for FXR ligand development.

For the characterization of antagonistic FXR ligands, it is useful to perform qPCR experiments with the antagonists alone and in co-incubation with the most potent physiological FXR ligand CDCA, since this resembles the physiological setting in liver.

3. Cell-free assays

Assays that are not performed in a cellular setting have the advantage of providing more direct information on molecular target–ligand interactions. Additionally, such assays are usually considerably quicker since no transfection is necessary and the incubation period with the test compounds is shorter than in cell-based assays. On the other hand, the purified target protein is necessary for cell-free assays and it has to be recombinantly expressed in bacteria. Cell-free assays can provide information on functional activities of test compounds such as coactivator recruitment or constants for binding affinity.

3.1 Coactivator recruitment assays

In contrast to the reporter gene assays that determine the transactivation of a gene transcription under the control of FXR, coactivator recruitment assays measure the spatial proximity of a coactivator that binds to coactivator to the nuclear receptor. Theoretically, the incubation of the FXR protein with a ligand leads to binding of the ligand which induces conformational changes in FXR. This, in turn, allows a coactivator to bind FXR. By labeling FXR and the coactivator with, for example, fluorophores or radiators makes this proximity measurable.

3.1.1 Time-resolved fluorescence resonance energy transfer

Fluorescence resonance energy transfer (FRET) was first discovered in 1927 and has acquired various uses in biological chemistry. FRET is based on the transfer of energy via electrodynamic interactions from an excited donor fluorophore to an acceptor fluorophore. Since this phenomenon is only possible within a small distance (around 3 – 7 nm), FRET can be used to determine the spatial proximity of two fluorophores [37].

The most common way to determine coactivator recruitment of FXR is a time-resolved FRET (TR-FRET) assay which is commercially available. It contains a FXR–glutathione-*S*-transferase (GST) fusion protein, fluorophore-labeled SRC2-2 as FRET acceptor and a terbium-labeled anti-GST antibody as FRET donor. When these peptides are incubated together, the anti-GST antibody binds to the FXR–GST fusion protein but without an FXR ligand the labeled SRC2-2 is not bound to FXR. When terbium is excited with 340 nm light, it emits light at 495 nm. However, without spatial proximity, the fluorophore of SRC2-2 is not excited.

By addition of an agonistic FXR ligand as test compound that enables recruitment of the coactivator SRC2-2 to FXR, the fluorophore of the labeled coactivator is brought in spatial proximity of the excited terbium and FRET takes place. The coactivator fluorophore is excited by terbium and emits light at a wavelength of 520 nm. Thereby, the emission of terbium (495 nm) is reduced and the emission at 520 nm increases [38]. When the respective test compounds are applied in varying concentrations with constant amounts of the proteins, a sigmoidal curve can be detected that provides an EC_{50} value for coactivator recruitment.

Another FRET-based coactivator recruitment assay for FXR uses differently labeled proteins but follows the same principle. It contains allophycocyanin (APC)-labeled FXR as FRET acceptor and europium-labeled SRC-1 as FRET donor. APC, a fluorescent protein (excitation 633 nm and emission 680 nm) and europium (excitation 320 /340 nm and emission 615 nm) are each bound to streptavidin and coupled to FXR and SRC-1 via biotin (biotinylated SRC-1/biotin-SRC-1) [39-43]. Streptavidin has an extraordinarily high affinity to biotin.

The mixture of both assay systems is described as well. It uses a GST-fused FXR–LBD, an europium-labeled anti-GST antibody as FRET donor and APC-labeled streptavidin bound to biotin-SRC-1 as FRET acceptor [44,45].

3.1.2 Amplified luminescent proximity homogeneous assay

As FRET, the amplified luminescent proximity homogeneous assay (alpha screen) technology is based on activation by illumination and energy transfer from the activated donor to an acceptor in spatial proximity. In contrast to FRET where the energy is transferred via dipole–dipole interactions, in alpha screen, chemical energy (in form of $^1O_2$) is released by the donor and consumed by the acceptor to emit light. Donor and acceptor are coatable beads containing distinct chemicals. Donor beads contain the photosensitizer phthalocyanine, which on illumination (680 nm) converts ambient oxygen to singlet oxygen – an oxygen species with one excited electron. With a half-life of 4 µs, this excited singlet oxygen can diffuse around 200 nm in solution. If it reaches an acceptor bead containing a thioxene derivative in this proximity, energy is transferred and light (520 – 620 nm) is emitted.

For FXR, an alpha screen assay uses streptavidin-coated donor beads binding to biotin-SRC-1 and acceptor beads coated with anti-GST antibodies that bind to a GST–FXR–LBD fusion protein. When a FXR agonist enables recruitment of SRC-1 to FXR–LBD, donor and acceptor beads are in proximity and on illumination with 680 nm singlet oxygen is released and the acceptor beads emit light (520 – 620 nm) [28,30,31,46].

The alpha screen technology has some advantages over FRET. Since donor and acceptor beads contain many molecules of the photosensitizer or the acceptor and not only one fluorophore as in FRET the signal intensity is stronger and the sensitivity of the assay is enhanced. The long wavelengths provide low interference with biomolecules so that the background is low and the signal: noise ratio is high. High sensitivity and robustness allow miniaturization and cost-effectiveness.

Comparable to reporter gene assays, coactivator recruitment assays can be used to characterize FXR antagonists by co-incubating test compounds with a known potent FXR agonist.

3.2 Binding assays

The literature does not describe many direct binding assays for FXR. Most assays have a functional readout that involves interaction with other proteins, for example, coactivators. Since there is no radioligand for FXR, there is no radioligand binding assay.

3.2.1 Surface plasmon resonance

Surface plasmon resonance (SPR) is an optical technique that allows measurement of ligand–target interactions. For this purpose, the target/receptor protein is immobilized on a metal

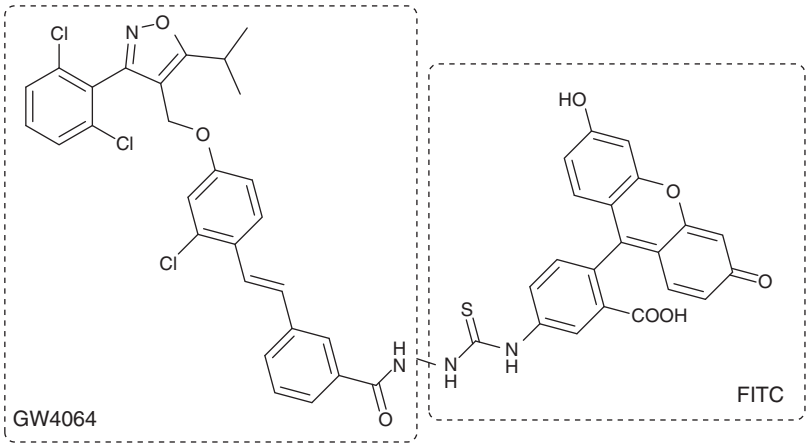

3

Figure 2. Schematic representation of FRET binding assay FITC-labeled derivative DY246.

surface and incubated with potential ligands in solution that passes the surface with target protein. When a ligand molecule is bound to the immobilized target, a change in the SPR signal can be detected. With this method, binding kinetics and affinity can be determined [47] Choi *et al.* [48] described a SPR experiment for FXR to measure direct binding of test compounds to the FXR–LBD. In this method, a soluble human FXR-LBD (no data about construct and expression/purification method) is incubated with test compounds for 1 h. Then, the mixture is injected over the sensor chip on which the coactivator SCR-1 was immobilized. Hence, this test system reminds more of a coactivator recruitment assay than of a direct binding assay.

3.2.2 *Scintillation proximity assay*

A true ligand binding assay for FXR ligands is a scintillation proximity experiment [49,50], which is derived from a similar assay for peroxisome proliferator-activated receptor-γ (PPARγ) [51]. In scintillation proximity assays (SPAs), the target protein is immobilized on beads that contain a scintillator which is a molecule that is excited to emit light by radiation. When a radiolabeled ligand is bound to the immobilized target, the radiator is in spatial proximity to the scintillator and light is emitted. When the radioligand is displaced by a competitor, the emission of light is reduced since the radiator is removed from the scintillator.

In the SPA experiments for FXR and PPARγ, the ligand-binding domain of the respective receptor is expressed in bacteria as His-tagged protein, purified and biotinylated. The resulting biotin-LBD is then bound to the scintillation beads via streptavidin. While for PPARγ, a high-affinity radioligand is published, however, the literature does not describe a radiolabeled ligand for FXR and the papers that mention the SPA experiments [49,50] provide no information about the ligand used. As result, IC_{50} values for inhibition of radioligand binding are obtained since SPA is applied in a competitive binding assay.

3.2.3 *Fluorescence polarization*

Fluorescence polarization-based competition experiments represent another binding assay which is relatively facile and suitable for high throughput [52]. It also uses recombinantly expressed His-tagged FXR–LBD and fluorescein isothiocyanate (FITC)-labeled CDCA as ligand. The FITC fluorophore is excited with polarized light of 494 nm and emitted light is measured at a right angle to the excitation light parallel and perpendicular to the original excitation light plane. When the ligand (FITC-CDCA) is bound to the FXR–LBD, its free rotation is hindered and diminished and the plane of emitted fluorescence light is maintained in the original plane of excitation light. When FITC-CDCA is displaced from the receptor by a competitor, it can rotate freely and the fluorescence intensity in the plane of excitation light is decreased which indicates binding of another ligand. Incubation of test compounds at varying concentrations with the FXR–LBD and FITC-CDCA at constant concentrations allows the determination of IC_{50} values for competitive displacement of the labeled ligand which can be used as an approximation for the binding constant. With appropriate instruments, such assay can be performed in miniature formats which enables high throughput and cost-effectiveness.

3.2.4 *Time-resolved fluorescence resonance energy transfer*

So far the most advanced FXR binding assay in literature is a FRET-based system [53]. In contrast to FRET-based coactivator recruitment assays, it uses a fluorescence-labeled FXR ligand instead of the labeled coactivator. The test system is, therefore, comparable to abovementioned fluorescence polarization binding assay with a different readout. For the FRET binding assay, FITC-labeled derivative DY246 (**Figure 2**) (**3**)

was developed from GW4064 (**2**). DY246 (**3**) has an EC_{50} value of 550 nM in a reporter gene assay which is only a slight loss in affinity compared to GW4064 (**2**, EC_{50} = ~ 90 nM). For the FRET binding assay, compound **3** was used as FRET acceptor, while a terbium-labeled anti-GST antibody acted as FRET donor. As third component for the assay, a GST–FXR–LBD fusion protein was necessary. Hence, the test system differs from the commercially available FRET-based coactivator recruitment assay only in the use of DY246 (**3**) instead of fluorescein-labeled SRC2-2 as FRET acceptor. When compound **3** is bound to the receptor–antibody complex, FRET (excitation: 340 nm and emission: 490 nm/520 nm) can take place. When a competitor displaces compound **3** from its binding, the distance between FRET donor and acceptor is increased and FRET intensity is decreased. The decrease in FRET intensity can then serve as readout. By detection of the FRET signal in presence of varying test compound concentrations, an IC_{50} value for competition with compound **3** is determined which can be used as an approximation for the binding constant.

4. Comparison and conclusion

A number of *in vitro* assay systems for FXR are described in the literature that can determine many characteristics of FXR ligands. A selection of important FXR ligands with their *in vitro* characteristics is depicted in **Table 3**. For functional characterization, meaning the effect of a ligand on the expression of FXR target genes reporter gene assays, qPCR and coactivator recruitment assays are available. Reporter gene assays provide information on the efficacy of a ligand, that is, the maximum relative FXR activation or inhibition and on the effective concentrations expressed as EC_{50} or IC_{50}. These values do not express the actual affinity of a ligand but can be a reference for affinity. In qPCR experiments, the effects on distinct FXR target genes can be evaluated which gives valuable information for eventual *in vivo* activities of a test compound. Coactivator recruitment assays stand between functional and binding assays. They determine the binding of a coactivator to the nuclear receptor after activation by a ligand. Hence, they can characterize a ligand as agonist or antagonist and provide an EC_{50} or IC_{50} value, but they cannot define a maximum relative FXR activation or inhibition.

The three available FXR binding assays are all based on competition of test compounds with known FXR ligands. For this purpose, labeled FXR ligands have been developed including FITC-labeled CDCA and GW4064 as well as a radioligand which is not specified, however.

The *in vitro* characterization of FXR targeting compounds hence can provide data on their efficacy and affinity as well as the pattern of affected target genes. More detailed information such as recruitment of coactivators distinct from SRC or influences on the phosphorylation state of the receptor are not available so far.

5. Expert opinion

The most widely used test systems concerning FXR ligand development are reporter gene assays. Modern FXR reporter gene assays should be based on the full-length receptor and should contain a control gene for transfection control. They can be performed in miniature formats and provide a considerably high throughput for screenings. The cellular background, on one hand, provides a more physiological setting than other *in vitro* test systems but, on the other hand, cellular influences on the assay cannot be excluded and may falsify the results. Further, compared with the analysis of FXR target genes, the test system is more artificial as it requires overexpression of FXR and RXR which might impair receptor signaling. Reporter gene assays provide quite much information as they characterize the maximum relative FXR activation and EC_{50} value of a ligand and can reveal toxic effects as well. Additionally, reporter gene assays are suitable for agonist and antagonist characterization.

A reporter gene assay in a stably transfected cell line is time- and cost-economic and very desirable. The only described stable cell line for such a FXR assay is actually missing a control gene which – though not necessary for transfection control – hinders good antagonist characterization, since the distinction between toxicity and antagonism may be difficult. In addition, this assay is based on the one-hybrid system that is not quite physiological.

A good alternative to reporter gene assays are coactivator recruitment assays. These test systems are fast and provide a high throughput. Although they fail to detect a maximum relative FXR activation, they can determine EC_{50} values and distinguish agonists and antagonists.

For antagonist characterization in reporter gene and coactivator recruitment assays, test compounds have to be examined in competitive experiments with a known agonist as competitor. Antagonistic activity can then be determined as a reduced reporter gene transactivation or a lower coactivator recruitment of the competitor.

The available FXR binding assays are based on modern techniques such as scintillation proximity or FRET and can provide high throughput. They can be used for screening purposes and can enhance the knowledge on FXR ligands but they provide considerably less information and cannot separate between agonists and antagonists. Additionally, they might fail to detect allosteric binders.

While reporter gene, coactivator recruitment or binding assays are a good basis for ligand screening, development and optimization, they miss information on how the FXR target genes are affected by a ligand. This, however, is necessary to make a first prediction on the possible physiological effects of a FXR-modulating compound. Therefore, advanced FXR ligands should be characterized by qPCR experiments.

For more predictive *in vitro* data, novel assays are required that could detect, for example, the response of hepatic cells or

Table 3. Selected FXR ligands with their *in vitro* pharmacological characteristics and used test systems.

Compound	Assay system for characterization	*In vitro* data	Ref.
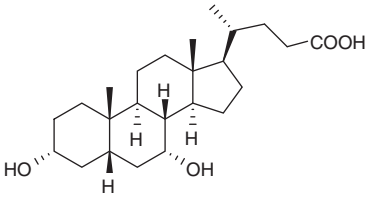 CDCA	Coactivator recruitment (FRET)	EC_{50} = 8.66 μM	[17]
	Coactivator recruitment (FRET)	EC_{50} = 3.4 μM	[18]
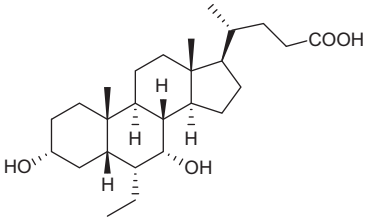 6-ECDCA	Coactivator recruitment (FRET)	EC_{50} = 99 nM (144% of CDCA)	[17]
	Reporter gene assay (flFXR in Huh7 cells)	EC_{50} = 85 nM	[17]
	Agonistic on TGR5 (EC_{50}(cAMP) = 20 μM; EC_{50}(transactivation) = 8 μM)		[31]
	Selective over other nuclear receptors at 1 μM		[17]
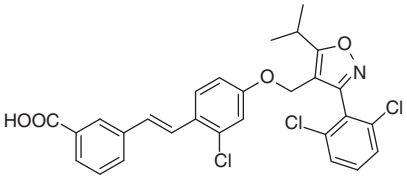 GW4064	Coactivator recruitment (FRET)	EC_{50} = 15 nM (140% of 50 μM CDCA)	[18]
	SPA-binding affinity	Affinity: 0.064 μM	[62]
	Reporter gene assay (chimeric)	EC_{50} = 0.9 μM	[62]
	Reporter gene assay	EC_{50} = 0.91 μM	[49]
	Coactivator recruitment (FRET)	EC_{50} = 37 nM (117% of CDCA)	[17]
	Selective over other nuclear receptors at 1 μM		[18]
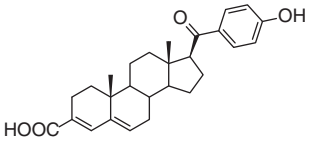 MFA-1	Coactivator recruitment (homogenous time-resolved FRET)	EC_{50} = 16.9 nM	[63]
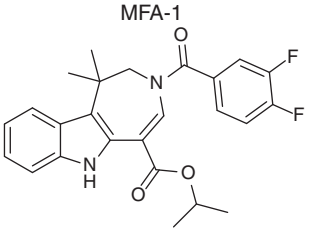 FXR-450	Reporter gene assay (flFXR in CV-1 cells)	EC_{50} = 4 nM (149% of 100 μM CDCA)	[61]
	Selective over PPARs, LXRs, RXRs, RAR, VDR		[61]
	SPA-binding affinity	Affinity: 0.07 μM	[49]
	Selective over PPARs, LXRs, RXRs inhibits hERG		[49,50]

islet cells *in vitro* on a FXR ligand. Such test systems would help to focus on desired physiological effects of test compounds than on affinity or transactivation efficiency. Although comparable experiments have already been performed [7], they are not yet suitable for regular compound characterization.

A major concern in any drug development process is the activity of novel active compounds on off-targets. For FXR ligands, the effects on other nuclear receptors should always be evaluated. Especially, the PPARs, pregnane X receptor, liver X receptor (LXR) and the vitamin D receptor (VDR) are important since they are physiologically linked to FXR. In addition, the membrane bile acid receptor TGR5 (a G-protein-coupled receptor) can be a desired target of FXR ligands or an off-target.

In recent years, it has been discovered that nuclear receptors are also affected in their activity by, for example, phosphorylation. For PPARs, modulating phosphorylations are known and the effects of ligands on the phosphorylation state can be determined in test systems. In addition, for FXR, post-translational modifications are described. In mice, FXR acetylation state which is catalyzed by p300 acetylase and SIRT1 deacetylase varies in fasted and fed state, and in obese animals FXR acetylation is elevated [54,55] The main site of FXR acetylation is Lys217 in the hinge region which leads to dissociation of FXR from RXR and the DNA and to decreased transactivation ability. In response to FXR-activating stimuli, the interaction of FXR with p300 and the acetylation state of the receptor are increased which might serve as a negative regulatory cycle. Besides acetylation of FXR, which is best investigated, phosphorylation of the nuclear receptor has consequences on its activity. FXR is phosphorylated, for example, by protein kinase C at Ser135 and Ser154 in the DBD which leads to increased interaction with the PPAR γ coactivator 1α and enhances transactivation activity [55,56]. However, the downstream effects of post-translational modifications of FXR on the pattern of target gene expression and whether they can be specifically modified by synthetic ligands is still uncertain and novel test systems to investigate these questions are required.

Altogether, many tools to characterize FXR ligands are available that can provide distinct information. The growing knowledge on nuclear receptor physiology, demonstrating that in addition to the presence of different coactivators and corepressors, phosphorylations [57] or SUMOylations influence their activity, suggests that the *in vitro* data from available assay systems may not roughly be sufficient to predict the physiological effects of a novel ligand. FXR is an emerging target especially for metabolic disorders and clinical trials with the first synthetic ligands are in progress. Hopefully, the growing knowledge on the physiology and pathophysiology of the nuclear receptor and the elaborate *in vitro* characterization systems will translate into novel drugs targeting FXR in the future.

Declaration of interest

The authors state no conflict of interest and have received no payment in preparation of this manuscript.

Bibliography

Papers of special note have been highlighted as either of interest (•) or of considerable interest (••) to readers.

1. Parks DJ, Blanchard SG, Bledsoe RK, et al. Bile acids: natural ligands for an orphan nuclear receptor. Science 1999;284(5418):1365-8
2. Makishima M, Okamoto AY, Repa JJ, et al. Identification of a nuclear receptor for bile acids. Science 1999;284(5418):1362-5
3. Wang H, Chen J, Hollister K, et al. Endogenous bile acids are ligands for the nuclear receptor FXR/BAR. Mol Cell 1999;3(5):543-53
4. Wang Y, Chen W, Moore DD, Huang W. FXR: a metabolic regulator and cell protector. Cell Res 2008;18(11):1087-95
5. Fiorucci S, Mencarelli A, Distrutti E, et al. Targetting farnesoid-X-receptor: from medicinal chemistry to disease treatment. Curr Med Chem 2010;17(2):139-59

• **Reviews physiological and pathophysiological roles of FXR.**

6. Cipriani S, Mencarelli A, Palladino G, Fiorucci S. FXR activation reverses insulin resistance and lipid abnormalities and protects against liver steatosis in Zucker (fa/fa) obese rats. J Lipid Res 2010;51(4):771-84
7. Düfer M, Hörth K, Wagner R, et al. Bile acids acutely stimulate insulin secretion of mouse β-cells via farnesoid X receptor activation and K(ATP) channel inhibition. Diabetes 2012;61(6):1479-89

• **Describes a potential role of FXR in diabetes and insulin resistance.**

8. Düfer M, Hörth K, Krippeit-Drews P, Drews G. The significance of the nuclear farnesoid X receptor (FXR) in β cell function. Islets 2012;4(5):333-8
9. Zhang Y, Lee FY, Barrera G, et al. Activation of the nuclear receptor FXR improves hyperglycemia and hyperlipidemia in diabetic mice. Proc Natl Acad Sci USA 2006;103(4):1006-11
10. Zhang Y, Yin L, Anderson J, et al. Identification of novel pathways that control farnesoid X receptor-mediated hypocholesterolemia. J Biol Chem 2010;285(5):3035-43
11. Renga B, Mencarelli A, Cipriani S, et al. The bile acid sensor FXR is required for immune-regulatory activities of TLR-9 in intestinal inflammation. PLoS One 2013;8(1):e54472
12. Nijmeijer RM, Gadaleta RM, van Mil SWC, et al. Farnesoid X receptor (FXR) activation and FXR genetic variation in inflammatory bowel disease. PLoS One 2011;6(8):e23745
13. Wildenberg ME, van den Brink GR. FXR activation inhibits inflammation and preserves the intestinal barrier in IBD. Gut 2011;60(4):432-3
14. Wang X, Fu X, van Ness C, et al. Bile acid receptors and liver cancer. Curr Pathobiol Rep 2013;1(1):29-35
15. Vaquero J, Briz O, Herraez E, et al. Activation of the nuclear receptor FXR enhances hepatocyte chemoprotection and liver tumor chemoresistance against genotoxic compounds. Biochim Biophys Acta 2013;1833(10):2212-19
16. Merk D, Steinhilber D, Schubert-Zsilavecz M. Medicinal chemistry of farnesoid X receptor ligands: from agonists and antagonists to modulators. Future Med Chem 2012;4(8):1015-36
17. Pellicciari R, Fiorucci S, Camaioni E, et al. 6alpha-ethyl-chenodeoxycholic acid (6-ECDCA): a potent and selective FXR agonist endowed with anticholestatic activity. J Med Chem 2002;45(17):3569-72

• **Discovery and in vitro characterization of 6-ECDCA – the farthest developed FXR ligand in clinical trials.**

18. Maloney PR, Parks DJ, Haffner CD, et al. Identification of a chemical tool for

the orphan nuclear receptor FXR. J Med Chem 2000;43(16):2971-4

- **Discovery and in vitro characterization of GW4064.**

19. Downes M, Verdecia MA, Roecker AJ, et al. A chemical, genetic, and structural analysis of the nuclear bile acid receptor FXR. Mol Cell 2003;11(4):1079-92
20. Tsai C, Liang J, Lin H. Sesquiterpenoids from Atractylodes macrocephala act as farnesoid X receptor and progesterone receptor modulators. Bioorgan Med Chem Lett 2012;22(6):2326-9
21. Lundquist JT, Harnish DC, Kim CY, et al. Improvement of physiochemical properties of the tetrahydroazepinoindole series of Farnesoid X Receptor (FXR) agonists: beneficial modulation of lipids in primates. J Med Chem 2010;53(4):1774-87
22. Mehlmann JF, Crawley ML, Lundquist JT, et al. Pyrrole[2,3-d] azepino compounds as agonists of the farnesoid X receptor (FXR). Bioorgan Med Chem Lett 2009;19(18):5289-92

- **Describes a reporter gene assay for FXR in stably transfected cells.**

23. Ginzinger DG. Gene quantification using real-time quantitative PCR: an emerging technology hits the mainstream. Exp Hematol 2002;30(6):503-12
24. Bustin SA. Quantification of mRNA using real-time reverse transcription PCR (RT-PCR): trends and problems. J Mol Endocrinol 2002;29(1):23-39
25. Putra MY, Bavestrello G, Cerrano C, et al. Polyhydroxylated sterols from the Indonesian soft coral Sinularia sp. and their effect on farnesoid X-activated receptor. Steroids 2012;77(5):433-40
26. Renga B, Mencarelli A, D'Amore C, et al. Discovery that theonellasterol a marine sponge sterol is a highly selective FXR antagonist that protects against liver injury in cholestasis. PLoS One 2012;7(1):e30443
27. Schuster D, Markt P, Grienke U, et al. Pharmacophore-based discovery of FXR agonists. Part I: model development and experimental validation. Bioorgan Med Chem 2011;19(23):7168-80
28. Marinozzi M, Carotti A, Sansone E, et al. Pyrazole[3,4-e][1,4]thiazepin-7-one derivatives as a novel class of Farnesoid X Receptor (FXR) agonists. Bioorgan Med Chem 2012;20(11):3429-45
29. Sepe V, Bifulco G, Renga B, et al. Discovery of sulfated sterols from marine invertebrates as a new class of marine natural antagonists of Farnesoid-X-Receptor. J Med Chem 2011;54(5):1314-20
30. Gioiello A, Macchiarulo A, Carotti A, et al. Extending SAR of bile acids as FXR ligands: Discovery of 23-N-(carbocinnamyloxy)-3α,7α-dihydroxy-6α-ethyl-24-nor-5β-cholan-23-amine. Bioorgan Med Chem 2011;19(8):2650-8
31. Rizzo G, Passeri D, de Franco F, et al. Functional characterization of the semisynthetic bile acid derivative INT-767, a dual Farnesoid X Receptor and TGR5 agonist. Mol Pharmacol 2010;78(4):617-30
32. de Marino S, Ummarino R, D'Auria MV, et al. 4-Methylenesterols from Theonella swinhoei sponge are natural pregnane-X-receptor agonists and farnesoid-X-receptor antagonists that modulate innate immunity. Steroids 2012;77(5):484-95

- **Contains exemplary information on qPCR experiments.**

33. Di Leva FS, Festa C, D'Amore C, et al. Binding mechanism of the Farnesoid X Receptor marine antagonist suvanine reveals a strategy to forestall drug modulation on nuclear receptors. design, synthesis, and biological evaluation of novel ligands. J Med Chem 2013;56(11):4701-17
34. de Marino S, Ummarino R, D'Auria MV, et al. Theonellasterols and conicasterols from theonella swinhoei. novel marine natural ligands for human nuclear receptors. J Med Chem 2011;54(8):3065-75
35. Grienke U, Mihály-Bison J, Schuster D, et al. Pharmacophore-based discovery of FXR-agonists. Part II: identification of bioactive triterpenes from Ganoderma lucidum. Bioorgan Med Chem 2011;19(22):6779-91
36. Iguchi Y, Kihira K, Nishimaki-Mogami T, Une M. Structure–activity relationship of bile alcohols as human farnesoid X receptor agonist. Steroids 2010;75(1):95-100
37. Hohng S, Lee S, Lee J, Jo MH. Maximizing information content of single-molecule FRET experiments: multi-color FRET and FRET combined with force or torque. Chem Soc Rev 2014; Epub ahead of print
38. Li G, Lin W, Araya JJ, et al. A tea catechin, epigallocatechin-3-gallate, is a unique modulator of the farnesoid X receptor. Toxicol Appl Pharmacol 2012;258(2):268-74
39. Akwabi-Ameyaw A, Bass JY, Caldwell RD, et al. Conformationally constrained farnesoid X receptor (FXR) agonists: naphthoic acid-based analogs of GW 4064. Bioorgan Med Chem Lett 2008;18(15):4339-43
40. Akwabi-Ameyaw A, Bass JY, Caldwell RD, et al. FXR agonist activity of conformationally constrained analogs of GW 4064. Bioorgan Med Chem Lett 2009;19(16):4733-9
41. Bass JY, Caldwell RD, Caravella JA, et al. Substituted isoxazole analogs of farnesoid X receptor (FXR) agonist GW4064. Bioorgan Med Chem Lett 2009;19(11):2969-73
42. Bass JY, Caravella JA, Chen L, et al. Conformationally constrained farnesoid X receptor (FXR) agonists: heteroaryl replacements of the naphthalene. Bioorgan Med Chem Lett 2011;21(4):1206-13
43. Abel U, Schlüter T, Schulz A, et al. Synthesis and pharmacological validation of a novel series of non-steroidal FXR agonists. Bioorgan Med Chem Lett 2010;20(16):4911-17
44. Urizar NL, A. natural product that lowers cholesterol as an antagonist ligand for FXR. Science 2002;296(5573):1703-6
45. Huang H, Yu Y, Gao Z. et al. Discovery and optimization of 1,3,4-trisubstituted-pyrazolone derivatives as novel, potent, and nonsteroidal Farnesoid X Receptor (FXR) selective antagonists. J Med Chem 2012;55(16):7037-53
46. Marinozzi M, Carotti A, Sardella R, et al. Asymmetric synthesis of the four diastereoisomers of a novel non-steroidal farnesoid X receptor (FXR) agonist: role of the chirality on the biological activity. Bioorgan Med Chem 2013;21(13):3780-9
47. Patching SG. Surface plasmon resonance spectroscopy for characterisation of membrane protein-ligand interactions and its potential for drug discovery. Biochim Biophys Acta 2013;

doi: 10.1016/j.bbamem.2013.04.028; Epub ahead of print

48. Choi H, Hwang H, Chin J, et al. Tuberatolides, potent FXR antagonists from the korean marine tunicate botryllus tuberatus. J Nat Prod 2011;74(1):90-4

• **Describes SPR experiments with FXR.**

49. Richter HG, Benson GM, Blum D, et al. Discovery of novel and orally active FXR agonists for the potential treatment of dyslipidemia & diabetes. Bioorgan Med Chem Lett 2011;21(1):191-4

50. Richter HG, Benson G, Bleicher K, et al. Optimization of a novel class of benzimidazole-based farnesoid X receptor (FXR) agonists to improve physicochemical and ADME properties. Bioorgan Med Chem Lett 2011;21(4):1134-40

51. Nichols JS, Parks DJ, Consler TG, Blanchard SG. Development of a scintillation proximity assay for peroxisome proliferator-activated receptor gamma ligand binding domain. Anal Biochem 1998;257(2):112-19

52. Han K, Kim JH, Kim K, et al. Identification of farnesoid X receptor modulators by a fluorescence polarization-based interaction assay. Anal Biochem 2010;398(2):185-90

• **Describes a fluorescence polarization-based FXR binding assay.**

53. Yu DD, Lin W, Chen T, Forman BM. Development of time resolved fluorescence resonance energy transfer-based assay for FXR antagonist discovery. Bioorgan Med Chem 2013;21(14):4266-78

• **Development of a FRET-based binding assay with a labeled FXR ligand.**

54. Kemper JK, Xiao Z, Ponugoti B, et al. FXR acetylation is normally dynamically regulated by p300 and SIRT1 but constitutively elevated in metabolic disease states. Cell Metab 2009;10(5):392-404

55. Kemper JK. Regulation of FXR transcriptional activity in health and disease: emerging roles of FXR cofactors and post-translational modifications. Biochim Biophys Acta BBAMol Basis Dis 2011;1812(8):842-50

•• **Reviews post-translational modifications of FXR.**

56. Gineste R, Sirvent A, Paumelle R, et al. Phosphorylation of farnesoid X receptor by protein kinase c promotes its transcriptional activity. Mol Endocrinol 2008;22(11):2433-47

57. Choi JH, Banks AS, Kamenecka TM, et al. Antidiabetic actions of a non-agonist PPARγ ligand blocking Cdk5-mediated phosphorylation. Nature 2011;477(7365):477-81

58. Sepe V, Ummarino R, D'Auria M, et al. Preliminary structure-activity relationship on theonellasterol, a new chemotype of FXR antagonist, from the marine sponge theonella swinhoei. Mar Drugs 2012;10(12):2448-66

59. Lin H. Identification of liver X receptor and farnesoid X receptor dual agonists from Tithonia diversifolia. Med Chem Res 2013;22(7):3270-81

60. Suzuki T, Nishimaki-Mogami T, Kawai H, et al. Screening of novel nuclear receptor agonists by a convenient reporter gene assay system using green fluorescent protein derivatives. Phytomedicine 2006;13(6):401-11

61. Flatt B, Martin R, Wang T, et al. Discovery of XL335 (WAY-362450): a highly potent, selective, and orally active agonist of the Farnesoid X Receptor (FXR). J Med Chem 2009;52(4):904-7

62. Feng S, Yang M, Zhang Z, et al. Identification of an N-oxide pyridine GW4064 analog as a potent FXR agonist. Bioorgan Med Chem Lett 2009;19(9):2595-8

63. Soisson SM, Parthasarathy G, Adams AD, et al. Identification of a potent synthetic FXR agonist with an unexpected mode of binding and activation. Proc Natl Acad Sci USA 2008;105(14):5337-42

Affiliation

Daniel Merk†, Dieter Steinhilber & Manfred Schubert-Zsilavecz
†Author for correspondence
Goethe-University Frankfurt, Institute of Pharmaceutical Chemistry, Max-von-Laue-Str. 9, D-60438 Frankfurt am Main, Germany
E-mail: merk@pharmchem.uni-frankfurt.de

Bioorganic & Medicinal Chemistry 22 (2014) 2447–2460

Contents lists available at ScienceDirect

Bioorganic & Medicinal Chemistry

journal homepage: www.elsevier.com/locate/bmc

Anthranilic acid derivatives as novel ligands for farnesoid X receptor (FXR)

Daniel Merk [a,*], Matthias Gabler [a], Roberto Carrasco Gomez [a,b], Daniel Flesch [a], Thomas Hanke [a], Astrid Kaiser [a], Christina Lamers [a], Oliver Werz [c], Gisbert Schneider [b], Manfred Schubert-Zsilavecz [a]

[a] Institute of Pharmaceutical Chemistry, Goethe-University Frankfurt, Max-von-Laue-Str. 9, D-60438 Frankfurt am Main, Germany
[b] Institute of Pharmaceutical Sciences, ETH Zürich, Wolfgang-Pauli-Str. 10, CH-8093 Zürich, Switzerland
[c] Institute of Pharmacy, University of Jena, Philosophenweg 14, 07743 Jena, Germany

ARTICLE INFO

Article history:
Received 4 December 2013
Revised 24 February 2014
Accepted 28 February 2014
Available online 15 March 2014

Keywords:
Metabolic disorder
Glucose homeostasis
Farnesoid X receptor
Nuclear receptor
Bile acids

ABSTRACT

Nuclear farnesoid X receptor (FXR) has important physiological roles in various metabolic pathways including bile acid, cholesterol and glucose homeostasis. The clinical use of known synthetic non-steroidal FXR ligands is restricted due to toxicity or poor bioavailability. Here we report the development, synthesis, in vitro activity and structure–activity relationship (SAR) of anthranilic acid derivatives as novel FXR ligands. Starting from a virtual screening hit we optimized the scaffold to a series of potent partial FXR agonists with appealing drug-like properties. The most potent derivative exhibited an EC_{50} value of 1.5 ± 0.2 μM and 37 ± 2% maximum relative FXR activation. We investigated its SAR regarding polar interactions with the receptor by generating derivatives and computational docking.

1. Introduction

The ligand-activated transcription factor farnesoid X receptor (FXR) is a member of the nuclear receptor superfamily. It is predominantly expressed in liver, intestine and kidney and binds to specific DNA response elements as monomer or as a heterodimer with the retinoid X receptor (RXR). When physiologically activated by bile acids such as chenodeoxycholic acid (CDCA, 1a) FXR regulates a large number of target genes affecting metabolism and homeostasis of bile acids, lipids and glucose.[1,2]

Several pathophysiological conditions have been discovered in which FXR is involved. Both in vitro and in vivo models suggest a possible use of FXR ligands for treatment of metabolic[3–6] and inflammatory[7–11] diseases as well as a role of FXR in the development and growth of certain cancer cells.[12] FXR ligands might be beneficial for the treatment of primary biliary cirrhosis (PBC), diabetes, dyslipidemia, cancer and other disorders.[2]

Intensive research on FXR ligands has yielded several potent steroidal and non-steroidal compounds (reviewed in Ref. [13]). CDCA (**1a**) is the most potent bile acid physiologically activating FXR. Medicinal chemistry efforts have optimized **1a** to obtain 6-ethyl-CDCA[14] (INT-747, **1b**) and **1c**[15] which contains an elongated side chain in addition to the 6α-ethyl moiety. Among the non-steroidal FXR agonists GW4064[16] (**2**) and its derivatives are most potent so far.

Compounds **1b**, **1c** and **2** constitute full FXR agonists with low nanomolar EC_{50} values. Compound **1b** was effective in a co-activator recruitment assay (EC_{50} = 99 nM) and a reporter gene assay (EC_{50} = 85 nM). Compound **1c** is characterized as very potent FXR agonist with an EC_{50} value of 15 nM (290% of 20 μM CDCA) in a co-activator recruitment assay.[15] GW4064 (**2**) showed low nanomolar EC_{50} values in co-activator recruitment (15 nM and 37 nM respectively) and a binding affinity of 64 nM in a scintillation proximity assay (SPA) while its EC_{50} value in reporter gene assays was higher with around 0.9 μM (reviewed in Ref. 17).

However, several of the existing non-steroidal FXR agonists either do not possess acceptable bioavailability, are non-selective or exhibit toxicity.[13,18–21] Consequently their clinical utility is limited and novel FXR ligands are required. So far the only FXR agonists in clinical development are **1b**,[14] which has reached phase IIb (NCT01265498) for the treatment of non-alcoholic

Abbreviations: SAR, structure–activity-relationship; FXR, farnesoid X receptor; RXR, retinoid X receptor; DMEM, Dulbecco's modified eagle medium; FCS, fetal calf serum; DMSO, dimethyl sulfoxide; NAFLD, non-alcoholic fatty liver disease; PBC, primary biliary cirrhosis; PCC, pyridinium chlorochromate; SP, sodium pyruvate; PS, penicillin/streptomycin; RLU, relative light units; AF2, activation function 2.

* Corresponding author. Tel.: +49 6979829806.
E-mail address: merk@pharmchem.uni-frankfurt.de (D. Merk).

http://dx.doi.org/10.1016/j.bmc.2014.02.053
0968-0896/

steatohepatitis (NASH), and primary biliary cirrhosis (PBC) as well as a derivative of **2** that has recently entered early clinical development (NCT01899703). Compound **1b** was also investigated in a phase II trial (NCT00501592) in patients with type **2** diabetes and non-alcoholic fatty liver disease (NAFLD) where it showed promising results on insulin sensitivity and liver fibrosis and was generally well tolerated.[22] Hence, INT-747 (**1b**) appears to be effective and non-toxic and may be the first marketed FXR-targeting drug (for preclinical and clinical data see Ref. 5). As a general consideration, it is however questionable whether full agonism on FXR may actually be beneficial for all conditions that might be treatable by FXR ligands. In vivo data indicates that full agonism is not crucial for in vivo efficacy[23] and may even have undesirable effects.[24] Therefore our approach was to develop novel FXR ligands that only partially and moderately activate this nuclear receptor.

Virtual screening of a compound collection using an in silico model of FXR[25] yielded several hits with low potency that were confirmed in our cell-based FXR full-length transactivation assay. We selected one of these hits, the anthranilic acid derivative **3** (Fig. 1), for optimization by medicinal chemistry and automated computational docking studies. The optimization yielded a set of FXR agonists with considerable in vitro potency in the FXR transactivation assay and favorable physicochemical properties. Here we describe the synthesis, SAR and in vitro pharmacology of anthranilic acid derivatives as FXR ligands.

2. Results

Lead structure **3** possesses partial agonistic activity at FXR with 11% activity at 30 μM in a cell-based FXR full-length transactivation assay compared to the activity of **2** (3 μM, 100%).

An initial docking analysis of **3** (Fig. 2) indicated that the butyric acid side chain might be suitable for FXR activation and placed the acidic head group near Arg_{268} and Arg_{335}. Docking also suggested that enlargement of the lipophilic acyl substituent (4-methylbenzoyl moiety in **3**) might improve binding to FXR since the relatively small 4-methylbenzoyl residue did not fill the large lipophilic pocket. Therefore our optimization study started with a variation of the lipophilic acyl substituent.

2.1. Chemistry

Anthranilic acid derivatives were generated in a two-step synthesis using isatoic anhydride (**4a**) as origin of the anthranilic acid core. Compound **4a** was reacted with various amino acids (**5a**, **c**–**h**) and ester **5b** to introduce the acidic side chains by nucleophilic substitution (Scheme 1). To improve the yield of the required *o*-aminobenzoyl derivatives **6a**–**i** 4-(dimethylamino)pyridine (**7**) served as catalyst with an amount of 10 mol%, as described by Venuti.[26] We optimized the reaction by varying solvent, reaction time and temperature (Supporting information Table 1). The highest yield was achieved with a mixture of pyridine/DMF/NEt_3 at 80 °C over 16 h. With aliphatic amino acids as nucleophiles, the optimized conditions lead to yields of around 72%.

Anthranilic acid derivatives **6a**–**j** were subsequently reacted with suitable acyl chlorides (**8a**–**p**) to introduce the mostly lipophilic acyl substituents of the test compounds **15a**–**p**, **16**–**24** (Supporting information Scheme 1).

To investigate the necessity of the amide hydrogens in the anthranilic acid core for interaction with FXR, monomethylated derivatives **23** and **24** were generated with the same synthetic strategy using either *N*-methyl isatoic anhydride (**4b**) or 4-(methylamino)butyric acid (**5i**) as methylated starting material

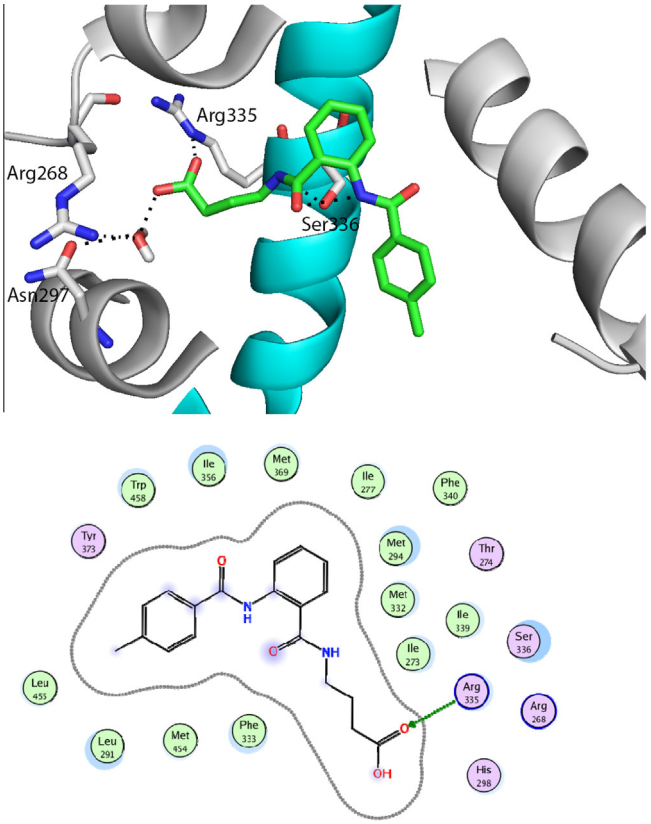

Figure 2. Docking analysis of lead structure **3**.

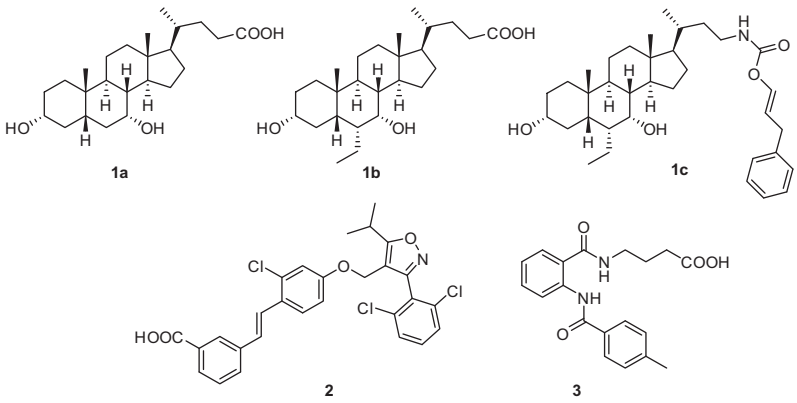

Figure 1. Important FXR ligands CDCA (**1a**) 6-ECDCA (**1b**) and GW4064 (**2**), and lead structure **3**.

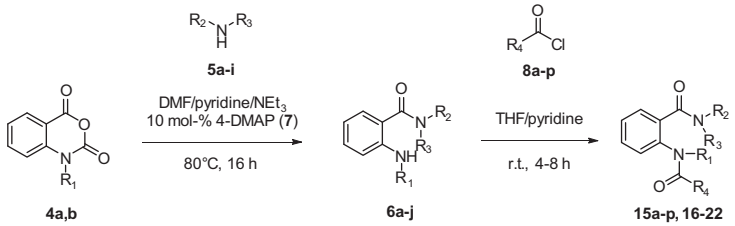

Scheme 1. General synthetic procedure: *Ortho*-aminobenzoylation of amino acids **5a**–**i** with isatoic anhydride derivatives **4a** and **b** and acylation with acyl chlorides **8a**–**p**.

(Scheme 2). We also examined the requirement of the amide carbonyl groups for interaction with the receptor by replacing the amides with a sulfonic amide (**25**) or secondary amines (**26**, and **27**). Sulfonic amide **25** was synthetized using sulfonic acid chloride **9** instead of an acyl chloride (Supporting information Scheme 2).

Secondary amine **26** was generated by reductive amination using 2-naphthaldehyde **10** and anthranilic acid derivative **6a** (Scheme 2).

For the preparation of amine **27** a different synthetic strategy was required. The secondary amine of the acidic side chain had to be introduced in the last step since it would exhibit higher nucleophilicity than the aromatic amine of the anthranilic acid core, which was supposed to react with an acyl chloride. For the generation of **27** 2-aminobenzyl alcohol (**11**) was therefore used as starting material, which we selectively oxidized to 2-aminobenzaldehyde (**12**) using pyridinium chlorochromate (PCC, **13**). **12** subsequently reacted with acyl chloride **8j** to form aldehyde **14** which was then suitable for a reductive amination with 4-aminobutyric acid (**5a**) yielding amine **27** (Scheme 3).

2.2. Biological evaluation

FXR activation by the described compounds was tested in a HeLa cell-based full-length FXR transactivation assay with a firefly luciferase as reporter gene and a constitutively expressed renilla luciferase as control. Maximal relative FXR activation of the compounds refers to the activity of GW4064 (**2**) at 3 μM, which we defined as 100%.

In the first structural optimization study the acyl substituent in the lipophilic backbone of the anthranilic acid derivatives was varied (**15a**–**p**, Table 1). The more polar 3,5-dinitrobenzoyl derivative **15a** showed no activity at FXR as well as **15b** with a 4-methoxybenzoyl moiety, all biphenyl derivatives (**15e**–**g**) and the highly lipophilic and sterically demanding diphenylacetyl (**15l**) and diphenylpropanoyl (**15m**) derivatives. Introduction of an aromatic heterocycle as lipophilic substituent in **15h** and **15i** also led to lack of activity.

A 2-naphthoyl moiety (**15j**) as lipophilic substituent produced partial FXR transactivation of 37 ± 2% with an EC_{50} value of 8.6 ± 1.3 μM. Interestingly, both its 1-naphthoyl (**15k**) and 2-naphthylacetyl (**15p**) derivatives were inactive.

Lower EC_{50} values with reduced partial transactivation of FXR were measured for the 4-ethylbenzoyl (**15c**) and the 4-*t*-butylbenzoyl moiety (**15d**). Compound **15c** exhibited partial FXR activation of 28 ± 2% with an EC_{50} value of 5.8 ± 1.0 μM while **15d** activated FXR to an extent of 19 ± 1% with EC_{50} = 2.5 ± 0.4 μM.

The lowest EC_{50} value of 0.72 ± 0.01 μM within this series was observed for cinnamoyl derivative **15n** combined with a FXR transactivation of 12.39 ± 0.02%. The saturated dihydrocinnamoyl derivative **15o** was inactive.

After optimization of the acyl substituent, the acidic head group was varied (**16**–**22**, Table 1). For this SAR investigation the 2-naphthoyl moiety of **15j** was selected as lipophilic substituent since it produced the highest relative FXR activation although **15j** had the poorest EC_{50} value among the series **15c**, **15d**, **15j** and **15n**. The higher relative FXR activation of **15j** is preferred since in a cell-based assay there is the risk of false-negatives when the relative activation is too low.

The methyl ester **16** of **15j** turned out to be still active with a comparable EC_{50} value but led to lower maximum relative activation of 19.0 ± 0.6%. Elongation of the acidic side chain from C4 (**15j**) over C5 (**17**) to C6 (**18**) led to a moderate improvement in the EC_{50} value with 8.3 ± 1.0 μM for **17** and 4.4 ± 0.6 μM for **18** but at the same time the relative activation considerably dropped to 11.4 ± 0.4% and 10.4 ± 0.4%, respectively.

Introduction of aromatic moieties in the acidic head group improved the EC_{50} value compared to **15j**. Within the series of aromatic carboxylic acids, the *p*-benzoic acid derivative **19** showed the best EC_{50} value of 1.0 ± 0.2 μM with 23 ± 1% maximum relative FXR activation. The *m*-benzoic acid derivative **20** relatively activated FXR to an extent of 37 ± 1% with a slightly higher EC_{50} value of 1.5 ± 0.2 μM. Compound **21** with an additional methylene group between aromatic ring and carboxylic acid and phenylacetic acid derivative **22** yielded EC_{50} values in the same range with 1.3 ± 0.1 μM for **21** and 3.1 ± 0.3 μM for **22** but their maximum relative FXR activation activities were lower (10.02 ± 0.04% for **21** and 9.8 ± 0.4% for **22**).

Then we blocked selected polar functions in compounds **23**–**27** to investigate hypothetical interactions of the anthranilic acid derivatives with the FXR ligand binding site (**23**–**27**, Table 2). For this purpose amide nitrogen atoms were methylated (**23** and **24**) and amides were reduced to secondary amines (**26** and **27**). In addition, sulfonic amide **25** was investigated which has a different acidity and geometry than the respective amide **15j**.

All derivatives **23**–**27** were inactive up to concentrations of 30 μM suggesting that the polar functions and the geometry of the anthranilic acid core might be important for ligand-FXR interaction.

Compounds **15j** and **20** turned out as the most potent derivatives. Therefore we investigated their activity on common *off*-targets and physicochemical properties. Since anthranilic acid derivatives such as the NSAIDs mefenamic acid and flufenamic acid are known to interact with the arachidonic acid cascade we studied **15j** on several enzymes of this pathway. The compound did not inhibit cyclooxygenases I and II, 5-lipoxygenase and mPGES-1 up to a concentration of 10 μM. Additionally, **15j** and **20** were soluble in various solvents including water at alkaline pH. For both compounds **15j** an **20** no toxic effects occurred in the HeLa cell based reporter gene assay up to the highest used concentration of 60 μM. In a cell proliferation assay (WST-1) in HepG2 cells **15j** showed no significant toxicity up to 100 μM while **20** slightly inhibited proliferation starting from 30 μM which increased with higher concentrations (60 μM and 100 μM; for values see experimental section). **15j** and **20** furthermore passed computational tests on ADME and toxicological properties (FAF*Drugs*2,[27] standard algorithms) which confirms the drug-likeness of the compounds and indicates that no known toxic pharmacophores are included. With the optimization of **15j** yielding **20** ligand efficiency (LE)

Table 1
In vitro activities of compounds **15a–p** and **16–22**

#	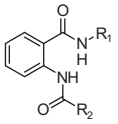		**EC_{50}** [μM] (max. rel activation [%])
	R_1	R_2	
3	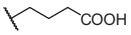		11% at 30 μM
15a	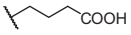	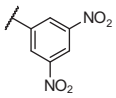	i.a. at 30 μM
15b	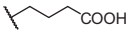	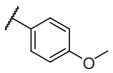	i.a. at 3 μM*
15c	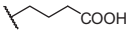	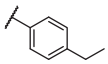	**5.8 ± 1.0** (28 ± 2)
15d	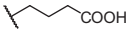	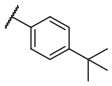	**2.5 ± 0.4** (19 ± 1)
15e	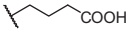	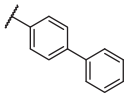	i.a. at 3 μM*
15f	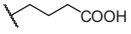	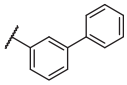	i.a. at 30 μM
15g	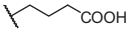	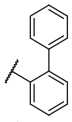	i.a. at 30 μM
15h	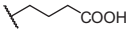		i.a. at 30 μM
15i	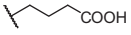		i.a. at 3 μM*
15j	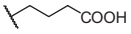	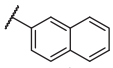	**8.6 ± 1.3** (37 ± 2)
15k	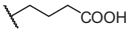		i.a. at 30 μM
15l	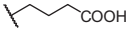	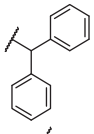	i.a. at 3 μM*
15m	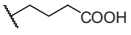	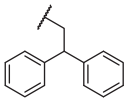	i.a. at 30 μM
15n	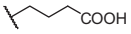	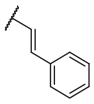	**0.72 ± 0.01** (12.39 ± 0.02)
15o	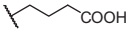	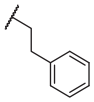	i.a. at 30 μM
15p	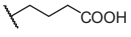	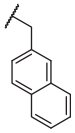	i.a. at 30 μM
16	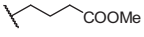	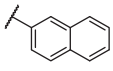	**7.1 ± 0.6** (19.0 ± 0.6)

Table 1 (*continued*)

#	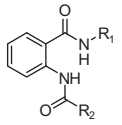		**EC$_{50}$** [μM] (max. rel activation [%])
	R_1	R_2	
17	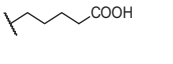	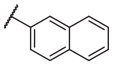	**8.3 ± 1.0** (11.4 ± 0.4)
18	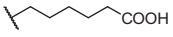	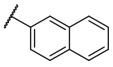	**4.4 ± 0.6** (10.4 ± 0.4)
19	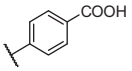	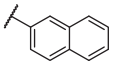	**1.0 ± 0.2** (23 ± 1)
20	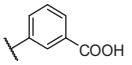	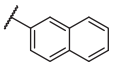	**1.5 ± 0.2** (37 ± 1)
21	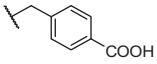	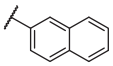	**1.3 ± 0.1** (10.02 ± 0.04)
22	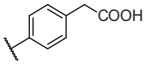	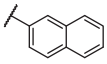	**3.1 ± 0.3** (9.8 ± 0.4)

Values are expressed as mean ± SEM. n = 3–6. i.a. inactive.

* Compounds **15b**, **15e**, **15i**, **15l** showed toxicity at concentrations ⩾10 μM. Therefore no statistically significant relative FXR activation at higher concentrations could be determined.

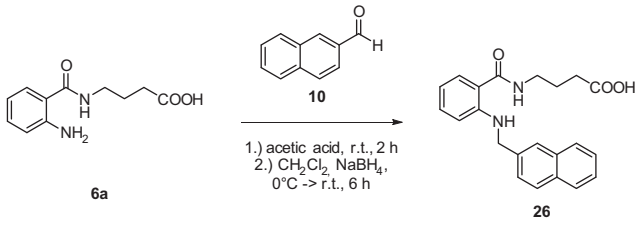

Scheme 2. Synthesis of amine **26** from anthranilic acid derivative **6a** and aldehyde **10** by reductive amination.

and size independent ligand efficiency (SILE) were slightly improved (**15j**: LE = 0.25; SILE = 1.87; **20**: LE = 0.26; SILE = 2.08). We also determined the aqueous solubility of **15j** and **20** and investigated their metabolic stability by incubation with liver microsomes of Sprague–Dawley rats. For **15j** an aqueous solubility of 45 mg/L was measured and the compound was highly stable against metabolic degradation by liver microsomes with 92 ± 2% of **15j** being detectable after 60 min. Compound **20** showed an aqueous solubility of 0.3 mg/L and moderate metabolic stability. After 60 min incubation with liver microsomes 61 ± 2% of the compound were detectable. (Fig. 3)

2.3. Receptor-ligand docking

Docking (Fig. 4A) of **15j** into the ligand binding site of FXR (model derived from PDB ID: 3OLF,[23] full agonist conformation) suggested prominent polar interactions between the carboxylic acid head group and Arg_{335} in activation function 2 (AF2) as well as Arg_{268}.

In the model, three water molecules were found to participate in this cluster of interactions. A further polar interaction was formed between the benzamide nitrogen and Ser_{336}, and an

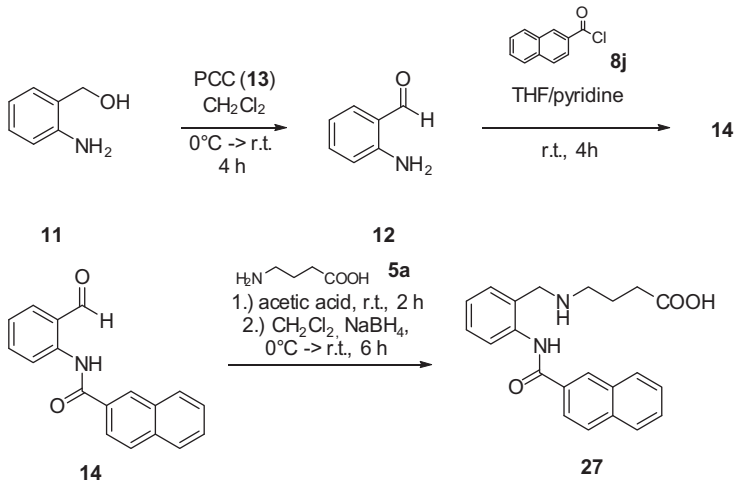

Scheme 3. Synthesis of amine **27**. Alcohol **11** was oxidized to aldehyde **12** which was acylated with **8j** to yield **14**. Compound **27** was generated from **14** and **5a** by reductive amination.

Table 2
In vitro activities of compounds **23–27**

#	R_1	R_2	X	Y	**EC_{50}** [μM] (max. rel activation [%])
15j	H	H	C=O	C=O	**8.6 ± 1.3** (37 ± 2)
23	CH_3	H	C=O	C=O	i.a. at 30 μM
24	H	CH_3	C=O	C=O	i.a. at 30 μM
25	H	H	C=O	SO_2	i.a. at 30 μM
26	H	H	C=O	CH_2	i.a. at 30 μM
27	H	H	CH_2	C=O	i.a. at 30 μM

Values are mean ± SEM. n = 3–6. i.a. inactive.

intramolecular hydrogen bridge between benzamide carbonyl oxygen and the second amide nitrogen. The lipophilic 2-naphthoyl substituent was buried in a deep apolar pocket lined by Ile_{277}, Leu_{291}, Ile_{356}, Ile_{361} and Trp_{458}.

Compound **20** showed a similar binding pose in the docking experiment (Fig. 4B) with the exception that the interaction with Ser_{336} was not visible. Additionally, its lipophilic tail was placed deeper into the hydrophobic subpocket (Fig. 4).

Cinnamoyl derivative **15n** had a similar docking pose (Fig. 4C) as **15j** with the cinnamic amide residue placed in the same pocket as the 2-naphthoyl moiety. Docking revealed no additional interactions that could explain the significant difference in the activities of **15n** and **15j** but shows Ser_{336} and Tyr_{373} in a range of 3.9 and 4.6 Å around the double bond of **15n**.

Compared to the binding mode of GW4064 (**2**) in its co-crystal structure (Fig. 4D) on which the docking analysis is based, the docking suggests a similar polar interaction of the acidic head groups of compounds **3**, **15j**, **15n** and **20** with Arg_{335} as it is present in the co-crystal structure of **2**. Additionally the lipophilic tails were placed in the same pocket as the dichlorobenzene moiety of GW4064 (**2**). However, there is no polar interaction between Ser_{336} and GW4064 (**2**) that is comparable to the interaction of the benzamide nitrogen of **15j** with Ser_{336} in the docking.

The Gibbs energies of the docking poses were −6.9 J/mol for **3**, −7.1 J/mol for **15j**, −8.1 J/mol for **20** and −21.6 J/mol for **15n** which is in congruence with the rank order of potency of the compounds concerning their EC_{50} values.

Our initial docking study suggested additional space for larger lipophilic substituents might be available in the hydrophobic subpocket where the 4-methylbenzoyl moiety of lead structure **3** was placed automatically. This hypothesis was not confirmed since large rigid substituents such as biphenyl residues are not tolerated. The compounds' rank order according to potency and the beneficial introduction of an aromatic moiety in the acidic head group however, are in agreement with the docking model.

3. Discussion

To explore the SAR of anthranilic acid derivatives derived from **3** as FXR ligands we varied the two substituents of the anthranilic acid core. First we investigated the acyl substituent at the aniline nitrogen. By replacing the 4-methylbenzoyl moiety of **3** with more polar (**15a** and **15b**) or small heteroaromatic substituents such as thiophene (**15i**) or pyridine (**15h**) activity was lost. Similarly, all large and rigid biphenyl derivatives (**15e–g**) as well as the sterically even more demanding diphenylacetyl (**15l**) and diphenylpropanoyl (**15m**) derivatives were also inactive. In contrast to more polar residues at the aromatic acyl substituent larger lipophilic substituents in the 4-position of the aromatic ring strongly improved the potency of compound **3**. The 4-ethylbenzoyl derivative **15c** and the 4-*t*-butylbenzoyl derivative **15d** showed the desired moderate FXR transactivation at low micromolar concentrations. Introduction of a cinnamoyl moiety in **15n** lead to a favorable EC_{50} value but the maximum relative FXR activation turned out to be low with ~12%. We found the best overall characteristics for further optimization in the 2-naphthoyl derivative **15j** with a low micromolar EC_{50} value, moderate FXR transactivation, lack of toxicity in our cell-based assay and in HepG2 cells, good aqueous solubility and low molecular weight.

The fact that 1-naphthoyl derivative **15k**, 2-naphtylacetyl derivative **15p** and dihydrocinnamoyl derivative **15o** were inactive indicates that the SAR is steep. The results suggest that π-electrons

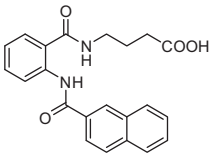

15j

FXR transactivation: EC_{50} = 8.55±1.33 μM (37±2% max.)

molecular weight = 376

H-bond donors: 3; H-bond acceptors: 6

clogP = 3.35, aqueous solubility: 45 mg/L

LE = 0.25; SILE = 1.87

inactive at COX, 5-LO, mPGES-1 up to 10 μM (for details see supporting information)

not toxic up to 60 μM in HeLa and HepG2 cells

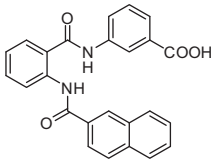

20

FXR transactivation: EC_{50} = 1.54±0.19 μM (37±1% max.)

molecular weight = 410

H-bond donors: 3; H-bond acceptors: 6

clogP = 4.96, aqueous solubility: 0.3 mg/L

LE = 0.26; SILE = 2.08

not toxic up to 60 μM in HeLa cells and up to 30 μM in HepG2 cells

Figure 3. Properties of optimized structures **15j** and **20**.

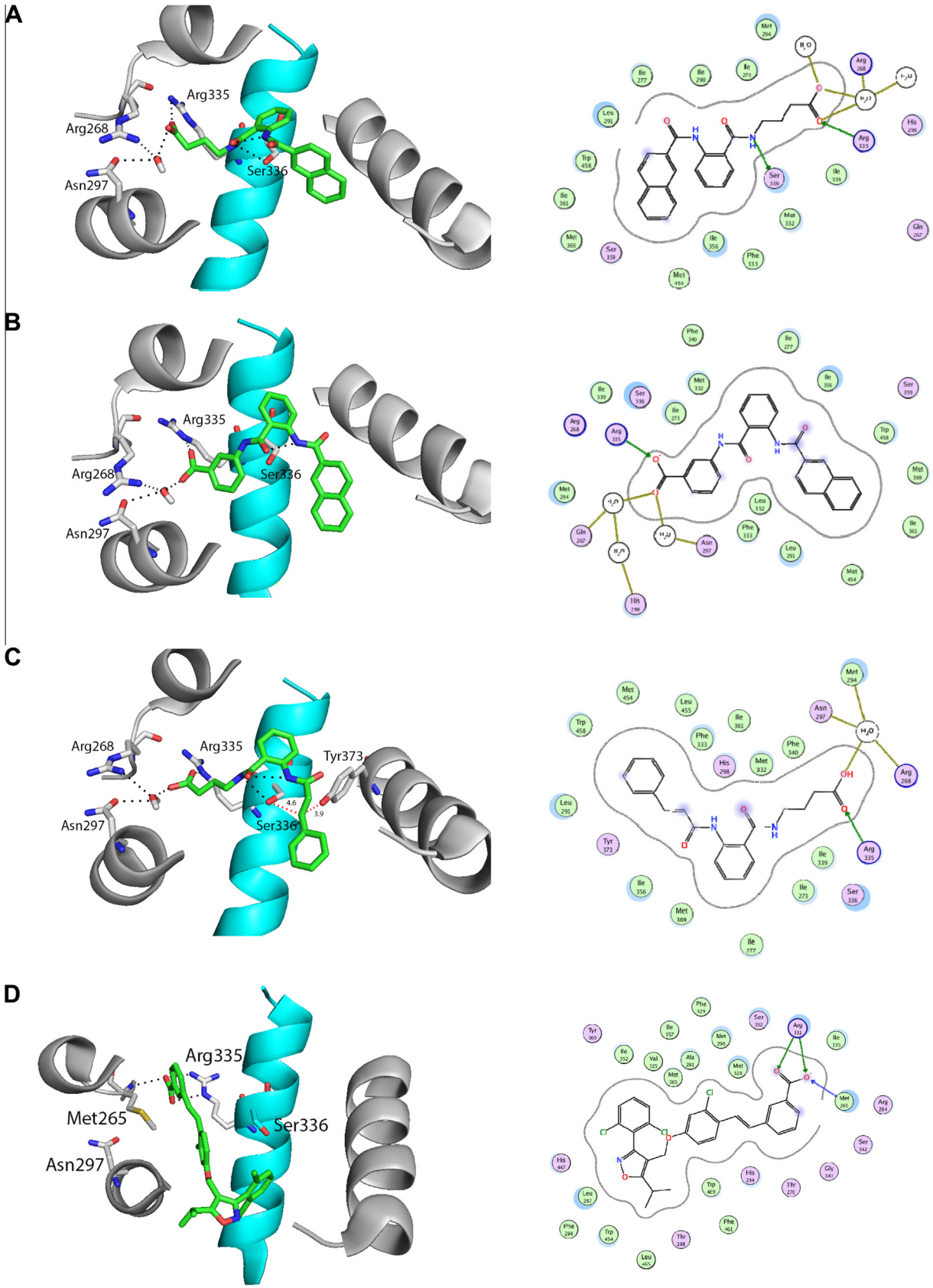

Figure 4. Docking poses of **15j** (A), **20** (B) and **15n** (C) and binding mode of **2** (D) in the co-crystal structure 3OLF[23] on which the docking is based for comparison. Helix 12 (AF2) in blue.

next to the acyl aniline moiety might be necessary since only derivatives with an aromatic moiety or a double bond in conjugation with the amide were active. In accordance with this hypothesis, cinnamoyl derivative **15n** was active while dihydrocinnamoyl derivative **15o** was inactive. Another possible but speculative explanation for the low EC_{50} value of **15n** and the inactivity of the saturated analog **15o** might be a covalent bond to the target. The cinnamoyl moiety of **15n** constitutes a Michael acceptor system that is lost when its double bond is hydrated. It could react with nucleophilic centers within the FXR binding site such as the alcohol functions of serine, threonine and tyrosine or the thiol of a cysteine. Docking analysis of **15n** suggests that Ser_{336} and Tyr_{373} surround the electrophilic Michael acceptor in a range of 3.9 and 4.6 Å. However, the actual possibility of covalent bond formation to FXR has to be further investigated.

For exploration of the SAR of the acidic head group the 2-naphthoyl residue of **15j** was selected as aromatic acyl substituent. With the 2-naphthoyl residue as acyl substituent the aliphatic C_4-side chain of the head group was elongated or replaced by various aromatic carboxylic acids. Elongation of the aliphatic carboxylic acid of **15j** by one (**17**) or two (**18**) carbon atoms improved the EC_{50} value but decreased relative FXR activation. Improvement of the EC_{50} value was also achieved by introduction of an additional aromatic moiety (compounds **19**–**22**). 4-aminobenzoic acid derivative **19** yielded the lowest EC_{50} value with 1.0 ± 0.2 μM, which is an approximately 10-fold improvement over the butyric acid side chain (**15j**). However, at the same time maximal relative FXR activation was diminished to 23 ± 1%. More flexible aromatic head groups with an additional methylene spacer between amide and aromatic ring (**21**) or between aromatic ring and carboxylic acid (**22**) only slightly changed the EC_{50} value (1.3 ± 0.1 μM for **21** and 3.1 ± 0.3 μM for **22**) but further diminished maximal relative FXR activation to ~10%. 3-Aminobenzoic acid derivative **20** showed the best overall characteristics with an EC_{50} of 1.6 ± 0.2 μM and 37 ± 1% maximal relative FXR activation.

We investigated the role of the amides in the anthranilic acid core by selective methylation, which eliminates the possibility to act as hydrogen bridge donors. In addition, the acyl anilide moiety was replaced by a sulfonic amide, which allows polar interactions but features a different geometry and bears strong N–H acidity. Both methylated derivatives **23** and **24** were inactive suggesting that both amide nitrogen functions might contribute to binding to the nuclear receptor via hydrogen bridges. The docking pose of **15j** shows an intramolecular hydrogen bond that includes the hydrogen of the acyl anilide and cannot be formed in compound **24**. Potentially, this interaction is crucial to maintain an appropriate geometry for receptor binding.

4. Conclusion

Our SAR study of anthranilic acid derivatives as FXR agonists revealed that the anthranilic acid core constitutes a promising scaffold for the development of novel FXR ligands. All functional groups of the anthranilic acid moiety seem to be crucial for FXR activation. By replacement or blockade of any of these groups activity was lost. By enlargement of the lipophilic tail as exemplified in compounds **15c**, **d**, **j**, we were able to improve both the EC_{50} value and maximal relative FXR activation. By introduction of an aromatic moiety within the acidic head group the potency was further enhanced. The resulting compound **20** constitutes a potent partial FXR agonist with an EC_{50} value of 1.5 ± 0.2 μM and 37 ± 1% maximal relative FXR activation. Further structural optimization and SAR studies should also tend to improve solubility and metabolic stability of this class of FXR ligands. Compound **20** provides a promising structure for further optimization.

5. Experimental section

General All chemicals and solvents were of reagent grade and used without further purification, unless otherwise specified. ^1H NMR and ^{13}C NMR spectra were measured in DMSO-d_6, on a Bruker AV 500 spectrometer. Chemical shifts are reported in parts per million (ppm) with tetramethylsilane (TMS) as an internal standard. Mass spectra were obtained on a Fisons Instruments VG PlattformII measuring in the positive- or negative-ion mode (ESI-MS system). The purity of the final compounds was determined by combustion analysis, which was performed by the Microanalytical Laboratory of the Institute of Organic Chemistry and Chemical Biology, Goethe-University Frankfurt, on an Elementar Vario Micro Cube. All tested compounds described here have a purity ⩾95%. Intermediates were not analyzed.

Docking simulations were performed using the Molecular Operating Environment (MOE) (Version 2012.10; The Chemical Computing Group, Montreal, Canada). The crystal structure of FXR (PDB ID: 3OLF[23]) was downloaded from the Protein Data Bank (PDB).[23] Prior to ligand docking one monomer of the dimer crystal structure was isolated and the crystallized ligand was removed. Subsequently, the structure was prepared with Protonate 3D and the active site was isolated using MOE Site Finder. The structures were placed in the site with the Triangle Matcher method, and then ranked with the London dG scoring function. For the energy minimization in the pocket MOE Forcefield Refinement was used and ranked with the GBVI/WSA dG scoring function.

5.1. Synthesis

5.1.1. General Procedures

(a) Ortho-aminobenzoylation with isatoic anhydride: Isatoic anhydride derivative (**4a**/**b**, 1.0 equiv) and 4-*N*,*N*-dimethylaminopyridine (**7**, 0.1 equiv) were dissolved in a mixture of pyridine (2 mL/mmol **4a**/**b**) and DMF (0.5 mL/mmol **4a**/**b**) and heated to 80 °C. After a clear brown solution had formed, the respective amine (**5a**–**i**, 1.1 equiv) was added in one portion. With addition of NEt_3 (0.5 mL/mmol **4a**/**b**) the formation of carbon dioxide started. The reaction mixture was kept at 80 °C for 16 h. Then the solvents were evaporated in vacuum and the crude product dissolved in ethyl acetate. The organic phase was washed twice with 10% hydrochloric acid and brine and dried over Na_2SO_4. Further purification was performed by recrystallization or column chromatography on silica.

(b) Acylation of anthranilic acid derivatives: Anthranilic acid derivative (**6a**–**j**, 1.0 equiv) was dissolved in THF (3 mL/mmol **6a**–**j**) and pyridine (3.0 equiv) was added. After a clear solution had formed, the respective acyl chloride (**8a**–**p**, 1.3 equiv) was added in THF (2 mL/mmol **6a**–**j**). The reaction mixture was kept at room temperature for 4–8 h and the reaction progress was monitored by TLC. When anthranilic acid derivative (**6a**–**j**) was consumed, the reaction mixture was diluted with ethyl acetate, washed three times with 10% hydrochloric acid and dried over Na_2SO_4. Further purification was performed by column chromatography on silica.

5.1.1.1. 4-(2-(3,5-Dinitrobenzamido)benzamido)butanoic acid (15a). Preparation according to general procedure b using **6a** and 3,5-dinitrobenzoyl chloride (**8a**). Yield 44.6%. R_f (pentane/ethyl acetate 1:1 + 2% acetic acid) = 0.44. ^1H NMR (500 MHz, DMSO) δ 12.66 (s, 1H), 12.03 (s, 1H), 9.04 (d, J = 2.0 Hz, 2H), 9.03–9.01 (m, 1H), 8.88 (t, J = 5.6 Hz, 1H), 8.40 (dd, J = 8.3, 1.0 Hz, 1H), 7.84 (dd, J = 7.9, 1.4 Hz, 1H), 7.64–7.58 (m, 1H), 7.30 (td, J = 7.7, 1.1 Hz, 1H), 3.32 (s, 2H), 2.29 (t, J = 7.4 Hz, 2H), 1.78 (p,

J = 7.1 Hz, 2H). ^{13}C NMR (125 MHz, DMSO) δ 206.28, 173.77, 167.77, 160.19, 147.80, 137.18, 136.70, 131.29, 127.66, 126.57, 123.42, 120.85, 120.54, 29.79, 29.37, 22.76. $C_{18}H_{16}N_4O_8$. MS (ESI−): m/z 415.2 ((M−H)$^-$, 100). Combustion analysis: measured (calculated): C 51.64 (51.93); H 3.84 (3.87); N 13.25 (13.46).

5.1.1.2. 4-(2-(4-Methoxybenzamido)benzamido)butanoic acid (15b). Preparation according to general procedure b using **6a** and 4-methoxybenzoyl chloride (**8b**). Yield 62.5%. R_f (pentane/ethyl acetate 1:1 + 2% acetic acid) = 0.45. ^{1}H NMR (500 MHz, DMSO) δ 12.50 (s, 1H), 8.93 (s, 1H), 8.65 (d, J = 8.2 Hz, 1H), 7.90 (d, J = 8.7 Hz, 2H), 7.83 (d, J = 7.7 Hz, 1H), 7.55 (t, J = 7.6 Hz, 1H), 7.17 (t, J = 7.6 Hz, 1H), 7.13 (d, J = 8.7 Hz, 2H), 3.85 (s, 3H), 3.32–3.30 (m, 2H), 2.30 (t, J = 7.2 Hz, 2H), 1.78 (p, J = 7.0 Hz, 2H). ^{13}C NMR (125 MHz, DMSO) δ 173.85, 168.25, 163.40, 161.69, 139.00, 131.48, 128.12, 127.46, 125.92, 121.71, 119.28, 119.22, 113.40, 54.30, 29.85, 29.37, 22.83. $C_{19}H_{20}N_2O_5$. MS (ESI+): m/z 379.60 ((M+Na)$^+$, 100). Combustion analysis: measured (calculated): C 63.96 (64.04); H 5.63 (5.66); N 7.63 (7.86).

5.1.1.3. 4-(2-(4-Ethylbenzamido)benzamido)butanoic acid (15c). Preparation according to general procedure b using **6a** and 4-ethylbenzoyl chloride (**8c**). Yield 64.8%. R_f (pentane/ethyl acetate 1:1 + 2% acetic acid) = 0.44. ^{1}H NMR (500 MHz, DMSO) δ 12.53 (s, 1H), 12.10 (s, 1H), 8.89 (t, J = 5.4 Hz, 1H), 8.66 (dd, J = 8.4, 0.9 Hz, 1H), 7.88–7.81 (m, 3H), 7.56 (td, J = 1.3, 7.9 Hz, 1H), 7.42 (d, J = 8.3 Hz, 2H), 7.19 (td, J = 1.2, 7.5 Hz, 1H), 3.33–3.30 (m, 2H), 2.69 (q, J = 7.5 Hz, 2H), 2.31 (t, J = 7.3 Hz, 2H), 1.79 (p, J = 7.1 Hz, 2H), 1.22 (t, J = 7.5 Hz, 3H). ^{13}C NMR (125 MHz, DMSO) δ 173.78, 168.20, 163.83, 147.67, 138.85, 131.49, 131.35, 127.63, 127.47, 126.48, 126.30, 121.88, 119.37, 37.42, 29.75, 26.72, 22.81, 13.85. $C_{20}H_{22}N_2O_4$. MS (ESI−): m/z 353.22 ((M−H)$^-$, 100). Combustion analysis: measured (calculated): C 67.47 (67.78); H 6.04 (6.26); N 7.85 (7.90).

5.1.1.4. 4-(2-(4-(*tert*-Butyl)benzamido)benzamido)butanoic acid (15d). Preparation according to general procedure b using **6a** and 4-*tert*-butylbenzoyl chloride (**8d**). Yield 69.3%. R_f (pentane/ethyl acetate 1:1 + 2% acetic acid) = 0.46. ^{1}H NMR (500 MHz, DMSO) δ 12.55 (s, 1H), 12.09 (s, 1H), 8.92 (t, J = 5.1 Hz, 1H), 8.66 (dd, J = 8.4, 1.0 Hz, 1H), 7.89–7.85 (m, 2H), 7.83 (dd, J = 8.0, 1.4 Hz, 1H), 7.64–7.59 (m, 2H), 7.58–7.53 (m, 1H), 7.19 (td, J = 7.8, 1.2 Hz, 1H), 3.32–3.30 (m, 2H), 2.31 (t, J = 7.3 Hz, 2H), 1.78 (p, J = 7.1 Hz, 2H), 1.32 (s, 9H). ^{13}C NMR (126 MHz, DMSO) δ 174.72, 169.15, 164.82, 155.48, 140.01, 132.68, 132.33, 128.69, 127.28, 126.30, 123.14, 120.55, 39.18, 35.24, 31.58, 31.37, 24.66. $C_{22}H_{26}N_2O_4$. MS (ESI−): m/z 381.24 ((M−H)$^-$, 100). Combustion analysis: measured (calculated): C 68.96 (69.09); H 6.65 (6.85); N 7.12 (7.32).

5.1.1. 5. 4-(2-([1,1′-Biphenyl]-4-carboxamido)benzamido)butanoic acid (15e). Preparation according to general procedure b using **6a** and [1,1′-biphenyl]-4-carbonyl chloride (**8e**). Yield 66.0%. R_f (pentane/ethyl acetate 1:1 + 2% acetic acid) = 0.42. ^{1}H NMR (500 MHz, DMSO) δ 12.65 (s, 1H), 12.11 (s, 1H), 8.93 (t, J = 5.5 Hz, 1H), 8.68 (dd, J = 8.3, 1.1 Hz, 1H), 8.05–8.00 (m, 2H), 7.93–7.88 (m, 2H), 7.85 (ddd, J = 8.0, 3.4, 1.5 Hz, 1H), 7.79–7.76 (m, 2H), 7.61–7.55 (m, 1H), 7.55–7.49 (m, 2H), 7.46–7.41 (m, 1H), 7.25–7.19 (m, 1H), 3.34–3.31 (m, 2H), 2.41 (t, J = 7.4 Hz, 2H), 1.83 (dt, J = 14.2, 7.1 Hz, 2H). ^{13}C NMR (125 MHz, DMSO) δ 172.67, 168.23, 163.52, 142.93, 138.78, 138.26, 132.58, 131.54, 128.37, 127.53, 127.50, 126.88, 126.44, 126.22, 122.05, 119.51, 119.44, 37.31, 29.40, 22.73. $C_{24}H_{22}N_2O_4$. MS (ESI−): m/z 401.2 ((M−H)$^-$, 100). Combustion analysis: measured (calculated): C 71.82 (71.63); H 5.83 (5.51); N 6.56 (6.96).

5.1.1.6. 4-(2-([1,1′-Biphenyl]-3-carboxamido)benzamido)butanoic acid (15f). Preparation according to general procedure b using **6a** and [1,1′-biphenyl]-3-carbonyl chloride (**8f**). Yield 61.4%. R_f (pentane/ethyl acetate 1:1 + 2% acetic acid) = 0.42. ^{1}H NMR (500 MHz, DMSO) δ 12.71 (s, 1H), 9.15 (s, 1H), 8.66 (dd, J = 8.4, 1.0 Hz, 1H), 8.21 (t, J = 1.7 Hz, 1H), 7.92 (dd, J = 10.7, 4.6 Hz, 2H), 7.86 (dd, J = 7.9, 1.3 Hz, 1H), 7.76 (dd, J = 8.2, 1.1 Hz, 2H), 7.69 (t, J = 7.7 Hz, 1H), 7.60–7.55 (m, 1H), 7.53 (dd, J = 10.5, 4.8 Hz, 2H), 7.43 (t, J = 7.4 Hz, 1H), 7.24–7.18 (m, 1H), 3.32 (dd, J = 12.1, 6.7 Hz, 2H), 2.29 (t, J = 7.2 Hz, 2H), 1.79 (p, J = 7.0 Hz, 2H). ^{13}C NMR (125 MHz, DMSO) δ 174.15, 168.13, 163.84, 140.13, 138.69, 138.64, 134.72, 131.46, 129.51, 128.98, 128.42, 127.52, 127.26, 126.09, 125.08, 124.63, 122.13, 119.72, 119.47, 30.55, 29.37, 22.85. $C_{24}H_{22}N_2O_4$. MS (ESI−): m/z 401.2 ((M−H)$^-$, 100). Combustion analysis: measured (calculated): C 71.76 (71.63); H 5.58 (5.51); N 6.93 (6.96).

5.1.1.7. 4-(2-([1,1′-Biphenyl]-2-carboxamido)benzamido)butanoic acid (15g). Preparation according to general procedure b using **6a** and [1,1′-biphenyl]-2-carbonyl chloride (**8g**). Yield 62.0%. R_f (pentane/ethyl acetate 1:1 + 2% acetic acid) = 0.43. ^{1}H NMR (500 MHz, DMSO) δ 12.09 (s, 1H), 11.47 (s, 1H), 8.68 (d, J = 5.1 Hz, 1H), 8.39 (d, J = 8.3 Hz, 1H), 7.66 (dd, J = 7.9, 1.2 Hz, 1H), 7.64 (dd, J = 7.6, 1.2 Hz, 1H), 7.60 (td, J = 7.6, 1.4 Hz, 1H), 7.52 (td, J = 7.5, 1.3 Hz, 1H), 7.47 (dd, J = 11.8, 4.4 Hz, 2H), 7.41–7.37 (m, 2H), 7.37–7.32 (m, 2H), 7.30–7.26 (m, 1H), 7.13 (td, J = 7.7, 1.2 Hz, 1H), 3.18 (q, J = 6.9 Hz, 2H), 2.26 (t, J = 7.4 Hz, 2H), 1.70 (p, J = 7.2 Hz, 2H). ^{13}C NMR (125 MHz, DMSO) δ 173.78, 167.42, 166.85, 139.08, 138.62, 138.07, 136.03, 131.12, 129.64, 127.58, 127.55, 127.29, 127.00, 126.89, 126.59, 122.05, 119.98, 119.29, 37.30, 29.76, 22.81. $C_{24}H_{22}N_2O_4$. MS (ESI−): m/z 401.1 ((M−H)$^-$, 100). Combustion analysis: measured (calculated): C 71.50 (71.63); H 5.54 (5.51); N 7.03 (6.96).

5.1.1.8. 4-(2-(Isonicotinamido)benzamido)butanoic acid (15h). Preparation according to general procedure b using **6a** and isonicotinoyl chloride (**8h**). Yield 48.7%. R_f (pentane/ethyl acetate 1:1 + 2% acetic acid) = 0.19. ^{1}H NMR (500 MHz, DMSO) δ 12.76 (s, 1H), 12.09 (s, 1H), 8.94 (t, J = 5.3 Hz, 1H), 8.85 (dd, J = 4.4, 1.7 Hz, 2H), 8.60 (dd, J = 8.3, 1.0 Hz, 1H), 7.87 (dd, J = 8.0, 1.4 Hz, 1H), 7.82 (dd, J = 4.4, 1.7 Hz, 2H), 7.63–7.57 (m, 1H), 7.25 (td, J = 7.7, 1.1 Hz, 1H), 3.33–3.31 (m, 2H), 2.31 (t, J = 7.3 Hz, 2H), 1.78 (p, J = 7.1 Hz, 2H). ^{13}C NMR (125 MHz, DMSO) δ 173.79, 168.03, 162.26, 150.26, 140.88, 138.12, 131.59, 127.55, 122.71, 120.00, 119.92, 119.71, 37.44, 29.73, 22.79. $C_{17}H_{17}N_3O_4$. MS (ESI+): m/z 328.18 ((M+H)$^+$, 100). Combustion analysis: measured (calculated): C 62.25 (62.38); H 5.33 (5.23); N 12.76 (12.84).

5.1.1.9. 4-(2-(Thiophene-2-carboxamido)benzamido)butanoic acid (15i). Preparation according to general procedure b using **6a** and thiophene-2-carbonyl chloride (**8i**). Yield 51.9%. R_f (pentane/ethyl acetate 1:1 + 2% acetic acid) = 0.37. ^{1}H NMR (500 MHz, DMSO) δ 12.62 (s, 1H), 12.09 (s, 1H), 8.92 (t, J = 5.5 Hz, 1H), 8.53 (dd, J = 8.4, 1.0 Hz, 1H), 7.91 (dt, J = 4.5, 2.2 Hz, 1H), 7.84 (dd, J = 8.0, 1.4 Hz, 1H), 7.72 (dd, J = 3.8, 1.2 Hz, 1H), 7.59–7.52 (m, 1H), 7.28–7.25 (m, 1H), 7.22–7.16 (m, 1H), 3.32 (d, J = 6.9 Hz, 2H), 2.33–2.27 (m, 2H), 1.84–1.73 (m, 2H). ^{13}C NMR (125 MHz, DMSO) δ 173.78, 168.14, 158.70, 139.21, 138.51, 131.59, 131.56, 127.75, 127.74, 127.51, 122.02, 119.29, 119.16, 29.74, 29.37, 22.80. $C_{16}H_{16}N_2O_4S$. MS (MALDI): m/z 332.7 ((M+1), 100), 333.7 (34), 334.7 (20). Combustion analysis: measured (calculated): C 57.73 (57.82); H 4.89 (4.85); N 8.01 (8.43); S 9.63 (9.65).

5.1.1.10. 4-(2-(2-Naphthamido)benzamido)butanoic acid (15j). Preparation according to general procedure b using **6a** and 2-naphthoyl chloride (**8j**). Yield 55.0%. Rf (pentane/ethyl

acetate 1:1 + 2% acetic acid) = 0.43. ^{1}H NMR (500 MHz, DMSO) δ 12.70 (s, 1H), 8.98 (s, 1H), 8.68 (dd, J = 8.3, 0.8 Hz, 1H), 8.55 (d, J = 0.9 Hz, 1H), 8.12 (d, J = 8.3 Hz, 2H), 8.03 (t, J = 6.0 Hz, 1H), 7.99 (dd, J = 8.6, 1.8 Hz, 1H), 7.86 (dd, J = 7.9, 1.2 Hz, 1H), 7.70–7.56 (m, 4H), 7.25–7.20 (m, 1H), 3.29–3.23 (m, 2H), 2.32 (t, J = 7.3 Hz, 2H), 1.80 (p, J = 7.1 Hz, 2H). ^{13}C NMR (126 MHz, DMSO) δ 174.80, 169.15, 164.96, 139.87, 134.90, 132.73, 132.66, 132.43, 129.63, 129.19, 128.73, 128.62, 128.31, 128.19, 127.57, 123.71, 123.37, 120.99, 120.86, 39.30, 31.76, 24.69. $C_{22}H_{20}N_2O_4$. MS (ESI−): m/z 375.21 ((M−H)$^-$, 100). Combustion analysis: measured (calculated): C 69.95 (70.20); H 5.44 (5.36); N 7.12 (7.44).

5.1.1.11. 4-(2-(1-Naphthamido)benzamido)butanoic acid (15k). Preparation according to general procedure b using **6a** and 1-naphthoyl chloride (**8k**). Yield 58.7%. R_f (pentane/ethyl acetate 1:1 + 2% acetic acid) = 0.43. ^{1}H NMR (500 MHz, DMSO) δ 12.09 (s, 1H), 8.85 (t, J = 5.5 Hz, 1H), 8.66 (d, J = 8.2 Hz, 1H), 8.38–8.34 (m, 1H), 8.12 (d, J = 8.3 Hz, 1H), 8.06–8.02 (m, 1H), 7.85 (dd, J = 7.1, 1.1 Hz, 1H), 7.82 (dd, J = 7.9, 1.4 Hz, 1H), 7.66–7.59 (m, 4H), 7.24 (td, J = 7.7, 1.2 Hz, 1H), 3.23 (dd, J = 12.6, 6.9 Hz, 2H), 2.26 (t, J = 7.3 Hz, 2H), 1.73 (p, J = 7.2 Hz, 2H). ^{13}C NMR (125 MHz, DMSO) δ 173.77, 167.83, 166.18, 138.37, 133.57, 132.67, 131.32, 130.23, 128.87, 127.71, 127.48, 126.46, 125.81, 124.55, 124.45, 124.37, 122.40, 120.44, 119.83, 29.77, 29.37, 22.78. $C_{22}H_{20}N_2O_4$. MS (ESI−): m/z 375.20 ((M−H)$^-$, 100). Combustion analysis: measured (calculated): C 70.11 (70.20); H 5.59 (5.36); N 7.09 (7.44).

5.1.1.12. 4-(2-(2,2-Diphenylacetamido)benzamido)butanoic acid (15l). Preparation according to general procedure b using **6a** and 2,2-diphenylacetyl chloride (8 l). Yield 64.8%. R_f (pentane/ethyl acetate 1:1 + 2% acetic acid) = 0.42. ^{1}H NMR (500 MHz, DMSO) δ 12.69 (s, 1H), 11.39 (s, 1H), 8.70 (s, 1H), 8.36 (d, J = 8.0 Hz, 1H), 7.66 (dd, J = 7.9, 1.4 Hz, 1H), 7.50–7.45 (m, 1H), 7.40–7.31 (m, 8H), 7.28–7.23 (m, 2H), 7.14 (t, J = 7.5 Hz, 1H), 5.19 (s, 1H), 3.20 (dd, J = 12.6, 6.8 Hz, 2H), 2.37–2.30 (m, 2H), 1.72 (p, J = 7.2 Hz, 2H). ^{13}C NMR (125 MHz, DMSO) δ 172.65, 169.58, 167.56, 138.89, 137.71, 130.95, 127.93, 127.71, 127.26, 126.19, 122.19, 121.05, 119.97, 50.07, 37.14, 29.40, 29.36, 22.75. $C_{25}H_{24}N_2O_4$. MS (ESI−): m/z 415.26 ((M−H)$^-$, 100). Combustion analysis: measured (calculated): C 71.97 (72.10); H 6.08 (5.81); N 6.92 (6.73).

5.1.1.13. 4-(2-(3,3-Diphenylpropanamido)benzamido)butanoic acid (15m). Preparation according to general procedure b using **6a** and 3,3-diphenylpropanoyl chloride (**8m**). Yield 68.3%. R_f (pentane/ethyl acetate 1:1 + 2% acetic acid) = 0.44. ^{1}H NMR (500 MHz, DMSO) δ 12.13 (s, 1H), 11.28 (s, 1H), 8.71 (t, J = 5.4 Hz, 1H), 8.24 (d, J = 8.3 Hz, 1H), 7.66 (d, J = 7.9 Hz, 1H), 7.44–7.38 (m, 1H), 7.35 (d, J = 7.4 Hz, 4H), 7.26 (dd, J = 10.5, 4.9 Hz, 4H), 7.18–7.12 (m, 2H), 7.09 (td, J = 7.7, 1.1 Hz, 1H), 4.53 (t, J = 7.9 Hz, 1H), 3.32–3.28 (m, 2H), 3.15 (d, J = 8.0 Hz, 2H), 2.31 (t, J = 7.2 Hz, 2H), 1.78 (p, J = 7.0 Hz, 2H). ^{13}C NMR (125 MHz, DMSO) δ 173.81, 168.57, 167.70, 143.40, 137.88, 130.92, 127.68, 127.24, 126.81, 125.48, 121.77, 120.35, 119.68, 45.65, 41.78, 37.32, 29.77, 22.91. $C_{26}H_{26}N_2O_4$. MS (ESI−): m/z 429.26 ((M−H)$^-$, 100). Combustion analysis: measured (calculated): C 72.72 (72.54); H 5.98 (6.09); N 6.22 (6.51).

5.1.1.14. 4-(2-Cinnamamidobenzamido)butanoic acid (15n). Preparation according to general procedure b using **6a** and cinnamoyl chloride (**8n**). Yield 50.2%. R_f (pentane/ethyl acetate 1:1 + 2% acetic acid) = 0.42. ^{1}H NMR (500 MHz, DMSO) δ 12.10 (s, 1H), 11.51 (s, 1H), 8.79 (t, J = 5.6 Hz, 1H), 8.59 (d, J = 7.5 Hz, 2H), 8.50 (t, J = 8.8 Hz, 1H), 8.01 (dd, J = 7.9, 1.6 Hz, 2H), 7.57–7.50 (m, 2H), 7.20–7.15 (m, 1H), 7.13 (t, J = 7.4 Hz, 1H), 6.86 (d, J = 1.7 Hz, 1H), 6.82 (d, J = 1.6 Hz, 1H), 3.28–3.24 (m, 2H), 2.30 (t, J = 7.3 Hz, 2H), 1.78 (p, J = 7.2 Hz, 2H). ^{13}C NMR (126 MHz, DMSO) δ 174.72, 168.74, 164.11, 134.97, 132.22, 131.64, 130.43, 129.41, 128.64, 128.58, 123.24, 123.04, 122.95, 70.26, 68.35, 31.57, 31.17, 24.73. $C_{20}H_{20}N_2O_4$. MS (MALDI): m/z 352.9 ((M+1), 100). Combustion analysis: measured (calculated): C 67.90 (68.17); H 5.88 (5.72); N 8.14 (7.95).

5.1.1.15. 4-(2-(3-Phenylpropanamido)benzamido)butanoic acid (15o). Preparation according to general procedure b using **6a** and 3-phenylpropanoyl chloride (**8o**). Yield 71.2%. R_f (pentane/ethyl acetate 1:1 + 2% acetic acid) = 0.41. ^{1}H NMR (500 MHz, DMSO) δ 12.06 (s, 1H), 11.25 (s, 1H), 8.73 (t, J = 5.4 Hz, 1H), 8.36 (d, J = 8.2 Hz, 1H), 7.69 (dd, J = 7.9, 1.3 Hz, 1H), 7.48–7.44 (m, 1H), 7.29–7.22 (m, 3H), 7.17 (ddd, J = 8.5, 6.4, 4.0 Hz, 2H), 7.12 (td, J = 7.8, 1.1 Hz, 1H), 3.27 (dd, J = 12.7, 6.8 Hz, 2H), 2.92 (t, J = 7.6 Hz, 2H), 2.66 (t, J = 7.7 Hz, 2H), 2.29 (t, J = 7.3 Hz, 2H), 1.75 (p, J = 7.2 Hz, 2H). ^{13}C NMR (126 MHz, DMSO) δ 174.71, 170.61, 168.71, 141.23, 139.18, 135.58, 132.19, 130.90, 128.78, 128.72, 126.47, 122.99, 46.07, 39.07, 33.17, 31.60, 31.08, 24.71. $C_{20}H_{22}N_2O_4$. MS (ESI−): m/z 353.4 ((M−H)$^-$, 100). Combustion analysis: measured (calculated): C 68.12 (67.78); H 6.33 (6.26); N 7.50 (7.90).

5.1.1.16. 4-(2-(2-(Naphthalen-2-yl)acetamido)benzamido)butanoic acid (15p). Preparation according to general procedure b using **6a** and 2-(naphthalen-2-yl)acetyl chloride (**8p**). Yield 65.0%. R_f (pentane/ethyl acetate 1:1 + 2% acetic acid) = 0.48. ^{1}H NMR (500 MHz, DMSO) δ 11.30 (s, 1H), 8.71 (s, 1H), 8.34 (d, J = 8.3 Hz, 1H), 7.94–7.83 (m, 4H), 7.66 (d, J = 7.6 Hz, 1H), 7.55–7.42 (m, 4H), 7.12 (t, J = 7.5 Hz, 1H), 3.86 (s, 2H), 3.20 (q, J = 6.3 Hz, 2H), 2.25 (t, J = 7.2 Hz, 2H), 1.70 (p, J = 6.9 Hz, 2H). ^{13}C NMR (126 MHz, DMSO) δ 174.74, 169.58, 168.56, 139.01, 133.55, 133.37, 132.43, 132.10, 128.45, 128.42, 128.32, 128.14, 127.97, 126.63, 126.19, 123.21, 122.09, 120.96, 45.03, 39.06, 31.61, 24.67. $C_{23}H_{22}N_2O_4$. MS (ESI−): m/z 389.21 ((M−H)$^-$, 100). Combustion analysis: measured (calculated): C 70.51 (70.75); H 5.63 (5.68); N 6.92 (7.17).

5.1.1.17. Methyl 4-(2-(2-naphthamido)benzamido)butanoate (16). Preparation according to general procedure b using **6b** and 2-naphthoyl chloride (**8j**). Yield 74.0%. R_f (pentane/ethyl acetate 1:1 + 2% acetic acid) = 0.62. ^{1}H NMR (500 MHz, DMSO) δ 12.66 (s, 1H), 8.93 (t, J = 5.4 Hz, 1H), 8.67 (d, J = 7.7 Hz, 1H), 8.55 (s, 1H), 8.12 (t, J = 8.4 Hz, 2H), 8.04 (d, J = 7.8 Hz, 1H), 7.99 (dd, J = 8.6, 1.6 Hz, 1H), 7.88–7.83 (m, 1H), 7.66 (qd, J = 6.9, 3.4 Hz, 2H), 7.63–7.58 (m, 1H), 7.27–7.20 (m, 1H), 3.55 (s, 3H), 3.39–3.35 (t, J = 7.0 Hz, 2H), 2.42 (t, J = 7.3 Hz, 2H), 1.84 (p, J = 7.1 Hz, 2H). ^{13}C NMR (126 MHz, DMSO) δ 173.60, 169.17, 164.97, 139.82, 134.90, 132.74, 132.69, 132.43, 129.60, 129.17, 128.71, 128.61, 128.31, 128.19, 127.57, 123.70, 123.39, 121.07, 120.96, 51.71, 39.06, 31.22, 24.62. $C_{23}H_{22}N_2O_4$. MS (ESI+): m/z 391.24 ((M+H)$^+$, 100). Combustion analysis: measured (calculated): C 70.51 (70.75); H 5.68 (5.68); N 7.08 (7.17).

5.1.1.18. 5-(2-(2-Naphthamido)benzamido)pentanoic acid (17). Preparation according to general procedure b using **6c** and 2-naphthoyl chloride (**8j**). Yield 58.2%. R_f (pentane/ethyl acetate 1:1 + 2% acetic acid) = 0.46. ^{1}H NMR (500 MHz, DMSO) δ 12.72 (s, 1H), 8.92 (t, J = 5.5 Hz, 1H), 8.69 (dd, J = 8.4, 1.0 Hz, 1H), 8.55 (d, J = 1.1 Hz, 1H), 8.13 (d, J = 8.2 Hz, 2H), 8.04 (d, J = 7.7 Hz, 1H), 7.99 (dd, J = 8.6, 1.8 Hz, 1H), 7.86 (dd, J = 8.0, 1.3 Hz, 1H), 7.70–7.62 (m, 2H), 7.62–7.58 (m, 1H), 7.23 (td, J = 7.9, 1.2 Hz, 1H), 3.32 (d, J = 3.6 Hz, 2H), 2.26 (t, J = 6.9 Hz, 2H), 1.58 (dt, J = 6.9, 3.6 Hz, 4H). ^{13}C NMR (125 MHz, DMSO) δ 173.95, 168.06, 163.97, 138.74, 133.73, 131.55, 131.48, 131.25, 128.42, 128.00, 127.47, 127.41, 127.10, 126.98, 126.36, 122.45, 122.13, 119.73, 119.62, 37.63, 31.95, 26.97, 20.60. $C_{23}H_{22}N_2O_4$. MS (ESI−): m/z

389.22 ((M−H)⁻, 100). Combustion analysis: measured (calculated): C 70.41 (70.75); H 5.55 (5.68); N 6.91 (7.17).

5.1.1.19. 6-(2-(2-Naphthamido)benzamido)hexanoic acid (18). Preparation according to general procedure b using **6d** and 2-naphthoyl chloride (**8j**). Yield 59.0%. R_f (pentane/ethyl acetate 1:1 + 2% acetic acid) = 0.47. ^{1}H NMR (500 MHz, DMSO) δ 12.70 (s, 1H), 11.99 (s, 1H), 8.89 (t, J = 5.4 Hz, 1H), 8.67 (dd, J = 8.3, 0.7 Hz, 1H), 8.54 (s, 1H), 8.12 (d, J = 8.5 Hz, 2H), 8.02 (t, J = 9.6 Hz, 1H), 7.98 (dd, J = 8.6, 1.7 Hz, 1H), 7.85 (dd, J = 7.9, 1.2 Hz, 1H), 7.70–7.62 (m, 2H), 7.62–7.57 (m, 1H), 7.27–7.19 (m, 1H), 3.31–3.30 (m, 2H), 2.20 (t, J = 7.4 Hz, 2H), 1.61–1.48 (m, 4H), 1.39–1.29 (m, 2H). ^{13}C NMR (126 MHz, DMSO) δ 174.93, 168.99, 164.94, 139.83, 134.90, 132.73, 132.63, 132.42, 129.62, 129.20, 128.67, 128.62, 128.31, 128.19, 127.59, 123.68, 123.39, 121.11, 120.91, 34.02, 31.18, 29.00, 26.45, 24.69. $C_{24}H_{24}N_2O_4$. MS (ESI−): m/z 403.21 ((M−H)⁻, 100). Combustion analysis: measured (calculated): C 71.67 (71.27); H 5.98 (5.98); N 6.89 (6.93).

5.1.1.20. 4-(2-(2-Naphthamido)benzamido)benzoic acid (19). Preparation according to general procedure b using **6e** and 2-naphthoyl chloride (**8j**). Yield 54.6%. R_f (pentane/ethyl acetate 1:1 + 2% acetic acid) = 0.49. ^{1}H NMR (500 MHz, DMSO) δ 12.78 (s, 1H), 11.48 (s, 1H), 10.81 (s, 1H), 8.54 (s, 1H), 8.35 (dt, J = 8.3, 4.1 Hz, 1H), 8.12–8.05 (m, 2H), 8.02 (d, J = 8.0 Hz, 1H), 7.98–7.86 (m, 6H), 7.69–7.60 (m, 3H), 7.34 (td, J = 7.7, 1.1 Hz, 1H). ^{13}C NMR (125 MHz, DMSO) δ 167.03, 166.41, 164.42, 142.32, 137.48, 133.70, 131.51, 131.46, 131.15, 129.50, 128.42, 128.33, 127.79, 127.33, 126.97, 126.30, 125.05, 123.66, 122.92, 122.82, 121.45, 119.13, 119.03. $C_{25}H_{18}N_2O_4$. MS (ESI−): m/z 409.22 ((M−H)⁻, 100). Combustion analysis: measured (calculated): C 73.10 (73.16); H 4.56 (4.42); N 6.63 (6.83).

5.1.1.21. 3-(2-(2-Naphthamido)benzamido)benzoic acid (20). Preparation according to general procedure b using **6f** and 2-naphthoyl chloride (**8j**). Yield 56.8%. R_f (pentane/ethyl acetate 1:1 + 2% acetic acid) = 0.50. ^{1}H NMR (500 MHz, DMSO) δ 13.02 (s, 1H), 11.63 (s, 1H), 10.72 (s, 1H), 8.54 (s, 1H), 8.42 (dd, J = 18.2, 9.5 Hz, 2H), 8.09 (t, J = 7.0 Hz, 2H), 8.04–7.93 (m, 4H), 7.71 (d, J = 7.6 Hz, 1H), 7.64 (dd, J = 15.9, 7.6 Hz, 3H), 7.49 (t, J = 7.9 Hz, 1H), 7.33 (t, J = 7.5 Hz, 1H). ^{13}C NMR (125 MHz, DMSO) δ 166.95, 166.62, 164.36, 138.27, 137.67, 133.71, 131.50, 131.48, 131.19, 130.52, 128.31, 128.21, 127.83, 127.34, 127.16, 126.97, 126.32, 124.28, 124.14, 123.08, 122.80, 122.77, 121.17, 120.90, 120.80. $C_{25}H_{18}N_2O_4$. MS (ESI−): m/z 409.4 ((M−H)⁻, 100). Combustion analysis: measured (calculated): C 72.94 (73.16); H 4.50 (4.42); N 6.54 (6.83).

5.1.1.22. 4-((2-(2-Naphthamido)benzamido)methyl)benzoic acid (21). Preparation according to general procedure b using **6g** and 2-naphthoyl chloride (**8j**). Yield 57.9%. R_f (pentane/ethyl acetate 1:1 + 2% acetic acid) = 0.50. ^{1}H NMR (500 MHz, DMSO) δ 12.32 (s, 1H), 11.83 (s, 1H), 10.56 (s, 1H), 8.54 (s, 1H), 8.50 (d, J = 8.0 Hz, 1H), 8.10 (t, J = 7.6 Hz, 2H), 8.02 (d, J = 7.8 Hz, 1H), 7.96 (dd, J = 14.0, 5.2 Hz, 2H), 7.65 (dt, J = 14.9, 7.4 Hz, 5H), 7.32 (t, J = 7.1 Hz, 1H), 7.25 (d, J = 8.4 Hz, 2H), 3.54 (s, 2H). ^{13}C NMR (125 MHz, DMSO) δ 172.32, 166.80, 164.20, 137.94, 136.38, 133.71, 131.51, 131.14, 130.39, 130.34, 128.88, 128.38, 128.27, 127.91, 127.36, 127.17, 126.96, 126.33, 122.62, 122.43, 120.80, 120.21, 120.08, 38.97. $C_{26}H_{20}N_2O_4$. MS (ESI−): m/z 423.19 ((M−H)⁻, 100). Combustion analysis: measured (calculated): C 73.51 (73.57); H 4.89 (4.75); N 6.82 (6.60).

5.1.1.23. 2-(4-(2-(2-Naphthamido)benzamido)phenyl)acetic acid (22). Preparation according to general procedure b using **6h** and 2-naphthoyl chloride (**8j**). Yield 58.0%. R_f (pentane/ethyl acetate 1:1 + 2% acetic acid) = 0.47. ^{1}H NMR (500 MHz, DMSO) δ 12.90 (s, 1H), 12.56 (s, 1H), 9.55 (t, J = 5.9 Hz, 1H), 8.68 (dt, J = 8.3, 2.1 Hz, 1H), 8.50 (d, J = 1.2 Hz, 1H), 8.09 (dd, J = 8.7, 3.4 Hz, 1H), 8.06 (dd, J = 7.8, 0.6 Hz, 1H), 8.01 (t, J = 6.2 Hz, 1H), 7.95 (dd, J = 8.5, 1.7 Hz, 2H), 7.92 (d, J = 8.3 Hz, 2H), 7.68–7.60 (m, 3H), 7.49 (d, J = 8.4 Hz, 2H), 7.26 (tt, J = 4.0, 2.0 Hz, 1H), 4.62 (d, J = 5.8 Hz, 2H). ^{13}C NMR (125 MHz, DMSO) δ 168.33, 166.66, 164.06, 143.49, 138.77, 138.61, 133.72, 131.77, 131.51, 131.21, 128.74, 128.36, 127.96, 127.56, 127.40, 127.07, 126.97, 126.92, 126.47, 126.42, 126.34, 122.49, 122.30, 119.87, 119.66, 41.27. $C_{26}H_{20}N_2O_4$. MS (ESI−): m/z 423.22 ((M−H)⁻, 100). Combustion analysis: measured (calculated): C 73.43 (73.57); H 4.78 (4.75); N 6.81 (6.60).

5.1.1.24. 4-(2-(2-Naphthamido)-*N*-methylbenzamido)butanoic acid (23). Preparation according to general procedure b using **6i** and 2-naphthoyl chloride (**8j**). Yield 51.3%. R_f (pentane/ethyl acetate 1:1 + 2% acetic acid) = 0.50. ^{1}H NMR (500 MHz, DMSO) δ 12.13 (s, 1H), 10.45 (s, 1H), 8.16–7.96 (m, 4H), 7.82–7.64 (m, 3H), 7.59–7.50 (m, 1H), 7.42 (dd, J = 23.5, 11.6 Hz, 1H), 7.34 (t, J = 7.5 Hz, 1H), 3.46 (dd, J = 13.6, 6.5 Hz, 2H), 2.99 (s, 3H), 2.32 (t, J = 7.3 Hz, 2H), 1.85 (dt, J = 14.4, 7.1 Hz, 2H). ^{13}C NMR (126 MHz, DMSO) δ 174.69, 169.36, 165.72, 135.81, 134.79, 132.58, 132.06, 131.42, 130.01, 129.47, 128.59, 128.48, 128.36, 128.13, 128.06, 127.35, 125.80, 125.35, 124.57, 46.55, 37.51, 31.59, 22.41. $C_{23}H_{22}N_2O_4$. MS (ESI−): m/z 389.22 ((M−H)⁻, 100). Combustion analysis: measured (calculated): C 70.56 (70.75); H 5.59 (5.68); N 6.87 (7.17).

5.1.1.25. 4-(2-(*N*-Methyl-2-naphthamido)benzamido)butanoic acid (24). Preparation according to general procedure b using **6j** and 2-naphthoyl chloride (**8j**). Yield 44.7%. R_f (pentane/ethyl acetate 1:1 + 2% acetic acid) = 0.54. ^{1}H NMR (500 MHz, DMSO) δ 12.07 (s, 1H), 8.28 (s, 1H), 7.95 (d, J = 6.0 Hz, 1H), 7.79 (dd, J = 12.5, 4.8 Hz, 1H), 7.76 (t, J = 8.3 Hz, 1H), 7.66 (d, J = 8.5 Hz, 1H), 7.54–7.43 (m, 2H), 7.41–7.35 (m, 1H), 7.27 (t, J = 7.2 Hz, 1H), 7.24–7.18 (m, 2H), 3.31 (s, 3H), 3.30–3.25 (m, 2H), 2.30 (t, J = 7.4 Hz, 2H), 1.80–1.68 (m, 2H). ^{13}C NMR (126 MHz, DMSO) δ 174.73, 169.74, 167.31, 142.86, 134.47, 134.29, 133.34, 132.26, 131.07, 130.26, 128.98, 128.78, 128.65, 127.93, 127.61, 127.48, 127.28, 126.81, 125.72, 38.98, 38.23, 31.61, 21.53. $C_{23}H_{22}N_2O_4$. MS (ESI−): m/z 389.22 ((M−H)⁻, 100). Combustion analysis: measured (calculated): C 70.39 (70.75); H 5.62 (5.68); N 7.00 (7.17).

5.1.1.26. 4-(2-(Naphthalene-2-sulfonamido)benzamido)butanoic acid (25). Compound **6a** (670 mg, 3 mmol, 1.0 equiv) was dissolved in CH_2Cl_2 (15 mL, abs.) triethylamine (1.3 mL, 9 mmol, 3.0 equiv) was added and the solution was cooled to 0 °C. Naphthalene-2-sulfonyl chloride (**9**, mg, mmol, 1.3 equiv) was dissolved in CH_2Cl_2 and drop wise added to the solution of **6a**. The reaction mixture was kept at 0 °C and the reaction was monitored by TLC. After 4 h the mixture was diluted with 50 mL ethyl acetate, washed three times with 10% hydrochloric acid (50 mL) and dried over Na_2SO_4. Yield 68.9%. R_f (pentane/ethyl acetate 1:1 + 2% acetic acid) = 0.31. ^{1}H NMR (500 MHz, DMSO) δ 12.13 (s, 1H), 11.77 (s, 1H), 8.71 (t, J = 5.4 Hz, 1H), 8.46 (d, J = 1.7 Hz, 1H), 8.13 (d, J = 8.0 Hz, 1H), 8.05 (d, J = 8.8 Hz, 1H), 7.98 (d, J = 8.1 Hz, 1H), 7.71–7.61 (m, 4H), 7.58 (dd, J = 8.3, 1.0 Hz, 1H), 7.48–7.42 (m, 1H), 7.12–7.06 (m, 1H), 3.19 (dd, J = 12.6, 6.9 Hz, 2H), 2.22 (t, J = = 7.3 Hz, 2H), 1.65 (p, J = 7.2 Hz, 2H). ^{13}C NMR (125 MHz, DMSO) δ 173.70, 167.51, 137.41, 134.93, 133.65, 131.72, 130.81, 128.86, 128.58, 128.48, 127.60, 127.57, 127.07, 127.05, 122.83, 120.98, 120.22, 119.27, 37.29, 29.63, 22.65. $C_{21}H_{20}N_2O_5S$. MS (ESI−): m/z 411.4 ((M−H)⁻, 100). Combustion analysis: measured (calculated): C 61.35 (61.15); H 4.95 (4.89); N 6.56 (6.79).

5.1.1.27. 4-(2-((Naphthalen-2-ylmethyl)amino)benzamido)butanoic acid (26). Compound **6a** (670 mg, 3 mmol, 1.0 equiv) and 2-naphthaldehyde (10, 470 mg, 3 mmol, 1.0 equiv) were dissolved in acetic acid (9 mL) and stirred for 2 h at room temperature. CH_2Cl_2 (15 mL, abs.) was added and the mixture was cooled to 0 °C. $NaBH_4$ (450 mg, 12 mmol, 4.0 equiv) was added in small portions over 1 h. The mixture was stirred for an additional hour at 0 °C and overnight at room temperature. Saturated NH_4Cl solution (5 mL) was added and the mixture was stirred at room temperature for additional 15 min. The mixture was then partitioned between ethyl acetate (50 mL) and water (50 mL) and the aqueous layer was extracted twice with ethyl acetate (2*50 mL). The combined organic layers were dried (Na_2SO_4) and concentrated in vacuum. The crude product was purified by column chromatography on silica. Yield 52.3%. R_f (pentane/ethyl acetate 1:1 + 2% acetic acid) = 0.31. ^{1}H NMR (500 MHz, DMSO) δ 12.08 (s, 1H), 7.94–7.84 (m, 3H), 7.74 (s, 1H), 7.67 (d, J = 7.4 Hz, 1H), 7.56–7.44 (m, 4H), 7.19 (dd, J = 11.1, 4.2 Hz, 1H), 6.65 (dd, J = 12.0, 7.8 Hz, 2H), 6.02 (d, J = 2.2 Hz, 1H), 4.05–3.96 (m, 1H), 2.84 (dt, J = 7.6, 6.8 Hz, 1H), 2.31–2.18 (m, 2H), 1.89–1.69 (m, 2H). ^{13}C NMR (125 MHz, DMSO) δ 173.60, 161.85, 145.58, 137.78, 132.52, 132.05, 131.65, 127.81, 127.23, 126.79, 126.71, 125.83, 125.64, 124.04, 123.37, 116.36, 114.13, 113.46, 69.10, 42.61, 29.69, 21.76. $C_{22}H_{22}N_2O_3$. MS (ESI−): m/z 361.6 ($(M-H)^-$, 100). Combustion analysis: measured (calculated): C 72.95 (72.91); H 5.80 (6.12); N 7.65 (7.73).

5.1.1.28. 4-((2-(2-Naphthamido)benzyl)amino)butanoic acid (27). Compound **14** (1.4 g, 5 mmol, 1.0 equiv) and 4-aminobutyric acid (**5a**, 520 mg, 5 mmol, 1.0 equiv) were dissolved in acetic acid (15 mL) and stirred for 2 h at room temperature. CH_2Cl_2 (25 mL, abs.) was added and the mixture was cooled to 0 °C. $NaBH_4$ (750 mg, 20 mmol, 4.0 equiv) was added in small portions over 1 h. The mixture was stirred for an additional hour at 0 °C and overnight at room temperature. Saturated NH_4Cl solution (8 mL) was added and the mixture was stirred at room temperature for additional 15 min. The mixture was then partitioned between ethyl acetate (50 mL) and water (50 mL) and the aqueous layer was extracted twice with ethyl acetate (2*50 mL). The combined organic layers were dried (Na_2SO_4) and concentrated in vacuum. The crude product was purified by column chromatography on silica. Yield 54.6%. R_f (pentane/ethyl acetate 1:1 + 2% acetic acid) = 0.18. ^{1}H NMR (500 MHz, DMSO) δ 10.49 (s, 1H), 8.67 (s, 1H), 8.15–7.98 (m, 4H), 7.75–7.56 (m, 3H), 7.41–7.35 (m, 1H), 7.34–7.31 (m, 1H), 7.26 (td, J = 7.5, 1.0 Hz, 1H), 5.76 (s, 2H), 3.39–3.36 (m, 2H), 2.29 (t, J = = 8.1 Hz, 2H), 1.98–1.90 (m, 2H). ^{13}C NMR (126 MHz, DMSO) δ 175.26, 166.05, 136.75, 134.81, 132.60, 132.20, 131.10, 129.70, 129.50, 128.69, 128.45, 128.32, 128.13, 127.28, 126.58, 126.03, 124.86, 42.99, 31.18, 30.65, 17.93. $C_{22}H_{22}N_2O_3$. MS (ESI−): m/z 361.6 ($(M-H)^-$, 100). Combustion analysis: measured (calculated): C 72.57 (72.91); H 5.86 (6.12); N 8.05 (7.73).

5.1.2. Intermediates

5.1.2.1. 4-(2-Aminobenzamido)butanoic acid (6a). Preparation according to general procedure a using isatoic anhydride (**4a**) and 4-aminobutyric acid (**5a**). The crude product was purified by recrystallization from 2-propanol and 10% hydrochloric acid. Yield 71.6%. ^{1}H NMR (500 MHz, DMSO) δ 8.71 (s, 1H), 7.72 (d, J = 7.8 Hz, 1H), 7.44 (t, J = 7.7 Hz, 1H), 7.25–7.17 (m, 1H), 7.13 (t, J = 6.8 Hz, 1H), 3.27 (q, J = 6.3 Hz, 2H), 2.29 (t, J = = 7.4 Hz, 2H), 1.76 (p, J = 7.2 Hz, 2H). ^{13}C NMR (126 MHz, DMSO) δ 174.72, 167.57, 138.69, 132.40, 129.01, 123.45, 123.11, 122.06, 38.97, 31.65, 24.82. $C_{11}H_{14}N_2O_3$. MS (ESI−): m/z 221.5 ($(M-H)^-$, 100).

5.1.2.2. Methyl 4-(2-aminobenzamido)butanoate (6b). Preparation according to general procedure a using isatoic anhydride (**4a**) and methyl 4-aminobutanoate (**5b**). The crude product was purified by column chromatography on silica. Yield 69.8%. R_f (pentane/ethyl acetate 1:1 + 2% acetic acid) = 0.65. ^{1}H NMR (500 MHz, DMSO) δ 8.21 (t, J = 5.3 Hz, 1H), 7.46 (d, J = 7.9 Hz, 1H), 7.14–7.09 (m, 1H), 6.68 (d, J = 8.2 Hz, 1H), 6.54–6.46 (m, 1H), 6.37 (s, 2H), 3.57 (s, 3H), 3.22 (q, J = 6.8 Hz, 2H), 2.36 (t, J = 7.2 Hz, 2H), 1.76 (p, J = 7.2 Hz, 2H). ^{13}C NMR (126 MHz, DMSO) δ 173.66, 169.41, 162.78, 150.03, 132.03, 128.48, 116.74, 115.00, 38.54, 36.24, 31.30, 24.97. $C_{12}H_{16}N_2O_3$. MS (ESI+): m/z 237.6 ($(M+H)^+$, 100).

5.1.2.3. 5-(2-Aminobenzamido)pentanoic acid (6c). Preparation according to general procedure a using isatoic anhydride (**4a**) and 5-aminopentanoic acid (**5c**). The crude product was purified by recrystallization from 2-propanol and 10% hydrochloric acid. Yield 76.7%. ^{1}H NMR (500 MHz, DMSO) δ 8.82 (s, 1H), 7.75 (dd, J = 18.6, 4.7 Hz, 1H), 7.48 (t, J = 7.7 Hz, 1H), 7.29 (t, J = 9.0 Hz, 1H), 7.21 (t, J = 7.0 Hz, 1H), 3.25 (d, J = 5.3 Hz, 2H), 2.25 (t, J = 6.4 Hz, 2H), 1.58–1.50 (m, 4H). ^{13}C NMR (126 MHz, DMSO) δ 174.85, 167.19, 142.04, 132.39, 129.05, 127.84, 124.67, 122.92, 39.18, 34.44, 28.83, 22.47. $C_{12}H_{16}N_2O_3$. MS (ESI−): m/z 235.1 ($(M-H)^-$, 100).

5.1.2.4. 6-(2-Aminobenzamido)hexanoic acid (6d). Preparation according to general procedure a using isatoic anhydride (**4a**) and 6-aminohexanoic acid (**5d**). The crude product was purified by recrystallization from 2-propanol and 10% hydrochloric acid. Yield 71.8%. ^{1}H NMR (500 MHz, DMSO) δ 8.74 (s, 1H), 7.78–7.71 (m, 1H), 7.52–7.40 (m, 1H), 7.34–7.12 (m, 2H), 3.24 (q, J = 6.7 Hz, 2H), 2.21 (t, J = 7.4 Hz, 2H), 1.57–1.48 (m, 4H), 1.35–1.28 (m, 2H). ^{13}C NMR (126 MHz, DMSO) δ 174.92, 167.19, 132.37, 128.99, 127.80, 123.91, 122.38, 107.42, 39.37, 34.09, 29.09, 26.48, 24.71. $C_{13}H_{18}N_2O_3$. MS (ESI−): m/z 248.8 ($(M-H)^-$, 100).

5.1.2.5. 4-(2-Aminobenzamido)benzoic acid (6e). Preparation according to general procedure a using isatoic anhydride (**4a**) and 4-aminobenzoic acid (**5e**). The crude product was purified by column chromatography on silica. Yield 62.4%. R_f (pentane/ethyl acetate 1:1 + 2% acetic acid) = 0.57. ^{1}H NMR (500 MHz, DMSO) δ 10.62 (s, 1H), 7.95–7.91 (m, 2H), 7.91–7.86 (m, 2H), 7.80 (d, J = 7.6 Hz, 1H), 7.42 (t, J = 7.3 Hz, 1H), 7.14 (d, J = 7.2 Hz, 1H), 7.03 (d, J = 5.8 Hz, 1H). ^{13}C NMR (126 MHz, DMSO) δ 167.42, 167.30, 143.70, 132.94, 132.46, 130.63, 129.73, 129.64, 126.24, 125.96, 120.35, 120.10. $C_{14}H_{12}N_2O_3$. MS (ESI−): m/z 255.0 ($(M-H)^-$, 100).

5.1.2.6. 3-(2-Aminobenzamido)benzoic acid (6f). Preparation according to general procedure a using isatoic anhydride (**4a**) and 3-aminobenzoic acid (**5f**). The crude product was purified by column chromatography on silica. Yield 64.0%. R_f (pentane/ethyl acetate 1:1 + 2% acetic acid) = 0.58. ^{1}H NMR (500 MHz, DMSO) δ 10.54 (s, 1H), 8.44 (d, J = 1.2 Hz, 1H), 7.96 (t, J = 8.8 Hz, 1H), 7.82 (d, J = 7.8 Hz, 1H), 7.71–7.66 (m, 1H), 7.48 (t, J = 7.9 Hz, 1H), 7.46–7.41 (m, 1H), 7.26–7.15 (m, 1H), 7.07 (d, J = 6.6 Hz, 1H). ^{13}C NMR (126 MHz, DMSO) δ 167.64, 167.02, 139.72, 133.08, 132.81, 131.64, 130.58, 129.63, 129.28, 128.29, 125.09, 125.01, 121.78, 120.83. $C_{14}H_{12}N_2O_3$. MS (ESI−): m/z 254.9 ($(M-H)^-$, 100).

5.1.2.7. 4-((2-Aminobenzamido)methyl)benzoic acid (6g). Preparation according to general procedure a using isatoic anhydride (**4a**) and 4-(aminomethyl)benzoic acid (**5g**). The crude product was purified by column chromatography on silica. Yield 70.7%. $\boldsymbol{R_f}$ (pentane/ethyl acetate 1:1 + 2% acetic acid) = 0.58. $^{\mathbf{1}}$H NMR (500 MHz, DMSO) $\boldsymbol{\delta}$ 9.97 (s, 1H), 7.69–7.56 (m, 3H), 7.25–7.15 (m, 3H), 6.74 (dd, $\boldsymbol{J}$ = 8.2, 0.9 Hz, 1H), 6.63–6.54 (m, 1H), 6.32 (s, 2H), 3.52 (s, 2H). $^{\mathbf{13}}$C NMR (126 MHz, DMSO) $\boldsymbol{\delta}$ 173.31, 168.23, 150.20, 138.25, 132.54, 130.44, 129.87, 129.14, 120.93, 116.82, 115.69, 115.15, 40.62. $\boldsymbol{C_{15}H_{14}N_2O_3}$. MS (ESI−): $\boldsymbol{m/z}$ 269.0 ($(M-H)^-$, 100).

5.1.2.8. 2-(4-(2-Aminobenzamido)phenyl)acetic acid (6h). Preparation according to general procedure a using isatoic anhydride (**4a**) and 4-(aminophenyl)acetic acid (**5h**). The crude product was purified by column chromatography on silica. Yield 62.8%. R_f (pentane/ethyl acetate 1:1 + 2% acetic acid) = 0.59. ^{1}H NMR (500 MHz, DMSO) δ 9.39 (s, 1H), 7.91 (d, J = 8.3 Hz, 2H), 7.85 (t, J = 9.2 Hz, 1H), 7.46 (t, J = 8.0 Hz, 3H), 7.26–7.22 (m, 1H), 7.14 (t, J = 7.7 Hz, 1H), 4.53 (d, J = 5.7 Hz, 2H). ^{13}C NMR (126 MHz, DMSO) δ 167.73, 167.64, 144.97, 139.35, 132.67, 129.86, 129.78, 129.66, 129.09, 127.76, 123.33, 122.11, 42.76. $C_{15}H_{14}N_2O_3$. MS (ESI−): m/z 269.0 ((M−H)$^-$, 100).

5.1.2.9. 4-(2-Amino-*N*-methylbenzamido)butanoic acid (6i). Preparation according to general procedure a using isatoic anhydride (**4a**) and 4-(methylamino)butanoic acid (**5i**). The crude product was purified by recrystallization from acetone. Yield 61.5%. ^{1}H NMR (500 MHz, DMSO) δ 7.09–7.04 (m, 1H), 6.96 (d, J = 7.3 Hz, 1H), 6.69 (d, J = 8.0 Hz, 1H), 6.55 (td, J = 7.5, 1.0 Hz, 1H), 3.32–3.28 (m, 2H), 2.69 (s, 3H), 2.20–2.14 (m, 2H), 1.93–1.85 (m, 2H). ^{13}C NMR (126 MHz, DMSO) δ 174.28, 170.38, 145.86, 130.15, 127.82, 120.75, 115.97, 115.92, 39.31, 30.58, 29.47, 17.68. $C_{12}H_{16}N_2O_3$. MS (ESI−): m/z 234.8 ((M−H)$^-$, 100).

5.1.2.10. 4-(2-(Methylamino)benzamido)butanoic acid (6j). Preparation according to general procedure a using ***N***-methylisatoic anhydride (**4b**) and 4-aminobutanoic acid (**5a**). The crude product was purified by column chromatography on silica. Yield 50.4%. R_f (pentane/ethyl acetate 1:1 + 2% acetic acid) = 0.41. ^{1}H NMR (500 MHz, DMSO) δ 12.07 (s, 1H), 8.29 (t, J = 5.5 Hz, 1H), 7.62 (d, J = 4.2 Hz, 1H), 7.51 (dd, J = 7.8, 1.4 Hz, 1H), 7.27 (ddd, J = 8.5, 7.3, 1.5 Hz, 1H), 6.61 (d, J = 8.1 Hz, 1H), 6.58–6.51 (m, 1H), 3.22 (dd, J = 12.7, 6.8 Hz, 2H), 2.76 (d, J = 4.3 Hz, 3H), 2.26 (t, J = 7.4 Hz, 2H), 1.73 (p, J = 7.2 Hz, 2H). ^{13}C NMR (126 MHz, DMSO) δ 174.77, 169.62, 150.49, 132.72, 128.62, 115.64, 114.36, 110.89, 38.72, 31.65, 29.73, 24.98. $C_{12}H_{16}N_2O_3$. MS (ESI−): m/z 235.16 ((M−H)$^-$, 100).

5.1.2.11. 2-Aminobenzaldehyde (12). 2-(Aminophenyl)ethanol (11, 2.4 g, 20 mmol, 1.0 equiv) was dissolved in CH_2Cl_2 (40 mL, abs.) and cooled to 0 °C. Pyridiniumchlorochromate (PCC, 13, 6.5 g, 30 mmol, 1.5 equiv) was added in small portions. The mixture was kept at 0 °C for 1 h and then stirred for 4 h at room temperature. Silica was added to the mixture and the solvent was evaporated. Purification was performed by distillation. Yield 71.9%. ^{1}H NMR (500 MHz, DMSO) δ 6.60 (s, 2H), 6.66 (d, J = 8.1 Hz, 1H), 6.73–6.77 (m, 1H), 7.27–7.32 (m, 1H), 7.45 (d, J = 8.2, 1H), 9.89 (s, 1H). ^{13}C NMR (126 MHz, DMSO) δ 115.5, 116.2, 118.4, 134.9, 135.5, 149.3, 193.1. C_7H_7NO. MS (ESI+): m/z 122.6 (4.5, (M+H)$^+$), 144.6 (100, (M+Na)$^+$). (agrees with[28])

5.1.2.12. *N*-(2-Formylphenyl)-2-naphthamide (14). Preparation according to general procedure b using **12** and 2-naphthoyl chloride (**8j**). Purification was performed by recrystallization from pentane/acetone. Yield 80.1%. ^{1}H NMR (500 MHz, DMSO) δ 11.87 (s, 1H), 10.09 (s, 1H), 8.61 (s, 1H), 8.53 (d, J = 8.2 Hz, 1H), 8.14 (d, J = 8.3 Hz, 2H), 8.09–8.02 (m, 2H), 7.99 (dd, J = 7.7, 1.5 Hz, 1H), 7.83–7.74 (m, 1H), 7.74–7.59 (m, 2H), 7.45–7.37 (m, 1H). ^{13}C NMR (126 MHz, DMSO) δ 196.16, 166.02, 140.53, 136.22, 135.17, 135.03, 132.67, 131.76, 129.62, 129.21, 128.80, 128.61, 128.22, 127.66, 124.49, 124.39, 123.95, 121.13. $C_{18}H_{13}NO_2$. MS (ESI−): m/z 274.13 ((M−H)$^-$, 100).

5.2. Reporter gene assay

5.2.1. Cell culture

HeLa cells were grown in DMEM high glucose, supplemented with 10% fetal calf serum (FCS), 1% sodium pyruvate (SP) and 1% penicillin/streptomycin (PS) at 37 °C and 5% CO_2.

5.2.2. Plasmids for full length FXR transactivation assay

pcDNA3-hFXR contains the sequence of human FXR and was already published elsewhere,[29] pGL3basic (Promega, Mannheim, Germany) was used as a reporter plasmid, with a shortened construct of the promotor of the bile salt export pump (BSEP, sequence of construct from[30]) cloned into the SacI/NheI cleavage site in front of the luciferase gene. pRL-SV40 (Promega) was transfected as a control for normalization of transfection efficacy and cell growth. pSG5-hRXR was already published elsewhere as well.[31]

5.2.4. Full length FXR transactivation assay

24 h before transfection, HeLa cells were seeded in 96-well plates with a density of 8000 cells per well. 3, 5 h before transfection, medium was changed to DMEM high glucose, supplemented with 1% SP, 1% PS and 0.5% charcoal-stripped FCS. Transient transfection of HeLa cells with BSEP-pGL3, pRL-SV40 and the expression plasmids pcDNA3-hFXR and pSG5-hRXR was carried out using calcium phosphate transfection method. 16 h after transfection, medium was changed to DMEM high glucose, supplemented with 1% SP, 1% PS and 0.5% charcoal-stripped FCS. 24 h after transfection, medium was changed to DMEM without phenol red, supplemented with 1% SP, 1% PS, 1% L-glutamate and 0.5% charcoal-stripped FCS, now additionally containing 0.1% DMSO and the respective test compound or 0.1% DMSO alone as untreated control. Each concentration was tested in triplicate wells and each experiment was repeated independently at least three times. Following 24 h incubation with the test compounds, cells were assayed for luciferase activity using Dual-Glo™ Luciferase Assay System (Promega) according to the manufacturer's protocol. Luminescence was measured with a Tecan Infinite M200 luminometer (Tecan Deutschland GmbH, Crailsheim, Germany). Normalization of transfection efficacy and cell growth was done by division of firefly luciferase data by renilla luciferase data resulting in relative light units (RLU). Fold activation was obtained by dividing the mean RLU of the tested compound at a respective concentration by the mean RLU of untreated control. Relative activation was obtained by dividing the fold activation of the tested compound at a respective concentration by the fold activation of FXR full agonist GW4064 (**2**) at 3 μM. EC_{50} and standard error of the mean values were calculated with the mean relative activation values of at least three independent experiments by SigmaPlot 10.0 (Systat Software GmbH, Erkrath, Germany) using a four parameter logistic regression.

6. Metabolism assay

The solubilized test compounds (5 μL, final concentration 10 μM in DMSO) were preincubated at 37 °C in 432 μL of phosphate buffer (0.1 M, pH 7.4) together with a 50 μL NADPH regenerating system (30 mM glucose-6-phosphate, 4 U/mL glucose-6-phosphate dehydrogenase, 10 mM NADP, 30 mM $MgCl_2$). After 5 min, the reaction was started by the addition of 13 μL of microsome mix from the liver of Sprague–Dawley rats (Invitrogen, Darmstadt, Germany; 20 mg protein/mL in 0.1 M phosphate buffer) in a shaking water bath at 37 °C. The reaction was stopped by addition of 250 μL of ice-cold methanol at 0, 15, 30, and 60 min. The samples were diluted with 250 μL of DMSO and centrifuged at 10,000*g* for 5 min at 4 °C. The supernatants were analyzed, and test compounds were quantified by HPLC: mobile phase,

MeOH 83%/H_2O 17%/formic acid 0.1%; flow-rate, 1 mL/min; stationary phase, MultoHigh Phenyl phase, 5 μm, 250 × 4 precolumn, phenyl, 5 μm, 20 × 4; detection wavelength, 330 and 254 nm; injection volume, 50 μL. Control samples were performed to check the stability of the compounds in the reaction mixture: first control was without NADPH, which is needed for the enzymatic activity of the microsomes, second control was with inactivated microsomes (incubated for 20 min at 90 °C), third control was without test compounds (to determine the baseline). The amounts of the test compounds were quantified by an external calibration curve, where data are expressed as means ± SEM of single determinations obtained in three independent experiments. The metabolism experiments showed the following curves: **15j** (n = 4): 0 min–96 ± 2%; 15 min–93 ± 2%; 30 min–93 ± 2%; 60 min–92 ± 2%; 20 (n = 3): 0 min–100 ± 1%; 15 min–86 ± 2%; 30 min–76 ± 4%; 60 min–61 ± 2%.

7. WST-1 assay in HepG2 cells

The WST-1 assay from Roche was performed according to manufacturer's protocol (Roche Diagnostics, Mannheim, Germany). In brief, HepG2 cells were seeded in 96-well plates (30,000 cells per well) in DMEM containing 1% PS and 1% FCS. After 24 h cells were incubated with compounds **15j**, **20** (final concentrations 10 μM, 30 μM, 60 μM 100 μM), Revlotron (100 μM, Sigma Aldrich) as positive control, and Zileuton (100 μM, Sigma Aldrich) and DMEM + 1% DMSO as negative controls. After 48 h WST reagent (Roche) was added to each well according to manufacturer's instructions. After 45 min incubation absorption (450 nm/reference: 620 nm) was determined with a TEACAN Infinite M200 luminometer. Each experiment was repeated three times in triplicates. Results (expressed as percent of untreated control): **15j**: 10 μM = 92 ± 8%; 30 μM = 90 ± 7%; 60 μM = 81 ± 1%; 100 μM = 84 ± 4%. **20**: 10 μM = 93 ± 5%; 30 μM = 65 ± 1%; 60 μM = 50 ± 7%; 100 μM = 46 ± 9%. Values are expressed as mean ± SEM; n = 3.

Supplementary data

Supplementary data associated with this article can be found, in the online version, at http://dx.doi.org/10.1016/j.bmc.2014.02.053.

References and notes

1. Fiorucci, S.; Mencarelli, A.; Distrutti, E.; Palladino, G.; Cipriani, S. *Curr. Med. Chem.* **2010**, *17*, 139.
2. Fiorucci, S.; Mencarelli, A.; Distrutti, E.; Zampella, A. *Future Med. Chem.* **2012**, *4*, 877.
3. Düfer, M.; Hörth, K.; Krippeit-Drews, P.; Drews, G. *Islets* **2012**, *4*, 333.
4. Li, Y.; Jadhav, K.; Zhang, Y. *Biochem. Pharmacol.* **2013**, *86*, 1517.
5. Adorini, L.; Pruzanski, M.; Shapiro, D. *Drug Discovery Today* **2012**, *17*, 988.
6. Musso, G.; Gambino, R.; Cassader, M. *Progress Lipid Res.* **2013**, *52*, 175.
7. Nijmeijer, R. M.; Gadaleta, R. M.; van Mil, S. W.; van Bodegraven, A. A.; Crusius, J. B.; Dijkstra, G.; Hommes, D. W.; de Jong, D. J.; Stokkers, P. C.; Verspaget, H. W.; Weersma, R. K.; van der Woude, C. J.; Stapelbroek, J. M.; Schipper, M. E.; Wijmenga, C.; van Erpecum, K. J.; Oldenburg, B. *PLoS ONE* **2011**, *6*, e23745.
8. Hollman, D.; Milona, A.; van Erpecum, K.; van Mil, S. *Biochim. Biophys. Acta* **2012**, *1821*, 1443.
9. Wildenberg, M. E.; van den Brink, G. R. *Gut* **2011**, *60*, 432–433.
10. Hageman, J.; Herrema, H.; Groen, A.; Kuipers, F. *Arterioscler. Thromb. Vasc. Biol.* **2010**, *30*, 1519.
11. Mencarelli, A.; Fiorucci, S. *J. Cell. Mol. Med.* **2010**, *14*, 79.
12. Wang, X.; Fu, X.; van Ness, C.; Meng, Z.; Ma, X.; Huang, W. *Curr. Pathobiol. Rep.* **2013**, *1*, 29.
13. Merk, D.; Steinhilber, D.; Schubert-Zsilavecz, M. *Future Med. Chem.* **2012**, *4*, 1015.
14. Pellicciari, R.; Fiorucci, S.; Camaioni, E.; Clerici, C.; Costantino, G.; Maloney, P. R.; Morelli, A.; Parks, D. J.; Willson, T. M. *J. Med. Chem.* **2002**, *45*, 3569.
15. Gioiello, A.; Macchiarulo, A.; Carotti, A.; Filipponi, P.; Costantino, G.; Rizzo, G.; Adorini, L.; Pellicciari, R. *Bioorg. Med. Chem.* **2011**, *19*, 2650.
16. Maloney, P. R.; Parks, D. J.; Haffner, C. D.; Fivush, A. M.; Chandra, G.; Plunket, K. D.; Creech, K. L.; Moore, L. B.; Wilson, J. G.; Lewis, M. C.; Jones, S. A.; Willson, T. M. *J. Med. Chem.* **2000**, *43*, 2971.
17. Merk, D.; Steinhilber, S.; Schubert-Zsilavecz, M. *Expert Opin. Drug Discov.* **2014**, *9*, 27.
18. Akwabi-Ameyaw, A.; Bass, J. Y.; Caldwell, R. D.; Caravella, J. A.; Chen, L.; Creech, K. L.; Deaton, D. N.; Jones, S. A.; Kaldor, I.; Liu, Y.; Madauss, K. P.; Marr, H. B.; McFadyen, R. B.; Miller, A. B.; Iii, F. N.; Parks, D. J.; Spearing, P. K.; Todd, D.; Williams, S. P.; Wisely, G. B. *Bioorg. Med. Chem. Lett.* **2008**, *18*, 4339.
19. Chiang, P. C.; Thompson, D. C.; Ghosh, S.; Heitmeier, M. R. *J. Pharm. Sci.* **2011**, *100*, 4722.
20. Howarth, D. L.; Law, S. H.; Law, J. M.; Mondon, J. A.; Kullman, S. W.; Hinton, D. E. *Toxicol. Appl. Pharmacol.* **2010**, *243*, 111.
21. Flatt, B.; Martin, R.; Wang, T. L.; Mahaney, P.; Murphy, B.; Gu, X. H.; Foster, P.; Li, J.; Pircher, P.; Petrowski, M.; Schulman, I.; Westin, S.; Wrobel, J.; Yan, G.; Bischoff, E.; Daige, C.; Mohan, R. *J. Med. Chem.* **2009**, *52*, 904.
22. Mudaliar, S.; Henry, R.; Sanyal, A.; Morrow, L.; Marschall, H.; Kipnes, M.; Adorini, L.; Sciacca, C.; Clopton, P.; Castelloe, E.; Dillon, P.; Pruzanski, M.; Shapiro, D. *Gastroenterology* **2013**, *145*, 574.
23. Richter, H. G.; Benson, G. M.; Bleicher, K. H.; Blum, D.; Chaput, E.; Clemann, N.; Feng, S.; Gardes, C.; Grether, U.; Hartman, P.; Kuhn, B.; Martin, R. E.; Plancher, J. M.; Rudolph, M. G.; Schuler, F.; Taylor, S. *Bioorg. Med. Chem. Lett.* **2011**, *21*, 1134. http://www.rcsb.org/pdb/ PDB-ID: 3OLF.
24. Watanabe, M.; Horai, Y.; Houten, S.; Morimoto, K.; Sugizaki, T.; Arita, E.; Mataki, C.; Sato, H.; Tanigawara, Y.; Schoonjans, K.; Itoh, H.; Auwerx, J. *J. Biol. Chem.* **2011**, *286*, 26913.
25. Achenbach, J.; Gabler, M.; Steri, R.; Schubert-Zsilavecz, M.; Proschak, E. *Med. Chem. Commun.* **2013**, *4*, 920.
26. Venuti, M. C. *Synthesis* **1982**, *4*, 266.
27. Miteva, M. A.; Violas, S.; Montes, M.; Gomez, D.; Tuffery, P.; Villoutreix, B. O. *Nucleic Acids Res.* **2006**, *34*, W738. http://bioserv.rpbs.univ-paris-diderot.fr/Help/FAFDrugs.html.
28. Maddani, M. R.; Moorthy, S. K.; Prabhu, K. R. *Tetrahedron* **2010**, *66*, 329.
29. Steri, R.; Achenbach, J.; Steinhilber, D.; Schubert-Zsilavecz, M.; Proschak, E. *Biochem. Pharmacol.* **2012**, *83*, 1674.
30. Ananthanarayanan, M.; Balasubramanian, N.; Makishima, M.; Mangelsdorf, D. J.; Suchy, F. J. *J. Biol. Chem.* **2001**, *276*, 28857.
31. Seuter, S.; Väisänen, S.; Rådmark, O.; Carlberg, C.; Steinhilber, D. *Biochim. Biophys. Acta* **2007**, *1771*, 864.

Journal of Medicinal Chemistry

Article

pubs.acs.org/jmc

Extending the Structure–Activity Relationship of Anthranilic Acid Derivatives As Farnesoid X Receptor Modulators: Development of a Highly Potent Partial Farnesoid X Receptor Agonist

Daniel Merk,*[,†] Christina Lamers,[†] Khalil Ahmad,[†] Roberto Carrasco Gomez,[†] Gisbert Schneider,[‡] Dieter Steinhilber,[†] and Manfred Schubert-Zsilavecz[†]

[†]Institute of Pharmaceutical Chemistry, Goethe University Frankfurt, Max-von-Laue-Strasse 9, 60438 Frankfurt, Germany

[‡]Department of Chemistry and Applied Biosciences, ETH Zürich, Vladimir-Prelog-Weg 1-5/10, 8093 Zürich, Switzerland

Supporting Information

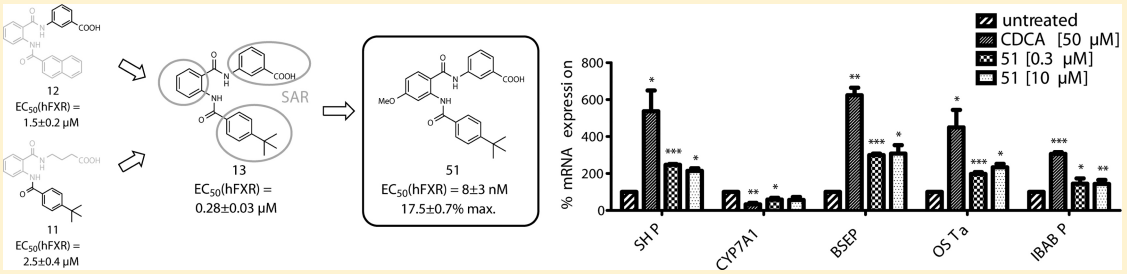

ABSTRACT: The ligand activated transcription factor nuclear farnesoid X receptor (FXR) is involved as a regulator in many metabolic pathways including bile acid and glucose homeostasis. Therefore, pharmacological activation of FXR seems a valuable therapeutic approach for several conditions including metabolic diseases linked to insulin resistance, liver disorders such as primary biliary cirrhosis or nonalcoholic steatohepatitis, and certain forms of cancer. The available FXR agonists, however, activate the receptor to the full extent which might be disadvantageous over a longer time period. Hence, partial FXR activators are required for long-term treatment of metabolic disorders. We here report the SAR of anthranilic acid derivatives as FXR modulators and development, synthesis, and characterization of compound **51**, which is a highly potent partial FXR agonist in a reporter gene assay with an EC_{50} value of 8 ± 3 nM and on mRNA level in liver cells.

INTRODUCTION

As a ligand activated transcription factor, nuclear farnesoid X receptor (FXR) regulates several metabolic pathways involved in bile acid, triglyceride, and glucose homeostasis. It binds to specific response elements on the DNA as monomer or as heterodimer with RXR and controls the transcription of genes especially involved in bile acid synthesis and metabolism when activated by its physiological ligands, the bile acids.[1,2]

Modulation of FXR may be a valuable therapeutic approach for various pathophysiological conditions. FXR activation showed promising results in vitro and in vivo for the treatment of metabolic,[3−8] neoplastic,[9] as well as inflammatory[10−15] diseases such as diabetes and inflammatory bowel disease. Clinical development of FXR agonists for the treatment of the liver disorders primary biliary cirrhosis (PBC), nonalcoholic steatohepatitis (NASH), and nonalcoholic fatty liver disease (NAFLD) is ongoing.[6,16,17] Most recently, an in vivo model indicated that the very beneficial metabolic effects of vertical sleeve gastrectomy in adipose individuals could be due to activation of FXR.[18]

A number of synthetic steroidal and nonsteroidal FXR agonists has been developed so far (reviewed in ref 19). By introduction of an additional ethyl residue in the most potent physiological FXR ligand chenodeoxycholic acid (CDCA, **1**, Scheme 1), 6α-ethyl-CDCA[20] (6-ECDCA, obeticholic acid, INT-747, **2**, Scheme 1) was discovered, which is presently being investigated in clinical phase II and III trials for PBC, NASH, and NAFLD.[17] The most important and widely used nonsteroidal FXR agonist is GW4064[21] (**3**, Scheme 1), which served as a model or reference compound in many experiments. **3** and several other synthetic nonsteroidal FXR agonists, however, have a poor bioavailability or show toxic effects which limit their clinical utility.[19,22−25] In addition, a recent study indicated that GW4064 (**3**) is active on several off-targets.[26]

CDCA (**1**), 6-ECDCA (**2**), and GW4064 (**3**) all constitute full FXR agonists. For GW4064 (**3**), the EC_{50} value varies in literature depending on the applied test system from 15 nM in a coactivator recruitment assay to 0.9 μM in a reporter gene assay. 6-ECDCA (**2**) was characterized with an EC_{50} value of 99 nM for coactivator recruitment and 85 nM in a reporter gene assay (reviewed in ref 27).

Given the fact that conditions which might be treatable with FXR ligands are predominantly metabolic diseases that require

Received: June 20, 2014
Published: September 13, 2014

   dx.doi.org/10.1021/jm500937v | J. Med. Chem. 2014, 57, 8035−8055

Scheme 1. Important FXR Agonists CDCA (1), 6-ECDCA (2), and GW4064 (3)

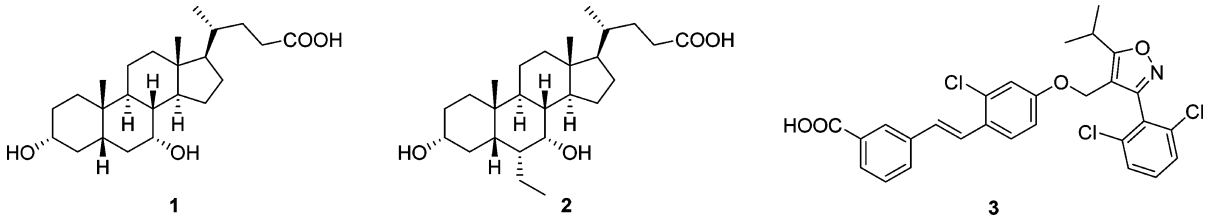

Scheme 2. Synthesis Routes for Preparation of the Tested Acylanthranilic Amides

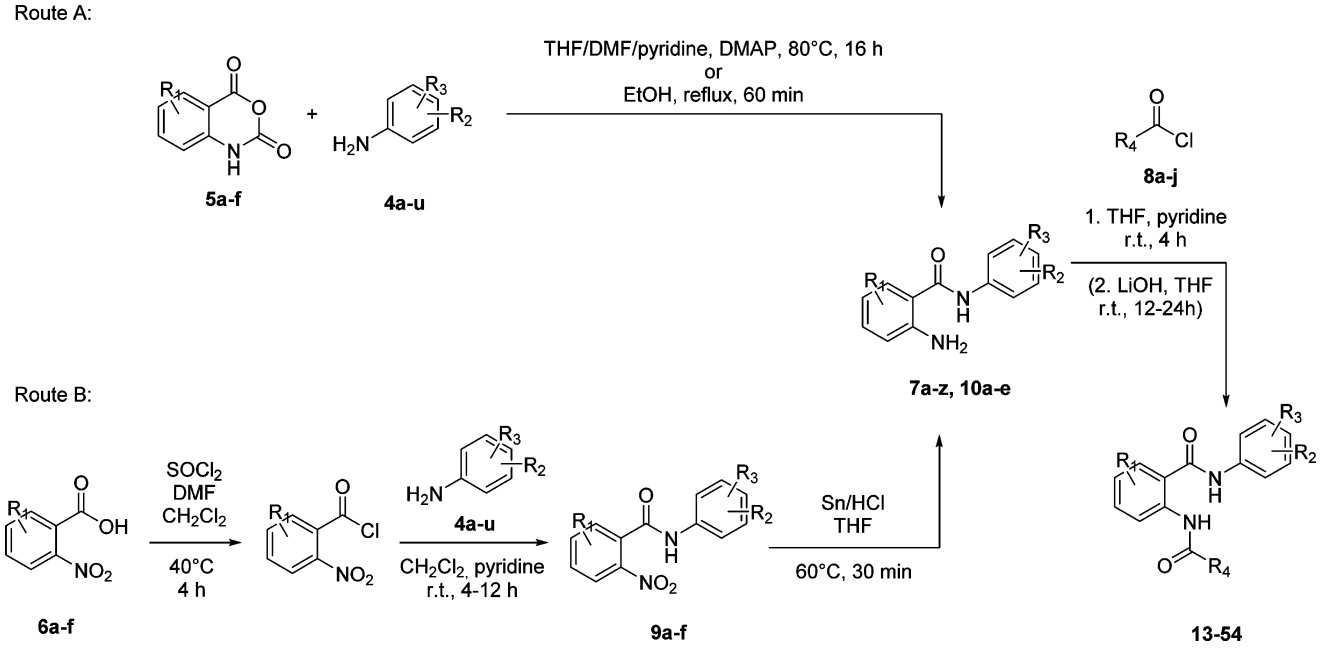

a stable long-term therapy, well tolerated agents are required that can be applied over long time. Many of the known FXR ligands, however, exhibit toxicity and show poor bioavailability.[19,22−25] In addition, targeting of nuclear receptors involved in metabolic processes such as FXR and PPARγ has taught that full activation of a ligand activated transcription factor may lead to various side effects in long-term treatment and that full activation is not necessarily required for beneficial effects.[25] New potent FXR modulators are therefore needed that do not exhibit full agonism but only activate the nuclear receptor to a partial extent.

We recently described the discovery and development of anthranilic acid derivatives as novel FXR agonists.[28,29] Here we report the optimization of the anthranilic acid scaffold to highly potent FXR partial agonists by structure−activity relationship (SAR) studies and molecular docking. Optimized compound **51** constitutes a potent partial FXR agonist with an EC_{50} value of 8 ± 3 nM and a maximum relative FXR activation of 17.5 ± 0.7% in a FXR reporter gene assay.

RESULTS

Chemistry. Anthranilic acid derivatives were generated via two different synthetic strategies depending on the reactivity and availability of starting materials.

Synthetic route A involved the *ortho*-aminobenzoylation of an aniline derivative (**4a−u**) with a derivative of isatoic anhydride (**5a−f**) to introduce the acidic headgroup at the anthranilic acid core structure. We previously reported this *ortho*-aminobenzoylation of amines or anilines in a mixture of DMF and pyridine at 80 °C and in the presence of 4-DMAP as a catalyst.[28] For several substituted anilines that were necessary for our SAR, these conditions however led to very poor yields. Better yields could be achieved when the reaction was carried out in absolute ethanol under reflux with an excess of the isatoic anhydride derivative (**5a−f**). The better performance of this reaction in ethanol may probably be due to better solubility and the presence of a protic solvent (Scheme 2).

For some aniline derivatives as headgroup substituents that showed a very poor nucleophilicity, another synthetic strategy was necessary. In addition, some isatoic anhydride derivatives containing certain substituents were not commercially available. In these cases, synthetic route B was used.

Synthetic route B started with *ortho*-nitrobenzoic acid derivatives (**6a−f**), which were activated by chlorination with thionyl chloride in methylene chloride in the presence of catalytic amounts of DMF and subsequently reacted with the respective aniline derivatives (**4a−u**) in THF/pyridine to introduce the headgroup substituents. By reduction of the nitro group of the resulting derivatives **9a−f** with tin and hydrochloric acid in THF, the required *ortho*-aminobenzoylaniline derivaties (**7a−z, 10a−e**) were available (Scheme 2).

Finally, the *ortho*-aminobenzoylaniline derivatives **7a−z** and **10a−e** from route A or B were reacted with various acyl chlorides (**8a−j**) to introduce the acyl substituent at the aniline group of the anthranilic acid core structure. For some compounds, a final alkaline ester hydrolysis was necessary

dx.doi.org/10.1021/jm500937v | J. Med. Chem. 2014, 57, 8035−8055

Scheme 3. Synthesis of Tetrazole Derivative 27 and Amide 28

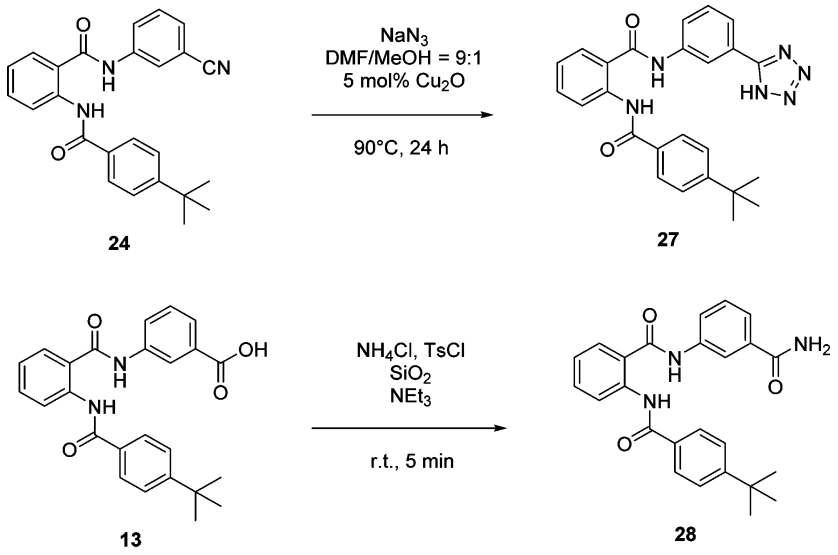

Scheme 4. Development of Compound 13

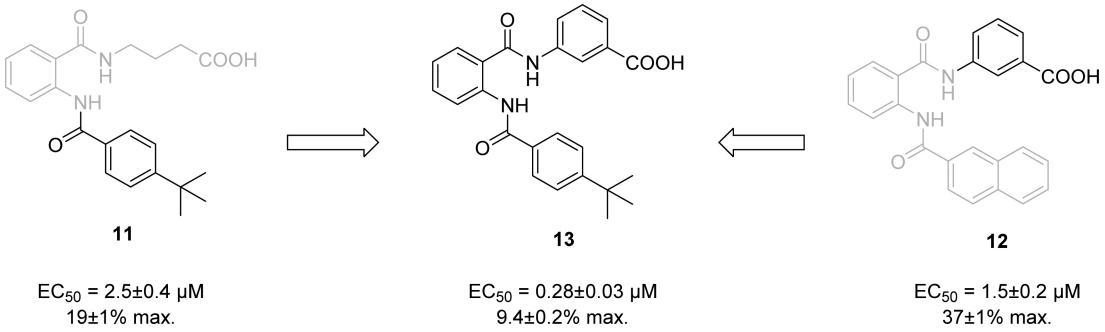

after this synthesis procedure to yield the test compound (Scheme 2).

The bioisosteric derivatives **27** and **28** were generated by different strategies. Tetrazole derivative **27** was obtained by cycloaddition of sodium azide and nitrile **24** in DMF/MeOH in the presence of catalytic amounts copper(I) oxide.[30] For the preparation of amide **28**, the respective carboxylic acid derivative **13** was used as starting material and reacted with silica supported ammonium chloride in the presence of tosyl chloride and triethyl amine as described previously[31] (Scheme 3).

Biological Evaluation and Structure–Activity Relationships. In our first SAR study, we discovered compounds **11** (EC_{50} = 2.5 ± 0.4 μM, 19 ± 1% max) and **12** (EC_{50} = 1.5 ± 0.2 μM, 37 ± 1% max) as FXR partial agonists with moderate potency. Recombination of the 3-aminobenzoic acid of **12** as headgroup and the 4-*tert*-butylbenzoyl moiety of **11** as lipopholic acyl substituent in compound **13** resulted in improved potency and provided the starting point of this SAR study (**13**, EC_{50} = 0.28 ± 0.03 μM, 9.4 ± 0.2% max, Scheme 4). With compound **13** as the starting point, we investigated the SAR of the lipophilic acyl substituent, the acidic headgroup, and the anthranilic acid core structure.

FXR activity was determined in a full-length FXR reporter gene assay in HeLa cells that were transiently transfected with hFXR (constitutively expressed, CMV promoter), hRXR (constitutively expressed, CMV promoter), a firefly luciferase (reporter gene) under the control of a minimum BSEP promoter, and a constitutively expressed renilla luciferase with SV40 promoter as internal control for transfection efficiency and toxicity. As reference compound, GW4064 (**3**) was used in a concentration of 3 μM, which we set as 100% FXR activation. The assay was validated with CDCA (**1**), which had an EC_{50} of 18 ± 1 μM with 88 ± 3% maximum relative FXR activation and 6-ECDCA (**2**), which showed an EC_{50} of 0.16 ± 0.02 μM (87 ± 3% max).

We first analyzed fragments of the lead compound **13** to evaluate the possibility of reducing the size of the compounds. Fragment **7a** without lipophilic acyl substituent and anthranilic acid were inactive, however. We then inverted both amide bonds of compound **13**, resulting in **14**, which was inactive on FXR as well.

In case of the lipophilic acyl substituent, the SAR was equally steep as we have already observed in our first SAR study.[28] Replacement of the 4-*tert*-butyl moiety of **13** by comparably large and lipophilic residues such as a trifluoromethyl group (**15**) or a bromine atom (**16**) strongly reduced the potency. In our first SAR study, also a 2-naphthoyl substituent (**12**) showed potent FXR activating results. We therefore investigated potential bioisosters and homologues of this moiety. A methylenedioxo residue (**17**), a dihydrobenzodioxine residue (**18**), and a 4-trifluoromethyl-3-fluorobenzyl moiety (**19**) were significantly less active than the 2-naphthoyl substituent (**12**). Moving the substitution from 4-position of the aromatic ring to 3- and 5-positions in **20** or the introduction of additional carbon atoms between amide group and aromatic ring in **21**

dx.doi.org/10.1021/jm500937v | J. Med. Chem. 2014, 57, 8035–8055

Table 1. In Vitro Activities of 7a and 13−22 in the Full-Length FXR Transactivation Assay[a]

#	R	EC_{50} [μM] (max. rel. activation [%])	#	R	EC_{50} [μM] (max. rel. activation [%])
13	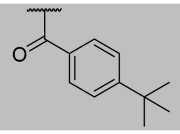	0.28±0.03 (9.4±0.2)	**18**	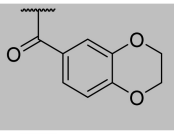	4.9±0.4 (23.3±0.4)
7a	H	i.a. (30 μM)	**19**	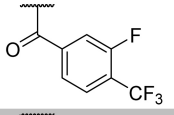	5.0±0.2 (32.4±0.5)
15	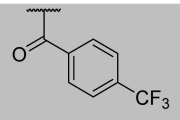	6.9±0.2 (26.2±0.4)	**20**	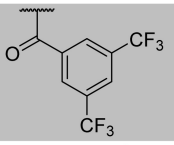	i.a. (30 μM)
16	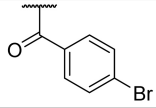	3.7±0.9 (14.3±0.9)	**21**	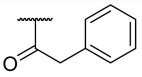	i.a. (30 μM)
17	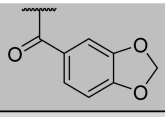	10.0±0.2 (12.2±0.5)	**22**	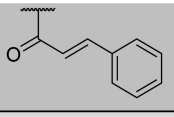	5.2±0.9 (15.6±0.5)
14	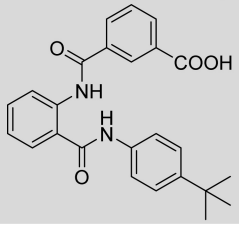				i.a.

[a]Values are expressed as mean ± SEM. i.a.: inactive.

and **22** reduced potency as well. Summarizing the above, the 4-*tert*-butylbenzoyl moiety of lead compound **13** proved to be the best substituent in this position (Table 1).

As next step, we investigated the SAR of the acidic headgroup. Therefore, we replaced the carboxylic acid with suitable bioisosters of the carboxylic acid and introduced additional carbon atoms between aromatic ring and carboxylic acid. Bioisosteric replacement of the carboxylic acid with a methyl ketone (**23**), a nitrile group (**24**), a methoxy group (**25**), or a methylmercaptan moiety (**26**) did not significantly change the potency of the compounds. A 1*H*-tetrazolyl moiety (**27**) as headgroup significantly enhanced the maximum relative activation activity at FXR, but the EC_{50} value was worsened by a factor 10. Replacement of the carboxylic acid by a carboxylic amide (**28**) improved the potency at FXR, but unfortunately the compound was quite toxic to the HeLa cells in our assay system, so we did not further investigate the amide moiety. The potency could also be improved by introduction of a second methoxy group as hydrogen bond acceptor in 2-position of the aromatic ring (**29**), while a third methoxy group (**30**) completely disrupted activity (Table 2).

By replacing the benzoic acid residue of **13** with a phenyl acetic acid (**31**), potency was slightly lowered while a 3-phenlylpropionic acid (**32**) increased the activity on FXR (Table 2).

To discover additional space for further substituents in the binding pocket, we introduced additional residues at the aromatic ring of the headgroup. A methyl group in 6-position (**33**) disrupted FXR activation activity, while a methyl group on either side of the carboxylic acid in 2- and 6-positions (**34** and **35**) strongly improved the potency of the compounds. Because docking of compound **13** into the FXR ligand binding site had suggested additional space for substituents in 4-position of the aromatic ring of the headgroup, we also investigated other residues than the methyl group (**33**), which was inactive. Introduction of a methoxy group (**36**), a fluorine (**37**), or chlorine atom (**38**) retained low FXR activating activity, but all compounds **36**−**38** showed lower potency than the lead compound. This worse activity might also be due to steric clashes between 4-substituent and the amide group, which makes the aromatic ring of the headgroup flip out of the plane of the central aromatic ring. This effect might however be generated by a larger substituent in the 2-position (compound **34**) as well (Table 3).

The best position for further substitution therefore seemed to be the 6-position (**35**) next to the carboxylic acid. We replaced the methyl group of **35**, which had strongly improved the potency of compound **13** by various other residues. However, the SAR was quite steep again. While the introduction of a methoxy group (**39**) retained the low

dx.doi.org/10.1021/jm500937v | J. Med. Chem. 2014, 57, 8035−8055

Table 2. In Vitro Activities of 23−32 in the Full-Length FXR Transactivation Assay[a]

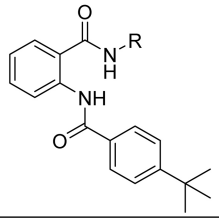

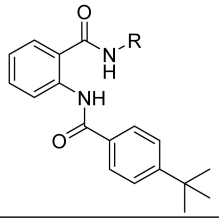

#	R	EC_{50} [μM] (max. rel. activation [%])	#	R	EC_{50} [μM] (max. rel. activation [%])
23	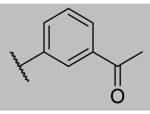	0.48±0.07 (18.8±0.5)	**28**	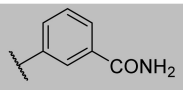	0.074±0.011 (14.8±0.3)
24	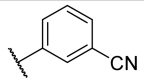	0.23±0.05 (17.5±0.8)	**29**	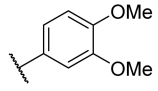	0.071±0.022 (12.7±0.2)
25	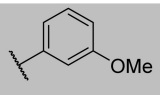	0.38±0.06 (13.3±0.7)	**30**	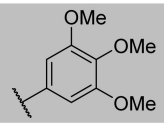	i.a. (30 μM)
26	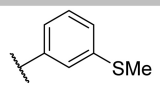	0.20±0.03 (8.6±0.3)	**31**	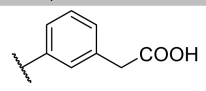	0.42±0.13 (26.4±1.4)
27	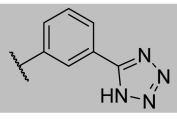	2.9±0.8 (39±4)	**32**	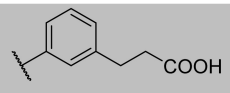	0.064±0.013 (21.8±0.6)

[a]Values are expressed as mean ± SEM. i.a.: inactive.

Table 3. In Vitro Activities of 33−42 in the Full-Length FXR Transactivation Assay[a]

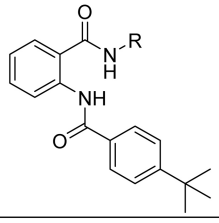

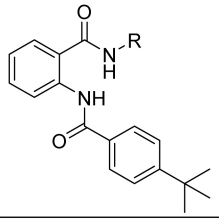

#	R	EC_{50} [μM] (max. rel. activation [%])	#	R	EC_{50} [μM] (max. rel. activation [%])
33	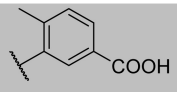	i.a. (30 μM)	**35**	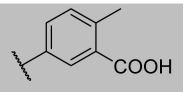	0.045±0.009 (22.4±0.5)
34	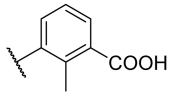	0.042±0.001 (19.0±0.2)	**39**	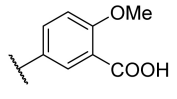	0.047±0.001 (19.1±0.5%)
36	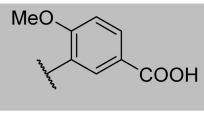	4.7±0.3 (14.9±0.2)	**40**	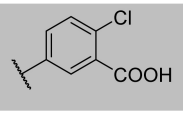	0.28±0.04 (18.7±0.4)
37	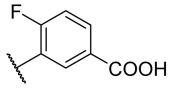	0.48±0.14 (12.0±0.4)	**41**	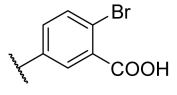	0.15±0.01 (16.4±0.2)
38	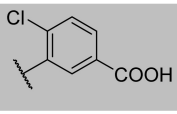	1.1±0.3 (15.6±0.7)	**42**	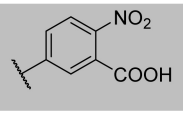	i.a. (30 μM)

[a]Values are expressed as mean ± SEM. i.a.: inactive.

dx.doi.org/10.1021/jm500937v | J. Med. Chem. 2014, 57, 8035−8055

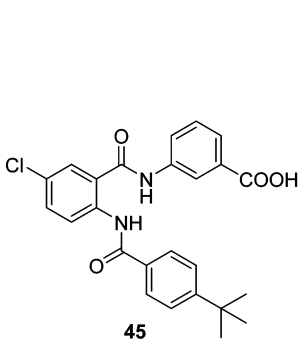

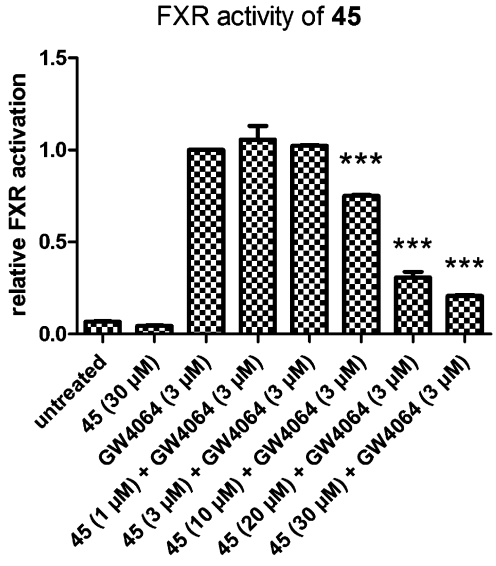

Figure 1. Antagonistic activity of **45** in competition with GW4064 (**3**) in the reporter gene assay. * $p < 0.05$; ** $p < 0.01$; *** $p < 0.001$.

Table 4. In Vitro Activities of 43−51 in the Full-Length FXR Transactivation Assay[a]

#	R_1 = COOH; R_2 = O	EC_{50} [μM] (max. rel. activation [%])	#	R_1 = COOH; R_2 = O	EC_{50} [μM] (max. rel. activation [%])
13	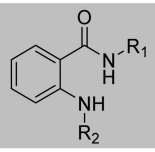	0.28±0.03 (9.4±0.2)	**47**	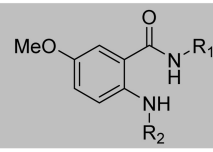	*antagonistic* IC_{50} = 15.1±0.1 μM (10±1% min.)
43	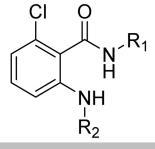	i.a. (30 μM)	**48**	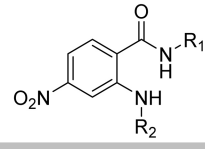	i.a. (30 μM)
44	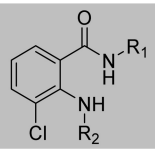	i.a. (30 μM)	**49**	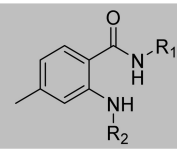	0.061±0.014 (21±1)
45	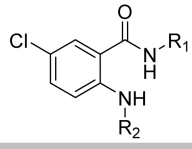	*antagonistic* IC_{50} = 12.3±0.6 μM (15±4% min.)	**50**	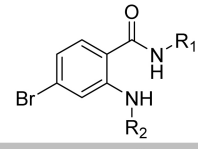	0.048±0.016 (15.4±0.9)
46	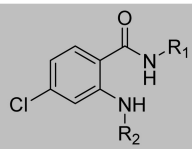	0.047±0.001 (19.1±0.5)	**51**	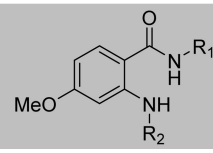	0.008±0.003 (17.5±0.7)

[a]Values are expressed as mean ± SEM. i.a.: inactive.

nanomolar activity of **35**, a chlorine (**40**) or bromine atom (**41**) reduced the potency by about 6-fold and 3-fold, respectively. Introduction of a nitro group (**42**) even completely disrupted the activity (Table 3).

dx.doi.org/10.1021/jm500937v | J. Med. Chem. 2014, 57, 8035−8055

At last we also investigated the availability of additional space around the anthranilic acid core structure of lead compound **13** by introducing chlorine atoms in every position of the aromatic ring. An additional chlorine atom in 3- or 6-positions of the anthranilic acid moiety (**43** and **44**) led to inactivity on FXR, which might be due to steric clashes with the amide groups that causes a different geometry. Chlorine substitution in the 5-position (**45**) interestingly led to moderate antagonistic activity on FXR (Figure 1), while a chlorine atom in the 4-position (**46**) improved the agonistic activity (Table 4).

In the next step, we replaced the chlorine atom in 4-position of compound **46** with various other substituents. In this case, the SAR was less steep than before. While the 4-nitro derivative **48** was inactive, the 4-methyl (**49**) as well as the 4-bromo derivative (**50**) were more potent than the 4-chloro derivative **46**. Introduction of a methoxy group in 4-position (**51**) finally led to the desired improvement of potency to a low nanomolar EC_{50} value (Table 4).

To confirm the antagonistic activity of **45**, we prepared derivative **47** with a methoxy group in the 5-position which exhibited a comparable antagonistic activity. Further investigation of this antagonism shall, however, be performed and discussed elsewhere (Table 4).

Finally, we investigated the possibility to recombine the best moieties of our SAR studies to further improve the potency. Therefore, we tested derivative **52** containing the 4-chloro substituent at the anthranilic acid core and the 6-methyl residue at the headgroup. Although potent on FXR, this compound (**52**) could not outmatch the derivatives **35** and **46** with only one of the substituents but was more or less equally potent. When the best residues, in particular the 4-methoxy group at the central aromatic ring and the 6-methyl group at the headgroup aromatic ring, were combined in **53**, potency was even slightly diminished. We assumed this might be due to steric clashes with the receptor by the double substitution and prepared the smallest possible compound with two substitutions (**54**) which contained a 4-methyl group at the anthranilic acid residue and a 6-methyl substituent at the headgroup. However, this derivative was again equally potent as the derivatives bearing only one of the methyl groups (**35** and **49**). Hence, **51** remained the best anthranilic acid derivative as FXR agonist (Tables 3, 4, and 5).

In Vitro Characterization of Compound 51. To further investigate the FXR agonist activity of compound **51**, we determined its effect on FXR target genes in the liver carcinoma cell line HepG2 and the colorectal adenocarcinoma cell line HT-29 by quantitative PCR experiments at the concentrations 0.1, 0.3, 1, 3, and 10 μM. **51** showed statistically significant partial agonist activity on FXR target genes. The mRNA of small heterodimer partner (SHP) was induced by about 2-fold (untreated, 100%; CDCA, 537 ± 113%; **51**, 0.1 μM 239 ± 88%, 0.3 μM 247 ± 4%, 1 μM 181 ± 12%, 3 μM 185 ± 18%, 10 μM 214 ± 14%) and mRNA of CYP7A1 (untreated, 100%; CDCA, 33 ± 8%; **51**, 0.1 μM 52 ± 17%, 0.3 μM 59 ± 9%, 1 μM 55 ± 11%, 3 μM 67 ± 10%, 10 μM 57 ± 16%), which is not a direct FXR target gene but affected via SHP induction, was repressed by about 2-fold. Also on the organic solute transporter α (OSTα: untreated, 100%; CDCA, 450 ± 94%; **51**, 0.1 μM 151 ± 11%, 0.3 μM 198 ± 10%, 1 μM 140 ± 14%, 3 μM 149 ± 13%, 10 μM 234 ± 19%), the bile salt export protein (BSEP: untreated, 100%; CDCA 624 ± 40%; **51**, 0.1 μM 294 ± 16%; 0.3 μM 300 ± 8%; 1 μM 319 ± 46%; 3 μM 326 ± 58%; 10 μM 308 ± 46%; GW4064 (**3**, 3 μM) 1523 ± 187%), and the ileal bile acid binding protein (IBABP: untreated, 100%; CDCA, 288 ± 15%; **51**, 0.1 μM 188 ± 42%, 0.3 μM 145 ± 29%, 1 μM 161 ± 12%, 3 μM 168 ± 29%, 10 μM 144 ± 22%), **51** showed a concentration independent partial agonistic activity. For all investigated target genes, this effect reached a maximum of about 40% of the effect produced by CDCA (**1**, 50 μM). The fact that **51** exhibited a constant effect on the target genes in a concentration range from 0.1 to 10 μM shows that **51** has a partial FXR agonistic activity not only in the reporter gene assay but on FXR target genes on mRNA level as well (Figure 2).

Table 5. In Vitro Activities of 52−54 in the Full-Length FXR Transactivation Assay[a]

#	R =	EC_{50} [μM] (max. rel. activation [%])
52	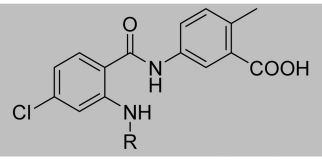	0.11±0.02 (20.1±0.5)
53	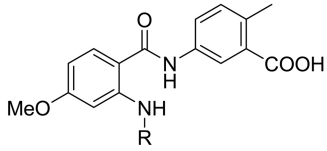	0.087±0.020 (22.3±0.7)
54	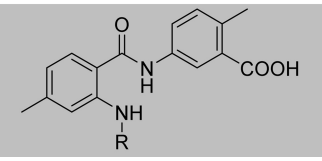	0.043±0.007 (16.8±0.3)

[a]Values are expressed as mean ± SEM. i.a.: inactive.

To characterize the pharmacological profile of **51**, we also investigated its activity on common off-targets. Compound **51** was inactive on the membrane bile acid receptor TGR5 (30 μM) and on PPARδ (3 μM). A slight activity on PPARγ and PPARα was observed (EC_{50}(PPARγ) = 2.99 ± 0.10 μM (81 ± 2% max); EC_{50} (PPARα) > 10 μM), which makes **51** about 375-fold selective for FXR over PPARγ and >1000-fold over PPARα, PPARδ, and the membrane bile acid receptor TGR5 (Figure 3A).

Furthermore, **51** showed an aqueous solubility of 2.6 mg/L and was quite stable against metabolism by liver microsomes in vitro. After 60 min incubation, 80.2 ± 0.2% of the compound were still detectable (Figure 3B).

Finally, we determined the toxicity of compound **51** which showed slight toxic effects on HeLa cells in the reporter gene assay starting from 30 μM. In HepG2 cells, **51** had an antiproliferative effect at concentrations of 30 μM and above in a WST-1 assay and exhibited acute toxicity at the same concentrations in an LDH assay (Figure 3C,D).

Receptor−Ligand Docking. Among the 25 available cocrystal structures of the FXR-LBD, the complex (PDB ID: 3OLF[32]) with the benzimidazole-based partial agonistic ligand **55** (EC_{50} = 0.5 μM, 51% max)[32] seemed most suited for docking studies on the here reported partial FXR agonists. Comparison of benzimidazole-based cocrystal structures (complexes of **55** (3OLF) and related derivatives (PDB IDs:

dx.doi.org/10.1021/jm500937v | J. Med. Chem. 2014, 57, 8035−8055

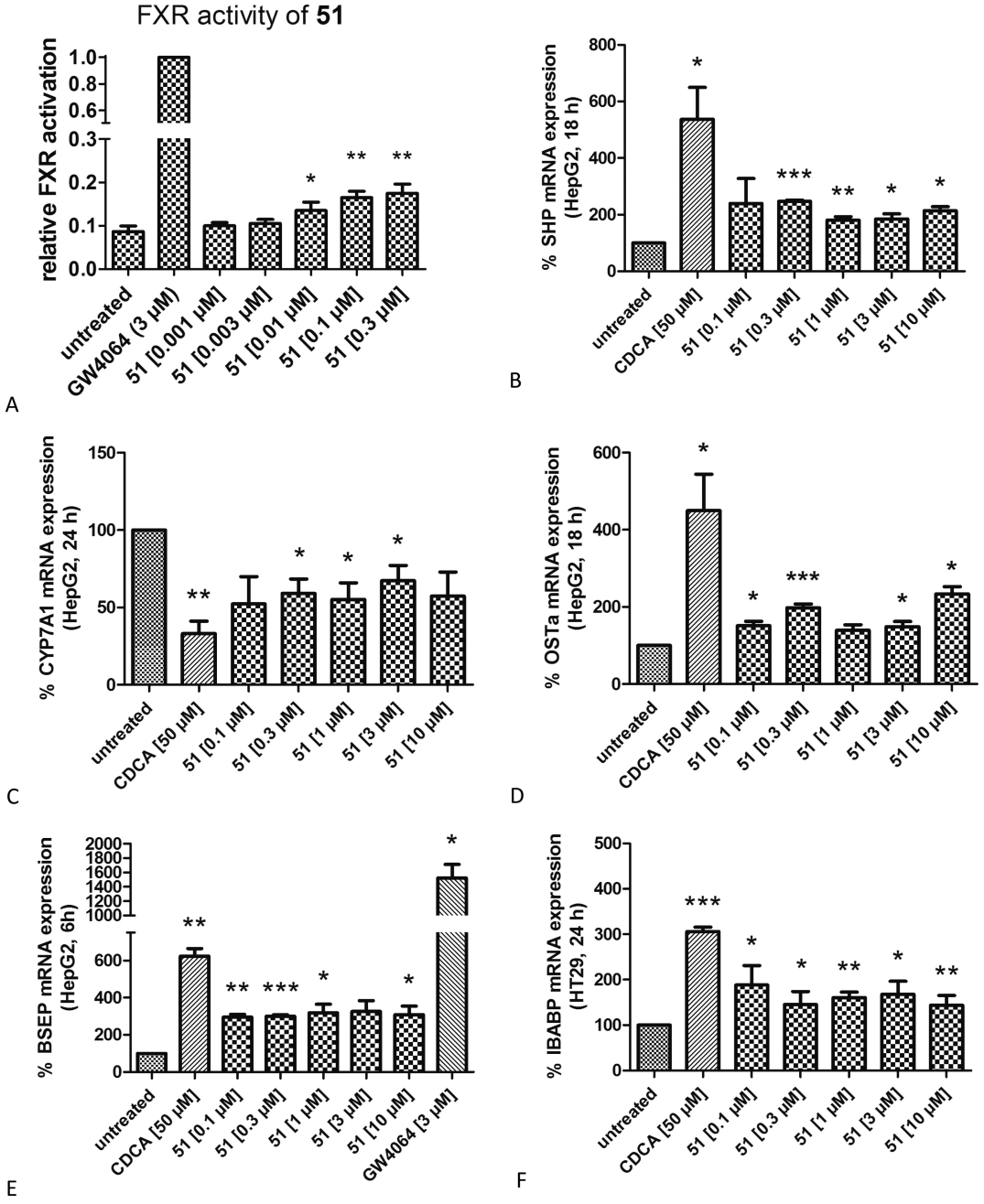

Figure 2. In vitro pharmacological activity of compound **51**. (A) Relative FXR activation of 51 in the reporter gene assay compared to 3 μM GW4064 (**3**), which is set as 100%. Nonlinear regression yielded an EC_{50} value of 8 $\pm$ 3 nM with 17.5% max rel activation; n = 5. (B) Effect of **51** on mRNA expression of direct FXR target gene SHP in HepG2 cells. Partial FXR agonist **51** (0.1, 0.3, 1, 3, 10 μM) induces SHP expression by about 2-fold (physiologic FXR agonist CDCA: 5.4-fold); effect independent from concentration; n = 4. (C) Effect of **51** (0.1, 0.3, 1, 3, 10 μM) on mRNA expression of indirect FXR target gene CYP7A1 in HepG2 cells. Partial FXR agonist **51** represses CYP7A1 expression to about 60% (physiologic FXR agonist CDCA: 33%); effect independent from concentration; n = 4. (D) Effect of **51** (0.1, 0.3, 1, 3, 10 μM) on mRNA expression of direct FXR target gene OSTα in HepG2 cells. Partial FXR agonist **51** induces OSTα expression by about 1.8-fold (physiologic FXR agonist CDCA: 4.5-fold); effect independent from concentration; n = 4. (E) Effect of **51** (0.1, 0.3, 1, 3, 10 μM) on mRNA expression of direct FXR target gene BSEP in HepG2 cells. Partial FXR agonist **51** induces BSEP expression by about 3-fold (physiologic FXR agonist CDCA, 6.5-fold; GW4064, 15-fold); effect independent from concentration; n = 4. (F) Effect of **51** (0.1, 0.3, 1, 3, 10 μM) on mRNA expression of direct FXR target gene IBABP in HT-29 cells. Partial FXR agonist **51** induces IBABP expression by about 1.7-fold (physiologic FXR agonist CDCA: 3-fold); effect independent from concentration; n = 4. * $p < 0.05$; ** $p < 0.01$; *** $p < 0.001$.

3OKH, 3OKI, 3OMK, 3OMM, 3OOF, 3OOK)) with the cocrystal structure of the GW4064-analogue **56** (PDB-ID: 3RUT[33]) revealed significant differences in the protein structure and in the form of the ligand binding pocket (Figure 4A). Especially, the helices 3 and 7 which form the ligand binding pocket are in significantly shifted positions. This influences the geometry of the ligand binding site. While the complexes of the partial agonistic benzimidazoles such as **55** reveal a triangular ligand binding pocket, the pocket of full agonistic ligands such as **56** is long and narrow. Docking of the here reported partial agonistic anthranilic acid derivatives in a model of the FXR-LBD derived from 3OLF[32] yielded sound

dx.doi.org/10.1021/jm500937v | J. Med. Chem. 2014, 57, 8035−8055

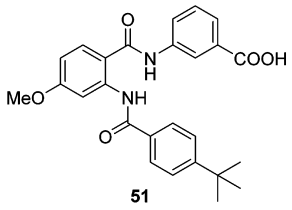

51

EC_{50}(hFXR) = 8±3 nM (17.5±0.7%); pEC_{50} = 8.1

molecular weight: 446
aqueous solubility: 2.6 mg/L; ***clogP***: 4.95
tPSA: 104.7;
H-bond donors: 3; ***H-bond-acceptors***: 7
LE: 0.24; ***SILE***: 2.83

selective over PPARs and membrane BA rec. TGR5 (***PPARα***: EC_{50} > 10 μM (not determined due to toxicity), selectivity > 1000-fold; ***PPARγ***: EC_{50} = 2.99±0.10 μM (81±2% max.), selectivity ~375-fold; ***PPARδ***: inactive (3 μM); ***TGR5***: inactive (30 μM))

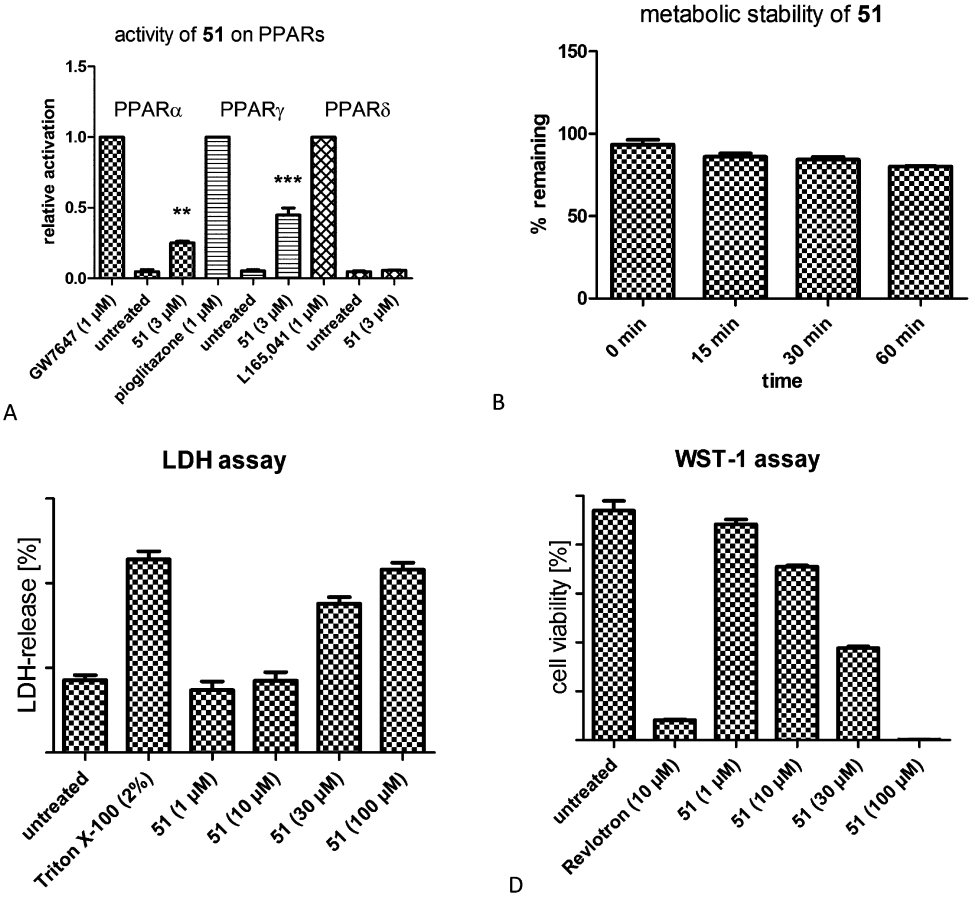

Figure 3. In vitro characterization of **51**. (A) off-target activity of compound **51**: **51** is highly selective over PPARs and the membrane bile acid receptor TGR5. (B) In vitro metabolism of **51** with Sprague Wistar Rat liver microsomes: after 60 min, 80.2 ± 0.2% of the compound were still detectable; $n = 4$. (C) LDH activity of HepG2 cells after 48 h treatment with compound **51**: **51** showed acute toxicity starting from 30 μM; $n = 4$. (D) WST-1 assay in HepG2 cells: 51 exhibited significant antiproliferative effects starting from 30 μM; $n = 4$.

docking poses. Accordingly, models derived from other benzimidazole-based FXR-LBD complexes led to equal results. However, docking of the anthranilic acid derivatives into models derived from FXR-LBD cocrystal structures with full agonistic ligands such as **56** revealed no reasonable docking poses in contrast. Therefore, the complex 3OLF[32] was used to generate the model for our docking studies.

Docking of lead compound **13** into the ligand binding site of FXR (model derived from PDB ID: 3OLF[32]) suggested prominent polar interactions of the benzoic acid with Arg_{335} and with Arg_{268} via a near water cluster formed by two water molecules. The lipophilic substituent was buried in a hydrophobic pocket formed by Phe_{333}, Leu_{291}, Leu_{455}, Met_{454}, and Trp_{458} (Figure 5A). Through elongation of the benzoic acid in **13** to phenylacetic acid (**31**), these interactions were weakened because the distances for polar interactions were not optimal. The Gibbs energies for the poses of **31** and **13** were however comparable (−8.9 and −8.7; Figure 5B). According to our docking, further elongation to phenylpropionic acid in **32** on the other hand strengthened the interactions with Arg_{335} and with Arg_{268} and led to displacement of one water molecule from the cluster (Figure 5C), which explains the rank order of potency of **13**, **31**, and **32**. Additionally, the Gibbs energy for the pose of **32** was significantly lower with −9.2 than for **31**.

Additionally, docking of **45** yielded an explanation for its antagonistic activity. Introduction of a chlorine substituent in 5-postion of the central aromatic ring in **45** seemed to shift the whole compound toward helix 7 and make a polar interaction with Tyr_{373} possible (Figure 5D,E). A comparable interaction of

dx.doi.org/10.1021/jm500937v | J. Med. Chem. 2014, 57, 8035−8055

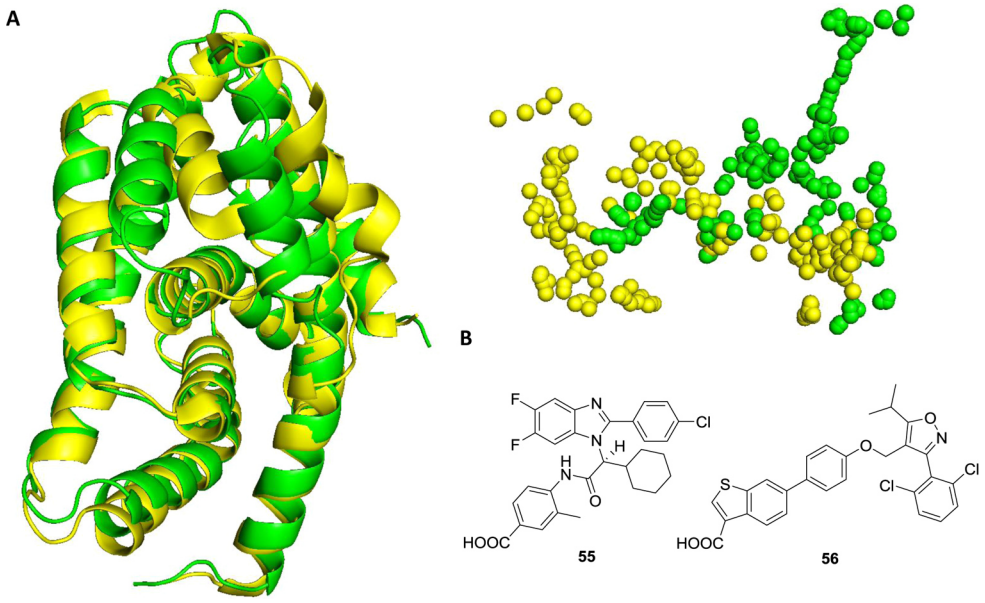

Figure 4. Comparison of the conformation (A) and pocket form (B) of the FXR-LBD cocrystal structures in complex with the partial agonist **55** (green, 3OLF) and the full agonist **56** (yellow, 3RUT). Helices 3 and 7 are shifted, which makes the ligand binding pocket of the partial agonistic conformation triangular, while in the full agonistic conformation, the pocket is long and narrow.

FXR antagonists with helix 7 has already been described previously.[33]

With an additional substituent in the 4-position of the headgroup aromatic ring (compounds **33** and **36**–**38**), the compounds cannot form the same docking pose as, e.g., **13** because the 4-substituent and the amide oxygen would form a steric clash. In the docking pose, both amide groups were flipped, and with this different geometry, a good binding pose and many beneficial interactions seemed to be lost (Figure 5F).

An additional substituent in the 4-position of the central aromatic ring (compounds **46** and **48**–**51**) in the docking was placed between helix 3 and helix 7, which slightly changed the whole binding mode of the compounds and led to a docking pose quite similar to the pose of phenylpropionic acid derivative **32**. The interactions with Arg_{335} and Arg_{268} as well as with the associated water cluster were strengthened, and one water molecule was displaced. Additionally, the docking pose suggested a further cation–π interaction of the headgroup aromatic ring with Met_{294} (Figure 5G/H). The displacement of one water molecule together with the more favorable relative position of the carboxylic acid function to Arg_{335} and Arg_{268} can explain the high rise in potency of compounds **46**, **49**, **50**, and **51**. There was no further polar interaction for compound **51**, but in addition to the displacement of one water molecule, the methoxy group and the *tert*-butylbenzoyl moiety were buried more deeply in lipophilic pockets, probably leading to the additional rise in potency (Figure 5I,J).

Substituents in the ortho-position of the carboxylic acid (6-position of headgroup, compounds **35** and **39**–**42**) also seemed to displace one water molecule from the water cluster associated with Arg_{335} and Arg_{268}, thereby increasing the potency of the compounds (Figure 5K). There seemed however not to be enough space for large substituents such as bromine (**41**) or a nitro group (**42**), which explains their loss in potency. On the other hand, the docking poses of **35** and **51** can explain why the combination of both beneficial substitutions in compounds **52** and **54** could not further improve the potency but led to approximately equally potent derivatives because one substitution alone is sufficient to displace a water from the cluster. The double substituted derivative **54** (green) was slightly twisted compared to the poses of **35** (pink) and **46** (blue). The Gibbs energies also support this thesis, with values of −9.6 for **35** and −8.3 for **53** (Figure 5K,L).

Finally, we tried to dock the optimized compound **51** in different models of the FXR-LBD derived from complexes of other compound classes than the benzimidazoles related to **55** on which our docking was based. Docking of **51** in FXR-LBD models derived from cocrystals of full FXR agonists such as **56** (PDB-ID: 3RUT[33]), which display a long and narrow binding pocket, yielded no reasonable docking poses however. The fact that **51** could only reasonably be docked in FXR models based on the partial agonistic benzimidazoles related to **55** further confirms the partial FXR agonistic activity of the acylanthranilic acid scaffold.

DISCUSSION AND CONCLUSIONS

We have intensively investigated the SAR of anthranilic acid derivatives as partial FXR agonists. Starting from compound **13**, which resulted from recombination of the best moieties in our first SAR study,[28] all structural features of the acyl anthranilamide scaffold and their impact on FXR activity have been evaluated. Inversion of the amide bonds (**14**) disrupted the activity on FXR, and we found no comparable or better lipophilic backbone substituent (compounds **15**–**22**) than the 4-*tert*-butylbenzoyl residue (**13**).

Interestingly, the acidic headgroup of **13** could be replaced by several bioisosteric moieties such as a nitrile (**24**), a methyl ketone (**23**), or even a methoxy group (**25**) without a significant change in potency. However, none of the bioisosteric groups improved the potency either and for reasons of solubility the carboxylic acid remained the most convenient residue.

By elongation of the acidic headgroup side chain from a benzoic acid (**13**) to phenylacetic acid (**31**) potency was slightly diminished, while further elongation to phenylpropionic

dx.doi.org/10.1021/jm500937v | J. Med. Chem. 2014, 57, 8035–8055

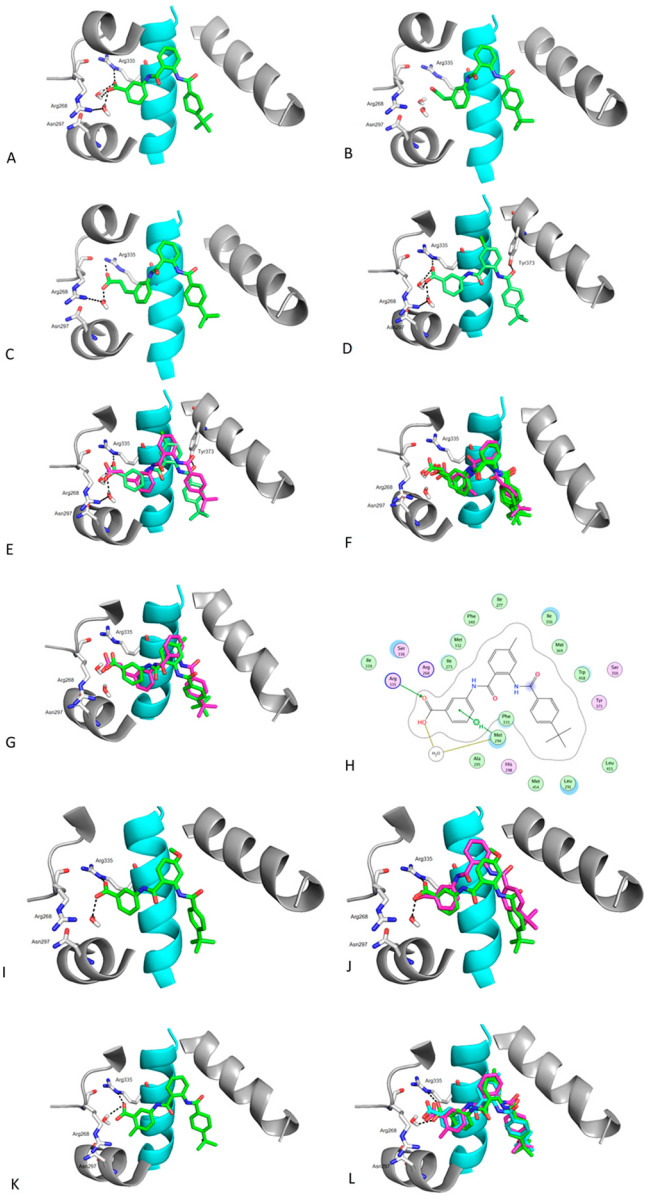

Figure 5. Docking poses of compounds docked to the FXR-LBD derived from 3OLF.[32] (A) lead compound **13**. (B) **31** with elongated side chain: the distances and angles of the acidic headgroup to Arg_{335}, Arg_{268}, and the associated water molecules are inappropriate for polar interactions. (C) **32** with further elongated side chain: **32** forms potent polar interactions with Arg_{335}, Arg_{268}, and the associated water molecules and displaces one water molecule from the cluster. (D) Antagonistic compound **45**. (E) **45** (green) in comparison with **32** (pink): **45** forms a different docking pose than the agonistic compounds and is shifted toward helix 7. (F) Introduction of an additional methyl substituent in the 4-position of the aromatic ring of the headgroup in **33** (pink) leads to a different docking pose in which the amide bonds are flipped and beneficial interactions are lost. (G) Methyl group in the 4-position of the central aromatic ring in **49** (green) leads to a docking pose similar to **32** (pink) with displacement of one water molecule from the cluster. (H) Additionally, in the docking pose, an additional interaction of **49** with Met_{294} is present. (I) Compound **51** displaces one water molecule from the water cluster and forms potent interactions with Arg_{335}, Arg_{268}, and the associated water molecule; furthermore, the lipophilic 4-*tert*-butylbenzoyl substituent is deeply buried in a lipophilic pocket and the methoxy group is placed in a lipophilic pocket next to helix 7. (J) Superimposed docking poses of **13** (pink) and **35** (green). (K) Methyl group in 6-position of the headgroup aromatic ring (**35**) also seems to displace one water molecule and forms a similar docking pose as **32** and **51**. (L) Superimposed docking poses of **35** (pink), **49** (light blue), and **54** (green): introduction of two methyl groups (4-position of the central aromatic ring and 6-position of the headgroup aromatic ring) does not lead to a more beneficial docking pose because each methyl group alone is sufficient to displace one water from the cluster associated with Arg_{335} and Arg_{268}.

acid (**32**) strongly improved the potency. This rank order of potency is best explained by interaction of the headgroup with a water cluster associated with Arg_{335} and Arg_{268} as suggested by the docking pose. While the benzoic acid (**13**) can well interact with the water cluster, for the phenylacetic acid moiety (**31**), angles and distances might be inappropriate for good interaction, and finally, the phenylpropionic acid (**32**) seems to form potent interactions with Arg_{335} and Arg_{268} and to displace one water molecule from the cluster.

By selectively substituting all free positions of the headgroup (**33**−**42**) and central aromatic ring (**43**−**51**), we discovered positions that through substitution either disrupted the activity of the compounds on FXR or strongly improved their potency. Additional substituents on the central aromatic moiety next to the amide bonds (**43** and **44**) led to inactivity which is probably due to steric clashes with the amide bonds and a consequently different geometry of the compounds. Substituents in the 4-position of the headgroup aromatic ring (**33**, **36**−**38**) strongly reduced the potency as well. The fact that a fluorine atom, which constitutes the smallest substituent in this series, retained most activity indicates that the loss of potency is as well due to steric interactions with the amide group in proximity.

Substituents in the 4-position of the central aromatic ring (**46**, **49**−**51**) and in the 6-position of the headgroup (**35**, **39**−**41**) both strongly improved the potency of the compounds. In the case of the headgroup, the SAR was quite steep because only a methyl (**35**) and a methoxy group (**39**) were highly potent while larger substituents were less active. Our docking studies suggest that the gain in potency of **35** and **39** might be due to displacement of one water molecule from the water cluster associated with Arg_{335} and Arg_{268}.

Furthermore, in the case of 5-substituted derivatives (**45** and **47**) of the central aromatic ring, we found two FXR antagonists. According to our docking studies, the additional substituent seems to change slightly the binding mode of the whole scaffold and make a polar interaction of the *tert*-butylbenzoylamide oxygen with Tyr_{373} in helix 7 possible. It has been suggested[34] that interaction with helix 7 might lead to antagonistic activity on FXR, which here seems to be true as well.

The strongest improvement in agonistic activity was gained by introduction of substituents in the 4-position of the central aromatic ring. A methyl group (**49**), a chlorine atom (**46**), and a bromine atom (**50**) in this position led to equally potent derivatives, which is according to our docking studies due to a slight shift in the binding mode toward Arg_{335} and Arg_{268} and the associated water cluster. The docking pose of **49** is similar to the pose of phenylpropionic acid derivative **32** and reveals better angles and distances for polar interactions with Arg_{335} and Arg_{268} as well as displacement of one water molecule. A methoxy group (**51**) in the 4-position of the central aromatic ring showed even more potency on FXR and a very favorable docking pose.

dx.doi.org/10.1021/jm500937v | *J. Med. Chem.* 2014, 57, 8035−8055

The resulting compound **51** of this SAR study constitutes a highly potent and selective partial FXR agonist (EC_{50} = 8 ± 3 nM, 17.5 ± 0.7% max) with good physicochemical properties, acceptable solubility, high metabolic stability, and acceptable toxicity compared to its potency. The fact that the effect of **51** on FXR target genes was not concentration dependent in the investigated range from 0.1 to 10 μM shows that **51** exhibits true partial FXR agonism which might be of therapeutic value for metabolic disorders because full activation of nuclear receptors over long-term treatment has been observed to cause negative effects as well, e.g., for full FXR agonists, promoting effects on proliferation and migration of several forms of cancer have been observed[35−40] and FXR agonism might induce impaired cholesterol homeostasis[41] because the conversion of cholesterol to bile acids and their elimination are inhibited by FXR activation. Overactivation of the nuclear receptor might also evoke a cholestatic condition,[2] and finally FXR agonism can cause serious liver damage in cholestasis.[42] The development of FXR targeting drugs therefore must either find the right balance between beneficial FXR activation and disadvantageous overactivation or discover target gene selective FXR modulators that similarly to the selective estrogen-receptor modulators (SERMs) exhibit differential effects on different target genes. The here reported highly potent FXR partial agonist **51** constitutes a novel FXR targeting agent that only moderately activates the nuclear receptor and might display one possible way to overcome the handicaps of full FXR agonists.

EXPERIMENTAL SECTION

General. All chemicals and solvents were of reagent grade and used without further purification unless otherwise specified. ^{1}H NMR and ^{13}C NMR spectra were measured in DMSO-d_6 on a Bruker AV 500, Bruker AV 400, Bruker AV 300, or Bruker am250xp spectrometer. Chemical shifts are reported in parts per million (ppm), with tetramethylsilane (TMS) as an internal standard. Mass spectra were obtained on a Fisons Instruments VG Plattform II measuring in the positive- or negative-ion mode (ESI−MS system). The purity of the final compounds was determined by combustion analysis, which was performed by the Microanalytical Laboratory of the Institute of Organic Chemistry and Chemical Biology, Goethe University Frankfurt, on an Elementar Vario Micro Cube. All tested compounds described here have a purity ≥95%. Intermediates were not analyzed.

Synthesis. General Procedures. *a. ortho-Aminobenzoylation with Isatoic Anhydride Derivatives.* Isatoic anhydride derivative (**5a−f**, 1.0 equiv) and 4-*N*,*N*-dimethylaminopyridine (0.1 equiv) were dissolved in a mixture of pyridine (2 mL/mmol **5a−f**) and DMF (0.5 mL/mmol **4a**,**b**) and heated to 80 °C. After a clear brown solution had formed, the respective aniline derivative (**4a−u**, 1.1 equiv) was added in one portion. With addition of NEt_3 (0.5 mL/mmol **5a−f**), the formation of carbon dioxide started. The reaction mixture was kept at 80 °C for 16 h. Then the solvents were evaporated in vacuum and the crude product dissolved in ethyl acetate. The organic phase was washed twice with 10% hydrochloric acid and brine and dried over Na_2SO_4. Further purification was performed by recrystallization or column chromatography on silica.

Aniline derivative (**4a−u**, 1.0 equiv) was dissolved in EtOH (abs, 5 mL/mmol **4a−u**) and heated to reflux. When the mixture had cleared and reached at least 80 °C, isatoic anhydride derivative (**5a−f**, 2.0 equiv) was added in one portion with the immediate formation of carbon dioxide. The reaction mixture was stirred under reflux for 60 min. After cooling to room temperature, volume was reduced in vacuum until crystallization of the product initiated and the crude product was filtered off. When no crystallization was possible, the crude product was partitioned between ethyl acetate and 10% hydrochloric acid, the aqueous layer was extracted with additional ethyl acetate three times, the combined organic layers were dried over Na_2SO_4, and solvent was evaporated in vacuum. The crude product was further purified by recrystallization or column chromatography on silica.

b. ortho-Nitrobenzoylation with Benzoic Acid Derivatives. *ortho*-Nitrobenzoic acid derivative (**6a−f**, 1.0 equiv) was dissolved in CH_2Cl_2 (abs, 5 mL/mmol **6a−f**) and DMF (abs, 0.1 mL/mmol **6a−f**). Thionyl chloride (1.3 equiv) was added slowly at room temperature, and the mixture was stirred 4 h under reflux. Solvents were evaporated in vacuum, and the crude product (**9a−f**) was dried in ultravacuum. Without further purification the crude product (**9a−f**) was used for reaction with aniline derivatives (**4a−u**): for this purpose aniline derivative (**4a−u**, 1.3 equiv) was dissolved in CH_2Cl_2 (abs, 5 mL/mmol **6a−f**) and pyridine (abs, 1 mL/mmol **6a−f**), and the crude *ortho*-nitrobenzoyl chloride derivative (**9a−f**) in CH_2Cl_2 (abs, 5 mL/mmol **6a−f**) was added dropwise. The mixture was stirred at room temperature until TLC indicated consumption of starting material (4−12 h). The reaction mixture was then poured into an equal volume 10% hydrochloric acid, phases were separated, and the aqueous phase was extracted three times with ethyl acetate. Combined organic layers were dried over Na_2SO_4, and solvent was evaporated in vacuum. Further purification was performed by recrystallization or column chromatography on silica.

c. Reduction of ortho-Nitrobenzoylaniline Derivatives. *ortho*-Nitrobenzoylaniline derivative (**10a−e**, 1.0 equiv) was dissolved in THF (abs, 10 mL/mmol), tin (3.5 equiv) was added, and the mixture was heated to 50 °C. Hydrochloric acid (36%, 7 equiv) was added slowly, and the mixture was stirred under reflux for 60 min, then filtered, diluted with an equal volume ethyl acetate, and washed twice with water. The combined aqueous layers were extracted three times with ethyl acetate, and the combined organic layers were dried over Na_2SO_4 and solvent was evaporated in vacuum. Further purification was performed by recrystallization or column chromatography on silica.

d. Acylation of Anthranilic Acid Derivatives. Anthranilic acid derivative (**7a−z**, **10a−e**, 1.0 equiv) was dissolved in THF (3 mL/mmol **7a−z**, **10a−e**), and pyridine (3.0 equiv) was added. After a clear solution had formed, the respective acyl chloride (**8a−j**, 1.3 equiv) was added in THF (2 mL/mmol **7a−z**, **10a−e**). The reaction mixture was kept at room temperature for 4−8 h, and the reaction progress was monitored by TLC. When anthranilic acid derivative (**7a−z**, **10a−e**) was consumed, the reaction mixture was diluted with ethyl acetate and washed three times with 10% hydrochloric acid, and dried over Na_2SO_4. Further purification was performed by column chromatography on silica and recrystallization.

e. Alkaline Ester Hydrolysis. The respective ester was dissolved in THF (9 mL/mmol), and aqueous LiOH solution (10%, 1 mL/mmol) was added slowly. The mixture was then stirred at room temperature or at 40 °C until TLC indicated complete conversion of the starting material (12−24 h). The mixture was then poured into 10% aqueous hydrochloric acid, an equal volume of ethyl acetate was added, and phases were separated. The aqueous layer was extracted three times with ethyl acetate, the combined organic layers were dried over Na_2SO_4, and solvent was evaporated in vacuum. Further purification was performed by recrystallization or column chromatography on silica.

Test Compounds. *3-(2-(4-(tert-Butyl)benzamido)benzamido)-benzoic Acid (**13**).* Preparation according to general procedure d using **7a** and *tert*-butylbenzoyl chloride (**8a**). After column chromatography on silica with hexane/ethyl acetate/acetic acid (89:9:2) as mobile phase, the product was recrystallized from hexane/ethyl acetate to give **13** as white solid in 77% yield. R_f (hexane/ethyl acetate/acetic acid (49:49:2)) = 0.58. ^{1}H NMR (500 MHz, DMSO) δ = 13.03 (s, 1H), 11.55 (s, 1H), 10.70 (s, 1H), 8.32 (t, J = 1.8 Hz, 1H), 8.00−7.96 (m, 1H), 7.95 (dd, J = 7.9, 1.2 Hz, 1H), 7.87−7.84 (m, 1H), 7.78 (d, J = 8.5 Hz, 1H), 7.74−7.71 (m, 1H), 7.59 (d, J = 8.5 Hz, 2H), 7.51 (t, J = 7.9 Hz, 1H), 7.48−7.45 (m, 1H), 7.32−7.28 (m, 2H), 1.31 (s, 9H). ^{13}C NMR (126 MHz, DMSO) δ = 168.08, 167.58, 165.08, 155.48, 139.26, 132.83, 132.23, 131.72, 129.56, 129.43, 127.39, 126.21, 126.04, 125.69, 125.47, 123.69, 123.20, 122.32, 121.79, 35.22, 31.34. $C_{25}H_{24}N_2O_4$. MS (ESI−): m/z 415.9 ([M − HM

dx.doi.org/10.1021/jm500937v | J. Med. Chem. 2014, 57, 8035−8055

− H]⁻, 100). Combustion analysis measured (calculated): C 72.17 (72.10); H 6.21 (5.81); N 6.64 (6.73).

*3-((2-((4-(tert-Butyl)phenyl)carbamoyl)phenyl)carbamoyl)-benzoic Acid (**14**).* Preparation according to general procedure e using **14a**. After column chromatography on silica with hexane/ethyl acetate/acetic acid (89:9:2) as mobile phase, the product was recrystallized from hexane/ethyl acetate to give **14** as white solid in 89% yield. R_f (hexane/ethyl acetate/acetic acid (49:49:2)) = 0.60. ^{1}H NMR (500 MHz, DMSO) δ = 13.32 (s, 1H), 11.81 (s, 1H), 10.50 (s, 1H), 8.52 (s, 1H), 8.42 (d, J = 8.1 Hz, 1H), 8.15 (dd, J = 14.2, 7.8 Hz, 2H), 7.92 (d, J = 7.6 Hz, 1H), 7.72 (t, J = 7.7 Hz, 1H), 7.63 (t, J = 7.2 Hz, 3H), 7.38 (d, J = 8.6 Hz, 2H), 7.32 (t, J = 7.5 Hz, 1H), 1.28 (s, 9H). ^{13}C NMR (126 MHz, DMSO) δ = 167.64, 167.10, 164.32, 147.11, 138.76, 136.37, 135.32, 133.02, 132.58, 131.93, 131.55, 129.87, 129.36, 128.55, 125.75, 124.05, 123.98, 122.10, 121.33, 34.58, 31.65. $C_{25}H_{24}N_2O_4$. MS (ESI−): m/z 415.26 ([M − H]⁻, 100), 451.24 ([M + Cl]⁻, 46). Combustion analysis measured (calculated): C 72.01 (72.10); H 6.18 (5.81); N 6.72 (6.73).

*2-Methyl-5-(2-(4-(trifluoromethyl)benzamido)benzamido)-benzoic Acid (**15**).* Preparation according to general procedure d using **7a** and 4-(trifluoromethyl)benzoyl chloride (**8b**). After column chromatography on silica with hexane/ethyl acetate/acetic acid (89:9:2) as mobile phase, the product was recrystallized from hexane/ethyl acetate to give **15** as white solid in 78% yield. R_f (hexane/ethyl acetate/acetic acid (49:49:2)) = 0.54. ^{1}H NMR (500 MHz, DMSO) δ = 13.00 (s, 1H), 11.56 (s, 1H), 10.70 (s, 1H), 8.34−8.30 (m, 2H), 8.11 (d, J = 8.2 Hz, 2H), 7.95 (dd, J = 11.5, 8.2 Hz, 4H), 7.71 (d, J = 7.7 Hz, 1H), 7.67−7.62 (m, 1H), 7.49 (t, J = 7.9 Hz, 1H), 7.35 (dd, J = 11.1, 4.1 Hz, 1H). ^{13}C NMR (126 MHz, DMSO) δ = 167.75, 167.60, 164.18, 139.36, 138.83, 138.30, 132.63, 132.28, 132.03, 131.79, 129.57, 129.38, 128.57, 126.38, 126.35, 125.50, 125.37, 124.82, 124.46, 123.23, 122.63, 122.18, 21.54. $C_{23}H_{17}F_3N_2O_4$. MS (ESI−): m/z 427.8 ([M − H]⁻, 100). Combustion analysis measured (calculated): C 61.32 (61.69); H 3.58 (3.53); N 6.48 (6.54).

*3-(2-(4-Bromobenzamido)benzamido)benzoic Acid (**16**).* Preparation according to general procedure d using **7a** and 4-bromobenzoyl chloride (**8c**). After column chromatography on silica with hexane/ethyl acetate/acetic acid (89:9:2) as mobile phase, the product was recrystallized from hexane/ethyl acetate to give **16** as white solid in 30% yield. R_f (hexane/ethyl acetate/acetic acid (49:49:2)) = 0.51. ^{1}H NMR (500 MHz, DMSO) δ = 11.48 (s, 1H), 10.69 (s, 1H), 8.33 (d, J = 8.3 Hz, 1H), 8.32 (s, 1H), 7.96 (d, J = 8.1 Hz, 1H), 7.94−7.91 (m, 1H), 7.87−7.82 (m, 2H), 7.79 (d, J = 8.6 Hz, 2H), 7.71 (d, J = 7.8 Hz, 1H), 7.66−7.60 (m, 1H), 7.49 (t, J = 7.9 Hz, 1H), 7.32 (dd, J = 11.0, 4.2 Hz, 1H). ^{13}C NMR (126 MHz, DMSO) δ = 168.64, 167.84, 167.58, 164.38, 139.32, 138.56, 134.12, 132.66, 132.37, 129.68, 129.55, 129.39, 126.27, 125.55, 125.39, 124.36, 124.19, 122.41, 122.21. $C_{21}H_{15}BrN_2O_4$. MS (ESI+): m/z 461.29 ([M + Na]⁺, 95); 463.29 ([M + Na]⁺, 100). Combustion analysis measured (calculated): C 57.21 (57.42); H 3.70 (3.44); N 6.19 (6.38).

*3-(2-(Benzo[d][1,3]dioxole-5-carboxamido)benzamido)benzoic Acid (**17**).* Preparation according to general procedure d using **7a** and benzo[*d*][1,3]dioxole-5-carbonyl chloride (**8d**). After column chromatography on silica with hexane/ethyl acetate/acetic acid (89:9:2) as mobile phase, the product was recrystallized from hexane/ethyl acetate to give **17** as white solid in 45% yield. R_f (hexane/ethyl acetate/acetic acid (49:49:2)) = 0.41. ^{1}H NMR (500 MHz, DMSO) δ = 13.03 (s, 1H), 11.40 (s, 1H), 10.69 (s, 1H), 8.40 (d, J = 7.6 Hz, 1H), 8.33 (t, J = 1.8 Hz, 1H), 7.97 (dd, J = 8.1, 1.1 Hz, 1H), 7.93 (dd, J = 7.9, 1.1 Hz, 1H), 7.74−7.70 (m, 1H), 7.64−7.59 (m, 1H), 7.53−7.47 (m, 2H), 7.40 (d, J = 1.7 Hz, 1H), 7.29 (td, J = 7.8, 1.0 Hz, 1H), 7.09 (d, J = 8.1 Hz, 1H), 6.14 (s, 2H). ^{13}C NMR (126 MHz, DMSO) δ = 168.01, 167.58, 164.37, 150.91, 148.23, 139.31, 139.07, 132.74, 131.71, 129.54, 129.42, 128.97, 125.60, 125.42, 123.73, 123.58, 122.63, 122.22, 122.01, 108.81, 107.62, 102.45. $C_{22}H_{16}N_2O_6$. MS (ESI+): m/z 405.37 ([M + H]⁺, 23), 427.37 ([M + Na]⁺, 100). Combustion analysis measured (calculated): C 64.96 (65.35); H 4.28 (3.99); N 6.77 (6.93).

*3-(2-(2,3-Dihydrobenzo[b][1,4]dioxine-6-carboxamido)-benzamido)benzoic Acid (**18**).* Preparation according to general procedure d using **7a** and 2,3-dihydrobenzo[*b*][1,4]dioxine-6-carbonyl chloride (**8e**). After column chromatography on silica with hexane/ethyl acetate/acetic acid (89:9:2) as mobile phase, the product was recrystallized from hexane/ethyl acetate to give **18** as white solid in 41% yield. R_f (hexane/ethyl acetate/acetic acid (49:49:2)) = 0.34. ^{1}H NMR (500 MHz, DMSO) δ = 13.04 (s, 1H), 11.44 (s, 1H), 10.69 (s, 1H), 8.42 (d, J = 7.7 Hz, 1H), 8.32 (s, 1H), 7.97 (dd, J = 8.1, 1.0 Hz, 1H), 7.95−7.91 (m, 1H), 7.72 (d, J = 7.8 Hz, 1H), 7.64−7.59 (m, 1H), 7.51 (t, J = 7.9 Hz, 1H), 7.44−7.39 (m, 2H), 7.31−7.26 (m, 1H), 7.03 (d, J = 8.4 Hz, 1H), 4.31 (dd, J = 10.7, 5.1 Hz, 4H). ^{13}C NMR (126 MHz, DMSO) δ = 168.07, 167.57, 164.32, 147.24, 143.73, 139.27, 139.18, 132.78, 131.73, 129.55, 129.43, 127.87, 125.66, 125.45, 123.63, 123.27, 122.29, 121.85, 120.94, 117.85, 116.59, 64.86, 64.48. $C_{23}H_{18}N_2O_6$. MS (ESI+): m/z 419.37 ([M + H]⁺, 16), 441.37 ([M + Na]⁺, 100). Combustion analysis measured (calculated): C 65.57 (66.03); H 4.62 (4.34); N 6.93 (6.70).

*3-(2-(3-Fluoro-4-(trifluoromethyl)benzamido)benzamido)-benzoic Acid (**19**).* Preparation according to general procedure d using **7a** and 3-fluoro-4-(trifluoromethyl)benzoyl chloride (**8f**). After column chromatography on silica with hexane/ethyl acetate/acetic acid (89:9:2) as mobile phase, the product was recrystallized from hexane/ethyl acetate to give **19** as white solid in 73% yield. R_f (hexane/ethyl acetate/acetic acid (49:49:2)) = 0.53. ^{1}H NMR (500 MHz, DMSO) δ = 13.01 (s, 1H), 11.46 (s, 1H), 10.69 (s, 1H), 8.34 (s, 1H), 8.21 (d, J = 8.2 Hz, 1H), 8.03 (t, J = 7.7 Hz, 1H), 7.95 (d, J = 10.2 Hz, 2H), 7.91 (d, J = 8.0 Hz, 2H), 7.70 (d, J = 7.6 Hz, 1H), 7.65 (t, J = 7.8 Hz, 1H), 7.48 (t, J = 7.9 Hz, 1H), 7.37 (t, J = 7.5 Hz, 1H). ^{13}C NMR (126 MHz, DMSO) δ = 167.60, 167.52, 163.00, 141.73, 139.45, 137.72, 132.49, 131.74, 129.58, 129.37, 128.78, 125.76, 125.37, 125.30, 124.86, 124.16, 124.13, 123.11, 122.04, 121.67, 116.65, 116.47. $C_{22}H_{14}F_4N_2O_4$. MS (ESI+): m/z 469.38 ([M + Na]⁺, 100). Combustion analysis measured (calculated): C 58.97 (59.20); H 3.17 (3.16); N 6.38 (6.28).

*3-(2-(3,5-Bis(trifluoromethyl)benzamido)benzamido)benzoic Acid (**20**).* Preparation according to general procedure d using **7a** and 3,5-bis(trifluoromethyl)benzoyl chloride (**8g**). After column chromatography on silica with hexane/ethyl acetate/acetic acid (89:9:2) as mobile phase, the product was recrystallized from hexane/ethyl acetate to give **20** as white solid in 66% yield. R_f (hexane/ethyl acetate/acetic acid (49:49:2)) = 0.57. ^{1}H NMR (500 MHz, DMSO) δ = 12.95 (s, 1H), 11.33 (s, 1H), 10.63 (s, 1H), 8.50 (s, 2H), 8.38 (s, 2H), 7.98 (d, J = 8.1 Hz, 1H), 7.94 (d, J = 8.0 Hz, 1H), 7.85 (d, J = 7.1 Hz, 1H), 7.68−7.65 (m, 1H), 7.65−7.62 (m, 1H), 7.44 (t, J = 7.9 Hz, 1H), 7.39 (td, J = 7.7, 0.9 Hz, 1H). ^{13}C NMR (126 MHz, DMSO) δ = 167.59, 167.11, 162.91, 139.70, 137.43, 136.83, 132.07, 131.69, 131.29, 131.02, 129.53, 129.24, 128.69, 125.87, 125.38, 125.04, 124.83, 124.57, 124.22, 121.58. $C_{23}H_{14}F_6N_2O_4$. MS (ESI+): m/z 519.4 ([M + Na]⁺, 100). Combustion analysis measured (calculated): C 55.55 (55.66); H 2.76 (2.84); N 5.63 (5.64).

*3-(2-(2-Phenylacetamido)benzamido)benzoic Acid (**21**).* Preparation according to general procedure d using **7a** and phenylacetyl chloride (**8h**). After column chromatography on silica with hexane/ethyl acetate/acetic acid (89:9:2) as mobile phase, the product was recrystallized from hexane/ethyl acetate to give **21** as white solid in 72% yield. R_f (hexane/ethyl acetate/acetic acid (49:49:2)) = 0.43. ^{1}H NMR (500 MHz, DMSO) δ = 13.02 (s, 1H), 10.56 (s, 1H), 10.45 (s, 1H), 8.40 (s, 1H), 8.11 (d, J = 8.3 Hz, 1H), 7.90 (t, J = 14.3 Hz, 1H), 7.77 (d, J = 7.7 Hz, 1H), 7.71 (d, J = 7.7 Hz, 1H), 7.51 (dt, J = 12.8, 7.7 Hz, 2H), 7.36−7.26 (m, 4H), 7.26−7.21 (m, 2H), 3.70 (s, 2H). ^{13}C NMR (126 MHz, DMSO) δ = 169.75, 167.68, 167.30, 139.56, 137.91, 135.79, 132.07, 131.68, 129.83, 129.30, 129.09, 128.85, 127.16, 125.34, 125.18, 125.11, 123.87, 122.45, 121.77, 44.20. $C_{22}H_{18}N_2O_4$. MS (ESI+): m/z 375.38 ([M + H]⁺, 20), 397.36 ([M + Na]⁺, 100). Combustion analysis measured (calculated): C 70.50 (70.58); H 4.97 (4.85); N 7.43 (7.48).

*3-(2-Cinnamamidobenzamido)benzoic Acid (**22**).* Preparation according to general procedure d using **7a** and cinnamoyl chloride (**8i**). After column chromatography on silica with hexane/ethyl acetate/acetic acid (89:9:2) as mobile phase, the product was recrystallized from hexane/ethyl acetate to give **22** as white solid in 42% yield. R_f (hexane/ethyl acetate/acetic acid (49:49:2)) = 0.48. ^{1}H

dx.doi.org/10.1021/jm500937v | J. Med. Chem. 2014, 57, 8035−8055

NMR (500 MHz, DMSO) δ = 13.02 (s, 1H), 10.66 (d, J = 12.5 Hz, 1H), 10.59 (s, 1H), 8.42 (s, 1H), 8.28 (d, J = 8.2 Hz, 1H), 8.01−7.92 (m, 1H), 7.82 (dd, J = 7.7, 1.0 Hz, 1H), 7.74−7.66 (m, 3H), 7.62−7.55 (m, 2H), 7.49 (t, J = 7.9 Hz, 1H), 7.46−7.38 (m, 3H), 7.31−7.25 (m, 1H), 6.93 (d, J = 15.7 Hz, 1H). ^{13}C NMR (126 MHz, DMSO) δ = 167.64, 167.46, 164.14, 141.44, 139.61, 138.11, 135.01, 132.17, 131.70, 130.37, 129.39, 129.33, 128.54, 125.24, 125.21, 123.93, 122.75, 122.65, 121.88. $C_{23}H_{18}N_2O_4$. MS (ESI−): m/z 485.24 ([M − H]$^-$, 100). Combustion analysis measured (calculated): C 71.11 (71.49); H 4.75 (4.70); N 7.32 (7.25).

N-(3-Acetylphenyl)-2-(4-(tert-butyl)benzamido)benzamide (**23**). Preparation according to general procedure d using **7b** and *tert*-butylbenzoyl chloride (**8a**). After column chromatography on silica with hexane/ethyl acetate/acetic acid (89:9:2) as mobile phase, the product was recrystallized from hexane/ethyl acetate to give **23** as white solid in 27% yield. R_f (hexane/ethyl acetate (4:1)) = 0.63. ^{1}H NMR (500 MHz, DMSO) δ = 11.59 (s, 1H), 10.72 (s, 1H), 8.48 (dd, J = 8.3, 0.8 Hz, 1H), 8.26 (t, J = 1.8 Hz, 1H), 8.03 (dd, J = 8.1, 1.2 Hz, 1H), 7.95 (dt, J = 14.9, 7.5 Hz, 1H), 7.90−7.82 (m, 2H), 7.79−7.74 (m, 1H), 7.67−7.60 (m, 1H), 7.60−7.57 (m, 2H), 7.55 (dd, J = 10.0, 5.9 Hz, 1H), 7.30 (td, J = 7.7, 1.1 Hz, 1H), 2.59 (s, 3H), 1.31 (s, 9H). ^{13}C NMR (126 MHz, DMSO) δ = 198.08, 168.12, 165.06, 155.47, 139.39, 139.25, 137.73, 132.87, 132.21, 129.59, 129.51, 127.40, 126.19, 126.10, 124.73, 123.67, 123.10, 121.79, 120.88, 35.21, 31.33, 27.25. $C_{26}H_{26}N_2O_3$. MS (ESI−): m/z 413.25 ([M − H]$^-$, 100). Combustion analysis measured (calculated): C 75.16 (75.34); H 6.32 (6.32); N 6.56 (6.76).

2-(4-(tert-Butyl)benzamido)-N-(3-cyanophenyl)benzamide (**24**). Preparation according to general procedure d using **7c** and *tert*-butylbenzoyl chloride (**8a**). After column chromatography on silica with hexane/ethyl acetate/acetic acid (89:9:2) as mobile phase, the product was recrystallized from hexane/ethyl acetate to give **24** as white solid in 59% yield. R_f (hexane/ethyl acetate/acetic acid (49:49:2)) = 0.74. ^{1}H NMR (500 MHz, DMSO) δ = 11.38 (s, 1H), 10.80 (s, 1H), 8.40 (dd, J = 11.6, 3.9 Hz, 1H), 8.16 (s, 1H), 8.04−7.97 (m, 1H), 7.91 (dd, J = 7.8, 1.3 Hz, 1H), 7.88−7.83 (m, 2H), 7.66−7.62 (m, 1H), 7.62−7.58 (m, 4H), 7.32 (td, J = 7.7, 1.0 Hz, 1H), 1.32 (s, 9H). ^{13}C NMR (126 MHz, DMSO) δ = 168.17, 165.15, 155.48, 140.01, 139.00, 132.93, 132.16, 130.66, 129.53, 128.09, 127.46, 126.18, 125.99, 124.11, 123.85, 123.60, 122.14, 119.17, 111.94, 35.22, 31.35. $C_{25}H_{23}N_3O_2$. MS (ESI−): m/z 396.7 ([M − H]$^-$, 100). HRMS (MALDI+) measured for [M + K]$^+$ (calculated): 436.14240 (436.14219). HPLC purity 100% (H_2O/MeOH gradient, 25 min).

2-(4-(tert-Butyl)benzamido)-N-(3-methoxyphenyl)benzamide (**25**). Preparation according to general procedure d using **7d** and *tert*-butylbenzoyl chloride (**8a**). After column chromatography on silica with hexane/ethyl acetate/acetic acid (89:9:2) as mobile phase, the product was recrystallized from hexane/ethyl acetate to give **25** as white solid in 52% yield. R_f (hexane/ethyl acetate/acetic acid (39:9:2)) = 0.35. ^{1}H NMR (500 MHz, DMSO) δ = 11.67 (s, 1H), 10.50 (s, 1H), 8.52 (s, 1H), 7.92 (d, J = 7.8 Hz, 1H), 7.86 (d, J = 8.3 Hz, 2H), 7.65−7.57 (m, 3H), 7.35 (d, J = 8.4 Hz, 2H), 7.29 (t, J = 7.6 Hz, 2H), 6.76−6.72 (m, 1H), 3.76 (s, 3H), 1.30 (d, J = 8.5 Hz, 9H). ^{13}C NMR (126 MHz, DMSO) δ = 167.97, 164.97, 159.87, 155.49, 140.10, 139.28, 132.76, 132.18, 129.94, 129.46, 127.35, 126.22, 123.58, 123.03, 121.60, 113.86, 109.99, 107.56, 55.53, 35.21, 31.33. $C_{25}H_{26}N_2O_3$. MS (ESI−): m/z 401.14 ([M − H]$^-$, 100). Combustion analysis measured (calculated): C 74.41 (74.60); H 6.56 (6.51); N 6.83 (6.96).

2-(4-(tert-Butyl)benzamido)-N-(3-(methylthio)phenyl)benzamide (**26**). Preparation according to general procedure d using **7e** and *tert*-butylbenzoyl chloride (**8a**). After column chromatography on silica with hexane/ethyl acetate/acetic acid (89:9:2) as mobile phase, the product was recrystallized from hexane/ethyl acetate to give **26** as white solid in 58% yield. R_f (hexane/ethyl acetate/acetic acid (49:49:2)) = 0.79. ^{1}H NMR (500 MHz, DMSO) δ = 11.58 (s, 1H), 10.53 (s, 1H), 8.48 (d, J = 8.2 Hz, 1H), 7.94−7.89 (m, 1H), 7.86 (t, J = 7.6 Hz, 2H), 7.66−7.58 (m, 4H), 7.55 (d, J = 8.1 Hz, 1H), 7.34−7.27 (m, 2H), 7.05 (dd, J = 7.9, 0.9 Hz, 1H), 2.48 (s, 3H), 1.31 (s, 9H). ^{13}C NMR (126 MHz, DMSO) δ = 167.98, 165.02, 155.49, 139.52, 139.18, 138.97, 132.78, 132.20, 129.66, 129.47, 127.39, 126.22, 123.66, 123.25, 122.07, 121.74, 118.67, 118.06, 35.22, 31.35, 15.12. $C_{25}H_{26}N_2O_2S$. MS (ESI+): m/z 419.46 ([M + H]$^+$, 15); 441.44 ([M + Na]$^+$, 100). Combustion analysis measured (calculated): C 71.78 (71.74); H 5.96 (6.26); N 6.79 (6.69); S 7.33 (7.66).

N-(3-(1H-Tetrazol-5-yl)phenyl)-2-(4-(tert-butyl)benzamido)-benzamide (**27**). **24** (199 mg, 0.5 mmol, 1.0 equiv) was dissolved in 5 mL of DMF/MeOH (9:1), and Cu_2O (3.6 mg, 5 mol %) and NaN_3 (297 mg, 3.0 mmol, 6.0 equiv) were added. The mixture was stirred at 90 °C for 24 h. After cooling to room temperature, 15 mL of 5% aqueous hydrochloric acid and 10 mL of CH_2Cl_2 were added and the mixture was vigorously stirred for another 30 min. Phases were then separated, and the aqueous phase was extracted with equal volumes of ethyl acetate three times. The combined aqueous layers were dried over Na_2SO_4, and the solvents were evaporated in vacuum. Further purification was performed by column chromatography on silica with hexane/ethyl acetate/acetic acid and recrystallization from acetone/water to obtain **27** as white solid in 20% yield. R_f (hexane/ethyl acetate/acetic acid (49:49:2)) = 0.15. ^{1}H NMR (500 MHz, DMSO) δ = 11.53 (s, 1H), 10.79 (s, 1H), 8.49 (t, J = 1.8 Hz, 1H), 8.46 (dd, J = 8.3, 0.9 Hz, 1H), 7.97 (dd, J = 7.9, 1.3 Hz, 1H), 7.93−7.89 (m, 1H), 7.88−7.84 (m, 2H), 7.79 (d, J = 7.8 Hz, 1H), 7.67−7.57 (m, 4H), 7.32 (td, J = 7.7, 1.1 Hz, 1H), 1.31 (s, 9H). ^{13}C NMR (126 MHz, DMSO) δ = 192.78, 168.15, 165.11, 155.48, 139.97, 139.17, 132.88, 132.20, 130.33, 129.59, 127.42, 126.21, 124.06, 123.75, 123.33, 123.05, 121.91, 119.88, 35.22, 31.34. $C_{25}H_{24}N_6O_2$. MS (ESI−): m/z 439.8 ([M − H]$^-$, 100). Combustion analysis measured (calculated): C 67.82 (68.17); H 5.57 (5.49); N 18.91 (19.08).

2-(4-(tert-Butyl)benzamido)-N-(3-carbamoylphenyl)benzamide (**28**). **13** (417 mg, 1.0 mmol, 1.0 equiv) was added to a mixture of silica gel and NH_4Cl (5:1, 1.3 g). After TsCl (210 mg, 1.1 mmol, 1.1 equiv) was added, the mixture was treated with 2.2 mL of triethylamine mixed with a spatula for 5 min. Then the mixture was added to 30 mL of ethyl acetate, and silica was filtered off. The filtrate was washed with 1% aqueous hydrochloric acid, and the aqueous layer was extracted with additional ethyl acetate three times. The combined aqueous layers were dried over Na_2SO_4, and the solvents were evaporated in vacuum. Further purification was performed by column chromatography on silica with hexane/ethyl acetate/acetic acid and recrystallization from acetone/water to obtain **28** as white solid in 38% yield. R_f (hexane/ethyl acetate/acetic acid (49:49:2)) = 0.34. ^{1}H NMR (500 MHz, DMSO) δ = 11.70 (s, 1H), 10.67 (s, 1H), 8.58−8.48 (m, 1H), 8.19 (t, J = 1.7 Hz, 1H), 8.01−7.95 (m, 2H), 7.88−7.83 (m, 3H), 7.67−7.62 (m, 2H), 7.62 7.58 (m, 2H), 7.46 (t, J = 7.9 Hz, 1H), 7.40 (s, 1H), 7.30 (td, J = 7.8, 1.0 Hz, 1H), 1.31 (s, 9H). ^{13}C NMR (126 MHz, DMSO) δ = 168.19, 168.09, 165.01, 155.51, 139.42, 138.94, 135.44, 132.90, 132.21, 129.53, 128.99, 127.35, 126.26, 124.49, 123.59, 123.53, 122.69, 121.57, 121.39, 35.22, 31.34. $C_{25}H_{25}N_3O_3$. MS (ESI−): m/z 414.26 ([M − H]$^-$, 100). Combustion analysis measured (calculated): C 71.93 (72.27); H 6.06 (6.07); N 9.76 (10.11).

2-(4-(tert-Butyl)benzamido)-N-(3,4-dimethoxyphenyl)benzamide (**29**). Preparation according to general procedure d using **7f** and *tert*-butylbenzoyl chloride (**8a**). After column chromatography on silica with hexane/ethyl acetate/acetic acid (89:9:2) as mobile phase, the product was recrystallized from hexane/ethyl acetate to give **29** as white solid in 70% yield. R_f (hexane/ethyl acetate/acetic acid (49:49:2)) = 0.57. ^{1}H NMR (500 MHz, DMSO) δ = 11.83 (s, 1H), 10.41 (s, 1H), 8.55 (d, J = 8.3 Hz, 1H), 7.93 (d, J = 7.7 Hz, 1H), 7.86 (d, J = 8.3 Hz, 2H), 7.63−7.58 (m, 3H), 7.35−7.25 (m, 3H), 6.96 (d, J = 8.6 Hz, 1H), 3.76 (s, 6H), 1.32 (s, 9H). ^{13}C NMR (126 MHz, DMSO) δ = 167.65, 164.92, 155.49, 148.94, 146.24, 139.38, 132.68, 132.22, 132.14, 129.28, 127.34, 126.24, 123.50, 122.72, 121.40, 114.03, 112.27, 106.96, 56.19, 55.95, 35.22, 31.34. $C_{26}H_{28}N_2O_4$. MS (ESI+): m/z 455.53 ([M + Na]$^+$, 100). Combustion analysis measured (calculated): C 71.87 (72.20); H 6.46 (6.53); N 6.46 (6.48).

2-(4-(tert-Butyl)benzamido)-N-(3,4,5-trimethoxyphenyl)-benzamide (**30**). Preparation according to general procedure d using **7g** and *tert*-butylbenzoyl chloride (**8a**). After column chromatography on silica with hexane/ethyl acetate/acetic acid (89:9:2) as mobile phase, the product was recrystallized from hexane/ethyl acetate to give **30** as white solid in 74% yield. R_f (hexane/ethyl acetate/acetic acid

(49:49:2)) = 0.54. ^{1}H NMR (500 MHz, DMSO) δ = 11.59 (s, 1H), 10.43 (s, 1H), 8.47 (d, J = 8.3 Hz, 1H), 7.88 (dd, J = 12.9, 8.2 Hz, 3H), 7.64−7.56 (m, 3H), 7.29 (t, J = 7.4 Hz, 1H), 7.09 (s, 2H), 3.77 (s, 6H), 3.65 (s, 3H), 1.32 (s, 9H). ^{13}C NMR (126 MHz, DMSO) δ = 167.74, 165.02, 155.49, 153.10, 139.06, 134.91, 134.79, 132.66, 132.17, 129.36, 127.43, 126.20, 123.67, 123.48, 121.80, 99.73, 60.60, 56.32, 35.22, 31.35. $C_{27}H_{30}N_2O_5$. MS (ESI+): m/z 463.52 ([M + H]$^+$, 51); 485.51 ([M + Na]$^+$, 51). Combustion analysis measured (calculated): C 69.85 (70.11); H 6.47 (6.54); N 6.21 (6.06).

*2-(3-(2-(4-(tert-Butyl)benzamido)benzamido)phenyl)acetic Acid (**31**).* Preparation according to general procedure d using **7h** and *tert*-butylbenzoyl chloride (**8a**). After column chromatography on silica with hexane/ethyl acetate/acetic acid (89:9:2) as mobile phase, the product was recrystallized from hexane/ethyl acetate to give **31** as white solid in 72% yield. R_f (hexane/ethyl acetate/acetic acid (49:49:2)) = 0.48. ^{1}H NMR (500 MHz, DMSO) δ = 12.37 (s, 1H), 11.68 (s, 1H), 10.55 (s, 1H), 8.52 (d, J = 8.3 Hz, 1H), 7.94 (d, J = 7.8 Hz, 1H), 7.85 (d, J = 8.4 Hz, 2H), 7.66−7.62 (m, 2H), 7.60 (d, J = 8.2 Hz, 3H), 7.33 (t, J = 7.8 Hz, 1H), 7.29 (t, J = 7.6 Hz, 1H), 7.06 (d, J = 7.6 Hz, 1H), 3.58 (s, 2H), 1.32 (s, 9H). ^{13}C NMR (126 MHz, DMSO) δ = 173.06, 167.96, 165.00, 155.48, 139.33, 138.87, 135.98, 132.77, 132.22, 129.52, 127.37, 126.24, 125.92, 123.57, 122.92, 122.54, 121.54, 120.13, 67.49, 41.28, 35.22, 31.35. $C_{26}H_{26}N_2O_4$. MS (ESI−): m/z 429.17 ([M − H]$^-$, 100). Combustion analysis measured (calculated): C 72.35 (72.54); H 6.27 (6.09); N 6.19 (6.51).

*3-(3-(2-(4-(tert-Butyl)benzamido)benzamido)phenyl)propanoic Acid (**32**).* Preparation according to general procedure d using **7i** and *tert*-butylbenzoyl chloride (**8a**). After column chromatography on silica with hexane/ethyl acetate/acetic acid (89:9:2) as mobile phase, the product was recrystallized from hexane/ethyl acetate to give **32** as white solid in 72% yield. R_f (hexane/ethyl acetate/acetic acid (49:49:2)) = 0.55. ^{1}H NMR (500 MHz, DMSO) δ = 12.16 (s, 1H), 11.69 (s, 1H), 10.50 (s, 1H), 8.51 (d, J = 8.3 Hz, 1H), 7.96−7.91 (m, 1H), 7.85 (d, J = 8.4 Hz, 2H), 7.64−7.57 (m, 3H), 7.52 (s, 1H), 7.29 (ddd, J = 8.3, 3.1, 1.7 Hz, 2H), 7.03 (d, J = 7.6 Hz, 1H), 2.83 (t, J = 7.6 Hz, 2H), 2.55 (t, J = 7.6 Hz, 2H), 1.31 (s, 9H). ^{13}C NMR (126 MHz, DMSO) δ = 174.14, 167.92, 164.99, 155.49, 141.85, 139.31, 138.87, 132.75, 132.20, 129.47, 129.08, 127.36, 126.24, 124.74, 123.58, 122.97, 121.55, 121.54, 119.56, 35.55, 35.22, 31.34, 30.83. $C_{27}H_{28}N_2O_4$. MS (ESI+): m/z 467.52 ([M + Na]$^+$, 100). Combustion analysis measured (calculated): C 73.32 (72.95); H 6.50 (6.35); N 5.88 (6.30).

*3-(2-(4-(tert-Butyl)benzamido)benzamido)-4-methylbenzoic Acid (**33**).* Preparation according to general procedure d using **7j** and *tert*-butylbenzoyl chloride (**8a**). After column chromatography on silica with hexane/ethyl acetate/acetic acid (89:9:2) as mobile phase, the product was recrystallized from hexane/ethyl acetate to give **33** as white solid in 64% yield. R_f (hexane/ethyl acetate/acetic acid (49:49:2)) = 0.58. ^{1}H NMR (500 MHz, DMSO) δ = 12.96 (s, 1H), 12.03 (s, 1H), 10.38 (s, 1H), 8.61 (d, J = 8.3 Hz, 1H), 8.07 (d, J = 7.7 Hz, 1H), 7.91 (d, J = 1.2 Hz, 1H), 7.83 (d, J = 8.5 Hz, 2H), 7.79 (dd, J = 7.9, 1.5 Hz, 1H), 7.65 (t, J = 7.8 Hz, 1H), 7.58 (d, J = 8.5 Hz, 2H), 7.44 (d, J = 8.0 Hz, 1H), 7.30 (t, J = 7.6 Hz, 1H), 2.32 (s, 3H), 1.29 (s, 9H). ^{13}C NMR (126 MHz, DMSO) δ = 168.35, 167.38, 164.96, 155.48, 140.12, 139.94, 136.47, 133.11, 132.19, 131.23, 129.47, 129.41, 128.35, 127.77, 127.30, 126.25, 123.53, 121.44, 121.26, 40.57, 40.48, 40.41, 40.32, 40.24, 40.15, 40.07, 39.98, 39.91, 39.81, 39.65, 39.48, 35.20, 31.32, 31.17, 18.56. $C_{26}H_{26}N_2O_4$. MS (ESI−): m/z 429.9 ([M − H]$^-$, 100). Combustion analysis measured (calculated): C 72.21 (72.54); H 6.12 (6.09); N 6.41 (6.51).

*3-(2-(4-(tert-Butyl)benzamido)benzamido)-2-methylbenzoic Acid (**34**).* Preparation according to general procedure d using **7k** and *tert*-butylbenzoyl chloride (**8a**). After column chromatography on silica with hexane/ethyl acetate/acetic acid (89:9:2) as mobile phase, the product was recrystallized from hexane/ethyl acetate to give **34** as white solid in 71% yield. R_f (hexane/ethyl acetate/acetic acid (49:49:2)) = 0.57. ^{1}H NMR (500 MHz, DMSO) δ = 12.17 (s, 1H), 10.43 (s, 1H), 8.66 (d, J = 8.3 Hz, 1H), 8.09 (d, J = 7.7 Hz, 1H), 7.83 (d, J = 8.5 Hz, 2H), 7.74−7.69 (m, 1H), 7.68−7.62 (m, 1H), 7.58 (d, J = 8.5 Hz, 2H), 7.49 (d, J = 7.2 Hz, 1H), 7.35 (t, J = 7.8 Hz, 1H), 7.32−7.27 (m, 1H), 2.39 (s, 3H), 1.29 (s, 9H). ^{13}C NMR (126 MHz, DMSO) δ = 169.48, 168.48, 164.92, 155.51, 140.16, 137.30, 135.52, 133.27, 133.21, 132.17, 132.12, 131.11, 129.34, 128.58, 127.25, 126.29, 123.45, 121.08, 120.86, 35.20, 31.31, 15.74. $C_{26}H_{26}N_2O_4$. MS (ESI−): m/z 429.8 ([M − H]$^-$, 100). Combustion analysis measured (calculated): C 72.10 (72.54); H 6.06 (6.09); N 6.17 (6.51).

*5-(2-(4-(tert-Butyl)benzamido)benzamido)-2-methylbenzoic Acid (**35**).* Preparation according to general procedure d using **7l** and *tert*-butylbenzoyl chloride (**8a**). After column chromatography on silica with hexane/ethyl acetate/acetic acid (89:9:2) as mobile phase, the product was recrystallized from hexane/ethyl acetate to give **35** as white solid in 66% yield. R_f (hexane/ethyl acetate/acetic acid (49:49:2)) = 0.58. ^{1}H NMR (500 MHz, DMSO) δ = 12.91 (s, 1H), 11.65 (s, 1H), 10.61 (s, 1H), 8.50 (d, J = 8.3 Hz, 1H), 8.17 (d, J = 1.9 Hz, 1H), 7.94 (d, J = 7.8 Hz, 1H), 7.88−7.80 (m, 3H), 7.61 (dd, J = 17.6, 8.1 Hz, 3H), 7.29 (dd, J = 14.6, 7.8 Hz, 2H), 1.32 (s, 9H). ^{13}C NMR (126 MHz, DMSO) δ = 168.87, 167.96, 165.03, 155.48, 139.29, 136.73, 135.30, 132.80, 132.25, 130.94, 129.48, 127.37, 126.23, 124.89, 123.61, 123.44, 122.93, 121.63, 40.57, 40.48, 40.41, 40.32, 40.24, 40.15, 40.07, 39.98, 39.91, 39.81, 39.65, 39.48, 35.22, 31.35, 21.27. $C_{26}H_{26}N_2O_4$. MS (ESI+): m/z 431.46 ([M + H]$^+$, 16); 453.45 ([M + Na]$^+$, 100). Combustion analysis measured (calculated): C 72.19 (72.54); H 6.08 (6.09); N 6.43 (6.51).

*3-(2-(4-(tert-Butyl)benzamido)benzamido)-4-methoxybenzoic Acid (**36**).* Preparation according to general procedure d using **7m** and *tert*-butylbenzoyl chloride (**8a**). After column chromatography on silica with hexane/ethyl acetate/acetic acid (89:9:2) as mobile phase, the product was recrystallized from hexane/ethyl acetate to give **36** as white solid in 38% yield. R_f (hexane/ethyl acetate/acetic acid (49:49:2)) = 0.54. ^{1}H NMR (500 MHz, DMSO) δ = 11.83 (s, 1H), 9.93 (s, 1H), 8.49 (d, J = 8.3 Hz, 1H), 8.22 (t, J = 5.4 Hz, 1H), 8.01 (d, J = 7.7 Hz, 1H), 7.87−7.83 (m, 3H), 7.64 (t, J = 7.5 Hz, 1H), 7.58 (d, J = 8.4 Hz, 2H), 7.29 (t, J = 7.6 Hz, 1H), 7.20 (d, J = 8.7 Hz, 1H), 3.83 (s, 3H), 1.30 (s, 9H). ^{13}C NMR (126 MHz, DMSO) δ = 167.87, 167.29, 165.16, 156.35, 155.52, 139.36, 133.01, 132.11, 129.44, 128.98, 127.37, 127.09, 126.36, 126.22, 123.87, 123.20, 122.48, 121.89, 111.81, 56.52, 35.21, 31.33. $C_{26}H_{26}N_2O_5$. MS (ESI−): m/z 445.24 ([M − H]$^-$, 100). Combustion analysis measured (calculated): C 69.54 (69.94); H 5.92 (5.87); N 6.01 (6.27).

*3-(2-(4-(tert-Butyl)benzamido)benzamido)-4-fluorobenzoic Acid (**37**).* Preparation according to general procedure d using **7n** and *tert*-butylbenzoyl chloride (**8a**). After column chromatography on silica with hexane/ethyl acetate/acetic acid (89:9:2) as mobile phase, the product was recrystallized from hexane/ethyl acetate to give **37** as white solid in 51% yield. R_f (hexane/ethyl acetate/acetic acid (49:49:2)) = 0.59. ^{1}H NMR (500 MHz, DMSO) δ = 13.18 (s, 1H), 11.81 (s, 1H), 10.58 (s, 1H), 8.56 (d, J = 8.2 Hz, 1H), 8.15 (dd, J = 7.3, 2.0 Hz, 1H), 8.01 (t, J = 10.3 Hz, 1H), 7.90 (ddd, J = 8.4, 4.6, 2.1 Hz, 1H), 7.83 (d, J = 8.5 Hz, 2H), 7.68−7.63 (m, 1H), 7.58 (d, J = 8.4 Hz, 2H), 7.49−7.43 (m, 1H), 7.30 (dd, J = 11.2, 4.0 Hz, 1H), 1.30 (s, 9H). ^{13}C NMR (126 MHz, DMSO) δ = 168.29, 166.60, 165.08, 155.51, 139.78, 133.34, 132.17, 129.65, 129.38, 129.31, 129.13, 127.77, 127.33, 126.24, 125.87, 125.77, 123.62, 121.48, 121.33, 116.99, 116.82, 35.20, 31.32. $C_{25}H_{23}FN_2O_4$. MS (ESI+): m/z 435.44 ([M + H]$^+$, 13); 457.45 ([M + Na]$^+$, 100). Combustion analysis measured (calculated): C 68.92 (69.11); H 5.24 (5.34); N 6.49 (6.45).

*3-(2-(4-(tert-Butyl)benzamido)benzamido)-4-chlorobenzoic Acid (**38**).* Preparation according to general procedure d using **7o** and *tert*-butylbenzoyl chloride (**8a**). After column chromatography on silica with hexane/ethyl acetate/acetic acid (89:9:2) as mobile phase, the product was recrystallized from hexane/ethyl acetate to give **38** as white solid in 35% yield. R_f (hexane/ethyl acetate/acetic acid (49:49:2)) = 0.61. ^{1}H NMR (500 MHz, DMSO) δ = 13.33 (s, 1H), 11.87 (s, 1H), 10.56 (s, 1H), 8.57 (d, J = 8.3 Hz, 1H), 8.12 (d, J = 1.8 Hz, 1H), 8.06 (d, J = 7.6 Hz, 1H), 7.88 (dd, J = 8.4, 1.8 Hz, 1H), 7.84 (d, J = 8.3 Hz, 2H), 7.73 (d, J = 8.4 Hz, 1H), 7.66 (t, J = 7.6 Hz, 1H), 7.58 (d, J = 8.3 Hz, 2H), 7.31 (t, J = 7.6 Hz, 1H), 1.30 (s, 9H). ^{13}C NMR (126 MHz, DMSO) δ = 168.37, 166.65, 165.06, 155.51, 139.85, 135.32, 135.26, 133.35, 132.15, 130.86, 130.56, 129.94, 129.46, 129.04, 127.35, 126.24, 123.66, 121.49, 121.33, 35.21, 31.32. $C_{25}H_{23}ClN_2O_4$.

dx.doi.org/10.1021/jm500937v | J. Med. Chem. 2014, 57, 8035−8055

MS (ESI+): m/z 474.44 ([M + H]$^+$, 100). Combustion analysis measured (calculated): C 66.38 (66.59); H 5.17 (5.14); N 6.14 (6.21).

*5-(2-(4-(tert-Butyl)benzamido)benzamido)-2-methoxybenzoic Acid (**39**).* Preparation according to general procedure d using **7p** and *tert*-butylbenzoyl chloride (**8a**). After column chromatography on silica with hexane/ethyl acetate/acetic acid (89:9:2) as mobile phase, the product was recrystallized from hexane/ethyl acetate to give **39** as white solid in 60% yield. R_f (hexane/ethyl acetate/acetic acid (49:49:2)) = 0.40. ^{1}H NMR (500 MHz, DMSO) δ = 11.76 (s, 1H), 10.53 (s, 1H), 8.53 (d, J = 7.7 Hz, 1H), 7.97 (d, J = 2.6 Hz, 1H), 7.94 (dd, J = 7.9, 1.2 Hz, 1H), 7.87−7.82 (m, 3H), 7.64−7.58 (m, 3H), 7.28 (td, J = 7.8, 1.1 Hz, 1H), 7.15 (d, J = 9.1 Hz, 1H), 3.82 (s, 3H), 1.32 (s, 9H). ^{13}C NMR (126 MHz, DMSO) δ = 167.78, 167.50, 164.99, 155.49, 155.36, 139.40, 132.78, 132.25, 131.34, 129.37, 127.34, 126.56, 126.25, 124.37, 123.55, 122.60, 121.47, 113.25, 56.48, 35.23, 31.35. $C_{26}H_{26}N_2O_5$. MS (ESI−): m/z 445.9 ([M − H]$^-$, 100). Combustion analysis measured (calculated): C 69.77 (69.94); H 5.93 (5.87); N 5.93 (6.27).

*5-(2-(4-(tert-Butyl)benzamido)benzamido)-2-chlorobenzoic Acid (**40**).* Preparation according to general procedure d using **7q** and *tert*-butylbenzoyl chloride (**8a**). After column chromatography on silica with hexane/ethyl acetate/acetic acid (89:9:2) as mobile phase, the product was recrystallized from hexane/ethyl acetate to give **40** as white solid in 63% yield. R_f (hexane/ethyl acetate/acetic acid (49:49:2)) = 0.50. ^{1}H NMR (500 MHz, DMSO) δ = 11.42 (s, 1H), 10.74 (s, 1H), 8.41 (d, J = 7.9 Hz, 1H), 8.17 (d, J = 2.6 Hz, 1H), 7.91 (dd, J = 8.7, 2.3 Hz, 2H), 7.85 (d, J = 8.5 Hz, 2H), 7.65−7.61 (m, 1H), 7.59 (d, J = 8.5 Hz, 2H), 7.55 (d, J = 8.7 Hz, 1H), 7.33−7.27 (m, 1H), 1.32 (s, 9H). ^{13}C NMR (126 MHz, DMSO) δ = 172.49, 168.03, 166.91, 165.13, 155.46, 139.02, 138.08, 132.85, 131.77, 131.44, 129.52, 127.44, 126.79, 126.17, 125.07, 123.77, 123.52, 123.37, 122.03, 35.22, 31.35. $C_{25}H_{23}ClN_2O_4$. MS (ESI−): m/z 449.9 ([M − H]$^-$, 100). Combustion analysis measured (calculated): C 66.53 (66.59); H 5.19 (5.14); N 6.23 (6.21).

*2-Bromo-5-(2-(4-(tert-butyl)benzamido)benzamido)benzoic Acid (**41**).* Preparation according to general procedure d using **7r** and *tert*-butylbenzoyl chloride (**8a**). After column chromatography on silica with hexane/ethyl acetate/acetic acid (89:9:2) as mobile phase, the product was recrystallized from hexane/ethyl acetate to give **41** as white solid in 54% yield. R_f (hexane/ethyl acetate/acetic acid (49:49:2)) = 0.48. ^{1}H NMR (500 MHz, DMSO) δ = 11.40 (s, 1H), 10.73 (s, 1H), 8.41 (t, J = 7.3 Hz, 1H), 8.13 (d, J = 2.6 Hz, 1H), 7.91 (d, J = 7.7 Hz, 1H), 7.83 (dd, J = 13.6, 5.5 Hz, 3H), 7.71 (d, J = 8.7 Hz, 1H), 7.63 (t, J = 7.8 Hz, 1H), 7.59 (d, J = 8.4 Hz, 2H), 7.30 (t, J = 7.4 Hz, 1H), 1.32 (s, 9H). ^{13}C NMR (126 MHz, DMSO) δ = 168.03, 167.52, 165.14, 155.47, 139.00, 138.62, 134.58, 134.09, 132.85, 132.21, 129.52, 127.44, 126.17, 125.03, 123.79, 123.58, 123.21, 122.06, 114.61, 35.22, 31.35. $C_{25}H_{23}BrN_2O_4$. MS (ESI−): m/z 494.0 ([M − H]$^-$, 99), 495.9 ([M − H]$^-$, 100). Combustion analysis measured (calculated): C 60.93 (60.62); H 5.11 (4.68); N 5.60 (5.66).

*5-(2-(4-(tert-Butyl)benzamido)benzamido)-2-nitrobenzoic Acid (**42**).* Preparation according to general procedure d using **7s** and *tert*-butylbenzoyl chloride (**8a**). After column chromatography on silica with hexane/ethyl acetate/acetic acid (89:9:2) as mobile phase, the product was recrystallized from hexane/ethyl acetate to give **42** as yellow solid in 31% yield. R_f (hexane/ethyl acetate/acetic acid (49:49:2)) = 0.51. ^{1}H NMR (500 MHz, DMSO) δ = 12.23 (s, 1H), 10.58 (s, 1H), 8.44 (d, J = 2.6 Hz, 1H), 8.25 (t, J = 1.8 Hz, 1H), 7.97 (t, J = 8.5 Hz, 1H), 7.94−7.91 (m, 1H), 7.86 (d, J = 8.5 Hz, 2H), 7.75−7.71 (m, 1H), 7.61 (d, J = 8.5 Hz, 2H), 7.55 (t, J = 7.9 Hz, 1H), 6.98 (dd, J = 8.9, 2.6 Hz, 1H), 1.32 (s, 9H). ^{13}C NMR (126 MHz, DMSO) δ = 174.03, 168.09, 167.60, 165.19, 162.65, 153.22, 142.08, 138.89, 134.14, 131.45, 129.87, 127.64, 126.67, 124.82, 125.61, 122.34, 113.12, 109.34, 106.03, 35.23, 31.33. $C_{25}H_{23}N_3O_6$. MS (ESI−): m/z 460.9 ([M − H]$^-$, 100). Combustion analysis measured (calculated): C 64.78 (65.07); H 4.97 (5.02); N 9.06 (9.11).

*3-(2-(4-(tert-Butyl)benzamido)-6-chlorobenzamido)benzoic Acid (**43**).* Preparation according to general procedure d using **7t** and *tert*-butylbenzoyl chloride (**8a**). After column chromatography on silica with hexane/ethyl acetate/acetic acid (89:9:2) as mobile phase, the product was recrystallized from hexane/ethyl acetate to give **43** as white solid in 68% yield. R_f (hexane/ethyl acetate/acetic acid (49:49:2)) = 0.47. ^{1}H NMR (500 MHz, DMSO) δ = 12.96 (s, 1H), 10.50 (s, 1H), 10.11 (s, 1H), 8.32 (s, 1H), 7.87 (t, J = 7.7 Hz, 3H), 7.75 (d, J = 8.0 Hz, 1H), 7.64 (t, J = 7.2 Hz, 2H), 7.49 (dd, J = 15.4, 8.0 Hz, 3H), 7.42 (t, J = 7.9 Hz, 1H), 1.30 (s, 9H). ^{13}C NMR (126 MHz, DMSO) δ = 167.60, 166.01, 165.55, 155.13, 139.86, 137.43, 133.59, 132.99, 131.72, 131.69, 131.52, 129.36, 128.42, 128.05, 127.73, 125.67, 124.86, 124.32, 121.01, 35.15, 31.37. $C_{25}H_{23}ClN_2O_4$. MS (ESI−): m/z 449.08 ([M − H]$^-$, 100). Combustion analysis measured (calculated): C 66.42 (66.59); H 5.10 (5.14); N 6.17 (6.21).

*3-(2-(4-(tert-Butyl)benzamido)-3-chlorobenzamido)benzoic Acid (**44**).* Preparation according to general procedure e using **44a**. After column chromatography on silica with hexane/ethyl acetate/acetic acid (89:9:2) as mobile phase, the product was recrystallized from hexane/ethyl acetate to give **44** as white solid in 86% yield. R_f (hexane/ethyl acetate/acetic acid (49:49:2)) = 0.46. ^{1}H NMR (500 MHz, DMSO) δ = 12.95 (s, 1H), 10.50 (s, 1H), 10.11 (s, 1H), 8.32 (s, 1H), 7.90−7.84 (m, 3H), 7.75 (dd, J = 8.1, 1.2 Hz, 1H), 7.67−7.61 (m, 2H), 7.52−7.46 (m, 3H), 7.42 (t, J = 7.9 Hz, 1H), 1.30 (s, 9H). ^{13}C NMR (126 MHz, DMSO) δ = 167.59, 166.01, 165.55, 155.13, 139.85, 137.43, 133.58, 132.98, 131.72, 131.69, 131.52, 129.36, 128.41, 128.05, 127.72, 125.67, 124.85, 124.32, 121.01, 35.15, 31.37. $C_{25}H_{23}ClN_2O_4$. MS (ESI−): m/z 449.7 ([M − H]$^-$, 100). Combustion analysis measured (calculated): C 66.48 (66.59); H 5.11 (5.14); N 6.12 (6.21).

*3-(2-(4-(tert-Butyl)benzamido)-5-chlorobenzamido)benzoic Acid (**45**).* Preparation according to general procedure d using **7u** and *tert*-butylbenzoyl chloride (**8a**). After column chromatography on silica with hexane/ethyl acetate/acetic acid (89:9:2) as mobile phase, the product was recrystallized from hexane/ethyl acetate to give **45** as pale-yellow solid in 44% yield. R_f (hexane/ethyl acetate/acetic acid (49:49:2)) = 0.65. ^{1}H NMR (500 MHz, DMSO) δ = 11.45 (s, 1H), 10.76 (s, 1H), 8.45 (d, J = 8.9 Hz, 1H), 8.30 (s, 1H), 8.01 (d, J = 2.4 Hz, 1H), 7.99−7.96 (m, 1H), 7.84 (d, J = 8.5 Hz, 2H), 7.73 (d, J = 7.8 Hz, 1H), 7.70 (dd, J = 8.9, 2.5 Hz, 1H), 7.59 (d, J = 8.5 Hz, 2H), 7.51 (t, J = 7.9 Hz, 1H), 1.31 (s, 9H). ^{13}C NMR (126 MHz, DMSO) δ = 167.55, 166.61, 165.16, 155.63, 139.08, 137.98, 132.39, 131.96, 131.77, 129.45, 129.15, 127.52, 127.47, 126.22, 125.64, 125.60, 125.12, 123.66, 122.33, 35.24, 31.33. $C_{25}H_{23}ClN_2O_4$. MS (ESI−): m/z 449.8 ([M − H]$^-$, 100). Combustion analysis measured (calculated): C 66.25 (66.59); H 4.96 (5.14); N 6.12 (6.21).

*3-(2-(4-(tert-Butyl)benzamido)-4-chlorobenzamido)benzoic Acid (**46**).* Preparation according to general procedure d using **7v** and *tert*-butylbenzoyl chloride (**8a**). After column chromatography on silica with hexane/ethyl acetate/acetic acid (89:9:2) as mobile phase, the product was recrystallized from hexane/ethyl acetate to give **46** as white solid in 61% yield. R_f (hexane/ethyl acetate/acetic acid (49:49:2)) = 0.63. ^{1}H NMR (500 MHz, DMSO) δ = 13.05 (s, 1H), 11.82−11.68 (m, 1H), 10.76 (s, 1H), 8.63 (d, J = 2.1 Hz, 1H), 8.32 (d, J = 16.3 Hz, 1H), 8.03−7.96 (m, 2H), 7.85 (d, J = 8.4 Hz, 2H), 7.74 (d, J = 7.8 Hz, 1H), 7.61 (d, J = 8.5 Hz, 2H), 7.52 (t, J = 7.9 Hz, 1H), 7.43−7.36 (m, 1H), 1.31 (s, 9H). ^{13}C NMR (126 MHz, DMSO) δ = 167.54, 167.28, 165.31, 155.82, 140.69, 139.04, 137.28, 131.81, 131.75, 131.33, 129.47, 127.46, 126.31, 125.82, 125.64, 123.32, 122.45, 121.28, 120.88, 35.26, 31.32. $C_{25}H_{23}ClN_2O_4$. MS (ESI−): m/z 449.8 ([M − H]$^-$, 100). Combustion analysis measured (calculated): C 66.68 (66.59); H 5.05 (5.14); N 6.08 (6.21).

*3-(2-(4-(tert-Butyl)benzamido)-5-methoxybenzamido)benzoic Acid (**47**).* Preparation according to general procedure e using **47a**. After column chromatography on silica with hexane/ethyl acetate/acetic acid (89:9:2) as mobile phase, the product was recrystallized from hexane/ethyl acetate to give **47** as white solid in 85% yield. R_f (hexane/ethyl acetate/acetic acid (49:49:2)) = 0.54. ^{1}H NMR (500 MHz, DMSO) δ = 13.04 (s, 1H), 11.13 (s, 1H), 10.64 (s, 1H), 8.31 (d, J = 1.7 Hz, 1H), 8.26 (d, J = 9.0 Hz, 1H), 8.00−7.94 (m, 1H), 7.83 (d, J = 8.5 Hz, 2H), 7.71 (d, J = 7.8 Hz, 1H), 7.57 (d, J = 8.5 Hz, 2H), 7.50 (t, J = 7.9 Hz, 1H), 7.45 (d, J = 2.9 Hz, 1H), 7.22 (dd, J = 9.0, 2.9 Hz, 1H), 3.87 (s, 3H), 1.31 (s, 9H). ^{13}C NMR (126 MHz, DMSO) δ = 167.57, 167.53, 164.88, 155.38, 155.21, 139.27, 132.32, 131.90,

131.68, 129.42, 127.34, 126.09, 125.61, 125.58, 125.42, 124.06, 122.24, 118.05, 114.42, 56.07, 35.18, 31.36. $C_{26}H_{26}N_2O_5$. MS (ESI−): m/z 446.1 ([M − H]$^-$, 100). Combustion analysis measured (calculated): C 69.83 (69.94); H 6.02 (5.87); N 6.05 (6.27).

*3-(2-(4-(tert-Butyl)benzamido)-4-nitrobenzamido)benzoic Acid (**48**).* Preparation according to general procedure d using **7w** and *tert*-butylbenzoyl chloride (**8a**). After column chromatography on silica with hexane/ethyl acetate/acetic acid (89:9:2) as mobile phase, the product was recrystallized from hexane/ethyl acetate to give **48** as yellow solid in 51% yield. R_f (hexane/ethyl acetate/acetic acid (49:49:2)) = 0.56. ^{1}H NMR (500 MHz, DMSO) δ = 11.50 (s, 1H), 10.95 (s, 1H), 9.24 (d, J = 2.2 Hz, 1H), 8.33 (s, 1H), 8.16 (d, J = 8.6 Hz, 1H), 8.12 (dd, J = 8.6, 2.3 Hz, 1H), 7.99 (dd, J = 8.1, 1.0 Hz, 1H), 7.88−7.85 (m, 2H), 7.76−7.73 (m, 1H), 7.62−7.59 (m, 2H), 7.52 (t, J = 7.9 Hz, 1H), 1.31 (s, 9H). ^{13}C NMR (126 MHz, DMSO) δ = 172.49, 167.52, 166.29, 165.57, 162.77, 155.92, 149.51, 139.71, 139.02, 131.77, 131.56, 131.08, 129.51, 129.25, 127.62, 126.25, 125.75, 125.63, 122.29, 118.13, 116.32, 35.26, 31.31. $C_{25}H_{23}N_3O_6$. MS (ESI−): m/z 460.9 ([M − H]$^-$, 100). Combustion analysis measured (calculated): C 64.80 (65.07); H 5.17 (5.02); N 9.06 (9.11).

*3-(2-(4-(tert-Butyl)benzamido)-4-methylbenzamido)benzoic Acid (**49**).* Preparation according to general procedure e using **49a**. After column chromatography on silica with hexane/ethyl acetate/acetic acid (89:9:2) as mobile phase, the product was recrystallized from hexane/ethyl acetate to give **49** as white solid in 82% yield. R_f (hexane/ethyl acetate/acetic acid (49:49:2)) = 0.60. ^{1}H NMR (500 MHz, DMSO) δ = 13.04 (s, 1H), 11.77 (s, 1H), 10.63 (s, 1H), 8.41 (s, 1H), 8.30 (s, 1H), 7.97 (dd, J = 9.0, 8.0 Hz, 1H), 7.88 (t, J = 7.3 Hz, 1H), 7.85 (d, J = 8.5 Hz, 2H), 7.72 (d, J = 7.8 Hz, 1H), 7.60 (d, J = 8.5 Hz, 2H), 7.51 (t, J = 7.9 Hz, 1H), 7.11 (d, J = 8.0 Hz, 1H), 2.42 (s, 3H), 1.32 (s, 9H). ^{13}C NMR (126 MHz, DMSO) δ = 168.20, 167.59, 164.97, 155.48, 143.26, 139.65, 139.20, 132.29, 129.52, 129.41, 127.31, 126.26, 125.79, 125.45, 124.18, 122.45, 121.81, 119.56, 35.23, 31.34, 21.94. $C_{26}H_{26}N_2O_4$. MS (ESI+): m/z 431.50 ([M + H]$^+$, 45), 453.49 ([M + Na]$^+$, 100). Combustion analysis measured (calculated): C 72.19 (72.54); H 6.33 (6.09); N 6.12 (6.51).

*3-(4-Bromo-2-(4-(tert-butyl)benzamido)benzamido)benzoic Acid (**50**).* Preparation according to general procedure d using **7x** and *tert*-butylbenzoyl chloride (**8a**). After column chromatography on silica with hexane/ethyl acetate/acetic acid (89:9:2) as mobile phase, the product was recrystallized from hexane/ethyl acetate to give **50** as white solid in 57% yield. R_f (hexane/ethyl acetate/acetic acid (49:49:2)) = 0.61. ^{1}H NMR (500 MHz, DMSO) δ = 11.70 (s, 1H), 10.76 (s, 1H), 8.76 (d, J = 2.0 Hz, 1H), 8.30 (t, J = 1.8 Hz, 1H), 7.97 (dt, J = 13.7, 6.8 Hz, 1H), 7.92 (d, J = 8.5 Hz, 1H), 7.85 (d, J = 8.5 Hz, 2H), 7.76−7.71 (m, 1H), 7.61 (d, J = 8.5 Hz, 2H), 7.52 (dd, J = 8.9, 7.1 Hz, 2H), 1.31 (s, 9H). ^{13}C NMR (126 MHz, DMSO) δ = 172.49, 167.54, 167.36, 165.29, 155.81, 140.62, 139.04, 131.80, 131.73, 131.39, 129.48, 127.46, 126.30, 126.09, 125.80, 125.63, 123.86, 122.43, 121.75, 35.26, 31.32. $C_{25}H_{23}BrN_2O_4$. MS (ESI+): m/z 517.47 ([M + Na]$^+$, 77), 519.46 ([M + Na]$^+$, 100). Combustion analysis measured (calculated): C 60.89 (60.62); H 4.72 (4.68); N 5.27 (5.66).

*3-(2-(4-(tert-Butyl)benzamido)-4-methoxybenzamido)benzoic Acid (**51**).* Preparation according to general procedure e using **51a**. After column chromatography on silica with hexane/ethyl acetate/acetic acid (89:9:2) as mobile phase, the product was recrystallized from hexane/ethyl acetate to give **51** as white solid in 83% yield. R_f (hexane/ethyl acetate/acetic acid (49:49:2)) = 0.56. ^{1}H NMR (500 MHz, DMSO) δ = 12.26 (s, 1H), 10.56 (s, 1H), 8.34 (d, J = 2.6 Hz, 1H), 8.26 (t, J = 1.8 Hz, 1H), 8.01 (t, J = 8.5 Hz, 1H), 7.99−7.95 (m, 1H), 7.86 (d, J = 8.5 Hz, 2H), 7.74−7.70 (m, 1H), 7.61 (d, J = 8.5 Hz, 2H), 7.50 (t, J = 7.9 Hz, 1H), 6.86 (dd, J = 8.9, 2.6 Hz, 1H), 3.88 (s, 3H), 1.32 (s, 9H). ^{13}C NMR (126 MHz, DMSO) δ = 168.18, 167.65, 165.13, 162.94, 155.62, 142.11, 139.13, 132.21, 131.32, 129.33, 127.29, 126.34, 125.82, 125.42, 122.63, 113.50, 108.95, 105.96, 55.99, 35.25, 31.33. $C_{26}H_{26}N_2O_5$. MS (ESI−): m/z 446.0 ([M − H]$^-$, 100). Combustion analysis measured (calculated): C 70.26 (69.94); H 5.88 (5.87); N 6.36 (6.27).

*5-(2-(4-(tert-Butyl)benzamido)-4-chlorobenzamido)-2-methylbenzoic Acid (**52**).* Preparation according to general procedure d using **7y** and *tert*-butylbenzoyl chloride (**8a**). After column chromatography on silica with hexane/ethyl acetate/acetic acid (89:9:2) as mobile phase, the product was recrystallized from hexane/ethyl acetate to give **52** as white solid in 74% yield. R_f (hexane/ethyl acetate/acetic acid (49:49:2)) = 0.63. ^{1}H NMR (500 MHz, DMSO) δ = 12.88 (s, 1H), 11.83 (d, J = 18.3 Hz, 1H), 10.67 (s, 1H), 8.65 (t, J = 2.6 Hz, 1H), 8.15 (t, J = 3.0 Hz, 1H), 8.00 (d, J = 8.5 Hz, 1H), 7.86−7.83 (m, 2H), 7.82 (dd, J = 8.3, 2.5 Hz, 1H), 7.61 (t, J = 6.4 Hz, 2H), 7.37 (dt, J = 13.0, 6.5 Hz, 1H), 7.30 (t, J = 11.2 Hz, 1H), 2.51 (s, 3H), 1.31 (s, 9H). ^{13}C NMR (126 MHz, DMSO) δ = 168.81, 167.16, 165.27, 155.82, 140.76, 137.25, 136.50, 135.53, 132.29, 131.80, 131.23, 130.94, 127.43, 126.31, 125.03, 123.58, 123.25, 121.00, 120.74, 35.26, 31.32, 21.28. $C_{26}H_{25}ClN_2O_4$. MS (ESI−): m/z 463.9 ([M − H]$^-$, 100). Combustion analysis measured (calculated): C 66.98 (67.17); H 5.73 (5.42); N 5.65 (6.03).

*5-(2-(4-(tert-Butyl)benzamido)-4-methoxybenzamido)-2-methylbenzoic Acid (**53**).* Preparation according to general procedure d using **7z** and *tert*-butylbenzoyl chloride (**8a**). After column chromatography on silica with hexane/ethyl acetate/acetic acid (89:9:2) as mobile phase, the product was recrystallized from hexane/ethyl acetate to give **53** as white solid in 63% yield. R_f (hexane/ethyl acetate/acetic acid (49:49:2)) = 0.59. ^{1}H NMR (500 MHz, DMSO) δ = 12.90 (s, 1H), 12.33 (s, 1H), 10.47 (s, 1H), 8.35 (d, J = 2.6 Hz, 1H), 8.13 (d, J = 2.4 Hz, 1H), 8.01 (d, J = 8.9 Hz, 1H), 7.88−7.84 (m, 2H), 7.83 (dd, J = 8.3, 2.4 Hz, 1H), 7.61 (d, J = 8.5 Hz, 2H), 7.31 (d, J = 8.4 Hz, 1H), 6.84 (dd, J = 8.9, 2.6 Hz, 1H), 3.88 (s, 3H), 2.51 (s, 3H), 1.31 (s, 9H). ^{13}C NMR (126 MHz, DMSO) δ = 168.87, 168.08, 165.11, 162.89, 155.60, 142.13, 136.69, 135.25, 132.23, 131.20, 130.91, 127.28, 126.33, 125.22, 123.73, 113.38, 108.91, 105.88, 55.97, 35.24, 31.33, 21.27. $C_{27}H_{28}N_2O_5$. MS (ESI−): m/z 459.2 ([M − H]$^-$, 100). Combustion analysis measured (calculated): C 70.12 (70.42); H 6.07 (6.13); N 5.89 (6.08).

*5-(2-(4-(tert-Butyl)benzamido)-4-methylbenzamido)-2-methylbenzoic Acid (**54**).* Preparation according to general procedure d using **7aa** and *tert*-butylbenzoyl chloride (**8a**). After column chromatography on silica with hexane/ethyl acetate/acetic acid (89:9:2) as mobile phase, the product was recrystallized from hexane/ethyl acetate to give **54** as white solid in 60% yield. R_f (hexane/ethyl acetate/acetic acid (49:49:2)) = 0.57. ^{1}H NMR (500 MHz, DMSO) δ = 11.86 (s, 1H), 10.54 (s, 1H), 8.43 (s, 1H), 8.15 (d, J = 2.3 Hz, 1H), 7.88 (d, J = 8.1 Hz, 1H), 7.85 (d, J = 8.5 Hz, 2H), 7.82 (dd, J = 8.5, 2.4 Hz, 1H), 7.60 (d, J = 8.5 Hz, 2H), 7.31 (d, J = 8.4 Hz, 1H), 7.10 (d, J = 8.0 Hz, 1H), 2.50 (s, 3H), 2.41 (s, 3H), 1.32 (s, 9H). ^{13}C NMR (126 MHz, DMSO) δ = 168.87, 168.08, 164.93, 155.48, 143.20, 139.70, 136.68, 135.27, 132.24, 131.56, 130.95, 129.42, 127.29, 126.27, 125.02, 124.12, 123.56, 121.68, 119.35, 35.22, 31.34, 21.94, 21.26. $C_{27}H_{28}N_2O_4$. MS (ESI−): m/z 444.0 ([M − H]$^-$, 100). Combustion analysis measured (calculated): C 72.95 (72.95); H 6.25 (6.35); N 5.91 (6.30).

Intermediates. *3-(2-Aminobenzamido)benzoic Acid (**7a**).* Preparation according to general procedure a1 using isatoic anhydride (**5a**) and 3-aminobenzoic acid (**4a**). The crude product was purified by column chromatography on silica with hexane/ethyl acetate/acetic acid (49:49:2) as mobile phase to obtain **7a** as white solid in 64% yield. R_f (hexane/ethyl acetate/acetic acid (49:49:2)) = 0.58. ^{1}H NMR (500 MHz, DMSO) δ = 13.16 (s, 1H), 7.96 (t, J = 8.0 Hz, 1H), 7.70 (dd, J = 9.1, 7.4 Hz, 1H), 7.65 (dd, J = 7.7, 1.2 Hz, 1H), 7.59 (t, J = 7.8 Hz, 1H), 7.53−7.49 (m, 1H), 7.37−7.31 (m, 1H), 7.05 (s, 1H), 6.79−6.70 (m, 2H). ^{13}C NMR (126 MHz, DMSO) δ = 167.26, 163.21, 147.09, 139.23, 135.33, 134.20, 132.11, 131.47, 129.79, 129.03, 128.32, 117.72, 115.09, 114.63. $C_{14}H_{12}N_2O_3$. MS (ESI−): m/z 255.0 ([M − H]$^-$, 100), as representative intermediate. For synthesis and analytical data of other intermediates, please see Supporting Information.

Docking. Docking simulations were performed using the Molecular Operating Environment (MOE) (version 2012.10; The Chemical Computing Group, Montreal, Canada). The crystal structure of FXR (PDB ID: 3OLF[32]) was downloaded from the Protein Data Bank (PDB). Prior to ligand docking, one monomer of the dimer crystal structure was isolated and the crystallized ligand was removed. Subsequently, the structure was prepared with Protonate 3D, and the active site was isolated using MOE Site Finder. The structures were

placed in the site with the Triangle Matcher method and then ranked with the London dG scoring function. For the energy minimization in the pocket, MOE Force Field Refinement was used and ranked with the GBVI/WSA dG scoring function.

In Vitro Biological Evaluation. *FXR Transactivation Assay. Cell Culture.* HeLa cells were grown in DMEM high glucose, supplemented with 10% fetal calf serum (FCS), 1 mM sodium pyruvate (SP), penicillin (100 U/mL), and streptomycin (100 μg/mL) at 37 °C and 5% CO_2.

Plasmids for Full-Length FXR Transactivation Aassay. pcDNA3-hFXR contains the sequence of human FXR and was already published elsewhere,[43] and pGL3basic (Promega, Mannheim, Germany) was used as a reporter plasmid, with a shortened construct of the promotor of the bile salt export pump (BSEP, sequence of construct from ref 44) cloned into the SacI/NheI cleavage site in front of the luciferase gene. pRL-SV40 (Promega) was transfected as a control for normalization of transfection efficiency and cell growth. pSG5-hRXR was already published elsewhere[45] as well.

Full-Length FXR Transactivation Assay. Twenty-four h before transfection, HeLa cells were seeded in 96-well plates with a density of 8000 cells per well. Then 3.5 h before transfection, medium was changed to DMEM high glucose supplemented with 1 mM SP, penicillin (100 U/mL), streptomycin (100 μg/mL), and 0.5% charcoal-stripped FCS. Transient transfection of HeLa cells with BSEP-pGL3, pRL-SV40, and the expression plasmids pcDNA3-hFXR and pSG5-hRXR was carried out using calcium phosphate transfection method. Then 16 h after transfection, medium was changed to DMEM high glucose, supplemented with 1 mM SP, penicillin (100 U/mL), streptomycin (100 μg/mL), and 0.5% charcoal-stripped FCS. Then 24 h after transfection, medium was changed to DMEM without phenol red, supplemented with 1 mM SP, penicillin (100 U/mL), streptomycin (100 μg/mL), 2 mM L-glutamate, and 0.5% charcoal-stripped FCS, now additionally containing 0.1% DMSO and the respective test compound or 0.1% DMSO alone as untreated control. Each concentration was tested in triplicate wells, and each experiment was repeated independently at least three times. Following 24 h incubation with the test compounds, cells were assayed for luciferase activity using Dual-Glo luciferase assay system (Promega) according to the manufacturer's protocol. Luminescence was measured with a Tecan Infinite M200 luminometer (Tecan Deutschland GmbH, Crailsheim, Germany). Normalization of transfection efficacy and cell growth was done by division of firefly luciferase data by renilla luciferase data, resulting in relative light units (RLU). Fold activation was obtained by dividing the mean RLU of the tested compound at a respective concentration by the mean RLU of untreated control. Relative activation was obtained by dividing the fold activation of the tested compound at a respective concentration by the fold activation of FXR full agonist GW4064 (**3**) at 3 μM. EC_{50} and standard error of the mean values were calculated with the mean relative activation values of at least three independent experiments by SigmaPlot 10.0 (Systat Software GmbH, Erkrath, Germany) using a four parameter logistic regression.

FXR Target Gene Quantification (qRT-PCR). *Cell Culture.* HepG2 cells were seeded and grown in DMEM high glucose, supplemented with 10% FCS, 1 mM SP, penicillin (100 U/mL), and streptomycin (100 μg/mL) at 37 °C and 5% CO_2 in 6-well plates (2×10^6 per well). HT-29 cells were seeded and grown in McCoys 5A medium supplemented with 10% FCS, penicillin (100 U/mL), and streptomycin (100 μg/mL) at 37 °C and 5% CO_2 in 6-well plates (2×10^6 per well). Then 24 h after seeding, medium was changed to MEM supplemented with 1% charcoal stripped FCS, penicillin (100 U/mL), streptomycin (100 μg/mL), and 2 mM L-glutamate. After an additional 24 h, medium was again changed to MEM now additionally containing the test compounds in DMSO or DMSO alone (final concentration 0.1% DMSO). Cells were incubated with the test compounds for 24 h, harvested, washed with cold PBS, and then directly used for RNA extraction or stored at −80 °C.

RNA Extraction and cDNA Synthesis. Two micrograms of total RNA were extracted from HepG2 or HT-29 cells by the Total RNA Mini Kit from Omega (R6834-02). RNA was reverse transcribed into cDNA using the High-Capacity cDNA Reverse Transcription Kit (Life Technologies: 4368814) according to the manufacturer's protocol.

q-RT PCR. FXR target gene expression was evaluated by quantitative PCR analysis with a StepOnePlus System (Life Technologies) using PowerSYBRGreen (Life Technologies; 12.5 μL per well) and the following primers (300 nM each): SHP, 5′-GCTGTCTGGAGTCCTTCTGG (forward) and 5′-CCAATGATAGGGCGAAAGAAGAG (reverse); CYP7A1, 5′-CACCTTGAGGACGGTTCCTA (forward) and 5′-CGATCCAAAGGGCATGTAGT (reverse); BSEP, 5′-CATGGTGCAAGAAGTGCTGAGT (forward) and 5′-AAGCGATGAGCAACTGAAATGAT (reverse); OSTα, 5′-TGCTGCTCACCAGGAAGAAG (forward) and 5′-ATAGAGCTGTGCTCCCCTCA (reverse); IBABP, 5′-TCAAGGCCACTGTGCAGATG (forward) and 5′-CAGCTTGTCACCCACGATCTC (reverse). Results were normalized to GAPDH *Ct* values. Sequences of the GAPDH primers were as follows: 5′-ATATGATTCCACCCATGGCA (forward) and 5′-GATGATGACCCTTTTGGCTC (reverse). Each sample was set up in duplicate and repeated in at least four independent experiments. The expression was quantified by comparative ΔΔ*Ct* method.

PPAR Transactivation Assay. *Cell Culture.* COS-7 cells were grown in DMEM high glucose, supplemented with 10% FCS, 1 mM sodium pyruvate (SP), penicillin (100 U/mL), and streptomycin (100 μg/mL) at 37 °C and 5% CO_2.

Plasmids for PPAR Transactivation Assay. The Gal4-fusion receptor plasmids pFA-CMV-PPARα-LBD, pFA-CMV-PPARδ-LBD, and pFA-CMV-PPARγ-LBD containing the hinge region and ligand binding domain (LBD) for each of the PPAR subtypes, respectively, were constructed by integrating cDNA fragments obtained from PCR amplification of human monocytes into the *Sma*I/*Xba*I cleavage site of the pFA-CMV vector (Stratagene, La Jolla, CA, USA) and have already been published.[46] The cDNA fragments consist of bps 499−1407 (NM_005 036), bps 412−1323 (NM_006 238) and bps 610−1518 (NM_015 869) for PPARα, PPARδ, and PPARγ, respectively. Frame and sequence of the fusion receptors were verified by sequencing. pFR-Luc (Stratagene) was used as reporter plasmid and pRL-SV40 (Promega) for normalization of transfection efficiency and cell growth.

PPAR Transactivation Assay. The day before transfection, COS-7 cells were seeded in 96-well plates with a density of 30000 cells per well. Transient transfection was carried out using Lipofectamine LTX reagent (Invitrogen, Carlsbad, CA, USA) according to the manufacturer's protocol with pFR-Luc (Stratagene), pRL-SV40 (Promega), and the Gal4-fusion receptor plasmids (pFA-CMV-hPPAR-LBD) of the respective PPAR subtype. Then 5 h after transfection, medium was changed to DMEM without phenol red and 10% FCS, supplemented with 1 mM SP, penicillin (100 U/mL), streptomycin (100 μg/mL), and 2 mM L-glutamate, now additionally containing 0.1% DMSO and the respective test compound or 0.1% DMSO alone as untreated control. Each concentration was tested in triplicate wells, and each experiment was repeated independently at least three times. Following overnight incubation with the test compounds, cells were assayed for luciferase activity using Dual-GloTM luciferase assay system (Promega) according to the manufacturer's protocol. Luminescence was measured with an Infinite M200 luminometer (Tecan Deutschland GmbH). Normalization of transfection efficacy and cell growth was done by division of firefly luciferase data by renilla luciferase data, resulting in relative light units (RLU). Fold activation was obtained by dividing the mean RLU of a test compound at a respective concentration by the mean RLU of untreated control. Relative activation was obtained by dividing the fold activation of a test compound at a respective concentration by the fold activation of PPARα full agonist GW 7647 at 1 μM, PPARδ full agonist L165,041 at 1 μM, or PPARγ full agonist pioglitazone at 1 μM, respectively. EC_{50} and standard error of the mean values were calculated with the mean relative activation values of at least three independent experiments by SigmaPlot 10.0 (Systat Software GmbH) using a four-parameter logistic regression.

TGR5 Assay. The activity of **51** on TGR5 was evaluated by measuring the level of cAMP using a HTR-FRET assay. In brief, NCI-H716 cells were cultured in DMEM supplemented with 10%FBS,

using 96-well plates coated with Matrigel (BD Biosciences). After 24 h, cells were stimulated with increasing concentrations of test compound **51** for 60 min at 37 °C in OptiMEM with 1 mM IBMX (Sigma). The level of intracellular cAMP was assessed using the Lance kit (PerkinElmer) according to the manufacturer's protocol.

Cytotoxicity Assays. *WST-1.* The WST-1 assay from Roche was performed according to manufacturer's protocol. In brief, HepG2 cells were seeded in DMEM supplemented with 1 mM SP, penicillin (100 U/mL), streptomycin (100 μg/mL), and 10% FCS in 96-well plates (3×10^4 cells/well). After 24 h, medium was changed to DMEM supplemented with penicillin (100 U/mL), streptomycin (100 μg/mL), and 1% FCS, and cells were incubated with compound **51** (final concentrations 1, 10, 30, and 100 μM), Revlotron (100 μM) as positive control, and Zileuton (100 μM) and DMEM/1% DMSO as negative controls. After 48 h, WST reagent (Roche) was added to each well according to manufacturer's instructions. After 45 min incubation, absorption (450 nm/reference: 620 nm) was determined with a TEACAN Infinite M200 luminometer. Each experiment was repeated three times in triplicates. Results (expressed as mean ± SEM; $n = 4$; untreated = 100%) **51**: 1 μM, 94 ± 2%; 10 μM, 76 ± 1%; 30 μM, 40 ± 1%; 100 μM, 0%.

LDH. LDH assay (Roche) was performed according to manufacturer's instructions. In brief, HepG2 cells were seeded in DMEM supplemented with 1 mM SP, penicillin (100 U/mL), streptomycin (100 μg/mL), and 10% FCS in 96-well plates (3×10^4 cells/well). After 24 h, medium was changed to DMEM supplemented with penicillin (100 U/mL), streptomycin (100 μg/mL), and 1% FCS, and cells were incubated with the respective compounds for 48 h. As positive control, TRITON X-100 (2%) was added 2 h before measurement. After incubation, supernatant of each well was transferred into a fresh plate and LDH substrate/reagent was added. After 20 min incubation, absorption at measurement (490 nM) and reference (690 nM) wavelength was determined with a TECAN infinite 200. All experiments were performed in triplicates and at least in three independent repeats. Results (expressed as mean ± SEM; $n = 4$; untreated = 0%, Triton X-100 (2%) = 100%) **51**: 1 μM, 0 ± 7%; 10 μM, 0 ± 7%; 30 μM, 63 ± 5%; 100 μM, 91 ± 6%.

Metabolism Assay. The solubilized test compounds (5 μL, final concentration 10 μM in DMSO) were preincubated at 37 °C in 432 μL of phosphate buffer (0.1 M, pH 7.4) together with a 50 μL of NADPH regenerating system (30 mM glucose-6-phosphate, 4 U/mL glucose-6-phosphate dehydrogenase, 10 mM NADP, 30 mM $MgCl_2$). After 5 min, the reaction was started by the addition of 13 μL of microsome mix from the liver of Sprague–Dawley rats (Invitrogen, Darmstadt, Germany; 20 mg protein/mL in 0.1 M phosphate buffer) in a shaking water bath at 37 °C. The reaction was stopped by addition of 250 μL of of ice-cold methanol at 0, 15, 30, and 60 min. The samples were diluted with 250 μL of DMSO and centrifuged at 10000*g* for 5 min at 4 °C. The supernatants were analyzed, and test compounds were quantified by HPLC: mobile phase, MeOH 83%/H_2O 17%/formic acid 0.1%; flow-rate, 1 mL/min; stationary phase, MultoHigh Phenyl phase, 5 μm, 250 × 4 precolumn, phenyl, 5 μm, 20 × 4; detection wavelength, 330 and 254 nm; injection volume, 50 μL. Control samples were performed to check the stability of the compounds in the reaction mixture: first control was without NADPH, which is needed for the enzymatic activity of the microsomes, second control was with inactivated microsomes (incubated for 20 min at 90 °C), third control was without test compounds (to determine the baseline). The amounts of the test compounds were quantified by an external calibration curve, where data are expressed as means ± SEM of single determinations obtained in three independent experiments. The metabolism experiments showed the following curves (expressed as mean ± SEM; $n = 4$) **51**: 0 min, 93.5 ± 2.4%; 15 min, 86.0 ± 1.8%; 30 min, 84.3 ± 1.4%; 60 min, 80.2 ± 0.2%.

■ ASSOCIATED CONTENT

Supporting Information

Preparation and analytical data of intermediate compounds. This material is available free of charge via the Internet at http://pubs.acs.org.

■ AUTHOR INFORMATION

Corresponding Author

*Phone: +49-69-798-29328. Fax: +49-69-798-29332. E-mail: merk@pharmchem.uni-frankfurt.de .

Notes

The authors declare no competing financial interest.

■ ACKNOWLEDGMENTS

We thank Prof. Dr. R. Pellicciari and Dr. D. Passeri for the generous in vitro characterization of compound **51** on TGR5. K.A. gratefully acknowledges financial support from Else Kröner-Fresenius-Stiftung (Dr. Hans Kröner-Graduiertenkolleg) and from CEF.

■ REFERENCES

(1) Fiorucci, S.; Mencarelli, A.; Distrutti, E.; Palladino, G.; Cipriani, S. Targeting farnesoid-X-receptor: from medicinal chemistry to disease treatment. *Curr. Med. Chem.* **2010**, *2*, 139–159.

(2) Fiorucci, S.; Mencarelli, A.; Distrutti, E.; Zampella, A. Farnesoid X receptor: from medicinal chemistry to clinical applications. *Future Med. Chem.* **2012**, *7*, 877–891.

(3) Düfer, M.; Horth, K.; Wagner, R.; Schittenhelm, B.; Prowald, S.; Wagner, T.; Oberwinkler, J.; Lukowski, R.; Gonzalez, F.; Krippeit-Drews, P.; Drews, G. Bile Acids Acutely Stimulate Insulin Secretion of Mouse-Cells via Farnesoid X Receptor Activation and KATP Channel Inhibition. *Diabetes* **2012**, *6*, 1479–1489.

(4) Düfer, M.; Hörth, K.; Krippeit-Drews, P.; Drews, G. The significance of the nuclear farnesoid X receptor (FXR) in β cell function. *Islets* **2012**, *5*, 333–338.

(5) Li, Y.; Jadhav, K.; Zhang, Y. Bile acid receptors in non-alcoholic fatty liver disease. *Biochem. Pharmacol.* **2013**, *11*, 1517–1524.

(6) Adorini, L.; Pruzanski, M.; Shapiro, D. Farnesoid X receptor targeting to treat nonalcoholic steatohepatitis. *Drug Discovery Today* **2012**, *17–18*, 988–997.

(7) Musso, G.; Gambino, R.; Cassader, M. Cholesterol metabolism and the pathogenesis of non-alcoholic steatohepatitis. *Prog. Lipid Res.* **2013**, *1*, 175–191.

(8) Renga, B.; Mencarelli, A.; Vavassori, P.; Brancaleone, V.; Fiorucci, S. The bile acid sensor FXR regulates insulin transcription and secretion. *Biochim. Biophys. Acta* **2010**, *3*, 363–372.

(9) Wang, X.; Fu, X.; van Ness, C.; Meng, Z.; Ma, X.; Huang, W. Bile Acid Receptors and Liver Cancer. *Curr. Pathobiol. Rep.* **2013**, *1*, 29–35.

(10) Nijmeijer, R. M.; Gadaleta, R. M.; van Mil, S. W. C.; van Bodegraven, A. A.; Crusius, J. B.; Dijkstra, G.; Hommes, D. W.; de Jong, D. J.; Stokkers, P. C.; Verspaget, H. W.; Weersma, R. K.; van der Woude, C. J.; Stapelbroek, J. M.; Schipper, M. E.; Wijmenga, C.; van Erpecum, K. J.; Oldenburg, B. Farnesoid X receptor (FXR) activation and FXR genetic variation in inflammatory bowel disease. *PLoS One* **2011**, *8*, e23745.

(11) Hollman, D. A. A.; Milona, A.; van Erpecum, K. J.; van Mil, S. W. C. Anti-inflammatory and metabolic actions of FXR: insights into molecular mechanisms. *Biochim. Biophys. Acta* **2012**, *11*, 1443–1452.

(12) Wildenberg, M. E.; van den Brink, G. R. FXR activation inhibits inflammation and preserves the intestinal barrier in IBD. *Gut* **2011**, *4*, 432–433.

(13) Hageman, J.; Herrema, H.; Groen, A. K.; Kuipers, F. A role of the bile salt receptor FXR in atherosclerosis. *Arterioscler. Thromb. Vasc. Biol.* **2010**, *8*, 1519–1528.

(14) Mencarelli, A.; Fiorucci, S. FXR an emerging therapeutic target for the treatment of atherosclerosis. *J. Cell. Mol. Med.* **2010**, *1*−*2*, 79−92.
(15) Fiorucci, S.; Cipriani, S.; Mencarelli, A.; Renga, B.; Distrutti, E.; Baldelli, F. Counter-regulatory role of bile acid activated receptors in immunity and inflammation. *Curr. Mol. Med.* **2010**, *6*, 579−595.
(16) Silveira, M. G.; Lindor, K. D. Obeticholic acid and budesonide for the treatment of primary biliary cirrhosis. *Expert Opin. Pharmacother.* **2014**, *3*, 365−372.
(17) Mudaliar, S.; Henry, R. R.; Sanyal, A. J.; Morrow, L.; Marschall, H. U.; Kipnes, M.; Adorini, L.; Sciacca, C. I.; Clopton, P.; Castelloe, E.; Dillon, P.; Pruzanski, M.; Shapiro, D. Efficacy and safety of the farnesoid X receptor agonist obeticholic acid in patients with type 2 diabetes and nonalcoholic fatty liver disease. *Gastroenterology* **2013**, *3*, 574−82.e1.
(18) Ryan, K. K.; Tremaroli, V.; Clemmensen, C.; Kovatcheva-Datchary, P.; Myronovych, A.; Karns, R.; Wilson-Pérez, H. E.; Sandoval, D. A.; Kohli, R.; Bäckhed, F.; Seeley, R. J. FXR is a molecular target for the effects of vertical sleeve gastrectomy. *Nature* **2014**, *509*, 183−188.
(19) Merk, D.; Steinhilber, D.; Schubert-Zsilavecz, M. Medicinal chemistry of farnesoid X receptor ligands: from agonists and antagonists to modulators. *Future Med. Chem.* **2012**, *8*, 1015−1036.
(20) Pellicciari, R.; Fiorucci, S.; Camaioni, E.; Clerici, C.; Costantino, G.; Maloney, P. R.; Morelli, A.; Parks, D. J.; Willson, T. M. 6alpha-Ethyl-chenodeoxycholic acid (6-ECDCA), a potent and selective FXR agonist endowed with anticholestatic activity. *J. Med. Chem.* **2002**, *17*, 3569−3572.
(21) Maloney, P. R.; Parks, D. J.; Haffner, C. D.; Fivush, A. M.; Chandra, G.; Plunket, K. D.; Creech, K. L.; Moore, L. B.; Wilson, J. G.; Lewis, M. C.; Jones, S. A.; Willson, T. M. Identification of a Chemical Tool for the Orphan Nuclear Receptor FXR. *J. Med. Chem.* **2000**, *16*, 2971−2974.
(22) Akwabi-Ameyaw, A.; Bass, J. Y.; Caldwell, R. D.; Caravella, J. A.; Chen, L.; Creech, K. L.; Deaton, D. N.; Jones, S. A.; Kaldor, I.; Liu, Y.; Madauss, K. P.; Marr, H. B.; McFadyen, R. B.; Miller, A. B.; Iii, F. N.; Parks, D. J.; Spearing, P. K.; Todd, D.; Williams, S. P.; Wisely, G. B. Conformationally constrained farnesoid X receptor (FXR) agonists: naphthoic acid-based analogs of GW 4064. *Bioorg. Med. Chem. Lett.* **2008**, *15*, 4339−4343.
(23) Chiang, P.; Thompson, D. C.; Ghosh, S.; Heitmeier, M. R. A formulation-enabled preclinical efficacy assessment of a farnesoid X receptor agonist, GW4064, in hamsters and cynomolgus monkeys. *J. Pharm. Sci.* **2011**, *11*, 4722−4733.
(24) Howarth, D. L.; Law, S. H. W.; Law, J. M.; Mondon, J. A.; Kullman, S. W.; Hinton, D. E. Exposure to the synthetic FXR agonist GW4064 causes alterations in gene expression and sublethal hepatotoxicity in eleutheroembryo medaka (*Oryzias latipes*). *Toxicol. Appl. Pharmacol.* **2010**, *1*, 111−121.
(25) Flatt, B.; Martin, R.; Wang, T. L.; Mahaney, P.; Murphy, B.; Gu, X. H.; Foster, P.; Li, J.; Pircher, P.; Petrowski, M.; Schulman, I.; Westin, S.; Wrobel, J.; Yan, G.; Bischoff, E.; Daige, C.; Mohan, R. Discovery of XL335 (WAY-362450), a highly potent, selective, and orally active agonist of the farnesoid X receptor (FXR). *J. Med. Chem.* **2009**, *4*, 904−907.
(26) Singh, N.; Yadav, M.; Singh, A. K.; Kumar, H.; Dwivedi, S. K.; Mishra, J. S.; Gurjar, A.; Manhas, A.; Chandra, S.; Yadav, P. N.; Jagavelu, K.; Siddiqi, M. I.; Trivedi, A. K.; Chattopadhyay, N.; Sanyal, S. Synthetic FXR Agonist GW4064 Is a Modulator of Multiple G Protein-Coupled Receptors. *Mol. Endocrinol.* **2014**, *5*, 659−673.
(27) Merk, D.; Steinhilber, D.; Schubert-Zsilavecz, M. Characterizing ligands for farnesoid X receptor—available in vitro test systems for farnesoid X receptor modulator development. *Expert Opin. Drug Discovery* **2014**, *1*, 27−37.
(28) Merk, D.; Gabler, M.; Gomez, R. C.; Flesch, D.; Hanke, T.; Kaiser, A.; Lamers, C.; Werz, O.; Schneider, G.; Schubert-Zsilavecz, M. Anthranilic acid derivatives as novel ligands for farnesoid X receptor (FXR). *Bioorg. Med. Chem.* **2014**, *8*, 2447−2460.
(29) Achenbach, J.; Gabler, M.; Steri, R.; Schubert-Zsilavecz, M.; Proschak, E. Identification of novel farnesoid X receptor modulators using a combined ligand- and structure-based virtual screening. *Med. Chem. Commun.* **2013**, *6*, 920−924.
(30) Jin, T.; Kitahara, F.; Kamijo, S.; Yamamoto, Y. Copper-catalyzed synthesis of 5-substituted 1*H*-tetrazoles via the [3 + 2] cycloaddition of nitriles and trimethylsilyl azide. *Tetrahedron Lett.* **2008**, *17*, 2824−2827.
(31) Khalafi-Nezhad, A.; Parhami, A.; Soltani Rad, M. N.; Zarea, A. Efficient method for the direct preparation of amides from carboxylic acids using tosyl chloride under solvent-free conditions. *Tetrahedron Lett.* **2005**, *40*, 6879−6882.
(32) Richter, H. G.; Benson, G. M.; Blum, D.; Chaput, E.; Feng, S.; Gardes, C.; Grether, U.; Hartman, P.; Kuhn, B.; Martin, R. E.; Plancher, J. M.; Rudolph, M. G.; Schuler, F.; Taylor, S.; Bleicher, K. H. Discovery of novel and orally active FXR agonists for the potential treatment of dyslipidemia and diabetes. *Bioorg. Med. Chem. Lett.* **2011**, *1*, 191−194.
(33) Akwabi-Ameyaw, A.; Caravella, J. A.; Chen, L.; Creech, K. L.; Deaton, D. N.; Madauss, K. P.; Marr, H. B.; Miller, A. B.; Navas, F., III; Parks, D. J.; Spearing, P. K.; Todd, D.; Williams, S. P.; Wisely, G. B. Conformationally constrained farnesoid X receptor (FXR) agonists: alternative replacements of the stilbene. *Bioorg. Med. Chem. Lett.* **2011**, *20*, 6154−6160.
(34) Di Leva, F. S.; Festa, C.; D'Amore, C.; De Marino, S.; Renga, B.; D'Auria, M. V.; Novellino, E.; Limongelli, V.; Zampella, A.; Fiorucci, S. Binding Mechanism of the Farnesoid X Receptor Marine Antagonist Suvanine Reveals a Strategy To Forestall Drug Modulation on Nuclear Receptors. Design, Synthesis, and Biological Evaluation of Novel Ligands. *J. Med. Chem.* **2013**, *11*, 4701−4717.
(35) De Gottardi, A.; Dumonceau, J. M.; Bruttin, F.; Vonlaufen, A.; Morard, I.; Spahr, L.; Rubbia-Brandt, L.; Frossard, J. L.; Dinjens, W. N.; Rabinovitch, P. S.; Hadengue, A. Expression of the bile acid receptor FXR in Barrett's esophagus and enhancement of apoptosis by guggulsterone in vitro. *Mol. Cancer* **2006**, *5*, 48.
(36) Capello, A.; Moons, L. M.; Van de Winkel, A.; Siersema, P. D.; van Dekken, H.; Kuipers, E. J.; Kusters, J. G. Bile Acid-Stimulated Expression of the Farnesoid X Receptor Enhances the Immune Response in Barrett Esophagus. *Am. J. Gastroenterol.* **2008**, *6*, 1510−1516.
(37) Lee, J. Y.; Lee, K. T.; Lee, J. K.; Lee, K. H.; Jang, K. T.; Heo, J. S.; Choi, S. H.; Kim, Y.; Rhee, J. C. Farnesoid X receptor, overexpressed in pancreatic cancer with lymph node metastasis promotes cell migration and invasion. *Br J. Cancer* **2011**, *6*, 1027−1037.
(38) De Gottardi, A.; Touri, F.; Maurer, C. A.; Perez, A.; Maurhofer, O.; Ventre, G.; Bentzen, C. L.; Niesor, E. J.; Dufour, J. F. The bile acid nuclear receptor FXR and the bile acid binding protein IBABP are differently expressed in colon cancer. *Dig. Dis. Sci.* **2004**, *6*, 982−989.
(39) Journe, F.; Durbecq, V.; Chaboteaux, C.; Rouas, G.; Laurent, G.; Nonclercq, D.; Sotiriou, C.; Body, J. J.; Larsimont, D. Association between farnesoid X receptor expression and cell proliferation in estrogen receptor-positive luminal-like breast cancer from postmenopausal patients. *Breast Cancer Res. Treat.* **2009**, *3*, 523−535.
(40) Silva, J.; Dasgupta, S.; Wang, G.; Krishnamurthy, K.; Ritter, E.; Bieberich, E. Lipids isolated from bone induce the migration of human breast cancer cells. *J. Lipid Res.* **2006**, *4*, 724−733.
(41) Qi, Y.; Jiang, C.; Cheng, J.; Krausz, K. W.; Li, T.; Ferrell, J. M.; Gonzalez, F. J.; Chiang, J. Y. Bile acid signaling in lipid metabolism: metabolomic and lipidomic analysis of lipid and bile acid markers linked to anti-obesity and anti-diabetes in mice. *Biochim. Biophys. Acta* **2014**, *14*, 1388−1981.
(42) Fiorucci, S.; Baldelli, F. Farnesoid X receptor agonists in biliary tract disease. *Curr. Opin. Gastroenterol.* **2009**, *3*, 252−259.
(43) Steri, R.; Achenbach, J.; Steinhilber, D.; Schubert-Zsilavecz, M.; Proschak, E. Investigation of imatinib and other approved drugs as starting points for antidiabetic drug discovery with FXR modulating activity. *Biochem. Pharmacol.* **2012**, *12*, 1674−1681.

(44) Ananthanarayanan, M. Human Bile Salt Export Pump Promoter Is Transactivated by the Farnesoid X Receptor/Bile Acid Receptor. *J. Biol. Chem.* **2001**, *31*, 28857−28865.
(45) Seuter, S.; Väisänen, S.; Rådmark, O.; Carlberg, C.; Steinhilber, D. Functional characterization of vitamin D responding regions in the human 5-lipoxygenase gene. *Biochim. Biophys. Acta* **2007**, *7*, 864−872.
(46) Rau, O.; Wurglics, M.; Paulke, A.; Zitzkowski, J.; Meindl, N.; Bock, A.; Dingermann, T.; Abdel-Tawab, M.; Schubert-Zsilavecz, M. Carnosic acid and carnosol, phenolic diterpene compounds of the labiate herbs rosemary and sage, are activators of the human peroxisome proliferator-activated receptor gamma. *Planta Med.* **2006**, *10*, 881−887.

Send Orders for Reprints to reprints@benthamscience.net

Medicinal Chemistry and Pharmacological Effects of Farnesoid X Receptor (FXR) Antagonists

Christina Lamers[1], Manfred Schubert-Zsilavecz[1] and Daniel Merk[1,*,#]

[1]*Institute of Pharmaceutical Chemistry, Goethe University Frankfurt, Max-von-Laue-Str. 9, 60438 Frankfurt (Main), Germany*

Abstract: The nuclear bile acid sensor farnesoid X receptor (FXR) constitutes a rising target for the treatment of a variety of diseases including metabolic disorders, inflammation and certain forms of cancer. While the research on FXR agonists has yielded many compounds and first clinical candidates, only few FXR antagonists have been discovered so far and the knowledge about their *in vivo* effects is quite narrow. We have evaluated available *in vitro* and *in vivo* studies with FXR antagonists as well as FXR knockout models to elucidate a potential pharmacological use of FXR antagonism. To date, the *in vitro* and *in vivo* data suggests that FXR inhibition by knockout or the use of antagonists causes beneficial effects on cholesterol metabolism, ameliorates liver toxicity in cholestasis and can reduce the proliferation and migration of some cancer cell lines. Unfortunately, also many disadvantageous effects are connected with FXR antagonists.

Keywords: Atherosclerosis, cancer, FXR antagonists, FXR knockout, glucose homeostasis, guggulsterone, lipid homeostasis, liver disorders, metabolic disorders, selective bile acid receptor modulators (SBARMs).

[#]**Author's Profile:** Daniel Merk is a pharmacist and currently works as a researcher at the Goethe University Frankfurt. His research interests focus on the physiologic and molecular function of nuclear receptors and the development of new small-molecule nuclear receptor ligands.

INTRODUCTION

Nuclear farnesoid X receptor (FXR) has gained intense research interest as potential pharmaceutical target soon after its identification as bile acid sensor in 1999 [1–4]. As a ligand activated transcription factor FXR is involved in many physiological processes. Activated by bile acids (BAs) as physiological ligands, FXR plays a role in metabolic pathways including bile acid, lipid and glucose homeostasis as well as in inflammation [5–10]. Additionally, FXR agonists are presently in clinical development for the treatment of the grave liver disorders primary billiary cirrhosis (PBC), non-alcoholic fatty liver disease (NAFLD) and non-alcoholic steatohepatitis (NASH) [11–13]. In recent years, also a potential role of the nuclear receptor in development and growth of certain tumors is discussed [14–18].

These various physiological functions make FXR a potentially valuable drug target and many synthetic ligands have been developed. Most synthetic FXR ligands are agonists however and most *in vitro* or *in vivo* studies concerning the nuclear receptor have been conducted with agonistic ligands [5, 19]. The development of FXR antagonists has long time been neglected but is coming into focus in recent years. This review shall give a brief overview over the known FXR antagonists described in the literature, gather available *in vitro* and *in vivo* data of FXR antagonists and FXR knockout models and finally evaluate the pharmacological potential of FXR antagonism.

MODULATION OF FXR WITH AGONISTS, ANTAGONISTS AND SELECTIVE MODULATORS

The ligand activated transcription factor FXR as heterodimer with RXR or as a monomer binds to its response elements (RE) on the DNA which are present in FXR controlled genes. In resting state, the FXR-RXR hetero-dimer is associated with co-repressors such as NCor. Upon agonist binding to the FXR ligand binding site which is flexible and able to accommodate many different ligands, the activation function 2 (AF-2) in helix 12 of the ligand binding domain is thought to close the ligand binding pocket. This in turn allows dissociation of co-repressors from FXR and binding of co-activators which makes transactivation of FXR target genes possible [1, 20, 21]. Activation of the receptor by an ***agonist*** hence causes transcription of target genes. The efficacy of this transcription initiation distinguishes ***full agonists*** such as GW4064 (**1**) which cause 100% transcription and ***partial agonists*** that only evoke a moderate amplitude of transcription [22].

An antagonist in contrast is thought to have a binding mode in which helix 12 cannot adopt a position that is suitable for co-activator binding. It has been suggested that antagonists merely interact with helix 7 than stabilize helix 12 thereby preventing co-activator binding. In addition, an antagonist might also stabilize the interaction of FXR with co-

*Address correspondence to this author at the Institute of Pharmaceutical Chemistry, Goethe University Frankfurt, Max-von-Laue-Str. 9, 60438 Frankfurt (Main), Germany; Tel: +49-69-79829806;
Fax: +49-69-79829332; E-mail: merk@pharmchem.uni-frankfurt.de

1873-5294/14 $58.00+.00

repressors such as NCoR [23, 24]. In contrast to agonists, an ***antagonist*** competitively inhibits the activation of FXR by e.g. the physiological agonist CDCA (**2a**). In absence of an agonist, an antagonist would produce no intrinsic effect, since without an agonist no activation of FXR takes place that could be inhibited by the antagonist [22].

The existence of different co-activator peptides forming different interactions with FXR also allows the existence of target gene selective FXR modulators, the so called ***selective bile acid receptor modulators (SBARMs)***. These modulators might partially stabilize helix 12 in a position between agonistic and antagonistic conformation in which one co-activator peptide can bind and another one fails to bind FXR. SBARMs such as guggulsterone (**3**) [25] reveal different activities on distinct target genes. They e.g. act agonistic on a subset of FXR target genes and antagonize the transcription of other target genes [22, 26].

Finally, an ***inverse agonist*** at FXR would stabilize the inactive state of FXR by increasing the receptor's interaction with co-repressors. It would therefore itself and even in absence of an agonist influence the expression profile of FXR target genes in the opposite direction of an agonist and lead to expression of FXR controlled genes below basal levels [22, 26].

Therapeutically, the concept of SBARMs might be most favorable since with a target gene selective FXR modulator only the desired effects on target genes that are beneficial for a certain condition could be induced while other genes that are associated with undesired effects would remain unaffected. If this concept can be realized it might have significant therapeutic relevance.

FXR Agonists, Antagonists and Modulators

Activation of FXR by an ***agonist*** causes transcription of target genes. Depending on the amplitude of transcription, there are ***full agonists*** and ***partial agonists***. FXR ***antagonists*** competitively inhibit the activation of the nuclear receptor by e.g. a physiological agonist. In absence of an agonist, an antagonist would produce no intrinsic effect. The so called ***selective bile acid receptor modulators (SBARMs)*** reveal different activities on distinct target genes by activating only a subset of target genes and antagonizing other target genes. Putative ***inverse agonists*** at FXR would themselves influence the expression profile of FXR target genes in the opposite direction of an agonist and therefore cause an effect even in absence of an agonist.

MEDICINAL CHEMISTRY OF FXR ANTAGONISTS

In contrast to a large and growing number of FXR agonists, only few FXR antagonists have been discovered so far. Comparable with agonistic FXR ligands there are steroidal and non-steroidal compounds with FXR antagonistic activity. FXR antagonists are usually characterized in typical FXR reporter gene assays or co-activator recruitment assays in competition with a known FXR ligand, mostly GW4064 (**1**) or CDCA (**2a**, Fig. **1**). Some development programs also use fluorescence based FXR binding assays but only for few putative FXR antagonists, data on their effect on FXR target genes is available.

Steroidal FXR Antagonists

The physiological ligands of FXR are bile acids and their metabolites. Amongst bile acids, chenodeoxycholic acid (CDCA, **2a**) is the most potent FXR agonist. While most bile acids and bile alcohols activate FXR there are antagonistic bile acid derivatives as well. Lithocholic acid (LCA, **4a**), a primary metabolite of CDCA (**2a**) is a potent FXR antagonist in reporter gene assays (IC_{50} = 1 μM) and on mRNA level. It inhibits FXR activation by CDCA (**2a**) or GW4064 (**1**) and diminishes expression of the FXR target gene BSEP in HepG2 cells [27]. Ursodeoxycholic acid (UDCA, **4b**) showed weak partial agonistic properties on FXR (EC_{50} > 50 μM, K_d = 38 μM) with an induction of the FXR target gene ileal bile acid binding protein (IBABP) of approximately 10% of CDCA (**2a**). In competition with **2a**, **4b** was however able to reduce the effects of CDCA (**2a**) to around 90% as well [28]. The predominantly murine bile acids α- and β-muricholic acid (MCA, **4c**, **4d**) and their tauro-conjugates are antagonistic on FXR [29, 30]. Bile alcohols bearing a hydroxyl group in α-orientation at carbon 5 of the steroid system such as 5α-cyprinol (**5**) or 5α-bufol (**6**) fail to activate FXR but also competitively antagonize FXR activation by CDCA (**2a**) or GW4064 (**1**) [31].

In addition to these human sterol metabolites a large number of natural and semi-synthetic sterols from other origins have been discovered as FXR antagonists. 4-methylene sterols such as swinhosterol B (**7a**) and theonellasterol (**7b**) [32–34], sulfated sterols such as **8** [35], scalarane sesterpenes such as **9** [36, 37], gorgosterol (**10**) [38] and sterol **11** [39] have recently been reported as steroids with marine origin and weak to moderate FXR antagonistic activity. In addition the soy derived phytosterol stigmasterol (**12**) [40] in competition with CDCA (**2a**) exhibited FXR antagonistic activity in a FXR reporter gene assay in HepG2 cells.

Guggulsterone (**3**) [41], another plant steroid was the first known FXR ligand with antagonistic properties. **3** originates from an extract of the gum resin of *Commiphora mukul* and exists in two isomers (*E* and *Z*) of which the Z-isomer has higher potency as FXR modulator [41–43]. Later experiments [25, 44] with guggulsterone (**3**) revealed, that the compound is actually a SBARM with agonistic and antagonistic activity on different FXR target genes. **3** acted as an antagonist in reporter gene assays and on most FXR target genes but induced the expression of BSEP which constitutes an FXR agonistic activity. Since BSEP transports bile acids out of hepatocytes and hence plays an important role in bile acid elimination, this effect is favorable when guggulsterone (**3**) is considered an anti-cholesterolemic agent. Virtual studies indicated that the modulatory activity of **3** might be due to allosteric binding [45].

Besides FXR, guggulsterone (**3**) modulates several other nuclear receptors such as the mineralocorticoid receptor, the glucocorticoid receptor, the androgen receptor, the estrogen receptor α and the pregnane X receptor [45–48]. Effects on metabolic and inflammatory genes that were observed for guggulsterone (**3**) therefore might be caused by its interaction with various ligand-activated transcription factors which makes their interpretation difficult. On the other hand, modulation of different nuclear receptors could also generate valu-

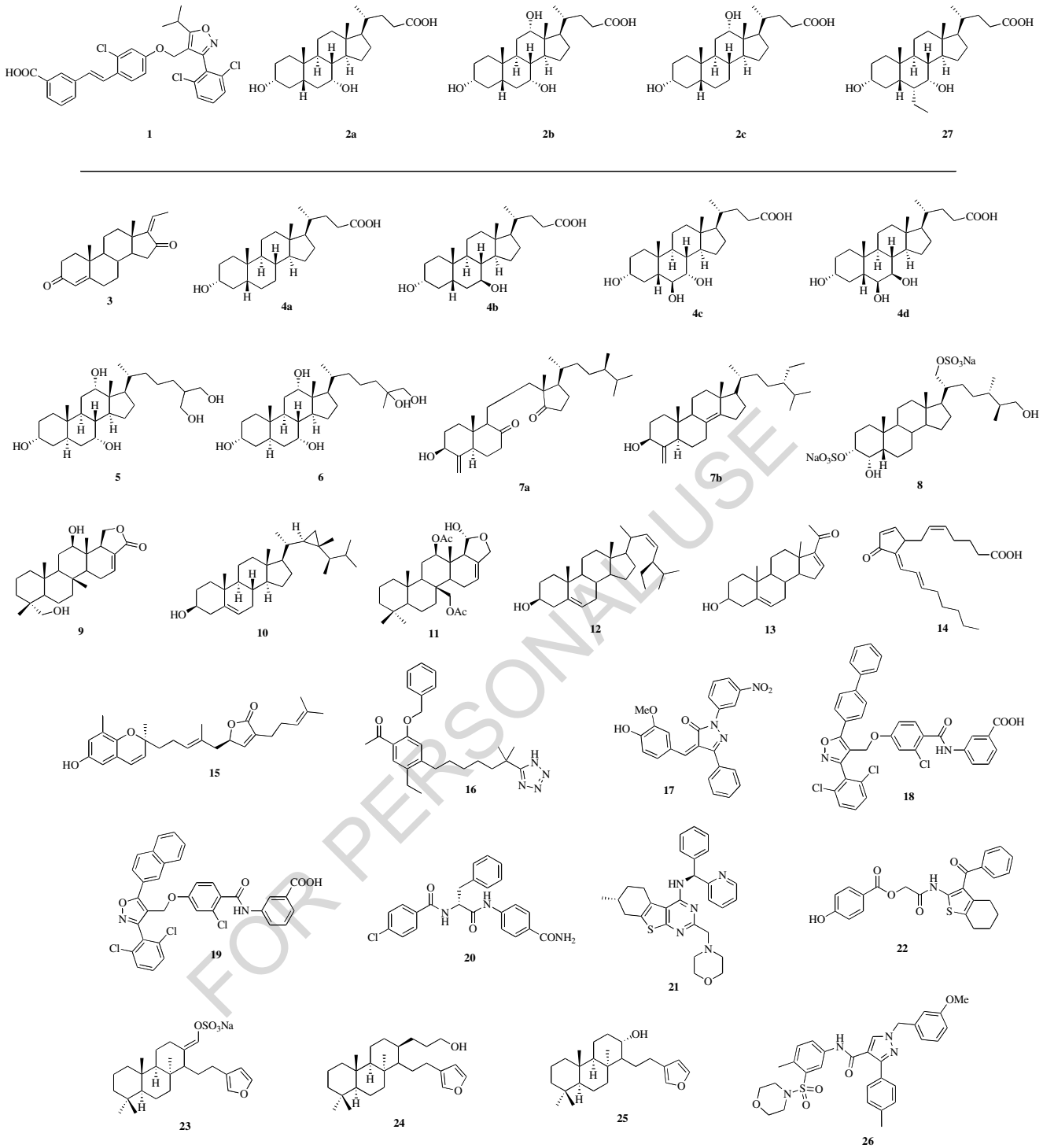

Fig. (1). FXR ligands: synthetic FXR agonists GW4064 (**1**) and 6-ECDCA (**27**), agonistic bile acids (**2a**-**c**), antagonistic bile acids (**4a-d**) and metabolites (**5**, **6**), steroidal (**7**-**13**) and non-steroidal FXR antagonists (**14**-**26**).

able synergistic effects [44]. In addition to its hypolipidemic effects, guggulsterone (**3**) is also coming into focus as an experimental anti-cancer agent [49–51].

The steroidal FXR antagonist 16-dehydropregnanolone (DHP, CDRI80/574, **13**) is structurally related to guggulsterone (**3**) and reported to have shown lipid-lowering effects in clinical trials in India. However, no detailed clinical data has been published yet [52].

Non-Steroidal FXR Antagonists

Besides the natural sterols that were discovered as FXR antagonists also some non-steroidal natural products exhibit FXR antagonistic activity. Especially the antagonistic activity of the arachidonic acid metabolite 15d-PGJ_2 (**14**) might be of interest since it occurs as major metabolite from PGD_2 in human and was also discovered as PPARγ ligand. 15d-PGJ_2 showed a K_d value for FXR binding of 3.47 μM and

antagonized FXR activation by CDCA in various assays with an IC_{50} value of 7.25 μM in a co-activator recruitment assay. On mRNA level, 15d-PGJ_2 did not act as a classical antagonist on FXR since it induced the expression of FXR target gene BSEP and repressed CYP7A1 expression [53]. Tuberatolides such as **15** from marine organisms share some structural similarity with PGJ_2 and also acted as moderately potent FXR antagonists in a FXR reporter gene assay [54]. Their effects on FXR target genes are not reported, however.

Several synthetic non-steroidal FXR antagonists have been discovered as well along with their SAR and *in vitro* properties. Their potency in reporter gene assays is varying with IC_{50} values between 0.47 μM and low micromolar values.

A hydroxyacetophenone scaffold has been optimized to compound **16** which is a FXR antagonist with an IC_{50} value of 1.1 μM in a homogenous time-resolved fluorescence (HTRF) based FXR co-activator recruitment assay with CDCA (**2a**) as reference agonist. The effect of **16** on FXR target genes is not described [55]. Another SAR study investigated the FXR antagonistic activity of trisubstituted pyrazolone derivatives [56] and discovered compound **17** as FXR antagonist in a HTRF assay with an IC_{50} value of 9 μM. *In vitro*, **17** increased the mRNA expression of CYP7A1 and decreased expression of SHP and SREBP-1c. Two FXR antagonists (**18** and **19**) [24] based on the isoxazole moiety of GW4064 (**1**) exhibit FXR antagonism in competition with CDCA (**2a**) with comparable IC_{50} values of around 4 μM but interestingly by two different mechanisms, either by stabilizing of the FXR-NCoR complex or by inhibiting co-activator recruitment. How the compounds affect mRNA expression of FXR target genes is not described however. Li *et al.* [57] have discovered **20**, **21**, and **22** as moderately potent FXR antagonists by a virtual screening. The structurally variable compounds were characterized in a FXR reporter gene assay in competition with CDCA and showed IC_{50} values of 13 μM (**20**), 8 μM (**21**) and 4 μM (**22**).

Di Leva *et al.* discovered the sesterpene suvanine (**23**) from a marine sponge as FXR antagonist and developed a series of suvanine derivatives with interesting properties on the nuclear receptor. Suvanine (**23**) is a FXR antagonist with an IC_{50} of 24 μM in a reporter gene assay in competition with CDCA (**2a**). **23** showed no intrinsic agonistic activity and did not affect the expression of FXR target genes OSTα, SHP or CYP7A1 alone but significantly antagonized the effect of CDCA on these genes. In contrast to suvanine, two semi-synthetic derivatives (**24** and **25**) of the natural product with varied side chain showed slight agonistic to no effects on FXR target genes but antagonized or enhanced the effect of CDCA (**2a**) depending on the gene with comparable half-maximal concentrations around 25 μM [23].

So far, the most potent FXR antagonist is a trisubstituted pyrazol derivative (**26**) [58]. It was optimized from a hit in a small screening program with a focused library of pyrazol derivatives inspired by **17**. After SAR studies and structural optimization, **26** was discovered as higly potent FXR antagonist *in vitro* with IC_{50} values of 7.5 nM in a competitive binding assay and 0.47 μM in a reporter gene assay in competition with GW4064 (**1**). It remains however unknown how **26** or any other antagonist of this scaffold influences FXR target gene expression *in vitro* and *in vivo*.

Antagonists and modulators of other nuclear receptors, especially the estrogen receptors (ER) [59] have gained clinical relevance yet. ER targeting drugs however predominantly constitute selective estrogen receptor modulators (SERMs) that exhibit (tissue) selective agonism and antagonism thereby avoiding side effects [22, 26]. A comparable concept of selective bile acid receptor modulators (SBARMs) [8, 60] has been discussed but so far (apart from guggulsterone (**3**)) no FXR ligand that shows these characteristics has successfully been developed.

PHARMACOLOGICAL POTENTIAL OF FXR ANTAGONISTS

To date, not many studies have been conducted with FXR antagonists. Besides their activity in *in vitro* assays and their influence on FXR target genes *in vitro*, little is known about the pharmacological effects of FXR antagonists and so far only few *in vivo* experiments are described. Furthermore, *in vivo* studies of FXR antagonists predominantly use guggulsterone (**3**) which was found to be a merely SBARM than a pure antagonist. For an evaluation of the pharmacological *in vivo* effects and a potential therapeutic benefit of FXR antagonists, mostly *in vitro* data and results from FXR knockout models have to be consulted.

In vivo Activity of FXR Antagonists

The first *in vivo* data on FXR antagonists were reported together with the discovery of guggulsterone (**3**) as FXR ligand with antagonistic properties. Guggulsterone (**3**) antagonizes the FXR activating effect of CDCA (**2a**) in reporter gene assays and in the transactivation of SHP expression. When guggulsterone (**3**) was fed to wild-type mice on high-cholesterol diet it reduced the intrahepatic cholesterol levels. In FXR knockout mice on high-chloesterol diet guggelsterone (**3**) had no effects however. The guggulsterone containing extract of guggul tree (*Commiphora mukul*) is known and used as LDL-cholesterol lowering agent in Ayurvedic medicine. A potential lipid lowering effect of FXR antagonists is however not yet fully investigated [41].

FXR is known to be the key regulator of genes involved in bile acid homeostasis and FXR activation leads to an increased expression of bile acid transporters (e.g. BSEP) and binding proteins (e.g. IBABP) as well as a diminished expression of enzymes involved in bile acid synthesis (CYP7A1). FXR antagonists – at least *in vitro* – affect these FXR target genes in the opposite way by reducing the expression of bile acid transport proteins and increasing the expression of bile acid forming enzymes. On one hand bile acids are important intestinal detergents helping digest and absorb molecules in the gastro-intestinal tract. In addition they act as signaling molecules with FXR and the membrane bile acid receptor TGR5 as targets. On the other hand bile acids are also the final product of cholesterol metabolism.

A potential antagonistic modulation of FXR target genes *in vivo* would cause an up-regulation of CYP7A1, the rate-limiting enzyme of bile acid synthesis from cholesterol which in turn would lead to a reduction in cholesterol levels

and increased levels of bile acids. In addition FXR antagonism would down-regulate the expression of BSEP and IBABP and thereby reduce the reuptake of bile acids from the gastro-intestinal tract in favor of increased bile acid elimination. The combination of increased bile acid synthesis from cholesterol and increased bile acid excretion could be beneficial in the treatment of hypercholesterolemia.

Table 1. Important genomic effects of FXR activation related to BA homeostasis. BA: bile acid; direct target genes in bold letters. According to [5].

BA synthesis		**FGF19 (human)↑ FGF15 (mouse)↑ and SHP↑ → CYP7A1↓**
BA transport	hepatic BA uptake	NTCP↓ OATP↓ (basolateral)
	hepatic BA efflux	**MRP-2↑ BSEP↑** (canalicular) MDR-3↑ MRP-3↑ **OSTA/β↑** (basolateral)
	intestinal BA efflux	**MRP-2↑** MRP-3↑
	renal BA efflux	**MRP-2↑ OSTA/β↑** (basolateral)
	(intestinal) BA binding	**IBABP↑**
BA detoxification		CYP3A4↑

Animal models suggest that FXR antagonism in fact leads to an increased bile acid pool by sort of a positive feedback mechanism. In CYP8B1 deficient mice which are not able to form cholic acid (CA, **2b**) the antagonistic bile acids UDCA (**4b**) and MCAs (**4c**, **4d**) accumulated and accounted for a positive feedback via inhibition of the downregulation of CYP7A1 and via downregulation of fibroblast growth factor 15 (FGF15). This increased the overall bile acid pool and decreased cholesterol levels. Since MCAs are not formed in humans it has to be investigated whether this positive feedback mechanism is also present in humans and which metabolites account for it [29]. Interestingly, MCAs have been found to be formed by gut microbiota which indicates that microbiota not only are involved in secondary bile acid metabolism but also affect bile acid synthesis in the liver. In germ free raised mice higher levels of T-β-MCA were observed along with increased total bile acid pool sizes [61]. Comparable effects were observed in CYP7A1 overexpressing mice on a high-fat diet that also accumulated T-β-MCA. Bile acid pool size was strongly increased and lipid homeostasis, insulin resistance as well as obesity were significantly improved [62]. With the fact that in obesity and many liver diseases the gut microbiota [63] (and eventually the bile acid pool size and composition) are altered, the link to humans and possible therapies is made. These experiments have shown the possibility to increase the bile acid pool and improve metabolic homeostasis by FXR antagonism *in vivo*. The underlying mechanisms and pathways have to be further elucidated, however.

Stedman *et al.* have investigated the changes in bile acid metabolism and transport after bile duct ligation which leads to obstructive cholestasis in mice. This hepatic disorder appears in the context of primary biliary cirrhosis and sclerosing cholangitis as well as with biliary stones or tumors and leads to serious liver injury. In cholestasis bile acid secretion is disturbed and a theoretical treatment is to enhance bile acid secretion from the basolateral membrane of hepatocytes. In the study, an increase of basolateral MRP-4 in hepatocytes of FXR knockout mice which transports bile acids (but not UCDA (**4b**)) to the blood was observed. The authors suggest that UDCA (**4b**), the only available agent to treat cholestasis might accumulate in liver cells and exhibit antagonistic effects on FXR also leading to enhanced expression of MRP4 [64].

The marine sponge sterol theonellasterol (**7b**) has also been investigated in an *in vivo* study for the treatment of obstructive cholestasis. When theonellasterol (**7b**) was administered to mice whose bile duct had been surgically ligated, the FXR antagonist protected the mice from liver injury. In contrast, administration of an FXR agonist in the same setting had no beneficial effects. Administration of **7b** after bile duct ligation reduced total bile acid amount and diminished liver necrosis determined by histological analysis and assessment of ALT/AST. Expression of FXR target genes in the livers of theonellesterol (**7b**) treated mice was significantly altered. Expression of OSTα, BSEP and SHP was reduced while MRP-4 was upregulated. Theonellasterol (**7b**) was intensively investigated *in vitro* previously and proven to be selective over other human nuclear receptors. **7b** showed no agonistic effect on FXR but antagonized the effect of CDCA (**2a**) on several FXR target genes *in vitro* [33].

Besides cholestasis, FXR also has a role in the response of hepatocytes on oxidative stress. In an animal model of oxidative liver damage (induced by H_2O_2 or CCl_4) poly(ADP-ribose) polymerase 1 (PARP1) exhibited inhibitory effects on FXR by poly(ADP-ribosyl)ation leading to dissociation from the FXR response elements on DNA. This in turn led to reduced transcription of FXR target genes and increased cell death of HepG2 cells and mouse hepatocytes from oxidative damage. Silencing of PARP1 in HepG2 cells by siRNA as well as the use of the FXR agonist GW4064 (**1**) protected liver cells from cell death. FXR antagonism therefore seems to have no liver protecting effect in oxidative stress [65].

Dai *et al.* investigated the impact of bile acids on the growth and viability of cholangiocarcinoma *in vitro* and *in vivo* [66, 67]. They observed that treatment of mice carrying xenograft tumors of the human cholangiocarcinoma cell line QBC939 with bile acids increased the expression of FXR in the tumor cells while conjugated bile acids had the inverse effect. Additionally, the cell growth was inversely proportional with FXR expression levels. The cell viability of tumor cells was strongly reduced when mice were treated with bile acids and this effect could be enhanced when GW4064 (**1**) was added to the bile acid treatment. When the FXR antagonist/modulator guggulsterone (**3**) was added to the bile acid treatment in contrast, the beneficial effect on the viability of tumor cells was lost. Overall the study showed a strong inhibitory effect of FXR agonists on the growth of xenograft cholangiocarcinoma in mice while guggulsterone (**3**) disrupted this beneficial effect. The strongest effect was achieved when mice with xenograft tumors were treated with a combination of CDCA (**2a**) and GW4064 (**1**). To translate

the results into human patients, the tumor tissue of 26 cholangiocarcinoma patients was investigated *ex vivo* and showed a pronounced downregulation of FXR in the tissue samples. This indicates that FXR antagonists are not a promising therapeutic strategy for cholangiocarcinoma. It is however difficult to translate these finding to other neoplastic diseases of FXR expressing tissues because of the highly complex biology of tumors [66, 67].

FXR seems to play a crucial role also in Barrett´s Esophagus, a premalignant disease of the esophagus in which the normal epithelium of the esophagus is replaced by intestinal epithelial cells to form a cylindrical Barrett's epithelium. An important factor for the development of Barrett's Esophagus is chronic reflux of intestinal fluids to the esophagus. While normal healthy esophagus epithelium is not expressing FXR, the nuclear receptor was recently found to be present in Barrett's epithelium and adenocarcinoma [68] and to play an important role in apoptosis [68] and inflammation associated with Barrett's Esophagus [69]. In esophagus epithelia (normal squamous epithelium and cylindrical Barrett's epithelium) of patients with Barrett's Esophagus the expression of FXR and of FXR target genes SHP and I-BABP was significantly increased. Additionally, high levels of the inflammatory cytokines MIP3α and IL-8 were detected in Barrett's esophagus but not in healthy subjects. When the esophageal cell line TE7 was incubated with the bile acid deoxycholic acid (DCA, **2c**) the mRNA levels of FXR, FXR target gene IBABP and the inflammatory cytokines MIP3α and IL-8 were significantly induced compared to untreated cells and interestingly this effect was efficiently antagonized when cells were additionally treated with guggulsterone (**3**). *In vitro* treatment of cells derived from Barrett's Esophagus epithelia with guggulsterone (**3**) alone increased caspase-3 activity and the number of apoptotic cells. FXR was furthermore found to be overexpressed in many human adenocarcinoma and this overexpression was associated with higher tumor size and grade and with lymph node metastasis [70]. FXR antagonist guggulsterone (**3**) reduced the growth and viability of adenoma cells and induced apoptosis *in vitro* and FXR knockout suppressed growth of xenograft adenoma [70]. In conclusion it seems that when esophageal epithelia are exposed to bile acids in refluxing intestinal fluids the bile acids activate FXR in epithelial cells and induce the transcription of inflammatory genes such as MIP3α and IL-8 which in turn leads to death of epithelial cells and inflammation. *In vitro* guggulsterone (**3**) was able to antagonize this proinflammatory response to bile acids indicating that FXR antagonists might have valuable therapeutic effects in the prevention and treatment of Barrett's Esophagus and resulting carcinoma.

In Vitro Activity of FXR Antagonists

Düfer *et al.* [71] have shown that glucose dependent insulin secretion from β-cells is FXR dependent *in vitro*. FXR agonists (taurodeoxycholic acid and GW4064 (**1**)) caused an increased insulin secretion which was antagonized by guggulsterone (**3**). When β-cells from FXR knockout mice were used, FXR agonists had no effect as well. Interestingly the observed effects occurred very fast after stimulation indicating that non-genomic mechanisms are involved, at least partially. The results suggest a potential therapeutic role of FXR agonists in diabetes and no desirable effects of FXR antagonism on insulin secretion from β-cells. Insulin secretion is however only one aspect of diseases linked to metabolic imbalance.

FXR also has a key role in the differentiation of preadipocytes to mature adipocytes. When the preadipocyte cell line 3T3-L1 is treated with the FXR agonist INT-747 (6-ECDCA, **27**) differentiation is strongly enhanced. This effect is however antagonized by guggulsterone (**3**) *in vitro* suggesting that FXR activity is required for adipocyte differentiation and energy storage. Since adipose tissue is crucial for the regulation of energy balance, FXR antagonism might disturb energy homeostasis and negatively affect the lipid-lowering *in vitro* effects of **3** *in vivo* [72]. The inhibition of adipogenesis caused by FXR antagonism might limit the hypothetic use of FXR antagonists for the treatment of metabolic disorders.

FXR is furthermore important for the differentiation of osteblastic cell lines BMSC and SaOS2 *in vitro*. CDCA (**2a**) accelerated the differentiation of these cell lines, calcium deposition and the expression of osteoblast marker genes such as alkaline phosphatase (ALP). Silencing of FXR quenched the effects of CDCA (**2a**). In addition, the association of RUNX2 to its DNA response element (OSE2) was improved by CDCA (**2a**) and decreased by guggulsterone (**3**). In presence of the FXR antagonist guggulsterone (**3**), the cells acquired a more adipocyte phenotype and accumulated lipids [73].

FXR seems therefore to be involved in a complex network with PPARγ and RUNX2 that controls osteoblast and adipocyte differentiation. FXR antagonism in osteoblasts caused an adipocyte phenotype which contradicts the results observed in adipocyte differentiation where FXR activity was required for adipogenesis. So far, FXR antagonism seems to delay bone formation [73].

Scholtes *et al.* observed a role of FXR in the replication of hepatitis C virus (HCV) in a HCV replication model in Huh7 cells and showed that bile acids promote virus replication while guggulsterone (**3**) antagonized this effect. Furthermore, **3** reduced the basal virus replication without stimulus by bile acids [74]. The underlying mechanisms of these observations are uncertain but the effects are in congruence with the fact that HCV patients with high bile acid levels often poorly respond to anti-viral therapy [75] and comparable data is described *in vivo* in an FXR knockout model [76]. The results indicate a possible use of FXR antagonists as co-medication for HCV patients who disply no satisfactory response to anti-viral therapy and have high bile acid levels.

Furthermore, FXR was found to be expressed in pancreatic cancer cells and to be linked to metastasis, cell migration and invasion [77]. *Ex vivo* samples of pancreatic cancer patients were investigated for their FXR expression level and in patients with lymph node metastasis, FXR was overexpressed and associated with poor prognosis. Furthermore, when FXR was silenced in a number of pancreatic cancer cell lines (MIA-PaCa2, PANC-1), cell proliferation, migration and invasion were decreased *in vitro*. A comparable effect was observed when pancreatic cancer cell lines were

treated with the FXR antagonist guggulsterone (**3**) while FXR agonist GW4064 (**1**) increased cell migration and invasion. The authors suggest that a decreased FXR activity reduces NF-κB-DNA binding and VEGF activity causing reduced proliferation and migration [77]. Similar data is described for colon cancer cells as well [78]. FXR is furthermore present in some breast cancer cell lines [79–81] and guggulsterone (**3**) caused reduced cell migration and enhanced apoptosis in the metastatic breast cancer cell line MDA-MB-231 *in vitro* [81]. In contrast to several other studies investigating the role of FXR on tumor proliferation and metastasis [82–84], FXR antagonism might therefore hold therapeutic potential in the treatment of pancreatic, breast and colon cancer as well as for Barrett's Esophagus and related adenocarcinoma.

Effects of FXR Knockout

To elucidate the impact of FXR antagonistic activity on physiological processes, also FXR deficient mice can be used. So far, only three different FXR deficient mouse models have been described (Table **2**). They differ not only in deletion technique but also in position and size of the deleted section on the allele. Gonzales *et al.* performed a targeted deletion which resulted in a truncated protein with still existing DNA-binding domain (DBD). On the other hand Deltagen Inc. deleted exon 2, which contains the DBD, but their allele still contains the ligand-binding domain (LBD), so binding of endogenous ligands, such as bile acids would still be possible. These variations may explain discrepancies in the outcome of FXR knockout studies.

Table 2. Available FXR knockout mouse models.

Developer		Reference
Deltagen Inc	A 292 bp long fragment corresponding to a segment of exon 2 was replaced with a phosphoglycerate kinase promoter-driven neomycin resistance cassette. The loss of 96 amino acids was anticipated to remove a part of the DNA-binding domain. No transcript detected	[85, 86]
F. Gonzalez	Targeted deletion of LBD and dimerization site (amino acids 406-484). But after deletion stable transcript containing intron sequences, 1663 bp long, resulting in a protein of 376 amino acids (451 in WT) resulted.	[14, 67, 71, 72, 83, 84, 87–110]
AstraZeneca	Lox-P site was inserted in intron 9 for targeted deletion of a 3326bp DNA segment of exon 9	[111]

Generally, $FXR^{-/-}$ mice were of normal phenotype and externally indistinguishable from their wildtype (WT) littermates. They showed normal development and weight gain and were fertile. No prenatal lethality was observed [89]. The mice showed normal cognitive function, normal behaviour and locomotor and had a normal core body temperature [111]. This inconspicuous phenotype dramatically changed when FXR deficient mice were fed a diet containing 1% cholic acid (CA). Then they showed severe wasting, hypothermia and absence of adipose tissue which was also recognized by progressive decrease in body weight. By day 7, 30% of the FXR deficient mice were dead since the CA diet resulted in hepatotoxity [89].

FXR Knockout and Lipid Homeostasis

FXR deficient mice showed higher levels of triglycerides (TG), phospholipids and cholesterolesters in plasma and liver [87, 89, 110]. Regarding the cholesterol profile, mice had higher HDL, LDL and VLDL levels [87, 89, 92, 103]. At an age of 21 weeks FXR deficient mice developed a statistically lower body weight and reduced FFA-levels compared to their WT littermates [111]. In accordance to that, body fat mass was reduced. Liver weight was however increased by 40% with indication of jaundice and serum levels of bilirubin and ALT were elevated [111]. These findings are in conflict to the study of Kok *et al.* who reported that their $FXR^{-/-}$ mice (3 month of age) had slightly higher body and liver weight without any changes of ALT, AST or bilirubin concentration compared to WT [86]. In addition Kok *et al.* found no significantly altered expression of SHP, CYP27, CYP8B1, MDR2, ABCG5, ABCG8, NTCP, OATP1, MRP-2, MRP-3 [86] which also contradicts other FXR knockout studies (Table **4**) [89, 111, 112].

Table 3. Role of FXR in tumorgenesis.

Cancer	FXR Normally Expressed	FXR in Tumorgenesis
Hepatocellular carcinoma	+	downregulated
Intestinal	+	downregulated
Gastric	+	downregulated
Esophageal	-	overexpressed
Pancreatic	-	overexpressed
Breast	+	overexpressed in some cell lines

The effect of FXR knockout on BA homeostasis is discussed controversially regarding levels of BA in plasma and liver. Most studies reported elevated plasma as well as hepatic levels [87, 89, 96, 110, 113] while Kok *et al.* discovered no altered plasma bile acid levels [86]. FXR deficient mice showed significantly increased hepatic CYP7A1 levels indicating a defective feedback inhibition of hepatic bile acid synthesis. This resulted in an elevated cholic acid (CA) pool, mostly conjugated to taurin. Coincidently, levels of α-muricholic acid (**4c**) and CDCA (**2a**) were decreased. Interestingly, though no IBABP was expressed in terminal ilea of $FXR^{-/-}$ mice, the absolute amount of bile salts reabsorbed from the intestine was not reduced. Taken together FXR de-

Table 4. Influence of FXR deletion on gene expression.

			Gene Expression	References
BA Homeostasis				
BA synthesis			CYP7A1↑, CYP8B1↑, CYP3A11↑, CYP2B10↑ CYP27↓, SHP↓	[86, 89, 111, 112]
BA transport			BSEP↓, I-BABP↓	[86, 89]
			NTCP↑, MDR2↑, MRP3↑, MRP4↑	[97, 112]
Cholesterol Homeostasis				
HDL uptake			SR-B1↓, LCAT↓, HL↓, CEH↓, SCP↓, LCAT↓, PLTP↓	[87, 92]
HDL building			ApoAI↓ ApoAIV↑	[87]
Cholesterol transport			ABCG5↓, ABCG8↓, ABCB11↓, ABCA1↑	[87, 89, 111]
Cholesterol synthesis			HMGCoA reductase↓, MTP↓	[87]
Glucose Homeostasis				
Glucose utilization			HK1↑, HK2↑, PDK4↑, LPK↑, PYK↑, GK↑	[85, 88, 95, 100, 102]
Glucose transport			GLUT1	[95]
Gluconeogenic			PEPCK↓, PGC-1↓, G6Pase↓	[88, 94, 102]
			FOXO1↓	[88]
Lipid Homeostasis				
Fatty acid metabolism			ACO↑, LCAD↑, CD36↑, L-FABP↑	[88]
Fatty acid synthesis	hepatic		FAS↑, ACC-1↑, SREBP-1c↑ PPARα↓	[100, 102, 104, 111]
	In muscle		PPARα↑, PPARδ↑, SREBP-1C↑	[95]
	Wat		HSL↓	[95]
Fatty acid uptake			FATP1↑,	[95]
Fatty acid oxidation	Hepatic		CPT1b↑, UCP-2↑, UCP3↑, LPL↑,	[95]
	In LDL$^{-/-}$/ FXR$^{-/-}$ mice	bepatic	PGC-1α↓, Cpt1a↓, Cpt2↓, Acox1↓, Acox2↓, Acox3↓, Mcad↓, Vlcad↓	[90]
		In muscle	PGC-1α↑, PGC-1β↑, Ucp3↑, Vlcad↑, Sirt1↑	
Adipogenesis				
Adipocyte differen-tiation			Perilipin↓, ADRP↓, Fsp27↓, sFRP5↓, sFRP1↓, β-Catenin↑	[107]
	WAT		c-EBPβ↑	[95]
Thermogenesis				
	In male mice		DIO2↑, UCP1↑	[93]
	BAT		PGC-1α↑	[93]
Atherosclerosis				
Macrophages			CD36↓, ADRP↓	[92, 104]
Atherosclerotic			ICAM-1↑, P-selectin↑, VCAM-1↑, TNFα↑, tPA↑	[92, 101]
Tumorgenesis				
Liver	Cell cycle		PCNA↓, c-myc↑, β-Catenin↑, Cyclin D1↑, Cylcin E1↑, Wnt4↑, Fzl1↑, Fzl4↑, Fzl7↑, Fzl8↑	[14, 96, 97, 108]

(Table 4) contd….

		Gene Expression	References
	proinflammatory	TNFα↑, INF ɣ ↑, IL-6↑, OPN↑	[76, 97]
Intestinal	proinflammatory	TNFα↑, INF ɣ ↑, IL-6↑	[84, 122]
	2 month	k-ras↑, p-53↑, ICAM↑, IL-6↑, Cyclin D1↑	[122]
	12 month	Pten↓, GADD45a↓, APC↓	[122]
Oxidative stress		Gsta2↑, Gstm3↑ Hmox1↑, Nqo1↑, Mt1↑	[106]
Fibronetic genes		SMA↑, TIMP-1↑, α1(I) collagen↑	[101, 109]
NASH		HO-1↑, Ccl5↑, Cd11c↑, Tlr4↑	[111]
Diabetic nephropathy		FAS↑, ACC↑, SCD-1↑, SREBP-1c↑, TGF-β↑	[100]

Table 5. Effects of FXR inhibition by antagonists, silencing or knockout.

	Lipid Metabolism	Glucose Metabolism	Cancer	Liver Protection	Cell Differentiation	Other
in vitro		- disruption of insulinotropic effects of FXR agonists on β-cells	+ decreased proliferation, migration and invasion of pancreatic and colon cancer cells + reduced migration and enhanced apoptosis of metastatic breast cancer cells		+/- reduction of adipocyte differentiation - reduction of osteoblast differentiation (shift to adipocyte phenotype)	+ reduced replication of HCV in Huh7 cells
in vivo	+ increased bile acid pool size and decreased cholesterol levels + improved lipid homeostasis + reduced obesity + reduction of intrahepatic cholesterol levels		+ induction of apoptosis (caspase-3 activity↑) and reduced inflammation in Barrett's Esophagus - disruption of antiproliferative effects of FXR agonists on cholangiocarcinoma	+ reduced liver injury in cholestasis (necrosis↓, ALT/AST↓) + reduced bile acid content in liver in chloestasis		
KO	- proatherogenic lipid profile (VLDL↑, LDL↑, HDL↑, FFA↑) Accumulation of TG and cholesterol + reduced atherogenic lesions + reduced adipocyte number and size	- impaired insulin signaling in muscle (and liver) + improved insulin sensitivity and glucose leels in obese mice	- increased tumor progression in intestinal and liver tumor + pancreatic and esophagal	- high BA levels toxic (focal necrosis, AST↑) - defective liver regeneration	+ reduction of adipocyte differentiation and lipid accumulation	- disruption of adaptive thermogenesis - defective intestinal barrier and bacterial translocation

ficiency was associated with an increased bile flow mainly due to defective feedback inhibition of hepatic BA synthesis but not to a decrease in enterohepatic circulation [86].

FXR Knockout and Atherosclerosis

FXR deficiency resulted in a pro-atherogenic phenotype with increased serum levels of TG, FFA and cholesterol. Triglyceride levels in FXR deficient mice were elevated due to induction of co-activators (apoC-II) and repression of inhibitors (apoC-III) of the lipoprotein-lipase (LPL) [7] as well as to up-regulation of SREBP1c and fatty-acid synthase (FAS) [114, 115]. Not only VLDL, LDL and HDL levels were elevated, but also HDL size was increased [87]. In liver, cholesterol and triglycerides accumulated due to severely increased absorption [87, 89, 103]. $FXR^{-/-}$ mice however showed an impaired HDL uptake to the liver which was the result of a decreased expression of SR-B1, LCAT and HL [87]. Interestingly, Hartmann *et al.* could prevent dyslipidemic serum profiles of $FXR^{-/-}$ mice in a SHP deficient mouse model. So it seems that loss of SHP protects against elevation of VLDL and LDL levels [110].

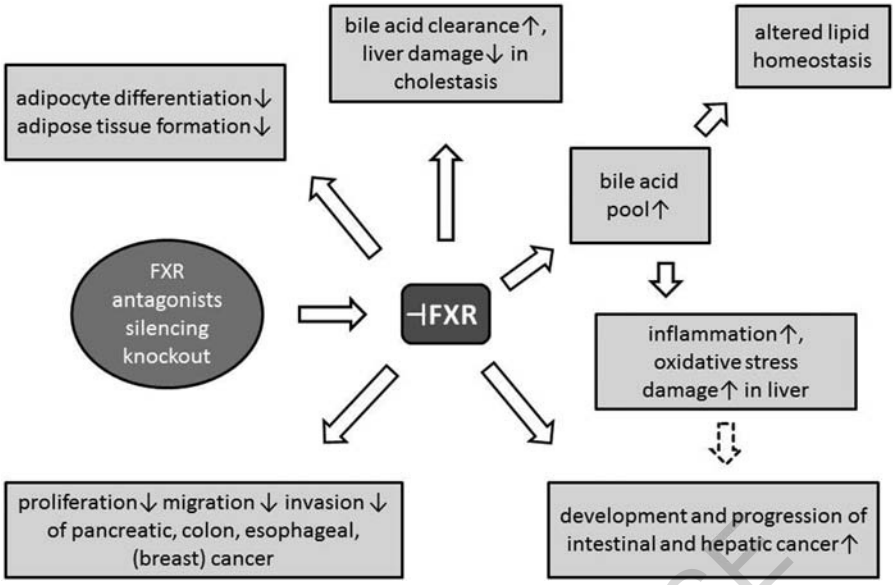

Fig. (2). Effects of FXR inhibition by antagonists, silencing or knockout.

Whether FXR has an impact on the development of atherosclerotic lesions was topic of many studies. Though FXR deficient mice display a pro-atherogenic lipid profile, $FXR^{-/-}$ mice did not develop atherosclerotic lesions even when they were fed a high fat/high cholesterol (HF/HC) diet [87]. As model for atherosclerosis, two mouse models were used in combination to FXR deficiency: ApoE deficient mice or LDLR deficient mice. $FXR^{-/-}/ApoE^{-/-}$ mice failed to gain weight on a HF/HC diet [103] but showed a severe pro-atherogenic lipid profile (VLDL and LDL increased, HDL decreased) besides an increased level of serum TG and increased hepatic lipid accumulation of cholesterol and TG. Furthermore they showed focal necrosis and elevated AST level. This phenotype was however more severe in $FXR^{-/-}$ than in $FXR^{-/-}/ApoE^{-/-}$ double knockout mice [103]. Nevertheless, FXR deficiency in addition to a HF/HC diet did not result in detectable atherosclerotic plaques after 12 weeks in contrast to $ApoE^{-/-}$ and $FXR^{-/-}/ApoE^{-/-}$ mice which showed about the double amount of atherosclerotic lesions [103]. In addition, Guo *et al.* observed significantly reduced atherosclerotic lesion in $FXR^{-/-}/ApoE^{-/-}$ double knockout mice compared to ApoE deficient mice [104]. Furthermore they could show that accumulation of ox-LDL in macrophages was reduced in $FXR^{-/-}$ mice compared to WT, probably due to decreased uptake of ox-LDL since the expression of CD36 on the macrophage surface was reduced [104]. Hanniman and Guo both detected no FXR expression in macrophages, indicating an indirect pathway of action. E.g. FXR deletion increased TNFα and INFγ secretion and INFγ is known to reduce the expression of CD36 and ApoE.

Zhang *et al.* studied atherosclerotic lesions in $LDLR^{-/-}$ and $FXR^{-/-}/LDLR^{-/-}$ double knockout mice. These mice showed decreased body weight, elevated TG and FFA levels and increased levels of LDL, VLDL and HDL. When they were fed a western diet, plasma HDL and LDL levels were reduced in male mice. Furthermore the male, but not female, double knockout mice showed reduced atherosclerosis [92]. Nevertheless hepatic expression of inflammatory and pro-fibrotic genes such as TNF-α, ICAM-1, P-selectin, VCAM-1, SAA2 and tissue plasminogen activator was induced in $FXR^{-/-}/LDR^{-/-}$ mice, so the reduction in atherosclerotic lesions was not a result of decreased expression of inflammatory genes [92]. Analyzing peritoneal macrophages Zhang *et al.* also reported decreased CD36 mRNA levels. Furthermore, expression of ADRP, a target gene of PPARδ, which is proposed to promote lipid droplet formation, was reduced in macrophages of $FXR^{-/-}/LDR^{-/-}$ double knockout mice [92]. Summing up, FXR deletion obviously showed a protective effect on atherosclerosis development regardless the pro-atherogenic serum lipid profile.

FXR Knockout and Metabolic Balance

Since hepatic FXR expression is regulated by glucose and insulin, FXR knockout could have an influence on carbohydrate metabolism and glucose homeostasis as well. A few FXR knockout studies examined the impact on carbohydrate metabolism but with different results. Zhang *et al.* observed unaltered fasting glucose levels besides a mild glucose intolerance and insulin resistance in FXR deficient mice [91]. In contrast, others detected hypoglycaemia in $FXR^{-/-}$ mice upon fasting linked to reduced glycogen stores [85, 94] besides lower fasting insulin levels [95, 111]. Furthermore FXR deficiency accelerated the entry into torpor [93] and caused a decrease in TG and FFA levels compared to baseline. Altogether this suggests a more rapid decrease of circulating metabolic fuel in $FXR^{-/-}$ mice upon fasting [93]. Leptin levels were drastically reduced in $FXR^{-/-}$ mice while adiponectin levels were unaffected [94, 99]. Again others reported that their FXR deficient mice had elevated serum glucose levels (30%) in combination with unaltered leptin [88] and insulin levels [102]. Basal glucose production was unaffected in comparison to WT mice but reduced after 9h fasting [102]. On molecular level, the expression of gluconeogenic genes (e.g. PEPCK) was decreased [88, 94, 102].

Nevertheless, FXR deficient mice displayed an attenuated inhibition of glucose production in liver in response to insulin [88, 91] indicating insulin resistance. Furthermore,

$FXR^{-/-}$ mice showed a decreased clearance of plasma glucose (20%) after i.v. glucose application [94] and impaired response on an oral glucose tolerance test [88, 95]. These findings might point to reduced hepatic insulin sensitivity [85]. In accordance to this, insulin signalling, such as phosphorylation of IRS-1, IRS-2 and Akt kinase, was decreased in livers of $FXR^{-/-}$ mice [88, 91]. Duran-Sandoval *et al.* however, did not observe altered insulin stimulated phosphorylation in the liver and Cariou *et al.* reported that endogenous blood glucose production rate after insulin infusion was suppressed to similar extent in both genotypes [95, 102]. Hence, hepatic insulin sensitivity seems not to be altered. Eventually, impaired glucose tolerance could instead be explained by a peripheral insulin resistance with impaired insulin signalling in muscle cells and adipose tissue [88, 95].

Intestinal glucose absorption in $FXR^{-/-}$ mice was delayed, but not reduced, which can be explained by an increased glucose phosphorylation in enterocytes. In accordance, expression of the glucose phosphorylating enzymes HK1 and HK2, but not SGLT1 and GLUT2, was increased in the proximal part of small intestine in FXR deficient mice [85]. Interestingly, at the age of 30 weeks FXR deficient mice showed lower fasting glucose and insulin levels besides an improved glucose control [111]. This positive effect of FXR deletion on glucose control was also observed in obese (ob/ob) mice [99] which showed attenuated weight gain, decreased fat mass and normal blood glucose levels. Glucose tolerance and insulin signalling in adipose tissue of $FXR^{-/-}$ mice were improved due to improved Akt phosphorylation [99]. These findings are interesting since in lean mice FXR deficiency impairs glucose homeostasis. And interestingly liver-specific FXR deficiency did not protect from diet-induced insulin-resistance [99] which indicates an important role of FXR in adaptation to obesity and its metabolic complications since global FXR deficiency in a mouse model of obesity (ob/ob) protected from excessive body weight gain [99].

FXR deficient mice revealed a reduced volume and size of adipocytes also when they were obese [95, 107, 111]. FXR is usually expressed in white adipose tissue (WAT) [72] and in adipocytes but not in preadipocytes. FXR knockout still caused delayed induction of adipogenic regulators such as PPARγ and c-EBPα [95]. On the other hand, expression of PPARα and PPARδ was increased in adipocytes of FXR deficient mice probably due to increased FFA levels [95]. Expression of lipoprotein lipase and FA transport protein-1 as well as CREBPβ and SREBP-1 but not TNFα was induced in WAT of FXR deficient mice [95]. This indicated anti-inflammatory effects of FXR deficiency and furthermore led to reduced size of lipid droplets in adipocytes [95]. Since genes involved in PPARγ-regulated adipocyte differentiation such as adiponectin, lipoproteinlipase, CD36 and Ap2 as well as genes involved in regulation of lipid droplet formation such as perilipin, ADRP and fsp27 were abolished in FXR deficient mice, FXR seems to be necessary to ensure full response of PPARγ in adipose tissue development [107].

In $FXR^{-/-}$ mice not only the PPARγ pathway in adipocyte differentiation was reduced but also β-catenin was increased. Over-activation of the Wnt/β-catenin pathway due to FXR deficiency resulted in reduced adipocyte differentiation [107]. Compared to $LDR^{-/-}$ mice, $LDR^{-/-}/FXR^{-/-}$ double knockout mice were highly resistant to diet-induced weight gain, with female mice being more resistant [90]. The mice showed a reduction of 30% of body fat content, especially WAT. Zhang *et al.* however detected a smaller size of adipocytes in brown adipose tissue (BAT) in contrast to normal adipocytes in WAT. This gives a lead for a role of FXR in adaptive thermogenesis. Though expression of neither FXR nor SHP was detectable in brown adipose tissue (BAT) [93], expression of thermogenic genes was altered in FXR deficient mice. mRNA levels of UCP-1, DIO2 [93], UCP-3, β_2-adrenergic receptor, PGC-1α and -β were induced in BAT and skeletal muscle [90]. Heat production, oxygen consumption and CO_2 production were increased in female mice indicating increased energy expenditure. In $LDR^{-/-}/FXR^{-/-}$ double knockout mice, fatty acids seemed to be the major fuel with a respiration quotient of 0.74-0.79. In line with this, genes involved in fatty acid oxidation were induced in muscle cells, whereas in liver they were reduced. Furthermore, expression of SREBP-1c and FAS was reduced in liver [90].

FXR Knockout and Inflammation/Regeneration

FXR knockout exacerbated hepatic and intestinal inflammation [9, 100] along with mucosal injury and bacterial translocation in intestine [116]. FXR deficiency furthermore resulted in progressive liver injury with up-regulation of inflammatory genes, such as INF-γ and osteoponin (OPN), an extracellular matrix glycoprotein known for its role in supporting adhesion and migration of inflammatory cells. Liver injury of these FXR knockout mice is characterized by hepatocyte vacuolization, lipid deposit and focal necrosis as histopathological evaluation demonstrated [76]. In a model of ConA induced hepatitis, FXR deficiency resulted in a markedly increased liver injury characterized by higher AST levels, higher mortality and elevated neutrophil accumulation [76]. Furthermore, FXR deficient mice fed a methionine- and choline deficient diet (MCD) showed higher ALT and AST levels than WT littermates, indicating more severe liver injury. They displayed a higher hepatic accumulation of TG but a lower degree of steatosis [117].

Also liver regeneration was impaired in FXR deletion. After CCl_4 treatment, FXR knockout mice displayed a defective liver regeneration, observed in reduced expression of Cyclin D1 and FoxM1b, a target gene in liver regeneration. In addition, the number of apoptotic hepatocytes and necrotic area were higher in CCl_4 treated FXR deficient mice [67]. Huang *et al.* suggest that the impaired liver regeneration of FXR deficient animals is a result of a defective BA homeostasis since activation of growth factor and cytokine responses are not lost in $FXR^{-/-}$ livers because diverting bile flow from the gut decreased liver re-growth and DNA synthesis in partial hepatectomicted rats [118] FXR deletion furthermore resulted in high serum and liver bile acid levels with toxic effects [119].

Furthermore, FXR deficiency resulted in dysregulation of intestinal immunity and tissue remodelling, as observed in higher expression of α1(I) collagen, TIMP-1, and α-smooth muscle actin [109]. In addition, an enhanced infiltration of the colonic mucosa by $CD11b^+$ cells was observed, which released either under basal conditions or in response to

stimulation with increased amounts of IL-1β, IL-6, INF-γ and TNFα [109]. Gadaleta *et al.* showed greater bacterial translocation in the intestine of FXR deficient mice due to higher basal intestinal permeability [9]. These results were confirmed by Inagaki *et al.* when they showed a higher bacterial translocation characterized by increased number of aerobic bacteria in mesenteric lymph nodes of FXR deficient mice. With the help of occluding staining, they indicated deterioration in the epithelial barrier of FXR knockout mice with bacteria and edema present in the junctions. This all indicates that lack of FXR results in mucosal injury and bacterial translocation [116].

FXR deficiency also accelerated diabetic nephropathy in a diabetic mouse model observed by tubular damage, elevated activity of NFκB, increased expression of pro-fibrotic growth factor TGF-β and accumulation of matrix proteins and lipids [100]. The accumulation of lipids was a result of increased expression of SREBP-1c and its target genes FAS, acetyl-CoA carboxylase (ACC) and stearoyl-CoA desaturase-1 (SCD-1) [100].

In a model of cholestasis, Stedman *et al.* in contrast observed benefits of FXR deletion. After bile duct ligation, a common model of obstructive cholestasis, FXR deficient mice had a survival and morbidity advantage. Reduced concentrations of bile acids and reduced expression of BSEP besides a marked induction of Mrp4 seemed to contribute to this protective effect [64].

FXR Knockout and Cancer

FXR deficient mice older than 12 months showed hepatomegalia and developed spontaneous hepatocellular carcinoma (HCC) [97, 113]. Histological examination revealed liver lesions consistent of hypertrophic and eosinophilic hepatocytes [113]. The mice had higher plasma ALT and AST levels as well as increased mRNA levels of pro-inflammatory factors such as IL-1β [113], INFγ, TNFα and IL-6 [106], whereas expression of COX-2 was not altered [97]. The amount of apoptotic cells and focal necrosis was increased which resulted in compensatory cell proliferation [97]. In accordance to that, expression of cyclin D1 and E1 was increased. Furthermore, β-catenin and c-myc levels were elevated [97, 113] and Wolfe *et al.* showed that activation of β-catenin occurs as result of activation of canonical Wnt signalling and loss of E-cadherin as well as GSK-3β, a negative regulator of β-catenin [108].

Wolfe *et al.* suppose that hepatocarcinogenesis occurs because of elevated BA levels, since hepato-specific FXR knockout mice with normal BA levels, did not develop HCC. They presume that the increase in β-catenin may be independent of the loss of FXR [108]. In older $FXR^{-/-}$ mice, increased amounts of Cyclin D1 mRNA were observed, which might also explain the appearance of HCC at the age of 12 month. Nomoto *et al.* suggested oxidative stress as cause for liver tumors in FXR deficient mice. They found significantly higher concentration of 8OHdG, TBARS and hydroperoxide as markers of oxidative stress [106]. In addition, levels of oxidative stress-related genes such as metallothionein 1 (Mt1), glutathione S-transferase mu3 (Gstm3), glutathione S-transferase α2 (Gsta2), NAD(P)H: quinone oxidoreductase 1 (Nqo1) and heme oxygenase (Hmox1), were significantly higher [106]. The increase of hepatic hydroperoxide, TBARS and 8OHdG showed a good correlation with increases in hepatic bile acid concentrations. Li *et al.* observed activation of further cell proliferative pathways in FXR deficiency. Phosphorylation of JAK2 and STAT3 was increased as a result of elevated IL-6 levels (induced by elevated BA levels) [14]. The expression of Survivin, a member of the inhibitor apoptosis protein (IAP) family, was also increased in $FXR^{-/-}$ mice with aging [14]. In conclusion hepatocellular carcinoma might be due to elevated BA levels which elevate oxidative stress [106], increased activation of the Wnt/β-catenin pathway [108] and increased inflammation in the liver.

Observations made on human HCC cells indicate that FXR down-regulation is associated with multiple malignant characteristics [120]. In the same way FXR seems to play a role in intestinal tumorigenesis. FXR is mainly expressed in fully differentiated cells of the surface epithelium in the intestine. In tumors of Adenomatous polyposis coli (APC) mice and in tumors of familial adenomatous patients (FAP), which is caused by mutations in the APC gene, this expression is reduced, however [84]. Loss of FXR in an APC mouse model and in chronic colitis mouse models resulted in early mortality and increased tumor progression [84].

High levels of BAs have also been linked to intestinal cancer in rodent models and human epidemiologic studies. Modica *et al.* however demonstrated by experiments with FXR knockout and cholestyramine administration that the absence of FXR and not merely elevated bile acid concentrations increased the susceptibility to tumorigenesis. In addition they showed that constitutively activated FXR increased apoptosis, reduced proliferation and blocked tumor growth [84]. No differences were observed in the expression of genes targeted by the nuclear β-catenin-TCF complex [84].

Maran *et al.* in contrast observed increased numbers of cells undergoing apoptosis in FXR deficient mice, which seemed to be more goblet cells, however [83]. Furthermore, they reported increased Cyclin D1, c-Myc and IL-6 levels and differently than Modica *et al.*, an increased activity of β-catenin [83].

The fact that studies on esophageal [70] and pancreatic cancer [121] revealed an overexpression of FXR in tumor cells [70] and FXR deletion by FXRshRNA or antagonism by gugglusterone significantly reduced tumor growth in mice [70] again points out that the role of FXR is thoroughly different in distinct forms of cancer.

CONCLUSION AND OUTLOOK

So far, it is difficult to assess the therapeutic value of FXR antagonists. The available data on FXR antagonists and FXR knockout is narrow and several experiments contradict each other. FXR inhibition by knockout or antagonists caused desirable and undesirable effects. In addition, for some compounds that behave as FXR antagonists in artificial settings such as reporter gene assays, it is not known how they affect FXR target genes. Depending on the desired effects both, an antagonist and an inverse agonist may be valuable. Development and *in vitro* characterization should however remember to investigate the effect of FXR ligands on the expression of FXR target genes.

Overall, the activity of FXR can be linked to three clusters of disorders. The nuclear receptor is crucially involved in metabolic balance including lipid and glucose homeostasis, it plays a role in inflammation and liver repair/protection and affects the development and progression of several forms of cancer and related disorders.

Concerning the metabolic balance, reduction of FXR activity displayed desirable effects especially on lipid homeostasis. FXR antagonism caused an increased overall bile acid pool and reduced cholesterol levels in circulation and in the liver. Lipid homeostasis was improved and adipogenesis as well as obesity were repressed. On the other hand, several FXR knockout models revealed a proatherogenic lipid profile that was combined with a protection against development of atherosclerotic lesions, however. *In vitro*, FXR antagonism inhibited glucose-dependent insulin secretion from β-cells and impaired glucose tolerance mostly due to reduced insulin sensitivity in muscle cells. Dependent on the knockout study, hepatic insulin resistance was also detected under reduced FXR activity. Nevertheless FXR deficiency in obese and older mice led to improved glucose homeostasis. Overall, FXR seems to be especially important for the adaption to obesity since FXR knockout displayed conflicting results in lean and obese mice. FXR antagonists might therefore protect from excessive obesity and weight gain but whether this effect can outweigh possible side effects is unclear.

FXR antagonism also affects several liver disorders. In obstructive cholestasis, FXR antagonists reduced the bile acid content in the liver and improved liver injury with lower levels of ALT/AST as well as reduced necrosis. This was also detected in a bile duct ligation model of steatosis where FXR knockout mice showed advantages in survival and morbidity. Under normal conditions however, FXR knockout led to hepatic steatosis, increased liver inflammation and higher lipid content of the liver which seems predominantly to be due to overall increased bile acid levels. Higher bile acid concentrations also caused stronger liver damage in oxidative stress in FXR deficient mice.

Promising effects of FXR antagonists were observed on several tumor cell lines *in vitro* and *in vivo*. Pancreatic, colon, esophageal and breast tumor cells revealed FXR overexpression and responded with reduced proliferation, reduced migration and enhanced apoptosis on FXR antagonism. In Barrett's epithelia, a pre-neoplastic disease, FXR antagonists caused reduced inflammation and enhanced apoptosis. Other cancer forms, especially liver tumors, in contrast seem to benefit from reduced FXR activity. The nuclear receptor was found to be downregulated in hepatocellular, intestinal and gastric tumors. Older FXR knockout mice furthermore spontaneously developed hepatocellular carcinoma. Epidemiologic studies in humans assist these findings. Experiments suggest that the higher prevalence of intestinal and hepatocellular cancer is not linked to higher bile acid concentrations but merely to FXR deficiency.

In cancer forms where FXR is overexpressed, FXR antagonists hold therapeutic potential. FXR antagonism might therefore be a strategy to delay the progression of pancreatic and colon cancer, Barrett's Esophagus and adenoma and eventually of some breast cancer forms. On the other hand, reduced FXR activity is also linked to tumor development and progression, especially in intestinal and hepatic cancer. This fact might strongly limit the potential therapeutic use of FXR antagonists to improve e.g. lipid homeostasis in metabolic disorders since long-term FXR antagonism bears the risk of cancerogenic effects. Besides FXR-overexpressing tumors, FXR antagonists might be promising for short-term treatment of (obstructive) cholestasis. The mayor drawback of complete FXR inhibition seen in knockout studies is the elevated BA level with its toxic impact on several tissues.

Antagonists on other nuclear receptors already have reached clinical significance. Especially antagonists on estrogen receptors (ER) have a long therapeutic tradition in the treatment of hormone receptor positive breast cancer [123]. Further research has generated the selective estrogen receptor modulators (SERMs) that exploit tissue selective agonism and antagonism helping them to play a therapeutic role in several estrogen receptor dependent disorders and to avoid systemic side effects by directly targeting only subpopulations of the nuclear receptor [59]. In contrast to FXR however, ER exists in two subtypes (ERα and ERβ) which alleviates selective modulation since the two subtypes respond differently to distinct ligands. The concept of (tissue) selective regulation of target genes by selective bile acid receptor modulators (SBARMs) may lead to more beneficial therapeutic effects [8, 60]. And for better understanding of the complex network of nuclear receptors and the co-activator and co-repressor peptides *in vivo* many more experiments and answers are necessary.

FXR constitutes a rising target for the treatment of many diseases but can also cause other disorders when overactivated or repressed. To find the right balance of FXR activating and FXR inhibiting effects will be crucial for the development of FXR targeting agents.

ABBREVIATIONS

ABCB	=	ATP-binding cassette transporter B
ACC-1	=	Acetyl-coenzyme A carboxylase-1
ACO	=	Acyl-CoA oxidase
ACOX	=	Acyl/coenyzm A oxidase
ADRP	=	Adipose differentiation-related protein
BAK1	=	Bcl-2 homologous antagonist killer 1
BSEP	=	Bile salt export protein
Casp9	=	Caspase 9
Ccl5	=	Chemokine (C-C-motif) ligand 5
Cd11c	=	Integrin alpha X (complement component 3 receptor 4 subunit)
CEH	=	Cholesterol ester hydrolase
CPT1b	=	Carnitine palmitoyltransferase 1B
FADD	=	Fas-Associated protein with Death Domain
FAP	=	Familial adenomatous patients
FAS	=	Fatty acid synthase
FOXO-1	=	Forkhead transcition factor 1

FSP27 = Fat-specific Protein 27
G6Pase = Glucose-6-phosphatase
GK = Glucokinase
GLUT1 = Glucose transporter 1
GSTa2 = Glutathione S-transferase alpha2
GSTm1 = Gluthation S-transferase mu1
HK1 = Hexokinase 1
HK2 = Hexokinase2
HL = Hepatic lipase
HMG-CoA = 3-hydroxy-3-methylglutaryl-coenzymeA
HO-1 /Hmox1 = Heme oxygenase
ICAM-1 = Intercellular adhesion molecule-1
KLF4 = Kruppel-like factor 4
k-ras = Kirsten rat sarcoma viral oncogene homolog
LCAD = Long-chain fatty acid dehydrogenase
LCAT = Lecithin cholesterol acyl transferase
L-FABP = Liver type FFA-binding protein
LPK = L-type pyruvate kinase
LPL = Lipoprotein lipase
MCAD = Medium chain acyl-CoA dehydrogenase
MCD = Methionine- and choline deficient diet
MT1 = Metallothionein 1
MTP = Microsomal triglyceride transfer protein
NTCP = Basolateral BA transporter into liver
Nqo1 = Nicotin adenine dinucleotide phosphatase quinone oxidoreductase 1
PCNA = Proliferating cell nuclear antigen
PDK4 = Phosphoinositide-dependent protein kinase 4
PGC-1 = PPARgamma coactivator-1alpha
PYK = Pyruvate kinase
SAA-2 = Serum amyloid A2
SCD-1 = Stearoyl-CoA desaturase-1
SCP = Sterol carrier protein
sFRP5 = Secreted frizzled-related protein 5
sFRP1 = Secreted frizzled-related protein 1
SMA = Alpha-smoth muscle actin
SRBI = Scavenger receptor BI
SREBP-1C = Sterol regulatory element-binding protein-1
Tlr4 = Toll like receptor4
TIMP-1 = Tissue inhibitor of metalloproteinase
tPA = Tissue plasminogen activator
UCP1 (2/3) = Uncoupling protein 1 (2/3)
VCAM-1 = Vascular cell adhesion molecule-1
VLCAD = Very long chain acyl-CoA dehydrogenase

CONFLICT OF INTEREST

The authors confirm that this article content has no conflict of interest.

ACKNOWLEDGEMENTS

Declared none.

REFERENCES

[1] Parks, D.J.; Blanchard, S.G.; Bledsoe, R.K.; Chandra, G.; Consler, T.G.; Kliewer, S.A.; Stimmel, J.B.; Willson, T.M.; Zavacki, A.M.; Moore, D.D.; Lehmann, J.M. Bile acids: natural ligands for an orphan nuclear receptor. *Science*, **1999**, *284*(5418), 1365–1368.
[2] Makishima, M.; Okamoto, A.Y.; Repa, J.J.; Tu, H.; Learned, R.M.; Luk, A.; Hull, M.V.; Lustig, K.D.; Mangelsdorf, D.J.; Shan, B. Identification of a nuclear receptor for bile acids. *Science*, **1999**, *284*(5418), 1362–1365.
[3] Forman, B.M.; Goode, E.; Chen, J.; Oro, A.E.; Bradley, D.J.; Perlmann, T.; Noonan, D.J.; Burka, L.T.; McMorris, T.; Lamph, W.W.; Evans, R.M.; Weinberger, C. Identification of a nuclear receptor that is activated by farnesol metabolites. *Cell*, **1995**, *81*(5), 687–693.
[4] Seol, W.; Choi, H.S.; Moore, D.D. Isolation of proteins that interact specifically with the retinoid X receptor: two novel orphan receptors. *Mol. Endocrinol.*, **1995**, *9*(1), 72–85.
[5] Fiorucci, S.; Mencarelli, A.; Distrutti, E.; Zampella, A. Farnesoid X receptor: from medicinal chemistry to clinical applications. *Future Med. Chem.*, **2012**, *4*(7), 877–891.
[6] Fiorucci, S.; Cipriani, S.; Baldelli, F.; Mencarelli, A. Bile acid-activated receptors in the treatment of dyslipidemia and related disorders. *Progress in Lipid Research*, **2010**, *49*(2), 171–185.
[7] Claudel, T.; Staels, B.; Kuipers, F. The Farnesoid X receptor: a molecular link between bile acid and lipid and glucose metabolism. *Arterioscler. Thromb. Vasc. Biol.*, **2005**, *25*(10), 2020–2030.
[8] Cariou, B.; Staels, B. FXR: a promising target for the metabolic syndrome? *Trends Pharmacol. Sci.*, **2007**, *28*(5), 236–243.
[9] Gadaleta, R.M.; van Erpecum, Karel J; Oldenburg, B.; Willemsen, Ellen C L; Renooij, W.; Murzilli, S.; Klomp, Leo W J; Siersema, P.D.; Schipper, Marguerite E I; Danese, S.; Penna, G.; Laverny, G.; Adorini, L.; Moschetta, A.; van Mil, Saskia W C. Farnesoid X receptor activation inhibits inflammation and preserves the intestinal barrier in inflammatory bowel disease. *Gut*, **2011**, *60*(4), 463–472.
[10] Düfer, M.; Hörth, K.; Krippeit-Drews, P.; Drews, G. The significance of the nuclear farnesoid X receptor (FXR) in β cell function. *Islets*, **2012**, *4*(5), 333–338.
[11] Adorini, L.; Pruzanski, M.; Shapiro, D. Farnesoid X receptor targeting to treat nonalcoholic steatohepatitis. *Drug Discov. Today*, **2012**, *17*(17-18), 988–997.
[12] Mudaliar, S.; Henry, R.R.; Sanyal, A.J.; Morrow, L.; Marschall, H.-U.; Kipnes, M.; Adorini, L.; Sciacca, C.I.; Clopton, P.; Castelloe, E.; Dillon, P.; Pruzanski, M.; Shapiro, D. Efficacy and safety of the farnesoid X receptor agonist obeticholic acid in patients with type 2 diabetes and nonalcoholic fatty liver disease. *Gastroenterology*, **2013**, *145*(3), 574-82.e1.
[13] Li, Y.; Jadhav, K.; Zhang, Y. Bile acid receptors in non-alcoholic fatty liver disease. *Biochem. Pharmacol.*, **2013**, *86*(11), 1517–1524.
[14] Li, G.; Kong, B.; Zhu, Y.; Le Zhan; Williams, J.A.; Tawfik, O.; Kassel, K.M.; Luyendyk, J.P.; Wang, L.; Guo, G.L. Small heterodimer partner overexpression partially protects against liver tumor development in farnesoid X receptor knockout mice. *Toxicol. Appl. Pharmacol.*, **2013**, *272*(2), 299–305.
[15] Zimber, A.; Gespach, C. Bile acids and derivatives, their nuclear receptors FXR, PXR and ligands: role in health and disease and their therapeutic potential. *Anticancer Agents Med. Chem.*, **2008**, *8*(5), 540–563.

[16] Koutsounas, I.; Giaginis, C.; Theocharis, S. Farnesoid X Receptor (FXR) from normal to malignant state. *Histol. Histopathol.*, **2012**, *27*(7), 835–853.

[17] Wang, X.; Fu, X.; van Ness, C.; Meng, Z.; Ma, X.; Huang, W. Bile Acid Receptors and Liver Cancer. *Curr. Pathobiol. Rep.*, **2013**, *1*(1), 29–35.

[18] Gadaleta, R.M.; Cariello, M.; Sabbà, C.; Moschetta, A. Tissue-specific actions of FXR in metabolism and cancer. *Biochim. Biophys. Acta*, **2014**.

[19] Merk, D.; Steinhilber, D.; Schubert-Zsilavecz, M. Medicinal chemistry of farnesoid X receptor ligands: from agonists and antagonists to modulators. *Future Med. Chem.*, **2012**, *4*(8), 1015–1036.

[20] Savkur, R.S.; Thomas, J.S.; Bramlett, K.S.; Gao, Y.; Michael, L.F.; Burris, T.P. Ligand-dependent coactivation of the human bile acid receptor FXR by the peroxisome proliferator-activated receptor gamma coactivator-1alpha. *J. Pharmacol. Exp. Ther.*, **2005**, *312*(1), 170–178.

[21] Fiorucci, S.; Mencarelli, A.; Distrutti, E.; Palladino, G.; Cipriani, S. Targetting farnesoid-X-receptor: from medicinal chemistry to disease treatment. *Curr. Med. Chem.*, **2010**, *17*(2), 139–159.

[22] Germain, P.; Staels, B.; Dacquet, C.; Spedding, M.; Laudet, V. Overview of nomenclature of nuclear receptors. *Pharmacol. Rev.*, **2006**, *58*(4), 685–704.

[23] Di Leva, Francesco Saverio; Festa, C.; D'Amore, C.; Marino, S. de; Renga, B.; D'Auria, M.V.; Novellino, E.; Limongelli, V.; Zampella, A.; Fiorucci, S. Binding Mechanism of the Farnesoid X Receptor Marine Antagonist Suvanine Reveals a Strategy To Forestall Drug Modulation on Nuclear Receptors. Design, Synthesis, and Biological Evaluation of Novel Ligands. *J. Med. Chem.*, **2013**, *56*(11), 4701–4717.

[24] Kainuma, M.; Makishima, M.; Hashimoto, Y.; Miyachi, H. Design, synthesis, and evaluation of non-steroidal farnesoid X receptor (FXR) antagonist. *Bioorg. Med. Chem.*, **2007**, *15*(7), 2587–2600.

[25] Cui, J. Guggulsterone Is a Farnesoid X Receptor Antagonist in Coactivator Association Assays but Acts to Enhance Transcription of Bile Salt Export Pump. *J. Biol. Chem.*, **2003**, *278*(12), 10214–10220.

[26] Gronemeyer, H.; Gustafsson, J.-A.; Laudet, V. Principles for modulation of the nuclear receptor superfamily. *Nat. Rev. Drug. Discov.*, **2004**, *3*(11), 950–964.

[27] Yu, J.; Lo, J.-L.; Huang, L.; Zhao, A.; Metzger, E.; Adams, A.; Meinke, P.T.; Wright, S.D.; Cui, J. Lithocholic acid decreases expression of bile salt export pump through farnesoid X receptor antagonist activity. *J. Biol. Chem.*, **2002**, *277*(35), 31441–31447.

[28] Campana, G.; Pasini, P.; Roda, A.; Spampinato, S. Regulation of ileal bile acid-binding protein expression in Caco-2 cells by ursodeoxycholic acid: role of the farnesoid X receptor. *Biochem. Pharmacol.*, **2005**, *69*(12), 1755–1763.

[29] Hu, X.; Bonde, Y.; Eggertsen, G.; Rudling, M. Muricholic bile acids are potent regulators of bile acid synthesis via a positive feedback mechanism. *J. Intern. Med.*, **2014**, *275*(1), 27–38.

[30] Sayin, S.I.; Wahlström, A.; Felin, J.; Jäntti, S.; Marschall, H.-U.; Bamberg, K.; Angelin, B.; Hyötyläinen, T.; Orešič, M.; Bäckhed, F. Gut Microbiota Regulates Bile Acid Metabolism by Reducing the Levels of Tauro-beta-muricholic Acid, a Naturally Occurring FXR Antagonist. *Cell Metab.*, **2013**, *17*(2), 225–235.

[31] Nishimaki-Mogami, T.; Kawahara, Y.; Tamehiro, N.; Yoshida, T.; Inoue, K.; Ohno, Y.; Nagao, T.; Une, M. 5α-Bile alcohols function as farnesoid X receptor antagonists. *Biochem. Biophys. Res. Commun.*, **2006**, *339*(1), 386–391.

[32] Marino, S. de; Ummarino, R.; D'Auria, M.V.; Chini, M.G.; Bifulco, G.; D'Amore, C.; Renga, B.; Mencarelli, A.; Petek, S.; Fiorucci, S.; Zampella, A. 4-Methylenesterols from Theonella swinhoei sponge are natural pregnane-X-receptor agonists and farnesoid-X-receptor antagonists that modulate innate immunity. *Steroids*, **2012**, *77*(5), 484–495.

[33] Renga, B.; Mencarelli, A.; D'Amore, C.; Cipriani, S.; D'Auria, M.V.; Sepe, V.; Chini, M.G.; Monti, M.C.; Bifulco, G.; Zampella, A.; Fiorucci, S.; Lobaccaro, J.-M.A. Discovery That Theonellasterol a Marine Sponge Sterol Is a Highly Selective FXR Antagonist That Protects against Liver Injury in Cholestasis. *PLoS ONE*, **2012**, *7*(1), e30443.

[34] Sepe, V.; Ummarino, R.; D'Auria, M.; Taglialatela-Scafati, O.; Marino, S.; D'Amore, C.; Renga, B.; Chini, M.; Bifulco, G.; Nakao, Y.; Fusetani, N.; Fiorucci, S.; Zampella, A. Preliminary Structure-Activity Relationship on Theonellasterol, a New Chemotype of FXR Antagonist, from the Marine Sponge Theonella swinhoei. *Marine Drugs*, **2012**, *10*(12), 2448–2466.

[35] Sepe, V.; Bifulco, G.; Renga, B.; D'Amore, C.; Fiorucci, S.; Zampella, A. Discovery of Sulfated Sterols from Marine Invertebrates as a New Class of Marine Natural Antagonists of Farnesoid-X-Receptor. *J. Med. Chem.*, **2011**, *54*(5), 1314–1320.

[36] Nam, S.-J.; Ko, H.; Shin, M.; Ham, J.; Chin, J.; Kim, Y.; Kim, H.; Shin, K.; Choi, H.; Kang, H. Farnesoid X-activated receptor antagonists from a marine sponge Spongia sp. *Bioorg. Med. Chem. Lett.*, **2006**, *16*(20), 5398–5402.

[37] Nam, S.-J.; Ko, H.; Ju, M.K.; Hwang, H.; Chin, J.; Ham, J.; Lee, B.; Lee, J.; Won, D.H.; Choi, H.; Ko, J.; Shin, K.; Oh, T.; Kim, S.; Rho, J.-R.; Kang, H. Scalarane Sesterterpenes from a Marine Sponge of the Genus Spongia and Their FXR Antagonistic Activity. *J. Nat. Prod.*, **2007**, *70*(11), 1691–1695.

[38] Putra, M.Y.; Bavestrello, G.; Cerrano, C.; Renga, B.; D'Amore, C.; Fiorucci, S.; Fattorusso, E.; Taglialatela-Scafati, O. Polyhydroxylated sterols from the Indonesian soft coral Sinularia sp. and their effect on farnesoid X-activated receptor. *Steroids*, **2012**, *77*(5), 433–440.

[39] Shin, K.; Chin, J.; Hahn, D.; Lee, J.; Hwang, H.; Won, D.H.; Ham, J.; Choi, H.; Kang, E.; Kim, H.; Ju, M.K.; Nam, S.-J.; Kang, H. Sterols from a soft coral, Dendronephthya gigantea as farnesoid X-activated receptor antagonists. *Steroids*, **2012**, *77*(5), 355–359.

[40] Carter, B.A.; Taylor, O.A.; Prendergast, D.R.; Zimmerman, T.L.; Furstenberg, R. von; Moore, D.D.; Karpen, S.J. Stigmasterol, a soy lipid-derived phytosterol, is an antagonist of the bile acid nuclear receptor FXR. *Pediatr. Res.*, **2007**, *62*(3), 301–306.

[41] Urizar, N.L. A Natural Product That Lowers Cholesterol As an Antagonist Ligand for FXR. *Science*, **2002**, *296*(5573), 1703–1706.

[42] Wu, J.; Xia, C.; Meier, J.; Li, S.; Hu, X.; Lala, D.S. The hypolipidemic natural product guggulsterone acts as an antagonist of the bile acid receptor. *Mol. Endocrinol.*, **2002**, *16*(7), 1590–1597.

[43] Yang, L.; Broderick, D.; Jiang, Y.; Hsu, V.; Maier, C.S. Conformational dynamics of human FXR-LBD ligand interactions studied by hydrogen/deuterium exchange mass spectrometry: insights into the antagonism of the hypolipidemic agent Z-guggulsterone. *Biochim. Biophys. Acta*, **2014**, *1844*(9), 1684–1693.

[44] Owsley, E.; Chiang, J.Y. Guggulsterone antagonizes farnesoid X receptor induction of bile salt export pump but activates pregnane X receptor to inhibit cholesterol 7α-hydroxylase gene. *Biochem. Biophys. Res. Commun.*, **2003**, *304*(1), 191–195.

[45] Meyer, U.; Costantino, G.; Macchiarulo, A.; Pellicciari, R. Is antagonism of E/Z-guggulsterone at the farnesoid X receptor mediated by a noncanonical binding site? A molecular modeling study. *J. Med. Chem.*, **2005**, *48*(22), 6948–6955.

[46] Owsley, E.; Chiang, John Y L. Guggulsterone antagonizes farnesoid X receptor induction of bile salt export pump but activates pregnane X receptor to inhibit cholesterol 7alpha-hydroxylase gene. *Biochem. Biophys. Res. Commun.*, **2003**, *304*(1), 191–195.

[47] Burris, T.P.; Montrose, C.; Houck, K.A.; Osborne, H.E.; Bocchinfuso, W.P.; Yaden, B.C.; Cheng, C.C.; Zink, R.W.; Barr, R.J.; Hepler, C.D.; Krishnan, V.; Bullock, H.A.; Burris, L.L.; Galvin, R.J.; Bramlett, K.; Stayrook, K.R. The hypolipidemic natural product guggulsterone is a promiscuous steroid receptor ligand. *Mol. Pharmacol.*, **2005**, *67*(3), 948–954.

[48] Deng, R. Therapeutic effects of guggul and its constituent guggulsterone: cardiovascular benefits. *Cardiovasc. Drug Rev.*, **2007**, *25*(4), 375–390.

[49] Shishodia, S.; Sethi, G.; Ahn, K.S.; Aggarwal, B.B. Guggulsterone inhibits tumor cell proliferation, induces S-phase arrest, and promotes apoptosis through activation of c-Jun N-terminal kinase, suppression of Akt pathway, and downregulation of antiapoptotic gene products. *Biochem. Pharmacol.*, **2007**, *74*(1), 118–130.

[50] Xiao, D.; Singh, S.V. z-Guggulsterone, a constituent of Ayurvedic medicinal plant Commiphora mukul, inhibits angiogenesis *in vitro* and *in vivo*. *Mol. Cancer Ther.*, **2008**, *7*(1), 171–180.

[51] Macha, M.A.; Rachagani, S.; Gupta, S.; Pai, P.; Ponnusamy, M.P.; Batra, S.K.; Jain, M. Guggulsterone decreases proliferation and metastatic behavior of pancreatic cancer cells by modulating JAK/STAT and Src/FAK signaling. *Cancer Lett.*, **2013**, *341*(2), 166–177.

[52] Kumar, D.; Khanna, A.K.; Pratap, R.; Sexana, J.K.; Bhatta, R.S. Dose escalation pharmacokinetics and lipid lowering activity of a novel farnesoid X receptor modulator: 16-Dehydropregnenolone. *Indian J. Pharmacol*, **2012**, *44*(1), 57–62.

[53] Xu, X.; Lu, Y.; Chen, L.; Chen, J.; Luo, X.; Shen, X. Identification of 15d-PGJ2 as an antagonist of farnesoid X receptor: Molecular modeling with biological evaluation. *Steroids*, **2013**, *78*(9), 813–822.

[54] Choi, H.; Hwang, H.; Chin, J.; Kim, E.; Lee, J.; Nam, S.-J.; Lee, B.C.; Rho, B.J.; Kang, H. Tuberatolides, Potent FXR Antagonists from the Korean Marine Tunicate Botryllus tuberatus. *J. Nat. Prod.*, **2011**, *74*(1), 90–94.

[55] Liu, P.; Xu, X.; Chen, L.; Ma, L.; Shen, X.; Hu, L. Discovery and SAR study of hydroxyacetophenone derivatives as potent, non-steroidal farnesoid X receptor (FXR) antagonists. *Bioorg. Med. Chem.*, **2014**, *22*(5), 1596–1607.

[56] Huang, H.; Yu, Y.; Gao, Z.; Zhang, Y.; Li, C.; Xu, X.; Jin, H.; Yan, W.; Ma, R.; Zhu, J.; Shen, X.; Jiang, H.; Chen, L.; Li, J. Discovery and Optimization of 1,3,4-Trisubstituted-pyrazolone Derivatives as Novel, Potent, and Nonsteroidal Farnesoid X Receptor (FXR) Selective Antagonists. *J. Med. Chem.*, **2012**, *55*(16), 7037–7053.

[57] Fu, J.; Si, P.; Zheng, M.; Chen, L.; Shen, X.; Tang, Y.; Li, W. Discovery of new non-steroidal FXR ligands via a virtual screening workflow based on Phase shape and induced fit docking. *Bioorg. Med. Chem. Lett.*, **2012**, *22*(22), 6848–6853.

[58] Yu, D.D.; Lin, W.; Forman, B.M.; Chen, T. Identification of trisubstituted-pyrazol carboxamide analogs as novel and potent antagonists of farnesoid X receptor. *Bioorg. Med. Chem.*, **2014**, *22*(11), 2919–2938.

[59] Komm, B.S.; Mirkin, S. An overview of current and emerging SERMs. *J. Steroid Biochem. Mol. Biol.*, **2014**, *143,* 207–222.

[60] Dussault, I.; Beard, R.; Lin, M.; Hollister, K.; Chen, J.; Xiao, J.-H.; Chandraratna, R.; Forman, B.M. Identification of gene-selective modulators of the bile acid receptor FXR. *J. Biol. Chem.*, **2003**, *278*(9), 7027–7033.

[61] Sayin, S.I.; Wahlström, A.; Felin, J.; Jäntti, S.; Marschall, H.-U.; Bamberg, K.; Angelin, B.; Hyötyläinen, T.; Orešič, M.; Bäckhed, F. Gut Microbiota Regulates Bile Acid Metabolism by Reducing the Levels of Tauro-beta-muricholic Acid, a Naturally Occurring FXR Antagonist. *Cell Metab.,* **2013**, *17*(2), 225–235.

[62] Qi, Y.; Jiang, C.; Cheng, J.; Krausz, K.W.; Li, T.; Ferrell, J.M.; Gonzalez, F.J.; Chiang, J.Y. Bile acid signaling in lipid metabolism: Metabolomic and lipidomic analysis of lipid and bile acid markers linked to anti-obesity and anti-diabetes in mice. *Biochim. Biophys. Acta*, **2014**, doi:10.1016/j.bbalip.2014.04.008

[63] Aron-Wisnewsky, J.; Gaborit, B.; Dutour, A.; Clement, K. Gut microbiota and non-alcoholic fatty liver disease: new insights. *Clin. Microbiol. Infect.*, **2013**, *19*(4), 338–348.

[64] Stedman, C.; Liddle, C.; Coulter, S.; Sonoda, J.; Alvarez, J.G.; Evans, R.M.; Downes, M. Benefit of farnesoid X receptor inhibition in obstructive cholestasis. *Proc. Natl. Acad. Sci. U.S.A.*, **2006**, *103*(30), 11323–11328.

[65] Wang, C.; Zhang, F.; Wang, L.; Zhang, Y.; Li, X.; Huang, K.; Du, M.; Liu, F.; Huang, S.; Guan, Y.; Huang, D. Poly(ADP-Ribose) Polymerase 1 Promotes Oxidative-Stress-Induced Liver Cell Death via Suppressing Farnesoid X Receptor. *Mol. Cell. Biol.*, **2013**, *33*(22), 4492–4503.

[66] Dai, J.; Wang, H.; Shi, Y.; Dong, Y.; Zhang, Y.; Wang, J. Impact of bile acids on the growth of human cholangiocarcinoma via FXR. *J. Hematol. Oncol.*, **2011**, *4*(1), 41.

[67] Meng, Z.; Wang, Y.; Wang, L.; Jin, W.; Liu, N.; Pan, H.; Liu, L.; Wagman, L.; Forman, B.M.; Huang, W. FXR regulates liver repair after CCl4-induced toxic injury. *Mol. Endocrinol.*, **2010**, *24*(5), 886–897.

[68] Gottardi, A. de; Dumonceau, J.-M.; Bruttin, F.; Vonlaufen, A.; Morard, I.; Spahr, L.; Rubbia-Brandt, L.; Frossard, J.-L.; Dinjens, Winand N M; Rabinovitch, P.S.; Hadengue, A. Expression of the bile acid receptor FXR in Barrett's esophagus and enhancement of apoptosis by guggulsterone *in vitro*. *Mol. Cancer*, **2006**, *5,* 48.

[69] Capello, A.; Moons, Leon M. G.; Van de Winkel, Anouk; Siersema, P.D.; van Dekken, H.; Kuipers, E.J.; Kusters, J.G. Bile Acid-Stimulated Expression of the Farnesoid X Receptor Enhances the Immune Response in Barrett Esophagus. *Am. J. Gastroenterology*, **2008**, *103*(6), 1510–1516.

[70] Guan, B.; Li, H.; Yang, Z.; Hoque, A.; Xu, X. Inhibition of farnesoid X receptor controls esophageal cancer cell growth *in vitro* and in nude mouse xenografts. *Cancer*, **2013**, *119*(7), 1321–1329.

[71] Düfer, M.; Horth, K.; Wagner, R.; Schittenhelm, B.; Prowald, S.; Wagner, T. F. J.; Oberwinkler, J.; Lukowski, R.; Gonzalez, F.J.; Krippeit-Drews, P.; Drews, G. Bile Acids Acutely Stimulate Insulin Secretion of Mouse ß-Cells via Farnesoid X Receptor Activation and KATP Channel Inhibition. *Diabetes*, **2012**, *61*(6), 1479–1489.

[72] Rizzo, G.; Disante, M.; Mencarelli, A.; Renga, B.; Gioiello, A.; Pellicciari, R.; Fiorucci, S. The farnesoid X receptor promotes adipocyte differentiation and regulates adipose cell function *in vivo*. *Mol. Pharmacol.*, **2006**, *70*(4), 1164–1173.

[73] Id Boufker, H.; Lagneaux, L.; Fayyad-Kazan, H.; Badran, B.; Najar, M.; Wiedig, M.; Ghanem, G.; Laurent, G.; Body, J.-J.; Journé, F. Role of farnesoid X receptor (FXR) in the process of differentiation of bone marrow stromal cells into osteoblasts. *Bone*, **2011**, *49*(6), 1219–1231.

[74] Scholtes, C.; Diaz, O.; Icard, V.; Kaul, A.; Bartenschlager, R.; Lotteau, V.; André, P. Enhancement of genotype 1 hepatitis C virus replication by bile acids through FXR. *J. Hepatol.*, **2008**, *48*(2), 192–199.

[75] Lebovics, E.; Seif, F.; Kim, D.; Elhosseiny, A.; Dworkin, B.M.; Casellas, A.; Clark, S.; Rosenthal, W.S. Pruritus in chronic hepatitis C: association with high serum bile acids, advanced pathology, and bile duct abnormalities. *Dig. Dis. Sci.*, **1997**, *42*(5), 1094–1099.

[76] Mencarelli, A.; Renga, B.; Migliorati, M.; Cipriani, S.; Distrutti, E.; Santucci, L.; Fiorucci, S. The bile acid sensor farnesoid X receptor is a modulator of liver immunity in a rodent model of acute hepatitis. *J. Immunol.*, **2009**, *183*(10), 6657–6666.

[77] Lee, J.Y.; Lee, K.T.; Lee, J.K.; Lee, K.H.; Jang, K.-T.; Heo, J.S.; Choi, S.H.; Kim, Y.; Rhee, J.C. Farnesoid X receptor, overexpressed in pancreatic cancer with lymph node metastasis promotes cell migration and invasion. *Br. J. Cancer*, **2011**, *104*(6), 1027–1037.

[78] Gottardi, A. de; Touri, F.; Maurer, C.A.; Perez, A.; Maurhofer, O.; Ventre, G.; Bentzen, C.L.; Niesor, E.J.; Dufour, J.-F. The bile acid nuclear receptor FXR and the bile acid binding protein IBABP are differently expressed in colon cancer. *Dig. Dis. Sci.*, **2004**, *49*(6), 982–989.

[79] Journe, F.; Durbecq, V.; Chaboteaux, C.; Rouas, G.; Laurent, G.; Nonclercq, D.; Sotiriou, C.; Body, J.-J.; Larsimont, D. Association between farnesoid X receptor expression and cell proliferation in estrogen receptor-positive luminal-like breast cancer from postmenopausal patients. *Breast Cancer Res. Treat.*, **2009**, *115*(3), 523–535.

[80] Swales, K.E.; Korbonits, M.; Carpenter, R.; Walsh, D.T.; Warner, T.D.; Bishop-Bailey, D. The farnesoid X receptor is expressed in breast cancer and regulates apoptosis and aromatase expression. *Cancer Res.*, **2006**, *66*(20), 10120–10126.

[81] Silva, J.; Dasgupta, S.; Wang, G.; Krishnamurthy, K.; Ritter, E.; Bieberich, E. Lipids isolated from bone induce the migration of human breast cancer cells. *J. Lipid Res.*, **2006**, *47*(4), 724–733.

[82] Ohno, T.; Shirakami, Y.; Shimizu, M.; Kubota, M.; Sakai, H.; Yasuda, Y.; Kochi, T.; Tsurumi, H.; Moriwaki, H. Synergistic growth inhibition of human hepatocellular carcinoma cells by acyclic retinoid and GW4064, a farnesoid X receptor ligand. *Cancer Lett.*, **2012**, *323*(2), 215–222.

[83] Maran, Rengasamy R M; Thomas, A.; Roth, M.; Sheng, Z.; Esterly, N.; Pinson, D.; Gao, X.; Zhang, Y.; Ganapathy, V.; Gonzalez, F.J.; Guo, G.L. Farnesoid X receptor deficiency in mice leads to increased intestinal epithelial cell proliferation and tumor development. *J. Pharmacol. Exp. Ther.*, **2009**, *328*(2), 469–477.

[84] Modica, S.; Murzilli, S.; Salvatore, L.; Schmidt, D.R.; Moschetta, A. Nuclear bile acid receptor FXR protects against intestinal tumorigenesis. *Cancer Res.*, **2008**, *68*(23), 9589–9594.

[85] van Dijk, Theo H; Grefhorst, A.; Oosterveer, M.H.; Bloks, V.W.; Staels, B.; Reijngoud, D.-J.; Kuipers, F. An increased flux through the glucose 6-phosphate pool in enterocytes delays glucose absorption in Fxr-/- mice. *J. Biol. Chem.*, **2009**, *284*(16), 10315–10323.

[86] Kok, T.; Hulzebos, C.V.; Wolters, H.; Havinga, R.; Agellon, L.B.; Stellaard, F.; Shan, B.; Schwarz, M.; Kuipers, F. Enterohepatic circulation of bile salts in farnesoid X receptor-deficient mice: effi-

cient intestinal bile salt absorption in the absence of ileal bile acid-binding protein. *J. Biol. Chem.*, **2003**, *278*(43), 41930–41937.

[87] Lambert, G.; Amar, Marcelo J A; Guo, G.; Brewer, H.B.; Gonzalez, F.J.; Sinal, C.J. The farnesoid X-receptor is an essential regulator of cholesterol homeostasis. *J. Biol. Chem.*, **2003**, *278*(4), 2563–2570.

[88] Ma, K.; Saha, P.K.; Chan, L.; Moore, D.D. Farnesoid X receptor is essential for normal glucose homeostasis. *J. Clin. Invest.*, **2006**, *116*(4), 1102–1109.

[89] Sinal, C.J.; Tohkin, M.; Miyata, M.; Ward, J.M.; Lambert, G.; Gonzalez, F.J. Targeted disruption of the nuclear receptor FXR/BAR impairs bile acid and lipid homeostasis. *Cell*, **2000**, *102*(6), 731–744.

[90] Zhang, Y.; Ge, X.; Heemstra, L.A.; Chen, W.-D.; Xu, J.; Smith, J.L.; Ma, H.; Kasim, N.; Edwards, P.A.; Novak, C.M. Loss of FXR protects against diet-induced obesity and accelerates liver carcinogenesis in ob/ob mice. *Mol. Endocrinol.*, **2012**, *26*(2), 272–280.

[91] Zhang, Y.; Lee, F.Y.; Barrera, G.; Lee, H.; Vales, C.; Gonzalez, F.J.; Willson, T.M.; Edwards, P.A. Activation of the nuclear receptor FXR improves hyperglycemia and hyperlipidemia in diabetic mice. *Proc. Natl. Acad. Sci. U.S.A.*, **2006**, *103*(4), 1006–1011.

[92] Zhang, Y.; Wang, X.; Vales, C.; Lee, F.Y.; Lee, H.; Lusis, A.J.; Edwards, P.A. FXR deficiency causes reduced atherosclerosis in Ldlr-/- mice. *Arterioscler. Thromb. Vasc. Biol.*, **2006**, *26*(10), 2316–2321.

[93] Cariou, B.; Bouchaert, E.; Abdelkarim, M.; Dumont, J.; Caron, S.; Fruchart, J.-C.; Burcelin, R.; Kuipers, F.; Staels, B. FXR-deficiency confers increased susceptibility to torpor. *FEBS Lett.*, **2007**, *581*(27), 5191–5198.

[94] Cariou, B.; van Harmelen, K.; Duran-Sandoval, D.; van Dijk, T.; Grefhorst, A.; Bouchaert, E.; Fruchart, J.-C.; Gonzalez, F.J.; Kuipers, F.; Staels, B. Transient impairment of the adaptive response to fasting in FXR-deficient mice. *FEBS Lett.*, **2005**, *579*(19), 4076–4080.

[95] Cariou, B.; van Harmelen, K.; Duran-Sandoval, D.; van Dijk, Theo H; Grefhorst, A.; Abdelkarim, M.; Caron, S.; Torpier, G.; Fruchart, J.-C.; Gonzalez, F.J.; Kuipers, F.; Staels, B. The farnesoid X receptor modulates adiposity and peripheral insulin sensitivity in mice. *J. Biol. Chem.*, **2006**, *281*(16), 11039–11049.

[96] Kim, I.; Morimura, K.; Shah, Y.; Yang, Q.; Ward, J.M.; Gonzalez, F.J. Spontaneous hepatocarcinogenesis in farnesoid X receptor-null mice. *Carcinogenesis*, **2007**, *28*(5), 940–946.

[97] Yang, F.; Huang, X.; Yi, T.; Yen, Y.; Moore, D.D.; Huang, W. Spontaneous development of liver tumors in the absence of the bile acid receptor farnesoid X receptor. *Cancer Res.*, **2007**, *67*(3), 863–867.

[98] Lian, F.; Xing, X.; Yuan, G.; Schäfer, C.; Rauser, S.; Walch, A.; Röcken, C.; Ebeling, M.; Wright, M.B.; Schmid, R.M.; Ebert, Matthias P A; Burgermeister, E. Farnesoid X receptor protects human and murine gastric epithelial cells against inflammation-induced damage. *Biochem. J.*, **2011**, *438*(2), 315–323.

[99] Prawitt, J.; Abdelkarim, M.; Stroeve, Johanna H M; Popescu, I.; Duez, H.; Velagapudi, V.R.; Dumont, J.; Bouchaert, E.; van Dijk, Theo H; Lucas, A.; Dorchies, E.; Daoudi, M.; Lestavel, S.; Gonzalez, F.J.; Oresic, M.; Cariou, B.; Kuipers, F.; Caron, S.; Staels, B. Farnesoid X receptor deficiency improves glucose homeostasis in mouse models of obesity. *Diabetes*, **2011**, *60*(7), 1861–1871.

[100] Wang, X.X.; Jiang, T.; Shen, Y.; Caldas, Y.; Miyazaki-Anzai, S.; Santamaria, H.; Urbanek, C.; Solis, N.; Scherzer, P.; Lewis, L.; Gonzalez, F.J.; Adorini, L.; Pruzanski, M.; Kopp, J.B.; Verlander, J.W.; Levi, M. Diabetic nephropathy is accelerated by farnesoid X receptor deficiency and inhibited by farnesoid X receptor activation in a type 1 diabetes model. *Diabetes*, **2010**, *59*(11), 2916–2927.

[101] Kong, B.; Luyendyk, J.P.; Tawfik, O.; Guo, G.L. Farnesoid X receptor deficiency induces nonalcoholic steatohepatitis in low-density lipoprotein receptor-knockout mice fed a high-fat diet. *J. Pharmacol. Exp. Ther.*, **2009**, *328*(1), 116–122.

[102] Duran-Sandoval, D.; Cariou, B.; Percevault, F.; Hennuyer, N.; Grefhorst, A.; van Dijk, Theo H; Gonzalez, F.J.; Fruchart, J.-C.; Kuipers, F.; Staels, B. The farnesoid X receptor modulates hepatic carbohydrate metabolism during the fasting-refeeding transition. *J. Biol. Chem.*, **2005**, *280*(33), 29971–29979.

[103] Hanniman, E.A.; Lambert, G.; McCarthy, T.C.; Sinal, C.J. Loss of functional farnesoid X receptor increases atherosclerotic lesions in apolipoprotein E-deficient mice. *J. Lipid Res.*, **2005**, *46*(12), 2595–2604.

[104] Guo, G.L.; Santamarina-Fojo, S.; Akiyama, T.E.; Amar, Marcelo J A; Paigen, B.J.; Brewer, B., JR; Gonzalez, F.J. Effects of FXR in foam-cell formation and atherosclerosis development. *Biochim. Biophys. Acta*, **2006**, *1761*(12), 1401–1409.

[105] Mencarelli, A.; Renga, B.; Distrutti, E.; Fiorucci, S. Antiatherosclerotic effect of farnesoid X receptor. *Am. J. Physiol. Heart Circ. Physiol.*, **2009**, *296*(2), H272-81.

[106] Nomoto, M.; Miyata, M.; Yin, S.; Kurata, Y.; Shimada, M.; Yoshinari, K.; Gonzalez, F.J.; Suzuki, K.; Shibasaki, S.; Kurosawa, T.; Yamazoe, Y. Bile acid-induced elevated oxidative stress in the absence of farnesoid X receptor. *Biol. Pharm. Bull.*, **2009**, *32*(2), 172–178.

[107] Abdelkarim, M.; Caron, S.; Duhem, C.; Prawitt, J.; Dumont, J.; Lucas, A.; Bouchaert, E.; Briand, O.; Brozek, J.; Kuipers, F.; Fievet, C.; Cariou, B.; Staels, B. The farnesoid X receptor regulates adipocyte differentiation and function by promoting peroxisome proliferator-activated receptor-gamma and interfering with the Wnt/beta-catenin pathways. *J. Biol. Chem.*, **2010**, *285*(47), 36759–36767.

[108] Wolfe, A.; Thomas, A.; Edwards, G.; Jaseja, R.; Guo, G.L.; Apte, U. Increased activation of the Wnt/beta-catenin pathway in spontaneous hepatocellular carcinoma observed in farnesoid X receptor knockout mice. *J. Pharmacol. Exp. Ther.*, **2011**, *338*(1), 12–21.

[109] Vavassori, P.; Mencarelli, A.; Renga, B.; Distrutti, E.; Fiorucci, S. The bile acid receptor FXR is a modulator of intestinal innate immunity. *J. Immunol.*, **2009**, *183*(10), 6251–6261.

[110] Hartman, H.B.; Lai, K.; Evans, M.J. Loss of small heterodimer partner expression in the liver protects against dyslipidemia. *J. Lipid Res.*, **2008**, *50*(2), 193–203.

[111] Bjursell, M.; Wedin, M.; Admyre, T.; Hermansson, M.; Bottcher, G.; Goransson, M.; Linden, D.; Bamberg, K.; Oscarsson, J.; Bohlooly-Y, M. Ageing Fxr deficient mice develop increased energy expenditure, improved glucose control and liver damage resembling NASH. *PLoS One*, **2013**, *8*(5), e64721.

[112] Schuetz, E.G.; Strom, S.; Yasuda, K.; Lecureur, V.; Assem, M.; Brimer, C.; Lamba, J.; Kim, R.B.; Ramachandran, V.; Komoroski, B.J.; Venkataramanan, R.; Cai, H.; Sinal, C.J.; Gonzalez, F.J.; Schuetz, J.D. Disrupted Bile Acid Homeostasis Reveals an Unexpected Interaction among Nuclear Hormone Receptors, Transporters, and Cytochrome P450. *J. Biol. Chem.*, **2001**, *276*(42), 39411–39418.

[113] Kim, I.; Ahn, S.-H.; Inagaki, T.; Choi, M.; Ito, S.; Guo, G.L.; Kliewer, S.A.; Gonzalez, F.J. Differential regulation of bile acid homeostasis by the farnesoid X receptor in liver and intestine. *J. Lipid Res.*, **2007**, *48*(12), 2664–2672.

[114] Moschetta, A.; Bookout, A.L.; Mangelsdorf, D.J. Prevention of cholesterol gallstone disease by FXR agonists in a mouse model. *Nat. Med.*, **2004**, *10*(12), 1352–1358.

[115] Watanabe, M.; Houten, S.M.; Wang, L.; Moschetta, A.; Mangelsdorf, D.J.; Heyman, R.A.; Moore, D.D.; Auwerx, J. Bile acids lower triglyceride levels via a pathway involving FXR, SHP, and SREBP-1c. *J. Clin. Invest.*, **2004**, *113*(10), 1408–1418.

[116] Inagaki, T.; Moschetta, A.; Lee, Y.-K.; Peng, L.; Zhao, G.; Downes, M.; Yu, R.T.; Shelton, J.M.; Richardson, J.A.; Repa, J.J.; Mangelsdorf, D.J.; Kliewer, S.A. Regulation of antibacterial defense in the small intestine by the nuclear bile acid receptor. *Proc. Natl. Acad. Sci. U.S.A.*, **2006**, *103*(10), 3920–3925.

[117] Wu, W.; Liu, X.; Peng, X.; Xue, R.; Ji, L.; Shen, X.; Chen, S.; Gu, J.; Zhang, S. Bile acids override steatosis in farnesoid X receptor deficient mice in a model of non-alcoholic steatohepatitis. *Biochem. Biophys. Res. Commun.*, **2014**, *448*(1), 50–55.

[118] Ueda, J.; Chijiiwa, K.; Nakano, K.; Zhao, G.; Tanaka, M. Lack of intestinal bile results in delayed liver regeneration of normal rat liver after hepatectomy accompanied by impaired cyclin E-associated kinase activity. *Surgery*, **2002**, *131*(5), 564–573.

[119] Huang, W. Nuclear Receptor-Dependent Bile Acid Signaling Is Required for Normal Liver Regeneration. *Science*, **2006**, *312*(5771), 233–236.

[120] Su, H.; Ma, C.; Liu, J.; Li, N.; Gao, M.; Huang, A.; Wang, X.; Huang, W.; Huang, X. Downregulation of nuclear receptor FXR is associated with multiple malignant clinicopathological characteris-

tics in human hepatocellular carcinoma. *Am. J. Physiol. Gastrointest. Liver Physiol.*, **2012**, *303*(11), G1245-53.

[121] Lee, J.Y.; Lee, K.T.; Lee, J.K.; Lee, K.H.; Jang, K.-T.; Heo, J.S.; Choi, S.H.; Kim, Y.; Rhee, J.C. Farnesoid X receptor, overexpressed in pancreatic cancer with lymph node metastasis promotes cell migration and invasion. *Br. J. Cancer*, **2011**, *104*(6), 1027–1037.

[122] Maran, Rengasamy R M; Thomas, A.; Roth, M.; Sheng, Z.; Esterly, N.; Pinson, D.; Gao, X.; Zhang, Y.; Ganapathy, V.; Gonzalez, F.J.; Guo, G.L. Farnesoid X receptor deficiency in mice leads to increased intestinal epithelial cell proliferation and tumor development. *J. Pharmacol. Exp. Ther.*, **2009**, *328*(2), 469–477.

[123] Ciruelos, E.; Pascual, T.; Arroyo Vozmediano, María Luisa; Blanco, M.; Manso, L.; Parrilla, L.; Muñoz, C.; Vega, E.; Calderón, M.J.; Sancho, B.; Cortes-Funes, H. The therapeutic role of fulvestrant in the management of patients with hormone receptor-positive breast cancer. *Breast*, **2014**, *23*(3), 201–208.

Received: June 16, 2014 **Revised: September 09, 2014** **Accepted: September 13, 2014**

Bioorganic & Medicinal Chemistry 23 (2015) 499–514

Contents lists available at ScienceDirect

Bioorganic & Medicinal Chemistry

journal homepage: www.elsevier.com/locate/bmc

Anthranilic acid derivatives as nuclear receptor modulators—Development of novel PPAR selective and dual PPAR/FXR ligands

Daniel Merk *,†, Christina Lamers †, Julia Weber, Daniel Flesch, Matthias Gabler, Ewgenij Proschak, Manfred Schubert-Zsilavecz

Institute of Pharmaceutical Chemistry, Goethe University Frankfurt, Max-von-Laue-Str. 9, D-60438 Frankfurt, Germany

ARTICLE INFO

Article history:
Received 15 September 2014
Revised 3 December 2014
Accepted 11 December 2014
Available online 19 December 2014

Keywords:
Nuclear receptors
Peroxisome proliferator activated receptors (PPAR)
Farnesoid X receptor (FXR)
Metabolic disorders
Lipid metabolism

ABSTRACT

Nuclear receptors, especially the peroxisome proliferator activated receptors (PPARs) and the farnesoid X receptor (FXR) fulfill crucial roles in metabolic balance. Their activation offers valuable therapeutic potential which has high clinical relevance with the fibrates and glitazones as PPAR agonistic drugs. With growing knowledge about the various functions of nuclear receptors in many disorders, new selective or dual ligands of these pharmaceutical targets are however still required. Here we report the class of anthranilic acid derivatives as novel selective PPAR or dual FXR/PPAR ligands. We identified distinct molecular determinants that govern selectivity for each PPAR subtype or FXR as well as the amplitude of activation of the respective receptors. We thereby discovered several lead compounds for further optimization and developed a highly potent dual PPARα/FXR partial agonist that might have a beneficial synergistic effect on lipid homeostasis by simultaneous activation of two nuclear receptors involved in lipid metabolism.

1. Introduction

Nuclear receptors (NR) are ligand-activated transcription factors which regulate key functions of development, cell differentiation and several metabolic pathways such as insulin signaling, lipid and cholesterol homeostasis as well as bile acid (BA) metabolism. The NR superfamily consists of 48 members that are activated by a broad range of endogenous or exogenous ligands such as steroid hormones, dietary lipids, bile acids and xenobiotics.[1]

Peroxisome proliferator activated receptors (PPARs) play a major role in metabolic regulation such as lipid and glucose homeostasis. Three subtypes are known which differ in expression and physiological role. All three subtypes are activated by fatty acids and eicosanoids underlining their regulatory role in lipid homeostasis and inflammation.[2–5]

PPARα is mainly expressed in liver and brown adipose tissue, besides small intestine, heart and kidney. It is the master regulator of hepatic nutrient metabolism in fasting and stimulates β-oxidation as well as ketogenesis of free fatty acids. Since the 1960s PPARα agonistic fibrates such as bezafibrate (**1**) are used to treat dyslipidemia.[6,7]

Expression of PPARγ is mainly found in adipose tissue and macrophages and with lower extent in skeletal muscle. In adipose tissue PPARγ controls adipogenesis and adipocyte differentiation besides its role in whole body lipid metabolism and insulin sensitivity. PPARγ agonistic thiazolidindiones (TZDs) such as rosiglitazone (**2**) are used in type 2 diabetes treatment.[6] Due to side effects their use has been restricted in many countries, nevertheless a recently published re-adjudication of the RECORD trial with rosiglitazone (**2**) supports their further therapeutic application.[8]

For PPARδ (also referred as PPARβ) in contrast, no ligand has entered the market yet. PPARδ is ubiquitously expressed and plays a major role in fatty acid oxidation in key metabolic tissues such as skeletal muscle. Furthermore the receptor is essential for the development and resolution of inflammation.[9] With growing knowledge of its physiological role PPARδ has gained interest as therapeutic target as it can be observed in patent literature.[10] First clinical studies with the PPARδ agonist GW501516 (**3**) provided encouraging findings such as decreased plasma triglyceride levels,[11] induction of HDL levels and improved insulin sensitivity in obese patients.[12] **3** was however cancerogenic in rats.[13]

Farnesoid X receptor (FXR), also a member of the NR superfamily, regulates bile acid (BA) homeostasis and has an impact on glucose and lipid metabolism. It is mainly expressed in liver, intestine and kidney.[14,15] Physiologically, FXR serves as BA sensor by controlling BA synthesis and elimination to protect the liver from

* Corresponding author.
E-mail address: merk@pharmchem.uni-frankfurt.de (D. Merk).
† D.M. and C.L. contributed equally to this work.

http://dx.doi.org/10.1016/j.bmc.2014.12.013
0968-0896/

overload of the potentially toxic BAs.[14,15] Modulation of FXR may be a valuable therapeutic approach for metabolic and inflammatory diseases and with 6-ECDCA (obeticholic acid, **4**) the first FXR agonist is currently in phase 3 of clinical trials for the treatment of the liver disorders primary biliary cirrhosis (PBC), non-alcoholic steatohepatitis (NASH) and non-alcoholic fatty liver disease (NAFLD) (Scheme 1).[16,17]

We recently reported the discovery, SAR and optimization of anthranilic acid derivatives as FXR ligands with the development of **5** as highly potent and selective partial FXR agonist.[18–20] In our efforts to optimize the potency and selectivity of the anthranilic acid derivatives towards FXR we also characterized selected compounds on PPARs. For two distinct reasons we therefore further investigated the SAR of anthranilic acid derivatives as PPAR ligands. On one hand we aimed to get rid of the off-target activity in the optimization of our recently reported highly potent FXR partial agonists. On the other hand we optimized the potency of anthranilic acid derivatives on PPARs and thereby generated new potent PPAR ligands as pharmacological tools and lead structures. We identified potent partial agonists, full agonists and superagonists on each PPAR subtype and discovered concrete molecular determinants in the acylanthranilamide scaffold that modulate selectivity of the compounds for PPAR subtypes or FXR.

2. Results and discussion

2.1. Chemistry

Compounds were prepared as published before.[19,20] In brief, two distinct synthetic routes were used for the preparation of the anthranilamide intermediates **6** carrying the acidic head group. Either isatoic anhydride derivatives (**7**) were reacted with the required amines or anilines (**8**) in a mixture of THF, DMF and pyridine in the presence of 4-*N*,*N*-dimethylaminopyridine (DMAP, **9**) as catalyst at 80 °C or in absolute ethanol under reflux without catalyst to introduce the head groups. When the nucleophilicity of the required anilines was too weak to give acceptable yields in this procedure or when the required isatoic anhydride derivative was not available, 2-nitrobenzoic acid derivatives (**10**) were used as starting material. 2-Nitrobenzoic acid derivatives (**10**) were activated (**11**) by chlorination with thionyl chloride in methylene chloride at 40 °C and then reacted with the required anilines (**8**) in methylene chloride in the presence of pyridine at room temperature. The resulting *o*-nitrobenzamides (**12**) were then reduced to yield the desired anthranilamide intermediates **6** using tin and hydrochloric acid in THF at 60 °C. The intermediates (**6**) were finally reacted with various acyl chlorides (**13**) in THF in the presence of pyridine at room temperature to yield the final acyl anthranilamide derivatives (**18**–**69**). The synthetic procedure is depicted in Scheme 2.

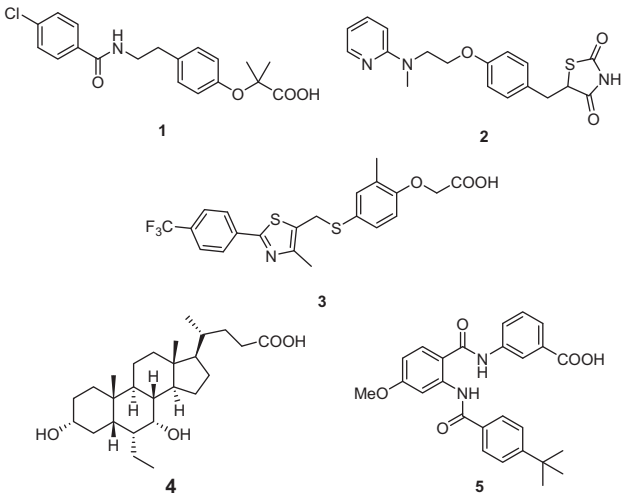

Scheme 1. Potent PPAR and FXR ligands: PPARα agonist bezafibrate (**1**), PPARγ agonist rosiglitazone (**2**), PPARδ agonist GW501516 (**3**), FXR agonist 6-ECDCA (**4**) and FXR partial agonist **5**.

2.2. Biological evaluation

Compounds were characterized in vitro in standard reporter gene assays as reported before.[21,22] The used PPAR subtype assays consisted of hybrid constructs of the respective PPAR ligand binding domain (LBD) fused to a Gal4 DNA binding domain (DBD). The assays were performed in Cos-7 cells which were transiently transfected with lipofectamine. Hybrid receptor constructs were under the control of a CMV promoter and constitutively expressed. A firefly luciferase under the control of a Gal4 promoter served as reporter gene. Additionally, a renilla luciferase under the control of a SV40 promoter was used for normalization and as control for transfection efficiency and toxicity. GW7647 (**14**, 1 μM, PPARα), pioglitazone (**15**, 1 μM, PPARγ) and L165,041 (**16**, 1 μM, PPARδ) served as reference compounds and their activity at the respective concentration was set as 100%.[22] FXR activity was determined in a full length FXR transactivation assay in HeLa cells containing FXR (CMV) and RXR (SV40), a firefly luciferase under the control of a BSEP promoter and a renilla luciferase (SV40) for normalization and transfection/toxicity control. For FXR, GW4064 (**17**, 3 μM) served as reference agonist (Scheme 3).[20]

2.3. Structure–activity relationship

We initially observed activity on PPARs for compound **18** which showed a very high maximum relative PPARγ activation with 432 ± 13% of pioglitazone (**15**) with a moderate EC_{50} value of 18 ± 1 μM but was inactive on other PPAR subtypes. We therefore systematically investigated the SAR of all parts of this scaffold on PPAR activity by varying either acyl substituent, acidic head group or the central anthranilic amide moiety.

The PPARγ-superagonistic activity of **18** was also present in 1-napthoyl isomer **19** with a slightly higher EC_{50}-value which was however inactive on FXR and showed minimal activity on PPARα. Introduction of smaller, monocyclic aromatic moieties as acyl substituents such as a 4-*tert*-butylbenzoyl (**22**) or a 4-ethylbenzoyl residue (**23**) strongly diminished the activity on PPARγ while **23** exhibited moderate PPARα agonistic activity. Since PPARγ activity seemed to require large aromatic substituents, we investigated the activity of biphenyl residues (**24**–**26**) as acyl substituents which were all inactive on FXR but showed partial to superagonistic activity on PPARγ. 4-Biphenyl derivative **24** activated PPARγ with the lowest EC_{50} amongst the biphenyl isomers while moving the phenyl substituent to 3-position in **25** increased maximum relative activation. 3-biphenyl derivative **25** was furthermore potent on PPARα. A diphenylacetyl substituent (**27**) which displays a comparable size, lipophilicity and electron density as the biphenyls was inactive on all PPARs and FXR probably due to its different geometry. These results indicated that already the various acyl substituents strongly modulate the activity profile of the acyl anthranilic acid derivatives on the nuclear receptors PPARα, PPARγ and FXR. While PPARγ was able to accommodate most lipophilic acyl substituents, PPARα was only activated by a small 4-ethylbenzoyl (**23**) and a 3-biphenyl derivative (**25**) and FXR preferred the 4-*tert*-butylbenzoyl residue in **22** as well as the 2-naphthoyl moiety in **18** (Table 1).

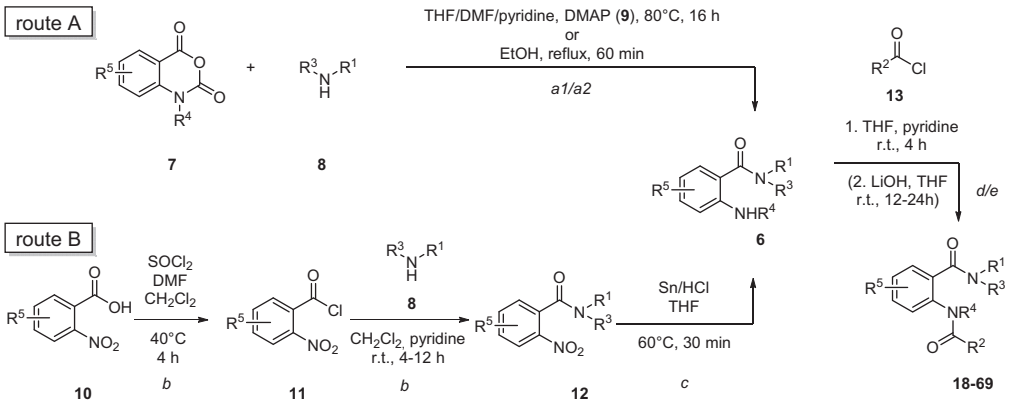

Scheme 2. Synthesis of acyl anthranilamides **18**–**69**. (Preparation by route A: **18**–**43**, **45**–**48**, **50**–**51**, **55**–**57**, **59**–**69**; route B: **5**, **49**, **52**–**54**, **58**; preparation of **44** is reported in Ref. 20).

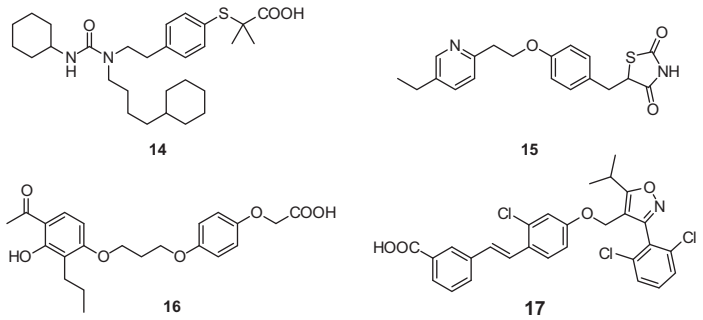

Scheme 3. Reference agonists for in vitro characterization of compounds **18**–**69**: PPARα agonist GW7647 (**14**), PPARγ agonist pioglitazone (**15**), PPARδ agonist L165,041 (**16**) and FXR agonist GW4064 (**17**).

When **18** was methylated at the nitrogen atoms of the amide bonds in **20** and **21**, activity on PPARγ and FXR was completely lost which might be due to a loss of polar interactions with the amide groups.

To elucidate the SAR of the acidic head group (Table 2) we introduced and characterized the activity of different carboxylic acid moieties while maintaining the 2-naphthoyl residue of **18** as acyl substituent. Elongation of the chain in the aliphatic acyl substituents by one (**28**) or two (**29**) methylene groups reduced the maximum relative activation on FXR without significant changes in the EC_{50} values and diminished activity on PPARγ. A strong improvement in the EC_{50} values on all receptors was achieved when an additional aromatic ring was introduced in the head group. 3-Aminobenzoic acid derivative **30** activated all PPARs and FXR with low micromolar EC_{50} values. When the carboxyl group was moved from *meta* to *para* position in **31**, activity on PPARα and PPARδ was lost, while on FXR it was hardly affected. On PPARγ however, **31** exhibited an even stronger superagonism than **18** and **19** with 639 ± 22% of pioglitazone (**15**). Introduction of additional methylene groups in 4-aminophenylacetic acid **32** and 4-aminomethylbenzoic acid derivative **33** diminished activity on all PPARs.

Summing up the results of the head group SAR, the 3-aminobenzoic acid of **30** was the most potent moiety on all PPARs and FXR. This on one hand did not improve the selectivity of our FXR partial agonists but provided a potent pan-PPAR agonist and a lead structure for the development of novel PPAR agonists. In addition, we discovered a potent and subtype selective PPARγ superagonist in compound **31** (Table 2).

With **30** as a new lead structure we again investigated the SAR of the acyl substituent by characterizing analogues of the 2-naphthoyl moiety of **30** and 4-substituted benzoyl residues (Table 3). The slightly more polar 3,4-methylenedioxobenzoyl residue (**34**) in place of the lipophilic 2-naphthoyl group diminished activity on all PPARs and FXR while the smaller 3-fluoro-4-trifluoromethylbenzoyl moiety in **35** as a minimal naphthoyl analogue showed comparable PPAR agonistic activity as **30** while its activity on FXR was diminished. When the substitution pattern was moved from a 3,4-disubstitution in **35** to a 3,5-disubstitution in **36**, activity on all PPARs and FXR was diminished.

With replacement of the 2-naphthoyl residue of **30** by a 4-*tert*-butylbenzoyl moiety (**37**), activity on FXR was strongly improved by about a factor 5, while it remained unchanged on PPARα as well as PPARγ and was lost on PPARδ. Other 4-substituted benzoyl derivatives did however not follow this trend. The sterically less demanding 4-trifluoromethyl derivative **38** was less active on FXR and PPARα than **30**, while it achieved a significantly higher maximum relative activation on PPARγ with a comparable EC_{50} value. On PPARδ, **38** showed a slightly improved EC_{50} value compared to **30**. Introduction of a large electron withdrawing 4-bromine substituent in **39** diminished the maximum relative activation on FXR, PPARα and especially on PPARγ and significantly worsened the potency on PPARδ.

Again, the acyl substituent significantly modulated the selectivity profile of the acyl anthranilamides. While the lipophilic 2-napthoyl residue (**30**) was equally potent on all PPARs and FXR, smaller monocyclic aromatic residues achieved more selectivity. The lipophilic and sterically demanding 4-*tert*-butylbenzoyl moiety (**37**) shifted the activity strongly towards FXR, while the sterically less demanding 4-trifluoromethyl-benzoyl residue (**38**) was most potent on PPARδ.

To investigate the availability of additional space in the ligand binding pockets of PPARs and FXR, we introduced additional

Table 1
In vitro activity of compounds **18–27** in reporter gene assays for PPARs and FXR

#	R_1	R_2	R_3	R_4	R_5	EC_{50} [μM] (max. rel activation [%]) PPARα	PPARγ	PPARδ	FXR
18	COOH	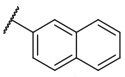	H	H	—	i.a.	18.1 ± 0.9 (432 ± 13)	i.a.	8.6 ± 1.3 (37 ± 2)
19	COOH	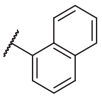	H	H	—	12 ± 3%	41 ± 5 (397 ± 39)	i.a.	i.a.
20	COOH	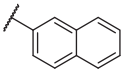	Me	H	—	i.a.	i.a.	i.a.	i.a.
21	COOH	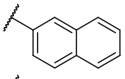	H	Me	—	i.a.	i.a.	i.a.	i.a.
22	COOH	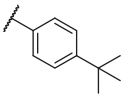	H	H	—	i.a.	i.a.	i.a.	2.5 ± 0.4 (19 ± 1)
23	COOH	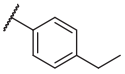	H	H	—	15.7 ± 2.7 (100 ± 11)	39 ± 10%	i.a.	5.8 ± 1.0 (28 ± 2)
24	COOH	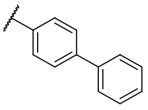	H	H	—	i.a.	13 ± 1 (135 ± 6)	i.a.	i.a.
25	COOH	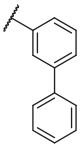	H	H	—	10 ± 1 (260 ± 5)	37 ± 11 (229 ± 44)	i.a.	i.a.
26	COOH	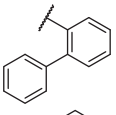	H	H	—	i.a.	23 ± 6 (45 ± 6)	i.a.	i.a.
27	COOH	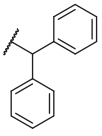	H	H	—	i.a.	i.a.	i.a.	i.a.

Results are expressed as mean ± SEM. n = 3–6; i.a. – inactive (30 μM). Percent values represent the activity at 10 μM when no EC_{50} value could be determined.

chlorine atoms on each position of the central aromatic ring of **37** (Table 3). Introduction of a chlorine atom in 3- (**40**) or 6-position (**41**) of the central aromatic ring led to inactivity on all PPARs and FXR which might be explained by steric clashes with the amide groups in proximity and a, thus, changed geometry. An additional chlorine atom in 4-position (**43**) further optimized the FXR selectivity, however, with a 2.5-fold improvement in potency on FXR, a significant loss of potency on PPARα and a reduced maximum relative activation on PPARγ. Chlorination of the 5-position of the central aromatic ring in **42** showed comparable effects on PPAR-activity as a chlorine atom in 4-position (**43**) but on FXR substitution of the 5-position led to antagonistic activity.[20]

Hence, FXR-selectivity could be achieved by introducing a 4-*tert*-butylbenzoyl moiety as acyl substituent and a chlorine atom in 4-position of the central aromatic ring in compound **43**. Overall, **43** was 75-fold selective over PPARγ and at least 100-fold selective over PPARα and PPARδ. With a methoxy residue in 4-position of the central aromatic ring, this selectivity profile could further be improved in **5**.[19,20]

Starting from **37** which robustly activated PPARα, PPARγ and FXR we next investigated the SAR of the acidic head group to discover structural changes that enhanced potency on PPARs. We evaluated the head group SAR by replacing the carboxylic acid with bioisosters, by elongation of the acidic side chain and by introducing additional substituents at the aromatic ring of the head group (Table 4).

Replacement of the carboxylic acid in **37** with bioisosters such as an amide (**44**) or a nitrile (**45**) lead to a complete loss of activity on all PPARs while the compounds remained equally potent as the carboxylic acid **37** on FXR. For FXR activity even a methoxy group (**46**) was sufficient. For activity on PPARs however, a carboxylic acid or at least an acidic moiety thus seemed to be crucial and the introduction of non-acidic bioisosters of the carboxylic acid such as an amide or a nitrile offered another way to improve the selectivity of the compounds for FXR.

Elongation of the acidic side chain of the head group from benzoic acid **37** to phenylacetic acid **47** did not affect activity on PPARγ but worsened the potency on PPARα and FXR. Furthermore,

Table 2
In vitro activity of compounds **28**–**33** in reporter gene assays for PPARs and FXR

#	R_1	R_2	R_3	R_4	R_5	EC_{50} [μM] (max. rel activation [%]) PPARα	PPARγ	PPARδ	FXR
28	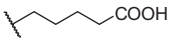	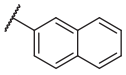	H	H	—	i.a.	26 ± 4 (269 ± 29)	i.a.	8.3 ± 1.0 (11.4 ± 0.4)
29	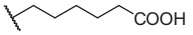	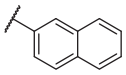	H	H	—	38 ± 9%	40 ± 10%	i.a.	4.4 ± 0.6 (10.4 ± 0.4)
30	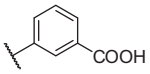	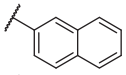	H	H	—	1.96 ± 0.13 (73 ± 2)	5.5 ± 0.6 (126 ± 19)	4.7 ± 0.6 (51 ± 5)	1.5 ± 0.2 (37 ± 1)
31	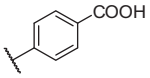	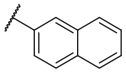	H	H	—	i.a.	21 ± 1 (639 ± 22)	i.a.	1.0 ± 0.2 (23 ± 1)
32	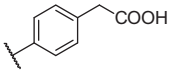	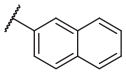	H	H	—	i.a.	25 ± 7%	i.a.	3.1 ± 0.3 (9.8 ± 0.4)
33	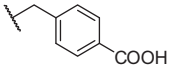	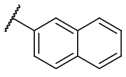	H	H	—	17 ± 9%	56 ± 5%	i.a.	1.3 ± 0.1 (10.0 ± 0.1)

Results are expressed as mean ± SEM. n = 3–6; i.a. – inactive (30 μM). Percent values represent the activity at 10 μM when no EC_{50} value could be determined.

phenylacetic acid **47** showed potent partial agonistic activity on PPARδ although all other derivatives with the 4-*tert*-butylbenzoyl substituent were inactive. Introduction of another methylene group in the acidic side chain leading to phenylpropionic acid **48** again did not significantly alter the activity on PPARα and PPARγ. On FXR however, **48** gained a factor 5 in potency compared to **37** and on PPARδ **48** was inactive.

We then introduced additional methyl groups at the head group aromatic ring of **37**. On FXR, methylation of position 2 (**49**) or 4 (**50**) had improved potency by a factor 7 while a methyl group in position 6 (**51**) caused inactivity. Interestingly, for PPARs the compounds revealed a different SAR. Concerning PPARα, methylation in 2- (**49**) and 4-position (**51**) led to complete loss of activity but derivative **50** with a methyl substituent in position 6 gained a factor 6 in potency and was a highly potent PPARα partial agonist. For PPARγ, none of the additional methyl groups (**49**–**51**) significantly altered the activity with the result that methylation in position 6 (**51**) which produced inactivity on PPARα and FXR made the compound a selective PPARγ superagonist. Hence, the substitution pattern of the head group aromatic ring significantly altered the activity and selectivity profile of the compounds with positions 2 and 6 improving potency on FXR, position 6 enhancing PPARα-activity and position 4 leading to selectivity for PPARγ.

To further investigate these substituent effects we also introduced other residues than the methyl groups in positions 4 and 6. The activity of **50** on PPARα was however diminished when the substituent in 6-position was varied from the small lipophilic methyl group of **50** to sterically more demanding and more polar residues such as a methoxy group (**52**), a chlorine (**53**) or a bromine (**54**) atom. PPARγ in contrast tolerated the replacement of the 4-methyl group of **51** by a larger methoxy group (**55**) and with the larger and more polar chlorine atom (**56**) in 4-position the activity was even improved. The potency enhancing effect of these 4-substitutions might also be due to a changed geometry that results from steric clashes with the amide group in proximity. Interestingly, introduction of a small but strongly electron withdrawing fluorine atom (**57**) in 4-position significantly enhanced the maximum relative activation to about 700% of pioglitazone (**15**). Hence, electron withdrawing halogen substituents in 4-position seemed to improve the potency on PPARγ but at the same time the activity on FXR and PPARα was increased and selectivity was diminished. **52** and **50** therefore remained the best compounds on PPARγ and PPARα, respectively. Concerning FXR, introduction of 4-substituents diminished potency which was probably due to steric reasons since the smallest substituent (**57**) retained most activity.

Besides discovering the PPARγ selective superagonist **51**, the dual PPARα/FXR partial agonist **50** and structural determinants leading to FXR selectivity (**5**, **43**), we finally explored the possibility to improve the compounds' potency and selectivity on PPARδ. Among the anthranilic amide derivatives discussed so far, only few showed activity on PPARδ. Concerning the acidic head group, only a 3-aminobenzoic acid and a 3-aminophenylacetic acid were active on PPARδ. Interestingly, 3-aminophenylacetic acid derivative **47** activated the nuclear receptor with the 4-*tert*-butylbenzoyl residue that in combination with 3-aminobenzoic acid (**37**) as head group was inactive. Thus, the 3-aminophenylacetic acid moiety seemed to be superior. In case of the acyl substituent four lipophilic moieties protruded for their activity on PPARδ, in particular a 2-naphthoyl group (**30**), a 4-bromobenzoyl group (**39**), a 3-fluoro-4-trifluoromethylbenzoyl residue (**35**) and especially a 4-trifluoromethylbenzoyl group (**38**). For activity on PPARδ large lipophilic 4- or 3,4-substituted benzoyl residues seemed to be required. Previous results indicated that for activity on PPARδ a 3-aminophenylacetic acid combined with a 4-substituted benzoyl group as acyl substituent was most suited. The space for substituents in 4-position of the acyl group seemed however limited since the small trifluoromethyl residue (**38**) was superior to the sterically more demanding bromine atom (**35**) and 4-*tert*-butylbenzoyl derivative **37** was inactive. We therefore combined the 3-aminophenylacetic acid head group with various small 4-substituted benzoyl residues with the aim to improve potency on PPARδ.

In addition, the SAR of substituents at the central aromatic ring (**40**–**43**) was not quite convincing for PPARδ since even the reference compound **37** without substituents was inactive on this receptor. To discover possible additional space in the ligand

Table 3
In vitro activity of compounds 34–43 in reporter gene assays for PPARs and FXR

#	R_1	R_2	R_3	R_4	R_5	EC_{50} [μM] (max. rel activation [%]) PPARα	PPARγ	PPARδ	FXR
34	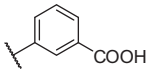	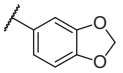	H	H	—	19 ± 2 (54 ± 2)	25 ± 5 (221 ± 59)	i.a.	10 ± 1 (12 ± 1)
35	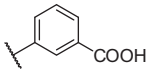	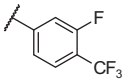	H	H	—	2.2 ± 0.3 (34 ± 2)	6.9 ± 0.4 (240 ± 14)	3.0 ± 0.3 (37 ± 2)	5.0 ± 0.2 (32 ± 1)
36	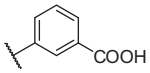	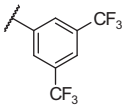	H	H	—	15 ± 6%	11 ± 2 (114 ± 17)	i.a.	i.a.
37	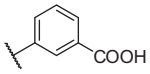	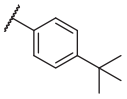	H	H	—	1.3 ± 0.3 (37 ± 3)	3.9 ± 0.5 (348 ± 26)	i.a.	0.28 ± 0.03 (9.4 ± 0.2)
38	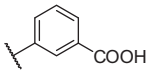	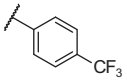	H	H	—	5.8 ± 2.8 (79 ± 15)	8.5 ± 0.5 (384 ± 13)	3.2 ± 0.7 (46 ± 5)	6.9 ± 0.2 (26 ± 1)
39	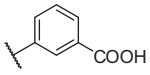	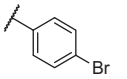	H	H	—	3.6 ± 0.1 (38 ± 1)	4.5 ± 1.9 (58 ± 12)	12 ± 1 (44 ± 2)	3.7 ± 0.9 (14.3 ± 0.9)
40	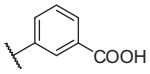	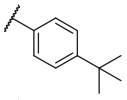	H	H	3-Cl	i.a.	i.a.	i.a.	i.a.
41	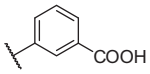	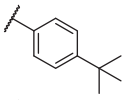	H	H	6-Cl	i.a.	i.a.	i.a.	i.a.
42	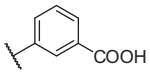	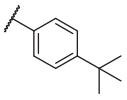	H	H	5-Cl	18 ± 1%	5.4 ± 0.3 (132 ± 5)	i.a.	Antagonistic
43	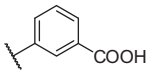	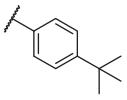	H	H	4-Cl	44 ± 1%	9 ± 1 (256 ± 16)	i.a.	0.12 ± 0.01 (22 ± 1)

Results are expressed as mean ± SEM. n = 3–6; i.a. – inactive (30 μM). Percent values represent the activity at 10 μM when no EC_{50} value could be determined.

binding pocket of PPARδ next to the anthranilic acid core structure we therefore also prepared chlorinated analogues (**58**–**60**) of **38** which had shown activity on PPARδ (Table 5).

Chlorination of the central aromatic moiety of **38** in 6-position (**58**) led to inactivity on all PPARs and FXR. An additional chlorine atom in 5-position (**59**) or in 4-position (**60**) reduced the potency on PPARα and PPARδ while the activity on PPARγ was hardly affected. In contrast, the additional chlorine substituent in 4-position (**60**) led to a slight improvement of the activity on FXR. Hence, these results are in congruence with the activity of the first series of chlorinated compounds **40**–**43** but offered no opportunity to improve the activity profile for PPARδ.

When the best residues for PPARδ so far, in particular the 3-aminophenylacetic acid and the 4-trifluoromethylbenzoyl moiety, were combined in **61**, potency on PPARδ was improved as expected (Table 5). **61** exhibited potent PPARδ partial agonism but was also active on PPARα, PPARγ and FXR. Interestingly, when **61** was enlarged on either side by elongation of the acidic side chain (**62**) or by replacement of the trifluoromethyl group with a phenyl substituent (**63**), the partial agonistic activity was turned into PPARδ-superagonism of up to 175% of L165,041 (**16**). **63** was however similarly potent on PPARα and PPARγ and constitutes a potent pan-PPAR superagonist with low micromolar EC_{50} values for each PPAR subtype.

We finally tried to shift the activity towards preference for PPARδ by varying the acyl substituent of **61** and replaced the 4-trifluoromethylbenzoyl residue with similar 4-substituted benzoyl groups. Larger and less lipophilic 4-substituents such as a methylmercapto group (**64**) and a trifluoromethylmercapto residue (**65**) also led to unselective activity on all PPAR subtypes while the small polar 4-cyanobenzoyl derivative **66** was inactive on all receptors. A 4-methoxybenzoyl residue (**67**) however generated a potent partial PPARδ agonist that was selective over FXR (inactive) and preferential over PPARα and PPARγ (EC_{50} >15 μM). Interestingly, the introduction of another methoxy group in 3-position (**68**) of the acyl substituent led to inactivity. The highest potency and selectivity on PPARδ was achieved by introduction of a large lipophilic 2-naphthoyl residue (**69**) as acyl substituent which generated potent PPARδ superagonism (147%) with an EC_{50} value of 1.3 μM. **69** was preferential for PPARδ over PPARα (factor 11) and PPARγ (factor 13) and selective over FXR since **69** showed only low partial agonism on FXR.

Table 4
In vitro activity of compounds **44**–**57** in reporter gene assays for PPARs and FXR

#	R_1	R_2	R_3	R_4	R_5	EC_{50} [μM] (max. rel activation [%]) PPARα	PPARγ	PPARδ	FXR
37	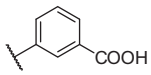	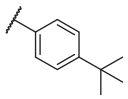	H	H	—	1.3 ± 0.3 (37 ± 3)	3.9 ± 0.5 (348 ± 26)	i.a.	0.28 ± 0.03 (9.4 ± 0.2)
44	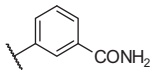	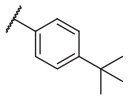	H	H	—	i.a.	i.a.	i.a.	0.07 ± 0.01 (15 ± 1)
45	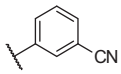	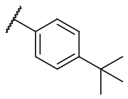	H	H	—	i.a.	i.a.	i.a.	0.23 ± 0.05 (18 ± 1)
46	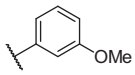	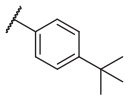	H	H	—	i.a.	i.a.	i.a.	0.38 ± 0.06 (13 ± 1)
47	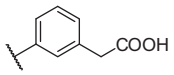	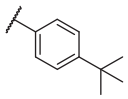	H	H	—	4.4 ± 0.5 (155 ± 11)	6.2 ± 0.8 (121 ± 1)	5.4 ± 0.3 (46 ± 1)	0.42 ± 0.13 (26 ± 1)
48	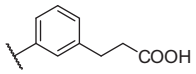	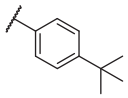	H	H	—	5.4 ± 0.7 (115 ± 12)	5.0 ± 0.8 (175 ± 23)	i.a.	0.06 ± 0.01 (22 ± 1)
49	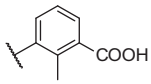	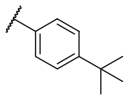	H	H	—	i.a.	13.5 ± 2.2 (70 ± 9)	i.a.	0.042 ± 0.001 (19.0 ± 0.2)
50	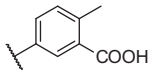	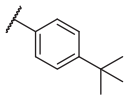	H	H	—	0.21 ± 0.02 (34 ± 1)	5.0 ± 0.2 (98 ± 3)	i.a.	0.045 ± 0.009 (22 ± 1)
51	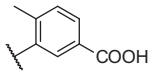	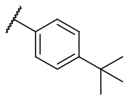	H	H	—	i.a.	6.3 ± 1.3 (163 ± 26)	i.a.	i.a.
52	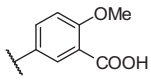	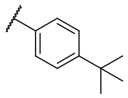	H	H	—	0.74 ± 0.09 (13.7 ± 0.4)	4.4 ± 1.0 (96 ± 12)	i.a.	0.047 ± 0.001 (19 ± 1)
53	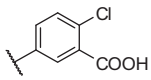	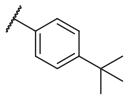	H	H	—	9.1 ± 1.0 (91 ± 6)	5.4 ± 0.3 (98 ± 6)	i.a.	0.28 ± 0.04 (19 ± 1)
54	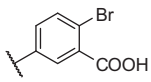	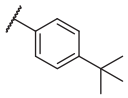	H	H	—	4.1 ± 0.5 (42 ± 4)	6.3 ± 1.1 (82 ± 15)	i.a.	0.15 ± 0.01 (16 ± 1)
55	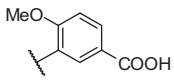	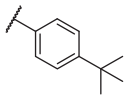	H	H	—	2.9 ± 0.3 (16 ± 1)	4.5 ± 1.6 (154 ± 36)	i.a.	4.7 ± 0.3 (15 ± 1)
56	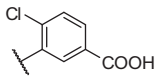	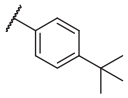	H	H	—	16 ± 4%	1.9 ± 0.5 (154 ± 23)	i.a.	1.1 ± 0.3 (16 ± 1)
57	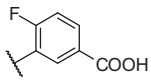	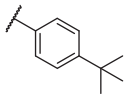	H	H	—	17 ± 2%	5.8 ± 1.6 (735 ± 112)	i.a.	0.48 ± 0.14 (12 ± 1)

Results are expressed as mean ± SEM. n = 3–6; i.a. – inactive (30 μM). Percent values represent the activity at 10 μM when no EC_{50} value could be determined.

Summing up, we identified distinct molecular determinants to modulate the activity of acyl anthranilamide derivatives on different metabolic nuclear receptors which are displayed in Figure 1. In addition, we discovered valuable lead structures for the development of PPARγ superagonists (**51**), PPARδ (super)agonists (**69**) and pan-PPAR (super)agonists (**63**) as well as a potent dual PPARα/FXR partial agonist (**50**) as pharmacological tool for in vitro or in vivo studies.

Table 5
In vitro activity of compounds **58**–**69** in reporter gene assays for PPARs and FXR

#	R_1	R_2	R_3	R_4	R_5	EC_{50} [μM] (max. rel activation [%]) PPARα	PPARγ	PPARδ	FXR
38	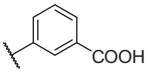	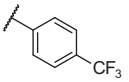	H	H	–	5.8 ± 2.8 (79 ± 15)	8.5 ± 0.5 (384 ± 13)	3.2 ± 0.7 (46 ± 5)	6.9 ± 0.2 (26 ± 1)
58	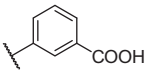	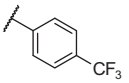	H	H	6-Cl	i.a.	i.a.	i.a.	i.a.
59	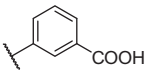	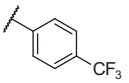	H	H	5-Cl	25 ± 2%	4.7 ± 1.4 (415 ± 49)	6.3 ± 0.4 (24 ± 1)	3.4 ± 0.5 (16.9 ± 0.5)
60	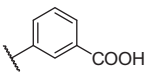	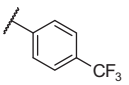	H	H	4-Cl	18.6 ± 0.5 (255 ± 11)	8.7 ± 1.3 (420 ± 49)	3.4 ± 0.3 (16.5 ± 0.5)	2.1 ± 0.3 (17.8 ± 1.0)
61	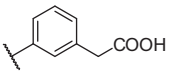	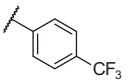	H	H	–	5.4 ± 1.4 (69 ± 9)	9.4 ± 3.4 (161 ± 37)	2.2 ± 0.1 (58 ± 1)	2.60 ± 0.02 (14.8 ± 0.1)
62	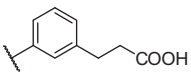	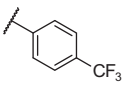	H	H	–	5.9 ± 0.4 (101 ± 1)	6.9 ± 0.3 (70 ± 3)	6.8 ± 2.2 (120 ± 23)	2.3 ± 0.1 (13.0 ± 0.1)
63	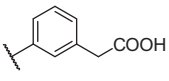	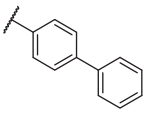	H	H	–	3.0 ± 0.2 (109 ± 5)	2.6 ± 0.2 (125 ± 7)	6.4 ± 1.0 (175 ± 23)	0.7 ± 0.1 (18.8 ± 0.3)
64	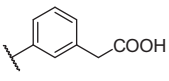	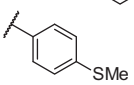	H	H	–	14.4 ± 3.6 (250 ± 47)	17.4 ± 1.7 (200 ± 15)	7.4 ± 0.6 (133 ± 6)	8.5 ± 2.0 (16.9 ± 1.3)
65	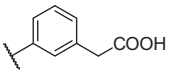	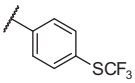	H	H	–	1.3 ± 0.2 (73 ± 3)	4.4 ± 0.1 (158 ± 2)	2.3 ± 0.5 (64 ± 6)	7.0 ± 2.5 (23 ± 2)
66	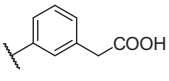	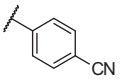	H	H	–	i.a.	i.a.	i.a.	i.a.
67	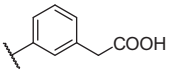	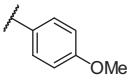	H	H	–	17.3 ± 0.2%	13.2 ± 0.6%	5.9 ± 0.5 (54 ± 2)	i.a.
68	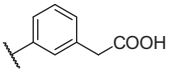	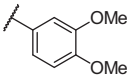	H	H	–	i.a.	i.a.	i.a.	i.a.
69	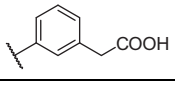	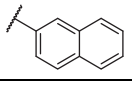	H	H	–	14.4 ± 2.5 (248 ± 22)	18.0 ± 4.7 (335 ± 58)	1.3 ± 0.1 (147 ± 3)	2.5 ± 0.2 (20.9 ± 0.3)

Results are expressed as mean ± SEM. n = 3–6; i.a. – inactive (30 μM). Percent values represent the activity at 10 μM when no EC_{50} value could be determined.

2.4. In vitro characterization of optimized compounds

To further characterize the properties of these 4 promising compounds, we expanded their in vitro profile and determined aqueous solubility, metabolic stability and in vitro toxicity.

The compounds showed a low aqueous solubility of around 1–2 mg/L but offer the possibility to improve their solubility by a salt formation of the free carboxylic acid. For the evaluation of metabolic stability, we selected **69** as model substance since with its naphthyl partial structure it offers the most points of attack for metabolism and ought to be the least stable derivative amongst the optimized compounds. **69** still showed high metabolic stability in vitro with 80.5 ± 0.3% of the compound remaining after 60 min. It can be assumed by their molecular structure that **50**, **51** and **63** are at least equally stable. As measured by their potency, **50**, **51**, **63** and **69** furthermore showed little to no toxicity on liver cells in vitro. Compounds **50**, **51** and **69** showed no anti-proliferative effect in the WST-1 assay up to a concentration of 50 μM and only a slight acute toxicity in the LDH assay at 50 μM. **63** was acutely toxic (LDH) and anti-proliferative (WST-1) at 50 μM. (Figs. 2 and 3)

2.5. Receptor ligand docking

To elucidate the binding mode of the most promising compounds **50** and **69** and understand their potency and selectivity, we docked **50** into the PPARα LBD and **69** into the PPARδ LBD.

The LBDs of the three PPAR subtypes PPARα, PPARγ and PPARδ have a sequence identity of 60–70% and form a Y-shaped ligand

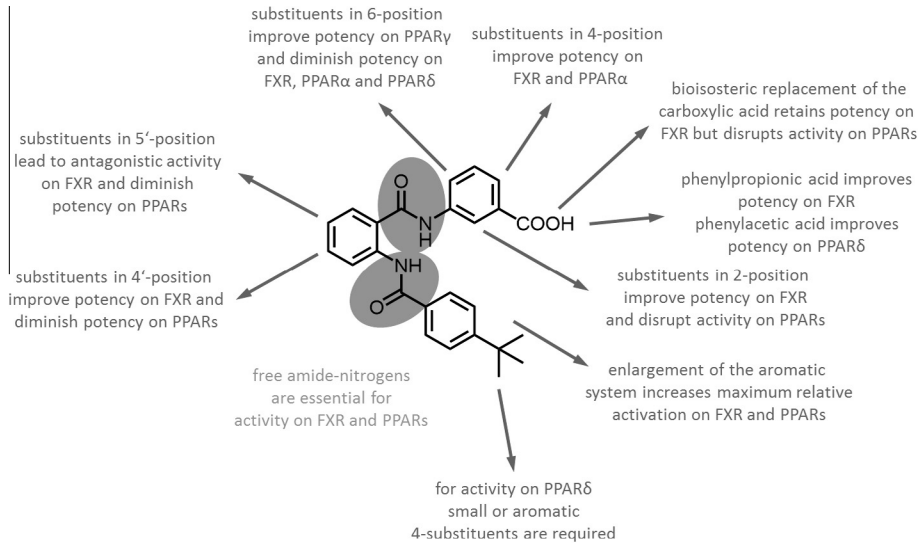

Figure 1. Structure activity relationships of acyl anthranilamides on PPARs and FXR.

binding pocket, that is, defined by three arms. The c-terminal arm I is highly conserved over all PPAR subtypes and offer a hydrogen bond network that complexes the carboxylate group of fatty acids and many synthetic ligands.[23–26] Arm II and arm III are mainly hydrophobic and contain the less conserved amino acids regarding the PPAR subtypes. Subtype selectivity therefore predominantly has to rely on different interactions with these regions of the ligand binding pocket .

For the most potent acyl anthranilamide derivative on PPARδ **69**, molecular docking (Fig. 4) suggests a binding mode similar to the selective PPARδ agonist **70** (LCI765, EC_{50} = 70 nM) (Scheme 4) which is co-crystallized with the PPARδ LBD (PDB code: 2J14).[27,28] **69** was placed in the Y-shaped pocket with its carboxylic head group forming potent hydrogen bonds to the side chains of H_{287}, H_{413}, T_{253} (not shown) and Y_{437}. The docking indicates that the length of the acidic side chain is important and that a shorter (benzoic acid, e.g., **38**, **30**) or longer (phenylpropionic acid, e.g., **62**) side chain cannot equally interact with H_{287}, H_{413}, T_{253} and Y_{437}. Further polar interactions incorporate the amide oxygen of the head group and the amide nitrogen of the acyl substituent which both form hydrogen bonds with the side chain of C_{249}. The lipophilic 2-naphthoyl residue is buried in arm II and interplays especially with V_{312} via hydrophobic contacts.

According to Batista et al.,[26] subtype selectivity for PPARδ can be achieved especially via the hydrophobic tail of ligands. They suggest that large and bulky lipophilic substituents with short linkers improve the selectivity for PPARδ since there are two lipophilic amino acids in arm II of the ligand binding pocket that differ from subtype to subtype.

While these amino acids are V_{312} and I_{328} in PPARδ at the same positions bulkier amino acids are found in PPARα (I_{339} and M_{355}) and in PPARγ (M_{376} and M_{392}). Due to these larger amino acids, PPARα and PPARγ might have difficulties in accommodating bulkier residues in arm II which seems also true for **69**, that is, preferential for PPARδ.

The selective PPARδ ligands **70** and **71** (GW0742, EC_{50} = 1 nM) (Scheme 4)[26] display a 3-fluoro-4-trifluoromethylbenzyl substituent in **71** and a 2,4-dichlorophenyl residue in **70** as lipophilic tails that both occupy arm II of the PPARδ ligand binding pocket (Fig. 5). The 3-fluoro-4-trifluoromethylphenyl residue of **71** is contained in our derivative **35** which also constitutes a potent though non-selective PPARδ ligand. The monocyclic system of **35** might however be too short to fill the pocket entirely which can explain the higher potency of 2-naphthyl derivative **69**. Eventually, the potency and selectivity of **69** could still be further improved by expanding the already bulky 2-naphthoyl moiety with lipophilic substituents such as fluorine, chlorine or trifluoromethyl residues. The inactivity of 3,4-dimethoxy derivative **68** indicates that the pocket of arm II requires very lipophilic substituents for beneficial interactions with V_{312} and does not tolerate methoxy groups. Additional residues in *ortho*-position to the amide bond might furthermore form steric clashes with the carbonyl group and disturb the coplanar orientation of amide bond and naphthyl system in the docking pose.

Docking (Fig. 6) of the dual PPARα/FXR partial agonist **50** revealed a similar binding mode with the carboxylic acid forming several hydrogen bonds to H_{440}, Y_{464}, S_{280} and Y_{314} while the rest of the molecule bound via hydrophobic contacts. The improvement in potency, that is, achieved by methylation in 4-position of the head group might emanate from lipophilic interactions between the methyl group of **50** and V_{444}. This contact might furthermore explain the selectivity for PPARα over PPARγ, that is, gained by methylation since at the tip of arm I PPARα offers the largest binding pocket with the relatively small V_{444}. PPARγ (L_{453}) and PPARδ (M_{417}) both display larger amino acids in the same position that diminish the size of the sub-pocket where the methyl group of **50** is placed. In addition, the additional methyl group via steric hindrance forces the carboxylic acid out of the plane of the aromatic ring which might also have an impact on receptor binding.

3. Discussion and outlook

We here report the discovery of the selective PPARγ superagonist **51**, the dual PPARα/FXR partial agonist **50**, the pan PPAR superagonist **63** and the PPARδ superagonist **69**. Compounds **51**, **63** and **69** can serve as potent lead structures for further optimization of their potency which according to our docking studies should be possible. Future optimization studies should also address an improvement of the compounds' aqueous solubility and, in case of **63**, toxicity since **63** showed substantial toxic effects starting from 50 μM.

The dual PPARα/FXR partial agonist **50** already possesses nanomolar potency on both targets, is selective over the other PPAR subtypes and displays low toxicity as measured by its potency. The high lipophilicity ($c\log P$ = 5.8) of the compound accounts for a quite low aqueous solubility of 4.9 μM which is still more than

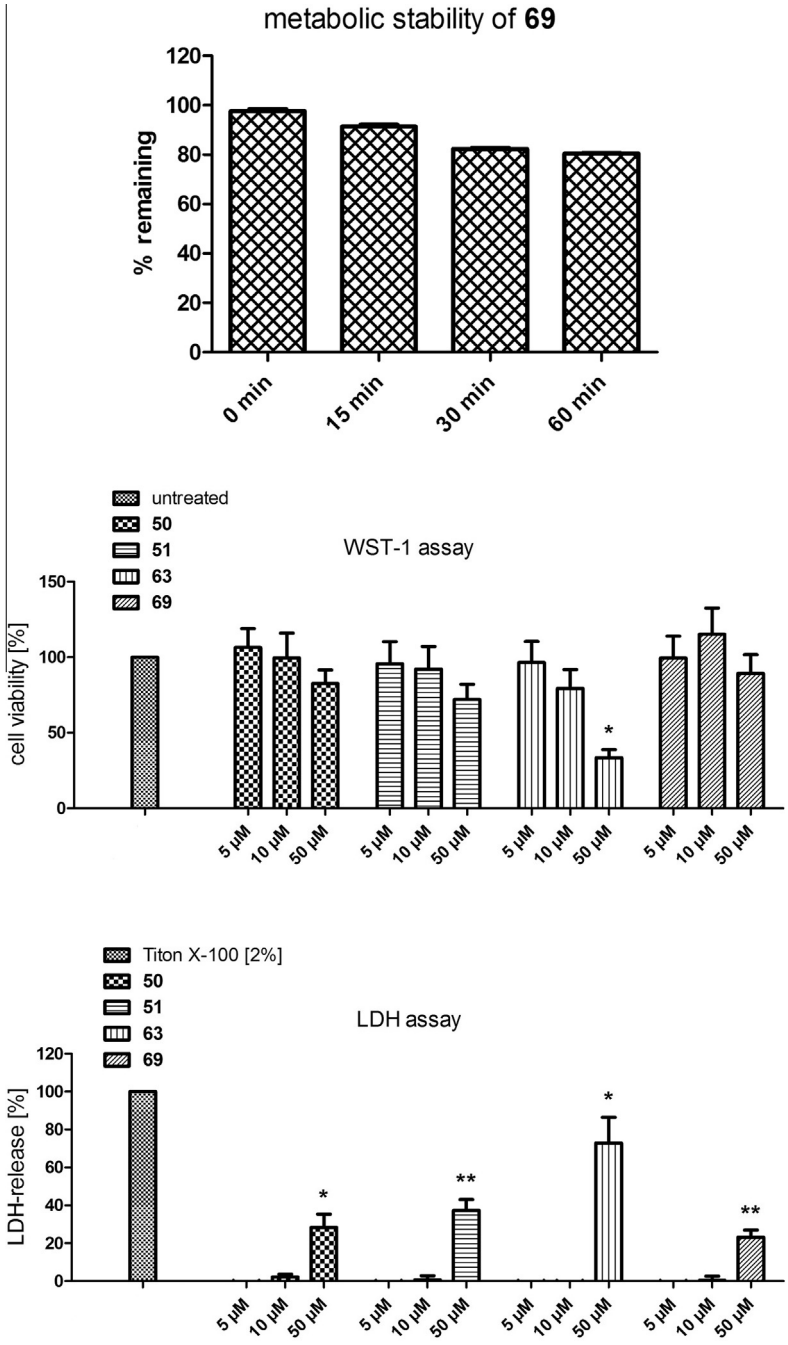

Figure 2. In vitro data of compounds **50**, **51**, **63** and **69**.

20-fold its worst EC_{50} value and probably sufficient for in vivo efficiency. However, the possible salt formation of the free carboxylic acid offers an opportunity to improve the compounds solubility. **50** might be useful to investigate eventual synergistic effects of slight FXR and PPARα activation on lipid profiles in vivo since both receptors play an important role in the regulation of lipid transport and metabolism.

The lipid-lowering and anti-atherosclerotic effects of PPARα are well-known and include amongst others the induction of target genes such as lipoprotein lipase (LPL), fatty acid transporters (FATP2, FATP4) and binding proteins (FATBP1), cholesterol transporters (SCARB1, ABCA1) and enzymes converting fatty acids into acetyl-CoA derivatives (acetyl-CoA synthases ACSL1, ACSL5).[29,30] FXR activation affects lipid metabolism by induction of, for example, the low-density lipoprotein receptor (LDL-R), the very low-density lipoprotein receptor (VLDL-R) and syndecan-1.[31] Via its target gene small hetero-dimer partner (SHP) FXR furthermore represses the sterol-regulatory-element-binding protein 1c (SREBP-1c) which controls lipogenic genes such as the fatty acid synthase (FAS).[31] FXR-SHP-dependent repression of SREBP-1c together with the induction of LDL-R, VLDL-R and syndecan-1 might beneficially amend the lipid-lowering effects of PPARα activation. In addition, PPARα itself is a target gene of FXR.[31]

Excessive supply of dietary fat and glucose induce several metabolic abnormalities such as obesity, type II diabetes and metabolic syndrome with increasing risk of cardiovascular diseases.[32] Also liver diseases such as NASH are due to lipid overload and inflammation. So far therapeutic intervention concentrates on lifestyle

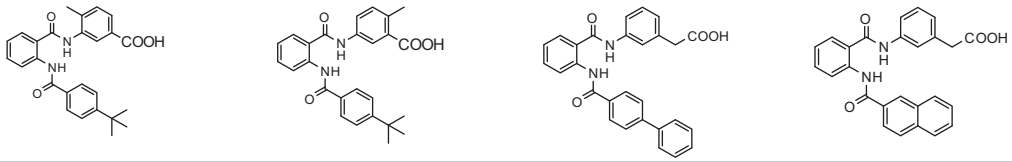

#	51	50	63	69
activity EC_{50} [μM] (max.act.[%])	PPARγ: 6.3±1.3 (163±26)	PPARα: 0.21±0.02 (34±1) FXR: 0.045±0.009 (22±1)	PPARα: 3.0±0.2 (109±5) PPARγ: 2.6±0.2 (125±7) PPARδ: 6.4±1.0 (175±23)	PPARδ: 1.3±0.1 (147±3)
profile/ selectivity	PPARγ superagonist selective over PPARα, PPARδ and FXR	dual PPARα/FXR partial agonist selective over PPARγ and PPARδ	pan-PPAR (super)agonist	PPARδ superagonist preferential over PPARα, PPARγ and FXR
toxicity (HepG)	not anti-proliferative up to 50 μM slightly toxic ≥ 50 μM	not anti-proliferative up to 50 μM slightly toxic ≥ 50 μM	anti-proliferative ≥ 50 μM toxic ≥ 50 μM	not anti-proliferative up to 50 μM slightly toxic ≥ 50 μM
aq. solubility [mg/L] ([μM])	1.1 (2.6)	2.1 (4.9)	0.8 (1.7)	2.5 (6.0)
metabolic stability	n.d.	n.d.	n.d.	80.5±0.3% left after 60 min
clogP	5.8	5.8	4.9	4.2
LipE	-0.6	0.8	0.6	1.7
SILE	0.17	0.22	0.17	0.20
tPSA	95.5	95.5	95.5	95.5

Figure 3. Most potent compounds **50**, **51**, **63** and **69** with their physicochemical and in vitro properties (n.d. – not detected).

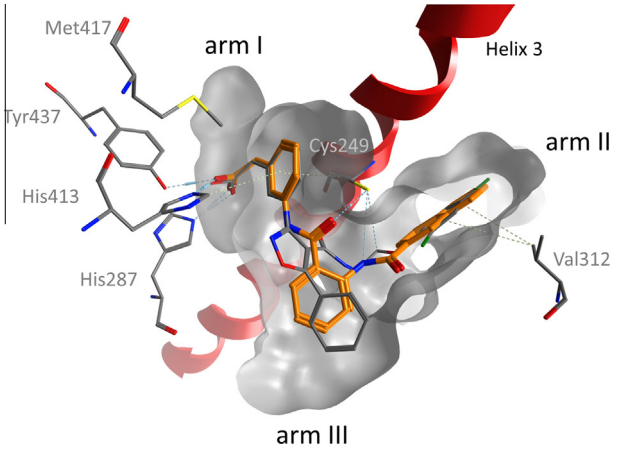

Figure 4. Docking conformation of compound **69** with hPPARδ: **69** (orange) forms a comparable binding pose as the co-crystallized ligand **70** (grey) within the LBD of PPARδ (PDB code: 2J14). The hydrogen bond network that holds the carboxylic acid head group consisting of the amino acids Y437, H413, T253 (not shown) and H287 is depicted as well as Helix 3 (red) and the shape of the binding pocket (grey).

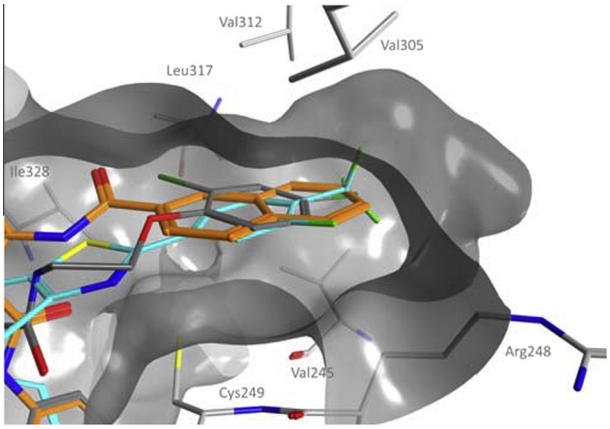

Figure 5. Hydrophobic arm II of PPARδ with compound **69** and two selective PPARδ agonists: The co-crystallized ligand **70** (grey, PDB code: 2J14), compound **69** (orange) and the superposed, co-crystallized structure of GW0742 (**71**, blue, PDB code: 3TKM, protein not shown) all reveal a large lipophilic moiety binding in arm II. The docking pose of **69** suggests that with additional lipophilic substituents at the naphthyl residue, the compounds potency on PPARδ could eventually be further improved.

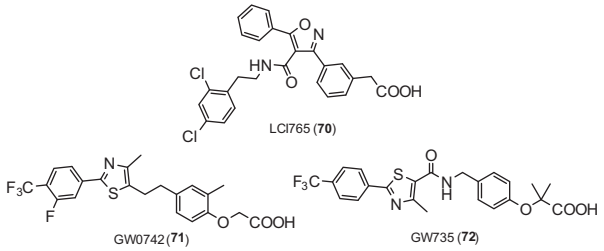

Scheme 4. Co-crystallized PPARδ ligands LCI765 (**70**) and GW0742 (**71**) and co-crystallized PPARα ligand GW735 (GW590735, **72**).

changes and pharmacological treatment of single symptoms. To overcome the problem of polypharmacy the development of new compounds which aim more than one target seems worthwhile.[33] A dual PPARα/FXR agonist such as **50** might favorably combine the liver protective and triglyceride lowering effects of FXR activation with the anti-inflammatory and lipid-lowering activity of PPARα and offer a new treatment strategy for lipid associated metabolic abnormalities.

In summary, we have further extended the SAR of acylanthranilamides as nuclear receptor ligands and show that their potency can be optimized not only towards FXR[19,20] but also towards all PPAR subtypes. With their variable activity on nuclear receptors, good stability and preferable drug-like properties, acylanthranilamides display a potent compound class for further in vitro and in vivo characterization.

4. Experimental

4.1. General

All chemicals and solvents were of reagent grade and used without further purification, unless otherwise specified. ^{1}H NMR and ^{13}C NMR spectra were measured in DMSO-d_6, on a Bruker AV 500, Bruker AV 400, Bruker AV 300 or Bruker am250xp

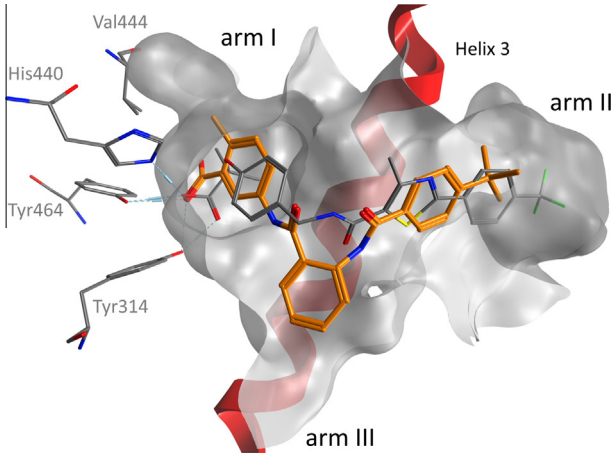

Figure 6. Docking conformation of compound **50** with the hPPARα-LBD (derived from the co-crystal structure of GW735 (**72**), grey, PDB code: 2P54): The carboxylic acid head group of **50** (orange) is complexed by the hydrogen network of H440, Y464, S280 (not shown) and Y314. The methyl group in 6-position of the head group fills a small pocket near V444 which might explain the selectivity of **50**. In PPARγ(L453) and PPARδ(M417) V444 of PPARα is substituted by larger amino acids that limit the pocket at the tip of arm I. (Helix 3 (red); shape of the binding pocket (grey).)

spectrometer. Chemical shifts are reported in parts per million (ppm) with tetramethylsilane (TMS) as an internal standard. Mass spectra were obtained on a Fisons Instruments VG Plattform II measuring in the positive- or negative-ion mode (ESI-MS system). The purity of the final compounds was determined by combustion analysis, which was performed by the Microanalytical Laboratory of the Institute of Organic Chemistry and Chemical Biology, Goethe-University Frankfurt, on an Elementar Vario Micro Cube. All tested compounds described here had a purity ⩾95%. Intermediates were not analyzed.

4.2. Synthesis

4.2.1. General procedures

4.2.1.1. *ortho*-Aminobenzoylation with isatoic anhydride derivatives (a1/a2). (a1) Isatoic anhydride derivative (**7**, 1.0 equiv) and 4-*N*,*N*-dimethylaminopyridine (**9**, 0.1 equiv) were dissolved in a mixture of pyridine (2 mL/mmol **7**) and DMF (0.5 mL/mmol **7**) and heated to 80 °C. After a clear brown solution had formed, the respective aniline derivative (**8**, 1.1 equiv) was added in one portion. With addition of NEt_3 (0.5 mL/mmol **7**) the formation of carbon dioxide started. The reaction mixture was kept at 80 °C for 16 h. Then the solvents were evaporated in vacuum and the crude product was dissolved in ethyl acetate. The organic phase was washed twice with 10% hydrochloric acid and brine and dried over Na_2SO_4. Further purification was performed by recrystallization or column chromatography on silica.

(a2) Aniline derivative (**8**, 1.0 equiv) was dissolved in EtOH (abs, 5 mL/mmol **8**) and heated to reflux. When the mixture had cleared and reached at least 80 °C isatoic anhydride derivative (**7**, 2.0 equiv) was added in one portion with the immediate formation of carbon dioxide. The reaction mixture was stirred under reflux for 60 min. After cooling to room temperature, volume was reduced in vacuum until crystallization of the product initiated and the crude product was filtered off. When no crystallization was possible, the crude product was partitioned between ethyl acetate and 10% hydrochloric acid, the aqueous layer was extracted with additional ethyl acetate three times, the combined organic layers were dried over Na_2SO_4 and solvent was evaporated in vacuum. The crude product was further purified by recrystallization or column chromatography on silica.

4.2.1.2. *ortho*-Nitrobenzoylation with benzoic acid derivatives (b). *ortho*-Nitrobenzoic acid derivative (**10**, 1.0 equiv) was dissolved in CH_2Cl_2 (abs, 5 mL/mmol **10**) and DMF (abs, 0.1 mL/mmol **10**). Thionyl chloride (1.3 equiv) was added slowly at room temperature and the mixture was stirred 4 h under reflux. Solvents were evaporated in vacuum and the crude product (**11**) was dried in ultra-vacuum. Without further purification the crude product (**11**) was used for reaction with aniline derivatives (**8**): for this purpose, the aniline derivative (**8**, 1.3 equiv) was dissolved in CH_2Cl_2 (abs, 5 mL/mmol **8**) and pyridine (abs, 1 mL/mmol **8**) and the crude *ortho*-nitrobenzoyl chloride derivative (**11**) in CH_2Cl_2 (abs, 5 mL/mmol **8**) was added drop wise. The mixture was stirred at room temperature until TLC indicated consumption of starting material (4–12 h). The reaction mixture was then poured into an equal volume 10% hydrochloric acid, phases were separated and the aqueous phase was extracted three times with ethyl acetate. Combined organic layers were dried over Na_2SO_4 and solvent was evaporated in vacuum. Further purification was performed by recrystallization or column chromatography on silica.

4.2.1.3. Reduction of *ortho*-nitrobenzoylaniline derivatives (c). *ortho*-Nitrobenzoylaniline derivative (**12**, 1.0 equiv) was dissolved in THF (abs, 10 mL/mmol **12**), Tin (3.5 equiv) was added and the mixture was heated to 50 °C. Hydrochloric acid (36%, 7 equiv) was added slowly, the mixture was stirred under reflux for 60 min, then filtrated, diluted with an equal volume ethyl acetate and washed twice with water. The combined aqueous layers were extracted three times with ethyl acetate and the combined organic layers were dried over Na_2SO_4 and solvent was evaporated in vacuum. Further purification was performed by recrystallization or column chromatography on silica.

4.2.1.4. Acylation of anthranilic acid derivatives (d). Anthranilic acid derivative (**6**, 1.0 equiv) was dissolved in THF (3 mL/mmol **6**) and pyridine (3.0 equiv) was added. After a clear solution had formed, the respective acyl chloride (**13**, 1.3 equiv) was added in THF (2 mL/mmol **6**). The reaction mixture was kept at room temperature for 4–8 h and the reaction progress was monitored by TLC. When the anthranilic acid intermediate (**6**) was consumed, the reaction mixture was diluted with ethyl acetate, washed three times with 10% hydrochloric acid and dried over Na_2SO_4. Further purification was performed by column chromatography on silica and recrystallization.

4.2.1.5. Alkaline ester hydrolysis (e). The respective ester was dissolved in THF (9 mL/mmol) and aqueous LiOH solution (10%, 1 mL/mmol) was added slowly. The mixture was then stirred at room temperature or at 40 °C until TLC indicated complete conversion of the starting material (12–24 h). The mixture was then poured into 10% aqueous hydrochloric acid, an equal volume of ethyl acetate was added and phases were separated. The aqueous layer was extracted three times with ethyl acetate, the combined organic layers were dried over Na_2SO_4 and solvent was evaporated in vacuum. Further purification was performed by recrystallization or column chromatography on silica.

4.3. Analytical data

Analytical data and preparation of all intermediates and test compounds **18**–**57** has already been reported.[19,20]

4.3.1. 3-(6-Chloro-2-(4-(trifluoromethyl)benzamido)benzamido) benzoic acid (58)

Preparation according to general procedure (d) using 3-(2-amino-6-chlorobenzamido)benzoic acid and 4-(trifluoromethyl) benzoyl chloride. The crude product was purified by column

chromatography on silica with hexane/ethyl acetate/acetic acid (79:19:2) as mobile phase to obtain **58** as colorless solid in 77% yield. ^{1}H NMR (500 MHz, DMSO) δ = 12.96 (s, 1H), 10.58 (s, 1H), 10.48 (s, 1H), 8.32 (s, 1H), 8.11 (d, J = 8.1 Hz, 2H), 7.89 (d, J = 8.2 Hz, 2H), 7.86 (d, J = 8.3 Hz, 1H), 7.77 (d, J = 8.0 Hz, 1H), 7.67 (d, J = 7.5 Hz, 1H), 7.64 (d, J = 7.7 Hz, 1H), 7.51 (t, J = 7.9 Hz, 1H), 7.43 (t, J = 7.9 Hz, 1H) ppm. ^{13}C NMR (126 MHz, DMSO) δ = 167.59, 165.47, 165.13, 139.84, 138.18, 137.28, 133.19, 132.88, 131.81, 131.67, 129.38, 129.06, 128.71, 127.78, 125.99, 125.97, 125.43, 124.91, 124.41, 123.27, 121.10 ppm. $C_{22}H_{14}ClF_3N_2O_4$. MS (ESI−): m/z 462.0 ([M−H]$^-$, 100). Combustion analysis: measured (calculated): C 57.22 (57.10); H 3.07 (3.05); N 5.91 (6.05).

4.3.2. 3-(5-Chloro-2-(4-(trifluoromethyl)benzamido)benzamido) benzoic acid (59)

Preparation according to general procedure (d) using 3-(2-amino-5-chlorobenzamido)benzoic acid and 4-(trifluoromethyl) benzoyl chloride. The crude product was purified by column chromatography on silica with hexane/ethyl acetate/acetic acid (79:19:2) as mobile phase to obtain **59** as colorless solid in 75% yield. ^{1}H NMR (500 MHz, DMSO) δ = 12.99 (s, 1H), 11.46 (s, 1H), 10.76 (s, 1H), 8.32–8.30 (m, 1H), 8.29 (d, J = 8.9 Hz, 1H), 8.10 (d, J = 8.2 Hz, 2H), 7.98 (t, J = 3.1 Hz, 1H), 7.96 (t, J = 6.4 Hz, 3H), 7.73–7.69 (m, 2H), 7.49 (t, J = 7.9 Hz, 1H) ppm. ^{13}C NMR (126 MHz, DMSO) δ = 167.55, 166.25, 164.28, 139.20, 138.56, 137.06, 132.18, 132.12, 131.73, 129.41, 129.19, 128.64, 128.36, 126.80, 126.37, 125.50, 125.48, 124.57, 123.21, 122.16 ppm. $C_{22}H_{14}ClF_3N_2O_4$. MS (ESI−): m/z 461.9 ([M−H]$^-$, 100). Combustion analysis: measured (calculated): C 57.29 (57.10); H 3.33 (3.05); N 6.02 (6.05).

4.3.3. 3-(4-Chloro-2-(4-(trifluoromethyl)benzamido)benzamido) benzoic acid (60)

Preparation according to general procedure (d) using 3-(2-amino-4-chlorobenzamido)benzoic acid and 4-(trifluoromethyl) benzoyl chloride. The crude product was purified by column chromatography on silica with hexane/ethyl acetate/acetic acid (79:19:2) as mobile phase to obtain **60** as colorless solid in 71% yield. ^{1}H NMR (500 MHz, DMSO) δ = 13.04 (s, 1H), 11.74 (s, 1H), 10.76 (s, 1H), 8.48 (d, J = 2.1 Hz, 1H), 8.30 (d, J = 1.6 Hz, 1H), 8.10 (d, J = 8.2 Hz, 2H), 7.97 (dd, J = 10.2, 5.5 Hz, 4H), 7.75–7.69 (m, 1H), 7.50 (t, J = 7.9 Hz, 1H), 7.44 (dd, J = 8.5, 2.2 Hz, 1H) ppm. ^{13}C NMR (126 MHz, DMSO) δ = 167.55, 166.96, 164.40, 139.84, 139.13, 138.43, 137.00, 131.75, 131.33, 129.44, 128.62, 126.43, 125.66, 125.56, 125.35, 124.08, 123.19, 122.82, 122.31, 121.74 ppm. $C_{22}H_{14}ClF_3N_2O_4$. MS (ESI−): m/z 462.0 ([M−H]$^-$, 100). Combustion analysis: measured (calculated): C 57.11 (57.10); H 3.09 (3.05); N 5.69 (6.05).

4.3.4. 2-(3-(2-(4-(Trifluoromethyl)benzamido)benzamido)phenyl) acetic acid (61)

Preparation according to general procedure (d) using 2-(3-(2-aminobenzamido)phenyl)acetic acid and 4-(trifluoromethyl) benzoyl chloride. The crude product was purified by column chromatography on silica with hexane/ethyl acetate/acetic acid (79:19:2) as mobile phase to obtain **61** as colorless solid in 69% yield. ^{1}H NMR (500 MHz, DMSO) δ = 12.36 (s, 1H), 11.70 (s, 1H), 10.55 (s, 1H), 8.38 (d, J = 8.2 Hz, 1H), 8.11 (d, J = 8.1 Hz, 2H), 7.96 (d, J = 8.3 Hz, 2H), 7.93 (d, J = 7.4 Hz, 1H), 7.63 (dd, J = 14.8, 7.8 Hz, 3H), 7.36–7.28 (m, 2H), 7.04 (d, J = 7.6 Hz, 1H), 3.57 (s, 2H) ppm. ^{13}C NMR (126 MHz, DMSO) δ = 173.06, 167.66, 164.07, 138.97, 138.82, 138.49, 135.95, 132.61, 132.29, 129.53, 128.99, 128.54, 126.42, 125.83, 125.40, 124.36, 124.32, 122.38, 122.32, 119.98, 41.29 ppm. $C_{23}H_{17}F_3N_2O_4$. MS (ESI−): m/z 397.8 ([M−CO$_2$−H]$^-$, 100), 442.0 ([M−H]$^-$, 38). Combustion analysis: measured (calculated): C 62.77 (62.44); H 4.33 (3.87); N 6.22 (6.33).

4.3.5. 3-(3-(2-(4-(Trifluoromethyl)benzamido)benzamido)phenyl) propanoic acid (62)

Preparation according to general procedure (d) using 3-(3-(2-aminobenzamido)phenyl)propanoic acid and 4-(trifluoromethyl) benzoyl chloride. The crude product was purified by column chromatography on silica with hexane/ethyl acetate/acetic acid (79:19:2) as mobile phase to obtain **62** as colorless solid in 65% yield. ^{1}H NMR (500 MHz, DMSO) δ = 12.04 (s, 1H), 11.73 (s, 1H), 10.50 (s, 1H), 8.39 (d, J = 8.2 Hz, 1H), 8.11 (d, J = 8.1 Hz, 2H), 7.96 (t, J = 8.2 Hz, 2H), 7.94–7.90 (m, 1H), 7.63 (td, J = 8.4, 4.1 Hz, 1H), 7.57 (t, J = 7.5 Hz, 1H), 7.54 (s, 1H), 7.33 (td, J = 7.5, 1.0 Hz, 1H), 7.27 (t, J = 7.8 Hz, 1H), 7.02 (d, J = 7.6 Hz, 1H), 2.82 (t, J = 7.6 Hz, 2H), 2.54 (t, J = 7.6 Hz, 2H) ppm. ^{13}C NMR (126 MHz, DMSO) δ = 174.14, 172.49, 167.63, 164.03, 141.83, 138.97, 138.79, 138.52, 132.61, 132.05, 129.51, 129.05, 128.53, 126.43, 126.40, 124.65, 124.30, 122.27, 121.38, 119.41, 35.55, 30.82 ppm. $C_{24}H_{19}F_3N_2O_4$. MS (ESI−): m/z 455.0 ([M−H]$^-$, 100). Combustion analysis: measured (calculated): C 63.04 (63.16); H 4.29 (4.20); N 6.02 (6.14).

4.3.6. 2-(3-(2-([1,1′-Biphenyl]-4-carboxamido)benzamido)phenyl) acetic acid (63)

Preparation according to general procedure (d) using 2-(3-(2-aminobenzamido)phenyl)acetic acid and [1,1′-biphenyl]-4-carbonyl chloride. The crude product was purified by column chromatography on silica with hexane/ethyl acetate/acetic acid (79:19:2) as mobile phase to obtain **63** as colorless solid in 64% yield. ^{1}H NMR (500 MHz, DMSO) δ = 12.38 (s, 1H), 11.75 (s, 1H), 10.57 (s, 1H), 8.51 (d, J = 8.3 Hz, 1H), 8.01 (d, J = 8.3 Hz, 2H), 7.95 (d, J = 7.8 Hz, 1H), 7.89 (d, J = 8.3 Hz, 2H), 7.77 (d, J = 7.6 Hz, 2H), 7.66–7.61 (m, 3H), 7.51 (t, J = 7.6 Hz, 2H), 7.43 (t, J = 7.3 Hz, 1H), 7.32 (dd, J = 16.6, 8.3 Hz, 2H), 7.05 (d, J = 7.6 Hz, 1H), 3.58 (s, 2H) ppm. ^{13}C NMR (126 MHz, DMSO) δ = 173.06, 167.93, 164.75, 144.00, 139.41, 139.16, 138.90, 136.00, 133.69, 132.75, 129.55, 129.02, 128.73, 128.21, 127.60, 127.42, 125.91, 123.76, 123.30, 122.53, 121.78, 120.13, 41.30 ppm. $C_{28}H_{22}N_2O_4$. MS (ESI−): m/z 405.8 ([M−CO$_2$−H]$^-$, 100), 450.0 ([M−H]$^-$, 12). Combustion analysis: measured (calculated): C 74.43 (74.65); H 5.07 (4.92); N 6.14 (6.22).

4.3.7. 2-(3-(2-(4-(Methylthio)benzamido)benzamido)phenyl) acetic acid (64)

Preparation according to general procedure (d) using 2-(3-(2-aminobenzamido)phenyl)acetic acid and 4-(methylthio)benzoyl chloride. The crude product was purified by column chromatography on silica with hexane/ethyl acetate/acetic acid (79:19:2) as mobile phase to obtain **64** as colorless solid in 76% yield. ^{1}H NMR (500 MHz, DMSO) δ = 12.37 (s, 1H), 11.67 (s, 1H), 10.55 (s, 1H), 8.53–8.44 (m, 1H), 7.93 (dd, J = 7.9, 1.3 Hz, 1H), 7.87–7.82 (m, 2H), 7.61 (dd, J = 12.3, 4.9 Hz, 3H), 7.43 (t, J = 5.4 Hz, 2H), 7.32 (t, J = 7.8 Hz, 1H), 7.29 (td, J = 7.8, 1.1 Hz, 1H), 7.05 (d, J = 7.7 Hz, 1H), 3.58 (s, 2H), 2.54 (s, 3H) ppm. ^{13}C NMR (126 MHz, DMSO) δ = 173.07, 167.95, 164.57, 144.30, 139.24, 138.88, 136.01, 132.74, 130.80, 129.52, 129.02, 127.97, 125.92, 125.79, 123.63, 123.10, 122.53, 121.68, 120.12, 41.31, 14.51 ppm. $C_{23}H_{20}N_2O_4S$. MS (ESI−): m/z 375.7 ([M−CO$_2$−H]$^-$, 100), 419.9 ([M−H]$^-$, 72). Combustion analysis: measured (calculated): C 65.72 (65.70); H 4.92 (4.79); N 6.72 (6.66); S 7.85 (7.62).

4.3.8. 2-(3-(2-(4-((Trifluoromethyl)thio)benzamido)benzamido) phenyl)acetic acid (65)

Preparation according to general procedure (d) using 2-(3-(2-aminobenzamido)phenyl)acetic acid and 4-((trifluoromethyl)thio) benzoyl chloride. The crude product was purified by column chromatography on silica with hexane/ethyl acetate/acetic acid (79:19:2) as mobile phase to obtain **65** as colorless solid in 70% yield. ^{1}H NMR (500 MHz, DMSO) δ = 12.29 (s, 1H), 11.71–11.61

(m, 1H), 10.55 (s, 1H), 8.36 (t, J = 6.5 Hz, 1H), 8.07–7.99 (m, 2H), 7.91 (t, J = 9.7 Hz, 3H), 7.68–7.58 (m, 3H), 7.36–7.27 (m, 2H), 7.04 (d, J = 7.6 Hz, 1H), 3.57 (s, 2H) ppm. ^{13}C NMR (126 MHz, DMSO) δ = 173.07, 167.65, 164.20, 138.98, 138.52, 137.59, 136.75, 135.98, 132.59, 131.17, 129.54, 128.98, 127.54, 125.81, 124.36, 124.27, 122.37, 122.30, 119.95, 41.32, 21.54 ppm. $C_{23}H_{17}F_3N_2O_4S$. MS (ESI−): m/z 429.8 ([M−CO_2−H]$^-$, 100), 474.0 ([M−H]$^-$, 77). Combustion analysis: measured (calculated): C 57.84 (58.23); H 3.77 (3.61); N 5.94 (5.90); S 6.84 (6.76).

4.3.9. 2-(3-(2-(4-Cyanobenzamido)benzamido)phenyl)acetic acid (66)

Preparation according to general procedure (d) using 2-(3-(2-aminobenzamido)phenyl)acetic acid and 4-cyanobenzoyl chloride. The crude product was purified by column chromatography on silica with hexane/ethyl acetate/acetic acid (79:19:2) as mobile phase to obtain **66** as colorless solid in 82% yield. ^{1}H NMR (500 MHz, DMSO) δ = 12.18 (s, 1H), 11.67 (s, 1H), 10.55 (s, 1H), 8.34 (d, J = 7.9 Hz, 1H), 8.06 (s, 4H), 7.96–7.88 (m, 1H), 7.68–7.56 (m, 3H), 7.33 (ddd, J = 15.1, 9.5, 4.4 Hz, 2H), 7.04 (d, J = 7.6 Hz, 1H), 3.57 (s, 2H) ppm. ^{13}C NMR (126 MHz, DMSO) δ = 173.07, 172.50, 167.60, 163.86, 139.02, 138.98, 138.32, 135.97, 133.41, 132.56, 129.54, 129.00, 128.46, 125.82, 124.63, 124.44, 122.44, 122.36, 119.96, 118.70, 114.67, 41.31 ppm. $C_{23}H_{17}N_3O_4$. MS (ESI−): m/z 354.7 ([M−CO_2−H]$^-$, 100); 398.8 ([M−H]$^-$, 44). Combustion analysis: measured (calculated): C 69.22 (69.17); H 3.98 (4.29); N 10.70 (10.52).

4.3.10. 2-(3-(2-(4-Methoxybenzamido)benzamido)phenyl)acetic acid (67)

Preparation according to general procedure (d) using 2-(3-(2-aminobenzamido)phenyl)acetic acid and 4-methoxybenzoyl chloride. The crude product was purified by column chromatography on silica with hexane/ethyl acetate/acetic acid (79:19:2) as mobile phase to obtain **67** as colorless solid in 74% yield. ^{1}H NMR (500 MHz, DMSO) δ = 12.36 (s, 1H), 11.62 (d, J = 12.8 Hz, 1H), 10.55 (s, 1H), 8.50 (d, J = 7.8 Hz, 1H), 7.93 (dd, J = 7.9, 1.2 Hz, 1H), 7.91–7.86 (m, 2H), 7.65–7.59 (m, 3H), 7.33 (t, J = 7.8 Hz, 1H), 7.29–7.25 (m, 1H), 7.14–7.09 (m, 2H), 7.05 (d, J = 7.7 Hz, 1H), 3.84 (s, 3H), 3.58 (s, 2H) ppm. ^{13}C NMR (126 MHz, DMSO) δ = 173.06, 168.02, 164.57, 162.69, 139.45, 138.88, 135.98, 132.75, 129.50, 129.42, 129.02, 127.02, 125.92, 123.42, 122.87, 122.53, 121.55, 120.12, 114.66, 55.95, 41.29 ppm. $C_{23}H_{20}N_2O_5$. MS (ESI−): m/z 403.8 ([M−H]$^-$, 100). Combustion analysis: measured (calculated): C 68.22 (68.31); H 5.09 (4.98); N 6.50 (6.93).

4.3.11. 2-(3-(2-(3,4-Dimethoxybenzamido)benzamido)phenyl) acetic acid (68)

Preparation according to general procedure (d) using 2-(3-(2-aminobenzamido)phenyl)acetic acid and 3,4-dimethoxybenzoyl chloride. The crude product was purified by column chromatography on silica with hexane/ethyl acetate/acetic acid (79:19:2) as mobile phase to obtain **68** as colorless solid in 78% yield. ^{1}H NMR (500 MHz, DMSO) δ = 12.36 (s, 1H), 11.67 (s, 1H), 10.55 (s, 1H), 8.49 (d, J = 8.3 Hz, 1H), 7.99–7.90 (m, 1H), 7.67 (s, 1H), 7.65–7.59 (m, 2H), 7.51 (dt, J = 4.3, 1.9 Hz, 2H), 7.32 (t, J = 7.8 Hz, 1H), 7.30–7.25 (m, 1H), 7.15 (d, J = 8.3 Hz, 1H), 7.05 (d, J = 7.6 Hz, 1H), 3.84 (d, J = 1.0 Hz, 6H), 3.57 (s, 2H) ppm. ^{13}C NMR (126 MHz, DMSO) δ = 173.05, 167.98, 164.64, 152.38, 149.09, 139.40, 138.95, 135.98, 132.75, 129.47, 129.00, 127.18, 125.88, 123.44, 122.96, 122.38, 121.47, 120.54, 119.93, 111.83, 110.85, 56.18, 55.90, 41.33 ppm. $C_{24}H_{22}N_2O_6$. MS (ESI−): m/z 434.0 ([M−H]$^-$, 100). Combustion analysis: measured (calculated): C 65.99 (66.35); H 5.13 (5.10); N 6.36 (6.45).

4.3.12. 2-(3-(2-(2-Naphthamido)benzamido)phenyl)acetic acid (69)

Preparation according to general procedure (d) using 2-(3-(2-aminobenzamido)phenyl)acetic acid and 2-naphthoyl chloride. The crude product was purified by column chromatography on silica with hexane/ethyl acetate/acetic acid (79:19:2) as mobile phase to obtain **69** as colorless solid in 67% yield. ^{1}H NMR (500 MHz, DMSO) δ = 12.36 (s, 1H), 11.76 (s, 1H), 10.57 (s, 1H), 8.55 (s, 1H), 8.47 (d, J = 8.2 Hz, 1H), 8.10 (d, J = 8.3 Hz, 2H), 8.02 (d, J = 7.9 Hz, 1H), 7.99–7.93 (m, 2H), 7.69–7.61 (m, 5H), 7.32 (td, J = 7.7, 3.4 Hz, 2H), 7.04 (d, J = 7.6 Hz, 1H), 3.57 (s, 2H) ppm. ^{13}C NMR (126 MHz, DMSO) δ = 173.06, 167.82, 165.24, 139.02, 139.00, 135.97, 134.88, 132.67, 132.64, 132.35, 129.57, 129.52, 129.08, 129.02, 128.57, 128.36, 128.18, 127.55, 125.81, 123.93, 123.90, 122.33, 122.13, 119.90, 41.31 ppm. $C_{26}H_{20}N_2O_4$. MS (ESI−): m/z 423.9 ([M−H]$^-$, 100). Combustion analysis: measured (calculated): C 73.23 (73.57); H 4.74 (4.75); N 6.54 (6.60).

4.4. In vitro biological evaluation

4.4.1. FXR transactivation assay

4.4.1.1. Cell culture. HeLa cells were grown in DMEM high glucose, supplemented with 10% fetal calf serum (FCS), 1 mM sodium pyruvate (SP), penicillin (100 U/mL) and streptomycin (100 μg/mL) at 37 °C and 5% CO_2.

4.4.1.2. Plasmids for full length FXR transactivation assay. pcDNA3-hFXR contains the sequence of human FXR and was already published elsewhere[34], pGL3basic (Promega, Mannheim, Germany) was used as a reporter plasmid, with a shortened construct of the promotor of the bile salt export pump (BSEP, sequence of construct from Ref. 35) cloned into the SacI/NheI cleavage site in front of the luciferase gene. pRL-SV40 (Promega) was transfected as a control for normalization of transfection efficacy and cell growth. pSG5-hRXR was already published elsewhere[36] as well.

4.4.1.3. Full length FXR transactivation assay. 24 h before transfection, HeLa cells were seeded in 96-well plates with a density of 8000 cells per well. 3, 5 h before transfection, medium was changed to DMEM high glucose, supplemented with 1 mM SP, penicillin (100 U/mL), streptomycin (100 μg/mL) and 0.5% charcoal-stripped FCS. Transient transfection of HeLa cells with BSEP-pGL3, pRL-SV40 and the expression plasmids pcDNA3-hFXR and pSG5-hRXR was carried out using calcium phosphate transfection method. 16 h after transfection, medium was changed to DMEM high glucose, supplemented with 1 mM SP, penicillin (100 U/mL), streptomycin (100 μg/mL) and 0.5% charcoal-stripped FCS. 24 h after transfection, medium was changed to DMEM without phenol red, supplemented with 1 mM SP, penicillin (100 U/mL), streptomycin (100 μg/mL), 2 mM L-glutamine and 0.5% charcoal-stripped FCS, now additionally containing 0.1% DMSO and the respective test compound or 0.1% DMSO alone as untreated control. Each concentration was tested in triplicate wells and each experiment was repeated independently at least three times. Following 24 h incubation with the test compounds, cells were assayed for luciferase activity using Dual-Glo™ Luciferase Assay System (Promega) according to the manufacturer's protocol. Luminescence was measured with a Tecan Infinite M200 luminometer (Tecan Deutschland GmbH, Crailsheim, Germany). Normalization of transfection efficacy and cell growth was done by division of firefly luciferase data by renilla luciferase data resulting in relative light units (RLU). Fold activation was obtained by dividing the mean RLU of the tested compound at a respective concentration by the mean RLU of untreated control. Relative activation was obtained by dividing the fold activation of the tested compound at a respective concentration by the fold activation of FXR full

agonist GW4064 (**17**) at 3 μM. EC_{50} and standard error of the mean values were calculated with the mean relative activation values of at least three independent experiments by SigmaPlot 10.0 (Systat Software GmbH, Erkrath, Germany) using a four parameter logistic regression.

4.4.2. PPAR transactivation assay

4.4.2.1. Cell culture. COS-7 cells were grown in DMEM high glucose, supplemented with 10% FCS, 1 mM sodium pyruvate (SP), penicillin (100 U/mL) and streptomycin (100 μg/mL) at 37 °C and 5% CO_2.

4.4.2.2. Plasmids for PPAR transactivation assay. The Gal4-fusion receptor plasmids pFA-CMV-PPARα-LBD, pFA-CMV-PPARδ-LBD and pFA-CMV-PPARγ-LBD containing the hinge region and ligand binding domain (LBD) for each of the PPAR subtypes, respectively, were constructed by integrating cDNA fragments obtained from PCR amplification of human monocytes into the SmaI/XbaI cleavage site of the pFA-CMV vector (Stratagene, La Jolla, CA, USA) and have already been published.[22] The cDNA fragments consist of bps 499–1407 (NM_005 036), bps 412–1323 (NM_006 238) and bps 610–1518 (NM_015 869) for PPARα, PPARδ and PPARγ, respectively. Frame and sequence of the fusion receptors were verified by sequencing. pFR-Luc (Stratagene) was used as reporter plasmid and pRL-SV40 (Promega) for normalization of transfection efficiency and cell growth.

4.4.2.3. PPAR transactivation assay. The day before transfection, COS-7 cells were seeded in 96-well plates with a density of 30,000 cells per well. Transient transfection was carried out using Lipofectamine LTX reagent (Invitrogen, Carlsbad, CA, USA) according to the manufacturer's protocol with pFR-Luc (Stratagene), pRL-SV40 (Promega) and the Gal4-fusion receptor plasmids (pFA-CMV-hPPAR-LBD) of the respective PPAR subtype. 5 h after transfection, medium was changed to DMEM without phenol red and 10% FCS, supplemented with 1 mM SP, penicillin (100 U/mL), streptomycin (100 μg/mL) and 2 mM L-glutamine, now additionally containing 0.1% DMSO and the respective test compound or 0.1% DMSO alone as untreated control. Each concentration was tested in triplicate wells and each experiment was repeated independently at least three times. Following overnight incubation with the test compounds, cells were assayed for luciferase activity using Dual-Glo™ Luciferase Assay System (Promega) according to the manufacturer's protocol. Luminescence was measured with an Infinite M200 luminometer (Tecan Deutschland GmbH). Normalization of transfection efficacy and cell growth was done by division of firefly luciferase data by renilla luciferase data resulting in relative light units (RLU). Fold activation was obtained by dividing the mean RLU of a test compound at a respective concentration by the mean RLU of untreated control. Relative activation was obtained by dividing the fold activation of a test compounds at a respective concentration by the fold activation of PPARα full agonist GW 7647 (**14**) at 1 μM, PPARδ full agonist L165,041 (**16**) at 1 μM or PPARγ full agonist pioglitazone (**15**) at 1 μM, respectively. EC_{50} and standard error of the mean values were calculated with the mean relative activation values of at least three independent experiments by SigmaPlot 10.0 (Systat Software GmbH) using a four parameter logistic regression.

4.4.3. Cytotoxicity

4.4.3.1. WST-1. WST-1 assay (Roche Diagnostics International AG, Rotkreuz, Schweiz) was performed according to manufacturer's protocol. In brief, HepG2 cells were seeded in DMEM supplemented with 1 mM SP, penicillin (100 U/mL), streptomycin (100 μg/mL) and 10% FCS in 96-well plates (3×10^4 cells/well). After 24 h, medium was changed to DMEM supplemented with penicillin (100 U/mL), streptomycin (100 μg/mL) and 1% FCS and cells were incubated with test compounds (final concentrations 5 μM, 10 μM and 50 μM), Revlotron (100 μM) as positive control, and Zileuton (100 μM) and DMEM/1% DMSO as negative controls. After 48 h, WST reagent (Roche) was added to each well according to manufacturer's instructions. After 45 min incubation absorption (450 nm/reference: 620 nm) was determined with a Tecan Infinite M200 luminometer. Each experiment was repeated four times in triplicates. Results (expressed as mean ± SEM; $n = 4$; untreated = 100%): **50**: 5 μM: 106.4 ± 12.6%; 10 μM: 99.6 ± 16.3%; 50 μM: 82.5 ± 9.0%. **51**: 5 μM: 95.7 ± 14.6%; 10 μM: 92.2 ± 14.9%; 50 μM: 72.0 ± 10.0%. **63**: 5 μM: 96.5 ± 13.9%; 10 μM: 79.5 ± 12.4%; 50 μM: 33.6 ± 5.2%. **69**: 5 μM: 99.5 ± 14.4%; 10 μM: 115.1 ± 17.4%; 50 μM: 89.3 ± 12.4%.

4.4.3.2. LDH. LDH assay (Roche) was performed according to manufacturer's instructions. In brief, HepG2 cells were seeded in DMEM supplemented with 1 mM SP, penicillin (100 U/mL), streptomycin (100 μg/mL) and 10% FCS in 96-well plates (3×10^4 cells/well). After 24 h, medium was changed to DMEM supplemented with penicillin (100 U/mL), streptomycin (100 μg/mL) and 1% FCS and cells were incubated with the respective compounds for 48 h. As positive control TRITON X-100 (2%) was added 2 h before measurement. After incubation, supernatant of each well was transferred into a fresh plate and LDH substrate/reagent was added. After 20 min incubation, absorption at measurement (490 nm) and reference (690 nm) wavelength was determined with a Tecan Infinite M200. All experiments were performed in triplicates and at least in four independent repeats. Results (expressed as mean ± SEM; $n = 4$; untreated = 0%, Triton X-100 (2%) = 100%): **50**: 5 μM: −0.1 ± 2.5%; 10 μM: 2.2 ± 1.4%; 50 μM: 28.4 ± 6.9%. **51**: 5 μM: −1.3 ± 2.2%; 10 μM: 0.7 ± 2.2%; 50 μM: 37.3 ± 5.8%. **63**: 5 μM: −4.5 ± 1.4%; 10 μM: −1.0 ± 1.9%; 50 μM: 72.9 ± 13.5%. **69**: 5 μM: −2.4 ± 1.5%; 10 μM: 0.3 ± 2.3%; 50 μM: 23.3 ± 3.6%.

4.4.4. Metabolism assay

The solubilized test compounds (5 μL, final concentration 10 μM in DMSO) were preincubated at 37 °C in 432 μL of phosphate buffer (0.1 M, pH 7.4) together with a 50 μL NADPH regenerating system (30 mM glucose-6-phosphate, 4 U/mL glucose-6-phosphate dehydrogenase, 10 mM NADP, 30 mM $MgCl_2$). After 5 min, the reaction was started by the addition of 13 μL of microsome mix from the liver of Sprague–Dawley rats (Invitrogen, Darmstadt, Germany; 20 mg protein/mL in 0.1 M phosphate buffer) in a shaking water bath at 37 °C. The reaction was stopped by addition of 250 μL of ice-cold methanol at 0, 15, 30, and 60 min. The samples were diluted with 250 μL of DMSO and centrifuged at 10,000*g* for 5 min at 4 °C. The supernatants were analyzed, and test compounds were quantified by HPLC: mobile phase, MeOH 83%/H_2O 17%/formic acid 0.1%; flow-rate, 1 mL/min; stationary phase, MultoHigh Phenyl phase, 5 μm, 250 × 4 precolumn, phenyl, 5 μm, 20 × 4; detection wavelength, 330 and 254 nm; injection volume, 50 μL. Control samples were performed to check the stability of the compounds in the reaction mixture: first control was without NADPH, which is needed for the enzymatic activity of the microsomes, second control was with inactivated microsomes (incubated for 20 min at 90 °C), third control was without test compounds (to determine the baseline). The amounts of the test compounds were quantified by an external calibration curve, where data are expressed as means ± SEM of single determinations obtained in three independent experiments. The metabolism experiments showed the following curve (expressed as mean ± SEM; $n = 4$): **69**: 0 min: 97.6 ± 0.8%; 15 min: 91.4 ± 0.7%; 30 min: 82.3 ± 0.4%; 60 min: 80.5 ± 0.3%

4.4.5. Molecular docking

Structure preparation and molecular docking studies were carried out using the software package Molecular Operating

Environment (MOE 2013.08).[37] The co-crystallized structures (PDB codes: 2J14[28], 2P54[38]) were protonated by means of the function Protonate 3D and energy minimized using the Amber12:EHT forcefield both implemented in MOE. As a docking placement method the Triangle Matcher was used and to score the generated conformations we used the scoring function Alpha HB. The conformation with lowest score was used to generate the figures.

References and notes

1. Gronemeyer, H.; Gustafsson, J.-Å.; Laudet, V. *Nat. Rev. Drug Disc.* **2004**, *3*, 950.
2. Keller, H.; Dreyer, C.; Medin, J.; Mahfoudi, A.; Ozato, K.; Wahli, W. *Proc. Natl. Acad. Sci. U.S.A.* **1993**, *90*, 2160.
3. Kliewer, S. A.; Sundseth, S. S.; Jones, S. A.; Brown, P. J.; Wisely, G. B.; Koble, C. S.; Devchand, P.; Wahli, W.; Willson, T. M.; Lenhard, J. M.; Lehmann, J. M. *Proc. Natl. Acad. Sci. U.S.A.* **1997**, *94*, 4318.
4. Xu, H. E.; Lambert, M. H.; Montana, V. G.; Parks, D. J.; Blanchard, S. G.; Brown, P. J.; Sternbach, D. D.; Lehmann, J. M.; Wisely, G. B.; Willson, T. M.; Kliewer, S. A.; Milburn, M. V. *Mol. Cell* **1999**, *3*, 397.
5. Forman, B. M.; Chen, J.; Evans, R. M. *Proc. Natl. Acad. Sci. U.S.A.* **1997**, *94*, 4312.
6. Staels, B.; Fruchart, J.-C. *Diabetes* **2005**, *54*, 2460.
7. Staels, B.; Dallongeville, J.; Auwerx, J.; Schoonjans, K.; Leitersdorf, E.; Fruchart, J. C. *Circulation* **1998**, *98*, 2088.
8. Mahaffey, K. W.; Hafley, G.; Dickerson, S.; Burns, S.; Tourt-Uhlig, S.; White, J.; Newby, L. K.; Komajda, M.; McMurray, J.; Bigelow, R.; Home, P. D.; Lopes, R. D. *Am. Heart J.* **2013**, *166*, 240.e1.
9. Neels, J. G.; Grimaldi, P. A. *Physiol. Rev.* **2014**, *94*, 795.
10. Lamers, C.; Schubert-Zsilavecz, M.; Merk, D. *Expert Opin. Ther. Pat.* **2012**, *22*, 803.
11. Sprecher, D. L.; Massien, C.; Pearce, G.; Billin, A. N.; Perlstein, I.; Willson, T. M.; Hassall, D. G.; Ancellin, N.; Patterson, S. D.; Lobe, D. C.; Johnson, T. G. *Arterioscler. Thromb. Vasc. Biol.* **2006**, *27*, 359.
12. Riserus, U.; Sprecher, D.; Johnson, T.; Olson, E.; Hirschberg, S.; Liu, A.; Fang, Z.; Hegde, P.; Richards, D.; Sarov-Blat, L.; Strum, J. C.; Basu, S.; Cheeseman, J.; Fielding, B. A.; Humphreys, S. M.; Danoff, T.; Moore, N. R.; Murgatroyd, P.; O'Rahilly, S.; Sutton, P.; Willson, T.; Hassall, D.; Frayn, K. N.; Karpe, F. *Diabetes* **2007**, *57*, 332.
13. Gupta, R. A.; Wang, D.; Katkuri, S.; Wang, H.; Dey, S. K.; DuBois, R. N. *Nat. Med.* **2004**, *10*, 245.
14. Fiorucci, S.; Mencarelli, A.; Distrutti, E.; Zampella, A. *Future Med. Chem.* **2012**, *4*, 877.
15. Fiorucci, S.; Mencarelli, A.; Distrutti, E.; Palladino, G.; Cipriani, S. *Curr. Med. Chem.* **2010**, *17*, 139.
16. Adorini, L.; Pruzanski, M.; Shapiro, D. *Drug Discovery Today* **2012**, *17*, 988.
17. Pellicciari, R.; Fiorucci, S.; Camaioni, E.; Clerici, C.; Costantino, G.; Maloney, P. R.; Morelli, A.; Parks, D. J.; Willson, T. M. *J. Med. Chem.* **2002**, *45*, 3569.
18. Achenbach, J.; Gabler, M.; Steri, R.; Schubert-Zsilavecz, M.; Proschak, E. *Med. Chem. Commun.* **2013**, *4*, 920.
19. Merk, D.; Gabler, M.; Gomez, R. C.; Flesch, D.; Hanke, T.; Kaiser, A.; Lamers, C.; Werz, O.; Schneider, G.; Schubert-Zsilavecz, M. *Bioorg. Med. Chem.* **2014**, *22*, 2447.
20. Merk, D.; Lamers, C.; Ahmad, K.; Carrasco Gomez, R.; Schneider, G.; Steinhilber, D.; Schubert-Zsilavecz, M. *J. Med. Chem.* **2014**, *57*, 8035.
21. Steri, R.; Kara, M.; Proschak, E.; Steinhilber, D.; Schneider, G.; Schubert-Zsilavecz, M. *Future Med. Chem.* **2010**, *2*, 575.
22. Rau, O.; Wurglics, M.; Paulke, A.; Zitzkowski, J.; Meindl, N.; Bock, A.; Dingermann, T.; Abdel-Tawab, M.; Schubert-Zsilavecz, M. *Planta Med.* **2006**, *72*, 881.
23. Fyffe, S. A.; Alphey, M. S.; Buetow, L.; Smith, T. K.; Ferguson, Michael A. J.; Sørensen, M. D.; Björkling, F.; Hunter, W. N. *J. Mol. Biol.* **2006**, *356*, 1005.
24. Xu, H. E.; Lambert, M. H.; Montana, V. G.; Plunket, K. D.; Moore, L. B.; Collins, J. L.; Oplinger, J. A.; Kliewer, S. A.; Gampe, R. T.; McKee, D. D.; Moore, J. T.; Willson, T. M. *Proc. Natl. Acad. Sci. U.S.A.* **2001**, *98*, 13919.
25. Markt, P.; Schuster, D.; Kirchmair, J.; Laggner, C.; Langer, T. *J. Comput. Aided Mol. Des.* **2007**, *21*, 575.
26. Batista, F.; Trivella, D.; Bernardes, A.; Gratieri, J.; Oliveira, P.; Figueira, A.; Webb, P.; Polikarpov, I. *PLoS ONE* **2012**, *7*, e33643.
27. Epple, R.; Russo, R.; Azimioara, M.; Cow, C.; Xie, Y.; Wang, X.; Wityak, J.; Karanewsky, D.; Gerken, A.; Iskandar, M.; Saez, E.; Seidel, M. H.; Tian, S.-S. *Bioorg. Med. Chem. Lett.* **2006**, *16*, 4376.
28. Epple, R.; Azimioara, M.; Russo, R.; Xie, Y.; Wang, X.; Cow, C.; Wityak, J.; Karanewsky, D.; Bursulaya, B.; Kreusch, A.; Tuntland, T.; Gerken, A.; Iskandar, M.; Saez, E.; Martin Seidel, H.; Tian, S.-S. *Bioorg. Med. Chem. Lett.* **2006**, *16*, 5488.
29. Kersten, S. *Mol. Metab.* **2014**, *3*, 354.
30. Feige, J. N.; Gelman, L.; Michalik, L.; Desvergne, B.; Wahli, W. *Prog. Lipid Res.* **2006**, *45*, 120.
31. Zhang, Y.; Edwards, P. A. *FEBS Lett.* **2008**, *582*, 10.
32. Eckel, R. H.; Grundy, S. M.; Zimmet, P. Z. *Lancet* **2005**, *365*, 1415.
33. Grundy, S. M. *Nat. Rev. Drug Disc.* **2006**, *5*, 295.
34. Steri, R.; Achenbach, J.; Steinhilber, D.; Schubert-Zsilavecz, M.; Proschak, E. *Biochem. Pharmacol.* **2012**, *83*, 1674.
35. Ananthanarayanan, M.; Balasubramanian, N.; Makishima, M.; Mangelsdorf, D. J.; Suchy, F. J. *J. Biol. Chem.* **2001**, *276*, 28857.
36. Seuter, S.; Väisänen, S.; Rådmark, O.; Carlberg, C.; Steinhilber, D. *Biochim. Biophys. Acta* **2007**, *1771*, 864.
37. Molecular Operating Environment (MOE), 2013.08; Chemical Computing Group Inc., 1010 Sherbooke St. West, Suite #910, Montreal, QC, Canada, H3A 2R7, 2013.
38. Sierra, M. L.; Beneton, V.; Boullay, A.-B.; Boyer, T.; Brewster, A. G.; Donche, F.; Forest, M.-C.; Fouchet, M.-H.; Gellibert, F. J.; Grillot, D. A.; Lambert, M. H.; Laroze, A.; Le Grumelec, C.; Linget, J. M.; Montana, V. G.; Nguyen, V.-L.; Nicodème, E.; Patel, V.; Penfornis, A.; Pineau, O.; Pohin, D.; Potvain, F.; Poulain, G.; Ruault, C. B.; Saunders, M.; Toum, J.; Xu, H. E.; Xu, R. X.; Pianetti, P. M. *J. Med. Chem.* **2007**, *50*, 685.